Integrated tectonic and quantitative thermochronometric investigation of the Xainza rift, Tibet

By

Christian Hager

Submitted to the graduate degree program in the Department of Geology and the Graduate Faculty of the University of Kansas in partial fulfillment of the requirements for the degree of Doctor of Philosophy.

Chairperson, Dr. J. Douglas Walker

Co-Chairperson, Dr. Daniel F. Stockli

Dr. Diane L. Kamola

Dr. George Tsoflias

Dr. Stephen Egbert

Date Defended: 05/12/2014

The Dissertation Committee for Christian Hager

certifies that this is the approved version of the following dissertation:

Integrated tectonic and quantitative thermochronometric investigation of the Xainza rift, Tibet

---

Chairperson Dr. J. Douglas Walker

Date approved: 06/09/2014

Abstract

Integrated tectonic and quantitative thermochronometric investigation of the Xainza rift, Tibet

By

Christian Hager

Department of Geology, April 2014

The University of Kansas

The Himalayan Tibetan orogeny is a superlative in many respects and has drawn a lot of attention because of its unrivaled landscape and geologic attractiveness. Many processes including ocean-continent and continent-continent collision, mountain building, plateau uplift, and E-W extension can be studied. This study utilizes a variety of different techniques to improve understanding of the history of the Lhasa terrane from its collision with the Qiangtang terrane to the north, subsequent amalgamation of the Indian subcontinent to the south, and late-stage extensional tectonics.

The Xainza rift in the central Lhasa terrane, an about 200 km long N-S trending structure, provides access to deeper crustal rocks enabling the study of magmatic evolution as well as timing and magnitude of footwall uplift during E-W extension. Zircon U/Pb dating reveals three distinct stages of magmatism at ~140-110 Ma, ~65-50 Ma, and ~15 Ma. The Cretaceous magmatism is triggered by southward subduction of the Bangong ocean slab whereas early Tertiary rocks are emplaced as a result of northward subduction of the Neo-Tethyan slab. The Miocene magmatic rocks result from additional heat influx following delamination of an over-thickened Lhasa lithosphere and show signs of significant assimilation of surrounding early

Tertiary plutons. Whole rock geochemistry reveals that the Lhasa terrane has ancient and thicker crust in its interior and more juvenile crust going outward, which has a first order effect on the observed isotopic ratios. Metamorphosed basaltic melts, under-plated during the early Tertiary, play a major role in the observed elemental patterns (high La/Yb and Sr/Y ratios) in post-collisional rocks.

Low-temperature thermochronology results from vertical transects as well as single samples, reveal that E-W extension initiated in the middle Miocene. Rift morphology combined with decreasing apatite (U-Th)/He ages from north to south support the proposed model of zipper-like opening of the rift triggered by right-lateral slip on the Gyaring Co fault. Major phase of rift shoulder uplift is constrained at ~12-10 Ma in the north and ~8 Ma in the southernmost segment. These dates coincide with the waning stages of south-directed thrusting along major faults in the Himalayas, suggesting a causal relationship between N-S shortening and E-W extension.

Thermal history modeling of (U-Th)/He data is a critical component of this study and the results are based on improved analysis of these data utilizing a newly developed software package. Modeling samples from vertical transects together provides superior control over the time-temperature evolution of the sampled crustal sections allowing for better constraint estimates of initiation and magnitude of rifting.

Acknowledgements

This work was funded by the United States National Science Foundation (grant EAR-0309976) awarded to Stockli. Additional funding was provided by the Geological Society of America and The University of Kansas Department of Geology (summer scholarships) awarded to Hager. Special thanks go to The University of Kansas for providing initial support in form of Patterson scholarships (2004-2006).

First and foremost I have to thank my advisor Daniel F. Stockli for giving me the opportunity to not only work in one of the most impressive regions on this planet but also for giving me the chance to grow academically and personally in unfamiliar surroundings. This work could not have been accomplished without the initial help and continued support of my fellow graduate students in the lab. Special thanks to Terrence Dewane, Kit Tincher, Terrence Blackburn, Jeff Schroeder, Eugene Szymanski, Melissa Wolfe, Markella Hoffman, Catherine Shirvell, Travis Glauser, Sarah Evans, Evan Bargnesi, and Kyle Gorynski for all your helpful hands, fruitful discussions, and time at the bar to blow off some steam when needed. Not to forget the "lab managers" Stephanie Brichau and Roman Kislitsyn whose attention to the lab instruments took a lot of responsibility off our shoulders. I also want to acknowledge the great support from the team at the Arizona Laserchron Laboratory during two successful visits to this facility as well as Douglas Walker's help with isotope analysis. Many thanks to the committee members Diane Kamola, Douglas Walker, George Tsoflias, Stephen Egbert, and the staff of the graduate school for being patient and allowing me to close this academic chapter of my life successfully. Finally, fieldwork in Tibet could not have been done without the logistic and linguistic support of Ding Lin and his students at the Institute of Tibetan Plateau Research as well as the help of my outstanding field assistants Terrence Dewane and Jack Desmond.

TABLE OF CONTENTS

LIST OF FIGURES AND TABLES

CHAPTER 1

CHAPTER 2

CHAPTER 3

CHAPTER 4

Page intentionally left blank

INTRODUCTION

This project was initiated by Daniel Stockli (The University of Kansas) to investigate timing and magnitude of Cenozoic E-W extension on the Lhasa terrane with focus on two major N-S trending rifts in the central part of the terrane (Tangra Yum-Co and Xainza rift). Chapters 1 and 2 outline the results from the Xainza rift and present interpretations for the evolution of this terrane from its early accretion history, collision with the Indian sub-continent, and E-W extension during the late Tertiary. Chapters 3 and 4 are focused on advancements in numerical modeling of (U-Th)/He thermochronology data that have been vital in addressing the timing of extension in the Xainza rift.

Chapter 1 is dedicated to the magmatic history of the Lhasa terrane and aims at constraining the architecture of the Lhasa terrane, subduction directions during closure, and timing of transition from ocean-continent to continent-continent collision. Samples collected from exhumed plutonic rocks as well as volcanic cover rocks from the Xainza rift and adjacent areas are analyzed using Laser Ablation Inductively Coupled Plasma Mass Spectrometry (LA-ICPMS) to derive estimates about timing of magmatism. Subsequent whole rock analysis provides quantitative measures of major element concentrations using X-ray fluorescence (XRF) spectrometry and trace element concentrations obtained from standard solution ICPMS. Together with isotopic analysis, possible source areas for magmatic rocks in the central Lhasa terrane are discussed in a spatiotemporal framework. Comparison with a large number of literature data suggests regional trends across the Lhasa terrane and allows for a conclusive but simplified model of the evolution of the Lhasa terrane from Cretaceous through Miocene times.

Chapter 2 focuses on the late-stage extensional history of the Lhasa terrane and presents results from structural mapping and (U-Th)/He thermochronology. Single samples and sample arrays predominately from plutonic basement rocks are utilized to gain insight into the thermal history of footwall as well as hanging wall units in the Xainza rift. Combined apatite and zircon analysis provide thermal sensitivities in the range of 40-80°C and 150-190°C respectively, allowing inferences on exhumation of shallow crustal rocks. Utilizing numerical modeling, uplift along rift bounding normal faults during the Miocene is constrained and estimates of pre-extensional geothermal gradients are given. The results are compared with estimates of inception and magnitude of rifting from other Lhasa terrane rifts. Finally, existing models of E-W extension are tested against the findings from this study.

Chapter 3 goes into great depths of analyzing uncertainties related to one of the most critical steps in (U-Th)/He dating, the F_T-correction (F_T). Numerical modeling using a newly developed He-Modeling Package (HeMP) illustrates the affects of inclusions and inhomogeneous parent concentrations for a variety of crystal geometries and sizes. The results are compared to F_T calculated using traditional parametric equations ignoring inhomogeneous parent concentrations improving knowledge of the range of uncertainties. Special treatment of F_T as a consequence of grain shape modifications is discussed in detail.

Chapter 4 illustrates how HeMP can be used to analyze a variety of (U-Th)/He datasets. Examples of forward modeling provide insights into the thermal sensitivities of apatite and zircon as a function of thermal history, grain size, and parent nuclide concentration. Inverse models are used to demonstrate HeMP's capabilities to extract meaningful thermal histories from analysis of single samples (single and multiple phases). Special attention is paid to modeling of sample arrays collected along vertical transects, either from boreholes or footwall transects in extensional settings. The latter has been instrumental in constraining initiation and magnitude of slip along normal fault bounded rift shoulders in the Xainza rift. Guidelines and workflows are presented to improve quantitative analyses of (U-Th)/He datasets.

CHAPTER 1:

Evolution of the Lhasa terrane from accretion to collision based on geochronological and geochemical investigations in the Xainza rift (south-central Tibet).

Abstract

The Indo-Asian collision zone is a natural laboratory to study processes involved in ocean-continent subduction and transition to continent-continent collision. New geochronological and geochemical data from the Xainza rift (central Lhasa terrane) add crucial insights into the evolution of the Lhasa terrane. Well-defined magmatic episodes with extensive magmatic gaps indicate that i) more than one subducting slab was involved in the generation of the plutonic and volcanic rocks, and ii) periods of slab roll-back and break-off are followed by magmatic quiescence related to lithospheric thickening. Isotope geochemistry reveals a thick, ancient basement in the center of the Lhasa terrane and more juvenile crust towards the Indus-Yarlung suture zone to the south and Bangong-Nujiang suture zone in the north prior to continent-continent collision. Extensive crustal contamination is reflected by highly negative eNd(t) values in the center of the terrane and observed zircon inheritance in Miocene plutonic and volcanic rocks of adakitic affinity indicates extensive assimilation of early Tertiary basement rocks. Presence of an eclogitic mafic lower crust is required in the southern part of the terrane to explain high La/Yb, Sr/Y adakitic rocks.

1.1 INTRODUCTION

The Himalayan-Tibetan orogen is a superlative with regard to the extent, peak heights, and plateau elevation. Following several episodes of terrane accretion in Mesozoic times, the main event of sculpting the Indo-Asian boundary and adjacent regions to how they appear today started in the early Tertiary with the closure of the Neo-Tethyan ocean and the collision of the Indian subcontinent with Asia. Drawn by the fascinating landscape and geology of this orogen, researchers from all over the world pursued to understand the evolution of this magnificent structure but as of today many pieces of the puzzle are either not found yet or their results are highly debated within the science community. Part of the problem, which in turn represents the attractiveness of working in this part of the world, is the remoteness and altitude of this area and all challenges that come along with that. Therefore, the current dataset for some areas might only resemble a rather coarse and punctual insight into the history of the entire Himalayan-Tibetan system. The magmatic history of the Tibetan plateau records a series of events related to the initial break-up of Gondwana, closing of oceans formed between micro-terranes, and the final collision of the Indian subcontinent with Asia. This makes the Himalayan-Tibetan orogen one of the prime studies areas to investigate tectonic and magmatic processes related to the transition from ocean-continent to continent-continent collision. Understanding the evolution of the Tibetan plateau is not only beneficial for investigations of other collision-related orogens around the world but also essential to evaluate the different models of uplift as well as subsequent E-W extension. Some of these models rely on gravitational collapse following uplift of the Tibetan plateau (England and Houseman, 1988, 1989; Harrison et al., 1992; Molnar et al., 1993), while others suggest that the present extensional processes are driven by lithospheric interactions (basal drag; McCaffrey and Nabelek, 1998; Seeber and Pecher, 1998). Within that context, the timing, distribution, and source of magmatism can provide valuable clues about the lithospheric portions involved in the Himalayan-Tibetan orogen, which in turn allows improved evaluation of the processes responsible for E-W extension. This study presents new insights into the crustal evolution of the Lhasa terrane prior and during the Indo-Asian collision based on new geochronological and geochemical analysis from the Xainza rift as well as adjacent areas.

1.2 GEOLOGIC BACKGROUND

1.2.1 Magmatism on the Lhasa terrane

The Lhasa terrane is one of several crustal blocks accreted to the Asian continent prior to the final collision of India at ~65 Ma (Allegre et al., 1984; Searle et al., 1987; Hodges, 2000; Yin and Harrison, 2000). It stretches along the present extent of the Himalayan arc and is bounded by the Bangong-Nujiang suture (BNS) in the north, and the Indus-Yarlung suture zone (IYSZ) in the south (see Fig. 1.1). The BNS formed as a result of collision of the Lhasa terrane with the Qiangtang terrane to the north and subsequent closure of the Bangong ocean in the middle Cretaceous (Dewey et al., 1988; Matte et al., 1996). The IYSZ represents the remnant of the Neo-Tethyan ocean that started to subduct northwards under the Lhasa terrane in the middle Cretaceous initiating arc magmatism within the Lhasa terrane (Durr 1996; Allegre et al., 1984; Harrison et al., 1992). Timing of initial collision of India with the Lhasa terrane is still debated and estimates predominately derived from the sedimentary record and changes in convergence rates range from ~55-70 Ma (Patriat and Achache, 1984; Klootwijk et al., 1992; Gaetani and Garzanti, 1991). Based on observed differences in sedimentary cover rocks, Zhu et al. (2009a) further subdivide the Lhasa terrane in a northern, central, and southern subterrane separated by the Shiquan River-Nam Tso Melange Zone (SNMZ) and Luobadui-Milashan Fault (LMF) respectively. These divisions are further corroborated by most negative εHf values in the central subterrane compared to more positive values towards the edges of the Lhasa terrane. Together, these observations led to the conclusion that the central Lhasa subterrane was a long-lived micro-continent that experienced addition of juvenile crust during its collisional history with the Qiangtang terrane and the Indian sub-continent (Zhu et al., 2011).

Guynn et al. (2006) report the oldest known age for exposed Tibetan basement from the Amdo region at the northern edge of the Lhasa terrane based on an upper intercept age of ~850 Ma. Recently, it has been proposed that the Amdo gneiss is not part of the Lhasa terrane but a small micro-terrane (Nyainrong terrane). Permian granitoids and proximal outcrops of eclogites of similar age within the central Lhasa terrane are interpreted as remnants of a Permian orogeny related to amalgamation of the Lhasa terrane to Australia (Gondwana) during the closure of the Paleo-Tethys ocean (Yang et al., 2009; Zhu et al., 2009a). The Gangdese Batholith and associated volcanic rocks represent the most extensive and voluminous remainders of magmatic activities and based on their spatial distribution are commonly divided into a northern and southern plutonic belt. The northern belt essentially consists of Cretaceous granitoids and associated volcanic rocks whereas late Cretaceous to Eocene granitoids dominate the southern belt. Extensive volcanism associated with the emplacement of the southern plutonic belt lasted from ~65-45 Ma and formed the Linzizong formation. There is consensus that late Cretaceous to Eocene rocks are the product of typical Andean-type magmatism related to the northward subduction of the Neo-Tethyan oceanic slab. On the other hand, contrasting models exist about the genesis of the northern Gangdese belt and it is still debated if the Cretaceous magmatism resulted from southward subduction of the Bangong oceanic slab (Pan et al., 2006; Zhu et al., 2006b, 2009a, 2011a, Chen et al., 2013; Sui et al., 2013) or represents the northernmost extent of magmatism related to northward subducting Neo-Tethyan slab (Coulon et al., 1986; Yin and Harrison, 2000; Kapp et al., 2003, 2007; Guynn et al., 2006).

Besides the widespread calc-alkaline and high-K calc-alkaline Cretaceous and early to middle Tertiary magmatic rocks, much attention has been focused on post-collisional rocks on the Lhasa terrane. Of special interest for the evolution of the Lhasa terrane within the last ~40 Myrs are ultrapotassic and adakitic rocks. Ultrapotassic rocks are generally defined by K2O/Na2O>2 but in this study the definition for ultrapotassic rocks after Foley et al. (1987) is adopted (K2O>3 wt%, MgO>3 wt%, and K2O/Na2O>2) and denoted as "UPR" to be able to compare differently treated literature data on an equal basis. Occurrences of these rocks are widespread across the Lhasa terrane and predominately consist of basaltic-trachyandesitic to trachyandesitic lava flows that unconformably overlay the Paleogene-Neogene volcano-sedimentary strata and commonly contain mantle xenoliths and xenocrysts (e.g. Miller et al., 1999; Gao et al., 2007b; Zhao et al., 2008a,b). They are primitive, clearly mantle-derived magmas but exhibit isotopic and elemental signatures that indicate extensive contamination of the source region. Miller et al. (1999) and Gao et al. (2007b) propose melting of a phlogopite-bearing lithospheric mantle that was previously contaminated by oceanic sediments as a source for UPR.

The second group is adakites, geochemically distinct magmas formed predominately between ~40-10 Ma across the southern Tibetan plateau but ages as old as 137 Ma are reported. After Defant and Drummond (1990), adakites are andesitic, dacitic to sodic rhyolitic rocks (as well as their intrusive equivalents (tonalites, trondhemites) with SiO_2 >56 wt%, Al_2O_3 >=15 wt%, MgO normally <3 wt%, Sr >400 ppm, Y <18 ppm, Yb <1.9 ppm, and $^{87}Sr/^{86}Sr$ usually <0.7045. They concluded that these rocks form predominately in arc settings where the subducting lithosphere is younger than 25 Myrs and melts are generated from melting of the down going, and consequently metamorphosed, basaltic slab leading to low concentrations of Y and heavy rare-earth elements (HREE) because of residual garnet or amphibole. This model is most consistent with the observed data but partial melting of the mantle wedge or interaction of slab melts with the overlying mantle peridotite is proposed as an alternative to be able to explain adakites with MgO exceeding 3 wt%. Based on the proposed geochemical as well as age constraints, none of the reported Tibetan adakites in the literature (Hou et al., 2004; Guo et al., 2007; Chung et al., 2009; Zhu et al., 2009a; Jiang et al., 2012; Guan et al., 2012) actually qualify as such, mostly related to the low 87Sr/86Sr constraint. The average 87Sr/86Sr values of the remnants of the Neo-Tethyan ocean along the IYSZ (0.7039, corrected for their Cretaceous age) are already close to the proposed maximum and the average value for the reported adakites on the Lhasa terrane is 0.7055. Therefore, the constraint on the isotopic Sr ratio is not enforced and going forward only samples that match the loosened constraints are presented, independent of the designation of other authors. Pre-collisional Tibetan adakites are considered the result of partial melting of (i) the Neo-Tethyan slab as a response to initiation of northward subduction (~137 Ma, Zhu et al., 2009a), ii) underplated mafic lower crust during low-angle subduction between ~100-80 Ma (Wen et al., 2008a, 2008b), and iii) the oceanic slab during mid-ocean ridge subduction (Guan et al., 2010; Zhang et al., 2010c). Origin of post-collisional adakites (~26-10 Ma) is attributed to partial melting of i) the basal portions of the over-thickened crust (Chung et al., 2003, 2005, 2009; Hou et al., 2004), ii) lower crust as a consequence of extensional collapse in S-Tibet (Guo et al., 2007), and iii) of mafic lower crust of the India (Xu et al., 2010; Jiang et al., 2011).

1.2.2 Deformational History

E-W trending thrusts and fold axes recording episodes of compressional tectonics are widespread on the Lhasa terrane and form a recognizable structural grain especially in the northern part of the terrane. Kapp et al. (2003) estimate shortening of the western Lhasa terrane (Shiquanhe area) exceeded 50% during predominately south-directed thrusting in late Cretaceous to early Tertiary times. Murphy et al. (1997) document a series of thrusts in the Coqin area (north-central Lhasa terrane) that accommodated ~60% of N-S shortening from the late Jurassic to the early Cretaceous. Further east, Kapp et al. (2007) estimate ~50% of shortening in the Cretaceous thrust belt in the Nima area just south of the BNS. Similar observations were made by Pan (1993) in the eastern part of the Lhasa terrane (Maqu area) and Leier et al. (2007) suggesting that the entire northern Lhasa terrane experienced significant N-S shortening during Cretaceous times. One of the key observations on the Lhasa terrane is that the undeformed volcanic rocks of the early Tertiary Linzizong formation (~65-45 Ma) unconformably overlay deformed Cretaceous strata constraining the cessation of this tectonic event by at least early Tertiary times.

Subsequent Tertiary N-S shortening is limited to the boundaries of the Lhasa terrane and expressed by southward thrusting along the Gangdese thrust (GT, 30-23 Ma) and north directed thrusting along the Great Counter thrust (GCT, 19-10 Ma) at its southern boundary (Yin et al., 1994; Quidelleur et al., 1997; Yin et al., 1999a; Harrison et al., 2000), and reactivation of Cretaceous structures in the Nima area in mid-Tertiary times (Kapp et al., 2007). Kapp et al. (2003a) suggests that Oligocene shortening along the S-verging Shiquanhe thrust, the only reported mid-Tertiary N-S contractional structure in the interior of the Lhasa terrane, is linked to the contemporaneous shortening along the GT and strike-slip along the Karakorum fault.

1.2.3 Geophysical Investigations

There has been a long history of geophysical investigations on the Tibetan plateau, some of the datasets are still re-evaluated, and the results improved. Although these techniques only provide a snapshot of the current configuration of the subsurface, they still deliver vital information that can be compared to other techniques to improve the coherency of tectono-magmatic models proposed based on geological investigations. One of the most ground-breaking studies in terms of progress in geophysical characterization of the Tibetan plateau is studies conducted during the International Deep Profiling of Tibet and the Himalaya (INDEPTH) projects. INDEPTH-I and INDEPTH-II revealed a strong north-dipping reflector, named the Main Himalayan Thrust (MHT), which serves as the main decollement on top of the under-thrusting Indian plate (Zhao et al., 1993; Brown et al., 1996; Yuan et al., 1997). Kumar et al. (2006) suggest that the base of the Indian Lithosphere dips northward to a depth of 220 km near the BNS and highlights an ~50 km vertical gap between the leading edges of the Indian lithosphere and lower crust which is filled by Asian lithosphere. Subduction angle of Indian plate is not uniform but steeper in the central Tibet and shallower at the eastern and western areas. Crustal thickness of the Tibetan plateau ranges from 70-75 km in the south to 60-65 km in the north and that the leading edge of the under-thrusting Indian lithosphere has reached the Tarim block in eastern Tibet while currently positioned at the BNS in central Tibet (e.g. Zhang et al., 2011). Towards the east, most of Tibet is underlain by Asian lithosphere. While many studies suggest that the Indian lithosphere is currently at the BNS in central Tibet where it steeply dives into the asthenospheric mantle (Owens and Zant, 1997; Kosarev et al., 1999; Tilman et al., 2003; Li et al., 2008), Zhou and Murphy (2005) suggest that it reaches as far as the Kunlun fault. He et al. (2010) positions the Indian lithosphere as far north as 34° (central Qiangtang terrane) based on 3-D P-wave velocity modeling. Significant for evaluation of direction of subduction at the BNS is south-directed subduction of Tibetan lithosphere beneath Lhasa terrane revealed by teleseismic from INDEPTH-III (Shi et al., 2004). Several seismic traverses across the main suture zones allow insights into the structure beneath Tibet based on analysis of P-wave velocities. In the Himalayan and Lhasa block, crustal thickening is observable in the middle and lower crust and overall crustal thickness remains constant along, as well as across the IYSZ. Along the BNS, Moho depths decrease by 10-15 km from west to east and in at the central traverse (~90°E) a high velocity anomaly in the lower portion of the crust indicates crust-mantle mixing (Zhang et al., 2011). Similar findings are provided by Teng et al. (1980a,b) who concluded from a N-S transect along ~90°E that the crust north of the ISYZ is 70-73 km thick and comprises a low-velocity layer between 45-55 km underlain by high-velocity crustal material ("crust-mantle mixture?"). Relatively low crustal densities (<3.2 g/cm^3) derived from the modeling do not support the existence of an eclogitic lower crust (3.15-3.6 g/cm^3) as suggested by Mengel and Kern (1990) beneath central-south Tibet. In contrast, Hetenyi et al. (2007) showed, based on a combination of seismic, gravity, and petrological data, that eclogitic lower crust is required beneath the Lhasa block. Compared to global averages (Christensen and Mooney, 1995), Tibetan crust shows lower velocities at all depths and is characterized by a high-velocity zone of changing thickness (10-20 km) throughout the plateau (Hirn et al., 1984a; Kind et al., 2002; Zhao et al., 1996; Owens and Zandt 1997; Zhao et al., 2001; Vergne et al., 2002). A low-velocity channel in the middle to lower crust of the Lhasa terrane is clearly inferred from waveform-modeling Vp results (Rapine et al., 2003; Kind et al., 1996; Cotte et al., 1999). This zone is not restricted to the N-S trending rifts in the Lhasa terrane but a regional phenomena suggesting widespread low-degree partial melts in the crust. Independent analysis using natural-source magnetotelluric (MT) data reveal zones of high conductance, further strengthening the concept of fluid-rich and/or partially molten crust (Wei et al., 2001; Li et al., 2003; Gokarn et al., 2002; Lemonnier et al., 1999; Unsworth et al., 2005; Kong et al., 1996).

1.3 ANALYTICAL METHODS

In order to address the question of timing and source of magmatism on the Lhasa terrane a subset of 27 samples was chosen for zircon U/Pb dating, whole rock geochemistry, and Pb/Nd/Sr isotopic compositions. Fig. 1.2 shows sample locations and magmatic ages where determined (see Fig. 1.3 for legend). In some cases either the sample quality was insufficient to allow for geochemical analysis (e.g. significant weathering), or the rock did not contain sufficient amounts of zircons for U/Pb dating. An overview of the analysed rock samples is given in Table 1.1.

1.3.1 Geochemical Background

The present chemical composition of magmatic rocks is the product of a sometimes simple, but often more complicated history of melt generation and subsequent rock formation. In the simplest case, melt is extracted from a uniform source rock and then emplaced at shallower levels without any or very little contamination from the surrounding country rock. The chemical composition of the newly formed rock is simply a function of the chemical composition of the source and the degree of melting (which in turn is a function of temperature, pressure, water saturation…). Unfortunately, this is only closely realized at mid-ocean ridges and areas of special interest like magmatism related to orogenic events as in this study, may involve many more processes before the final rock is emplaced. As an example, felsic plutons above a subduction zone can be the product of fluid extraction from the down going mafic oceanic crust which then interacts with the marine sediment cover, the lithospheric mantle, and a metamorphosed lower crust, all of which might contribute differently to the final chemical composition. Fortunately, the consequences of these interactions are not random but follow physical and chemical laws, which have been studied extensively and solved sufficiently well in many cases to allow for conclusive models. As a result, geochemical analyses of magmatic rocks can provide a characteristic fingerprint that can be used to extract information about the source and the underlying process that formed the sampled rock. A fundamental concept in geochemical studies is that the distribution of elements is closely related to their ionic radii and valence states, which determine their position in the crystal lattice. Small ions with low charges are preferred over larger ones or highly charged ions that lend to the nomenclature of compatible versus incompatible elements. In a solid-liquidus system like partial melting, compatible elements tend to remain in the solid mineral phase while incompatible elements preferentially go into the melt phase. The ratio of element concentrations in the mineral versus the melt, called the partition coefficient (McIntyre, 1963), is a simple way to quantify the compatibility of any element in a given mineral-melt system. Values > 1 indicate that the element preferentially remains in the mineral, values < 1 that the element will fractionate into the liquid phase. It is important to note that the partition coefficient is a function of the composition and elements can be incompatible in respect to one rock composition but compatible with another one. Fig. 1.4 shows partition coefficients for trace and rare-earth elements (REE) based on basaltic and rhyolitic melt compositions (data from Rollinson, 1993 and references therein). Of special interest for this study is the whole rock chemistry (major and trace elements) as well as isotopic ratios

(87Sr/86Sr, 143Nd/144Nd, 206Pb/204Pb, 207Pb/204Pb, 208Pb/204Pb) resulting from radioactive decay of their respective parent isotope.

Abundance of major elements, pressure, and temperature are the major factors controlling the mineral composition, which defines the type of rock formed during magmatic processes. Because these factors can be linked to specific tectonic settings, analysis of the major element composition can provide a first insight into the history of the samples of investigation.

Trace elements are defined as having concentrations less than 1000 ppm and occur as substitutions for major elements in the crystal lattice. According to their geochemical behavior, they are further classified into rare earth elements (REEs, atomic numbers 57-71), transition metals (atomic numbers 21-30 including the major elements Fe and Mn), and platinum group elements (PGEs, atomic numbers 44-46, 76-79). Other widely used trace elements include Rb, Sr, Y, Zr, Nb, Cs, Ba, Hf, Ta, P, Pb, Th, and U. Based on the ionic potential, the ratio of ionic radius and valence, trace elements (excluding transition metals and PGEs) are commonly grouped into high field strength (HFS, ionic potential > 2) and low field strength (LFS, ionic potential < 2; also known as large ion lithophile elements, LILE) elements.

The most important trace elements with respect to geochemical investigations are the REEs. With the exception of Eu and Ce, which additionally occur as 2+, respectively 4+ oxidation states, REE's are stable 3+ ions with similar ionic radii. As a consequence of their equal valence, differences in compatibility is a function of ionic radius and higher atomic number REEs are generally less compatible relative to the lower atomic number REEs.

Isotope ratios have been widely used as a dating technique (Rb/Sr, Sm/Nd, Pb/Pb) but with the advent or more accurate and precise methods like U/Pb dating have lost some of their appeal for geochronological studies. Nevertheless, analysis of the isotopic composition of a bulk rock sample provides exceptional insights into the history of rock formation. The same basic principles of compatibility/incompatibility apply as well but with the additional merit that another dimension, time, is added as an investigative tool. For the elements of interest the order of incompatibility is Rb > Th > U > Pb > Nd > (Sr, Sm).

The Rb/Sr system is based on the decay of 87Rb to 87Sr through single beta decay with a half-life of 48.8 Byr (Steiger and Jaeger, 1977). 86Sr is the stable isotope and the 87Sr/86Sr ratio is used to describe the radiogenic ingrowth over time. This system exhibits the most dramatic difference in compatibilities between parent and daughter and as a result, Rb is preferentially accumulated in the melt while Sr stays in the solid phase, which consequently leads to accelerated 87Sr/86Sr evolution in the newly formed rock compared to the Rb-depleted restite. With additional age information, the initial 87Sr/86Sr value (87Sr/86Sr(i)), which corresponds to the isotopic composition of the source rock at the time of the magmatic event, can be calculated and used to compare individual samples with each other. Analysis of basaltic achondrites led Papanastassiou et al. (1969) to propose a "basaltic achondrite best initial" or BABI of 0.69899±5 at 4.39±0.26 Byr that represents the initial 87Sr/86Sr value of the earliest earth. Based on the geochemical behavior, the present isotopic ratio might be the result of a convoluted history of magmatic events and the only information that can be gained is from the time of the last disturbance of closed system behavior.

The Sm/Nd system is based on the decay of 147Sm to 143Nd through single alpha decay with a half-life of 106 Byr (Lugmair and Marti, 1977). 144Nd is the stable isotope and the 143Nd/144Nd ratio is used to describe the radiogenic ingrowth over time. Contrary to the Rb/Sr system, Sm and Nd are both immobile REEs and show very similar chemical behavior. Consequently, there is very little fractionation of parent and daughter during crustal recycling and even high-grade metamorphic events. This circumstance elevated this technique to one of the prime investigative tool for source rock analysis. Similar to the Rb/Sr system, meteorites (chondritic) were used to establish a present-day 143Nd/144Nd value of 0.512638 and 147Sm/144Nd value of 0.1966 (Hamilton et al., 1983) for the so-called chondritic uniform reservoir (CHUR, DePaolo and Wasserburg, 1976a).

Contrary to above systems, radiogenic Pb isotopes are the product of several decay chains. 206Pb is the product of decay of 238U with a half-life of 4.47 Byr, 207Pb from 235U with a half-life of 0.704 Byr, and 208Pb from 232Th with a half-life of 14.01 Byr. The only non-radiogenic Pb isotope is 204Pb. U, Th, and Pb are concentrated in the upper crust due to their general incompatibility whereas U and Th are enriched compared to Pb. The geochemical behavior as well as the unique case of three parent isotopes decaying at much different rates has proven to be a viable tool to assess source regions.

1.3.2 Methodology

Samples for age determination underwent routinely applied mechanical and physical separation techniques at the Isotope Geochemistry Laboratory (IGL) at the University of Kansas to yield a purified zircon fraction. Laser ablation-multi-collector-inductively coupled plasma-mass spectrometry (LA-MC-ICP-MS) was utilized to gain insights into the magmatic evolution of the Lhasa terrane. Zircon populations from 25 samples were analyzed at the Arizona Laserchron Center at the University of Arizona using a GV Instrument Isoprobe coupled with a New Wave Instruments ArF excimer laser operating at a wavelength of 193 nm. Hand-picked zircon grains were mounted in epoxy, polished to expose the interior of the grain, and subsequently loaded in the laser chamber for in-situ U-Pb analysis. To ensure sufficient amounts of ablated material, the spot size of the laser was initially set to 30 μm but was changed to 20 μm for more detailed age mapping for some samples that showed inheritance. According to established lab procedures and based on sample size/quality, 20-30 analyzes per sample proved to yield statistically robust U/Pb ages with uncertainties within the limits of this procedure (1-3%). Where inheritance was detected, a greater number of analyses focusing on the center and the rim of the grains were needed to catch the multi-stage magmatic history of the zircon population. Isotope fractionation was corrected for by analyzing a well-known zircon standard every 4-5 unknowns. Final age calculation including all necessary corrections was accomplished with the in-house developed Microsoft Excel© macro.

After crushing the rocks to coarse cm sized chips, a representative split of visually unaltered rock was sent to the GeoAnalytical Lab at Washington State University (WSU) for further processing. Major elements were measured by X-ray fluorescence technique (XRF) on a ThermoARL AdvantXP+ automated sequential wavelength spectrometer and trace elements by conventional inductively coupled plasma–mass spectrometry (ICP-MS) on an Agilent4500+ quadrupole instrument. Nd/Sr/Pb isotope geochemistry was conducted at IGL on rock powder received from WSU after whole rock major and trace element procedures. Approximately 300 mg of sample was weighted into a microwave acid digestion vessel and mixed with a measured amount of Sr spike (~1 g) before adding 3 ml of HF and drying down on a hotplate. After adding 1 ml of 7N HNO3 and 5 ml of HF, this solution was heated in a microwave for 1.5 minutes and subsequently dried down on the hotplate. To ensure complete sample digestion, this process was repeated. Dissolution in 3 ml of 7N HNO3 and taking a 500 μl split for later Pb isotope analysis completed this process and gave way to further chemical separation techniques. In the first step, the solution was loaded on a cation exchange resin to separate the Sr isotopes from the rare earth elements (REE's). Sr was eluted with 2.5 N HCl and subsequently the REE's were extracted with 6.0 N HCl. REE solution underwent an additional column procedure to separate Sm from Nd isotopes. Several rinse steps with 0.18 N HCl were used to collect Nd and subsequent application of 0.5 N HCl eluted the Sm isotopes. After dry-down on the hotplate, all solutions were ready for thermal ionization mass spectrometry (TIMS).

1.4 RESULTS

Before going into the details of the analysis, it has to be pointed out that this study relies on extensive efforts to compile available literature data to be able to compare the results of this study with a larger dataset, which ultimately should allow for a conclusive regional picture of the evolution of the Lhasa terrane. Although great care was taken while summarizing the data, there is no guarantee for completeness or accuracy especially of sample locations. A large number of publications do not include geographic coordinates and much time was devoted to extract this valuable piece of information through georeferencing the available maps. For reference, Tables A.2-A.4 (Appendix A) provide sample names, lithologies, locations, magmatic ages, and geochemical analysis for the Lhasa terrane and Himalayan rocks sorted by author.

1.4.1 Zircon U/Pb dating

The results of the age analysis are given in Table 1.1 and Fig. 1.5-1.8, individual spot analysis for each sample is provided in Appendix A (Table A.1). Calculation of mean ages and plotting of results was accomplished using Isoplot v.4.3 Excel by Ludwig (2008). The sample set can be subdivided into four distinct age groups (206Pb/238U age) falling into the late

Triassic/early Jurassic, early Cretaceous, early Tertiary, and middle Miocene times, constituting the basis for subsequent discussion of geochemical results.

The oldest rocks exposed in the investigated areas are found in the central segment of the Xainza rift (05XI79; ~203 Myrs) and in the north of the Namling transect (05GB05; ~212 Myrs). Both samples show a wide spread in individual spot ages and a limited number of coherent analyses and the average age has to be used with caution. Additionally, the samples were heavily weathered and therefore did not qualify for whole rock geochemical analysis.

One of the major age populations ranges from ~111 to 131 Ma and is, besides one exclusion in the central segment (05XID68; ~129 Myrs), restricted to the northern segment and locations closer to the Bangong Nujiang suture zone to the north of the Xainza rift. By far the most prominent magmatic event happened in the early Tertiary when vast amounts of intrusives and effusives formed the voluminous Gangdese Batholith and Linzizong volcanic suite respectively. This period lasted from ~65-45 Ma and was predominant in the southern portion of the Xainza rift as well as along the Namling transect.

The youngest group of analyzed samples are middle Miocene in age and restricted to a fault-bounded granitoid in the southern segment, and an extensive tuff in the middle segment of the Xainza rift. All samples of this group show extensive inheritance with maximum ages overlapping with the major phase of magmatic activity in the early Tertiary.

1.4.2 Whole Rock Geochemistry

1.4.2.1 Major Elements

Results from XRF analysis are provided in Table 1.2. As presented in form of Harker diagrams in Fig. 1.9 for calc-alkaline rocks, the analyzed samples are of intermediate to acidic composition based on the SiO_2 content ranging from 60-85 weight percent (wt%). Al_2O_3 concentrations range from 9-18 wt%. Total iron expressed as FeO, CaO, Na_2O, as well as K_2O contents do not exceed 6 wt% whereas MgO concentrations stay below 3 wt%. Al_2O_3, FeO, MgO, and CaO show clear negative, K_2O slight positive, and Na_2O no correlation with SiO_2 content. None of these bivariate plots exhibits a clear relationship between oxide concentrations and age of the rocks. Fig. 1.10 compares the calc-alkaline rocks with Lhasa terrane adakites and UPR. While adakites show very similar major element concentrations as calc-alkaline rocks, UPR exhibit much higher K_2O values (a necessity based on their geochemical classification) and significantly lower Al_2O_3 and Na_2O values compared to calc-alkaline rocks of similar SiO_2 content.

Using total alkali versus silica (TAS) diagrams (see Fig. 1.11 for plutonic rocks ; Fig. 1.12 for volcanic rocks) after Le Maitre et al. (1989) and Cox et al. (1978) the volcanic rocks are exclusively classified as rhyolites and the plutonic rocks predominately as granites with a couple of samples plotting in the granodiorite and diorite field. Based on the K_2O vs. SiO_2 classification of Le Maitre et al. (1989), the samples fall into the High-K (calc-alkaline) series. The exceptions are the two mid-Miocene volcanic rocks (05XI75, 05XI77) that show a more shoshonitic affinity. Based on the molar ratios of $Al_2O_3/(Na_2O+K_2O)$ and $Al_2O_3/(Na_2O+CaO+K_2O)$ the samples range from metaluminous to peraluminous showing some differentiation in that the early Cretaceous plutons are predominately peraluminous whereas the early Tertiary plutons show a more metaluminous signature.

1.4.2.2 Trace Elements

Results from LA-ICPMS analysis are provided in Table 1.3. A variety of trace element concentration combinations is in use to classify granitoids into syn-collisional, volcanic-arc, within-plate, and ocean-ridge granites. Using the Rb vs. Y+Nb diagram (Fig. 1.11) after Pearce et al. (1984), all samples except the Miocene intrusive (05XIE82), which falls into the syn-collisional field, are volcanic-arc granites.

Fig. 1.13 shows primitive mantle normalized plots of trace elements as well as chondrite normalized REE patterns for the plutonic and volcanic rocks ordered by increasing compatibility in a small fraction melt of the mantle. The trace element plots show distinct negative anomalies in Ba, Nb, Ta, Sr, P, and Ti and overall the oldest age group exhibits the largest excursions. The Miocene granite has a relatively flat section between La and Sm and the lowest values of all samples for Tb and Y while showing one of the highest enrichments in Rb, Th, and U. The volcanic rocks show a similar pattern but the Cretaceous rocks follow the early Tertiary ones more closely. The most striking feature in this plot is the significant enrichment of Th and U in the Miocene volcanic rocks. The REE patterns for plutonic rocks indicate enrichment in LREE over HREE and with the exception of sample 04QT01 a relatively flat geometry at the heavier end. Two of the early Tertiary granites (05XI92, 05XI94) qualify as adakites showing the most depleted HREE pattern. The Miocene granite (05XIE82) exhibits almost identical trace element and REE patterns and upon further investigation the only threshold that is not met to be considered as an adakite is a slightly too low Al2O3 content (14.37 wt% versus the required >= 15.0 wt%). Going forward, this sample is not plotted using the adakites symbol for consistency reasons but it is noted that this sample shows highly adakitic affinities. A negative Eu anomaly is pronounced in the older rocks but very subdued in the Miocene granite. The volcanic rocks show a similar pattern but less pronounced Eu anomalies and contrary to the plutonic rocks, a clear separation between Cretaceous and Tertiary rocks is evident especially in the heavier end of the pattern. The Miocene volcanic rocks resemble the trend of the Tertiary rocks.

In order to make comparisons across the Tibetan plateau, the samples from this study are plotted together with other Lhasa terrane samples including adakites and ultrapotassic rocks as well as Himalayan granitoids (see Fig. 1.14-1.17). The Himalayan granitoids older than 165 Ma are a suite of ~500 Ma peraluminous granites and granodiorites derived from anatectic melting of continental crust (Miller et al., 2001). Strong negative Ba, Nb, Sr, Hf, and Ti as well as positive Ta and Nd anomalies are the most characteristic features in the trace element pattern. REE patterns show a pronounced negative Eu anomaly.

The 110-165 Ma age group can be further subdivided into three distinct groups. The first contains the plutonic and volcanic rocks from the Nidar ophiolitic complex (Ahmad et al., 2008), a remnant of the Neo-Tethyan Ocean that closed during northward migration and final collision of India with Asia. The gabbros show distinct positive Sr and Eu anomalies and overall relatively flat patterns. The basic volcanic rocks lack these strong peaks but otherwise share the flat and depleted character of the intrusive rocks. Including the Xainza samples already discussed above, the second group belongs to the widespread occurrence of the Cretaceous calc-alkaline series Gangdese Batholith. Sample 04QT01 collected near Nam Tso north of Lhasa is much different in its geochemical character than the rest of the analyzed samples in this age group. Negative anomalies in Ba, Sr, P, and Ti are more pronounced and values for Tb and Y are higher than any other samples from this study. The greatest difference is the strong positive anomaly in Ta paired with much more enrichment in Rb and Nb. An increase in HREE together with lower concentrations in LREE is opposite of the trend of other samples as well. Additionally, the by far strongest negative Eu anomaly is shown by this sample. These clearly different geochemical characteristics compare very well with samples from eastern Tibet categorized as "A-type" granites by Lin et al. (2012).

No magmatic rocks within 70-109 Ma are sampled during this study and this group represents a less abundant magmatic event in the Lhasa terrane overall. The majority of this population is adakitic plutonic rocks with no volcanic equivalents. Depletion in HREE and enrichment in LREE together with negative anomalies in Nb and Ta are the most consistent traits of the adakitic rocks. Additionally, some samples show a clear positive Sr peak.

The early Tertiary event is probably the most prominent magmatic phase within the Lhasa terrane and predominately consists of the large volume calc-alkaline plutonic rocks of the Gangdese belt and extensive intermediate-acidic volcanic rocks of the Linzizong formation. Trace element as well as REE patterns are very similar to the Cretaceous calc-alkaline rocks. Besides the familiar pattern, a number of volcanic samples show a very different trend in the trace elements. These samples are ~40 Myr old mafic, high-MgO picrites, basalts, and basaltic andesites characterized by positive anomalies in Sr and P and a very flat REE pattern less enriched in LREE (Gao et al., 2008). Magmatism in the Himalayas during this time period is localized in the Northern Himalayan Gneiss domes (NHG) and the trace element patterns show similar characteristics as the calc-alkaline Lhasa terrane rocks but less enrichment overall. More obvious is a separation in the REE pattern caused by a lesser enrichment in HREE that overlaps with adakitic varieties.

Past 40 Ma, magmatism on the Lhasa terrane is dominated by adakitic plutonism and adakitic and ultrapotassic volcanism. Adakitic varieties show the same characteristics discussed earlier, most noteworthy the lowest concentrations of HREE of all Lhasa terrane samples shown here. The ultrapotassic lavas are the most enriched samples and parallel the adakitic volcanic rocks for most part of the trace element pattern. The only difference is that adakitic dikes (0-19 Ma) show a positive Sr peak and less enrichment Rb, Ba, Th, U, and K which is more closely to the pattern of the intrusive adakites of similar age. This is opposite of the ultrapotassic rocks that display a clear negative Sr anomaly. In the Himalayas, magmatism within the NHG continues and leucogranites are emplaced beneath the STDS in the HHC. They are characterized by negative Sr and positive Ta and P anomalies. The REE patterns are less steep than adakitic plutonic rocks and show a clear Eu anomaly.

1.4.2.3 Whole Rock Isotopic Data

In Fig. 1.18, whole-rock isotopic data from the literature are plotted on the right-hand side, while samples analyzed during this study are plotted together with simplified outlines for comparison. The Cretaceous magmatic rocks are characterized by 87Sr/86Sr(i) ranging from 0.7089-0.7212 and εNd(t) between -7 and -13 with generally higher 87Sr/86Sr(i) and lower εNd(t) values for the volcanic compared to the plutonic rocks. Slightly higher 87Sr/86Sr(i) values between 0.7080-0.7128, similar to the lower ones of the early Cretaceous rocks, characterize the earliest stages of volcanic activity in the early Tertiary (~60-65 Ma), whereas lower values of 0.7047-0.7070 seem to represent the period between ~45-55 Ma dominated by plutonic rocks. This subdivision is further constraint by significantly different εNd values of -6.8 to -7.7 for rocks older than 60 Ma and -2.4 to 1.8 for the suite younger than 55 Ma. Again, the lowest values of the early Tertiary overlap with the highest values of the early Cretaceous rocks. Sr and Nd isotopic compositions of the middle Miocene plutonic and volcanic rocks are very similar to the older early Tertiary subgroup with 87Sr/86Sr(i) values of 0.7075 and 0.7087 and εNd(t) of -7.5 and -6.7. Similar to trace element and REE patterns, sample 04QT01 also falls slightly outside the trend showing a more radiogenic 87Sr/86Sr(i) value than other samples with comparable εNd(t). The Pb isotopes align with the Sr and Nd system confirming the overall trend of higher radiogenic values for the Cretaceous rocks compared to the early Tertiary ones and the observation that the Miocene rocks resemble more closely the isotopic character of Cretaceous and earliest Tertiary volcanic rocks.

In comparison with literature data from the Lhasa terrane, the Cretaceous rocks fall within the range of the published data whereas the earliest Tertiary volcanic rocks do show slightly lower εNd(t) values than time-equivalent Linzizong volcanic rocks. Furthermore, there is significant overlap with the isotopic ranges of UPR and adakites.

1.5 DISCUSSION

1.5.1 Geochemical variations in time and space

Because the goal of this study is to reveal the magmatic evolution over time and gain insight into the underlying processes, especially the transition from arc-magmatism to continent-continent collision, the dataset at hand must be evaluated in a temporal-spatial context. As shown in Fig.1.1, the Lhasa terrane and Himalayan samples are grouped into six areas (Q1-Q6) bounded by approximately arc-normal outlines. The definition of these areas is not based on any geological constraints but simply a function of data availability and an attempt to define areas of comparable width. Going forward, parameters of interest from samples within these quadrants are plotted against the normalized distances from the major terrane bounding structures (MFT, IYSZ, BNS). The normalized distance is simply the shortest distance of each sample from the terrane bounding structures expressed as fraction (e.g. a sample in the Lhasa terrane 100 km north of the IYSZ and 200 km south of the BNS plots at 1.334 where MFT = 0, IYSZ = 1, BNS = 2). Q1 and Q6 are excluded from the figures because of the severe deformation of the IYSZ within the eastern and western syntaxes which precludes this kind of analysis.

Figs. 1.15-1.18 summarize the available literature data and compare sample ages, 87Sr/86Sr(i), εNd(t) values, and Pb/Pb isotopic ratios for calc-alkaline rocks, adakites, and UPR separately based on their respective normalized distances from the sutures. Starting with the calc-alkaline suites (Fig. 1.19), magmatic ages > 100 Ma are predominately clustered in the northern portion of the Lhasa terrane whereas younger rocks are exposed in the southern half. This trend is best seen in Q3 and Q4 and less obvious in Q5. In the Xainza rift, there are clear breaks between the individual age groups and within the late Cretaceous/early Tertiary period the rocks are getting younger towards the IYSZ. Limited data are available in Q2 and the cluster of ~120 Ma samples with unradiogenic 87Sr/86Sr(i) and εNd(t) corresponds to the Nidar-Ophiolite complex within the IYSZ (Ahmad et al., 2008). One has to keep in mind that this display is based on present-day sample locations and the Cretaceous rocks could be "shifted" further north to account for N-S shortening at that time leading to a more linear decrease in ages from north to south.

Isotopic data reveal compelling evidence for changes in the source of magmatism and magma mixing processes across the Lhasa terrane. Most obvious in Q4 and Q5, the 87Sr/86Sr ratios increase from MORB-type values at the IYSZ to more radiogenic values in the interior of terrane and then decrease again towards the BNS. The opposite is true for eNd values that exhibit positive values close to the IYSZ gradually decreasing to highly negative values in the center of the terrane followed by an increase towards the BNS. It has to be noted that these trends are independent of the age of the magmatic rocks indicating that the composition of the Lhasa lithosphere above the dehydrating slab has the strongest control on the isotopic signature of the magmatic rocks. Harrison et al. (2010) investigated granitoids in the east-central portion of the terrane around Lhasa and showed the same trends in eNd values for rocks older than ~48 Myrs. They interpreted these results as evidence for decreasing magma flux in conjunction with increasing crustal thickness from <=20 km just north of the IYSZ to >50 km in the center of the terrane. The decreasing eNd values are therefore a result of increasing crustal assimilation to the point where granitoids with eNd less than -10 represent pure intra-crustal melts as suggested by Harrison et al. (2010). Further evidence for an ancient central Lhasa terrane flanked by more juvenile crust to the north and south is given by Zhu et al. (2011a). They concluded based on eHf isotopic studies that granitoids in the central Lhasa terrane are predominately the result of anatexis of mature continental crust whereas increasing contribution from mafic sources can be seen towards the edges of the terrane. Deviation from the overall eNd trend is most obvious in Q4 represented by Cretaceous basalts (Chen et al., 2013) with more positive values compared to contemporaneous intermediate and felsic magmatic rocks. This can be explained by faster ascend of less viscous basaltic magmas through the crust causing less extensive mixing with older continental material and therefore retaining much of their primary isotopic source character. Another deviation from this general behavior is represented by ~38 Myr old granitoids with gabbroic and dioritic enclaves from the Wolong area at the IYSZ (Q5, Guan et al., 2012). The host granodiorites and granites are adakitic (plotted in Fig. 1.21) and the enclaves with identical isotopic signatures are interpreted as restitic material. Based on these observations, Guan et al. (2012) suggest that these intrusives were derived from magma mixing of a parental mafic lithospheric magma with melts derived from a thickened (60-70 km) lower Lhasa crust. Limited Pb isotope data are available for the calc-alkaline rocks on the Lhasa terrane but the Xainza area samples show trends consistent with increasing crustal contamination towards the center of the terrane (Fig. 1.20). In comparison, the very low isotopic ratios at the IYSZ in Q4 correspond to the Xigaze ophiolites with values typical for oceanic basalts from a depleted mantle source (Zindler and Hart, 1986). On a final note, Fig. 1.19 highlights very distinct breaks in isotopic characters across the IYSZ suggesting that calc-alkaline series rocks were not affected by contamination with Himalayan crustal material.

Fig. 1.21 shows ages and isotopic ratios for adakites and UPR in comparison with the calc-alkaline series rocks. Adakites were formed since the Cretaceous but most occurrences fall within the 40-10 Ma timeframe and their geographic distribution is clearly restricted to the southern Lhasa terrane. 87Sr/86Sr(i) values are identical to adjacent calc-alkaline rocks but eNd(t) although within the same range as the Linzizong volcanic rocks (+5 through -5) are generally lower than calc-alkaline in the same position. Following Chung et al. (2009) and Guan et al. (2012), this shift towards lower values for similar distances from the IYSZ can be interpreted as a result of progressive thickening of the southern Lhasa terrane crust after ~40 Ma. Higher temperatures in the lower crust would allow for increased partial melting of older continental material which would result in lower eNd(t) values. Outcrops of UPR are most common in the eastern and central Lhasa terrane (Q3, Q4) and seem to be slighter older in the central parts compared to occurrences closer to the IYSZ (23-10 Ma). Similar to the adakites, the 87Sr/86Sr(i) values follow the trend of the calc-alkaline rocks but are slightly elevated. Values exceeding 0.73 are reported by Gao et al. (2007b) from the Chazi area as well as Williams et al. (2001) from a dike near Pabbai Zong. Contrary to all other examined rock types, UPR exhibit relatively uniform eNd(t) values overwhelmingly less than -10 lacking any correlation with distance. Pb isotopes for both, adakites and UPR are again in good agreement with the calc-alkaline series rocks (Fig. 1.22).

Ratios of compatible versus incompatible elements are another useful tool to investigate the geochemical characteristics of the magma source. Of special interest is the chondrite normalized ratio of La and Yb which provides a good measure of enrichment of LREE or depletion of HREE. The most efficient way to achieve depletion in HREE is melting of a source rock with garnet as residual phase. Across the REE range, garnet has a very steep increase in partition coefficients and the highest values for HREE compared to other common rock-forming minerals (see Fig. 1.4), which elevates this mineral to one of the most important constituents in controlling the whole-rock REE budget. Garnet as a rock-forming mineral is most commonly found in metamorphic rocks like garnet-amphibolites, eclogites, and granulites. In the framework of subduction zones, melting of i) the eclogitized basaltic slab itself, ii) eclogitized under-plated basalts that represent the restites of an earlier melt-extraction and fractionation process, or iii) eclogitic or granulitic lower crust can produce parental magmas with high La/Yb ratios. Fig. 1.23 illustrates the chondrite normalized La/Yb ratios and Sr/Y ratios for calc-alkaline rocks. In the Xainza rift (Q4) La/Yb ratios increase steadily towards the center of the terrane followed by a more or less sudden decrease and uniformly low values going further north with one exception (04QT02). The Miocene granite (05XIE82) as well as other samples collected from the same plutonic body ("Nanmuqie Granite"; Xu et al., 2010) display elevated values outside of the observed trend. This different behavior is also expressed in the very high Sr/Y ratios, which are otherwise uniformly low across. As in this study, Xu et al. (2010) reported inheritent U/Pb zircon ages up to ~50 Myrs indicating that the 15 Ma magmatic rocks suffered extensive contamination from surrounding early Tertiary granitoids. The trend in the La/Yb ratios seen in the Xainza samples is not clearly visible in Q5. Early Tertiary samples seem to increase towards the center of the terrane but there is also some indication of higher ratios towards the IYSZ. Post-collisional samples restricted to the southern half of the terrane show a wide range with the highest values at the IYSZ. Similar to Q4, ratios from Cretaceous rocks north of the terrane center are low. A much different picture is drawn by the Sr/Y ratios in Q5 compared to Q4. All Tertiary rocks show an increase towards the IYSZ, the 20-39 Ma plutonic rocks again represent the highest values. Cretaceous samples in the north are comparable to equivalent rocks in Q4. Within Q5, a group of ~84 Myr old plutonic rocks stands out because of elevated values especially in the Sr/Y plot compared to samples at equivalent distances. Actually, these are gabbroic and dioritic enclaves within host granodiorites of adakitic geochemistry (plotted in Fig. 1.24) from the Mamba area (Meng et al., 2013). The authors interpret this rock assemblage as result of magma mixing between melts of ancient thickened lower crust and enriched fluid-metasomatized mantle in a back-arc extensional setting. As required by the geochemical definition of adakites (high Sr, low Yb), they show generally more elevated values in both displays compared to the calk-alkaline series rocks (Fig. 1.24). UPR exhibit higher La/Yb and Sr/Y values in the center that decrease towards the sutures.

The idea that more negative eNd(t) values correlate with crustal thickness has already been discussed by means of supportive trends shown in Fig. 1.19. Based on studies in the Andes, Chung et al. (2009, and references therein) suggest that the La/Yb ratio can serve as proxy for crustal thickness and estimate that values around 20 correspond to 40 km thick crust and values around 50 to 50-55 km thick crust . To further investigate this idea, Fig. 1.25 shows La/Yb, Sr/Y, and eNd(t) plotted against the magmatic age. The color-coding in this case is not by age but by distance from the IYSZ bins to evaluate temporal trends at similar locations on the Lhasa terrane.

UPR are excluded from these illustrations because of their unique geochemical character that is a result of a metasomatized mantle source. Cretaceous samples from the central and northern terrane have low La/Yb indicating thin crust, which disagrees with the >50 km estimate of Harrison et al. (2010) based on highly negative eNd(t) values in the central Lhasa terrane. In Q4 an increase in La/Yb and Sr/Y ratios seems to correlate with younger ages but in Q5 a wide spread of values is rather inconclusive. The eNd(t) values on the other hand show better correlations than the REE ratios. In Q4 Cretaceous samples from the central and northern terrane (1.4-1.8 norm. distance) have the most negative eNd(t) values, the array of volcanic rocks ranging from ~0 to -5 are the already discussed basalts from the northern Xainza rift. Samples closest to the IYSZ (1.0-1.2 norm. distance) exhibit a well-defined trend from highly positive values in the Cretaceous to a minimum of -11 for Miocene adakites. Similar trends can be seen in Q5 with the exceptions that Cretaceous samples closest to the IYSZ do not have as positive, and Miocene adakites not as negative eNd(t) values. Furthermore, a much wider spread in the Miocene values is observed. Samples in the 1.2-1.4 normalized distance bin are offset towards more negative eNd(t) values compared to the samples closer to the IYSZ which aligns well with the interpretation of a gradually thickened crust towards the interior of the terrane. As in Q4, values from samples in the 1.6-1.8 normalized distance bin stay around -10 suggesting unchanged crustal thickness from the Cretaceous through the Miocene although it ahs to be noted that this is based on only a few samples. In summary, REE and trace element ratios are not suitable to derive at a conclusive answer to the question of evolution of crustal thickness through time and space. As pointed out earlier, crustal contamination plays an important role in the generation of many of the magmatic rocks within the Lhasa terrane and the eNd(t) seem to be less sensitive to this process. Nevertheless, elevated REE and trace element ratios predominately in the southern part of the terrane and more abundant in Tertiary rocks eludes to increasing contribution of garnet-bearing lithologies in the source area.

1.5.2 Magmatic evolution of the Lhasa terrane

Following, an attempt is made to synthesize the findings from the spatio-temporal variations in geochemical characteristics and an idealized model of the evolution of the Lhasa terrane is provided (Fig. 1.26-1.27). The model heavily relies on results from the investigated area but incorporates the data from other areas as well. From the above discussion, it is obvious that lateral variations across the Lhasa terrane do exist and extrapolation from one area to another might not be viable. Additionally, the dataset on hand has some limitations that are that not all samples have a complete suite of geochemical and age analysis. Furthermore, sample density is much higher towards the eastern part of the Lhasa terrane concentrated around Lhasa while it is difficult to extract convincing trends in the eastern areas of the plateau (Q2, Q3).

One of the least constrained topics concerning the long-lasting magmatic activity on the Lhasa terrane is the direction of subduction along the edges of the Lhasa terrane. The contrasting models are i) initial flat-slab subduction of the Neo-Tethyan slab that reached the northern edge of the Lhasa terrane followed by slab roll-back, or ii) southward subduction of the Bangong oceanic slab beneath the Lhasa terrane resulting in an early Cretaceous arc followed by slab roll-back of the Neo-Tethyan slab causing arc-type magmatism beginning in the late Cretaceous until the Eocene. The first model should result in a continuous trend of older ages in the north and younger ages in the south with no distinct breaks in magmatism whereas the second model should display two opposing trends of maximum ages in the interior getting younger towards the northern and southern boundaries of the terrane. The first model also implies that the Bangong oceanic slab subducted northwards under the Qiangtang terrane, consequently, one would expect a widespread Cretaceous arc along the southern boundary of the Qiangtang terrane. Such an indicator for northward subduction of the Bangong slab is missing but it cannot be ruled out that these rocks exist in the subsurface. As an additional cross-check, published conversion rates and estimates of initiation of subduction can be used to test if the Neo-Tethyan slab could have reached the northern extent of the Lhasa terrane to induce Cretaceous magmatism. Lee and Lawver (1995) proposed 100-120 mm/yr convergence rates during flat-slab subduction between ~70-90 Ma, which would enable the slab to travel the current width of the Lhasa terrane (~300 km) within 2-3 Myrs assuming similar rates for the early Cretaceous period. Even if the entire Lhasa terrane was shortened by 50-60%, the convergence rate was sufficiently high to position the slab beneath the northern Lhasa terrane within a few million years after initiation of subduction in the Cretaceous. The source of magmatism in subduction zones is primarily related to partial melting of the mantle wedge induced by dehydration of the down going slab. As a consequence, the isotopic ratios cannot be used as an argument for the direction of subduction because the basic processes of melt generation are identical and there is no reason to believe that the Neo-Tethyan and Bangong slab are significantly different in their geochemistry to be responsible for the observed trends. Strong support for the southward subduction of the Bangong slab is given by Chen et al. (2013) based on investigations at the northernmost edge of the Xainza rift. They conclude that widespread bimodal plutonism and volcanism at ~113 Ma indicates the final magmatic pulse as a result of slab break-off. This is not a localized event but similar suites of rocks with identical ages have been reported ~400 km to the west in Q3 near Yanhu (Sui et al., 2013). Evidence for slab roll-back of the Neo-Tethyan slab at ~85 Ma is given by Meng et al. (2013) from the Mamba area in the east-central Lhasa terrane. Host granodiorites (some exhibit adakitic geochemistries) and dioritic as well as gabbroic enclaves are interpreted as the result of magma mixing in a back-arc extensional setting. This observation implies that the Neo-Tethyan slab must have been at least under the central Lhasa terrane prior ~85 Ma. Zircon Hf isotopic studies as well as the eNd(t) data shown earlier are the best available indicators for ancient thickened Lhasa terrane crust. Consistently, these data confirm that the Lhasa terrane consists of ancient basement in the center flanked by more juvenile crust towards the suture zones. It seems highly unlikely that a northward subducting Neo-Tethyan slab would not be deflected downwards towards the asthenospheric mantle when encountering the thicker orogenic root beneath the central Lhasa terrane. Together with the observed magmatic gap between ~110-60 Ma as well as the indications for slab break-off at ~110 Ma below the present location of the northern Xainza rift, a southward subducting Bangong slab model is preferred over the single Neo-Tethyan flat-slab subduction model. Supporting evidence for this model is provided by teleseismic from the INDEPTH-III array that imaged a southward dipping mantle converter suggesting subduction of Asian lithosphere under the northern Lhasa terrane (Shi et al., 2004).

During the Cretaceous, the northern Gangdese plutonic and volcanic belt is formed because of southward subduction of the Bangong slab. Depending on the crustal thickness above the origin of parental melts, varying degrees of crustal contamination results in a spread of eNd(t) values. Closure of the Bangong ocean triggers crustal thickening of the northern Lhasa terrane expressed by fold and thrust belts along the northern edge of the terrane that accommodated up to 50% of horizontal shortening. At ~110 Ma, the Bangong slab detaches and upwelling hot asthenospheric material induces a last pulse of bimodal magmatism. Less viscous basaltic melts show less crustal contamination than contemporaneous felsic melts as indicated by more positive eNd(t) values. In the south, the Neo-Tethyan slab is subducting towards the north via flat-slab subduction until it arrives at the thicker continental root of the central Lhasa terrane where it is deflected downwards. The timing of arrival is questionable. Chung et al. (2005) propose transition from flat-slab subduction to slab roll-back at ~70 Ma based on accelerated convergence rates determined by Lee and Lawyer (1995). Meng et al. (2013) suggest that the occurrence of ~85 Ma adakitic granodiorites with mafic and gabbroic enclaves marks the onset of back-arc extension due to slab-rollback. While slab roll-back at ~70 Ma would fit quite well the Xainza data that show commencement of calc-alkaline magmatism at ~65 Ma, this event has to happen at least 15 Myrs earlier in eastern Tibet. This might be one of the mentioned cases where the model is either too simple, crucial data from the Xainza area are missing, or tectono-magmatic processes are just different along strike (in that case 200 km away). Emplacement of the voluminous southern Gangdese belt and equivalent volcanic rocks of the Linzizong formation characterize the early Tertiary. Between 45-55 Ma hard collision with the Indian subcontinent inferred from sudden decrease in convergence rates and initiation of shortening in the Tethyan Himalaya marks the cessation of Gangdese magmatism. Slow down of the slab ultimately leads to slab break-off triggering a last volcanic flare-up in the Linzizong volcanic rocks. The early Tertiary magmatic event is crucial for the following period of post-collisional magmatism because it provides the ingredients that ultimately define their geochemical characteristics. As shown above, especially the post-collisional adakitic rocks in the southern part of the terrane require a garnet-bearing source to end up with the observed high La/Yb and Sr/Y ratios and overall HREE depleted patterns. Underplated basaltic crust formed from restitic melts during emplacement of the southern Gangdese batholith represents a viable mechanism to explain the geochemistry of subsequent magmatism. After slab break-off, the Indian lithosphere starts pushing further north actively thickening the thermally weakened Tibetan lithosphere causing metamorphosis of the lower basaltic portion of the crust ultimately forming garnet. After thickening has reached a critical stage, a large portion of the lithospheric mantle detaches and upwelling asthenosphere delivers the necessary heat input to melt the lower mafic crust providing parental melts for adakites during Oligocene-Miocene times. UPR on the other hand are formed from melting of the metasomatised mantle itself. The removal of the lithospheric root also causes regional uplift of the southern Tibetan plateau and allows the Indian lithosphere to move under the Lhasa terrane and travel northwards to its present location at the BNS. Underplating of Indian lithosphere marks the cessation of magmatism in the Lhasa terrane.

1.6 CONCLUSION

Synthesis of geochemical and age data and their analysis within a tempo-spatial framework allows for a simplified yet coherent model of the magmatic history of the Lhasa terrane. It has been shown that isotopic ratios especially eNd(t) are the most sensitive data available to study source areas and crustal thickness and allow estimates of crustal contamination. The Lhasa terrane consists of a central ancient crustal block bounded by more juvenile crust prior to the Indo-Asian collision ultimately controlling trends of geochemical characteristics as well as subduction geometry. From the analysis of Xainza samples and auxiliary literature data, southward subduction of the Bangong slab seems the better model to explain an extensive magmatic gap and the overall distribution of Cretaceous rocks predominately in the north and Tertiary rocks clustered in the southern regions of the terrane. REE and trace element ratios are powerful tools in distinguishing petrological characteristics of melt sources and confirm underplated mafic crust that is metamorphosed during thickening of the lithospheric root during hard collision of India with the Lhasa terrane. Uplift of the Tibetan plateau is closely linked to deep processes and occurred prior to Oligocene times. Sample density and breath of analyses is limited especially in the eastern part of the Lhasa terrane limiting the ability to draw more regional conclusions or be able to improve the understanding of lateral variations.

CHAPTER 1: REFERENCES CITED

Ahmad, T., Tanaka, T., Sachan, H. K., Asahara, Y., Islam, R., and Khanna, P. P., 2008, Geochemical and isotopic constraints on the age and origin of the Nidar Ophiolitic Complex, Ladakh, India: Implications for the Neo-Tethyan subduction along the Indus suture zone: Tectonophysics, v. 451, no. 1-4, p. 206-224.

Ayres, M., and Harris, N., 1997, REE fractionation and Nd-isotope disequilibrium during crustal anatexis: constraints from Himalayan leucogranites: Chemical Geology, v. 139, no. 1-4, p. 249-269.

Booth, A. L., Zeitler, P. K., Kidd, W. S. F., Wooden, J., Liu, Y., Idleman, B., Hren, M., and Chamberlain, C. P., 2004, U-Pb zircon constraints on the tectonic evolution of southeastern Tibet, Namche Barwa Area: American Journal of Science, v. 304, no. 10, p. 889-929.

Chan, G. H. N., Waters, D. J., Searle, M. P., Aitchison, J. C., Horstwood, M. S. A., Crowley, Q., Lo, C. H., and Chan, J. S. L., 2009, Probing the basement of southern Tibet: evidence from crustal xenoliths entrained in a Miocene ultrapotassic dyke: Journal of the Geological Society, v. 166, no. 1, p. 45-52.

Chen, Y., Zhu, D.-C., Zhao, Z.-D., Meng, F.-Y., Wang, Q., Santosh, M., Wang, L.-Q., Dong, G.-C., and Mo, X.-X., 2013, Slab breakoff triggered ca. 113 Ma magmatism around Xainza area of the Lhasa Terrane, Tibet: Gondwana Research, no. in press.

Chiu, H.-Y., Chung, S.-L., Wu, F.-Y., Liu, D., Liang, Y.-H., Lin, I. J., Iizuka, Y., Xie, L.-W., Wang, Y., and Chu, M.-F., 2009, Zircon U–Pb and Hf isotopic constraints from eastern Transhimalayan batholiths on the precollisional magmatic and tectonic evolution in southern Tibet: Tectonophysics, v. 477, no. 1–2, p. 3-19.

Chung, S.-L., Chu, M.-F., Ji, J., O'Reilly, S. Y., Pearson, N. J., Liu, D., Lee, T.-Y., and Lo, C.-H., 2009, The nature and timing of crustal thickening in Southern Tibet: Geochemical and zircon Hf isotopic constraints from postcollisional adakites: Tectonophysics, v. 477, no. 1–2, p. 36-48.

Chung, S.-L., Liu, D., Ji, J., Chu, M.-F., Lee, H.-Y., Wen, D.-J., Lo, C.-H., Lee, T.-Y., Qian, Q., and Zhang, Q., 2003, Adakites from continental collision zones: Melting of thickened lower crust beneath southern Tibet: Geology, v. 31, no. 11, p. 1021-1024.

Coulon, C., Maluski, H., Bollinger, C., and Wang, S., 1986, Mesozoic and Cenozoic Volcanic Rocks from Central and Southern Tibet - Ar39/Ar40 dating, Petrological Characteristics and geodynamical Significance: Earth and Planetary Science Letters, v. 79, no. 3-4, p. 281-302.

D'Andrea Kapp, J. L. D., Harrison, T. M., Kapp, P., Grove, M., Lovera, O. M., and Lin, D., 2005, Nyainqentanglha Shan: A window into the tectonic, thermal, and geochemical evolution of the Lhasa block, southern Tibet: Journal of Geophysical Research: Solid Earth, v. 110, no. B8, p. B08413.

Dai, J., Yin, A., Liu, W., and Wang, C., 2008, Nd isotopic compositions of the Tethyan Himalayan Sequence in southeastern Tibet: Science in China Series D: Earth Sciences, v. 51, no. 9, p. 1306-1316.

Ding, L. I. N., Kapp, P., Zhong, D., and Deng, W., 2003, Cenozoic Volcanism in Tibet: Evidence for a Transition from Oceanic to Continental Subduction: J. Petrology, v. 44, no. 10, p. 1833-1865.

Gao, Y., Hou, Z., Kamber, B. S., Wei, R., Meng, X., and Zhao, R., 2007, Lamproitic Rocks from a Continental Collision Zone: Evidence for Recycling of Subducted Tethyan Oceanic Sediments in the Mantle Beneath Southern Tibet: J. Petrology, v. 48, no. 4, p. 729-752.

Gao, Y., Wei, R., Hou, Z., Tian, S., and Zhao, R., 2008, Eocene high-MgO volcanism in southern Tibet: New constraints for mantle source characteristics and deep processes: Lithos, v. 105, no. 1-2, p. 63-72.

Guan, Q., Zhu, D.-C., Zhao, Z.-D., Dong, G.-C., Zhang, L.-L., Li, X.-W., Liu, M., Mo, X.-X., Liu, Y.-S., and Yuan, H.-L., 2012, Crustal thickening prior to 38 Ma in southern Tibet: Evidence from lower crust-derived adakitic magmatism in the Gangdese Batholith: Gondwana Research, v. 21, no. 1, p. 88-99.

Guillot, S., Le Fort, P., Pêcher, A., Barman, M. R., and Aprahamian, J., 1995, Contact metamorphism and depth of emplacement of the Manaslu granite(Central Nepal). implications for Himalayan orogenesis: Tectonophysics, v. 241, p. 99-119.

Guo, Z., Wilson, M., and Liu, J., 2007, Post-collisional adakites in south Tibet: Products of partial melting of subduction-modified lower crust: Lithos, v. 96, no. 1-2, p. 205-224.

Guynn, J. H., Kapp, P., Pullen, A., Heizler, M., Gehrels, G., and Ding, L., 2006, Tibetan basement rocks near Amdo reveal "missing" Mesozoic tectonism along the Bangong suture, central Tibet: Geology, v. 34, no. 6, p. 505-508.

Harris, N. B. W., Ronghua, X., Lewis, C. L., and Chengwei, J., 1988a, Plutonic Rocks of the 1985 Tibet Geotraverse, Lhasa to Golmud: Philosophical Transactions of the Royal Society of London. Series A, Mathematical and Physical Sciences, v. 327, no. 1594, p. 145-168.

Harris, N. B. W., Ronghua, X., Lewis, C. L., Hawkesworth, C. J., and Yuquan, Z., 1988b, Isotope Geochemistry of the 1985 Tibet Geotraverse, Lhasa to Golmud: Philosophical Transactions of the Royal Society of London. Series A, Mathematical and Physical Sciences, v. 327, no. 1594, p. 263-285.

Harrison, T. M., Yin, A., Grove, M., and Lovera, O. M., 2000, The Zedong Window: A record of superposed Tertiary convergence in southeastern Tibet: Journal of Geophysical Research, v. 105, no. B8, p. 19211-19230.

He, S., Kapp, P., DeCelles, P. G., Gehrels, G. E., and Heizler, M., 2007, Cretaceous-Tertiary geology of the Gangdese Arc in the Linzhou area, southern Tibet: Tectonophysics, v. 433, no. 1-4, p. 15-37.

Hetzel, R., Dunkl, I., Haider, V., Strobl, M., von Eynatten, H., Ding, L., and Frei, D., 2011, Peneplain formation in southern Tibet predates the India-Asia collision and plateau uplift: Geology, v. 39, no. 10, p. 983-986.

Hou, Z.-Q., Zheng, Y.-C., Zeng, L.-S., Gao, L.-E., Huang, K.-X., Li, W., Li, Q.-Y., Fu, Q., Liang, W., and Sun, Q.-Z., 2012, Eocene–Oligocene granitoids in southern Tibet: Constraints on crustal anatexis and tectonic evolution of the Himalayan orogen: Earth and Planetary Science Letters, v. 349–350, no. 0, p. 38-52.

Hou, Z. Q., Gao, Y. F., Qu, X. M., Rui, Z. Y., and Mo, X. X., 2004, Origin of adakitic intrusives generated during mid-Miocene east-west extension in southern Tibet: Earth and Planetary Science Letters, v. 220, no. 1-2, p. 139-155.

Ji, W.-Q., Wu, F.-Y., Chung, S.-L., Li, J.-X., and Liu, C.-Z., 2009, Zircon U–Pb geochronology and Hf isotopic constraints on petrogenesis of the Gangdese batholith, southern Tibet: Chemical Geology, v. 262, no. 3–4, p. 229-245.

Ji, W.-Q., Wu, F.-Y., Chung, S.-L., and Liu, C.-Z., 2012, Identification of Early Carboniferous Granitoids from Southern Tibet and Implications for Terrane Assembly related to Paleo-Tethyan Evolution: Journal of Geology, v. 120, no. 5, p. 531-541.

Jiang, Z.-Q., Wang, Q., Li, Z.-X., Wyman, D. A., Tang, G.-J., Jia, X.-H., and Yang, Y.-H., 2012, Late Cretaceous (ca. 90 Ma) adakitic intrusive rocks in the Kelu area, Gangdese Belt (southern Tibet): Slab melting and implications for Cu–Au mineralization: Journal of Asian Earth Sciences, v. 53, no. 0, p. 67-81.

Kali, E., Leloup, P. H., Arnaud, N., Mahéo, G., Liu, D., Boutonnet, E., Van der Woerd, J., Liu, X., Liu-Zeng, J., and Li, H., 2010, Exhumation history of the deepest central Himalayan rocks, Ama Drime range: Key pressure-temperature-deformation-time constraints on orogenic models: Tectonics, v. 29, no. 2, p. TC2014.

Kapp, P., DeCelles, P. G., Gehrels, G. E., Heizler, M., and Ding, L., 2007, Geological records of the Lhasa-Qiangtang and Indo-Asian collisions in the Nima area of central Tibet: Geological Society of America Bulletin, v. 119, no. 7-8, p. 917-933.

Kapp, P., Murphy, M. A., Yin, A., Harrison, T. M., Ding, L., and Guo, J., 2003, Mesozoic and Cenozoic tectonic evolution of the Shiquanhe area of western Tibet: Tectonics, v. 22, no. 4.

Kapp, P., Taylor, M., Stockli, D., and Ding, L., 2008, Development of active low-angle normal fault systems during orogenic collapse: Insight from Tibet: Geology, v. 36, no. 1, p. 7-10.

Kapp, P., Yin, A., Harrison, T. M., and Ding, L., 2005, Cretaceous-Tertiary shortening, basin development, and volcanism in central Tibet: Geological Society of America Bulletin, v. 117, no. 7-8, p. 865-878.

Khan, S. D., Walker, D. J., Hall, S. A., Burke, K. C., Shah, M. T., and Stockli, L., 2009, Did the Kohistan-Ladakh island arc collide first with India?: Geological Society of America Bulletin, v. 121, no. 3-4, p. 366-384.

Lee, H.-Y., Chung, S.-L., Lo, C.-H., Ji, J., Lee, T.-Y., Qian, Q., and Zhang, Q., 2009, Eocene Neotethyan slab breakoff in southern Tibet inferred from the Linzizong volcanic record: Tectonophysics, v. 477, p. 20-35.

Leloup, P. H., Mahéo, G., Arnaud, N., Kali, E., Boutonnet, E., Liu, D., Xiaohan, L., and Haibing, L., 2010, The South Tibet detachment shear zone in the Dinggye area: Time constraints on extrusion models of the Himalayas: Earth and Planetary Science Letters, v. 292, no. 1-2, p. 1-16.

Lin, I. J., Chung, S.-L., Chu, C.-H., Lee, H.-Y., Gallet, S., Wu, G., Ji, J., and Zhang, Y., 2012, Geochemical and Sr–Nd isotopic characteristics of Cretaceous to Paleocene granitoids and volcanic rocks, SE Tibet: Petrogenesis and tectonic implications: Journal of Asian Earth Sciences, v. 53, no. 0, p. 131-150.

Mahoney, J. J., Frei, R., Tejada, M. L. G., Mo, X. X., Leat, P. T., and Nägler, T. F., 1998, Tracing the Indian Ocean Mantle Domain Through Time: Isotopic Results from Old West Indian, East Tethyan, and South Pacific Seafloor: Journal of Petrology, v. 39, no. 7, p. 1285-1306.

Meng, F.-Y., Zhao, Z., Zhu, D.-C., Mo, X., Guan, Q., Huang, Y., Dong, G., Zhou, S., DePaolo, D. J., Harrison, T. M., Zhang, Z., Liu, J., Liu, Y., Hu, Z., and Yuan, H., 2013, Late Cretaceous magmatism in Mamba area, central Lhasa subterrane: Products of back-arc extension of Neo-Tethyan Ocean?: Gondwana Research, v. In Press, Corrected Proof.

Miller, C., Schuster, R., Klötzli, U., Frank, W., and Grasemann, B., 2000, Late Cretaceous-Tertiary magmatic and tectonic events in the Transhimalaya batholith (Kailas area, SW Tibet): Schweizer mineralogische und petrographische Mitteilungen, v. 80, p. 1-20.

Miller, C., Schuster, R., Klötzli, U., Frank, W., and Purtscheller, F., 1999, Post-collisional potassic and ultrapotassic magmatism in SW Tibet: geochemical and Sr-Nd-Pb-O isotopic constraints for mantle source characteristics and petrogenesis: Journal of Petrology, v. 40, no. 9, p. 1399-1424.

Miller, C., Thoeni, M., Frank, W., Grasemann, B., Kloetzli, U., Guntli, P., and Draganits, E., 2001, The early Palaeozoic magmatic event in the Northwest Himalaya, India: source, tectonic setting and age of emplacement: Geological Magazine, v. 138, no. 03, p. 237-251.

Mo, X., Niu, Y., Dong, G., Zhao, Z., Hou, Z., Zhou, S., and Ke, S., 2008, Contribution of syncollisional felsic magmatism to continental crust growth: A case study of the Paleogene Linzizong volcanic Succession in southern Tibet: Chemical Geology, v. 250, no. 1-4, p. 49-67.

Murphy, M. A., 2007, Isotopic characteristics of the Gurla Mandhata metamorphic core complex: Implications for the architecture of the Himalayan orogen: Geology, v. 35, no. 11, p. 983-986.

Nomade, S., Renne, P. R., Mo, X., Zhao, Z., and Zhou, S., 2004, Miocene volcanism in the Lhasa block, Tibet: spatial trends and geodynamic implications: Earth and Planetary Science Letters, v. 221, no. 1–4, p. 227-243.

Parrish, R. R., and Hodges, K. V., 1996, Isotopic constraints on the age and provenance of the Lesser and Greater Himalayan sequences, Nepalese Himalaya: Geological Society of America Bulletin, v. 108, p. 904-911.

Richards, A., Parrish, R., Harris, N., Argles, T., and Zhang, L., 2006, Correlation of lithotectonic units across the eastern Himalaya, Bhutan: Geology, v. 34, no. 5, p. 341-344.

Sanchez, V. I., Murphy, M. A., Robinson, A. C., Lapen, T. J., and Heizler, M. T., 2013, Tectonic evolution of the India–Asia suture zone since Middle Eocene time, Lopukangri area, south-central Tibet: Journal of Asian Earth Sciences, v. 62, no. 0, p. 205-220.

Schärer, U., Xu, R.-H., and Allègre, C. J., 1984, U-Pb geochronology of Gangdese (Transhimalaya) plutonism in the Lhasa-Xigaze region, Tibet: Earth and Planetary Science Letters, v. 69, no. 2, p. 311-320.

Styron, R. H., Taylor, M. H., Sundell, K. E., Stockli, D. F., Oalmann, J. A. G., Möller, A., McCallister, A. T., Liu, D., and Ding, L., 2013, Miocene initiation and acceleration of extension in the South Lunggar rift, western Tibet: Evolution of an active detachment system from structural mapping and (U-Th)/He thermochronology: Tectonics, p. n/a-n/a.

Sui, Q.-L., Wang, Q., Zhu, D.-C., Zhao, Z.-D., Chen, Y., Santosh, M., Hu, Z.-C., Yuan, H.-L., and Mo, X.-X., 2013, Compositional diversity of ca. 110 Ma magmatism in the northern Lhasa Terrane, Tibet: Implications for the magmatic origin and crustal growth in a continent–continent collision zone: Lithos, v. 168–169, no. 0, p. 144-159.

Sundell, K. E., Taylor, M. H., Styron, R. H., Stockli, D. F., Kapp, P., Hager, C., Liu, D., and Ding, L., 2013, Evidence for constriction and Pliocene acceleration of east-west extension in the North Lunggar rift region of west central Tibet: Tectonics, v. 32, no. 5, p. 2013TC003331.

Upadhyay, R., Frisch, W., and Siebel, W., 2008, Tectonic implications of new U–Pb zircon ages of the Ladakh batholith, Indus suture zone, northwest Himalaya, India: Terra Nova, v. 20, no. 4, p. 309-317.

Valli, F., Leloup, P. H., Paquette, J.-L., Arnaud, N., Li, H., Tapponnier, P., Lacassin, R., Guillot, S., Liu, D., Deloule, E., Xu, Z., and Mahéo, G., 2008, New U-Th/Pb constraints on timing of shearing and long-term slip-rate on the Karakorum fault: Tectonics, v. 27, no. 5, p. TC5007.

Volkmer, J. E., Kapp, P., Guynn, J. H., and Lai, Q., 2007, Cretaceous-Tertiary structural evolution of the north central Lhasa terrane, Tibet: Tectonics, v. 26, no. 6, p. TC6007.

Wang, S., Fang, X., Lai, Q., Zheng, D., and Wang, Y., 2009, New radiometric dating constrains the time for initiation of the Karakorum fault zone (KFZ), SW Tibet: Tectonophysics, v. 475, no. 3-4, p. 503-513.

Wen, D.-R., Chung, S.-L., Song, B., Iizuka, Y., Yang, H.-J., Ji, J., Liu, D., and Gallet, S., 2008a, Late Cretaceous Gangdese intrusions of adakitic geochemical characteristics, SE Tibet: Petrogenesis and tectonic implications: Lithos, v. 105, no. 1-2, p. 1-11.

Wen, D.-R., Liu, D., Chung, S.-L., Chu, M.-F., Ji, J., Zhang, Q., Song, B., Lee, T.-Y., Yeh, M.-W., and Lo, C.-H., 2008b, Zircon SHRIMP U-Pb ages of the Gangdese Batholith and implications for Neotethyan subduction in southern Tibet: Chemical Geology, v. 252, no. 3-4, p. 191-201.

Williams, H., Turner, S., Kelley, S., and Harris, N., 2001, Age and composition of dikes in Southern Tibet: New constraints on the timing of east-west extension and its relationship to postcollisional volcanism: Geology, v. 29, no. 4, p. 339-a-342.

Xu, J.-F., and Castillo, P. R., 2004, Geochemical and Nd-Pb isotopic characteristics of the Tethyan asthenosphere: implications for the origin of the Indian Ocean mantle domain: Tectonophysics, v. 393, no. 1-4, p. 9-27.

Xu, W.-C., Zhang, H.-F., Guo, L., and Yuan, H.-L., 2010, Miocene high Sr/Y magmatism, south Tibet: Product of partial melting of subducted Indian continental crust and its tectonic implication: Lithos, v. 114, no. 3–4, p. 293-306.

Xu, Y.-G., Lan, J.-B., Yang, Q.-J., Huang, X.-L., and Qiu, H.-N., 2008, Eocene break-off of the Neo-Tethyan slab as inferred from intraplate-type mafic dykes in the Gaoligong orogenic belt, eastern Tibet: Chemical Geology, v. 255, no. 3-4, p. 439-453.

Zeng, L., Gao, L.-E., Xie, K., and Liu-Zeng, J., 2011, Mid-Eocene high Sr/Y granites in the Northern Himalayan Gneiss Domes: Melting thickened lower continental crust: Earth and Planetary Science Letters, v. 303, no. 3–4, p. 251-266.

Zeng, L., Liu, J., Gao, L., Xie, K., and Wen, L., 2009, Early Oligocene anatexis in the Yardoi gneiss dome, southern Tibet and geological implications: Chinese Science Bulletin, v. 54, no. 1, p. 104-112.

Zhang, H., Harris, N., Guo, L., and Xu, W., 2010, The significance of Cenozoic magmatism from the western margin of the eastern syntaxis, southeast Tibet: Contributions to Mineralogy and Petrology, v. 160, no. 1, p. 83-98.

Zhang, H., Harris, N., Parrish, R., Kelley, S., Zhang, L., Rogers, N., Argles, T., and King, J., 2004, Causes and consequences of protracted melting of the mid-crust exposed in the North Himalayan antiform: Earth and Planetary Science Letters, v. 228, no. 1-2, p. 195-212.

Zhao, Z., Mo, X., Dilek, Y., Niu, Y., DePaolo, D. J., Robinson, P., Zhu, D., Sun, C., Dong, G., and Zhou, S., 2009, Geochemical and Sr–Nd–Pb–O isotopic compositions of the post-collisional ultrapotassic magmatism in SW Tibet: petrogenesis and implications for India intra-continental subduction beneath southern Tibet: Lithos, v. 113, no. 1, p. 190-212.

Zhao, Z., Mo, X., Zhang, S., Guo, T., Zhou, S., Dong, G., and Wang, Y., 2001, Post-collisional magmatism in Wuyu basin, central Tibet: evidence for recycling of subducted Tethyan oceanic crust: Science in China Series D: Earth Sciences, v. 44, no. 0, p. 27-34.

Zheng, Y., Zhang, G., Xu, R., Gao, S., Pang, Y., Cao, L., Du, A., and Shi, Y., 2007, Geochronologic constraints on magmatic intrusions and mineralization of the Zhunuo porphyry copper deposit in Gangdese, Tibet: Chinese Science Bulletin, v. 52, no. 22, p. 3139-3147.

Zhou, S., Mo, X., Zhao, Z., Qiu, R., Niu, Y., Guo, T., and Zhang, S., 2010, 40Ar/39Ar geochronology of post-collisional volcanism in the middle Gangdese Belt, southern Tibet: Journal of Asian Earth Sciences, v. 37, no. 3, p. 246-258.

Zhu, D.-C., Mo, X.-X., Niu, Y., Zhao, Z.-D., Wang, L.-Q., Liu, Y.-S., and Wu, F.-Y., 2009a, Geochemical investigation of Early Cretaceous igneous rocks along an east–west traverse throughout the central Lhasa Terrane, Tibet: Chemical Geology, v. 268, no. 3–4, p. 298-312.

Zhu, D.-C., Mo, X.-X., Niu, Y., Zhao, Z.-D., Wang, L.-Q., Pan, G.-T., and Wu, F.-Y., 2009b, Zircon U-Pb dating and in-situ Hf isotopic analysis of Permian peraluminous granite in the Lhasa terrane, southern Tibet: Implications for Permian collisional orogeny and paleogeography: Tectonophysics, v. 469, no. 1-4, p. 48-60.

Zhu, D.-C., Mo, X.-X., Zhao, Z.-D., Niu, Y., Wang, L.-Q., Chu, Q.-H., Pan, G.-T., Xu, J.-F., and Zhou, C.-Y., 2010, Presence of Permian extension-and arc-type magmatism in southern Tibet: Paleogeographic implications: Geological Society of America Bulletin, v. 122, no. 7-8, p. 979-993.

Zhu, D.-C., Zhao, Z.-D., Niu, Y., Mo, X.-X., Chung, S.-L., Hou, Z.-Q., Wang, L.-Q., and Wu, F.-Y., 2011, The Lhasa Terrane: Record of a microcontinent and its histories of drift and growth: Earth and Planetary Science Letters, v. 301, no. 1-2, p. 241-255.

CHAPTER 1: FIGURES AND TABLES

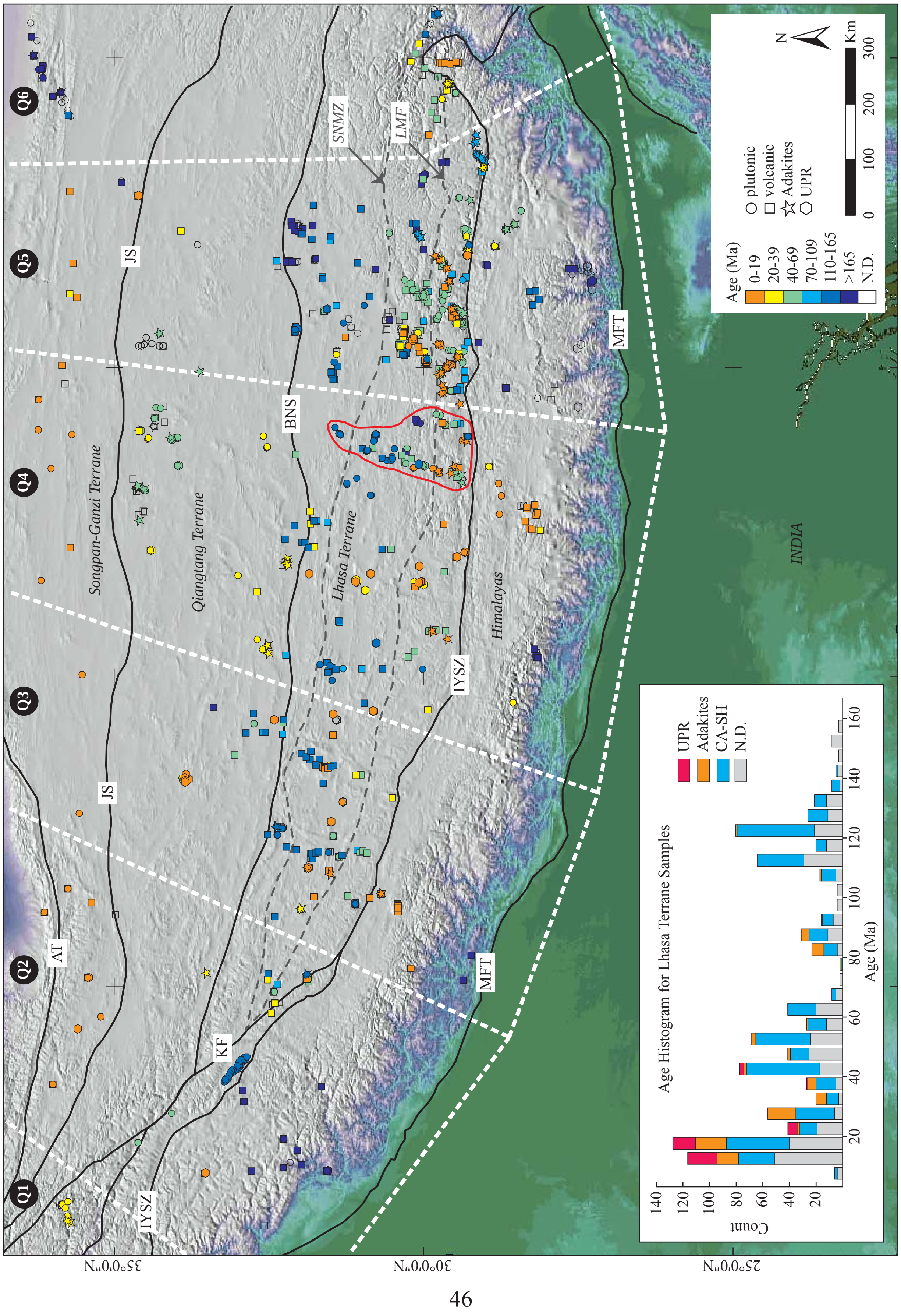
Q1
Q2
Q3
Q4
Q5
Q6
Songpan-Ganzi Terrane
Qiangtang Terrane
Lhasa Terrane
Himalayas
INDIA
JS
AT
BNS
SNMZ
LMF
IYSZ
KF
MFT
35°0'0"N
30°0'0"N
25°0'0"N
80°0'0"E
85°0'0"E
90°0'0"E
95°0'0"E
Age (Ma)
0-19
20-39
40-69
70-109
110-165
>165
N.D.
plutonic
volcanic
Adakites
UPR
N
Km
0
100
200
300
Age Histogram for Lhasa Terrane Samples
UPR
Adakites
CA-SH
N.D.
Count
Age (Ma)

Figure 1.1: Overview of the Tibetan plateau and Himalayas showing the main terranes and terrane bounding structures. Sample locations are plotted according to rock type and age. Study area is highlighted in red and quadrants (Q1-Q6) used to subdivide the dataset are outlined by dashed white lines. Inset shows age histogram for samples from the Lhasa terrane which was ultimately used to subdivide age populations according to the legend on the right. MFT – Main Frontal Thrust, IYSZ – Indus Yarlung Suture Zone, LMF - Luobadui-Milashan Fault, SNMZ - Shiquan River-Nam Tso Melange Zone, BNS – Bangong-Nujiang Suture, JS – Jinsha Suture, AT – Altyn Tagh fault, KF – Karakorum Fault.

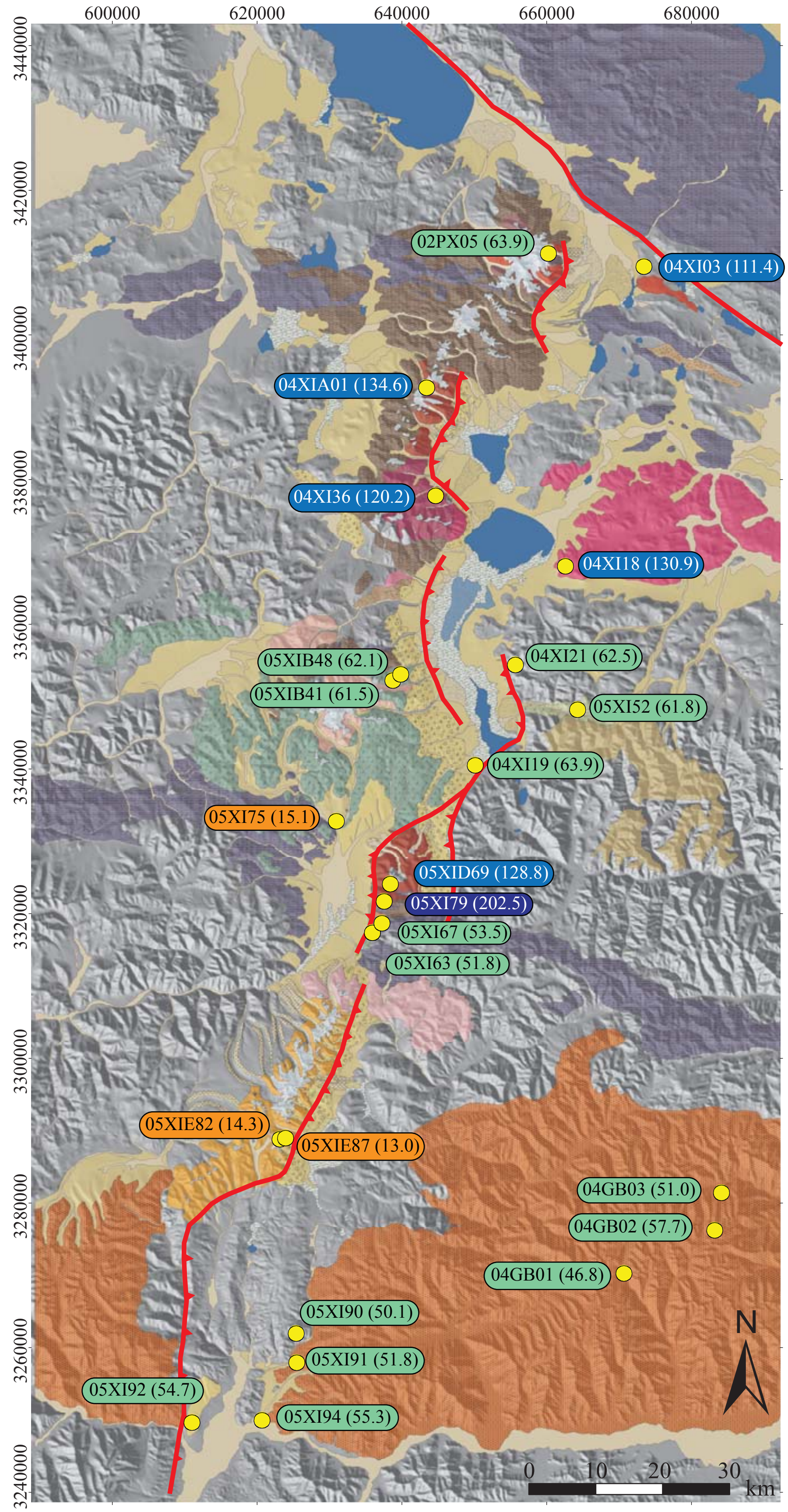
600000
620000
640000
660000
680000
3440000
3420000
3400000
3380000
3360000
3340000
3320000
3300000
3280000
3260000
3240000
02PX05 (63.9)
04XI03 (111.4)
04XIA01 (134.6)
04XI36 (120.2)
04XI18 (130.9)
05XIB48 (62.1)
05XIB41 (61.5)
04XI21 (62.5)
05XI52 (61.8)
04XI19 (63.9)
05XI75 (15.1)
05XID69 (128.8)
05XI79 (202.5)
05XI67 (53.5)
05XI63 (51.8)
05XIE82 (14.3)
05XIE87 (13.0)
04GB03 (51.0)
04GB02 (57.7)
04GB01 (46.8)
05XI90 (50.1)
05XI91 (51.8)
05XI92 (54.7)
05XI94 (55.3)
N
0
10
20
30
km

Figure 1.2: Geologic map of the Xainza rift showing zircon U/Pb sample ages analyzed during this study. Basemap is a shaded relief map created from 90m Shuttle Radar Topography Mission (SRTM) dataset.

QUATERNARY	Qice	
	Qlake	
	Qlake2	Dry Lakebed
	Qwet	Marsh/Wetlands
	Qal1	Active Alluvium (Drainages, Fans)
	Qaf1	
	Qal2	Older Alluvium (Drainages, Fans)
	Qaf2	
	Qal3	
	Qco	Colluvium
	Qlm	Lateral Moraine
	Qtm	Terminal Moraine
	Tal?	Quaternary/Tertiary ??? fluvial sediments, tilted!!!
	Tss	
TERTIARY	Tmg	Miocene granitic intrusion
	Tb	Basalt
	Tt1	Intermediate to acidic volcanics of the Linzizong Fm. (tuffs)
	Tt2	
	Tt3	
	Tv1	Intermediate to acidic volcanics of the Linzizong Fm. (andesites, dacites, rhyolites)
	Tv2	
	Tv3	
	Tv4	
	Tv6	
	Tv7	
	Thp	Qtz-porphyr
	Tgb	Granitic Intrusions
	Teg	
	Tpg	
Mz	Kv1	Undiff. volcanic
	Keg	Granite
	TRlg	Granite
	Mcgl	Conglomerate
Pz	Pcarb	Limestone (Crinoids)
	Pshale	Slate/Phyllite

Lower Hemisphere Plots

- metamorphic bedding (green line)
- volcanic flow layering (red line)
- sedimentary bedding (blue line)
- Slickensides / Joints (black line)
- ● Crenulation lineations / Fold axis
- ← Slickenlines

Figure 1.3: Geologic map - Legend.

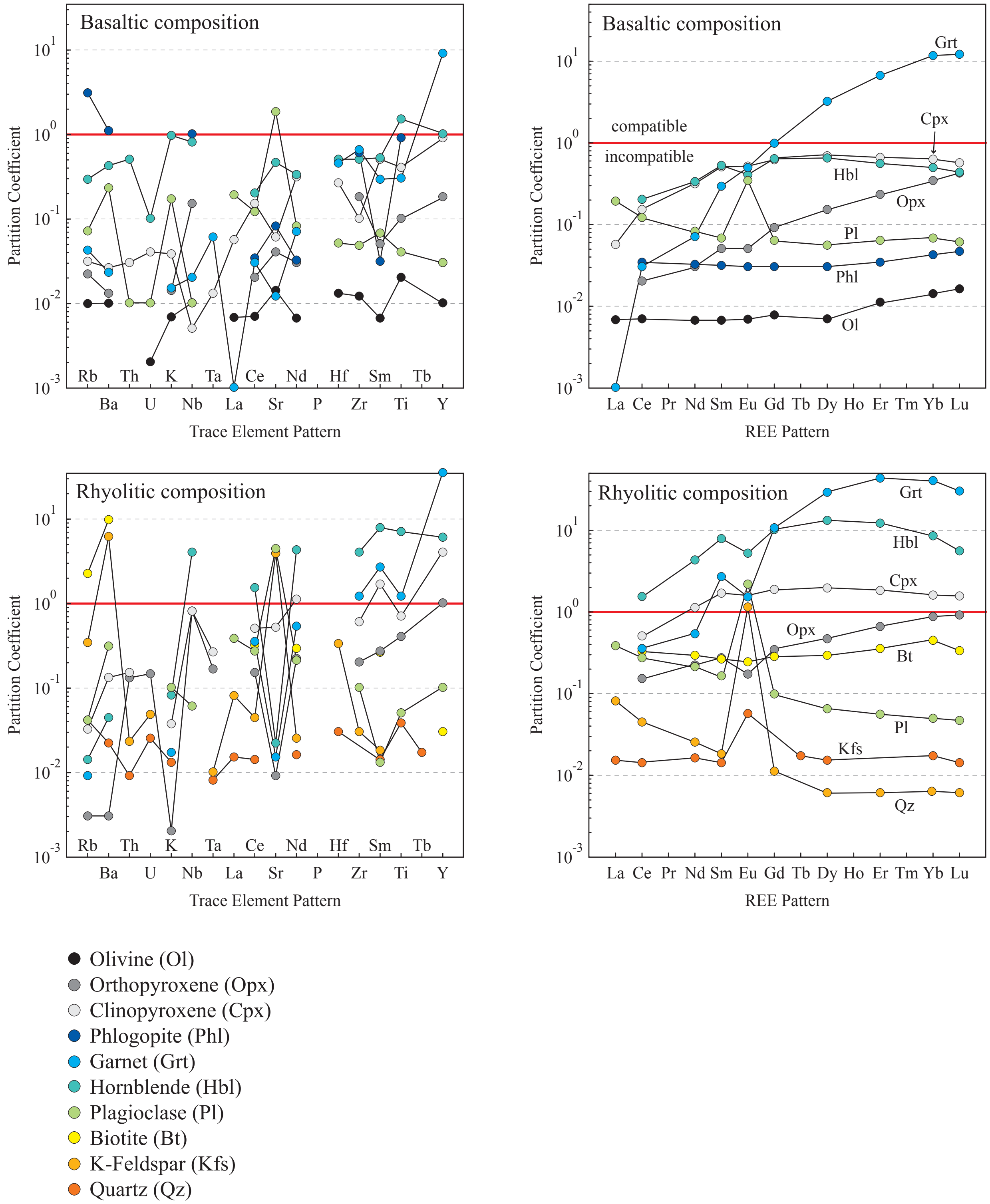

Basaltic composition
Rhyolitic composition
Partition Coefficient
Trace Element Pattern
REE Pattern
Rb Th K Ta Ce Nd Hf Sm Tb
Ba U Nb La Sr P Zr Ti Y
La Ce Pr Nd Sm Eu Gd Tb Dy Ho Er Tm Yb Lu
compatible
incompatible
Grt
Cpx
Hbl
Opx
Pl
Phl
Ol
Bt
Kfs
Qz
Olivine (Ol)
Orthopyroxene (Opx)
Clinopyroxene (Cpx)
Phlogopite (Phl)
Garnet (Grt)
Hornblende (Hbl)
Plagioclase (Pl)
Biotite (Bt)
K-Feldspar (Kfs)
Quartz (Qz)

Figure 1.4: Partition coefficients for trace element and REE in rock forming minerals based on melt composition (data from Rollinson, 1993 and references therein).

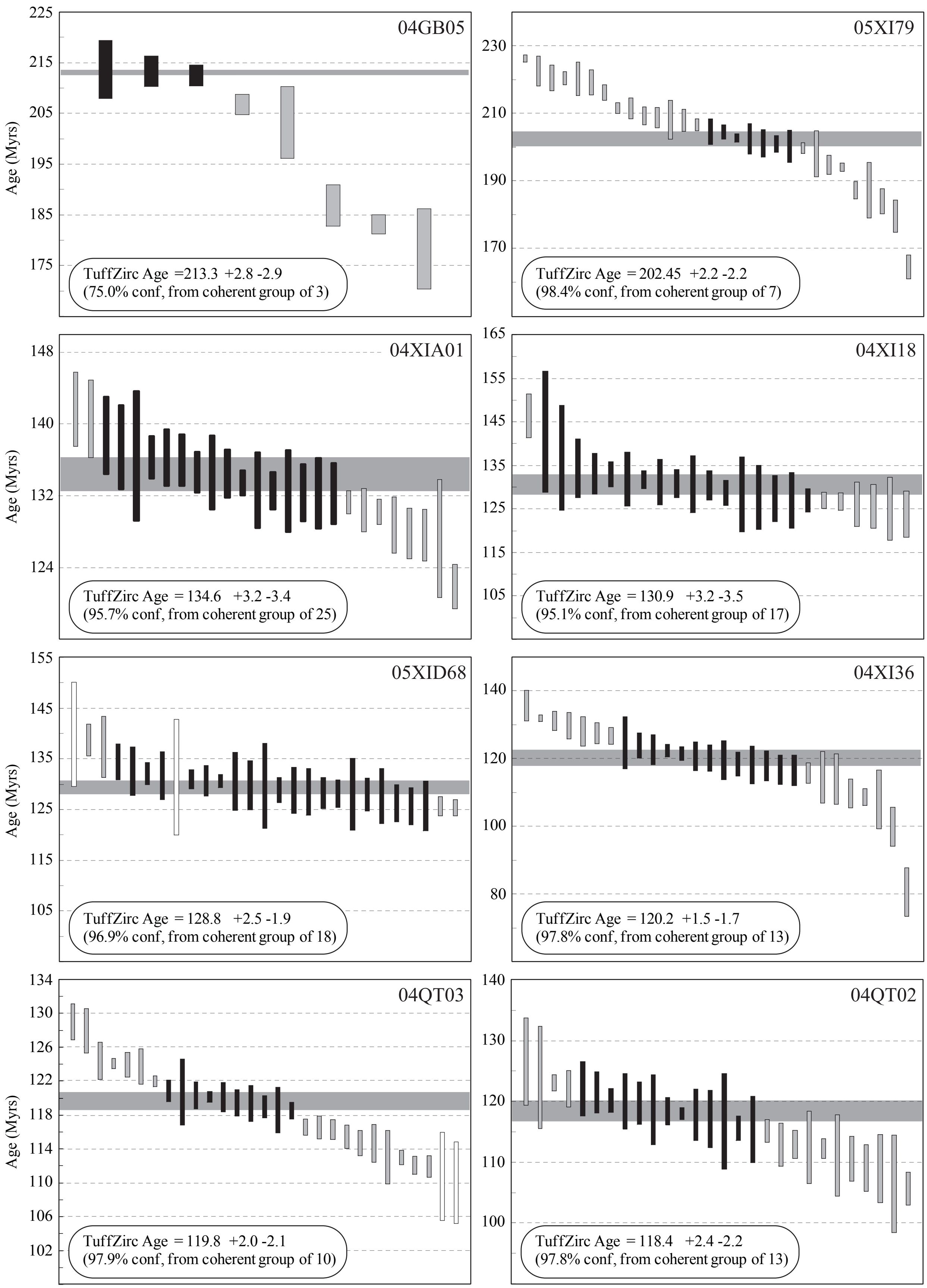
04GB05
Age (Myrs)
225 215 205 195 185 175
TuffZirc Age =213.3 +2.8 -2.9
(75.0% conf, from coherent group of 3)
05XI79
230 210 190 170
TuffZirc Age = 202.45 +2.2 -2.2
(98.4% conf, from coherent group of 7)
04XIA01
Age (Myrs)
148 140 132 124
TuffZirc Age = 134.6 +3.2 -3.4
(95.7% conf, from coherent group of 25)
04XI18
165 155 145 135 125 115 105
TuffZirc Age = 130.9 +3.2 -3.5
(95.1% conf, from coherent group of 17)
05XID68
Age (Myrs)
155 145 135 125 115 105
TuffZirc Age = 128.8 +2.5 -1.9
(96.9% conf, from coherent group of 18)
04XI36
140 120 100 80
TuffZirc Age = 120.2 +1.5 -1.7
(97.8% conf, from coherent group of 13)
04QT03
Age (Myrs)
134 130 126 122 118 114 110 106 102
TuffZirc Age = 119.8 +2.0 -2.1
(97.9% conf, from coherent group of 10)
04QT02
140 130 120 110 100
TuffZirc Age = 118.4 +2.4 -2.2
(97.8% conf, from coherent group of 13)

Figure 1.5: Results from zircon LA-MC-ICP-MS spot analysis plotted as vertical bars with size equivalent to uncertainty around the calculated spot age. Mean age calculated from group of coherent analysis (black bars). Grey bars indicate results not included in mean calculation and white bars are results with uncertainties exceeding the maximum allowed value (5%).

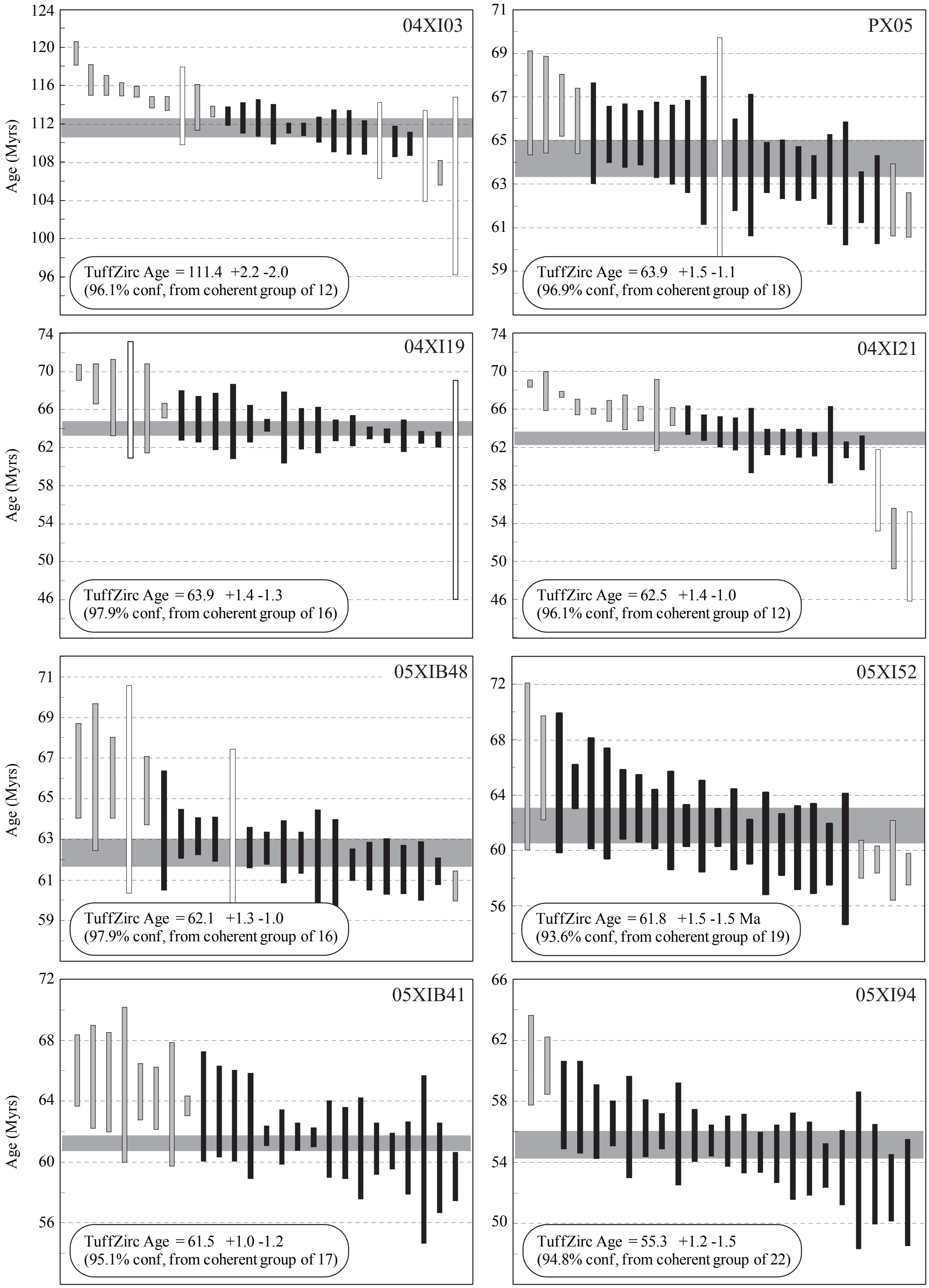
04XI03
Age (Myrs)
TuffZirc Age = 111.4 +2.2 -2.0
(96.1% conf, from coherent group of 12)
PX05
TuffZirc Age = 63.9 +1.5 -1.1
(96.9% conf, from coherent group of 18)
04XI19
Age (Myrs)
TuffZirc Age = 63.9 +1.4 -1.3
(97.9% conf, from coherent group of 16)
04XI21
TuffZirc Age = 62.5 +1.4 -1.0
(96.1% conf, from coherent group of 12)
05XIB48
Age (Myrs)
TuffZirc Age = 62.1 +1.3 -1.0
(97.9% conf, from coherent group of 16)
05XI52
TuffZirc Age = 61.8 +1.5 -1.5 Ma
(93.6% conf, from coherent group of 19)
05XIB41
Age (Myrs)
TuffZirc Age = 61.5 +1.0 -1.2
(95.1% conf, from coherent group of 17)
05XI94
TuffZirc Age = 55.3 +1.2 -1.5
(94.8% conf, from coherent group of 22)

Figure 1.6: Results from zircon LA-MC-ICP-MS spot analysis; continued

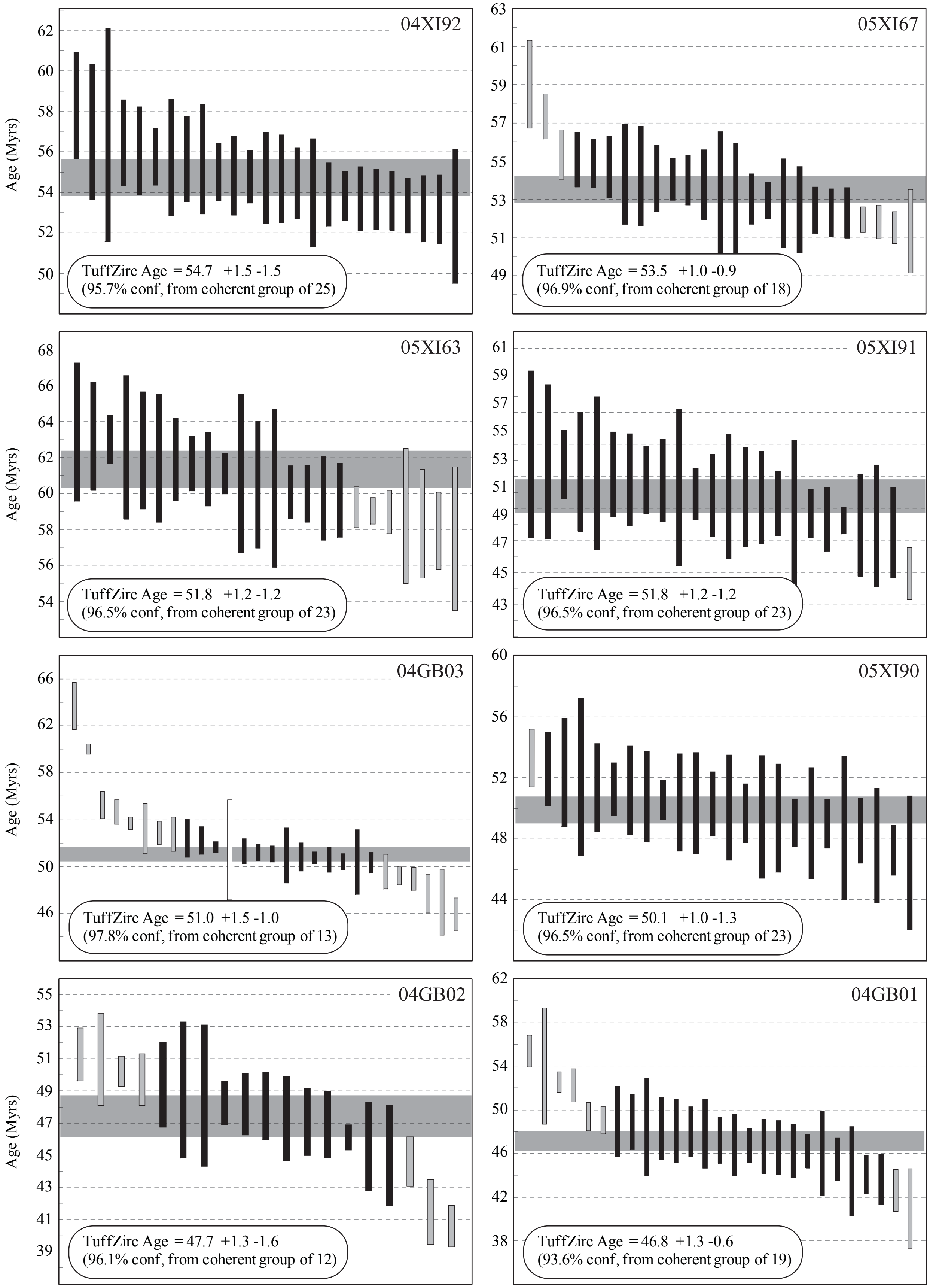
04XI92
Age (Myrs)
TuffZirc Age = 54.7 +1.5 -1.5
(95.7% conf, from coherent group of 25)
05XI67
TuffZirc Age = 53.5 +1.0 -0.9
(96.9% conf, from coherent group of 18)
05XI63
Age (Myrs)
TuffZirc Age = 51.8 +1.2 -1.2
(96.5% conf, from coherent group of 23)
05XI91
TuffZirc Age = 51.8 +1.2 -1.2
(96.5% conf, from coherent group of 23)
04GB03
Age (Myrs)
TuffZirc Age = 51.0 +1.5 -1.0
(97.8% conf, from coherent group of 13)
05XI90
TuffZirc Age = 50.1 +1.0 -1.3
(96.5% conf, from coherent group of 23)
04GB02
Age (Myrs)
TuffZirc Age = 47.7 +1.3 -1.6
(96.1% conf, from coherent group of 12)
04GB01
TuffZirc Age = 46.8 +1.3 -0.6
(93.6% conf, from coherent group of 19)

Figure 1.7: Results from zircon LA-MC-ICP-MS spot analysis; continued

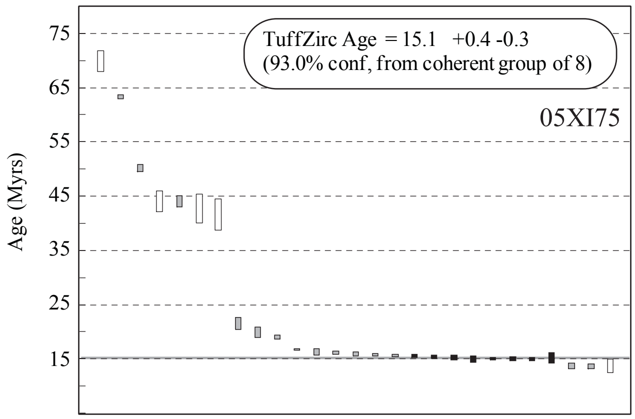
TuffZirc Age = 15.1 +0.4 -0.3
(93.0% conf, from coherent group of 8)
05XI75
Age (Myrs)
75
65
55
45
35
25
15

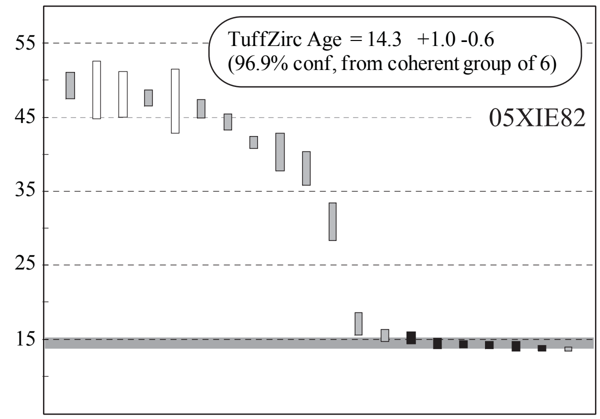
TuffZirc Age = 14.3 +1.0 -0.6
(96.9% conf, from coherent group of 6)
05XIE82
55
45
35
25
15

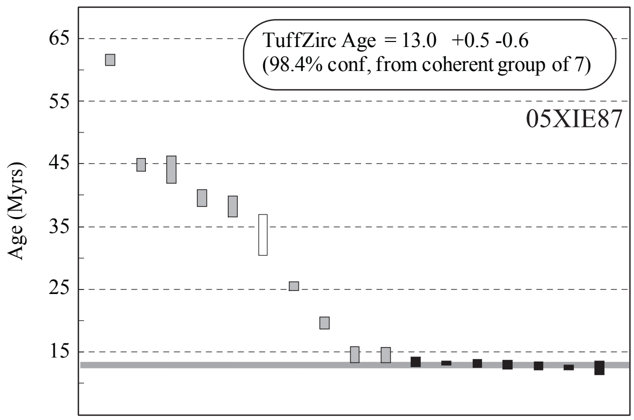
TuffZirc Age = 13.0 +0.5 -0.6
(98.4% conf, from coherent group of 7)
05XIE87
Age (Myrs)
65
55
45
35
25
15

Figure 1.8: Results from zircon LA-MC-ICP-MS spot analysis; continued

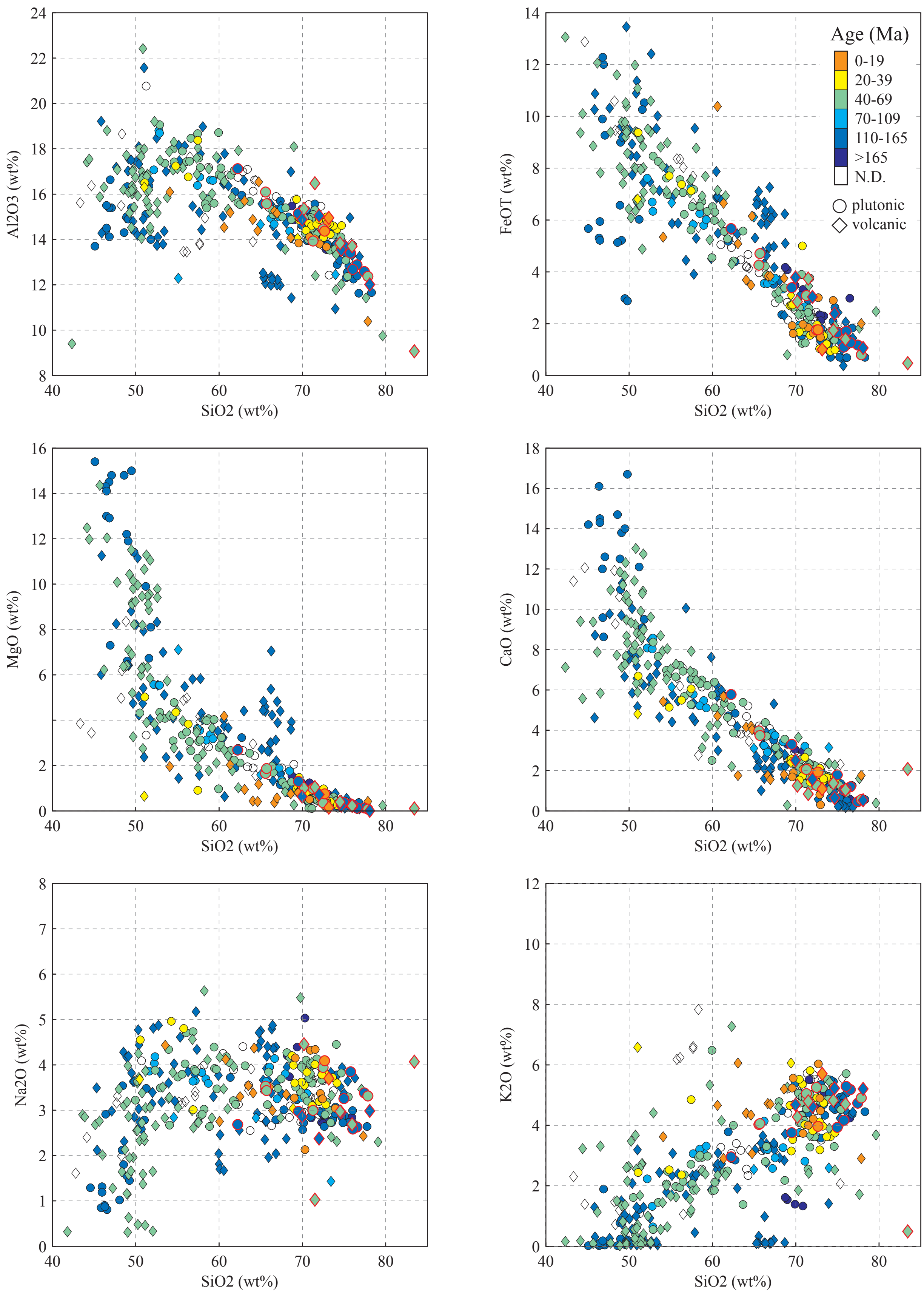

Al2O3 (wt%)
FeOT (wt%)
MgO (wt%)
CaO (wt%)
Na2O (wt%)
K2O (wt%)
SiO2 (wt%)
Age (Ma)
0-19
20-39
40-69
70-109
110-165
>165
N.D.
plutonic
volcanic

Figure 1.9: Harker diagrams plotting major element oxides against SiO_2 content for calc-alkaline rocks. Samples analyzed during this study are highlighted with red outlines.

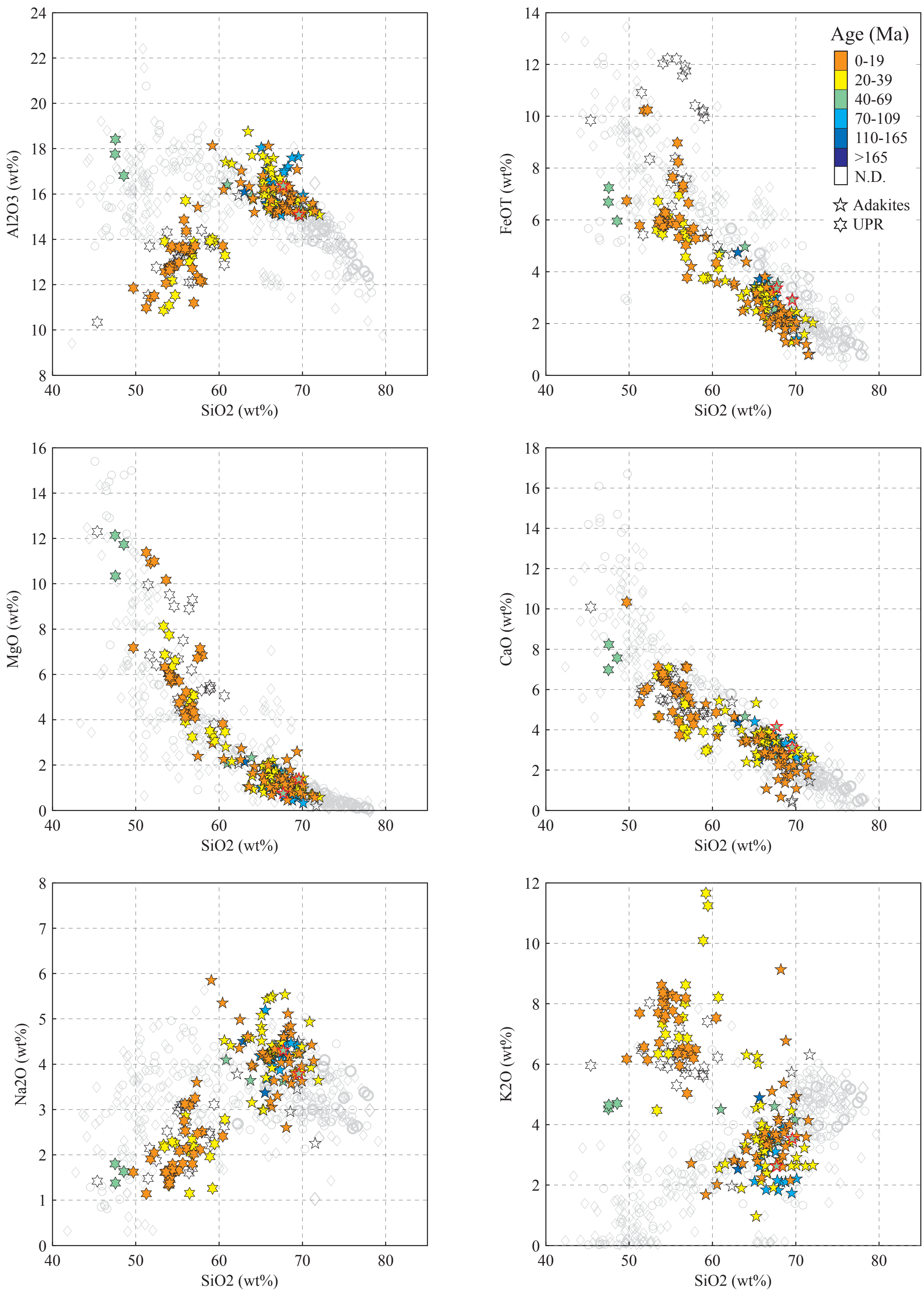

Al2O3 (wt%)
FeOT (wt%)
MgO (wt%)
CaO (wt%)
Na2O (wt%)
K2O (wt%)
SiO2 (wt%)
Age (Ma)
0-19
20-39
40-69
70-109
110-165
>165
N.D.
Adakites
UPR

Figure 1.10: Harker diagrams plotting major element oxides against SiO2 content for adakites and ultrapotassic rocks (UPR). Light grey symbols represent values for calc-alkaline rocks for comparison purposes.

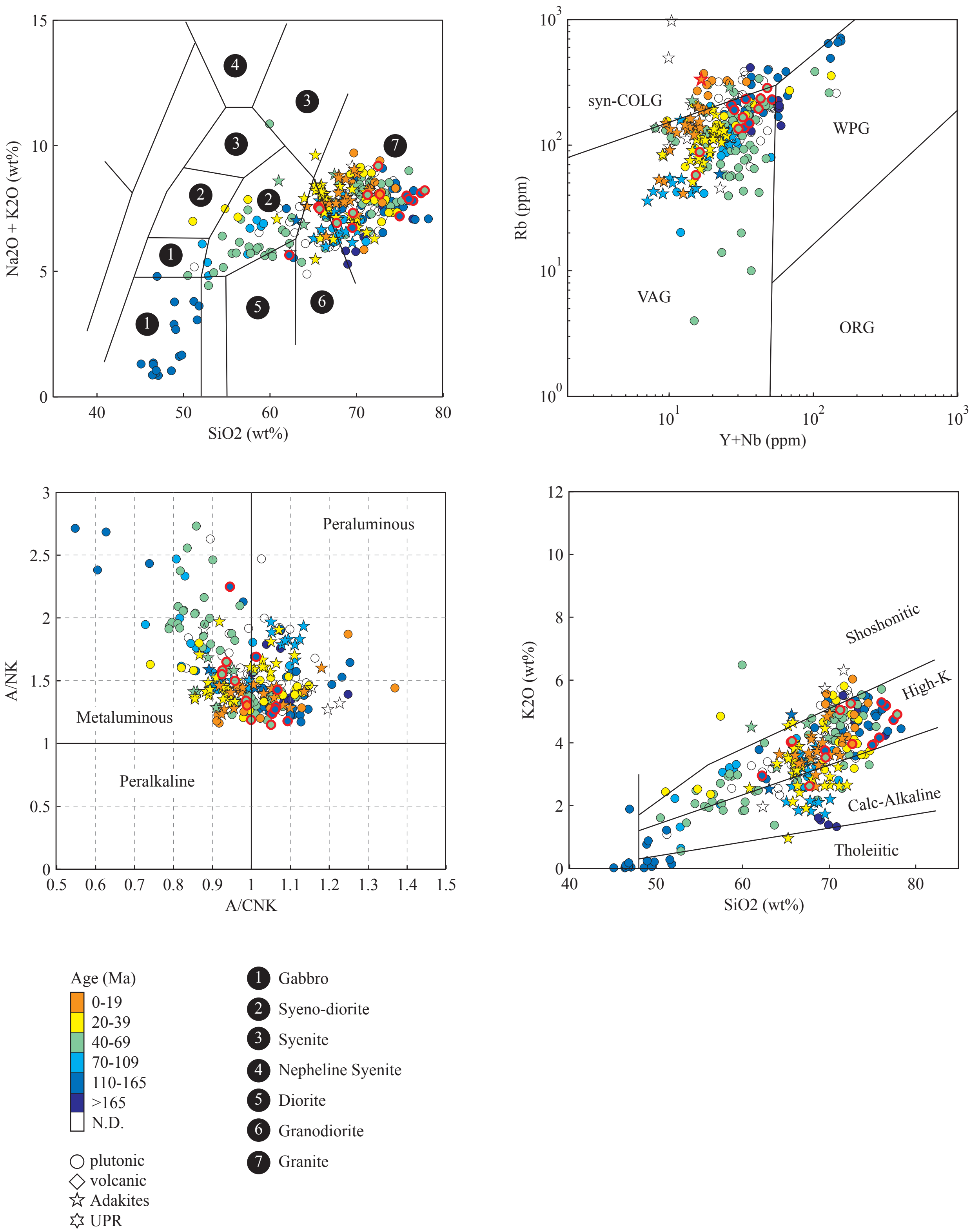
15
10
5
0
40
50
60
70
80
Na2O + K2O (wt%)
SiO2 (wt%)
1
2
3
4
5
6
7
syn-COLG
WPG
VAG
ORG
Rb (ppm)
Y+Nb (ppm)
Peraluminous
Metaluminous
Peralkaline
A/NK
A/CNK
Shoshonitic
High-K
Calc-Alkaline
Tholeiitic
K2O (wt%)
SiO2 (wt%)
Age (Ma)
0-19
20-39
40-69
70-109
110-165
>165
N.D.
plutonic
volcanic
Adakites
UPR
Gabbro
Syeno-diorite
Syenite
Nepheline Syenite
Diorite
Granodiorite
Granite

Figure 1.11: TAS, granitoid discrimination, A/NK vs. A/CNK, and K2O vs. SiO2 diagrams for plutonic rocks of the Lhasa terrane. Samples analyzed during this study are highlighted with red outlines.

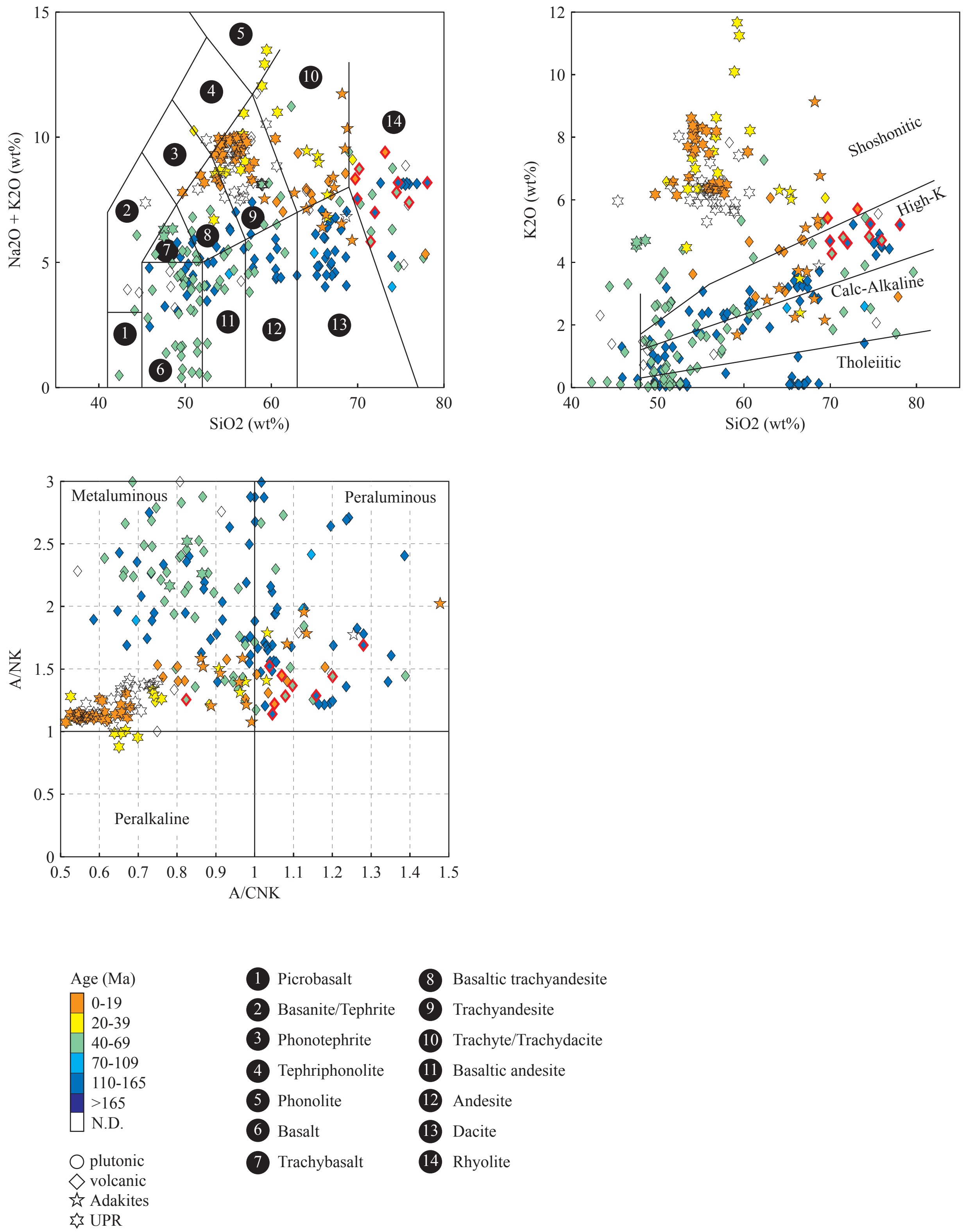

Na2O + K2O (wt%)
SiO2 (wt%)
K2O (wt%)
SiO2 (wt%)
Shoshonitic
High-K
Calc-Alkaline
Tholeiitic
A/NK
A/CNK
Metaluminous
Peraluminous
Peralkaline
Age (Ma)
0-19
20-39
40-69
70-109
110-165
>165
N.D.
plutonic
volcanic
Adakites
UPR
1 Picrobasalt
2 Basanite/Tephrite
3 Phonotephrite
4 Tephriphonolite
5 Phonolite
6 Basalt
7 Trachybasalt
8 Basaltic trachyandesite
9 Trachyandesite
10 Trachyte/Trachydacite
11 Basaltic andesite
12 Andesite
13 Dacite
14 Rhyolite

Figure 1.12: TAS, A/NK vs. A/CNK, and K2O vs. SiO2 diagrams for volcanic rocks of the Lhasa terrane. Samples analyzed during this study are highlighted with red outlines.

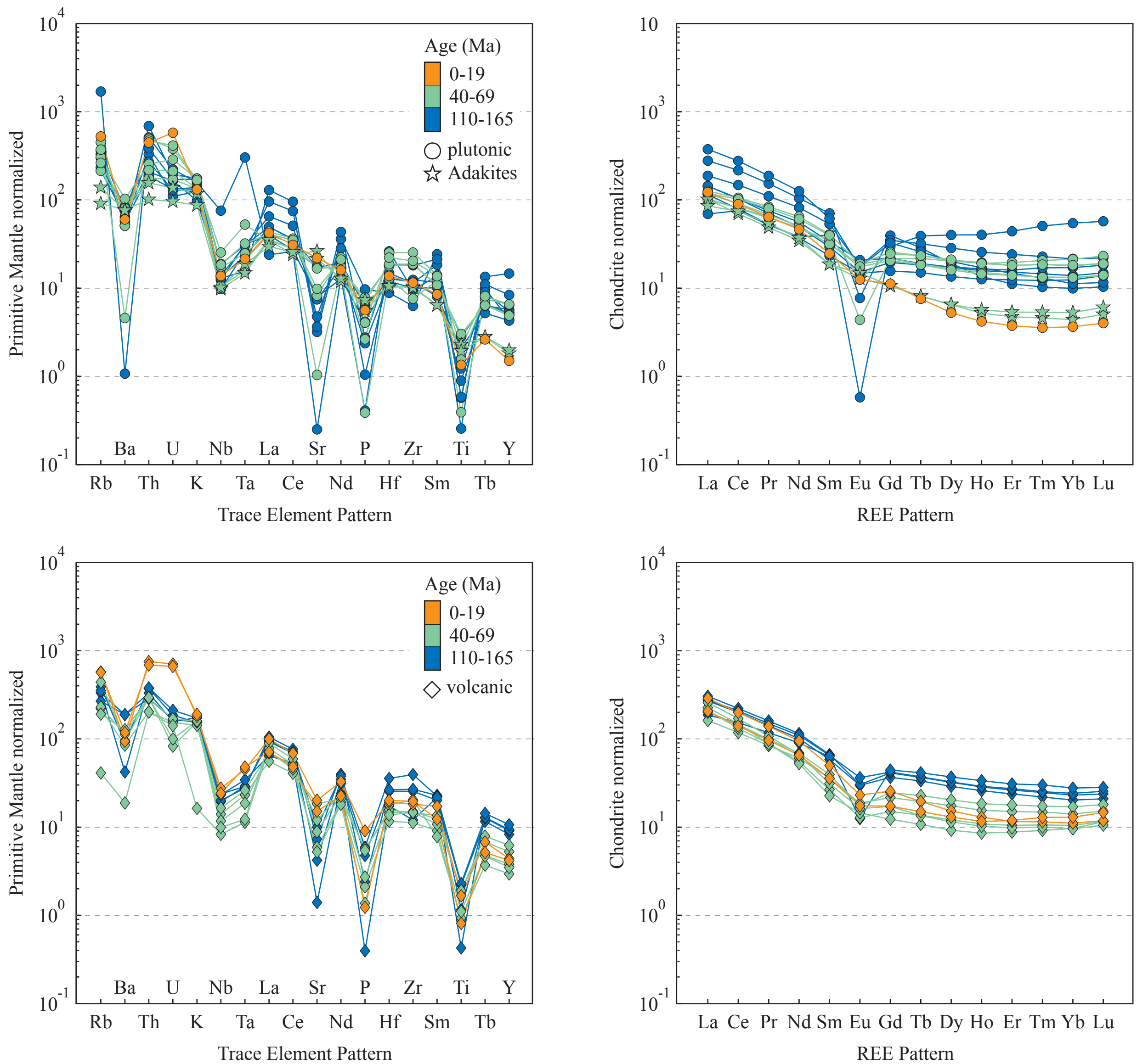
Age (Ma)
0-19
40-69
110-165
plutonic
Adakites
Primitive Mantle normalized
Rb Ba Th U K Nb Ta La Ce Sr Nd P Hf Zr Sm Ti Tb Y
Trace Element Pattern
Chondrite normalized
La Ce Pr Nd Sm Eu Gd Tb Dy Ho Er Tm Yb Lu
REE Pattern
Age (Ma)
0-19
40-69
110-165
volcanic
Primitive Mantle normalized
Rb Ba Th U K Nb Ta La Ce Sr Nd P Hf Zr Sm Ti Tb Y
Trace Element Pattern
Chondrite normalized
La Ce Pr Nd Sm Eu Gd Tb Dy Ho Er Tm Yb Lu
REE Pattern

Figure 1.13: Trace element and REE pattern for samples analyzed during this study grouped by plutonic and volcanic rocks

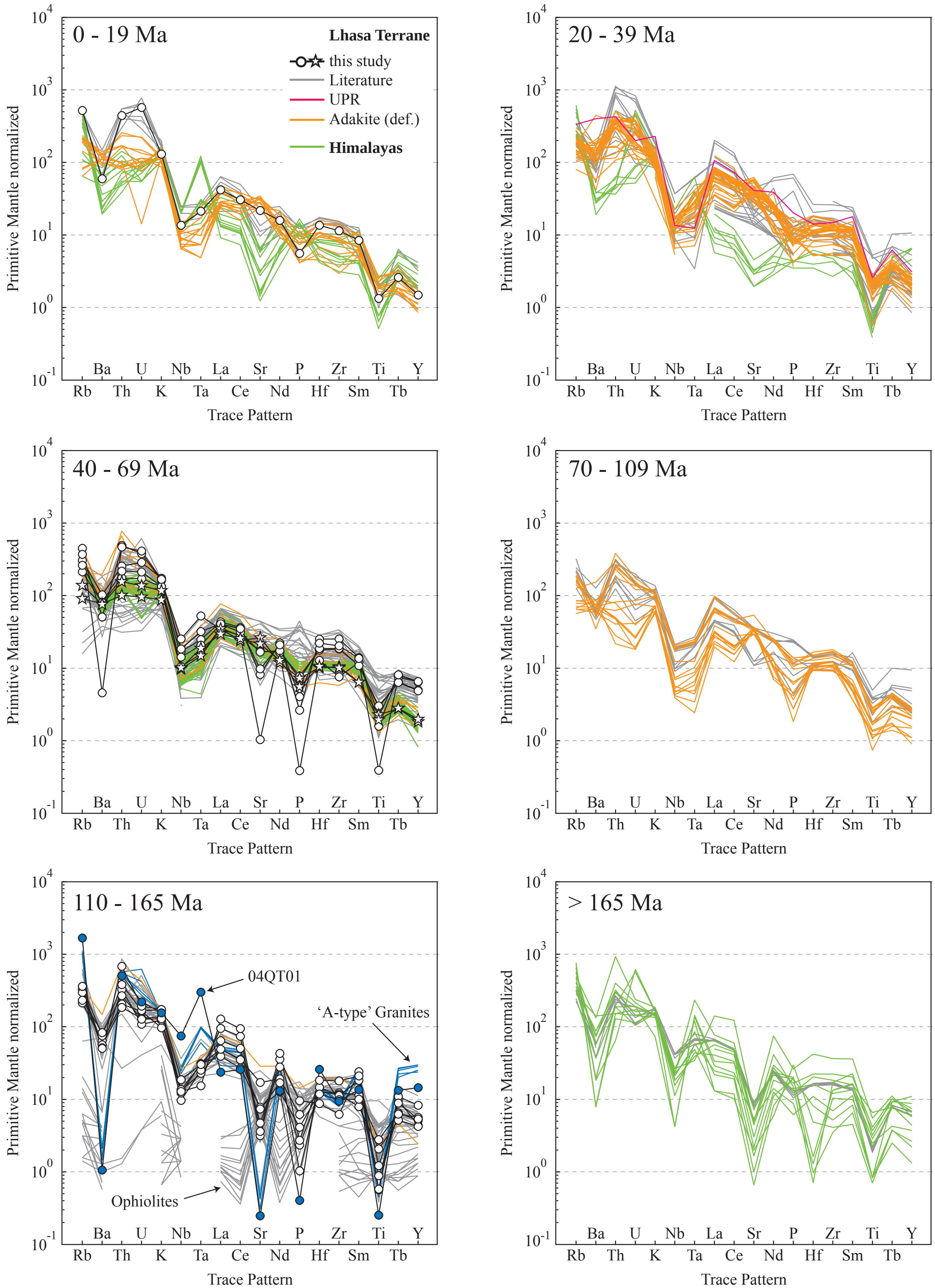
0 - 19 Ma
Lhasa Terrane
this study
Literature
UPR
Adakite (def.)
Himalayas
20 - 39 Ma
40 - 69 Ma
70 - 109 Ma
110 - 165 Ma
04QT01
'A-type' Granites
Ophiolites
> 165 Ma
Primitive Mantle normalized
Trace Pattern
Rb Ba Th U K Nb Ta La Ce Sr Nd P Hf Zr Sm Ti Tb Y

Figure 1.14: Trace element patterns for Lhasa terrane and Himalayan plutonic rocks subdivided into age groups. Samples analyzed during this study are highlighted (black lines with symbols). Besides the coloring indicating rock type or region, noteworthy trends are highlighted in blue or otherwise indicated.

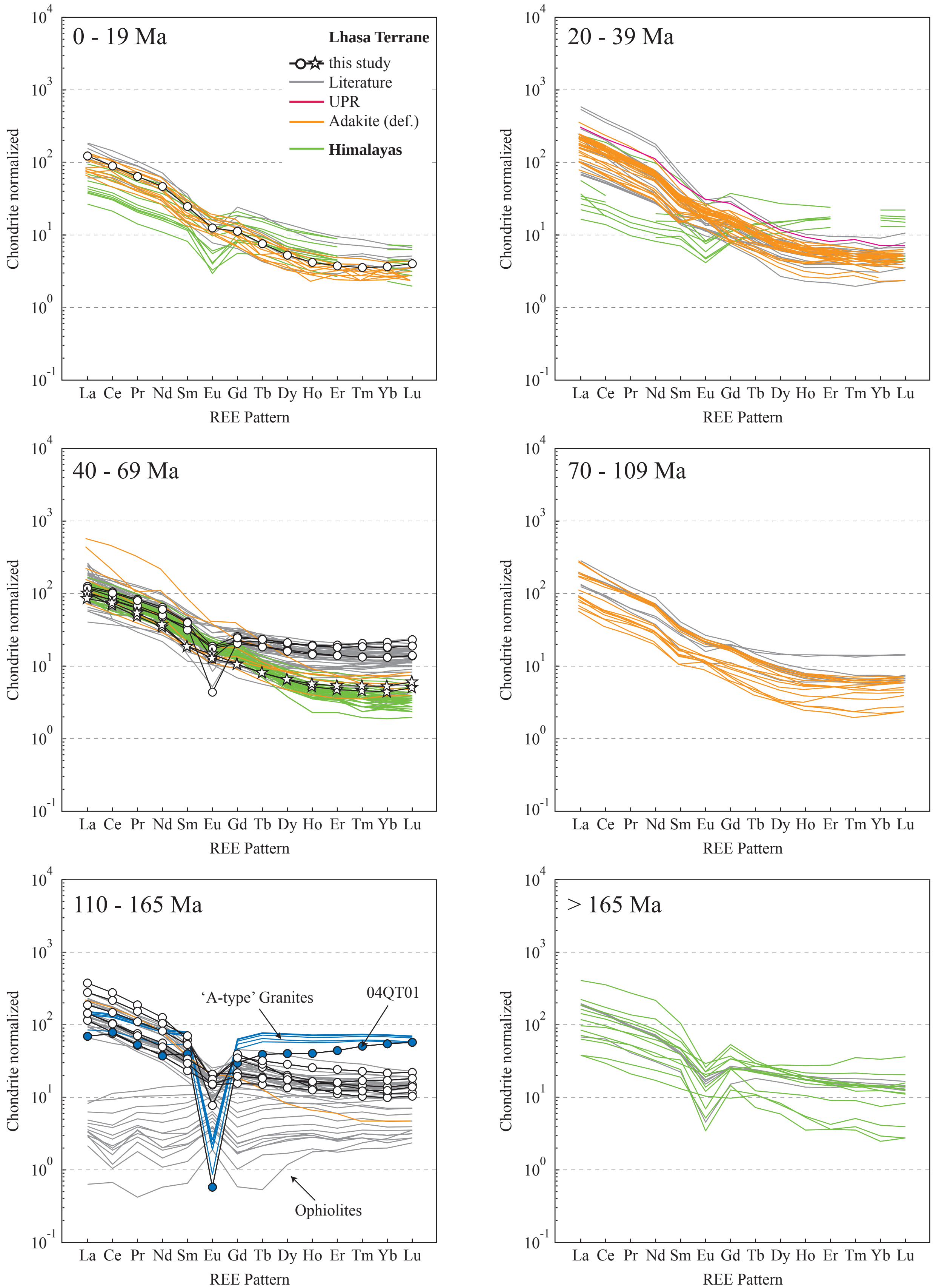
0 - 19 Ma
Lhasa Terrane
this study
Literature
UPR
Adakite (def.)
Himalayas
20 - 39 Ma
40 - 69 Ma
70 - 109 Ma
110 - 165 Ma
'A-type' Granites
04QT01
Ophiolites
> 165 Ma
Chondrite normalized
REE Pattern
La Ce Pr Nd Sm Eu Gd Tb Dy Ho Er Tm Yb Lu

Figure 1.15: REE patterns for Lhasa terrane and Himalayan plutonic rocks subdivided into age groups. Samples analyzed during this study are highlighted (black lines with symbols). Besides the coloring indicating rock type or region, noteworthy trends are highlighted in blue or otherwise indicated.

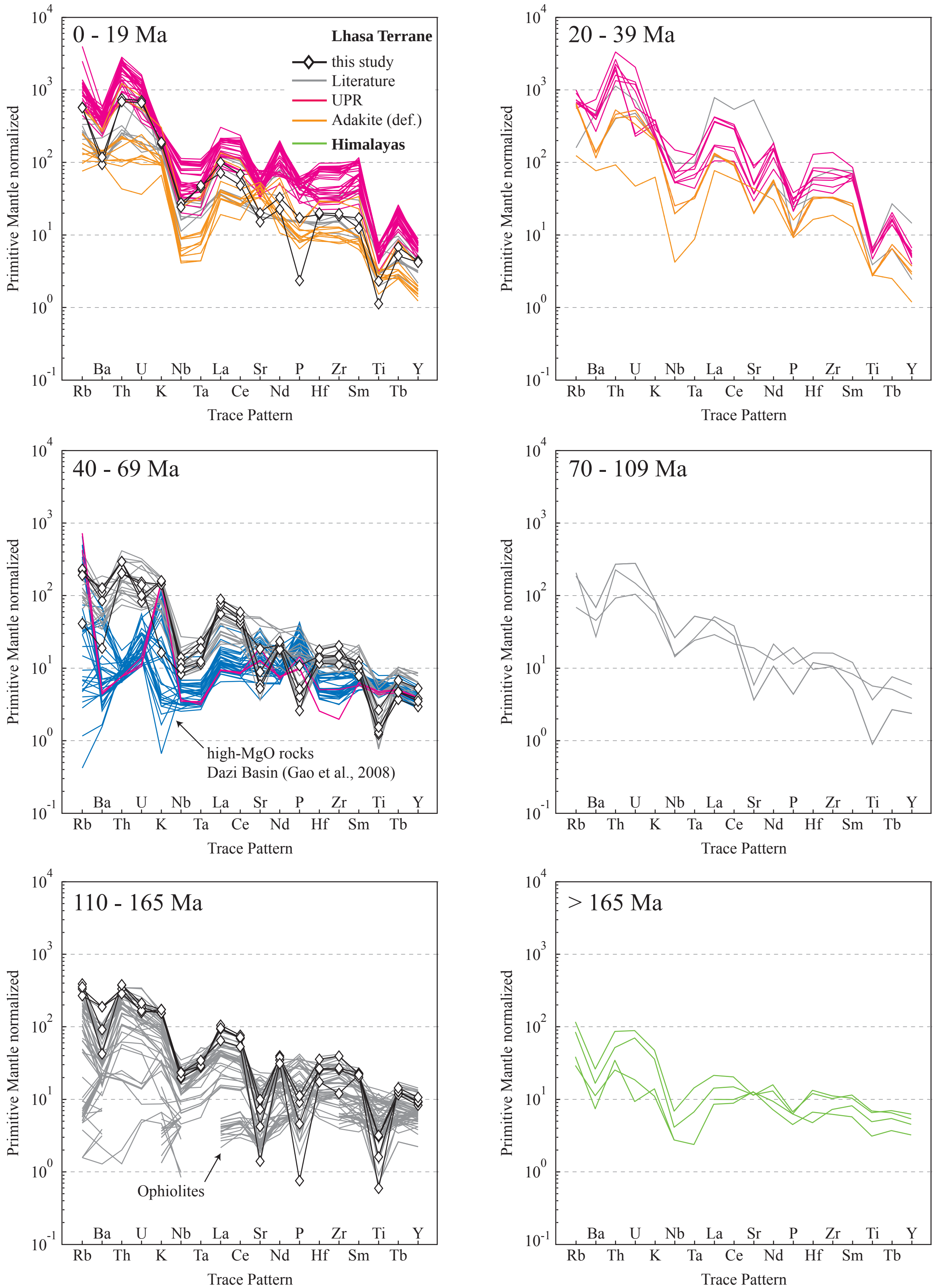

0 - 19 Ma
Lhasa Terrane
this study
Literature
UPR
Adakite (def.)
Himalayas
20 - 39 Ma
40 - 69 Ma
high-MgO rocks
Dazi Basin (Gao et al., 2008)
70 - 109 Ma
110 - 165 Ma
Ophiolites
> 165 Ma
Primitive Mantle normalized
Trace Pattern
Rb Ba Th U K Nb Ta La Ce Sr Nd P Hf Zr Sm Ti Tb Y

Figure 1.16: Trace element patterns for Lhasa terrane and Himalayan volcanic rocks subdivided into age groups. Samples analyzed during this study are highlighted (black lines with symbols). Besides the coloring indicating rock type or region, noteworthy trends are highlighted in blue or otherwise indicated.

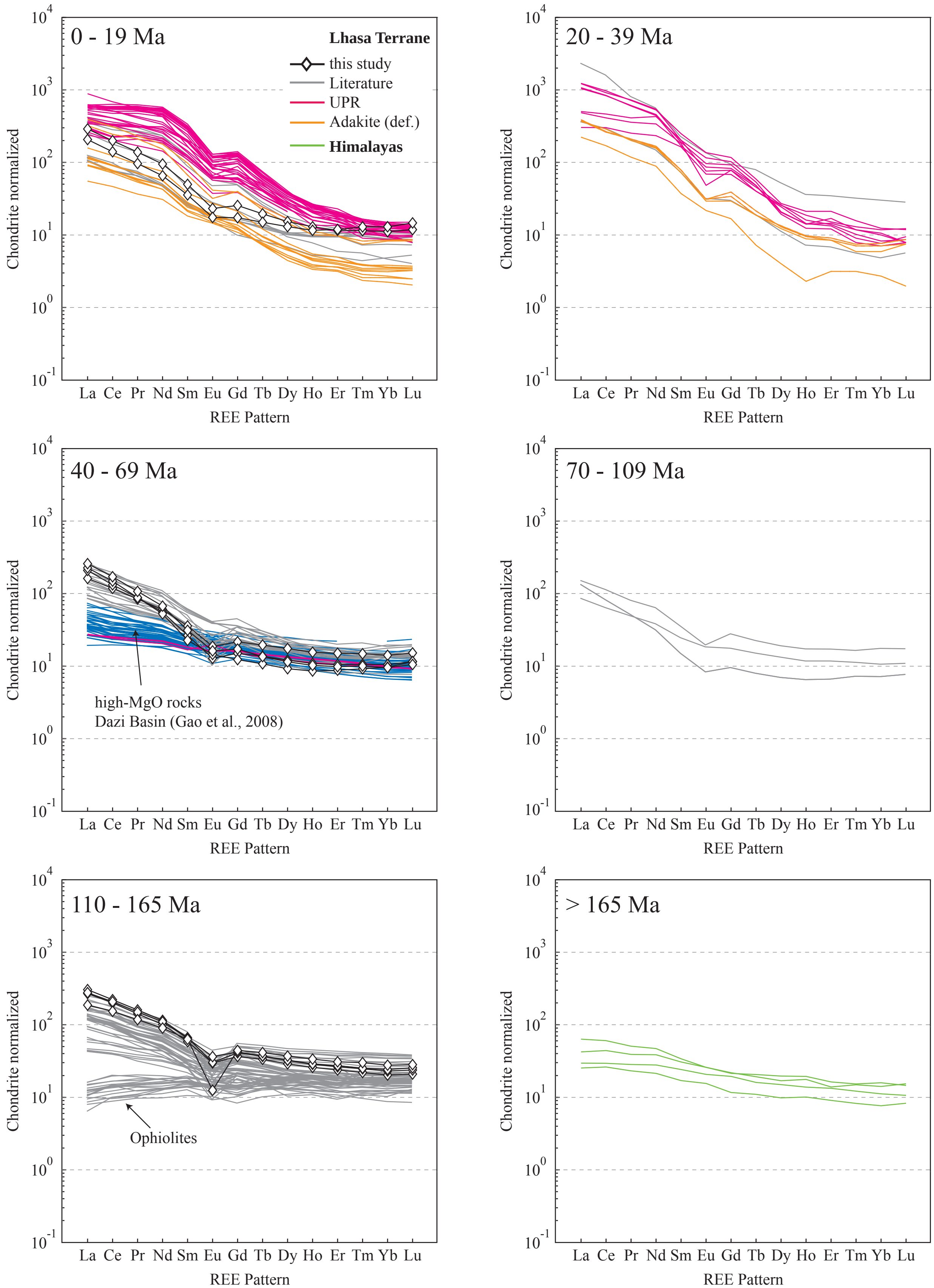
0 - 19 Ma
Lhasa Terrane
this study
Literature
UPR
Adakite (def.)
Himalayas
20 - 39 Ma
40 - 69 Ma
high-MgO rocks
Dazi Basin (Gao et al., 2008)
70 - 109 Ma
110 - 165 Ma
Ophiolites
> 165 Ma
Chondrite normalized
La Ce Pr Nd Sm Eu Gd Tb Dy Ho Er Tm Yb Lu
REE Pattern

Figure 1.17: REE patterns for Lhasa terrane and Himalayan volcanic rocks subdivided into age groups. Samples analyzed during this study are highlighted (black lines with symbols). Besides the coloring indicating rock type or region, noteworthy trends are highlighted in blue or otherwise indicated.

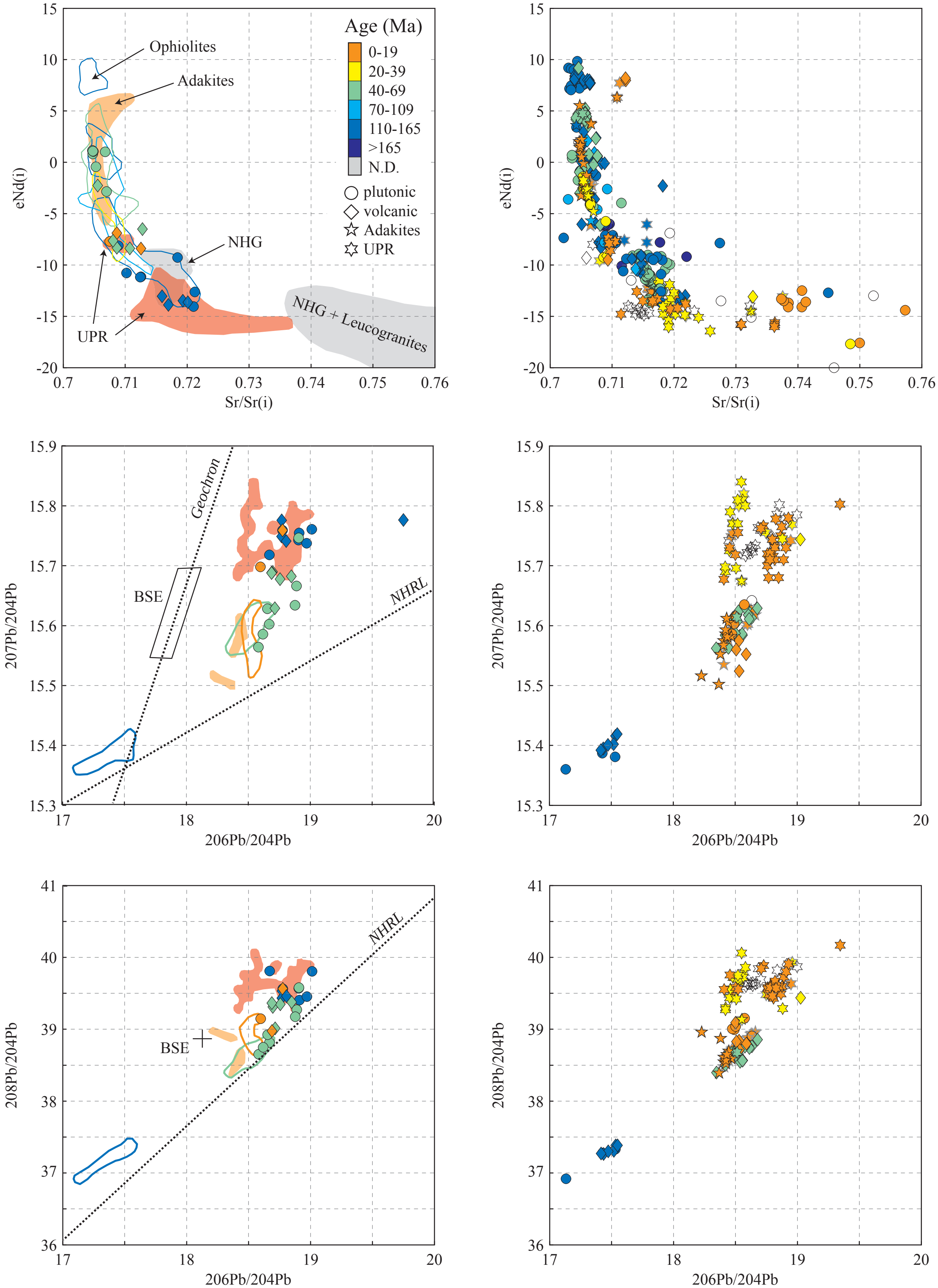

Age (Ma)
0-19
20-39
40-69
70-109
110-165
>165
N.D.
plutonic
volcanic
Adakites
UPR
Ophiolites
Adakites
NHG
UPR
NHG + Leucogranites
eNd(i)
Sr/Sr(i)
Geochron
BSE
NHRL
207Pb/204Pb
206Pb/204Pb
208Pb/204Pb

Figure 1.18: 87Sr/86Sr(i) vs. eNd(t), 207Pb/204Pb vs. 206Pb/204Pb, and 208Pb/204Pb vs. 206Pb/204Pb diagrams. Right-hand side shows all available literature data. Left-hand side compares samples from this study with the fields/outlines of literature data. BSE (Bulk Silicate Earth) and NHRL (Northern Hemisphere Reference Line) fields/lines are from Rollinson (1993) and references therein.

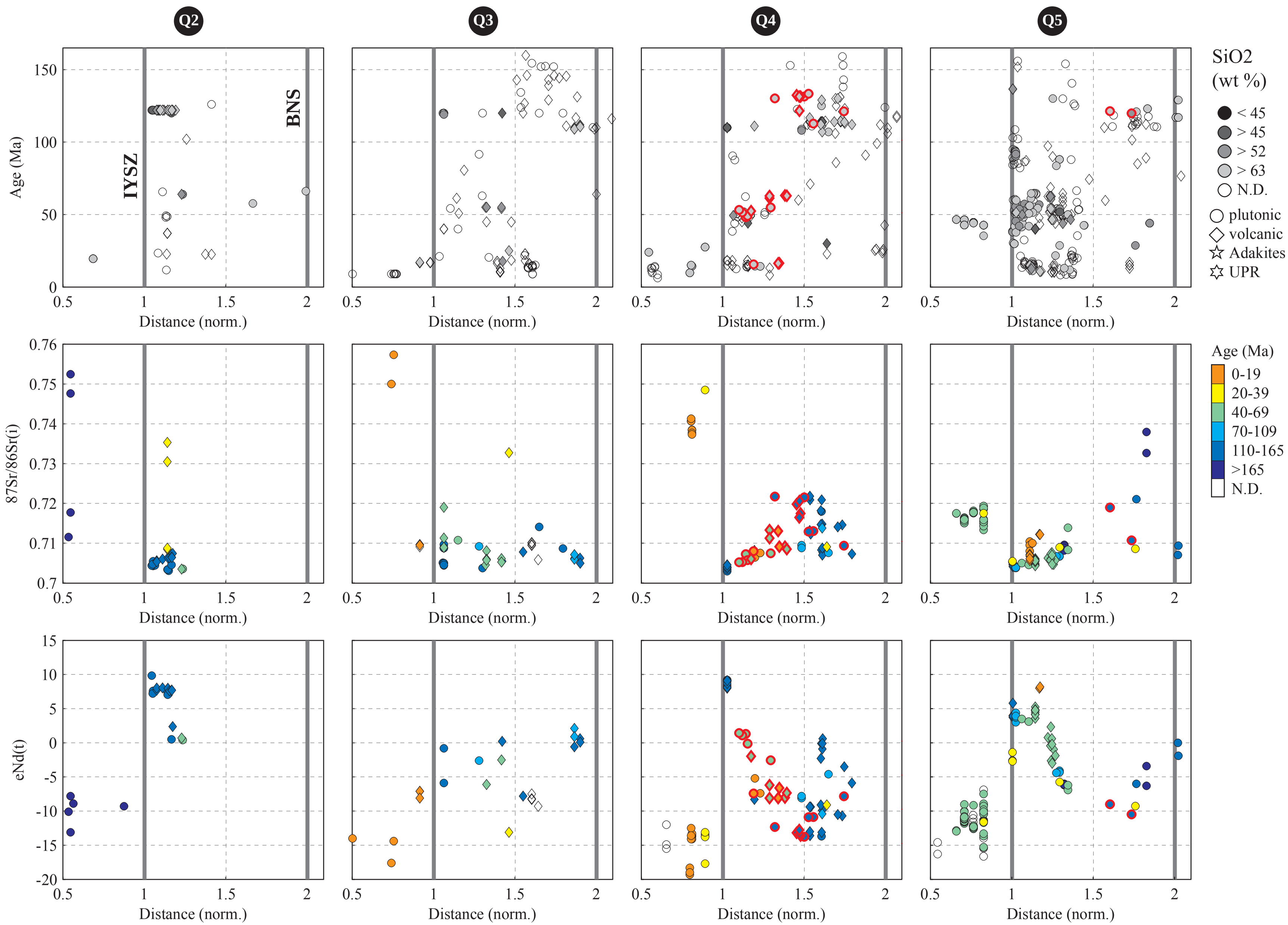

Q2
Q3
Q4
Q5
IYSZ
BNS
Age (Ma)
87Sr/86Sr(i)
eNd(t)
Distance (norm.)
SiO2
(wt %)
< 45
> 45
> 52
> 63
N.D.
plutonic
volcanic
Adakites
UPR
Age (Ma)
0-19
20-39
40-69
70-109
110-165
>165
N.D.

Figure 1.19: Magmatic age, 87Sr/86Sr(i), and eNd(t) for calc-alkaline rocks plotted against normalized distance from the sutures, which are highlighted as thick grey lines. Samples analyzed during this study are highlighted with red outlines.

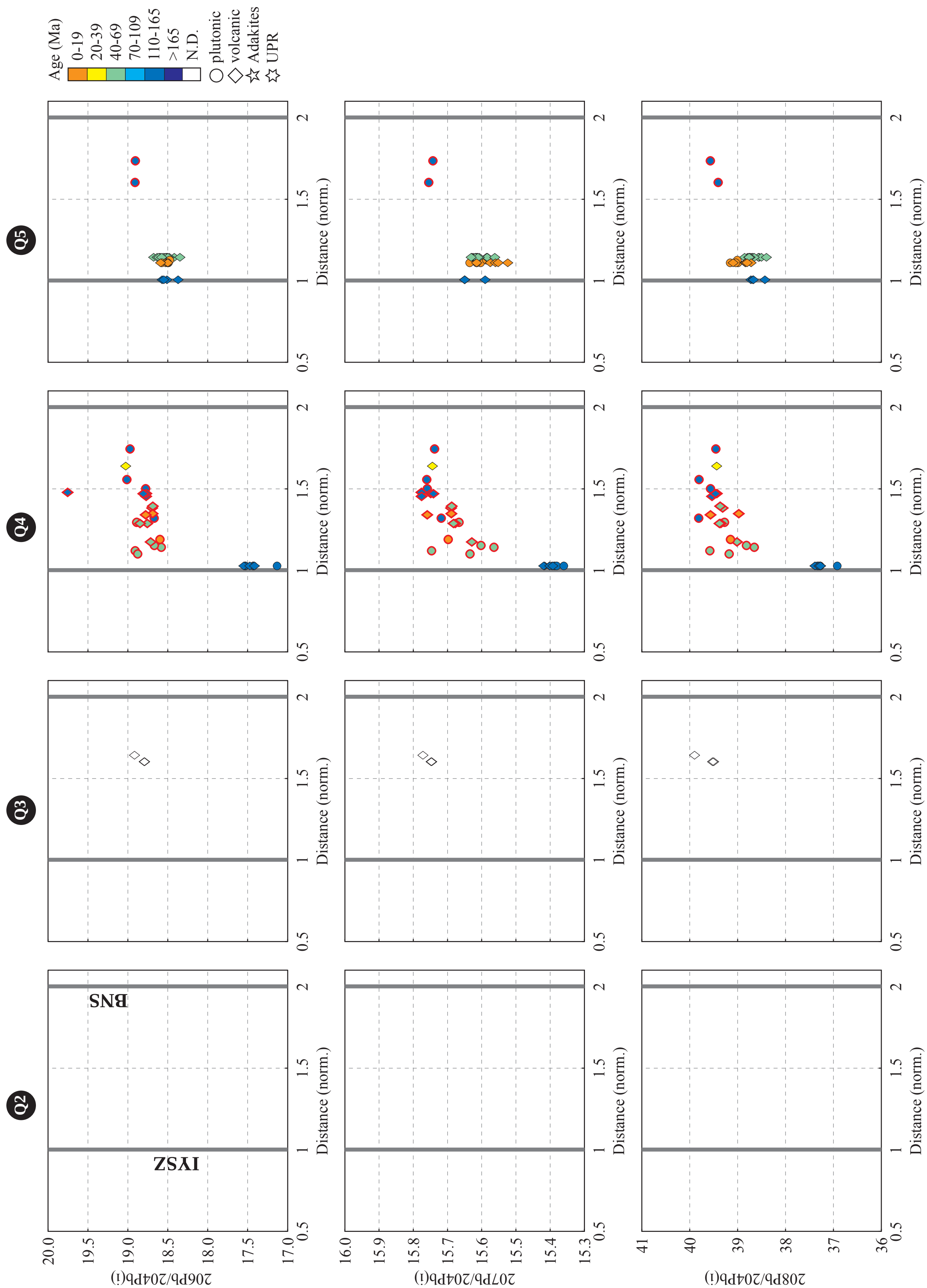

Q2
Q3
Q4
Q5
IYSZ
BNS
206Pb/204Pb(i)
207Pb/204Pb(i)
208Pb/204Pb(i)
Distance (norm.)
Age (Ma)
0-19
20-39
40-69
70-109
110-165
>165
N.D.
plutonic
volcanic
Adakites
UPR

Figure 1.20: Pb isotopes for calc-alkaline rocks plotted against normalized distance from the sutures, which are highlighted as thick grey lines. Samples analyzed during this study are highlighted with red outlines.

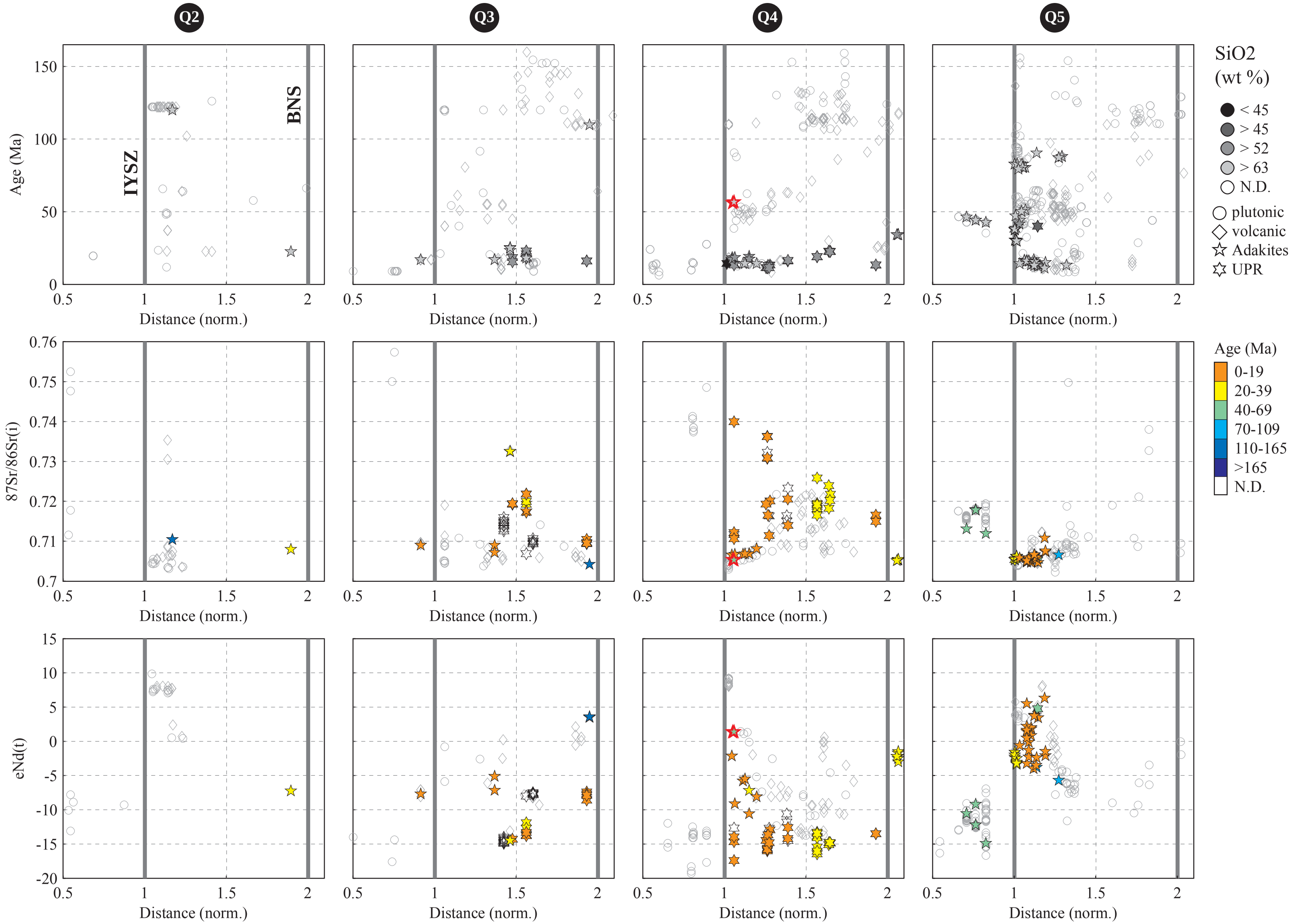
Q2
Q3
Q4
Q5
IYSZ
BNS
Age (Ma)
87Sr/86Sr(i)
eNd(t)
Distance (norm.)
SiO2
(wt %)
< 45
> 45
> 52
> 63
N.D.
plutonic
volcanic
Adakites
UPR
Age (Ma)
0-19
20-39
40-69
70-109
110-165
>165
N.D.

Figure 1.21: Magmatic age, 87Sr/86Sr(i), and eNd(t) for adakites and ultrapotassic rocks (UPR) plotted against normalized distance from the sutures, which are highlighted as thick grey lines. Samples analyzed during this study are highlighted with red outlines and calc-alkaline rocks are plotted with grey outlines for comparison.

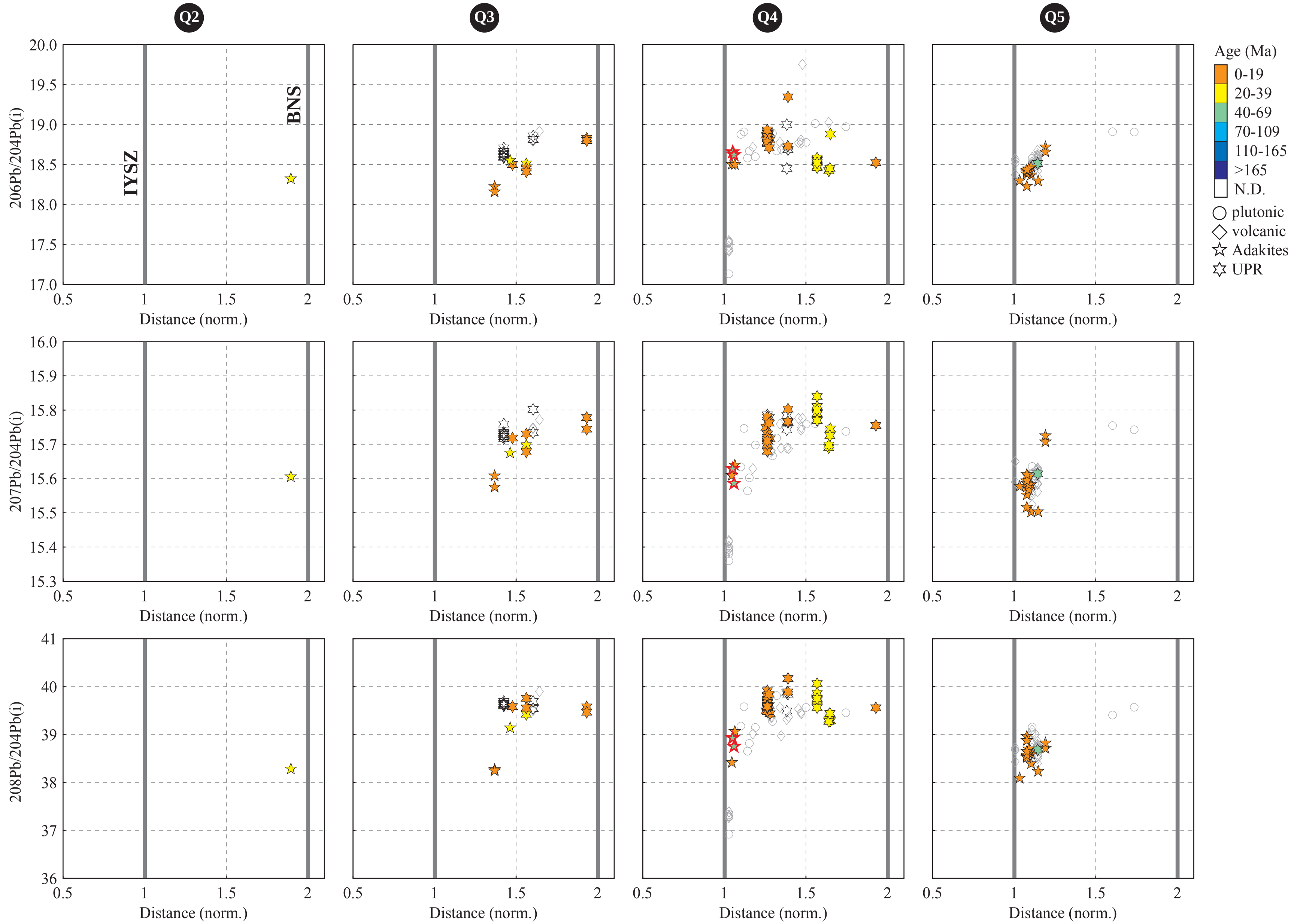

Q2
Q3
Q4
Q5
IYSZ
BNS
206Pb/204Pb(i)
207Pb/204Pb(i)
208Pb/204Pb(i)
Distance (norm.)
Age (Ma)
0-19
20-39
40-69
70-109
110-165
>165
N.D.
plutonic
volcanic
Adakites
UPR

Figure 1.22: Pb isotopes for adakites and ultrapotassic rocks (UPR) plotted against normalized distance from the sutures, which are highlighted as thick grey lines. Samples analyzed during this study are highlighted with red outlines.

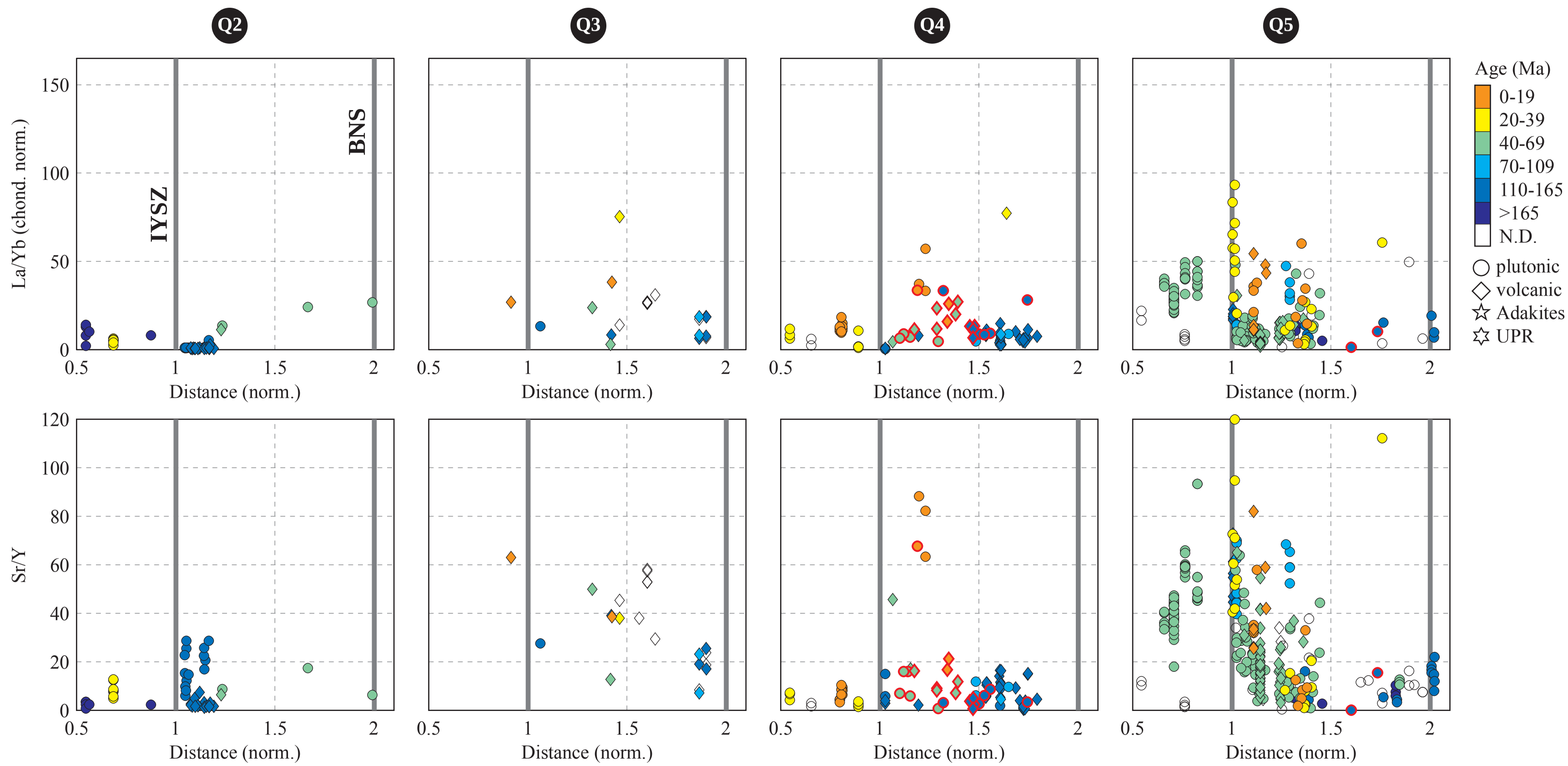
Q2
Q3
Q4
Q5
La/Yb (chond. norm.)
Sr/Y
Distance (norm.)
IYSZ
BNS
Age (Ma)
0-19
20-39
40-69
70-109
110-165
>165
N.D.
plutonic
volcanic
Adakites
UPR

Figure 1.23: Chondrite normalized La/Yb and measured Sr/Y ratios for calc-alkaline rocks plotted against the normalized distance from the sutures from the sutures, which are highlighted as thick grey lines. Samples analyzed during this study are highlighted with red outlines.

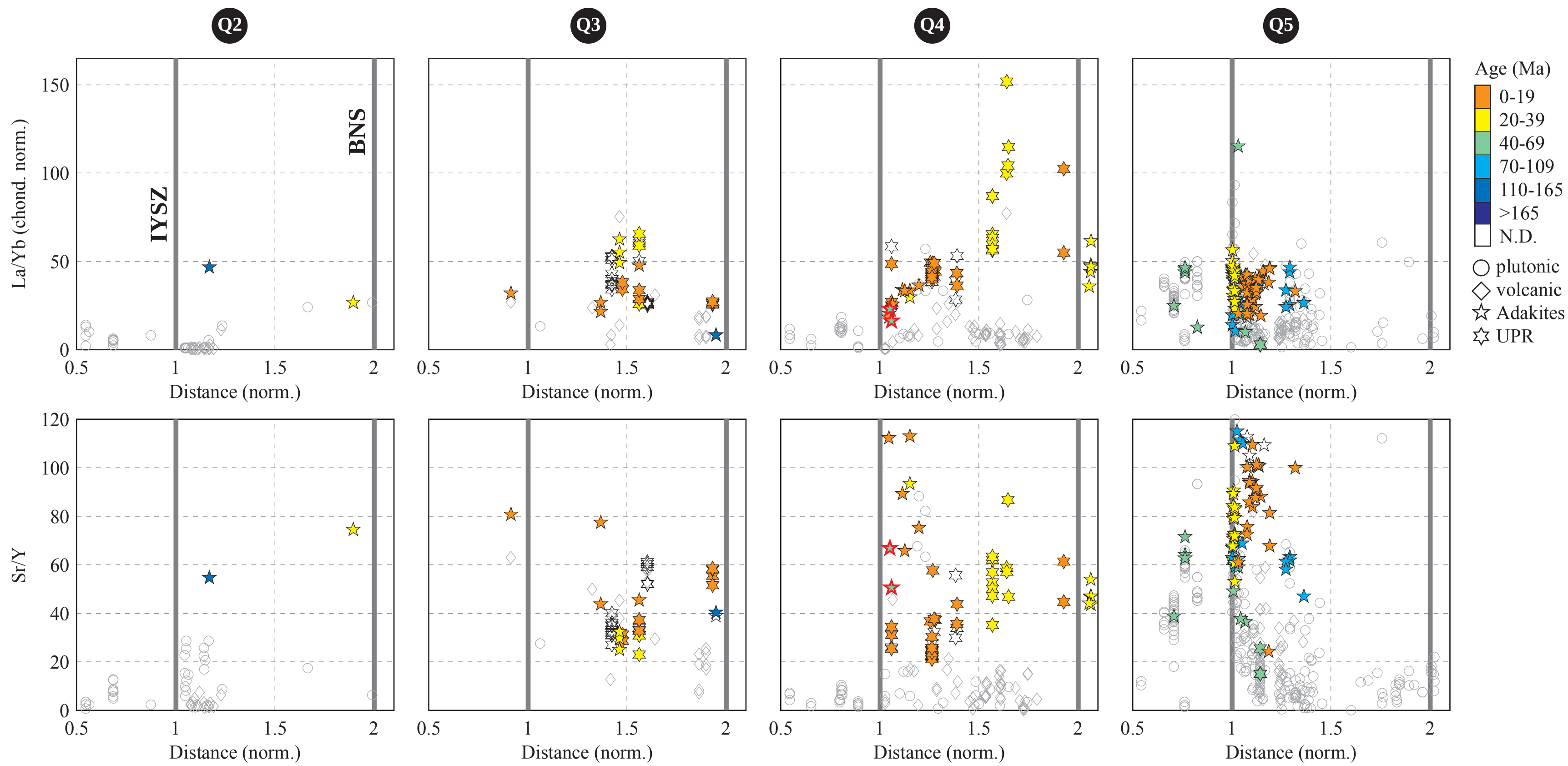
Q2
Q3
Q4
Q5
IYSZ
BNS
La/Yb (chond. norm.)
Sr/Y
Distance (norm.)
Age (Ma)
0-19
20-39
40-69
70-109
110-165
>165
N.D.
plutonic
volcanic
Adakites
UPR

Figure 1.24: Chondrite normalized La/Yb and measured Sr/Y ratios for adakites and ultrapotassic rocks (UPR) plotted against the normalized distance from the sutures from the sutures, which are highlighted as thick grey lines. Samples analyzed during this study are highlighted with red outlines and calc-alkaline rocks are plotted with grey outlines for comparison.

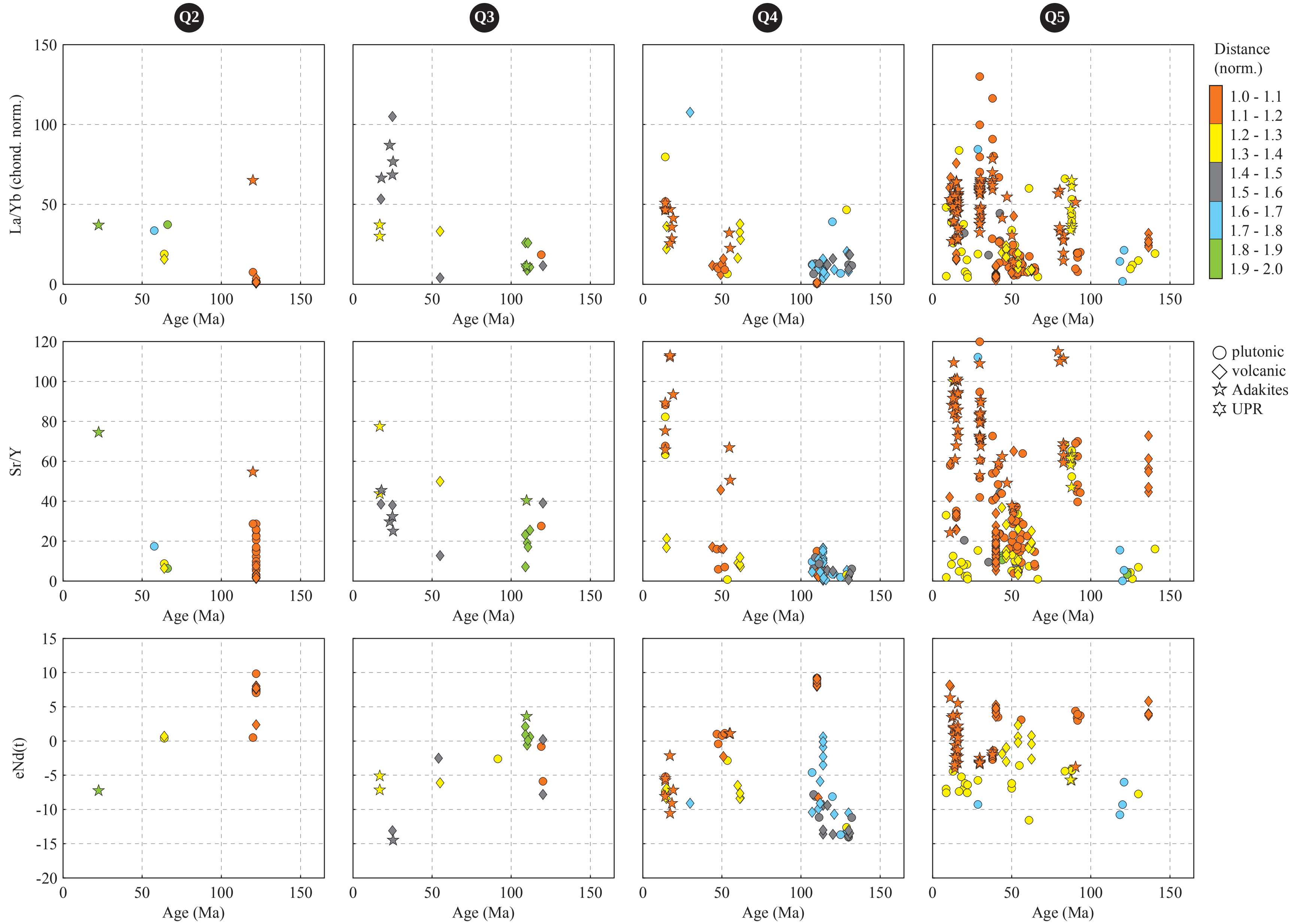
Q2
Q3
Q4
Q5
La/Yb (chond. norm.)
Sr/Y
eNd(t)
Age (Ma)
Distance
(norm.)
1.0 - 1.1
1.1 - 1.2
1.2 - 1.3
1.3 - 1.4
1.4 - 1.5
1.5 - 1.6
1.6 - 1.7
1.7 - 1.8
1.8 - 1.9
1.9 - 2.0
plutonic
volcanic
Adakites
UPR

Figure 1.25: La/Yb, Sr/Y, and eNd(t) plotted against the magmatic age. The color-coding in this case is not by age but by distance from the sutures based.

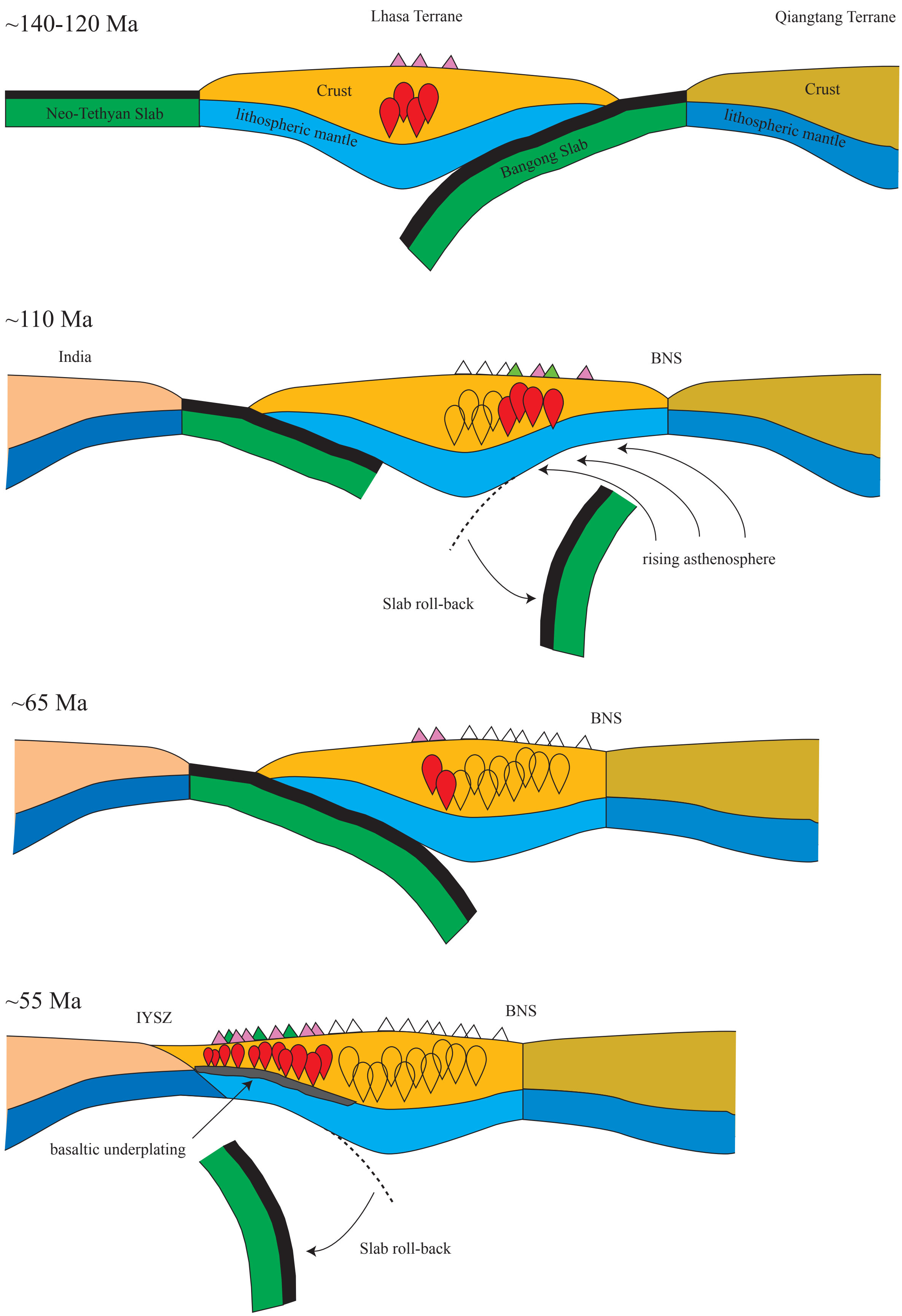

~140-120 Ma
Lhasa Terrane
Qiangtang Terrane
Crust
Neo-Tethyan Slab
lithospheric mantle
Bangong Slab
Crust
lithospheric mantle
~110 Ma
India
BNS
rising asthenosphere
Slab roll-back
~65 Ma
BNS
~55 Ma
IYSZ
BNS
basaltic underplating
Slab roll-back

Figure 1.26: Conceptual model of the evolution of the Lhasa terrane from Cretaceous through present times.

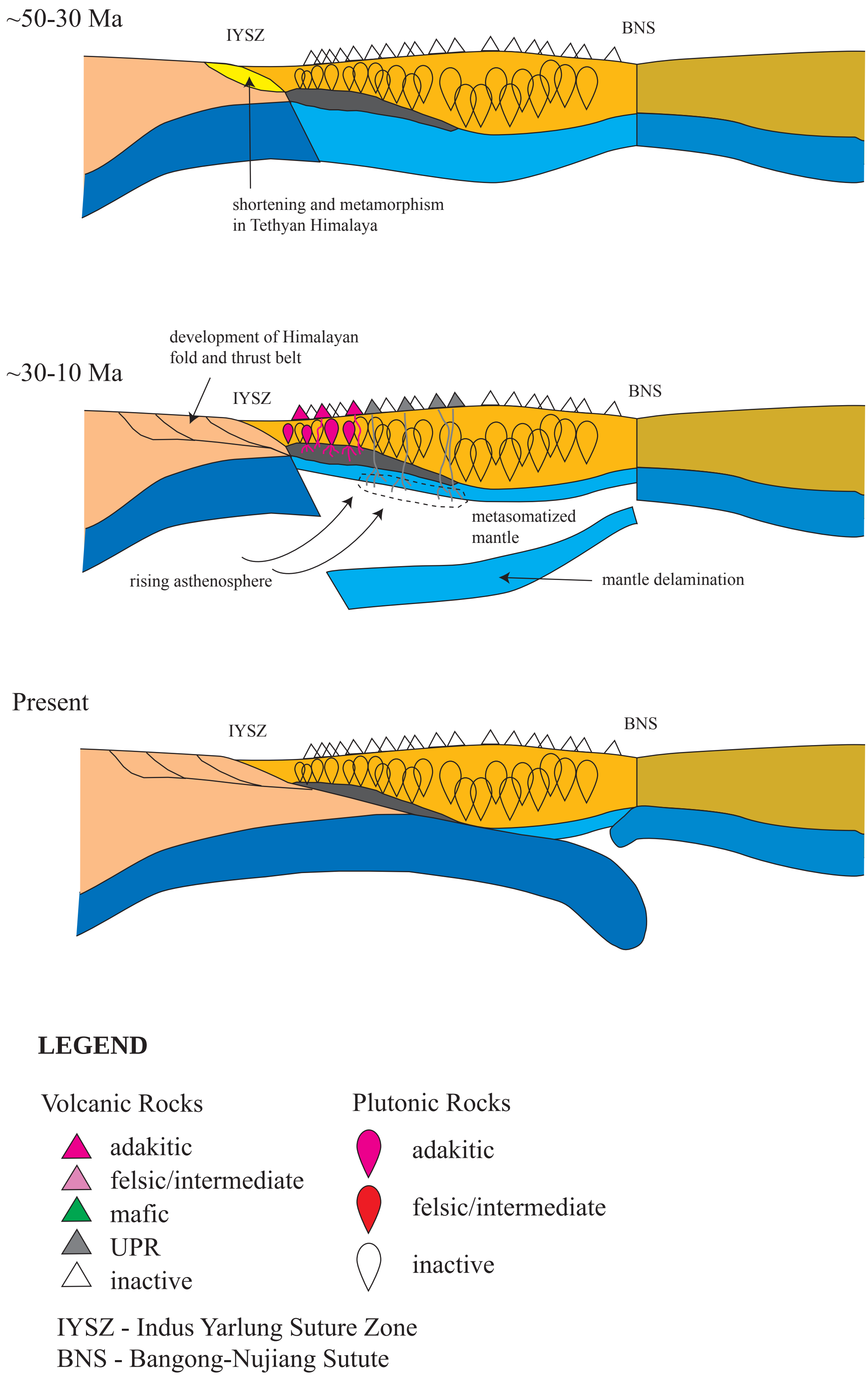
~50-30 Ma
IYSZ
BNS
shortening and metamorphism
in Tethyan Himalaya
development of Himalayan
fold and thrust belt
~30-10 Ma
IYSZ
BNS
metasomatized
mantle
rising asthenosphere
mantle delamination
Present
IYSZ
BNS
LEGEND
Volcanic Rocks
adakitic
felsic/intermediate
mafic
UPR
inactive
Plutonic Rocks
adakitic
felsic/intermediate
inactive
IYSZ - Indus Yarlung Suture Zone
BNS - Bangong-Nujiang Sutute

Figure 1.27: Conceptual model of the evolution of the Lhasa terrane from Cretaceous through present times - continued

Table 1.1: Overview of analyzed samples of the Xainza rift

Sample	Lithology	Latitude (dd)	Longitude (dd)	Age (Ma)	87Sr/86Sr(i)	eNd(t)	206Pb/204Pb(t)	207Pb/204Pb(t)	208Pb/204Pb(t)	WR - Chem.
02PX05	Granite	30.8038	88.6933	63.9						
04GB01	Granodiorite	29.6283	89.0618	46.8	0.7068	1.0	18.6	15.6	38.7	X
04GB02	Granite	29.7060	89.2246	47.7	0.7053	-0.4	18.7	15.6	38.8	X
04GB03	Rhyolite	29.7739	89.2369	51.0	0.7056	-2.3	18.7	15.6	39.0	X
04GB04	Metasandstone	30.0395	89.0932	500.0*	0.7487	-19.4	18.2	15.7	39.0	X
04GB05	Granite	30.0985	89.1351	213.3						
04QT01	Granite	30.9397	90.9993	120.0*	0.7185	-9.3	18.9	15.8	39.4	X
04QT02	Diorite	31.2809	90.7172	118.4	0.7102	-10.8	18.9	15.7	39.6	X
04QT03	Granite	31.4141	89.0234	119.8	0.7089	-8.1	19.0	15.7	39.5	X
04XI03	Granite	30.7888	88.8025	111.4	0.7126	-11.2	19.0	15.8	39.8	X
04XI04	Granite	30.5737	88.4925	130.0*	0.7210	-14.1	18.8	15.8	39.6	X
04XI12	Rhyolite	30.5096	88.4951	130.0*	0.7170	-13.9	19.8	15.8	41.4	X
04XI18	Rhyolite	30.4542	88.6869	130.9	0.7193	-13.5	18.8	15.8	39.5	X
04XI19	Rhyolite	30.1829	88.5236	63.9						
04XI20	Metasandstone	30.2665	88.6385	500.0						
04XI21	Rhyolite	30.3311	88.5794	62.5						
04XI36	Rhyolite	30.4894	88.5542	120.2	0.7201	-13.6	18.8	15.7	39.4	X
04XIA01	Granite	30.6538	88.5288	134.6						
04XIA04	Granite	30.6496	88.5294	134.6*	0.7125	-11.2				X
05XI52	Tuff (rhyolitic)	30.2503	88.6920	61.8	0.7087	-8.3	18.7	15.7	39.3	X
05XI62	Rhyolite	29.9818	88.4014	60.0*	0.7128	-6.5	18.8	15.7	39.3	X
05XI63	Rhyolite	29.9818	88.4014	51.8	0.7108	-8.4	18.8	15.7	39.4	X
05XI67	Granite	29.9993	88.4188	53.5	0.7070	-2.9	18.9	15.7	39.3	X
05XI75	Tuff (rhyolitic)	30.1541	88.3701	15.1	0.7087	-6.9	18.7	15.7	39.0	X
05XI77	Rhyolite	30.1332	88.3760	15.0*	0.7126	-8.4	18.8	15.8	39.6	X
05XI79	Granite	30.0388	88.4229	202.5						
05XI90	Granodiorite	29.5285	88.3143	50.1	0.7048	0.8	18.9	15.7	39.6	X
05XI91	Granite	29.4756	88.3159	51.8	0.7047	1.1	18.9	15.6	39.2	X
05XI92	Granite	29.3675	88.1270	54.7	0.7049	1.1	18.7	15.6	38.9	X
05XI94	Granite	29.3717	88.2533	55.3	0.7048	1.1	18.6	15.6	38.7	X
05XIB41	Rhyolite	30.2736	88.4508	61.5	0.7080	-7.6	18.7	15.7	39.4	X
05XIB48	Rhyolite	30.2845	88.4652	62.1						
05XIC55	Rhyolite	30.4856	88.5241	130.0*	0.7160	-13.1	18.8	15.7	39.5	X
05XID68	Granite	30.0696	88.4345	128.8						

Table 1.1: continued

Sample	Lithology	Latitude (dd)	Longitude (dd)	Age (Ma)	87Sr/86Sr(i)	eNd(t)	206Pb/204Pb(t)	207Pb/204Pb(t)	208Pb/204Pb(t)	WR - Chem.
05XID69	Granite	30.0707	88.4324	128.8*	0.7212	-12.6	18.7	15.7	39.8	X
05XIE82	Granite	29.7271	88.2860	14.3	0.7075	-7.7	18.6	15.7	39.1	X
05XIE87	Granite	29.7291	88.2953	13.0						

Sample ages denoted with (*) indicate assumed age for isotopic ratio corrections.

Table 1.2: Whole rock geochemistry (XRF - Major elements). All measurements reported in wt%

Sample	SiO2	TiO2	Al2O3	FeO	MnO	MgO	CaO	Na2O	K2O	P2O5	Total
04GB01	65.58	0.63	16.09	4.26	0.09	1.65	3.97	3.53	4.03	0.17	100.00
04GB02	72.49	0.35	14.46	1.76	0.06	0.36	1.27	3.94	5.25	0.06	100.00
04GB03	70.19	0.42	15.35	2.85	0.09	1.01	1.25	4.45	4.28	0.12	100.01
04GB04	92.75	0.19	3.82	0.83	0.03	0.23	0.22	0.74	1.17	0.03	100.01
04QT01	77.45	0.06	12.59	1.18	0.03	0.13	0.46	3.38	4.73	0.01	100.02
04QT02	62.24	0.61	17.12	5.67	0.12	2.69	5.78	2.68	2.96	0.14	100.01
04QT03	75.79	0.12	13.40	1.10	0.02	0.30	1.04	3.85	4.16	0.21	99.99
04XI03	69.52	0.46	15.14	3.39	0.07	1.30	3.30	2.97	3.76	0.09	100.00
04XI04	76.55	0.13	12.88	1.27	0.03	0.12	1.20	2.63	5.18	0.02	100.01
04XI12	72.00	0.48	15.05	3.04	0.04	0.72	1.57	2.37	4.62	0.10	99.99
04XI18	74.67	0.25	13.54	2.39	0.04	0.24	0.64	2.96	5.23	0.05	100.01
04XI36	69.97	0.50	14.88	3.78	0.06	0.63	2.51	2.86	4.68	0.13	100.00
04XIA04	74.98	0.19	13.72	1.66	0.06	0.37	1.78	3.26	3.93	0.05	100.00
05XI52	75.96	0.19	13.70	1.40	0.04	0.23	1.04	2.69	4.71	0.05	100.01
05XI62	71.51	0.41	16.48	3.74	0.04	1.05	0.84	1.03	4.79	0.12	100.01
05XI63	83.43	0.20	9.07	0.48	0.04	0.11	2.08	4.07	0.49	0.03	100.00
05XI67	77.87	0.09	12.37	0.80	0.02	0.08	0.56	3.31	4.90	0.01	100.01
05XI75	69.72	0.36	15.45	2.71	0.05	1.10	2.08	2.92	5.42	0.20	100.01
05XI77	73.18	0.18	14.95	1.01	0.03	0.14	1.09	3.70	5.70	0.03	100.01
05XI90	65.71	0.66	15.57	4.71	0.10	1.87	3.75	3.43	4.05	0.15	100.00
05XI91	71.27	0.47	13.93	3.09	0.06	0.99	2.06	3.00	5.05	0.09	100.01
05XI92	67.71	0.50	16.36	3.36	0.07	0.75	4.16	4.30	2.62	0.16	99.99
05XI94	69.59	0.42	15.08	2.91	0.05	1.38	3.13	3.79	3.53	0.12	100.00
05XIB41	74.51	0.24	13.82	1.75	0.06	0.39	1.37	2.97	4.82	0.06	99.99
05XIC55	78.08	0.09	12.02	1.07	0.02	0.01	0.52	2.98	5.20	0.01	100.00
05XID69	76.04	0.27	12.68	1.70	0.04	0.26	1.08	2.59	5.29	0.06	100.01
05XIE82	72.68	0.29	14.37	1.76	0.04	0.75	1.93	4.09	3.97	0.12	100.00

Table 1.3: Whole rock geochemistry (ICPMS - Trace elements). All measurements reported in ppm

Sample	Rb	Sr	Y	Zr	Nb	Ba	Pb	Sc	V	Cr	Ni	Cu	Zn	Ga	La	Ce	Pr
04GB01	135.14	363.48	22.75	206.33	7.49	557.86	12.08	10.62	81.70	10.90	0.00	6.50	53.00	15.60	24.57	49.29	5.91
04GB02	194.89	173.22	29.40	284.05	12.16	720.06	20.97	5.96	14.40	2.70	0.00	0.90	33.10	15.40	29.91	64.59	7.95
04GB03	140.15	387.78	23.96	168.76	10.01	592.85	16.46	6.27	36.80	3.20	0.00	0.90	51.90	15.80	38.26	72.23	7.99
04GB04	64.62	48.98	10.15	265.46	3.91	297.77	9.43	2.64	12.30	13.30	0.00	3.80	10.20	3.70	9.96	20.08	2.25
04QT01	1076.66	5.29	66.74	106.54	53.86	7.50	59.91	6.03	2.80	6.20	0.00	2.00	51.50	27.50	16.42	46.13	4.94
04QT02	137.04	364.74	23.64	139.01	9.59	452.85	17.48	15.39	129.70	16.90	3.04	22.80	77.10	17.50	33.84	63.94	7.17
04QT03	209.28	67.22	19.96	70.38	6.98	398.22	33.70	3.01	10.20	6.80	0.00	3.40	25.60	14.50	65.91	132.51	14.59
04XI03	190.75	167.03	19.45	132.44	8.79	363.83	23.40	9.10	68.60	11.40	0.00	2.30	47.50	16.10	27.21	48.26	5.04
04XI04	231.04	100.60	38.14	127.73	13.38	530.07	42.34	3.96	5.40	6.20	0.00	1.70	36.80	15.00	44.59	90.46	10.47
04XI12	247.09	88.88	37.69	285.61	13.87	638.13	3.75	9.05	39.90	11.30	0.49	0.00	61.80	21.60	63.89	122.62	13.45
04XI18	210.78	153.53	41.43	301.08	14.34	1317.29	43.61	6.78	8.10	9.20	0.00	2.80	62.40	17.10	72.07	135.46	15.20
04XI36	170.02	210.16	42.59	442.51	16.93	1320.16	34.70	11.11	30.80	9.70	0.00	5.60	79.20	19.60	65.70	127.41	14.19
04XIA04	149.23	157.34	25.99	111.80	9.87	586.47	31.30	4.48	13.70	2.30	0.00	0.40	37.70	14.60	34.13	62.79	6.70
05XI52	146.11	124.12	17.35	125.52	8.34	785.84	22.41	2.87	7.90	5.90	0.00	0.00	31.40	11.00	49.58	80.79	8.36
05XI62	280.08	254.13	28.22	162.16	11.74	666.15	14.08	8.07	28.50	10.90	2.09	5.50	62.90	17.10	47.60	89.13	9.42
05XI63	26.12	110.48	13.43	227.97	5.90	131.70	7.31	2.01	6.90	6.80	0.00	0.40	7.00	6.00	53.55	90.86	8.38
05XI67	285.69	21.86	29.68	85.20	18.10	32.15	20.90	3.54	2.70	2.30	0.00	0.00	13.60	14.20	23.61	50.20	6.08
05XI75	364.85	424.87	20.03	203.68	19.65	655.24	56.99	4.62	40.00	3.70	0.13	7.30	55.50	19.50	68.36	122.09	13.20
05XI77	360.83	319.97	19.11	219.55	17.26	823.55	56.11	2.15	8.60	7.50	0.00	0.00	44.90	16.40	48.85	85.86	9.17
05XI90	166.97	353.39	22.20	209.93	10.15	563.07	16.62	11.47	98.90	21.00	7.59	23.60	57.50	16.10	27.88	55.84	6.44
05XI91	235.75	207.69	29.86	228.17	13.14	355.56	18.48	7.50	52.70	12.00	2.66	13.40	39.50	14.20	28.10	62.26	7.59
05XI92	57.73	555.70	8.32	117.42	6.97	540.98	14.97	5.69	71.40	11.20	2.18	1.50	57.10	17.10	24.02	42.74	4.62
05XI94	88.04	455.11	9.02	112.98	7.23	529.48	10.05	5.10	62.90	11.80	3.75	8.80	42.00	14.80	20.28	45.51	5.13
05XIB41	121.09	187.55	15.91	165.10	7.07	887.88	17.58	3.11	9.40	4.50	0.00	0.00	31.30	12.30	61.23	104.68	10.20
05XIC55	225.26	29.51	48.43	134.56	16.57	295.64	39.33	4.97	1.90	6.10	0.00	0.00	38.50	16.80	44.15	94.09	11.18
05XID69	232.58	77.09	24.61	202.79	9.26	356.83	34.74	2.39	11.90	6.80	0.00	0.00	29.40	16.40	88.84	169.37	17.86
05XIE82	333.19	462.35	6.84	129.35	9.78	420.89	58.23	3.10	33.10	13.10	4.19	36.30	46.00	18.10	28.99	54.90	6.07

Table 1.3: continued

Sample	Nd	Sm	Eu	Gd	Tb	Dy	Ho	Er	Tm	Yb	Lu	Th	U	Cs	Hf	Ta
04GB01	22.67	4.86	1.08	4.44	0.70	4.22	0.86	2.33	0.34	2.26	0.35	14.96	3.60	5.47	5.51	0.65
04GB02	30.19	6.22	1.09	5.28	0.87	5.27	1.10	2.99	0.47	3.03	0.49	21.78	6.05	9.40	7.78	1.02
04GB03	28.22	5.48	1.08	4.45	0.73	4.44	0.88	2.49	0.38	2.41	0.39	17.30	3.22	7.94	4.52	0.95
04GB04	8.17	1.68	0.38	1.41	0.27	1.83	0.38	1.16	0.19	1.26	0.20	4.48	1.14	14.16	6.80	0.39
04QT01	17.80	6.10	0.03	6.08	1.46	10.20	2.28	7.28	1.29	9.27	1.45	43.34	4.68	43.25	8.08	12.45
04QT02	26.14	5.14	1.21	4.48	0.71	4.39	0.89	2.51	0.37	2.36	0.38	17.65	3.45	5.94	3.88	0.95
04QT03	48.88	10.77	0.45	8.11	1.07	4.82	0.76	1.85	0.26	1.68	0.26	15.89	2.77	8.90	2.73	1.05
04XI03	17.35	3.57	0.86	3.22	0.56	3.43	0.71	2.05	0.31	2.11	0.35	28.07	2.30	8.86	3.94	1.29
04XI04	38.19	8.16	1.03	7.16	1.19	7.26	1.45	4.00	0.58	3.66	0.56	32.71	3.57	10.11	4.59	1.26
04XI12	46.94	8.95	1.72	7.51	1.25	7.37	1.46	3.94	0.56	3.44	0.53	31.73	3.90	6.95	7.87	1.19
04XI18	53.71	10.17	1.76	8.45	1.37	8.18	1.61	4.36	0.63	3.91	0.60	28.23	3.31	4.32	8.16	1.13
04XI36	51.27	9.94	2.12	8.64	1.39	8.25	1.64	4.52	0.64	4.11	0.65	24.28	3.51	5.25	10.99	1.19
04XIA04	23.15	4.51	0.88	4.00	0.68	4.44	0.93	2.65	0.43	2.91	0.46	23.02	2.70	2.42	3.70	1.25
05XI52	25.97	4.06	0.74	3.09	0.51	3.07	0.61	1.73	0.27	1.78	0.30	25.12	1.73	8.08	3.60	0.76
05XI62	32.17	6.03	1.01	5.06	0.85	5.18	1.04	2.95	0.44	2.90	0.46	24.70	3.55	72.35	4.86	1.08
05XI63	24.50	3.47	0.84	2.53	0.40	2.34	0.49	1.45	0.23	1.64	0.29	17.22	2.98	4.26	5.51	0.46
05XI67	22.14	5.36	0.25	4.44	0.81	5.15	1.08	3.22	0.52	3.62	0.59	41.81	7.98	5.34	3.97	2.16
05XI75	44.39	7.65	1.34	5.24	0.73	3.89	0.73	1.91	0.29	1.89	0.30	64.03	14.83	14.96	5.92	1.85
05XI77	30.48	5.45	1.01	3.55	0.56	3.31	0.66	1.97	0.33	2.21	0.37	58.50	13.96	13.38	6.20	1.97
05XI90	23.59	4.83	1.02	4.20	0.69	4.07	0.82	2.31	0.34	2.24	0.36	18.55	4.46	11.51	5.77	0.86
05XI91	28.42	6.05	0.74	5.04	0.87	5.36	1.08	2.99	0.47	3.10	0.48	39.93	8.67	11.34	6.87	1.32
05XI92	16.11	2.84	0.86	2.20	0.30	1.64	0.30	0.78	0.12	0.75	0.13	8.62	2.02	13.69	3.14	0.61
05XI94	17.33	2.84	0.74	2.18	0.30	1.67	0.32	0.89	0.14	0.90	0.15	13.26	2.89	4.96	3.27	0.77
05XIB41	31.45	4.78	0.94	3.54	0.51	2.92	0.58	1.62	0.26	1.62	0.27	25.03	2.10	2.07	4.25	0.50
05XIC55	41.96	9.66	0.73	9.13	1.55	9.39	1.90	5.12	0.77	4.72	0.71	32.21	4.44	9.24	5.36	1.41
05XID69	58.66	9.45	1.00	6.68	0.97	5.10	0.96	2.43	0.33	1.91	0.30	58.47	4.10	2.48	5.73	0.64
05XIE82	21.76	3.78	0.72	2.31	0.28	1.34	0.24	0.62	0.09	0.62	0.10	38.08	12.16	22.80	4.26	0.88

Page left intentionally blank

CHAPTER 2:

Evolution of the Xainza rift revealed by structural investigations and (U-Th)/He thermochronology

Abstract

E-W extension on the Tibetan plateau is expressed by prominent N-S trending rifts in the Lhasa terrane documenting extensional tectonics in an overall compressional regime related to the ongoing Indo-Asian collision. A variety of conceptual models have been proposed to explain these somewhat counter-intuitive structures invoking deep processes like basal drag of the underthrusting Indian lithosphere, or gravitational collapse of the elevated Tibetan plateau to name a few. To be able to evaluate these models, timing as well as magnitude of rifting are key parameters. Low-temperature thermochronology is a powerful tool to assess thermal histories of normal fault bounded rift shoulder like the ones encountered in the area of interest (Xainza rift). The results from thermal modeling demonstrate that opening of the Xainza rift initiated in the middle Miocene (15-17 Ma) triggered by right-lateral strike-slip faulting along the northern boundary of the rift (Gyaring Co fault) was followed by intensified normal faulting from ~10-7 Ma. In agreement with geomorphological observations like highest relief and widest basin in the north, the (U-Th)/He data confirm progressive rift opening from north to south. This finding disagrees with proposed models of extension related to arc-parallel stretching as well as basal drag that would trigger a northward propagating mode but is most consistent with a distributed, constrictional shear model.

2.1 INTRODUCTION

Despite being our textbook example of a contractional orogenic zone, the salient features observed on satellite images of the Tibetan Plateau are N-S trending rift valleys. Since the recognition of active N-S trending rift systems in Tibet (Tapponnier and Molnar, 1977; Molnar and Tapponnier, 1978; Ni and York, 1978), numerous workers have investigated their development in an attempt to elucidate the uplift and elevation history of the Tibetan plateau and its potential influence on global climate dynamics. Our knowledge of the kinematics and spatial distribution of N-S rifting in Tibet is to a large extent based on interpretation of satellite imagery and earthquake focal-mechanisms (Molnar and Tapponnier, 1978; Ni and York, 1978; Rothery and Drury, 1984; Armijo et al., 1986; Molnar and Lyon-Caen, 1989). Active dextral strike-slip faults and associated N-S trending rifts at the terminations of strike-slip faults in the Lhasa terrane have been studied during the past two decades (Tapponnier et al., 1981; Armijo et al., 1986, 1989; Mercier et al., 1987; Burchfiel et al., 1991; Ratschbacher et al., 1994; Harrison et al., 1995; Cogan et al., 1998). However, these field-based investigations are predominately restricted to southern Tibet with an emphasis on neotectonics (Tapponnier et al., 1981; Armijo et al., 1986; Dewey et al., 1988; Pan and Kidd, 1992; Ratschbacher et al., 1994; Harrison et al., 1995).

Although stratigraphic and geomorphologic relationships indicate that the rift-bounding normal faults have been active in southern and central Tibet throughout the Pleistocene (Armijo et al., 1986), these relationships do not constrain the timing of the onset or any temporal variations or episodicity of rifting. This pertinent information is more readily obtained from thermochronological data from exhumed mid-upper crustal rocks.

2.2 E-W EXTENSION IN TIBET

2.2.1 Overview of the Indo-Asian collision

The current expression of the Tibetan plateau and the Himalayas to the south (Fig. 2.1) is the result of long-lived history of terrane accretion related to the closure of the Tethys ocean starting in Paleozoic times and subsequent collision of the Indian sub-continent with Eurasia (Yin and Harrison, 2000). The major tectonic units from north to south are the 1) Songpan-Ganzi terrane (northern Tibet), 2) Qiangtang terrane (central Tibet), 3) Lhasa terrane (southern Tibet), 4) Tethyan Himalaya, 5) Higher (Greater) Himalaya, 6) Lesser (Lower) Himalaya, and 7) Sub-Himalaya. Starting in the Paleozoic, the Songpan-Ganzi terrane was accreted to the Kunlun Shan along the Anyimaqen-Kunlun-Muztagh suture zone, followed by suturing of the Qiangtang terrane along the Jinsha suture (JNS) during the Jurassic to early Cretaceous, and subsequent accretion of the Lhasa terrane in the early Cretaceous along the Bangong-Nujiang suture zone (BNS). A best estimate for the timing of initial collision of India along the Indus-Yarlung suture zone (IYSZ) with the Lhasa terrane to the north is at ~65 Ma. Progressive and still ongoing underthrusting of India beneath Tibet led to a series of contractional structures accommodating at least 1400 km of shortening forming the current expression of the Himalayan orogenic arc. In the Indian part of the orogen, intense folding of the Tethyan Himalaya commenced by at least 50 Ma and lasted until ~17 Ma (Ratschbacher et al. 1994), followed by the development of one of the most important structures in the orogen, the Main Central Thrust (MCT) – Southern Tibetan Detachment System (STDS). Active between the early and middle Miocene, the MCT-STDS accommodated at least 140 km (maybe up to 500 km) of N-S shortening. Prograding southwards, the Main Boundary Thrust (MBT) places the Lesser Himalayan Units above Tertiary sediments starting at <5 Ma in the central Himalaya (DeCelles et al., 1998b). The southernmost active thrust fault, the Main Frontal Thrust (MFT) marks the boundary between the Himalayan orogen and the Indian foreland and juxtaposes the Neogene Siwalik group (Sub-Himalaya) on top of Quaternary sediments.

On the Tibetan plateau, separated from the Himalayas by the IYS, shortening related to several episodes of terrane accretion and final collision with the Indian sub-continent is predominantly accommodated by fold and thrust belts and large-scale strike slip systems. Total shortening within the Qiangtang and Lhasa terranes exceeded 470 km and took place mainly before the Indo-Asian collision (Kapp et al., 2005). During the Tertiary, shortening proceeded in the northern parts of the plateau but no tectonic expression of accommodation of N-S shortening related to the collision with India is reported from within Lhasa terrane. The northern termination of the Tibetan Plateau is marked by the Altyn Tagh strike-slip fault system which initiated between 60-45 Ma (Bally et al., 1986; Yin et al., 2002, 2008a) and accommodated from its eastern to western segments at total of ~470 km (Cowgill et al., 2003), ~360 km (Ritts and Biffi, 2000; Yang et al., 2001; Gehrels et al., 2003a,b), and ~230 km (Yin and Harrison, 2000) of left-lateral strike slip motion. At the western margin of the plateau, the conjugate right-lateral Karakorum fault extends over ~1000 km and links the Muji-Kongar Shan extensional system to the Gurla Mandhata metamorphic core complex within the Tethyan Himalaya (Ratschbacher et al., 1994; Murphy et al., 2002; Murphy and Copeland, 2005; Robinson et al., 2004, 2007). Slip estimates range from ~ 160 km (Robinson et al., 2009) in the north, ~120 km (Searle, 1996; Searle et al., 1998) at its central segment to ~65 km (Murphy et al., 2000, 2002) at its southern end. Fault initiation is believed to have started at 10-9 Ma (Murphy et al., 2002; Robinson et al., 2005, 2007), 16-14 Ma (Phillips et al., 2004; Phillips and Searle, 2007), and as early as 25-22 Ma (Lacassin et al., 2004, Valli et al., 2007, 2008). These two mega structures are one of the most recognizable features on the Tibetan plateau but not the only large-scale strike slip systems. A series of conjugate strike-slip faults (Karakorum–Jiali fault zone, KJFZ) emerge from the BNS and connect to rift systems in the Qiangtang as well as Lhasa terranes. The main phase of shearing along the right-lateral Jiali fault is constrained at 18-12 Ma (Lee et al., 2003). The left-lateral Kunlun fault in northern Tibet is an additional important structure that accommodates eastward extrusion of Tibet since the late Eocene (Jolivet et al., 2003). Trending along the entire northern edge of the Himalayan orogen, the south dipping Great Counter Thrust juxtaposes meta-sediments of the Tethyan Himalaya on top of IYS mélange rocks and in places on top of the Tibetan Gangdese batholith. Initiation age is unconstrained but this structure was active between ~25-9 Ma synchronously with the MCT-STD system to the south.

2.2.2 Initiation and Timing of rifting

A growing number of studies provide constraints on the timing of extensional faulting in central and southern Tibet and the northern flanks of the Himalayas but at this point it is still highly debated if rifting occurred synchronously across the entire Tibetan plateau or if the data suggests spatial and temporal variations in the evolution of these structures.

The maximum age for the initiation of E-W extension within the Lhasa terrane is proposed by Yin et al. (1994) and Williams et al. (2001) who used $^{40}Ar/^{39}Ar$ dating of N-S trending dyke swarms to constrain the earliest stages of extension to 18-13 Ma.

In the Nyainqentanglha range, the central portion of the prominent Yadong-Gulu rift, thermochronological data appear to constrain the initiation of normal faulting to be ~8 Ma (Harrison et al., 1995; D'Andrea Kapp et al., 2005). A maximum age of initiation of E-W extension in the northern Yadong graben at 11-12 Ma is provided by Ratschbacher et al.

(2011) based on the age of the Kari La granite which is cut by N-S tending normal faults. Investigating the northern portion of this rift system, the Gulu rift, Stockli et al. (2002) infer initiation of rifting at ~5 Ma based on apatite (U-Th)/He ages. Reproducible ages as young as 1.7 Ma from the structurally deepest samples also illustrate the substantial magnitude of Pliocene and younger exhumation and the continued rapid rift flank exhumation. This timing appears consistent with the field observation that the Yadong-Gulu rift cross-cuts a normal fault associated with the South Tibetan Detachment System (>11 Ma) and Northern Himalayan Gneiss domes (e.g., Edwards et al., 1996; Edwards and Harrison, 1997; Lee et al., 2000).

North of the Gulu rift, close to the BNS, the Pung Co rift exhibits sinistral-oblique low-angle brittle-ductile normal faulting overprinted by high-angle brittle normal faulting. These events are geochronologically not well resolved but occurred sometime between 18-7 Ma (Ratschbacher et al. 2011).

Detailed apatite and zircon (U-Th)/He data (from here on referred to as AHe and ZHe) from exhumed footwall rocks in central and northern Tangra Yum Co are generally characterized by either elevation-invariant ages clustering around ~6-5 Ma or marked inflection points in age-elevation plots at ~6-5 Ma, both indicative of rapid late Miocene/early Pliocene exhumation (Dewane et al., 2006). The structurally lowest samples from Xuro Co (central Tangra Yum Co) yield AHe ages as young as ~1 Ma illustrating continued rapid exhumation. Most strikingly though, combined AHe and ZHe data exhibit both middle Miocene and Pliocene inflection points suggesting two distinct episodes of rifting at ~15-13 Ma and ~6-5 Ma, with the latter being the more dominant pulse responsible for the modern rift topography. In the Kung Co rift (Fig. 2.1), which represents the continuation of the Tangra Yum Co rift across the IYSZ, no Pliocene cooling ages were observed. Lee et al. (2011) suggest rift initiation at ~13-12 Ma with accelerated exhumation starting ~10 Ma based on AHe and ZHe ages from a vertical transect. More recently, Mitsuishi et al. (2012) proposed an age of ~19 Ma as earliest initiation of ductile E-W extension in the Kung Co area.

Further west, the Lopukangri rift, part of a series of six left-stepping en-echelon basins, is thought to have initiated between 15-14 Ma based on U/Pb, $^{40}Ar/^{39}Ar$ thermochronology, and structural modeling by Murphy et al. (2010). Additionally, Sanchez et al. (2010) suggested a subsequent extensional event beginning of the Pliocene.

The westernmost expression of prominent rifting in the Lhasa terrane is represented by the Lunggar rift system. In the southern part, ZHe ages indicate rift inception between 12-8 Ma followed by rapid extension between 7-5 Ma (Styron et al., 2010). A slightly earlier rift initiation of 14-7 Ma and rapid exhumation at 4-3 Ma has been reported by Sundell et al. (2012) based on AHe and ZHe results from the northern Lunggar rift.

Within the Tethyan Himalaya, the age of the Thakkhola graben has been dated by means of $^{40}Ar/^{39}Ar$ analysis of fracture mineralization (Coleman and Hodges, 1995) and magnetostratigraphic analysis of syn-rift deposits (Garzione et al., 2000, 2003) yielding initiation ages of ~14 Ma and 11-8 Ma respectively.

The Ama Drime massif is thought to be part of the southward extension of the Xainza rift (referred to as Pum-Qu Xainza rift) within the Tethyan Himalaya. Bounded on either side by large-scale normal faults that cut the STDS, this rift segment exposes high-grade metamorphic rocks in its core. Using U-Th/Pb, $^{40}Ar/^{39}Ar$ and (U-Th)/He dating in combination with pressure-temperature estimates, Kali et al. (2010) constrained the initiation of E-W extension between 13-12 Ma. Similar to other rift systems, a second phase of exhumation was suggested to have started between 6-4 Ma.

Quite different from its southern counterparts, rift geometries within the Quiangtang terrane north of the BNS are not as distinctly developed. They trend in a more northeasterly direction and, as the rifts in the Lhasa terrane, seem to be linked to strike-slip faults of the KJFZ. Overall relief is less and extension appears to be more diffusively distributed north of the very discrete Lhasa terrane rifts. Two structures (Muga Purou rift, Gangma Co area) were investigated so far by Yin et al. (1999), Blisniuk et al. (2001) and Ratschbacher et al. (2011) with no age constraints available for the Gangma Co area. Yin et al. (1999) concluded, based on morphological analysis of fault scarps, that normal faults in the Shuang Hu graben were activated <4 Ma and accumulated less than 10 km of fault offset. Controversially, reported mineral cooling ages in Blisniuk et al. (2001) point towards ~13.5 Ma as a minimum estimate of graben formation in the Shuang Hu area.

2.2.3 Models explaining E-W extension

The pieces of the puzzle leading to a coherent picture of the evolution of rifts in Tibet are i) driving forces, ii) boundary conditions, iii) the state of the Tibetan crust, and iv) kinematics. Although this information seems to be increasingly accessible, their interplay in terms of timing and individual contributions is still highly debated. A multitude of different models have been proposed attempting to explain the mechanisms leading to the formation of N-S trending rifts within the Himalayan-Tibetan orogenic system. The various models are grouped into five "end member" categories that are illustrated in Fig. 2.2A-E. From each model, specific predictions about the timing of faulting, the spatial distribution and propagation of rifting, as well as the kinematic interplay of major Neogene structural elements of the Himalayan-Tibetan orogen can be extracted.

Traditionally, the onset of extension has been thought to represent the presence of a thickened crustal root (Molnar and Tapponnier, 1978; Dalmayrac and Molnar, 1981; Coney and Harms, 1984; Burchfiel and Royden, 1985; Dewey et al., 1988). Since elevation is a reflection of crustal thickness, the onset of late Cenozoic E-W extension in Tibet has been interpreted to represent the time when the plateau achieved its present elevation and started to undergo gravitational collapse or spreading (England and Houseman, 1988, 1989; Harrison et al., 1992; Molnar et al., 1993) (Fig. 2.2A). Dewey et al. (1988) proposed that the initial India-Eurasia convergence was taken up by S-directed thrusting in the Himalayas and northward propagating crustal shortening and thickening of Tibetan lithosphere during the time interval from 45-30 Ma. At the end of this period when crustal thickness was doubled, conjugate strike-slip faults started to accommodate shortening. Ongoing shortening further developed the Himalayan thrust belt and extended northwards into the Altyn Tagh and Tien Shan. Their model commenced with uplift of the Tibetan Plateau by about 2 km's at 5 Ma related to delamination of the over-thickened lithospheric root which marked the initiation of widespread E-W extension along N-S trending rifts due to gravitational collapse. Based on this model, the development of N-S trending extensional structures should be contemporaneous in Pliocene times and distributed across the entire plateau.

Armijo et al. (1989) proposed a lateral extrusion model for central Tibet in which active right-slip along the KJFZ decoupled deformation in northern and southern Tibet. Their hypothesis predicts little or no extension in northern Tibet (Fig. 2.2E), but suggests that left-lateral strike-slip faults are kinematically linked to and terminate in N-S trending rifts within the Lhasa terrane. Rifts evolving based on this process would be expected to propagate southward with increasing displacement on the strike-slip faults.

In light of recent results of geologic, geophysical, and geodetic investigations in Tibet, Taylor and others (2003) proposed a model in which significant N-S contraction occurs contemporaneously with N-S rifting in central Tibet and is accommodated by numerous interacting strike-slip and normal fault systems diffusely distributed over a wide region (Fig. 2.2D). This hypothesis appears to be an interesting alternative to the end-member models of lateral extrusion and distributed crustal thickening and implies that the conjugate set of the Altyn Tagh and Karakorum faults may only be one of many conjugate fault systems that have assisted in the distributed, syn-contractional eastward spreading of the Tibetan plateau (e.g., Searle, 1996, 1998, 1999; Murphy et al., 2000; Bendick et al., 2000). This distributed, constrictional shear model for central Tibet elegantly explains the kinematic interplay of strike-slip faults and N-S trending rifts at the terminations or extensional step-overs of these transcurrent faults in central Tibet. Both models, lateral extrusion as well as eastward spreading, are well suited to explain the evolution of rifts linked to the KJFZ. The eastward spreading model, however, does not yield any explanations or mechanisms for E-W extension within the Tethyan realm in southern Tibet and along the northern flank of the high Himalaya (e.g., Thakkola-Mustang, Kung Co, Pum-Qu, and Yadong rifts).

Several workers have suggested that extension in southern Tibet and the Himalayas may have resulted from southward expansion and stretching of the Himalayan arc during progressive shortening (Fig. 2.2C) (Klootwijk et al., 1985; Molnar and Lyon-Caen, 1989; Ratschbacher et al., 1994) or strain partitioning during oblique India-Asia convergence (McCaffrey and Nabelek, 1998; Seeber and Pecher, 1998) (Fig. 2.2B). In these models, E-W extension should be restricted to southern Tibet or at least decrease in magnitude from south to north (if unrelated to gravitational spreading of the entire plateau) and must coincide with times of tectonic activity along major S-verging thrust systems in the Himalayas. Assuming that the Ama Drime massif to the south is in fact part of a greater Xainza – Pum-Qu rift system, this model could infer that the southern segment in the Xainza rift constitutes the northernmost extent of an arc spreading related structure interlinking with the northern part that progressively opened from N-S. Recently, Li and Yin (2008) documented a broad zone of distributed left-slip systems (Dinggye-Chigu fault zone) that initiated at ~4-3 Ma and suggested that this zone transfers slip between the N-S trending rifts. Although the timing does not match the observed low-T constraints from the Xainza rift and Ama Drime massif, it demonstrates the effect of arc-spreading within the Tethyan Himalayas.

2.3 GEOLOGICAL SETTING OF THE XAINZA RIFT

2.3.1 Lithologic units and Rift Morphology

The NNE-SSW striking Xainza rift, located in the central part of the Lhasa terrane, stretches for ~180 km from the Gyaring Co strike-slip fault in the north to the IYSZ in the south (Fig. 2.3 and 2.4). It comprises predominantly Paleozoic and Mesozoic metasedimentary and metavolcanic rocks and syn-contractional Tertiary redbeds as well as Mesozoic granitoids and arc-related plutonic and volcanic rocks of the Gangdese batholith in the south. A clear WNW-ESE structural grain related to the pre-Tertiary contractional history of the Lhasa terrane is preserved by the Paleozoic metasediments throughout the rift. At the northern termination of the rift, E-dipping normal faults are kinematically linked to the NW-SE trending Gyaring Co strike-slip fault. The inception of strike-slip faulting along the Gyaring Co fault is inferred to be entirely late Cenozoic in age as it truncates a thrust system, which in turn cuts Tertiary strata (Taylor et al., 2003). The rift itself consists of several segments characterized by high- and low-angle normal faults with variable fault polarity and complex accommodation zones. For the ongoing discussion they will be referred to as northern, central, and southern segment (see Fig. 2.5). Location of cross sections (Fig. 2.6) as well as longitudinal profiles along the rift axes (Fig. 2.7) is provided in Fig. 2.5.

Terminated by the Gyaring Co strike-slip fault in the north, the northern segment (Fig. 2.8) shows an overall decrease in width and relief towards the south. The along-strike geometry can be further subdivided into three arc-shaped sub-segments. The two northern ones share the same characteristics exposing granitic basement in their central portions and volcanic and/or meta-sedimentary cover units at their terminations. Triangular facets and fault scarps situated right at the range front clearly define the trace of the ~NNE-trending normal faults. No granitic basement is visible in the southern sub-segment and contrary to above, abundant fault scarps are not located right at the footwall/basin interface but offset alluvial fan deposits distal from the range front in an impressive fashion. Both, the range front geometry as well as the trend of the fault scarps indicate a slight change from NNE to NNW trending normal faults. This area also marks the transition from fault slip along the so far dominating E-dipping normal faults to accommodation of E-W extension along a W-dipping fault on the eastern rift shoulder. After turning twice by almost 90°, the eastern fault strand loses its morphological expression within the realm of the Gangdese batholith, terminating the northern segment. Except for a small exposure of Cretaceous granite at the northernmost edge of this segment, the hanging wall exclusively consists of Paleozoic meta-sediments, Cretaceous volcanic rocks, and early Tertiary volcanic rocks of the Linzizong formation.

A pass, which constitutes the drainage divide between the northern segment that is drained towards Gyaring Co and the central and southern segments that drain southward towards the

Indus-Yarlung river, marks the transition zone between the northern and central segment of the rift. Bounded by an N-S trending, E-dipping normal fault on the eastern rift flank, this segment shares familiar features, like decreasing peak heights from north to south and fault scarps right at the range front, with its northern counterpart (Fig. 2.9). Granitic basement is exclusively exposed in the northern footwall and towards the south limestones, meta-sedimentary rocks, and volcanic cover rocks of the Linzizong formation are juxtaposed next to Quaternary basin fill. The hanging wall consists of the westward continuation of the Paleozoic sedimentary units partly covered by an extensive middle Miocene tuff, the youngest unit observed in the entire rift.

Separated from the central segment by another topographical high, the southern segment is structurally dominated by an E-dipping normal fault bounded exhumed block of middle Miocene granite. An almost 30 km straight array of triangular facets impressively marks the trace of this major NNE trending structure (Fig. 2.10). In contrast to the other segments, vast volumes of glacial sediments obliterate an otherwise maybe clearly delimited western boundary of the basin. Nevertheless, it has to be noted that this basin seems to be much narrower than the other ones to the north. The fault zone appears to be truncated at its northern termination by W-dipping normal faults of the central segment, exhibiting a clear overprinting relationship. The restriction of volcanic cover rocks to this transition zone implies that fault throw was not sufficient to expose underlying granitic basement suggesting that normal fault offsets are at a minimum in this particular area and increase towards the north, respectively the south in the adjacent segments. Approaching the southern termination of the Xainza rift near the IYSZ, displacement is transferred westward from the major E-dipping normal fault zone by a left-lateral accommodation zone and partitioned into a series of smaller E-dipping normal faults. The southern extent of normal faulting is not well defined, definitely extends south of the IYSZ but soon loses its clear morphological expression within the Flysch zone. It has been argued that the normal fault bounded Ama Drime massif, part of the Pum-Qu rift, marks the southern continuation of the Xainza rift, an observation in agreement with other rifts in central Tibet that connect southward with exhumed northern Himalayan gneiss domes (e.g. Kung Co half graben, Yadong rift).

Besides the main rift axes, there is another structure to the west of the northern segment that seems to be related to the evolution of the Xainza rift. Solely based on analysis of satellite imagery, this geomorphological low is interpreted as a pull-apart basin bounded by ~ENE trending strike-slip faults. The northern as well as southern ridges are predominantly covered by a ~15 Myr old tuff potentially constraining a maximum age for initiation of this structure although it has to be noted that no information about the age of the basin fill is available. There is no obvious geomorphic expression of the northern strand connecting through the rift flank but its extrapolated trace following a present river bed cuts the western rift flank right at the position where the geometry changes from NNE to NNW trending rift boundaries. The northern slope of the drainage paralleling the suggested fault trace is composed of an estimated 200 m thick sequence of inter-bedded conglomerates, sandstones, and mudstones (Fig. 2.11). The age of these fluvial sediments is unconstrained but their position well above the modern rift basin indicates that they significantly pre-date the modern alluvium. No other valley along this section of the northern segment exhibits a similar unit which could imply that these sediments were deposited by a paleo-river unrelated to the current drainage pattern. Further west, the fault strand defines a triangular area of low elevation as part of a conjugate strike-slip system together with the Gyaring Co fault.

2.3.2 Structural Geology

The structural evolution of the Lhasa terrane in the studied area is dominated by two generations of deformational events with very distinct characteristics. Paleozoic mudstones were slightly metamorphosed during development of a S-verging fold and thrust belt as a consequence of northward drift of the Lhasa terrane towards the Quiangtang terrane and the subsequent closure of the Bangong Ocean during the Jurassic. A penetrative ESE/SE trending crenulation cleavage as well as large and small scale folding is observable in the now phyllites and slates throughout the rift. Orientations of foliation planes vary dependant on the folding but show a general E-W trend. Crinoids-bearing limestones within the phyllites macroscopically lack deformational structures which might be attributed to strain partitioning into the weaker meta-mudstones. A minimum age of cessation of this early shortening event is given by the unconformable overlaying Linzizong volcanic sequence (~60-50 Ma) that does not exhibit any contractional structures. Sub horizontal flow layering and Fiammi's indicate little to no disturbance following their deposition during the early Tertiary.

The second, and of particular interest with respect to this study, deformational event is related to the opening of the rift along a ~N-S axes, crosscutting the older structural grain almost perpendicular. Slickensides, slickenlines, and joint orientations are consistent with normal faulting along the major rift bounding fault strands discussed above. In the central segment, dip-slip on ~N-S trending slickensides is well preserved in the carbonates but somewhat surprisingly, the majority of measured fault planes dip towards the E. This set either constitutes conjugate faults to the rift bounding, W-dipping master fault, or represents the northward extension of the E-dipping normal fault in the southern segment.

Within the southern segment, brittle style of deformation is manifested by a high density of steeply dipping normal faults that in most cases can be traced from the bottom to the top of the exposed range front. Slickenlines generally plunging at about 45º indicate that a considerable amount of strike-slip movement occurred along these faults.

Throughout the rift, no ductile structures related to E-W extension were observed, a crucial fact that has important implications for the later discussion of (U-Th)/He results, subsequent modeling as well as comparison to other rifts on the Tibetan plateau.

2.4 (U-Th)/He THERMOCHRONOLOGY

(U-Th)/He dating of a range of mineral phases is now a well-established thermochronological technique widely applied in geological, tectonic, and geomorphologic studies (e.g., Zeitler et al., 1987; Lippolt et al., 1994; Wolf et al., 1996, 1998; House et al., 1997, 1999; Farley, 2000; Reiners et al., 2000; Stockli et al., 2000; Reiners, 2002; Farley and Stockli, 2002; Ehlers and Farley, 2003; Carter et al., 2004). The method is based on the decay of ^{235}U, ^{238}U, and ^{232}Th by alpha (^{4}He nucleus) emission. According to experimentally derived diffusion kinetics, different mineral phases will show a characteristic response, that is total, partial, or no loss of ^{4}He, during a given t-T history. ^{4}He is completely expelled from apatite at temperatures above ~80°C and almost totally retained below ~40°C (termed the He partial retention zone, HePRZ) (Wolf et al., 1996, 1998; House et al., 1999; Stockli et al., 2000). The thermal sensitivity of this system is lower than that of any other widely used isotopic thermochronometer. Assuming a mean annual surface temperature of 10±5°C and a geothermal gradient of 25°C/km, the relevant temperature range is equivalent to depths of ~1 to 3 km. Thus, the apatite (U-Th)/He system can be applied to investigate a variety of geologic processes in the uppermost part of the crust, such as rifting, mountain building, erosional exhumation, and landscape evolution. Besides apatite, zircon is the most commonly used (U-Th)/He thermochronometer with a HePRZ ranging from ~190 to ~140°C (e.g., Reiners, 2005). Using the same geothermal gradient from above, zircon He dating allows insight into the time span when the samples resided at ~7-5 km crustal depths. Each mineral phase on its own can provide substantial information about the thermal history of the sample collected in the field but the true power of He-dating lies in the combination of samples from geologically meaningful sample arrays, each of the samples providing several mineral ages. Because of the characteristic temperature sensitivity of each mineral phase, (U-Th)/He ages are expected to vary systematically with depth in the stable crust (Wolf et al., 1996, 1998; House et al., 1999; Stockli et al., 2000). The increase in depth, and thus temperature, results in a measurable reduction of apparent ages by diffusive loss of He. In N-S trending rifts in central and southern Tibet, high- and low-angle normal faults have accommodated major crustal extension. The associated mountain ranges correspond to uplifted rift flanks that have been exhumed during normal faulting, exposing rocks brought from substantial depths. If fault slip has been rapid and of sufficient magnitude to exhume samples from the zero retention zones, (U-Th)/He will directly date the timing of faulting and footwall exhumation (e.g., Stockli et al., 2000; Stockli, 2005). At increasingly shallow paleo-depths, apparent ages will become older, because He at least partially accumulates within the mineral grains before exhumation commences. The observed (U-Th)/He ages in these exhumed partial retention zones may be used to estimate the pre-extension paleo-temperatures of samples from various depths and may also be used to estimate the pre-extensional geothermal gradient. Furthermore, these results constitute the basis for subsequent modeling to derive quantitative measures of exhumation rates and fault slip from compatible time-temperature evolutions.

This investigation relies on samples collected along vertical transects in rapidly exhumed footwall units as well as additional single samples from hanging wall and footwall outcrops. The extraction of valuable information regarding the evolution of the studied area and its implications for E-W extension on the Tibetan plateau is the ultimate goal of this study.

2.4.1 Analytical Methods

After mineral separation using various mechanical and physical techniques, 1-3 Inclusion-free, euhedral apatite grains with a minimum diameter of 60 µm were loaded into platinum packets and subsequently degassed for 5 minutes at ~1080°C with a Nd-YAG laser. For each sample, 3-6 packages (= aliquots) were analyzed. After adding 3He spike and gas purification, 4He/3He ratios were measured on a quadrupole mass spectrometer. A second heating cycle assured that all (>99%) of He was extracted from the mineral. Re-extracts higher than 1% usually indicate the presence of micro-inclusions not recognized during the selection process. In that case, these aliquot ages were not included in the final age calculation but still listed in the data tables and marked accordingly (*). Apatites were then dissolved in 100 µl ~25% HNO_3 U-Th-Sm Spike solution, cooked for 90 min at ~80°C, and diluted to a final 600 µl solution.

For zircon and titanite, only single grains were loaded into platinum jackets and heated for 10 minutes at ~1280°C. This routine was repeated until >99% of He was extracted. Dissolving these silicates is not as straightforward as for apatite and involves dissolution in special pressure digestion vessels at high temperatures, first in a 7N HNO_3-HF-Spike mix for 4 days at ~220°C, and subsequently (after dry-down) in 6N HCl for 12 hrs at ~180°C. Following dry-down, adding

100μl concentrated HNO_3 and heating for 45 minutes at ~90ºC assured dissolution of any formed compounds (e.g. Th salts). Diluting with 1 ml of H_2O finalized the procedure.

In the final step, parent isotopes were measured on a VG-PQ2 Inductively Coupled Plasma Mass Spectrometer (ICP-MS) and the He age was calculated from parent and daughter concentrations.

In the case of insufficient apatite quality (common because of inclusions), 6 grains were loaded in one platinum packet, completely degassed, and dissolved following the silicate dissolution procedure assuring recovery of parent nuclides that might reside in a non-apatite inclusion. This approach was used as a final resort but has the potential to give reproducible aliquot ages as shown by Vermeesch (2007) and analysis at the Isotope Geochemistry Laboratory at the University of Kansas (Stockli, pers. comm.).

2.4.2 (U-Th)/He Results

Fig. 2.12 presents the sample locations with their corresponding age information (average ages from multiple aliquot analyses) which consist of a combination of U/Pb, ZHe, AHe, and for one sample Ar/Ar data. The inset, a cross plot of all analyzed He ages versus sample elevations, shows a cluster of elevation invariant AHe ages centered around ~10 Ma whereas ZHe ages are more widely distributed over the entire age range. The individual aliquot analyses for apatite and zircon are given in Appendix B (Table B.1 and B.2).

The northern segment is characterized by early/middle Miocene zircon and middle/late Miocene AHe ages in the granitic footwall. An apparent increase in ZHe ages up to ~100 Ma towards the southern tip of the central sub-segment and the change in lithology from granitic basement to porphyritic rhyolite, clearly reflects the gradual decrease in magnitude of normal faulting along this fault strand. This is further supported by the aforementioned decrease in normal fault angles and occurrence of strike-slip faulting approaching the southern tip. The maximum ages at this location correspond well with analyzed samples from the volcanic footwall unit and although no U/Pb age is available, the proximity to the Cretaceous granite and Cretaceous ZHe ages points towards post-magmatic cooling above the zircon HePRZ. Samples collected along a vertical transect (VT-A) at the northern edge of the Cretaceous granite reveal an overall decrease of early Miocene zircon He ages at the top towards middle Miocene He ages at lower elevations. Within error elevation invariant apatite He ages suggest rapid cooling at ~10 Ma. Additional samples collected further to the south (04XI04, 04XI05) show comparable ages. Although vertical transects along normal fault bounded footwall units provide most insights into the initiation and magnitude of fault slip, hanging wall samples can add substantial information about the thermal state of the tectonically undisturbed crust prior to E-W extension. As expected, the samples collected from granitic as well as volcanic hanging wall units exhibit late Cretaceous to early Tertiary ZHe and AHe ages consistent with post-magmatic cooling and/or slow exhumation. Two samples, 04XI20 and 04GB04 are of special interest not only for E-W extension but also for the pre-extensional history of the Lhasa terrane. These meta-sandstones show abundant detrital zircon dated between ~500-3,300 Ma by Laser Ablation Inductively Coupled Plasma Mass Spectrometry (LA-ICPMS). Both samples yielded early Tertiary ZHe ages indicating complete thermal re-setting (= reheating above ~200ºC) during emplacement of the Gangdese batholith and Linzizong volcanic sequence between ~65-45 Ma. The proximity of 04XI20 to a 60 Myr old rhyolitic ash flow tuff (Sample 05XI52) with an identical ZHe age gives great confidence in that hypothesis. One might argue that He ages pre-dating this period of extensive plutonism and volcanism do not support this explanation but the range of zircon He ages from Cretaceous volcanics to the north as well as the fairly close AHe ages can be explained by only partial re-setting. Otherwise, ZHe and AHe ages should be relatively close to the magmatic age of the volcanic rocks but this theory will be further tested in the modeling section. ZHe ages from a vertical transect (VT-B) collected in the southern sub-segment of the northern rift segment are within error identical to the U-Pb crystallization age, thus revealing emplacement at a shallow crustal position well above the zircon HePRZ. No apatite data are available for this sample array to further constrain this by (U-Th)/He thermochronology but re-mineralized, flattened pumice clasts harden the evidence for rapid cooling at ~62 Ma related to sub-aerial emplacement.

Consistent with the observation from the north, elevation invariant late Miocene AHe ages results reveal rapid footwall exhumation in the central segment at ~10 Ma. In contrast, ZHe ages are generally older and span, clearly elevation dependant, from the early Oligocene to the early Miocene indicating that the exposed basement resided at shallower crustal levels earlier than the crustal section in the north.

Contrary to all other studied areas within the Xainza rift, elevation invariant late Miocene AHe and ZHe ages from a vertical transect in the southern segment (VT-D) allude to very rapid movement along a major N-S striking normal fault. Samples collected within the Gangdese batholith further south show similar AHe ages as footwall samples from throughout the rift. One exception is sample 05XI92 which is located right at the intersection of the Xainza rift with the Indus-Yarlung river gorge with unusually young apatite (2.4 Ma) together with a late Miocene ZHe age.

Not being able to define clear age-elevation inflection points in the analyzed vertical transects only allows a qualitative determination of times of rapid cooling, but the initiation of these events remains speculative at this point. In order to access this key piece of information, a more quantitative approach needs to be applied to get more insight in the evolution of these fault blocks.

2.4.3 Modeling Approach and Results

Over the last decade, increasing efforts to model the t-T evolution of fault blocks for quantifying exhumation rates and fault slips from (U-Th)/He data, led to a number of very powerful software packages. In general, they allow to forward model cooling ages calculated from user defined thermal histories and/or evaluation of randomly created t-T paths based on their goodness of fit for given ages (inverse modeling). Some of the drawbacks of these software packages are the restriction to single samples or even mineral phases, limitation to forward modeling only, accessibility as well as computational intensity. To accommodate the need to inverse model a suite of samples collected along a vertical transect for apatite and zircon (U-Th)/He dating, a new code called Helium Modeling Package (HeMP) was developed with the technical programming language MATLAB©. Utilizing the algorithms used by HeFTy© (Ketcham, 2005), the inverse modeling approach was modified in the following way. Instead of generating a random thermal history and compare the resulting model age with all sample ages, a temperature offset based on vertical sample spacing and user-defined geothermal gradient(s) is applied and subsequently these modified thermal histories are evaluated only against their corresponding samples. This approach results in better constraint thermal histories because of the linkage between samples of the entire transect utilizing a wider range of temperatures.

An important underlying assumption is that the geothermal gradient remains constant throughout the thermal history, which does not hold true in nature because of changes in erosion rates as a response to uplift along a normal fault and the effects on isotherms by an evolving topography. Given the lack of insight into the sedimentary record and geometry of the rift basins for the study area, as well as the increasing complexity of a model dealing with these additional parameters, the simplification of a fixed geothermal gradient is used in HeMP. During the discussion, the effects on the model results will be assessed in a qualitative fashion.

For all model runs, kinetic parameters of He diffusion in minerals listed in Ehlers et al. (2005, Table 3) were used. To incorporate the sample reproducibility, the 1σ standard deviation around the mean of all aliquots was utilized and the model results were classified into acceptable and good fit solutions based on the Kolmogorov-Smirnoff statistical test routine applied by Ketcham (2005). The lack of higher temperature sensitive thermochonologic data (e.g. $^{40}Ar/^{39}Ar$) for the majority of the samples but especially for the vertical transects renders the evaluation of the thermal history below the zircon HePRZ temperature interval almost impossible. To somehow be able to compare the vertical transects to each other, 50 Ma and 350°C was chosen as starting condition for the model runs based on the well documented volcanic flare-up between ~60-50 Ma and its likely perturbation of the thermal state of the crust at this time. Exempt from this setup is the southernmost vertical transect because of an additional constrain, a ~15 Ma U/Pb zircon crystallization age. All vertical transects were modeled with geothermal gradients ranging from 20-100ºC in 2ºC increments.

Fig. 2.13 summarizes the modeling results for all vertical transects. Left graph shows the t-T paths that lead to acceptable fits and a histogram of number of fits for each individual geothermal gradient. Fits for geothermal gradients of 24 and 26ºC/km are highlighted in blue and represent assumed pre-extensional values for stable crust. In red, t-T paths for the highest acceptable geothermal gradients are shown. Right graphs show the age versus elevation relationship of the analyzed samples and the colored lines represent the connections between the model ages for each t-T path using the same color scheme as above. Although each vertical transect model shows changes from slow to rapid cooling, the large number of overlying lines makes it difficult to define the earliest time of possible rift initiation. Fig. 2.14 shows the average thermal histories and cooling rates for each geothermal gradient as well as the derived exhumation rates and total accumulated exhumation. Higher geothermal gradients yield better defined inflection points in the model results and are pushed towards younger ages but peak values for cooling and exhumation rates overlap with the corresponding peaks of cooler geothermal gradients. Based on the average model results, initiation of E-W extension is chosen to be represented by increasing cooling rates for the pre-extensional geothermal gradient (24-26ºC/km) and is highlighted as thick dashed line in all the plots. As expected, the geothermal gradient does not have a major impact on the overall shape of the matching thermal histories in cases of fast cooling, but the resulting exhumation rates and accumulated exhumation calculated from the t-T paths and applied geothermal gradients vary drastically. Lacking control over emplacement depth and cooling path of the granitoids, the discussion of these derived values will focus on the time since rift inception. As a first order estimate, elevation invariant He ages can be used to determine a minimum amount of exhumation because i) all samples had to be at depths below their corresponding HePRZ, and ii) the entire sampled crustal section had to be moved/cooled through the HePRZ quickly enough so that the lowermost sample cooled to temperatures below the lower bound of the HePRZ at the same time or shortly after the samples above. As a consequence, the minimum amount of exhumation required equals the thickness of the HePRZ plus the elevation difference between the top and bottom sample of sampled section. With the modeled range of geothermal gradients the values for exhumation through the apatite HePRZ are 1.8-4.6 km's

(VT-A), 1.7-4.5 km's (VT-D), and 1.9-4.7 km's (VT-E). Because VT-E also exhibits elevation invariant ZHe ages equal to the AHe ages, this value increases to 3.7-10.7 km's.

Modeling results for VT-A show a change from slow to faster cooling between 17-16 Ma. Low exhumation rates of less than 0.2 km/Myrs increase towards peak values of 1-2 km/Myrs at ~10 Ma yielding 2-8 km of exhumation since rift initiation.

In the central segment (VT-D), a clear shift towards accelerated exhumation is less obvious but seems to happen around 15-14 Ma. As above, peak cooling rates are established ~10 Ma and accumulated exhumation ranges from less than 1 to 4 km's.

A combination of zircon U/Pb, biotite $^{40}Ar/^{39}Ar$, zircon (U/Th)/He, and apatite (U/Th)/He data for VT-E gives superb control over the thermal evolution of this footwall block. Starting with granite emplacement at 14-13 Ma, the granite cools down to 250-350ºC at ~12.5 Ma as constraint by $^{40}Ar/^{39}Ar$ data. After a period of slow cooling, rapid cooling commences at ~9 Ma moving the entire ~850 m thick crustal section quickly through the ~220-40ºC isotherms followed by slow cooling to an estimated average annual surface temperature of 5ºC. Peak cooling rates are obtained at ~7 Ma and exhumation is in the order of 3.5-11 km's.

For simple scenarios like exhumation along rift bounding faults as in the Xainza rift, the geothermal gradient has to increase over the period of accelerated exhumation due to advective heat transfer and compression of isotherms close to the surface. Estimates of pre-extensional geothermal gradients are sparse but based on the present α-β transition of quartz Mechie et al. (2004) suggested average values of 39°C/km and 25°C/km for the Quiangtang and Lhasa terrane. Styron et al. (2013) proposed 40°C/km as pre-extensional thermal gradient based on their preferred thermal modeling results from the Lunggar rift. As a result of these observations and the transient nature of the geothermal gradient during accelerated cooling, exhumation calculated from the lowest geothermal gradients must be the best estimate for maximum exhumation. Given the skew of number of fits towards lower geothermal gradients and a pronounced drop of fits at ~40°C/km (VT-D, VT-E) the pre-extensional geothermal gradients should fall within the range of 25-40°C/km with higher confidence in the lower values.

Besides vertical transects, a number of single samples with ZHe and AHe age pairs from footwall and hanging wall units are modeled using individual aliquot ages instead of aliquot means. Footwall sample model runs utilize the same setup as VT-A and VT-D, hanging wall samples are run with an initial constraint at 110 Ma and 350ºC and two additional constraint boxes that allow either monotonic cooling or re-heating past 85 Ma to account for the possibility of He age re-setting related to elevated temperatures during the extensive early Tertiary magmatism and volcanism. A total of 100,000 randomly created t-T paths are tested and Fig. 2.15-17 show the resulting acceptable fits color-coded by aliquot combinations. Sample names denoted with '*' indicate that the initial run yielded incomprehensive results based on too few aliquots that fit the same t-T path. In these cases, it was required to increase the 1σ age uncertainty from 3% to 4% to yield better defined thermal histories. Starting in the north with the only granitic hanging wall outcrop encountered in the northern and central segment, sample 04XI03 serves as the best estimate for cooling rates of crust that underwent no or little thermal disturbance related to rifting processes. Fitting t-T paths indicate that that the sample resided at temperatures at ~200ºC at ~60 Ma. Before that, it either cooled to temperatures as low as 40ºC and underwent reheating or just monotonically cooled. Past ~60 Ma, a well defined cluster of t-T paths show cooling rates of ~7ºC/Myr followed by less than 1.5ºC/Myr starting at ~40 Ma. Assuming a geothermal gradient of 25ºC/km, this equates to exhumation rates of ~0.3 km/Myr and 0.06 km/Myr respectively which is within the range of pre-extensional exhumation rates determined from the vertical transects for equivalent geothermal gradients. 04XI20 is a meta-sandstone collected close to the southeastern end of the northern segment. Similar to 04XI03, the sample resided at temperatures between 200-150°C at ~50 Ma and follows the same trend with initial higher cooling rates followed by slow cooling after ~40 Ma. These t-T histories are in excellent agreement with the results from the Bangoin gneiss NE of the Xainze rift (Hetzel et al., 2011) confirming the very low erosion rates in the interior of the plateau away from tectonically active regions since at least 40 Ma. Another meta-sandstone collected outside the rift (04GB04) provides another data point for the similar background cooling history of samples undisturbed by extensional processes within the rift. Close to the intersection of the main rift bounding normal fault and the Gyaring Co strike-slip fault, PX05 constitutes the northernmost analyzed footwall sample during this study. Very similar to the results obtained from VT-A, initiation of rifting seems to have occurred ~15 Ma. 04XI04 and 04XI05 are footwall samples collected along the granitic range front south of VT-A in the northern segment. Both yield acceptable solutions similar to VT-A indicating accelerated cooling ~15 Ma. 04XI04 demonstrates well the issues with single sample modeling that is that the solutions converge within the HePRZ temperature ranges of the analyzed phases (~140-190ºC for zircon, ~40-80ºC for apatite) but quickly diverge outside of them. In this example, initiation of rapid cooling could have started as early as 20 Ma or as late as 10 Ma. At the southern end of the range front, sample 04XI08 stems from an extensive hyperbyssal granitoid that exhibits ZHe ages that progressively increase in age towards the south. A wide range of acceptable thermal histories solutions makes it difficult to get insight into the thermal evolution of this sample. AHe ages are in agreement with the northern samples but the ZHe ages are well above the ones collected from the Cretaceous granite. Combining the available lithologic, structural, and thermochronological data, this part of the rift seems to represent a transition from larger magnitude uplift in the north exposing plutonic basement rocks to less exhumation on the southern tip of this fault strand.

In the southern segment, 05XI80 shows identical thermal evolution as VT-E. This sample was collected further up the valley and not along the triangular facet and therefore excluded from the VT-E model. Thermal history models for samples collected southward towards the IYSZ again show similar patterns as already discussed. 05XI91 and 05XI92 indicate rapid cooling from temperatures within the zircon HePRZ past 10 Ma similar to VT-E whereas 05XI90 and 05XI94 show a less clear trend but converge at ~20 Ma and ~170°C and ~10 Ma and ~60°C. Fig. 2.18 summarizes the modeling results showing their spatial distribution across the Xainza rift.

2.5 DISCUSSION

2.5.1 Evolution of the Xainza rift

Combining the morphologic expression of the Xainza rift with the results from thermal modeling gives an intriguing picture of the evolution of this structure. Based on the selection of initiation of E-W extension, a temporal trend from an early inception in the north to a later but more rapid episode of accelerated exhumation in the south is obvious. This finding is supported by the shape of the rift that suggests progressive, zipper-like opening from north to south triggered by the right-lateral Gyaring Co strike-slip fault. The extent of the ~ENE trending strike slip fault that created the pull-apart basin to the west is unconstrained but if it indeed represents a regional conjugate set to the Gyaring Co fault then it could have played an important role in the early history of the rift. On the basis of field observations integrated with the thermal history modeling results, a proposed model of the evolution of the Xainza rift is shown in Fig. 2.19. Starting as a early as 17-15 Ma, the primordial Xainza rift opened within a triangular zone bounded by the Gyaring Co fault in the north and a conjugate strand in the south. Extension most likely was diffuse across this zone but more localized along a series of small offset, arcuate normal faults at the western extent. The southern strike-slip fault represented a morphological low (similar to the modern trace of the Gyaring Co fault) and a paleo-river system drained into the early rift basin. Ongoing extension led to the abandonment of the southern strike-slip fault and the rift propagated further south along a SSE-trending axis to the present extent of the northern segment. Around 12-10 Ma, a left-lateral transfer fault initiated the central segment. At this point in time, the voluminous Miocene granitic body presently forming the backbone of the southern segment was already emplaced at depth. It is highly speculative if rifting would have proceeded in a similar fashion connecting separate basins through step-over transfer zones or if the rift would have terminated before reaching the IYSZ. The sudden change from W-directed faulting in the central segment to E-directed extension along a major normal fault at the eastern side of the southern segment suggests that the rift geometry is strongly influenced by the thermal anisotropy created by granite emplacement. This could be responsible for the mismatch between the proposed evolution which requires a gradual decrease towards zero fault throw in a, in map view, (ideally) V-shaped rift valley and the observed increase of fault throw towards the center of the southern segment. As this crustal anomaly disappears towards the south, the main fault strands splits into several fault splays whose surface expression disappears south of the IYSZ. Both, the northern and central segment show peak cooling rates at ~10 Ma which is interpreted as the main stage of rapid uplift and subsequent re-equilibration of the compressed isotherms. Prior to this event, strike-slip faulting was the dominant process and relief most probably was little. Normal faulting and rift shoulder uplift in the northern segment masked a possibly more pronounced geomorphic expression of the southern conjugate fault strand although this area is still the least elevated footwall portion in the entire rift. A newly developing drainage divide cut the paleo-river and the modern stream cut back into the fluvial deposits which are now exposed several hundred meters above the recent basin floor. In the southern segment it is very difficult to determine initiation of fault throw and surface uplift because it is unclear if a change of cooling rates is function of tectonics or simply post-magmatic cooling. Nevertheless, peak cooling rates related to normal faulting are established slightly later than in the north at ~7 Ma. Throughout the entire rift, abundant fault scarps directly along or parallel to the rift bounding normal faults indicate ongoing footwall uplift. This is not clearly reflected in the modeling results of the vertical transects which could be related to the fact that the lowest available outcrops are usually well above the current basin floor and the rocks exhibiting potentially younger He ages are buried under widespread glacial sediments. Sample 05XI92 collected just north of the IYSZ at the lowest elevations of the rift indicates how young the AHe ages can get and the single sample modeling results yield a more or less constant rate of fast cooling from ~8 Ma to present time. Observations from other rifts throughout Tibet (e.g. Armijo et al., 1986) and recent GPS studies (e.g. Zhang et al., 2004) confirm that rifts throughout the Lhasa terrane are actively extending.

If the estimated maximum cumulative exhumation in the Xainza rift (~11 km) is solely a result of movement along normal faults then ~5-8 km of horizontal extension must have been accommodated assuming fault angles of 45-60°. These values are less than the suggested slip on the Gyaring Co fault of 12.5 ± 4 km (Taylor et al., 2003) and do not compare either with the modern basin widths of 8-12 km. As a consequence, the high-angle normal faults need to flatten at depth to increase E-W extension. The arcuate nature of the normal faults in the northern segment as well as observations from other areas suggests that the high-angle normal faults are not crustal-scale structures but sole into a sub-horizontal detachment at mid-crustal levels.

2.5.2 Rifting in Southern Tibet

In comparison, the Xainza rift reveals similarities but also important differences with other prominent rifts within the Lhasa terrain. As other rifts, the Xainza rift is a composite structure with sub-basins connected through strike-slip transfer faults. This investigation confirms the proposed causal relationship between strike-slip faulting along strands of the KJFZ and rifting in southern Tibet and that extension indeed propagated from north to south. Comparing magnitudes of E-W extension, thermokinematic modeling revealed a total displacement of 21-26 km along the low-angle Nyainqentanglha fault that soles into a subhorizontal detachment at ~12 km depth (D'Andrea-Kapp, 2005). Sundell et al. (2013) and Styron et al. (2013) report net extension of 17-26 km in the northern, and 10-21 km in the southern Lunggar rift along low-angle detachment faults. Both observations exceed the estimated amount of E-W extension in the Xainza rift. The most striking difference is the absence of an exposed ductile detachment fault which has been observed in other areas like the Lunggar, Lopukangri, and Yadong Gulu rifts. Fault angles seem to be higher in the Xainza rift although there is some evidence for decreasing dips along strike from the northern segment. No such structure is reported from the southern Tangra Yum Co rift as well (pers. comm. Terrence J. Dewane) which raises the question if the rifts in the central portion of the Lhasa terrane underwent a different kinematic history than the structures to the east and west and magnitude of exhumation was insufficient to bring mid-crustal rocks up to the surface. Kapp et al. (2008) suggested that the Lunggar rift and Nyainqentanglha range are metamorphic core complexes (MCC's) in different stages of their evolution. The MCC model requires a thickened, hot crust in order to develop a low-angle detachment fault. In the Nyainqentanglha range as well as the Lunggar rift, Miocene granites are exposed along the detachment fault. Their emplacement might have pre-conditioned the thermal state of the upper crust to allow for low-angle detachment faulting. Neither the Tangra Yum Co nor the northern and central segments of the Xainza rift have Miocene granites exposed in their footwall units. Miocene volcanism is present in the Tangra Yum Co rift (unpublished data, pers. comm. Terrence J. Dewane) and only the footwall of the southern segment of the Xainza rift consists of a Miocene granitoid which lends itself to the conclusion that Miocene magmatism is a pre-requisite for development of MCC's but it's existence does not necessarily trigger their occurrence. As a consequence, the differences between the central and outboard rifts must be related to other factors.

2.5.3 Evaluation of kinematic models

With the information at hand, the previously presented end-member model for E-W extension on the Tibetan plateau can be further evaluated. The preferred model is the distributed, constrictional shear model of Tibet that initiates E-W extension linked to conjugate strike-slip faults along the KJFZ (Taylor et al., 2003). This model is consistent with the observed initiation in the northern part of the rift and progressive opening towards the south. It furthermore explains coeval rifting in northern Tibet. Arc-parallel stretching seems to play a subordinate role but represents a viable mechanism for E-W extension south of the IYSZ. The Pum-Qu rift for example consists of a central horst structure bounded by normal faults on either side that diverge from a common point in the northern part. Contrary to the proposed evolution of the Xainza rift, this morphology suggests opening from south to north. Another observation that does not fit this model is the trend of the individual rifts. If arc-parallel stretching is the dominant mechanism, then the rift axes should align with the radial traces perpendicular to the arc segment. Quite the opposite is true and rift axes actually trend ~NW-SE in the west (e.g. Lunggar rift) and ~NE-SW in the eastern part of the Lhasa terrane (e.g. Nyainqentanglha range). There is no indication that the crustal structure changes significantly going away from the central portion of the Lhasa terrane leading to kinematic variations as the root cause for the present day geometry. Kapp and Guynn (2004) proposed that the fanning pattern was a result of localized collisional stresses along a southern segment of the Himalayan arc. Arc normal pressures along the central part of the Himalayan arc produced principal stress trajectories ($\sigma 2$) consistent with the trend of major rifts in southern Tibet. They used emplacement ages of dyke swarms (~18-13 Ma) reported by Williams et al. (2001) as a proxy for rotation of $\sigma 1$ from horizontal to vertical but noted that vertical stresses were not sufficient to initiate E-W extension along large-scale rift systems at this point in time. This model relies on pressure relief outside the central part by slip on the Karakorum fault and thrusting within the Shillong plateau during rift activation. Biswas et al. (2007) determined that exhumation of the Shillong plateau started 15-7 Ma and the Karakorum fault has been active since at least ~15 Ma, both meeting this requirement. As suggested by Kapp and Guynn (2004) changes in deviatoric stress between 8-4 Ma finally allowed increasing rates of normal faulting leading to the initiation of ~N-S trending rifts in the Lhasa terrane. Similar to the arc-spreading model, the oblique convergence model would require the rifts to propagate from south to north following the northward propagating Indian lithosphere which exerts basal shear on the overlying Tibetan crust. Finally, wholesale collapse of the Tibetan plateau as a consequence of unsustainable plateau elevations needs to be evaluated. This model would require that all rifts initiated at the time when the plateau achieved its maximum elevation and concentrated at areas of maximum elevation. Initial paleoaltimetry studies from several regions using different techniques all suggested that the southern Tibetan plateau was at similar to modern elevations since ~15-11 Ma (e.g., Garzione et al., 2000; Rowley et al., 2001; Spicer et al., 2003; Currie et al., 2005). Rowley and Curry (2006) pushed this estimate further back in time and propose that much of Tibet was at or near its present elevation by Eocene times, undermining the causal relationship between the elevation evolution of the Tibetan Plateau and E-W extension. Although the gravitational potential of the Tibetan plateau undoubtedly influences rifting in Tibet, it acts in conjunction with other tectonic processes and cannot be solely responsible for the modern day observed morphologies.

At this point the different kinematic models have been discussed but why normal faulting occurred when it did is still in question. The Xainze rift seems to be characterized by an early strike-slip dominated phase that transitions to normal fault related accelerated cooling at ~10 Ma. Other studies report an early rift inception in the mid-Miocene followed by a second pulse in the late-Miocene (e.g. Kali et al., 2010, Styron et al., 2013; Sundell et al., 2013). Fig. 2.20 shows a compilation of age constraints on major structures within the Himalayan-Tibetan orogen. A first order observation is that major E-W trending contractional structures south of the Tibetan plateau like the MCT, STDS, and GCT are active during the early/mid-Miocene and estimates for rift initiation either post-date or overlap the latter half of their activity. Murphy et al. (2009) investigated E-W extension in the western part of the Tethyan Himalayas and suggested that the Zada basin was formed by topographic inversion from high mountains to a depression in less than 4 m.y. They concluded that this was triggered by inactivation of arc-normal shortening structures (MCT, STDS, and GCT) and establishment of arc-parallel stretching. Although arc-parallel stretching does not seem to be a significant contributor to E-W extension on the Tibetan plateau, the foreland propagating thrust system in the Himalayas and cessation of N-S shortening structures close to the southern fringes of the plateau could arguably have changed the boundary conditions enough to initiate accelerated E-W extension within the rifts post ~10 Ma.

2.6 CONCLUSIONS

Geological and thermochronological investigations suggest that the Xainza rift initiated at its northern boundary triggered by right-lateral movement along the Gyaring Co strike-slip fault. Timing of rift inception and main phases of rift shoulder uplift is constrained by modeling at ~15-17 Ma and ~12-8 Ma respectively. Furthermore, the results from three vertical transects indicate that the rift opened progressively from north to south, which is in excellent agreement with observations of increasing relief and noticeable wider basin geometries towards the Gyaring Co fault. Based on these findings, models of E-W extension like arc-parallel stretching and basal drag of the lithosphere as main drivers, which predict a south to north directed progression of rifting, cannot be solely responsible for extension on the Tibetan plateau. The constrictional shear model best fits the observations from the Xainza rift.

CHAPTER 2: REFERENCES CITED

Armijo, R., Tapponier, P., and Han, T., 1989, Late Cenozoic right-lateral strike-slip faulting in Southern Tibet: Journal of Geophysical Research, v. 94, p. 2787-2838.

Armijo, R., Tapponier, P., Mercier, J. L., and Tonglin, H., 1986, Quartenary extension in southern Tibet: field observations and tectonic implications: Journal of Geophysical Research, v. 91, p. 13803-13872.

Burchfiel, B. C., Chen, Z., Royden, L. H., Liu, Y., and Deng, C., 1991, Extensional development of Gabo Valley, southern Tibet: Tectonophysics, v. 194, no. 1–2, p. 187-193.

Coleman, M., and Hodges, K., 1995, Evidence for Tibetan plateau uplift before 14 Myr ago from a new minimum age for east-west extension: Nature, v. 374, p. 49-52.

Cowgill, E., Yin, A., Harrison, T. M., and Xiao-Feng, W., 2003, Reconstruction of the Altyn Tagh fault based on U-Pb geochronology: Role of back thrusts, mantle sutures, and heterogeneous crustal strength in forming the Tibetan Plateau: Journal of Geophysical Research: Solid Earth, v. 108, no. B7, p. 2346.

DeCelles, P. G., Gehrels, G. E., Quade, J., Ojha, T. P., Kapp, P. A., Upreti, B. N., Moss, S. J., McCarthy, A. J., DeCelles, P. G., and Giles, K. A., 1998, Neogene foreland basin deposits, erosional unroofing, and the kinematic history of the Himalayan fold-thrust belt, western Nepal. Foreland basin systems; discussion and reply: GSA Bulletin, v. 110, no. 1, p. 2-21.

Dewey, J. F., Shackleton, R. M., Chenfa, C., and Yiyin, S., 1988, The tectonic evolution of the Tibetan plateau: Royal Society of London Philosophical Transaction, v. A, no. 327, p. 301-320.

Edwards, M. A., and Harrison, T. M., 1997, When did the roof collapse? Late Miocene north-south extension in the high Himalaya revealed by Th-Pb monazitr dating of the Khula Kangri granite: Geology, v. 25, no. 6, p. 543-546.

Edwards, M. A., Kidd, W. S. F., Li, J., Yue, Y., and Clark, M., 1996, Multi-stage development of the southern Tibet detachment system near Khula Kangri. New data from Gonto La: Tectonophysics, v. 260, p. 1-19.

Garzione, C. N., DeCelles, P. G., Hodkinson, D. G., Ojha, T. P., Upreti, B. N., DeCelles, P. G., Robinson, D. M., and Zandt, G., 2003, East-west extension and Miocene environmental change in the southern Tibetan plateau: Thakkhola graben, central Nepal

Implications of shortening in the Himalayan fold-thrust belt for uplift of the Tibetan Plateau: GSA Bulletin, v. 115, no. 1, p. 3-20.

Garzione, C. N., Dettman, D. L., Quade, J., DeCelles, P. G., and Butler, R. F., 2000, High times on the Tibetan Plateau: Paleoelevation of the Thakkhola graben, Nepal: Geology, v. 28, no. 4, p. 339-342.

Gehrels, G. E., Yin, A., and Wang, X.-F., 2003a, Detrital-zircon geochronology of the northeastern Tibetan plateau: Geological Society of America Bulletin, v. 115, no. 7, p. 881-896.

-, 2003b, Magmatic history of the northeastern Tibetan Plateau: Journal of Geophysical Research: Solid Earth, v. 108, no. B9, p. 2423.

Harrison, T. M., Copeland, P., Kidd, W. S. F., and Lovera, O. M., 1995, Activation of the Nyainqentanghla Shear Zone: Implications for uplift of the southern Tibet plateau: Tectonics, v. 14, p. 658-676.

Jolivet, M., Brunel, M., Seward, D., Xu, Z., Yang, J., Malavieille, J., Roger, F., Leyreloup, A., Arnaud, N., and Wu, C., 2003, Neogene extension and volcanism in the Kunlun Fault Zone, northern Tibet: New constraints on the age of the Kunlun Fault: Tectonics, v. 22, no. 5, p. 1052.

Kali, E., Leloup, P. H., Arnaud, N., Mahéo, G., Liu, D., Boutonnet, E., Van der Woerd, J., Liu, X., Liu-Zeng, J., and Li, H., 2010, Exhumation history of the deepest central Himalayan rocks, Ama Drime range: Key pressure-temperature-deformation-time constraints on orogenic models: Tectonics, v. 29, no. 2, p. TC2014.

Kapp, P., Yin, A., Harrison, T. M., and Ding, L., 2005, Cretaceous-Tertiary shortening, basin development, and volcanism in central Tibet: Geological Society of America Bulletin, v. 117, no. 7-8, p. 865-878.

Lacassin, R., Valli, F., Arnaud, N., Leloup, P. H., Paquette, J. L., Haibing, L., Tapponnier, P., Chevalier, M.-L., Guillot, S., Maheo, G., and Zhiqin, X., 2004, Large-scale geometry, offset and kinematic evolution of the Karakorum fault, Tibet: Earth and Planetary Science Letters, v. 219, no. 3–4, p. 255-269.

Lee, H.-Y., Chung, S.-L., Wang, J.-R., Wen, D.-J., Lo, C.-H., Yang, T. F., Zhang, Y., Xie, Y., Lee, T.-Y., Wu, G., and Ji, J., 2003, Miocene Jiali faulting and its implications for Tibetan tectonic evolution: Earth and Planetary Science Letters, v. 205, no. 3–4, p. 185-194.

Lee, J., Hacker, B. R., Dinklage, W. S., Wang, Y., Gans, P., Calvert, A., Wan, J. L., and Chen, W., 2000, Evolution of the Kangmar Dome, southern Tibet: Structural, petrologic, and thermochronologic constraints: Tectonics, v. 19, no. 5, p. 872-.

Lee, J., Hager, C., Wallis, S. R., Stockli, D. F., Whitehouse, M. J., Aoya, M., and Wang, Y., 2011, Middle to late Miocene extremely rapid exhumation and thermal reequilibration in the Kung Co rift, southern Tibet: Tectonics, v. 30, no. 2, p. TC2007.

Mercier, J.-L., Armijo, R., Tapponnier, P., Carey-Gailhardis, E., and Lin, H. T., 1987, Change from Late Tertiary compression to Quaternary extension in southern Tibet during the India-Asia Collision: Tectonics, v. 6, no. 3, p. 275-304.

Molnar, P., and Lyon-Caen, H., 1989, Fault plane solutions of earthquakes and active tectonics of the Tibetan Plateau and its margins: Geophysical Journal International, v. 99, p. 123-153.

Molnar, P., and Tapponier, P., 1978, Active tectonics of Tibet: Journal of Geophysical Research, v. 83, p. 5361-5375.

Murphy, M. A., and Copeland, P., 2005, Transtensional deformation in the central Himalaya and its role in accommodating growth of the Himalayan orogen: Tectonics, v. 24, no. 4, p. TC4012.

Murphy, M. A., Yin, A., Kapp, P., Harrison, T. M., Lin, D., Jinghui, G., Deng, X., Ding, L., Liu, X., An, Y., Kapp, P. A., Murphy, M. A., and Manning, C. E., 2000, Southward propagation of the Karakoram fault system, southwest Tibet: Timing and magnitude of slip

The geochemistry characteristics of blueschist in the Gangmar area, Qingtang Block, Tibet: Geology, v. 28, no. 5, p. 451-454.

Murphy, M. A., Yin, A., Kapp, P., Harrison, T. M., Manning, C. E., Ryerson, F. J., Lin, D., and Jinghui, G., 2002, Structural evolution of the Gurla Mandhata detachment system, southwest Tibet: Implications for the eastward extent of the Karakoram fault system: Geological Society of America Bulletin, v. 114, no. 4, p. 428-447.

Ni, J., and York, J. E., 1978, Late Cenozoic tectonics of the Tibetan Plateau: Journal of Geophysical Research: Solid Earth, v. 83, no. B11, p. 5377-5384.

Pan, Y., and Kidd, W. S. F., 1992, Nyainqentanglha shear zone: A late Miocene extensional detachment in the southern Tibetan Plateau: Geology, v. 20, no. 9, p. 775-778.

Phillips, R. J., Parrish, R. R., and Searle, M. P., 2004, Age constraints on ductile deformation and long-term slip rates along the Karakoram fault zone, Ladakh: Earth and Planetary Science Letters, v. 226, no. 3–4, p. 305-319.

Phillips, R. J., and Searle, M. P., 2007, Macrostructural and microstructural architecture of the Karakoram fault: Relationship between magmatism and strike-slip faulting: Tectonics, v. 26, no. 3, p. TC3017.

Ratschbacher, L., Frisch, W., Liu, G., and Chen, C., 1994, Distributed deformation in southern and western Tibet during and after the India-Asia collision: Journal of Geophysical Research: Solid Earth, v. 99, no. B10, p. 19917-19945.

Ratschbacher, L., Krumrei, I., Blumenwitz, M., Staiger, M., Gloaguen, R., Miller, B. V., Samson, S. D., Edwards, M. A., and Appel, E., 2011, Rifting and strike-slip shear in central Tibet and the geometry, age and kinematics of upper crustal extension in Tibet: Geological Society, London, Special Publications, v. 353, no. 1, p. 127-163.

Ratschbacher, L. F. W. L. G. H. C. C. S., 1994, Distributed deformation in southern and western Tibet during and after the India-Asia collision: Journal of Geophysical Research, v. 99, no. B10, p. 19917-19945.

Ritts, B. D., and Biffi, U., 2000, Magnitude of post–Middle Jurassic (Bajocian) displacement on the central Altyn Tagh fault system, northwest China: Geological Society of America Bulletin, v. 112, no. 1, p. 61-74.

Robinson, A. C., 2009, Geologic offsets across the northern Karakorum fault: Implications for its role and terrane correlations in the western Himalayan-Tibetan orogen: Earth and Planetary Science Letters, v. 279, no. 1-2, p. 123-130.

Robinson, A. C., Yin, A., Manning, C. E., Harrison, T. M., Zhang, S.-H., and Wang, X.-F., 2004, Tectonic evolution of the northeastern Pamir: Constraints from the northern portion of the Cenozoic Kongur Shan extensional system, western China: Geological Society of America Bulletin, v. 116, no. 7-8, p. 953-973.

-, 2007, Cenozoic evolution of the eastern Pamir: Implications for strain-accommodation mechanisms at the western end of the Himalayan-Tibetan orogen: Geol Soc Am Bull, v. 119, no. 7-8, p. 882-896.

Rothery, D. A., and Drury, S. A., 1984, The neotectonics of the Tibetan Plateau: Tectonics, v. 3, no. 1, p. 19-26.

Searle, M. P., 1996a, Geological evidence against large-scale pre-Holocene offsets along the Karakoram Fault: Implications for the limited extrusion of the Tibetan plateau: Tectonics, v. 15, no. 1, p. 171-186.

-, 1996b, Geological evidence against large-scale pre-Holocene offsets along the Karakorum Fault: Implications for the limited extrusion of the Tibetan Plateau: Tectonics, v. 15, no. 1, p. 171-186.

Styron, R. H., Taylor, M. H., Sundell, K. E., Stockli, D. F., Oalmann, J. A. G., Möller, A., McCallister, A. T., Liu, D., and Ding, L., 2013, Miocene initiation and acceleration of extension in the South Lunggar rift, western Tibet: Evolution of an active detachment system from structural mapping and (U-Th)/He thermochronology: Tectonics, p. n/a-n/a.

Sundell, K. E., Taylor, M. H., Styron, R. H., Stockli, D. F., Kapp, P., Hager, C., Liu, D., and Ding, L., 2013, Evidence for constriction and Pliocene acceleration of east-west extension in the North Lunggar rift region of west central Tibet: Tectonics, v. 32, no. 5, p. 2013TC003331.

Tapponnier, P., and Molnar, P., 1977, Active faulting and tectonics in China: Journal of Geophysical Research, v. 82, no. 20, p. 2905-2930.

Valli, F., Arnaud, N., Leloup, P. H., Sobel, E. R., Mahéo, G., Lacassin, R., Guillot, S., Li, H., Tapponnier, P., and Xu, Z., 2007, Twenty million years of continuous deformation along the Karakorum fault, western Tibet: A thermochronological analysis: Tectonics, v. 26, no. 4, p. TC4004.

Valli, F., Leloup, P. H., Paquette, J.-L., Arnaud, N., Li, H., Tapponnier, P., Lacassin, R., Guillot, S., Liu, D., Deloule, E., Xu, Z., and Mahéo, G., 2008, New U-Th/Pb constraints on timing of shearing and long-term slip-rate on the Karakorum fault: Tectonics, v. 27, no. 5, p. TC5007.

Williams, H., Turner, S., Kelley, S., and Harris, N., 2001, Age and composition of dikes in Southern Tibet: New constraints on the timing of east-west extension and its relationship to postcollisional volcanism: Geology, v. 29, no. 4, p. 339-a-342.

Yin, A., 1994, Tertiary structural evolution of the Gangdese thrust system in southeastern Tibet: J. Geophys. Res., v. 99, p. 18175-18201.

Yin, A., Dang, Y.-Q., Wang, L.-C., Jiang, W.-M., Zhou, S.-P., Chen, X.-H., Gehrels, G. E., and McRivette, M. W., 2008, Cenozoic tectonic evolution of Qaidam basin and its surrounding regions (Part 1): The southern Qilian Shan-Nan Shan thrust belt and northern Qaidam basin: Geological Society of America Bulletin, v. 120, no. 7-8, p. 813-846.

Yin, A., and Harrison, T. M., 2000, Geologic Evolution of the Himalayan-Tibetan Orogen: Annual Review of Earth and Planetary Sciences, v. 28, p. 211-280.

Yin, A., Rumelhart, P. E., Butler, R., Cowgill, E., Harrison, T. M., Foster, D. A., Ingersoll, R. V., Qing, Z., Xian-Qiang, Z., Xiao-Feng, W., Hanson, A., and Raza, A., 2002, Tectonic history of the Altyn Tagh fault system in northern Tibet inferred from Cenozoic sedimentation: Geological Society of America Bulletin, v. 114, no. 10, p. 1257-1295.

CHAPTER 2: FIGURES AND TABLES

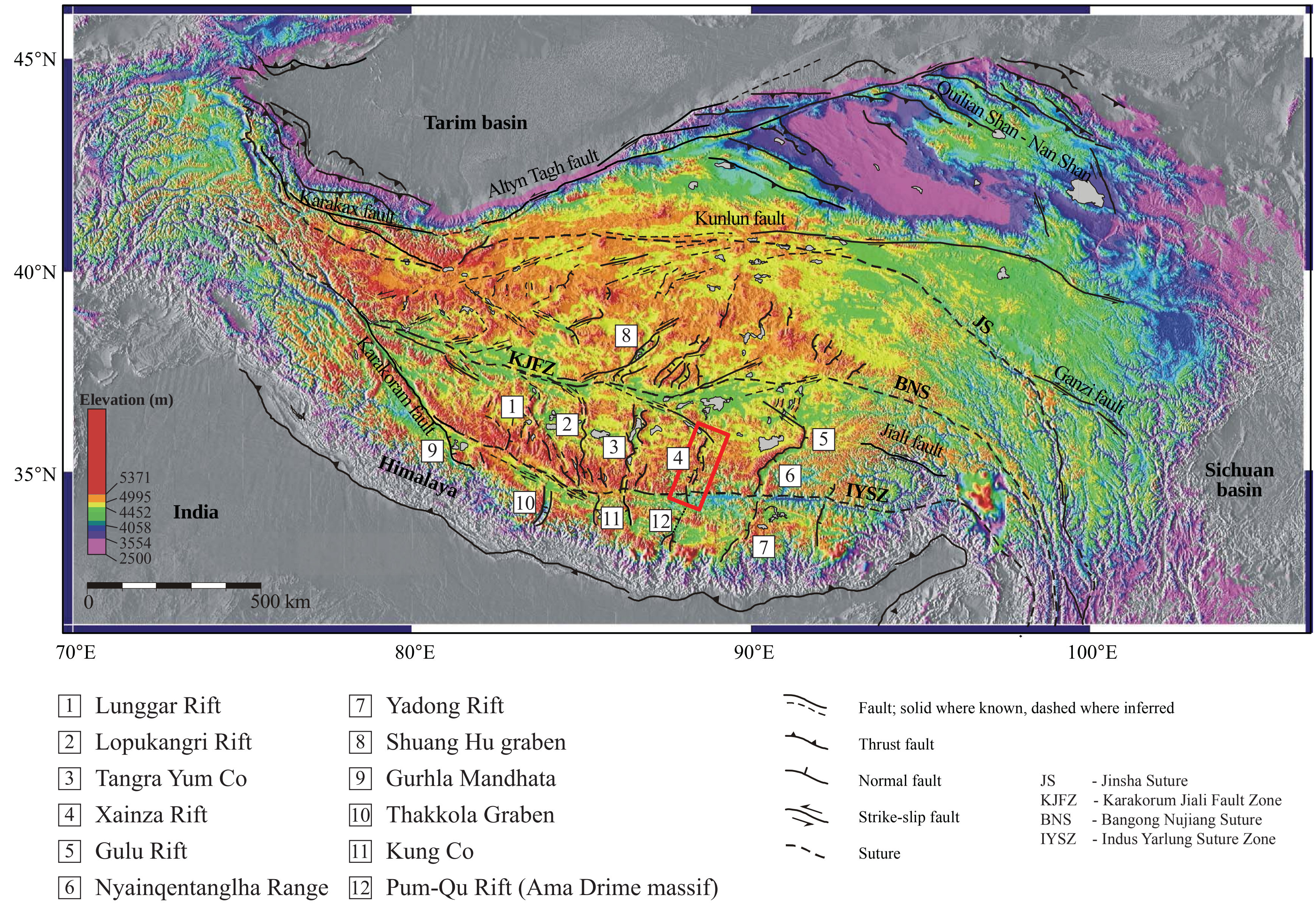
45°N
40°N
35°N
70°E
80°E
90°E
100°E
Tarim basin
Altyn Tagh fault
Karakax fault
Kunlun fault
Quilian Shan - Nan Shan
JS
Ganzi fault
BNS
KJFZ
Karakoram fault
Jiali fault
IYSZ
Himalaya
India
Sichuan basin
Elevation (m)
5371
4995
4452
4058
3554
2500
0
500 km
1 Lunggar Rift
2 Lopukangri Rift
3 Tangra Yum Co
4 Xainza Rift
5 Gulu Rift
6 Nyainqentanglha Range
7 Yadong Rift
8 Shuang Hu graben
9 Gurhla Mandhata
10 Thakkola Graben
11 Kung Co
12 Pum-Qu Rift (Ama Drime massif)
Fault; solid where known, dashed where inferred
Thrust fault
Normal fault
Strike-slip fault
Suture
JS - Jinsha Suture
KJFZ - Karakorum Jiali Fault Zone
BNS - Bangong Nujiang Suture
IYSZ - Indus Yarlung Suture Zone

Figure 2.1: Neotectonic map of the Himalayan-Tibetan orogen. Red box outlines the study area. Modified after Taylor et al. (2003).

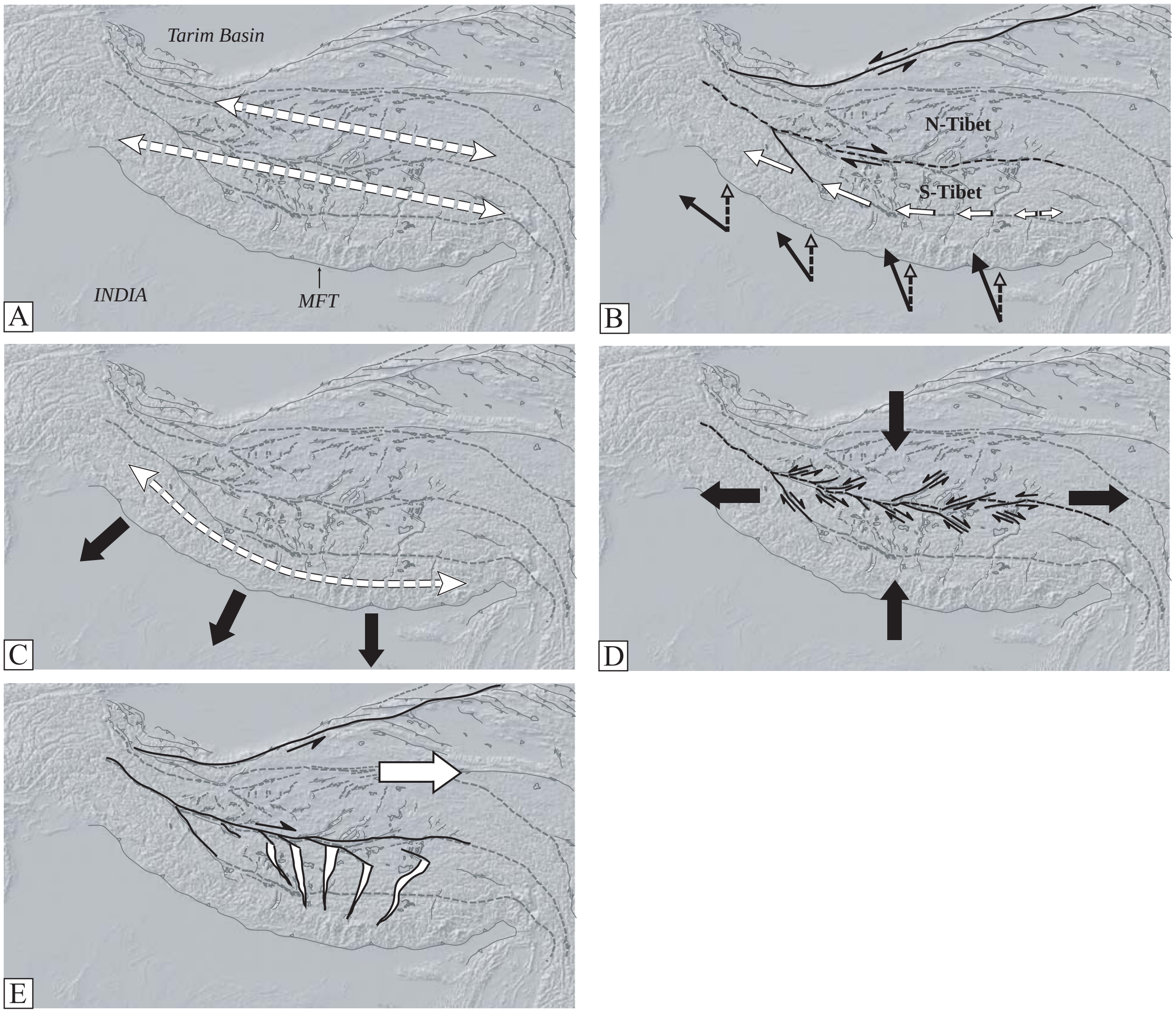

Tarim Basin
INDIA
MFT
A
N-Tibet
S-Tibet
B
C
D
E

Figure 2.2: Different models for E-W extension on the Tibetan plateau. A) Distributed extension related to gravitational collapse. B) Westward movement of S-Tibet relative to N-Tibet because of oblique convergence C) Rifting in S-Tibet due to southward propagation of the Himalayas and arc parallel extension. D) Eastward stretching of Tibet along conjugate strike-slip faults and linked rifts. E) Extrusion of N-Tibet and rifting in S-Tibet. See text for detailed description.

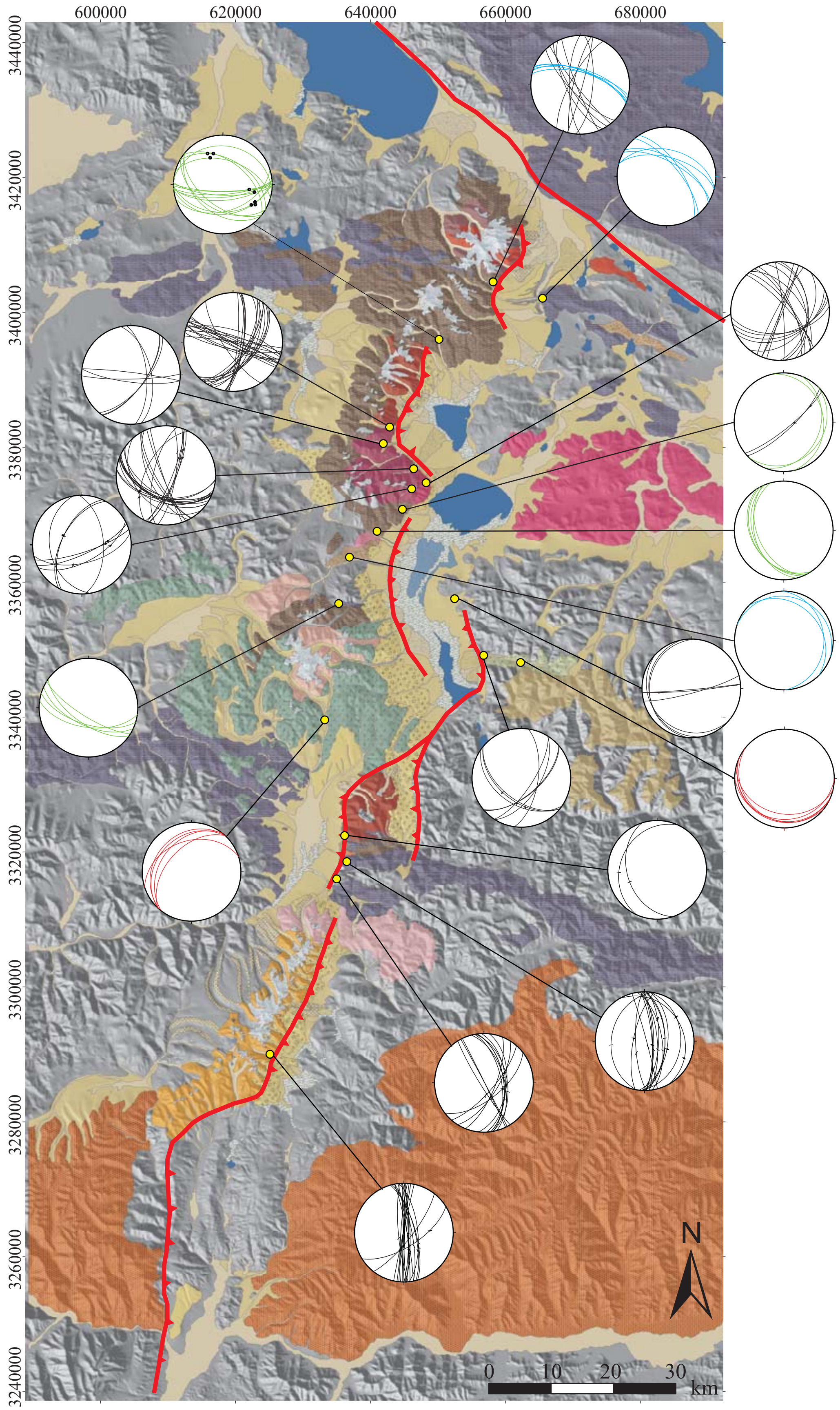
600000
620000
640000
660000
680000
3440000
3420000
3400000
3380000
3360000
3340000
3320000
3300000
3280000
3260000
3240000
N
0 10 20 30
km

Figure 2.3: Geologic map of the Xainza rift with lower hemisphere plots of structural measurements. Basemap is a shaded relief map created from 90 m Shuttle Radar Tomography Mission (SRTM) dataset.

Era	Unit	Description
QUATERNARY	Qice	
	Qlake	
	Qlake2	Dry Lakebed
	Qwet	Marsh/Wetlands
	Qal1	Active Alluvium (Drainages, Fans)
	Qaf1	
	Qal2	Older Alluvium (Drainages, Fans)
	Qaf2	
	Qal3	
	Qco	Colluvium
	Qlm	Lateral Moraine
	Qtm	Terminal Moraine
	Tal?	Quaternary/Tertiary ??? fluvial sediments, tilted!!!
	Tss	
TERTIARY	Tmg	Miocene granitic intrusion
	Tb	Basalt
	Tt1	Intermediate to acidic volcanics of the Linzizong Fm. (tuffs)
	Tt2	
	Tt3	
	Tv1	Intermediate to acidic volcanics of the Linzizong Fm. (andesites, dacites, rhyolites)
	Tv2	
	Tv3	
	Tv4	
	Tv6	
	Tv7	
	Thp	Qtz-porphyr
	Tgb	Granitic Intrusions
	Teg	
	Tpg	
Mz	Kv1	Undiff. volcanic
	Keg	Granite
	TRlg	Granite
	Mcgl	Conglomerate
Pz	Pcarb	Limestone (Crinoids)
	Pshale	Slate/Phyllite

Lower Hemisphere Plots

- metamorphic bedding
- volcanic flow layering
- sedimentary bedding
- Slickensides / Joints
- ● Crenulation lineations / Fold axis
- ← Slickenlines

Figure 2.4: Geologic map - Legend.

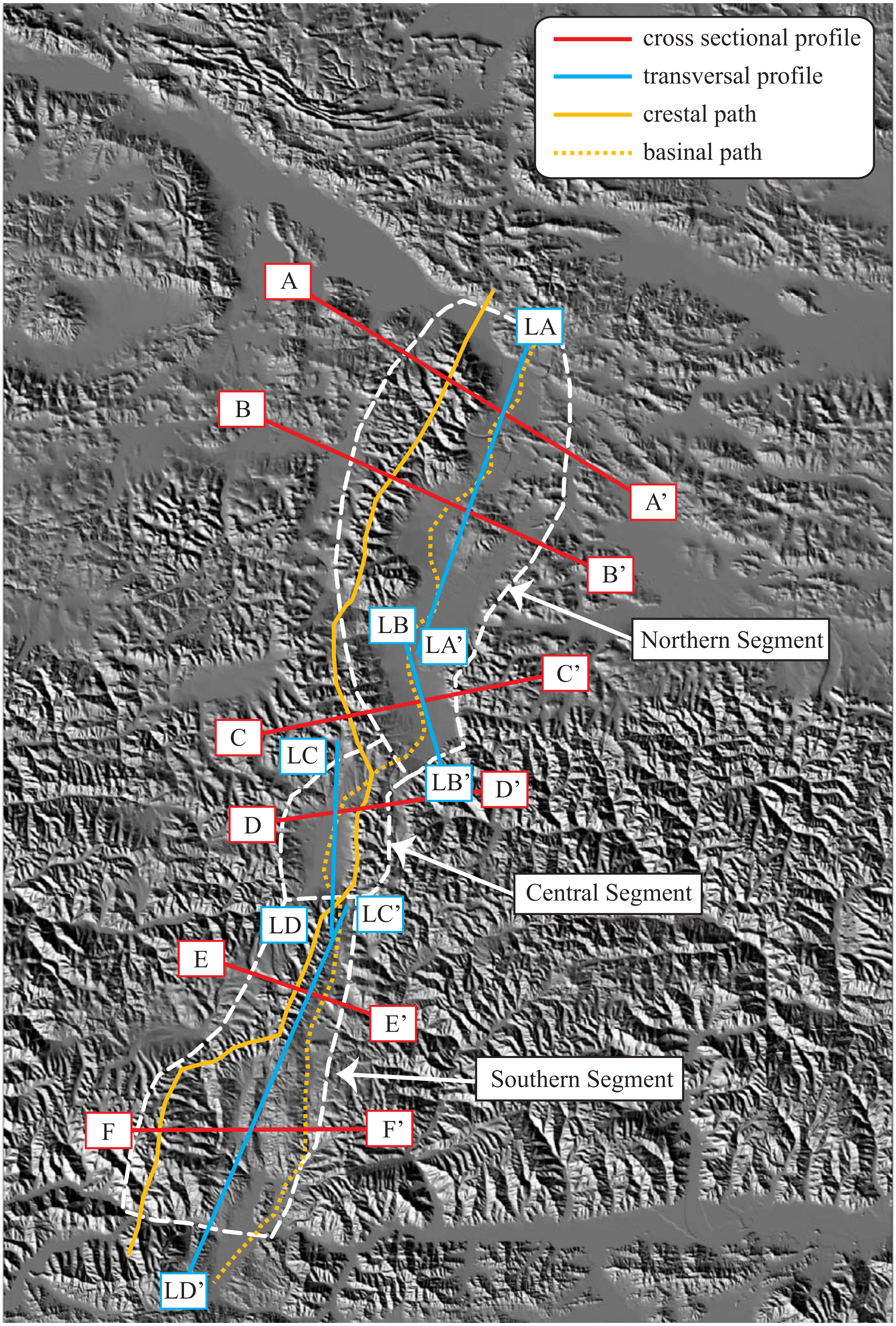
cross sectional profile
transversal profile
crestal path
basinal path
A
A'
B
B'
C
C'
D
D'
E
E'
F
F'
LA
LA'
LB
LB'
LC
LC'
LD
LD'
Northern Segment
Central Segment
Southern Segment

Figure 2.5: Location of cross sections (A-F) and along-strike section (LA-LE) as well as outlines for the northern, central, and southern segments for reference. Basemap is a digital elevation model created from 90 m Shuttle Radar Tomography Mission (SRTM) dataset.

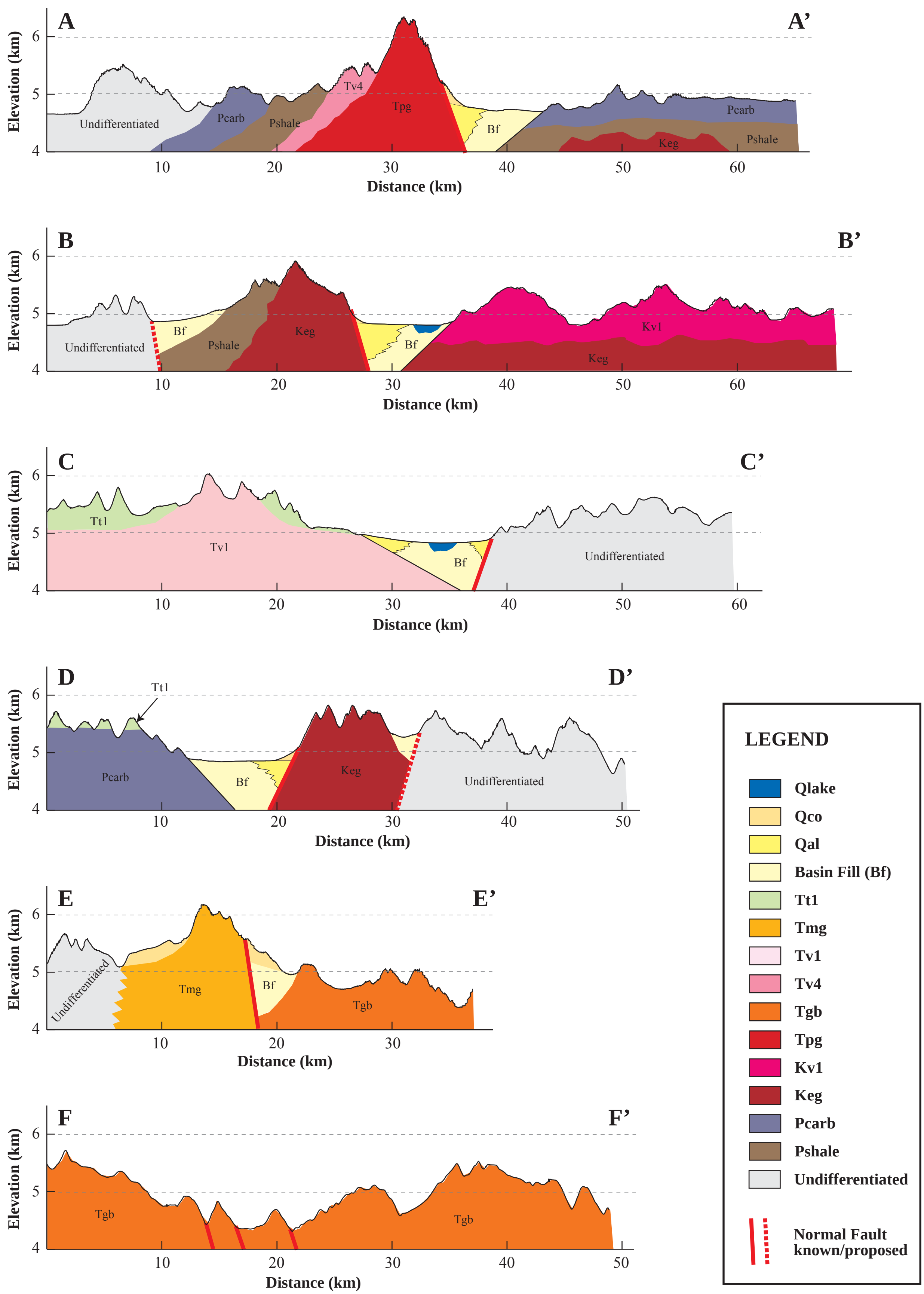
A
A'
Elevation (km)
Distance (km)
Undifferentiated
Pcarb
Pshale
Tv4
Tpg
Bf
Keg
B
B'
Bf
Keg
Kv1
C
C'
Tt1
Tv1
D
D'
Tt1
E
E'
Undifferentiated
Tmg
Tgb
F
F'
LEGEND
Qlake
Qco
Qal
Basin Fill (Bf)
Tt1
Tmg
Tv1
Tv4
Tgb
Tpg
Kv1
Keg
Pcarb
Pshale
Undifferentiated
Normal Fault
known/proposed

Figure 2.6: Cross sections through the Xainze rift at locations outlined in Fig.5. Vertical exaggeration is 5x.

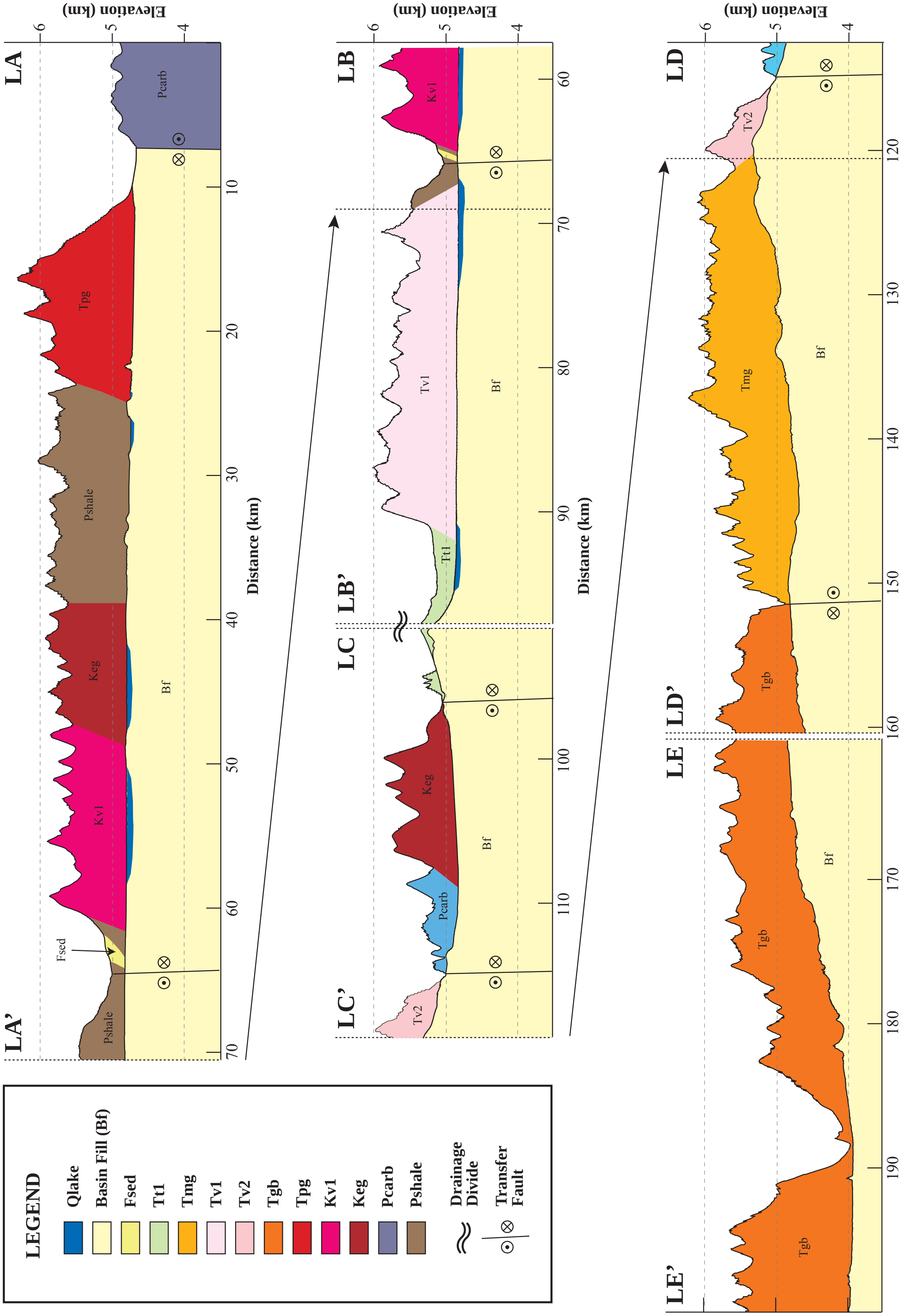
LEGEND
Qlake
Basin Fill (Bf)
Fsed
Tt1
Tmg
Tv1
Tv2
Tgb
Tpg
Kv1
Keg
Pcarb
Pshale
Drainage Divide
Transfer Fault
LA
LA'
LB
LB'
LC
LC'
LD
LD'
LE
LE'
Elevation (km)
Distance (km)
Pcarb
Tpg
Pshale
Keg
Kv1
Fsed
Bf
Tv1
Tt1
Tv2
Tmg
Tgb

Figure 2.7: Along-strike sections through the Xainze rift at locations outlined in Fig.5. Highest and lowest elevations (equivalent to dashed lines in Fig. 5) are projected perpendicular on profile lines LA-LE. Note that view is towards ~W for all sections for consistency. Vertical exaggeration is 5x.

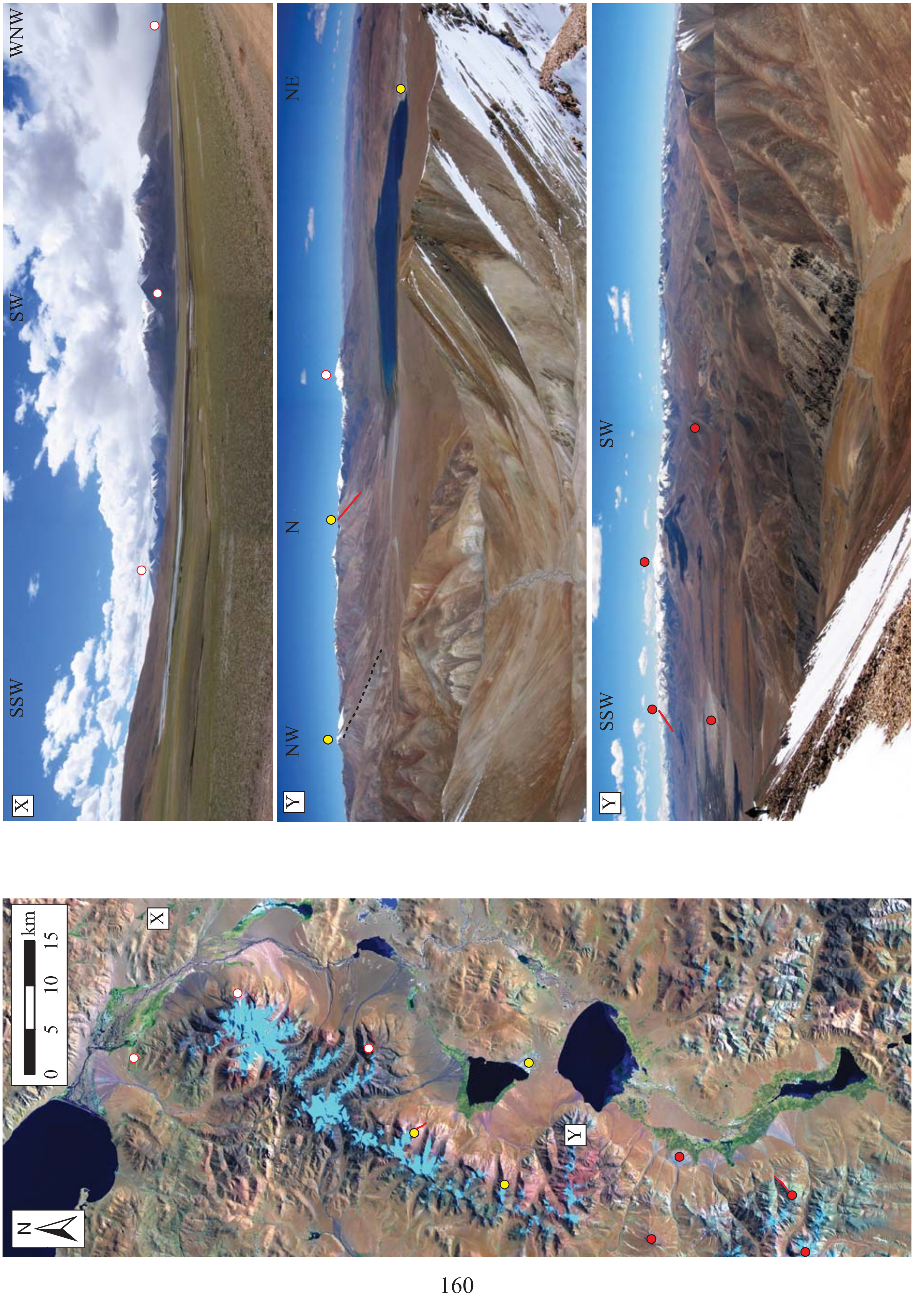
X
SSW
SW
WNW
Y
NW
N
NE
Y
SSW
SW
N
0
5
10
15
km
X
Y

Figure 2.8: Overview of the northern rift segment. Capital letters indicate approximate viewpoint and color-coded dots are shown for orientation purposes. Red lines mark approximate position of vertical sample transects. Basemap is false-color Landsat 7 dataset displaying bands 6-4-2 (RGB).

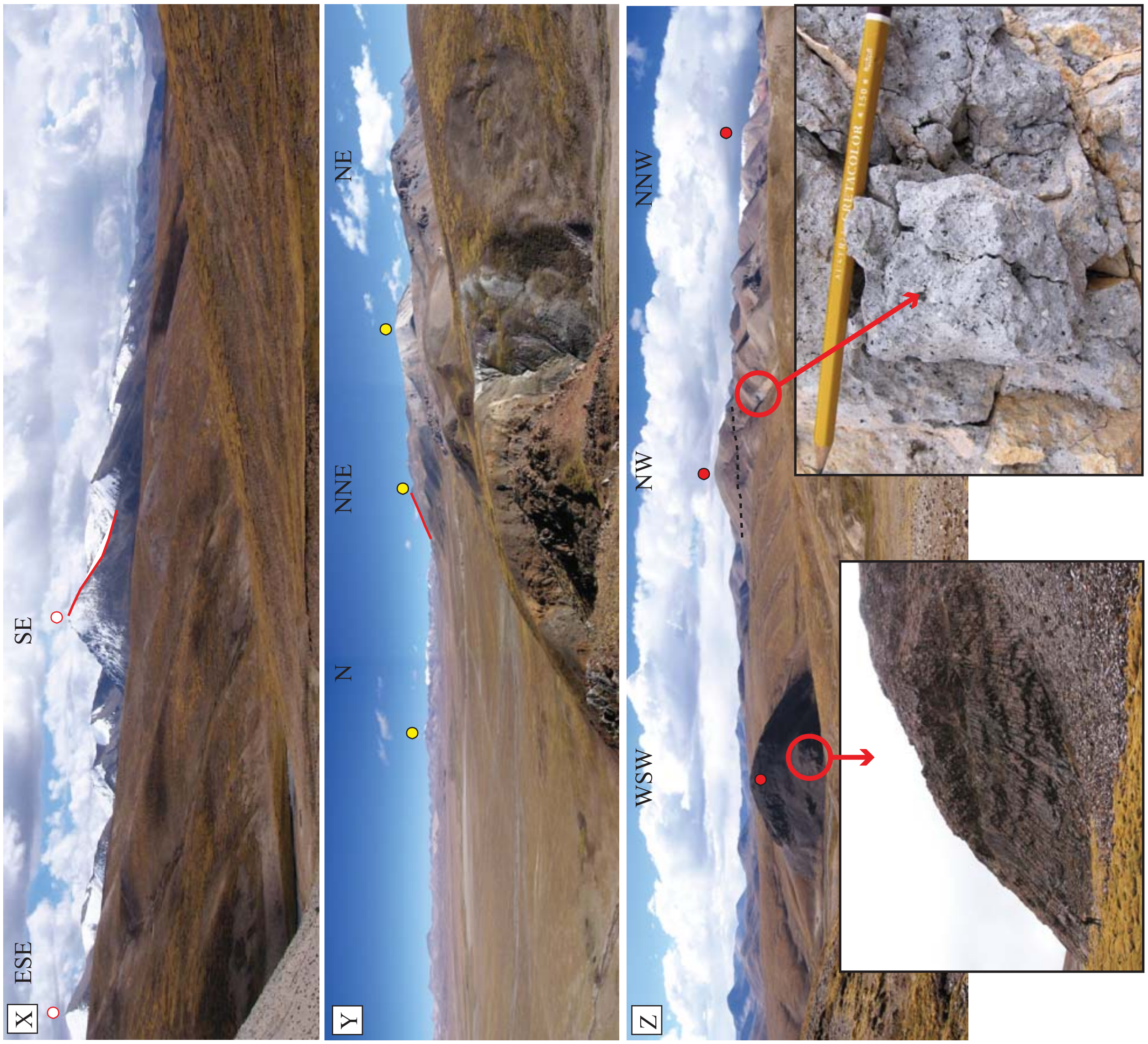
X
ESE
SE
Y
N
NNE
NE
Z
WSW
NW
NNW

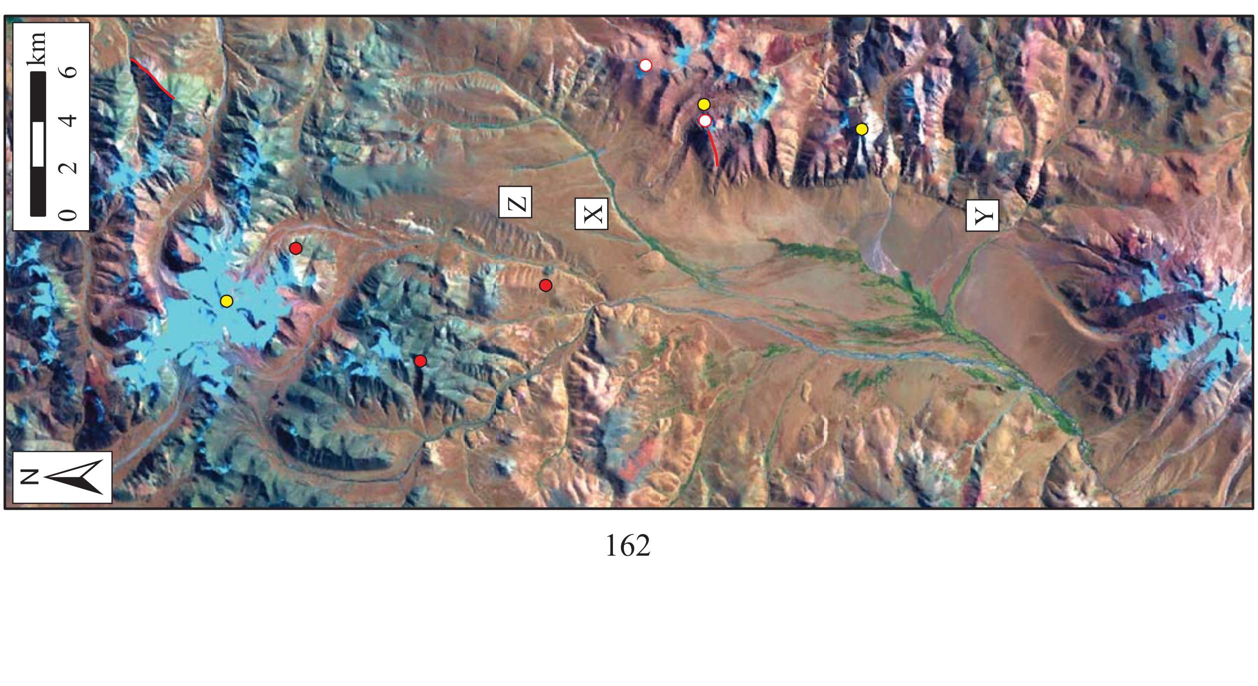
N
0 2 4 6 km
Z
X
Y

Figure 2.9: Overview of the central rift segment. Capital letters indicate approximate viewpoint and color-coded dots are shown for orientation purposes. Red lines mark approximate position of vertical sample transects. Bottom pictures (Z) show location of volcanic plug with columnar joints and a mid-Miocene rhyolitic tuff. Dashed black line follows a bedding plane. Basemap is false-color Landsat 7 dataset displaying bands 6-4-2 (RGB).

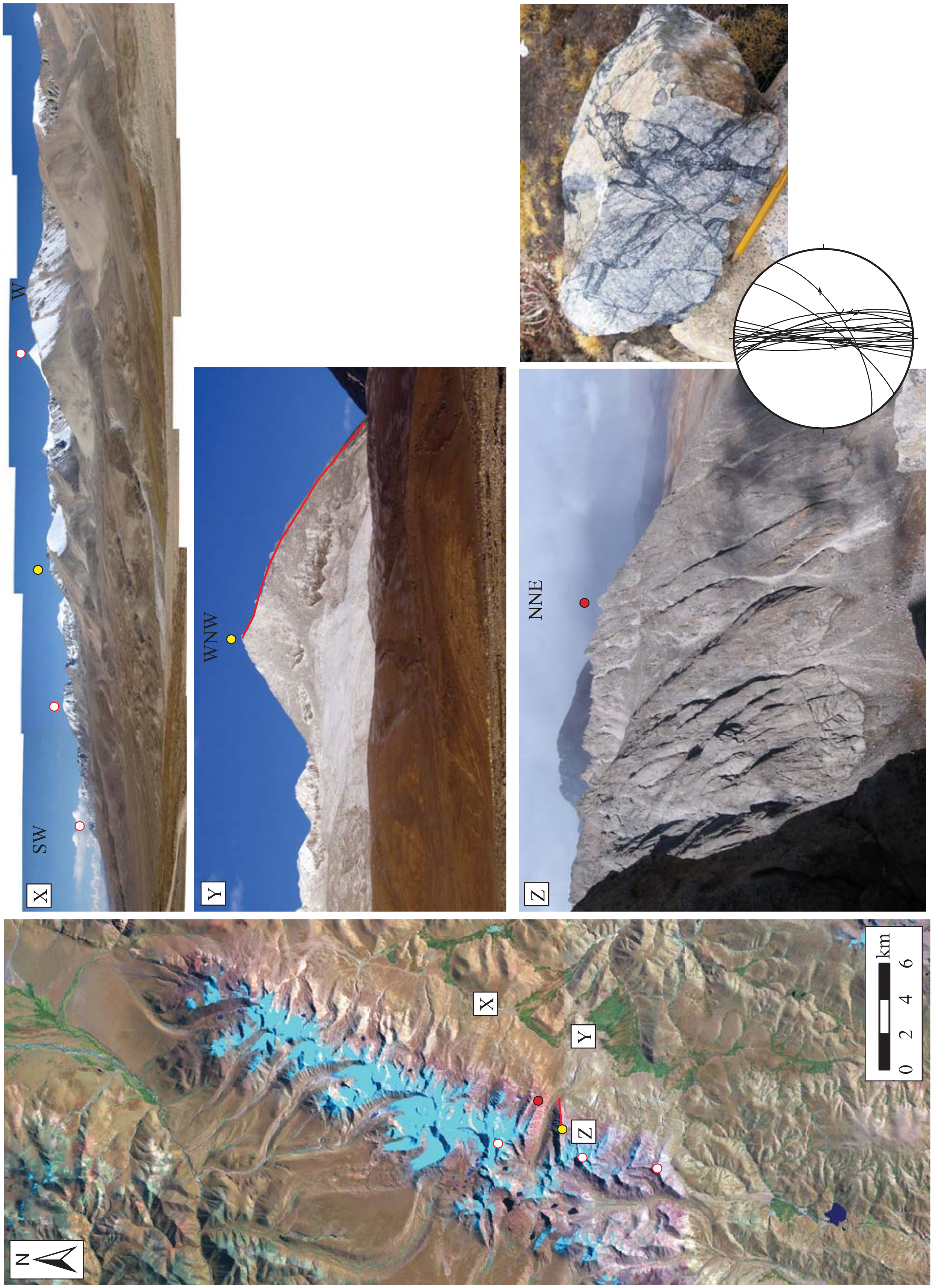
X
SW
W
Y
WNW
Z
NNE
N
0 2 4 6 km

Figure 2.10: Overview of the southern rift segment. Capital letters indicate approximate viewpoint and color-coded dots are shown for orientation purposes. Red lines mark approximate position of vertical sample transects. Lower right: Lower hemisphere plot showing trend of major slickensides. Pseudotachylite indicating earthquake related melt generation. Basemap is false-color Landsat 7 dataset displaying bands 6-4-2 (RGB).

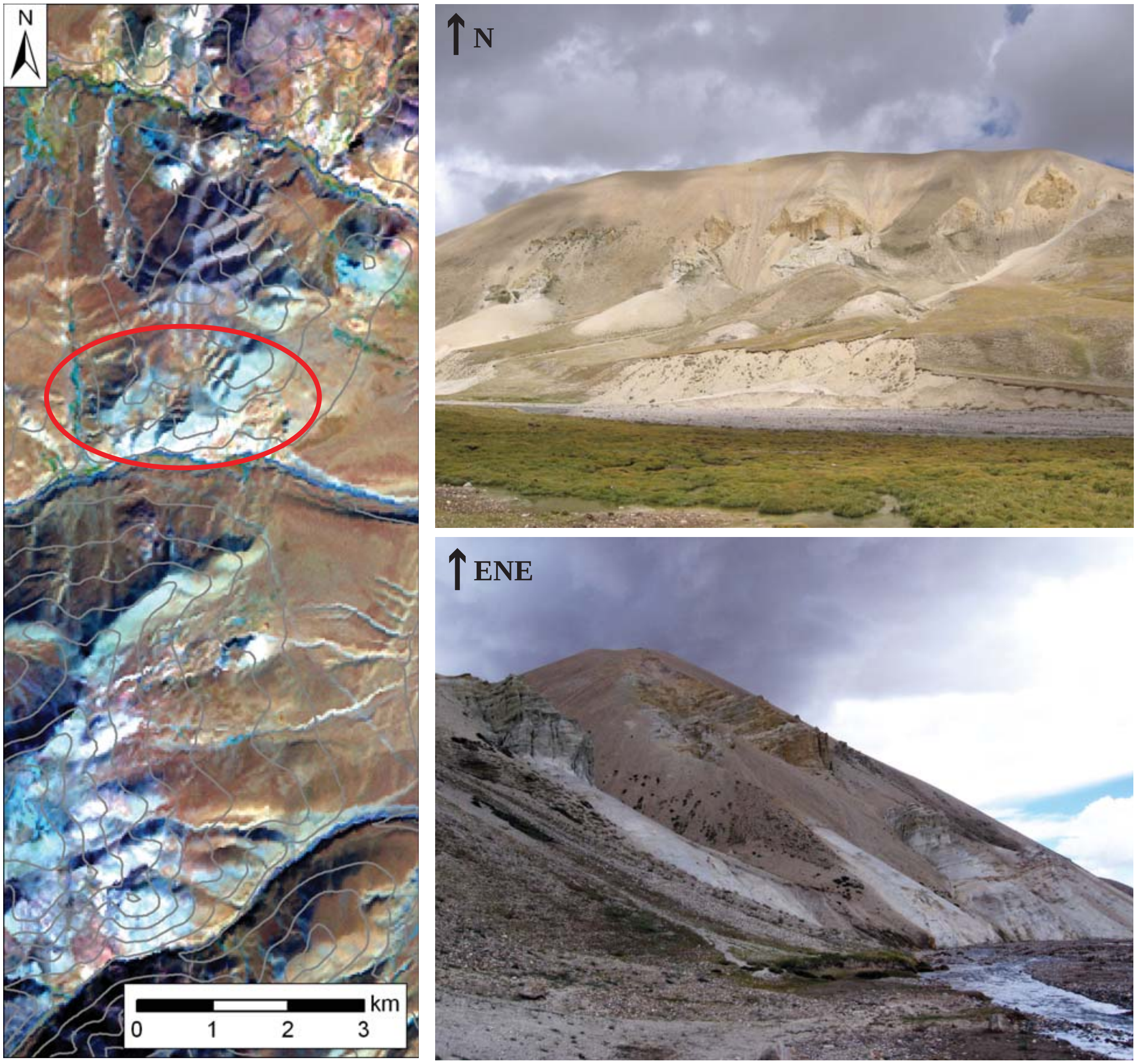
N
km
0
1
2
3
N
ENE

Figure 2.11: Location of thick fluvial sequence in the northern segment. Basemap is false-color Landsat 7 dataset displaying bands 6-4-2 (RGB).

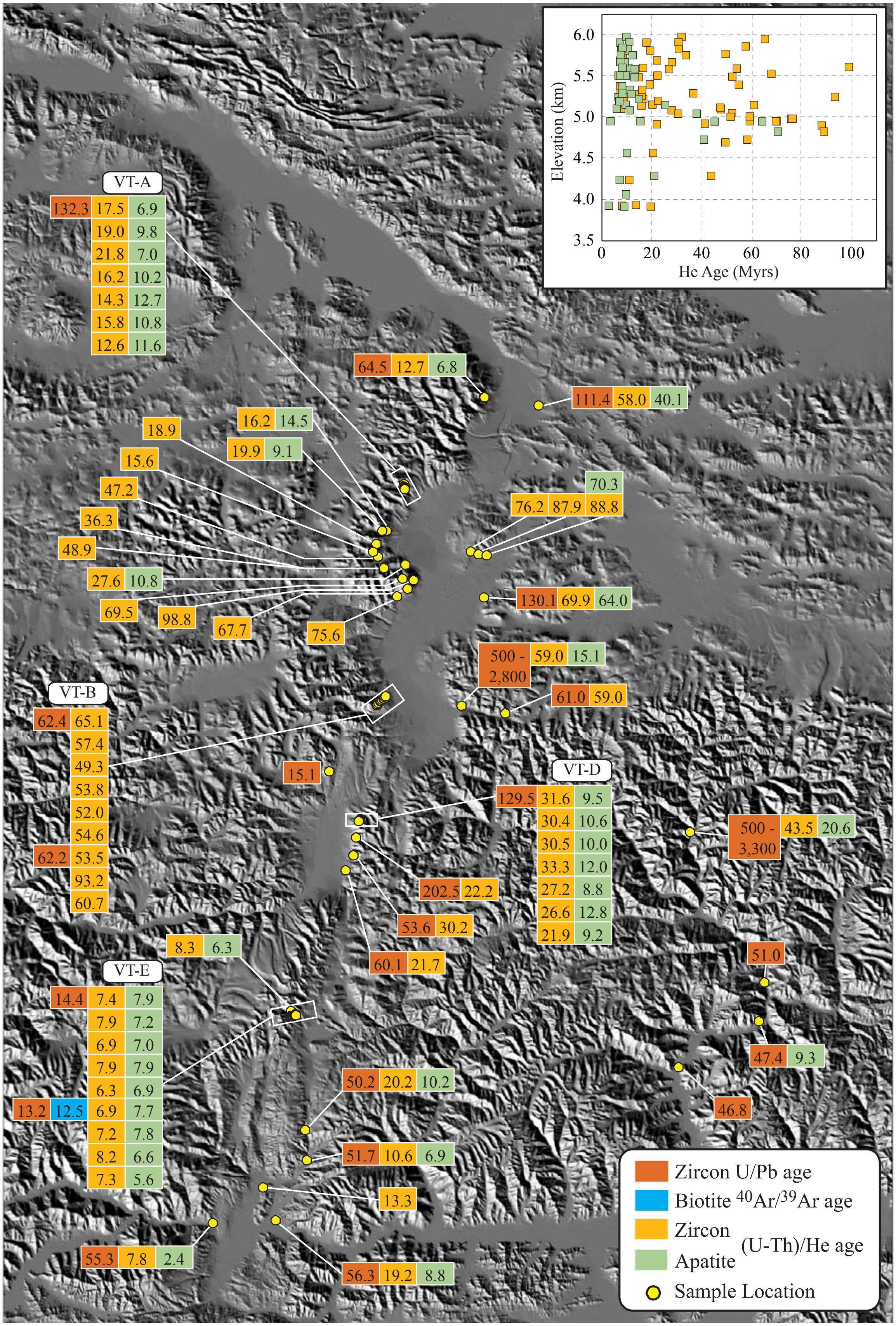

6.0
5.5
5.0
4.5
4.0
3.5
Elevation (km)
0
20
40
60
80
100
He Age (Myrs)
VT-A
132.3 17.5 6.9
19.0 9.8
21.8 7.0
16.2 10.2
14.3 12.7
15.8 10.8
12.6 11.6
64.5 12.7 6.8
111.4 58.0 40.1
16.2 14.5
19.9 9.1
18.9
15.6
47.2
36.3
48.9
27.6 10.8
69.5
98.8
67.7
75.6
70.3
76.2 87.9 88.8
130.1 69.9 64.0
500 - 2,800 59.0 15.1
61.0 59.0
VT-B
62.4 65.1
57.4
49.3
53.8
52.0
54.6
62.2 53.5
93.2
60.7
15.1
VT-D
129.5 31.6 9.5
30.4 10.6
30.5 10.0
33.3 12.0
27.2 8.8
26.6 12.8
21.9 9.2
500 - 3,300 43.5 20.6
202.5 22.2
53.6 30.2
60.1 21.7
8.3 6.3
VT-E
14.4 7.4 7.9
7.9 7.2
6.9 7.0
7.9 7.9
6.3 6.9
13.2 12.5 6.9 7.7
7.2 7.8
8.2 6.6
7.3 5.6
51.0
47.4 9.3
46.8
50.2 20.2 10.2
51.7 10.6 6.9
13.3
55.3 7.8 2.4
56.3 19.2 8.8
Zircon U/Pb age
Biotite $^{40}Ar/^{39}Ar$ age
Zircon
Apatite
(U-Th)/He age
Sample Location

Figure 2.12: Sample locations and corresponding mean ages based on several aliquot analyses. See Table B.1 and B.2 for details of (U/Th)/He analyses. Inset in the upper right corner shows He ages versus elevation relationship. Basemap is a shaded relief map created from 90 m Shuttle Radar Tomography Mission (SRTM) dataset.

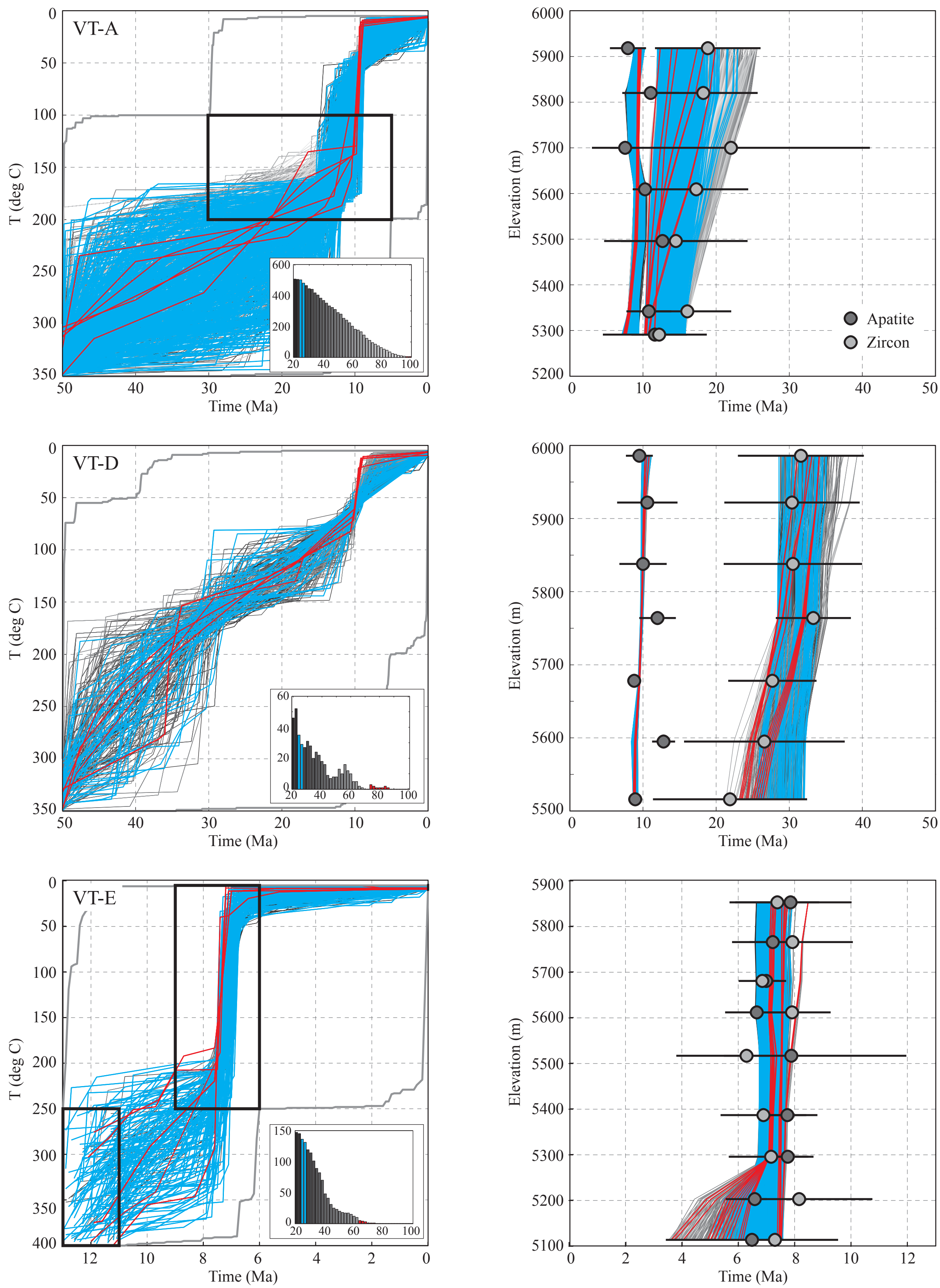

VT-A
T (deg C)
Time (Ma)
Elevation (m)
Apatite
Zircon
VT-D
VT-E

Figure 2.13: Results from thermal modeling for three vertical transects. Left-hand side shows the fitting thermal histories, on the right-hand side sample ages with their standard deviations are plotted against elevation. Black boxes represent model constraints. Lines represent the connections between the model ages calculated from the fitting thermal paths. Blue lines are fitting thermal histories based on geothermal gradients of 24 and 26°C/km, red lines for the maximum geothermal gradients. Bar graphs show the number of acceptable solutions color-coded by geothermal gradient.

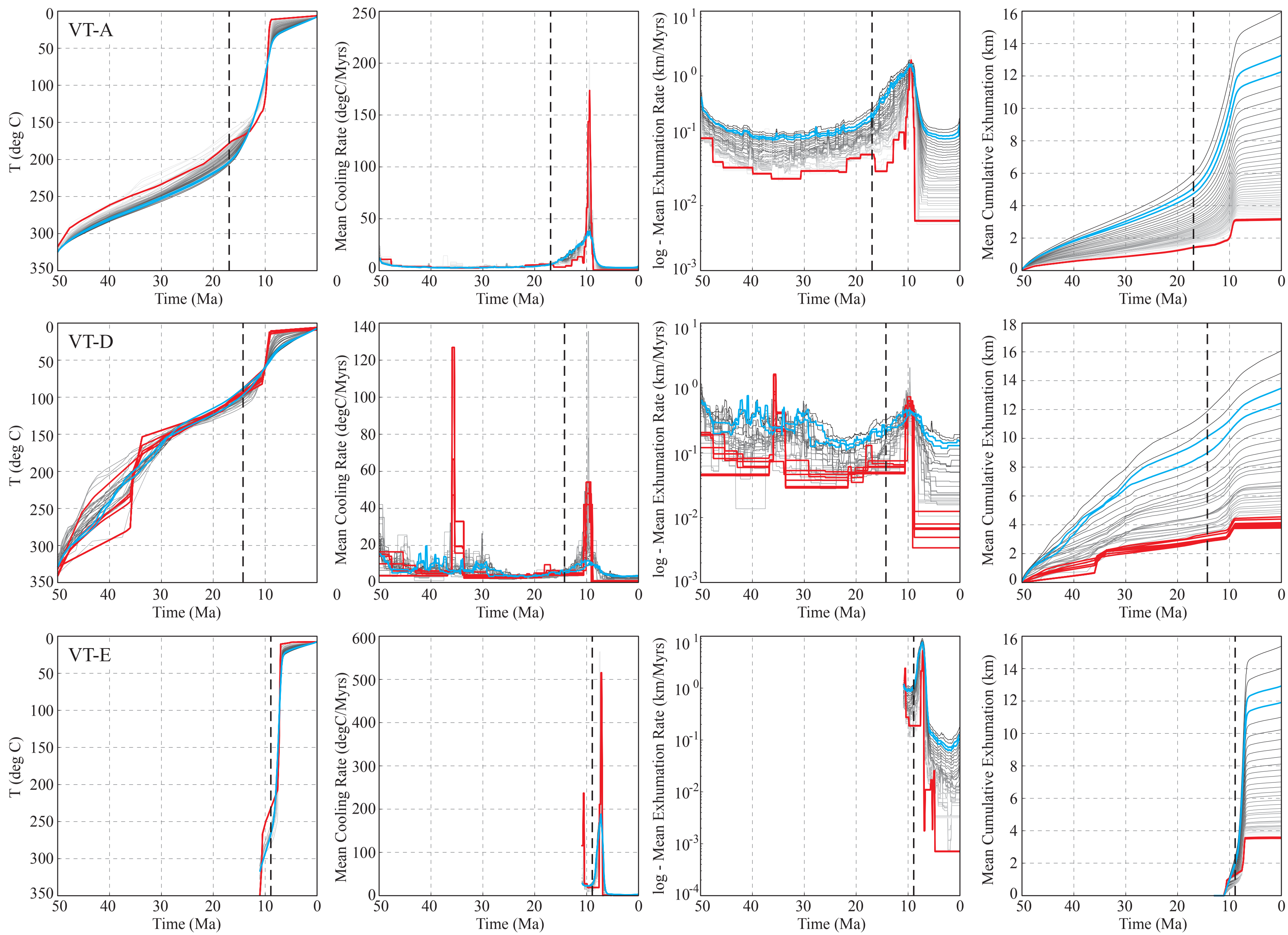
VT-A
VT-D
VT-E
T (deg C)
Mean Cooling Rate (degC/Myrs)
log - Mean Exhumation Rate (km/Myrs)
Mean Cumulative Exhumation (km)
Time (Ma)

Figure 2.14: Average t-T paths and cooling rates for each geothermal gradient based on the results shown in Fig. 2.13. Derived values of exhumation rates and total accumulated exhumation are shown on the right. Dashed lines indicate the suggested initiation of E-W extension.

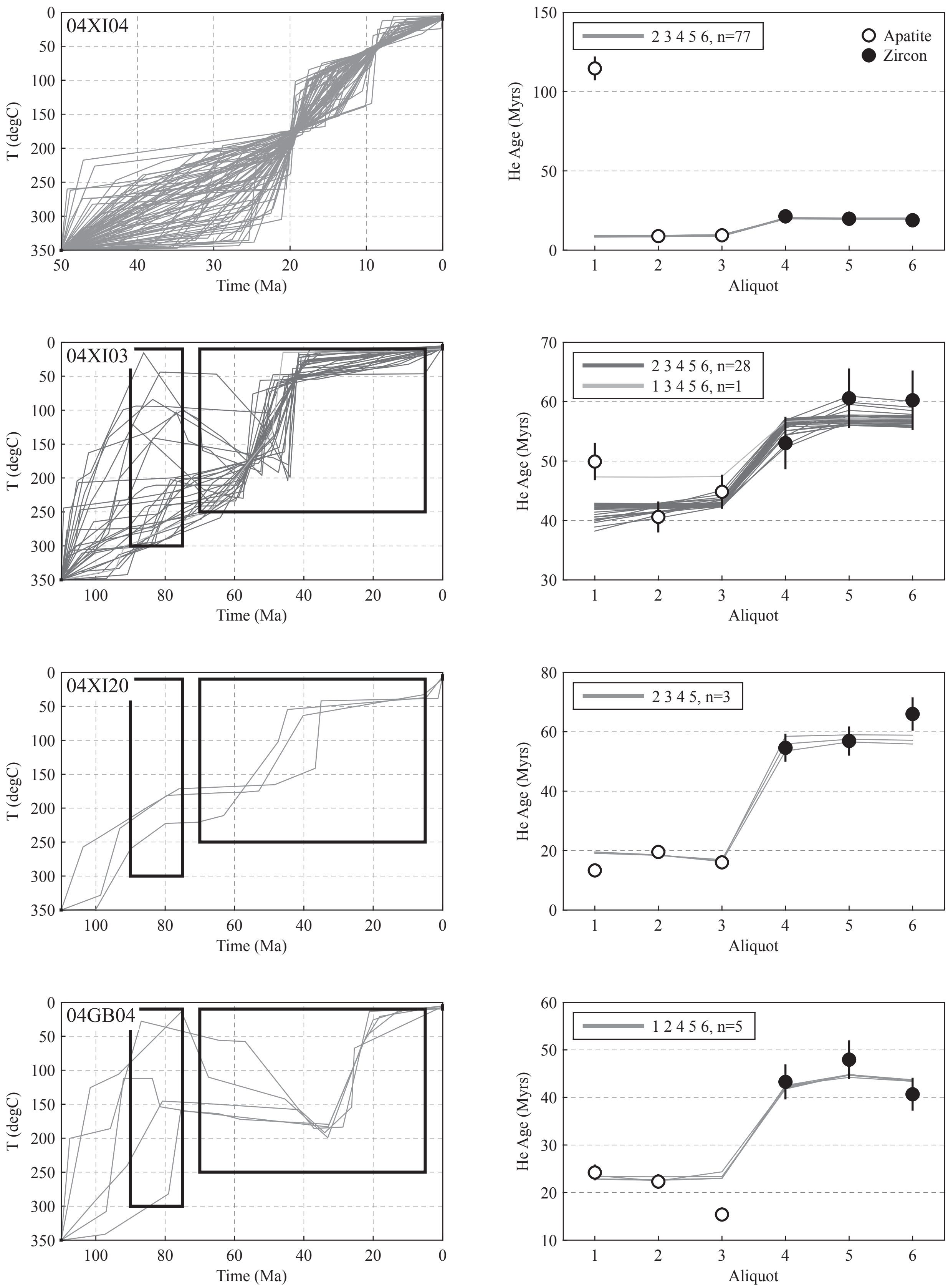
04XI04
T (degC)
Time (Ma)
He Age (Myrs)
Aliquot
2 3 4 5 6, n=77
Apatite
Zircon
04XI03
2 3 4 5 6, n=28
1 3 4 5 6, n=1
04XI20
2 3 4 5, n=3
04GB04
1 2 4 5 6, n=5

Figure 2.15: Compatible thermal histories for single sample modeling runs. Black boxes represent model constraints. Shades of grey correspond to fits for different aliquot combinations.

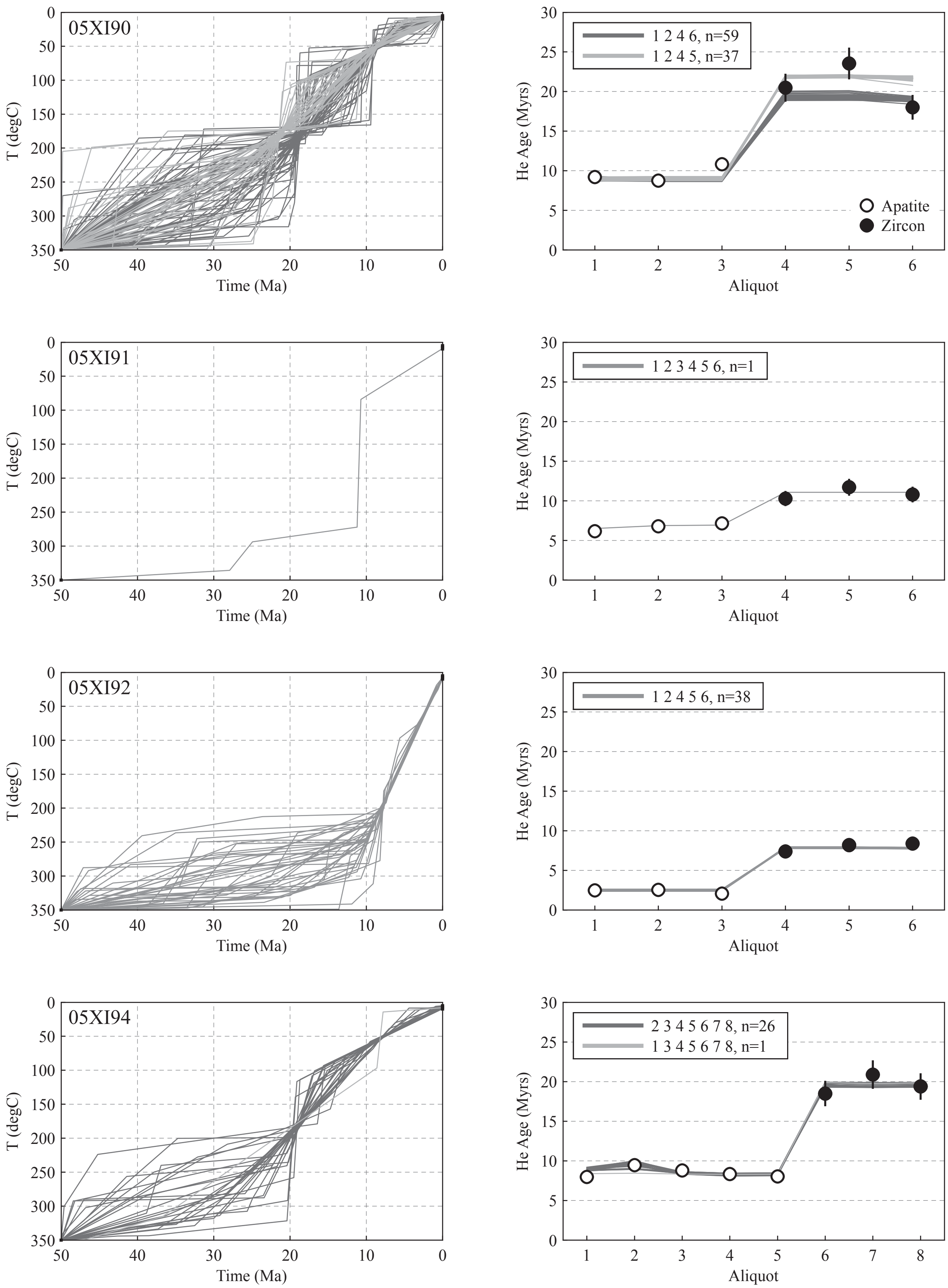

05XI90
T (degC)
Time (Ma)
1 2 4 6, n=59
1 2 4 5, n=37
He Age (Myrs)
Aliquot
Apatite
Zircon
05XI91
1 2 3 4 5 6, n=1
05XI92
1 2 4 5 6, n=38
05XI94
2 3 4 5 6 7 8, n=26
1 3 4 5 6 7 8, n=1

Figure 2.16: Compatible thermal histories for single sample modeling runs continued.

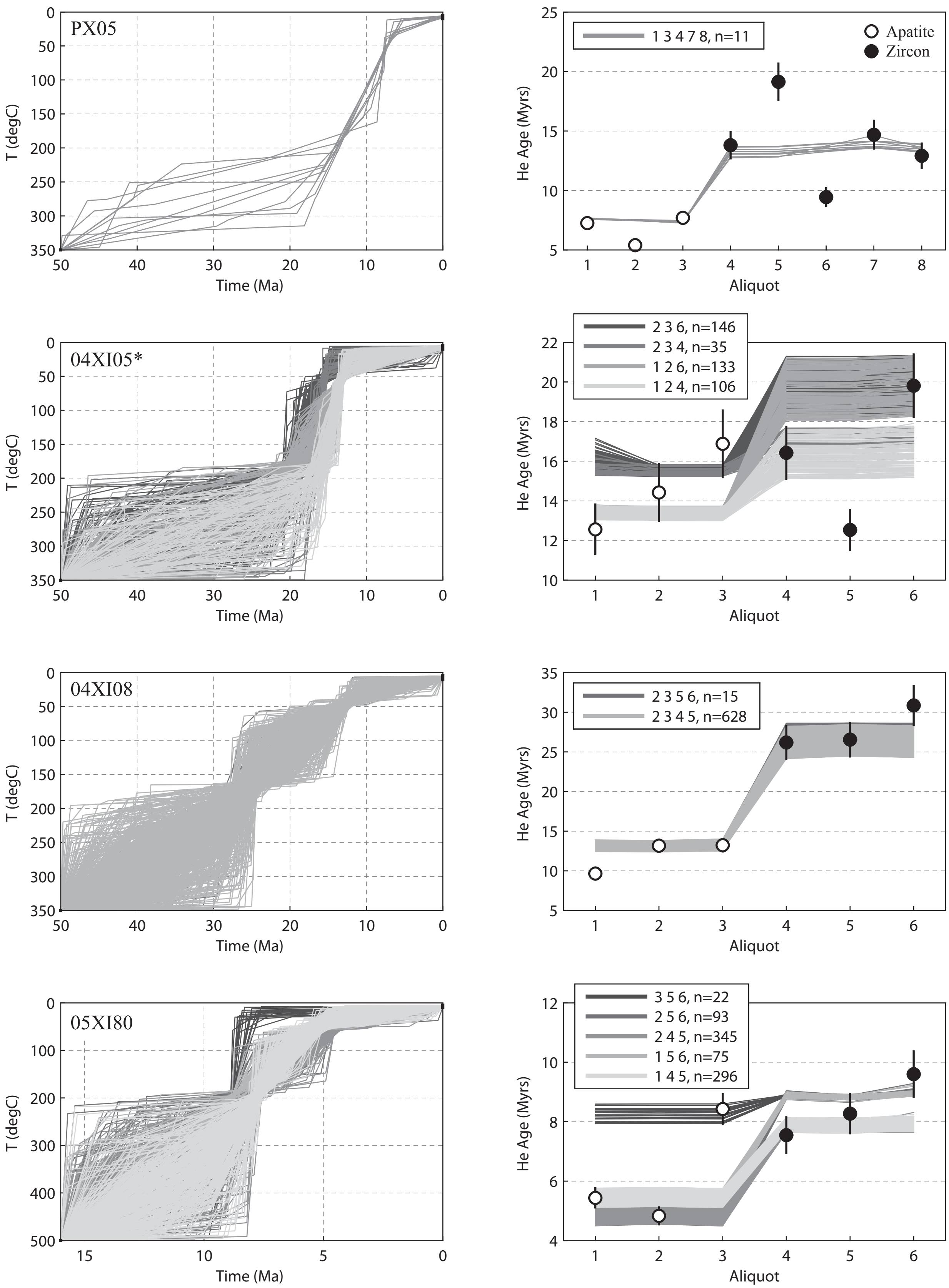
PX05
T (degC)
Time (Ma)
1 3 4 7 8, n=11
Apatite
Zircon
He Age (Myrs)
Aliquot
04XI05*
2 3 6, n=146
2 3 4, n=35
1 2 6, n=133
1 2 4, n=106
04XI08
2 3 5 6, n=15
2 3 4 5, n=628
05XI80
3 5 6, n=22
2 5 6, n=93
2 4 5, n=345
1 5 6, n=75
1 4 5, n=296

Figure 2.17: Compatible thermal histories for single sample modeling runs continued.

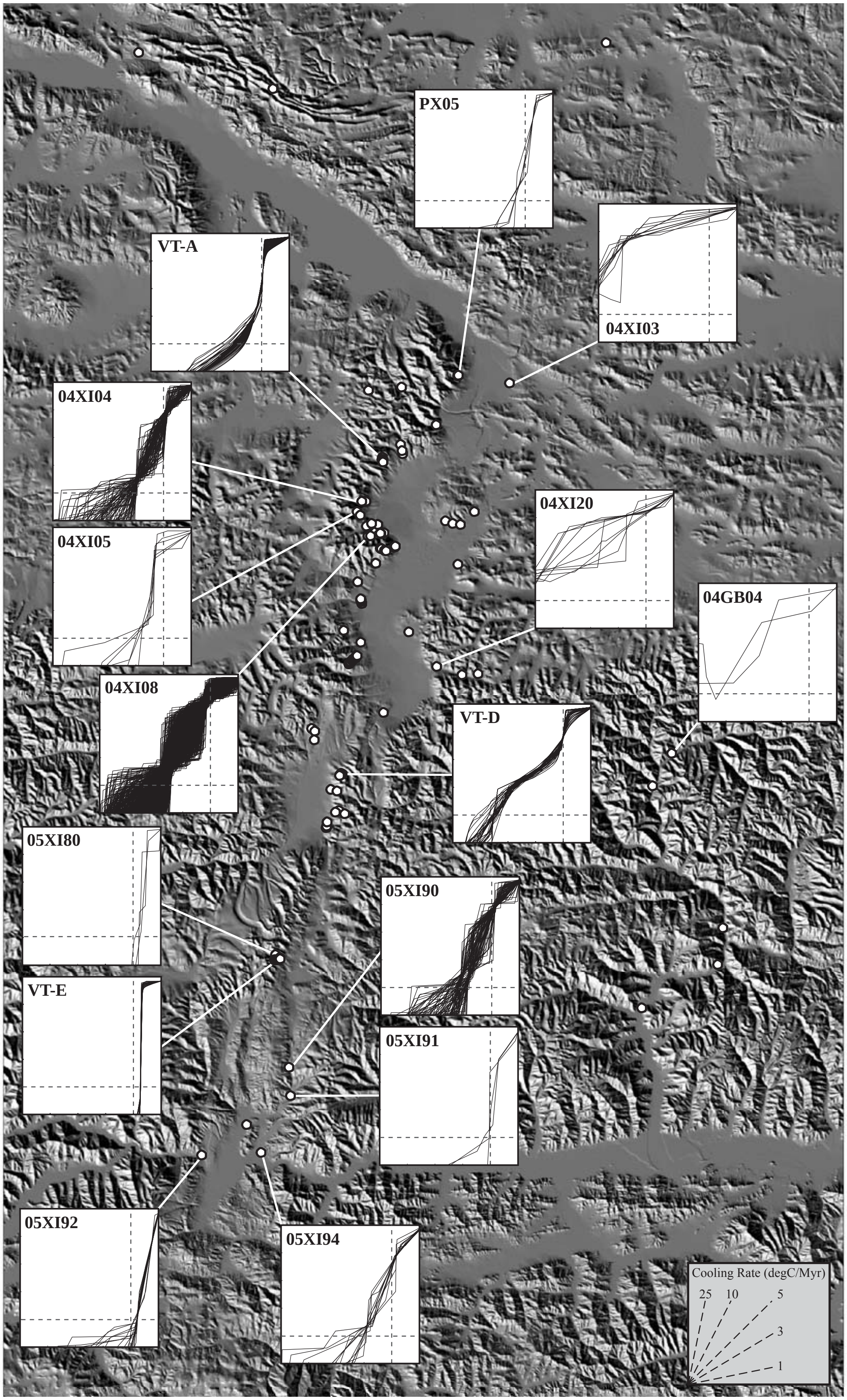

PX05
04XI03
VT-A
04XI04
04XI20
04XI05
04GB04
04XI08
VT-D
05XI80
05XI90
VT-E
05XI91
05XI92
05XI94
Cooling Rate (degC/Myr)
25
10
5
3
1

Figure 2.18: Summary of modeling results in a spatial context. All graphs range from 50-0 Ma and 0-250°C. Dashed lines mark 10 Ma and 200°C (the uppermost temperature limit for ZHe sensitivity) for reference.

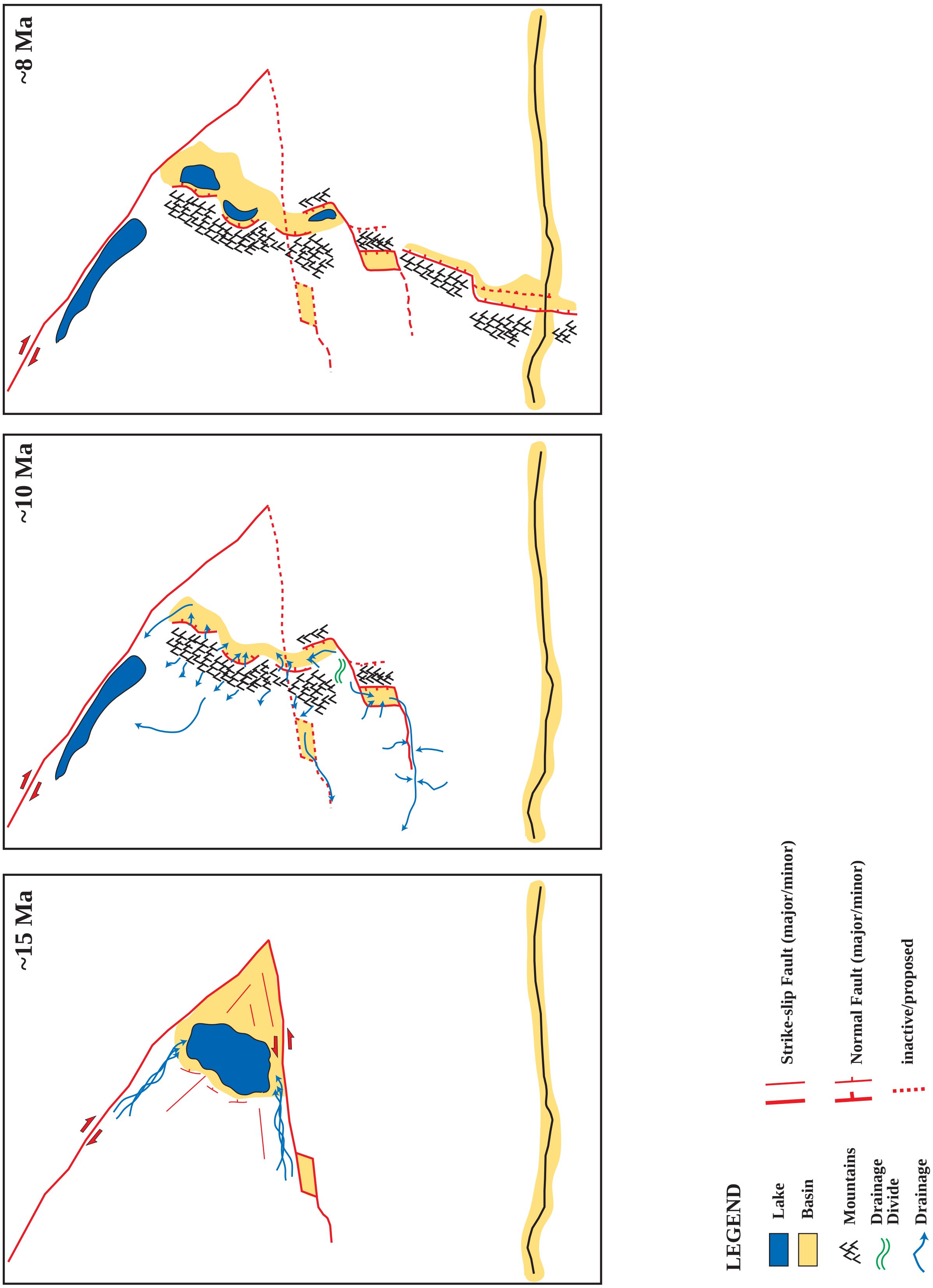
~8 Ma
~10 Ma
~15 Ma
LEGEND
Lake
Basin
Mountains
Drainage Divide
Drainage
Strike-slip Fault (major/minor)
Normal Fault (major/minor)
inactive/proposed

Figure 2.19: Evolution of E-W extension in the Xainza rift based on thermal history modeling and field observations.

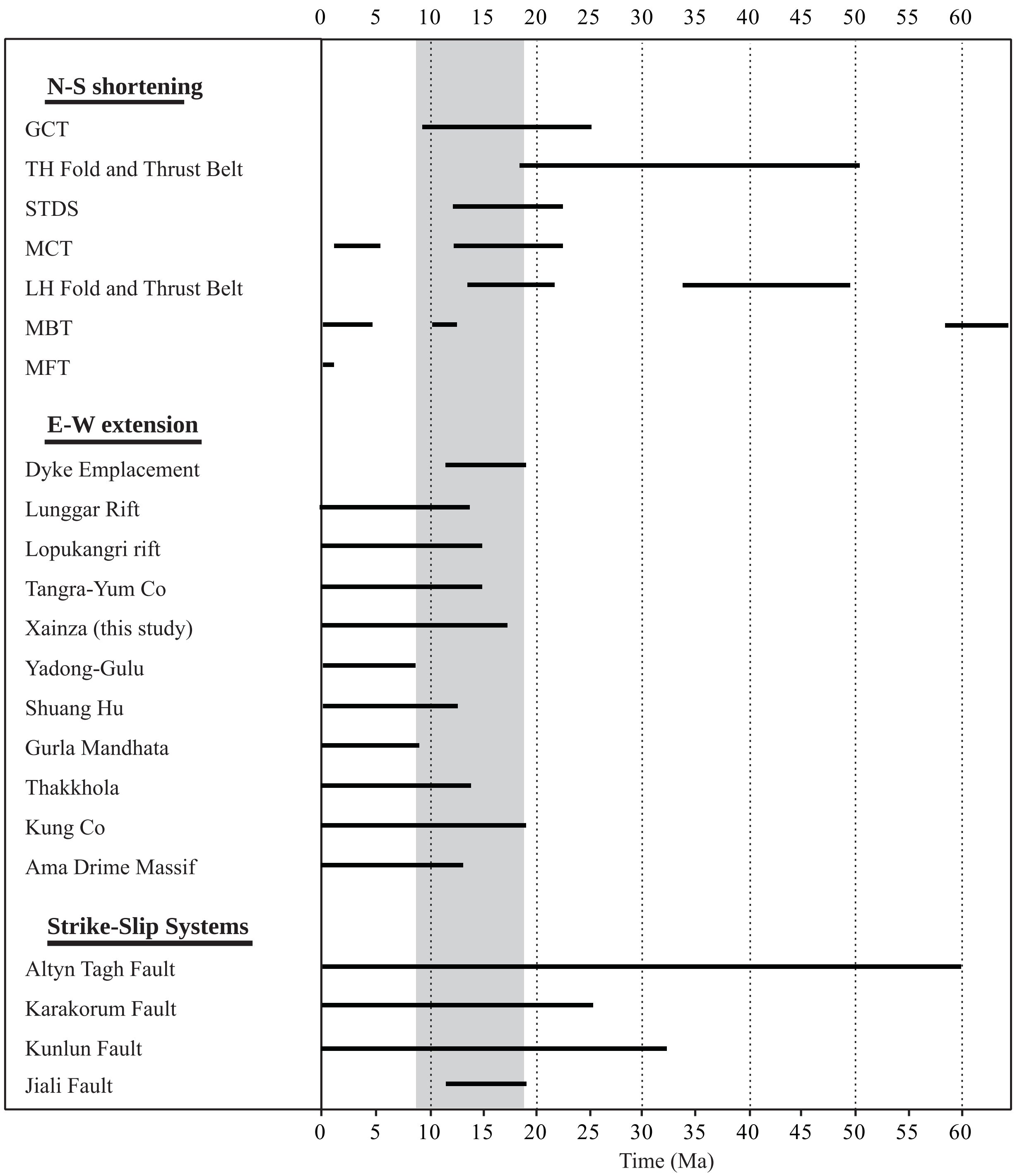
0 5 10 15 20 25 30 35 40 45 50 55 60
N-S shortening
GCT
TH Fold and Thrust Belt
STDS
MCT
LH Fold and Thrust Belt
MBT
MFT
E-W extension
Dyke Emplacement
Lunggar Rift
Lopukangri rift
Tangra-Yum Co
Xainza (this study)
Yadong-Gulu
Shuang Hu
Gurla Mandhata
Thakkhola
Kung Co
Ama Drime Massif
Strike-Slip Systems
Altyn Tagh Fault
Karakorum Fault
Kunlun Fault
Jiali Fault
0 5 10 15 20 25 30 35 40 45 50 55 60
Time (Ma)

Figure 2.20: Timing of major structures in the Himalayan-Tibetan orogen. See text for details.

Page left intentionally blank

CHAPTER 3:

Improvement of (U-Th)/He data analysis.

Part 1: Model-based determination of uncertainty in the F_T correction factor

Abstract

The (U-Th)/He technique is a widely used tool for investigating tectonic processes in a multitude of geological settings. Although very powerful, one of the drawbacks of this technique is the generally low precision compared to other geochronological and thermochronological methods. As a unique complication in (U-Th)/He dating, the small size of the daughter product (^{4}He) causes considerable amounts to be ejected out of the host crystal as a consequence of the high energy decay processes. To compensate for this loss, the F_T correction factor (F_T) is applied to the raw age determined by measured parent/daughter concentrations resulting in a final, corrected He age. Insufficient knowledge of the parent isotope distributions within the analyzed grain, inclusions, deviations from perfect idiomorphic crystal shapes, ^{4}He implantation from surrounding mineral phases as well as neglecting the generally minimally contributing parent Sm are the key factors inducing errors in the F_T, and consequently age calculation. Advances in parent isotope mapping and inclusion detection now allow for rigorous modeling of F_T instead of using parametric equations that assume homogenous parent isotope distributions. As an additional merit of this methodology, the effect of grain shape modifications (e.g. polishing, abrasion) can be assessed easily this allows for parent isotope mapping and subsequent (U-Th/He) analysis on the same mineral grain. Ultimately, uncertainties in (U-Th)/He ages could be addressed on a single grain basis with properly propagated errors from parent isotope

measurements and F_T instead of the common practice of assigning a more or less fixed uncertainty derived from analysis of standards.

3.1 INTRODUCTION

(U-Th)/He thermochronometry is a widely used technique to assess the low-temperature evolution of accessory minerals like apatite and zircon. Compared to other dating methods, the comparably small size of the daughter product 4He (called He thereafter) constitutes an additional complication for age determination. As a function of the decay energy and the crystal lattice of the host mineral, He can travel distances exceeding 20 µm before coming to a rest. Consequently, each parent isotope located less than the stopping distance away from a grain boundary potentially expels He out of the crystal. As a result, a certain percentage of daughter products are not measured during standard noble gas extraction and the calculated raw age based on parent/daughter concentrations needs to be corrected. This is routinely accomplished using the F_T correction factor (F_T) introduced by Farley et al. (1996). Utilizing Monte-Carlo simulation, they derived equations for simple geometries like spheres and cylinders that were later extended to tetragonal and hexagonal prisms to better represent the crystal shapes for the two most common used minerals zircon and apatite (Farley, 2002). Ketcham et al. (2011) provide the most recent update on F_T adding more grain geometries and using refined stopping distances (Ziegler, 2008; Ziegler et al., 2008). Besides the dependency on the grain geometry, F_T is a function of the parent isotope distribution that can be homogenous or inhomogeneous because of magmatic and/or metamorphic zonation. Special cases of heterogeneous parent distribution are represented by inclusions and He-implantation from nearby high-U/Th minerals that require a more sophisticated approach to derive a correct F_T. Once obtained, F_T can be used to calculate the corrected age of the analyzed sample by simply dividing the measured age by F_T (Farley et al., 1996). To account for the non-linearity of the decay equation and its effect on very old samples, Min et al. (2003) suggested dividing the measured amount of He instead. An even more accurate implementation of F_T is given by Ketcham et al. (2011) who calculate F_T for each individual parent isotope and use it directly in the age equation.

Although the analytical procedures measuring parent and daughter concentrations are able to produce results with a precision of ~2% (2σ), final (F_T-corrected) He ages from a single sample are usually much more dispersed. For the two most used laboratory standards, Durango apatite and Fish Canyon Tuff (FCT) zircon, the uncertainties are reported as 6% and 9% (2σ) based on reproducibility of a large number of single grain analysis (House et al., 2000; Farley and Stockli, 2002; Reiners, 2005). Durango apatite analysis is done on shards from cm-sized crystals whose rims are removed prior to crushing which eliminates a F_T correction because all shards are from within the mega-crystal at least one stopping distance away from any edges. Consequently, age reproducibility should fall within the analytical uncertainty. Given that this is not the case, inhomogeneous parent distribution must contribute to the deviation from the theoretical F_T value of 1 leading to much more dispersed He ages. Boyce et al. (2005) conducted an in-depth study on zonation of Durango apatite and could show that U-Th concentrations were indeed not homogenous. Contrary to Durango apatite, FCT zircon analysis relies on idiomorphic single crystals, which, as typical for zircon, show varying degrees of zonation. The observations on parent nuclide distributions imply that a significant amount of uncertainty is introduced during calculation of a standard, geometry based F_T ignoring zonation. It has to be noted that the nominal uncertainties of the standards are derived from quickly cooled volcanic samples where the measured He concentration is simply a function of time since rapid cooling and He loss due to ejection only. For other samples that resided a significant amount of time in the He partial retention zone (HePRZ) the combined effects of ejection and diffusive loss of He will amplify grain-to-grain differences in geometries and parent nuclide distributions potentially leading to much higher intra-sample dispersion of He ages. Fitzgerald et al. (2006) provide a summary of contributing factors for over-dispersed He ages.

Given the direct influence of the F_T on the He age, an accurate determination of this correction is critical to (U-Th)/He dating. Here, a new tool the *FT-Calculator* is presented which allows the calculation of F_T for the most commonly encountered grain shapes including versatile parent isotope distribution and grain shape modification modeling. Although the most recent stopping distances are included in the software, if not otherwise noted, the values provided by Farley et al. (1996) are used for comparison purposes throughout this study.

3.2 SOFTWARE OVERVIEW AND MODELING APPROACH

The *FT–Calculator* is one of a series of tools combined into a newly developed graphical user interface (GUI) based stand-alone He modeling package (HeMP). HeMP was created to provide an advanced platform for (U-Th)/He modeling and is available by request. In order to calculate F_T for a variety of grain geometries and parent isotope distributions the following approach was chosen (see Fig. 3.1 for a graphical representation of the workflow). Based on preset crystal shapes for the most commonly used minerals in (U-Th)/He dating (sphere, ellipsoid, cylinder, tetragonal prism with pyramidal terminations, hexagonal prism), a three-dimensional (3D) grid with node spacing of 1 μm (2 μm for grains where the smallest dimension exceeds 200 μm) is created. A rim equal to the longest stopping distance is attached at each side of the 3D grid to be able to add the ejection sphere matrix to each node within the grain (see below). Variation in parent distribution is simply accommodated by nodes of certain parent nuclide (^{238}U, ^{235}U, ^{232}Th, ^{147}Sm) concentration from which an individual He-production rate ($^{4}HeP_I$) can be calculated using following equation.

$$^4HeP_I = n_I * C_I * \lambda_I \qquad (1)$$

where n equals the number of He produced along the decay chain of each isotope (n = 8, 7, 6, 1), C the concentration in ppm, and λ the decay constant of each isotope (I).

In the next step, the ejection sphere around a point source (node) for each parent isotope is established by calculating the distance of each cell from the center. Each cell within the ejection sphere grid is assigned either a '1' (filled), or a '0' (empty) dependant on if a He nucleus stops within that cell or not. This approach is different from others in that it does not rely on a pre-defined number of ejection events (e.g. Hourigan et al., 2005; ~2,500 randomly created ejection vectors) but accounts for all possible resting places. Summing over the entire grid gives the number of filled cells (N_I). It is apparent that this number varies as a function of the stopping distance. Using the average stopping distances for zircon provided by Farley et al. (1996) and a 1 μm cell size, N_I equals 5234, 7298, 6962, 410 for U238, U235, Th232, and Sm147. In order to distribute the total He-production equally throughout all filled cells one must scale the He-production as follows

$$V_I = \frac{^4HeP_I}{N_I} \qquad (2)$$

Repeating this for all parent isotopes (I) gives four ejection spheres with a homogenous distribution of daughter products on their surface. Combining all four into a single ejection sphere grid (S) yields the overall He-distribution around a node with given parent concentrations. If the crystal is zoned (or has inclusions), each zone is represented by its unique ejection sphere grid (S_Z). The sum of the corresponding S_Z is assigned to each node and stored as the first required output, a He-production matrix (M_{HeP}). Moving S_Z through the crystal grid and adding all cells to the corresponding cells around each node provides the second output, the He-distribution matrix (M_{HeD}). The He-budget matrix (M_{HeB}), which represents the local F_T at each node, is calculated as

$$M_{HeB(x,y,z)} = \frac{M_{HeD(x,y,z)}}{M_{HeP(x,y,z)}} \qquad (3)$$

where x, y, z denote the node positions within the grid. The results can be plotted in the GUI and illustrate the redistribution of He within the grain. More importantly, F_T is calculated by summing over all grid nodes:

$$FT = \frac{\sum^{(x,y,z)} M_{HeD}}{\sum^{(x,y,z)} M_{HeP}} \qquad (4)$$

Upfront, it has to be noted that this approach is computationally intense and should not be used to obtain F_T for standard analysis. On the other hand, the tool allows for great versatility in creating different zonation patterns as well as inclusion distributions, the main application of this tool. Additionally, the availability of the entire production (M_{HeP}) and distribution (M_{HeP}) matrices is a pre-requisite for subsequent analysis of the effect of grain shape modifications on F_T.

Although this approach allows tracking of all the He produced in the grain which is critical to calculate F_T's for modified grain shapes (see "Applications" section), it is not necessary to go through this analysis to derive a F_T value for standard grain geometries. To avoid the long run times and provide a basis for quick modeling of inclusions or symmetrical parent zonation patterns, HeMP allows the generation of so-called "Library" files (Fig. 3.1). Because all grain shapes of interest are symmetrical around their long axis, only 1/8th (one sector) of the grain needs to be considered for F_T determination (see Hourigan et al., 2005). Contrary to the above workflow, the local F_T value (% He retained) for each isotope instead of the amount of accumulated He at each node is stored. These numbers are a function of the grain shape and the individual stopping distances only and independent of the parent concentrations. Additional improvement of computational efficiency is obtained by limiting the analysis to the rim equal to the maximum stopping distance because all nodes within the grain interior have $F_T = 1$. For prismatic shapes (cylinder, tetragonal/hexagonal prisms) the number of iterations can be further reduced because each cross section perpendicular to the longest axis (c-axis) and more than the maximum stopping distance away from any tip or corner has equal local F_T values. Any desired grain length can then be quickly constructed by just adding the required number of cross-sectional slabs. Final F_T values are simply calculated with user-defined concentrations that can vary from node to node based on desired zonation patterns or position of inclusions. A large number of these "Library" files for different grain geometries and dimensions modeled with the most current stopping distances (see Ketcham et al., 2011) are provided with the software.

3.3 FT DEPENDENCIES

3.3.1 Grain Shape

The geometry and size of the analyzed mineral grain has a direct effect on the final correction of He not measured due to ejection out of the grain. In general, the more edges or low-angle terminations (e.g. pyramidal tips) a crystal has, the lower the F_T (higher correction) will be. Considering the very simple case of a tetragonal prism with 90° angles between all sides, a parent isotope located on a surface at least one stopping distance away from any corners, will eject exactly 50% of the He out of the crystal. At a position along any edge, 75% of the He produced will come to rest outside the grain. The worst-case scenario, a parent isotope at the corner of the grain will eject 87.5% of the daughter. For any other locations, this percentage will vary as a function of the distance to the respective grain edges and the stopping distance. The majority of minerals analyzed during standard (U/Th)/He dating can be approximated by simple geometric shapes allowing derivation of analytical solution for F_T as a function of shape, size, and stopping distances. As stated above, the following calculations of F_T do not necessitate the use of the *FT-Calculator* but were needed to benchmark HeMP against the equations provided by Ketcham et al. (2011). F_T for apatite and zircon using common geometries of representative dimensions were modeled to assess the differences between this and the most commonly used approach, calculating F_T with analytically derived polynomial equations. The comparative plot against F_T obtained from Ketcham et al. (2011) is provided in Fig. 3.2.

The uncertainty in F_T for the simplest case of homogenous parent distribution is a function of grain selection and accurate measurements of their dimensions. The polynomial equations used to calculate F_T are based on idiomorphic crystal shapes and the user needs to make sure that the analyzed grain closely resembles the ideal case and all critical dimensions are measured. Fig. 3.3A illustrates the effects of measurement uncertainty for apatite and zircons assuming an absolute measurement error of ±2 μm. Only for very small grains, this uncertainty exceeds the analytical precision of 2% (2σ) as indicated by the grey shaded area. Insufficient capture of the three-dimensional geometry including pyramidal tips as in the case of zircon has much severe consequences on the other hand. Fig. 3.3B shows the results for zircons with height/width ratios ranging from 0.8-1.0 and pyramidal terminations included/ignored. It is clearly demonstrated that using a simple two-dimensional approach with just one width and length measurement will potentially result in highly inaccurate F_T values for a wide range of grain sizes. Even if the tips are included, ignoring a deviation from the ideal square cross section can yield values exceeding the analytical precision of the (U-Th)/He technique.

3.3.2 Parent Isotope Distribution

The examples shown so far represent F_T calculated based on He-distributions that are simply a function of shape and grain dimensions. Using the analytically derived equations is only valid for minerals with homogenous parent distribution, a condition that is violated more often than desired. Most naturally occurring zircon grains exhibit varying degrees of zoning ranging from simple symmetric growth zonation to sector zoning, or complicated combinations of both. Old cores overgrown by younger rims further increase the variety seen in parent isotope distribution in zircons. To fully appreciate this variability, see the examples provided by Corfu et al. (2003). Apatite, probably the most widely used mineral in (U-Th)/He thermochronology, is commonly treated as unzoned but mounting evidence from analysis of fission track distributions and LA-ICPMS measurements (e.g. Jolivet et al., 2003; Boyce and Hodges, 2005, Emmel et al., 2007, Emmel et al., 2008, Fitzgerald et al., 2009, Farley et al., 2011) clearly violates this assumption. Remedying the shortcomings of a simple calculation for zircon, Hourigan et al. (2005) developed a LabVIEW© code that calculates F_T for tetragonal prisms with pyramidal terminations (geometric model for idiomorphic zircon) and self-similar growth zonation. They demonstrated the impact on the He-distribution within the host grain and the resulting age biases if a traditional

F_T was applied. Their analysis of depleted/enriched rims for zircons with constant geometry (see Hourigan et al. 2005, Fig. 8C, p.3360) is used as a benchmark for HeMP's algorithm. Fig. 3.4 shows the results superimposed onto modeling results of Hourigan et al. (2005). Although some of the concentration gradients used for zircon zoning are unlikely for apatite, an identical model setup is applied to the hexagonal grain geometry and longer stopping distances of apatite for comparison. Results are shown in Fig. 3.4, which illustrates the expected shift of maximum values towards the grain interior because of longer stopping distances.

Besides the distribution of parent isotopes, the type of decaying isotope is important as well because of the differences in decay energies that lead to unique stopping distances. Neglected by Farley et al. (1999) and Farley (2002), Sm is included into the revised and extended F_T equations by Ketcham et al. (2011). Usually, this will have very minor effects on the correction because of the commonly low Sm concentrations, the by comparison very short stopping distance (~4-6 µm), and the longer half-live of Sm. As shown later in the application section, this is not true for some cases where the full suite of parent isotopes needs to be included to arrive at a correct F_T value.

3.3.3 Inclusions

Often addressed as the main cause for large scatter in apatite He ages, inclusions represent a major complication in (U-Th)/He dating of mineral phases with commonly low parent concentrations. As a special case of inhomogeneous parent concentration, inclusions constitute point sources whose location within the host mineral does not follow a pre-defined pattern like self-similar growth zonation, consequently not allowing for an analytical solution to F_T. For host grains with high-U/Th concentrations like zircons, the effect of inclusions will be negligible but for apatites, which can have zircon or monazite inclusions this, might have some effect on F_T. In the later case, the problem with inclusions is two-fold as they re-distribute He as halos of higher concentration compared to the host grain rendering the classic F_T calculation inaccurate, and secondly they are often not dissolved during standard HNO_3 treatment of apatites leading to "parentless" He and ages that are too old. Similarly, fluid inclusions with excess He will have the same effect.

3.3.4 He-Implantation

Also referred to as the "bad neighborhood" problem (Spencer et al., 2004), He implantation into the mineral of interest from surrounding high U/Th phases is another special case of inhomogeneous parent distribution. Similar to the inclusion case, a portion of the measured He is going to be "parentless" because only the host grain is analyzed. As a result, the measured He concentration is always going to be too high resulting in ages that are too old. The predicted He distribution for an unzoned host grain will be disturbed by a He implantation front that does not necessarily have to be spherical as in the case of micro-inclusions. If this process is responsible for large spreads in (U/Th) /He ages, it is usually not assessed because zonation and/or inclusions are brought forth as the usual suspects. If this cannot be verified by measuring the parent distribution by e.g. depth profiling, then more in-depth investigations like secondary electron microscopy (SEM) on thin sections need to be undertaken to assess if low-concentration phases of interest are proximal to high U/Th phases.

3.4 APPLICATIONS

3.4.1 Sm as major contributor to F_T

Before going into some more advanced analysis, the basic question of the influence of Sm on F_T needs to be addressed. The decay constant of Sm is comparatively small, it only contributes 1 out of 22 He particles, and it has a lower decay energy that translates to a relatively short stopping distance of ~4-6 µm (Ziegler, 2008). As a result, the contribution of Sm has been considered negligible in many publications but Belton et al. (2004b) showed that Sm can be responsible for >25% of the total measured He. Here the effect of very high Sm concentrations on F_T is determined using an adequate dataset from the Shillong Plateau (India). Some of the samples analyzed by Biswas et al. (2007) include apatites with surprisingly high Sm concentrations up to ~5,000 ppm, which might yield a significant deviation from a calculated F_T ignoring the contribution from Sm. Furthermore, neglecting the He contribution from Sm in the age equation must result in uncorrected ages that are already erroneous before F_T is applied. In general, including Sm into F_T calculations should always give higher values (smaller correction) because of the much shorter stopping distance consequently resulting in younger corrected He-ages. Ignoring Sm in the age calculation would have a similar effect because part of the He quantity measured in the lab will not be linked to Sm but attributed to the faster decaying U and Th isotopes leading to raw ages that are too old. The combined result of an already too old raw age divided by a too small F_T might lead to corrected ages that are significantly older than the "true" age of the sample. To quantify this, F_T for a total of 82 apatite aliquots from 12 samples is calculated using the equations provided by Ketcham et al. (2011) including and ignoring the measured Sm concentrations. In this dataset, the He contribution from Sm, calculated as the He production rate of Sm divided by the sum of all He production rates, ranges from ~0.3-28%

(mean at 3.4%, standard deviation of 5.6). In order to improve the comparison between individual aliquot analyses, the Sm contribution is normalized by the surface-to-volume ratio of the grain resulting in a grain dimension independent value. This quantity is plotted against the ratio of F_T including Sm (FT) versus F_T neglecting Sm (FT*) in Fig. 3.5 showing the increasing spread as a function of increasing Sm contribution. The vast majority of F_T's calculated incorporating Sm is within ~2% of the value ignoring Sm but deviations of up to ~9% for the highest Sm contributions are realized. Similarly, Fig. 3.5 shows the ratios of raw and corrected He ages calculated incorporating Sm (Age) and ignoring Sm (Age*). Somewhat surprising, the effect of Sm is much more critical in the age calculation. About 25% of raw ages are outside the accepted uncertainty range of apatite (U/Th)/He dating (2σ of 6%) reaching maximum deviations from the raw He age ignoring Sm of more than 35%. Combining this with the additional effect of the larger F_T values, the corrected He ages are further pushed towards lower values.

3.4.2 Grain Shape Modifications

Naturally, mineral shapes are altered during sedimentary transport and the original idiomorphic crystal shape is transformed to a more elliptical or even spherical geometry. Consequently, applying a standard F_T correction based on the measured grain dimensions has to lead to incorrect results because part of the grain edges where most of the ejection occurs has been removed. Assuming homogenous parent isotope distribution and ignoring ongoing decay during transport and deposition, an initially idiomorphic crystal with a certain F_T can be reduced to an elliptical grain with F_T of 1 if more than ~20 μm of the outer shell was removed by natural abrasion. In their study of He-Pb double-dating of Navajo Sandstone zircons, Rahl et al. (2003) used this assumption and considered only the post-depositional part of the grains history to calculate corrected He ages. This approach seems reasonably for highly abraded eolian zircons assuming homogenous parent concentration but cannot be applied to grains that did not undergo as extensive abrasion or violate the homogenous parent distribution requirement. To assess the effect of abrasion during sedimentary transport, the *FT-Calculator* incorporates a function that calculates F_T for each abrasion step. To simulate progressive rounding of grain tips, edges, and crystal faces, the grain is inscribed into an ellipsoid with an initially equal length to width ratio. During subsequent abrasion steps, this ratio is progressively minimized to 1 resulting in a spherical geometry. Fig. 3.6 and Fig. 3.7 illustrate this workflow by means of four examples from the zoned zircon and apatite model runs from above. F_T for each step is simply calculated using equation (4) but summing over the portion of the grid that is within the abrasion ellipsoid only. The evolution of F_T during progressive rounding is illustrated in Fig. 3.7 and Fig. 3.8. Both figures demonstrate that abrasion affects the F_T in a non-linear fashion as a function of concentration gradient and rim width. The He distribution can be quite complicated and grains abraded by more than the stopping distance show residual spherical volumes that do not have an F_T of 1. These examples confirm the violation of the assumption that abrasion leads to grain shapes that do not require an F_T correction.

Besides natural processes, grain shapes are often modified during standard lab procedures like preparation of grain mounts for U/Pb LA-ICPMS analysis where grains are polished to expose their cores. As a result of this destructive technique, it is not possible to calculate F_T for grains that underwent polishing with the standard equations. Recently, He-Pb double dating of detrital zircons has become increasingly popular for provenance studies (e.g. Rahl et al., 2003). The combination of crystallization age determined by U/Pb analysis with the low-T cooling age given by (U-Th)/He thermochronology of the same grain aids in the interpretation of possible source terranes for the investigated sediments. Avoiding the effect on F_T, in He-Pb double dating the grain is mounted on tape and the U/Pb age calculated from the concentrations ablated from the outer portion of the grain before (U/Th)/He analysis. Although this approach bypasses the need for a more rigorous determination of F_T, the material removal during ablation itself might affect F_T significantly. Given the re-distribution of He as much as ~20 μm away of its point of origin, parent and daughter products are not removed in the same quantities therefore, their resulting bulk ratios could yield erroneous F_T and age calculations. Using the well known Fish Canyon Tuff zircons, Rahl et al. (2003) could show that the ablation pit (~30 μm in diameter and ~20 μm deep) did not disturb the isotope distribution enough to cause significant age differences. The question on hand is if this finding holds true for other mineral phases and especially different zoning patterns. Utilizing the grids obtained from the modeling of apatite and zircon zonation in addition to the homogenous parent distribution model results, a more rigorous investigation of the influence of laser ablation is provided below. Using the same pit dimensions and placing the pit in the center of the grains outer surface, two values for F_T can be calculated. First, F_T is determined based on the standard lab protocol that the grain has not been degassed prior to LA-ICPMS analysis, and second based on the hypothetical case that the He concentration was measured prior to LA-ICPMS analysis in which case only the parent isotopes would be removed from the grain. Fig. 3.10A shows F_T after laser ablation (FT*) plotted against the original F_T (FT) for homogenous parent distribution and a variety of grain shapes and sizes. On the right, Fig. 3.10B compares these values for the zoned apatite and zircon grains with fixed size and varying rim width and concentration gradients. These results confirm that laser ablation prior to degassing does not affect the F_T correction significantly for commonly analyzed grain sizes.

Another grain shape modification is represented by mechanical abrasion in the laboratory removing the outer ~20μm of the grain prior analysis to completely circumvent the use of an F_T correction. As pointed out by Farley (2002), this technique should only be used for grains of known homogenous parent distribution and quickly cooled samples where the He concentration profile is a function of He ejection only. Violation of these requirements will certainly result in erroneous corrected ages. Spiegel et al. (2009), who conducted in-depth analysis not only on the analyzed grains itself but also on the surrounding matrix, provide a successful application of this technique. They show that depending on the severity of the "bad neighborhood" problem, mechanical abrasion is necessary to remove the effects of He-implantation. The majority of their dataset shows improved reproducibility as well as better alignment with AFT and biostratigraphic ages.

To show the effect of polishing on F_T, zoned apatite and zircon grains used previously are polished virtually along their shortest dimension (grain height) in 1 μm increments down to 25% of the original dimension and the resulting F_T (FT*) is plotted against the unpolished value (Fig. 3.11 for zircon, Fig. 3.12 for apatite). As anticipated, grains with an enriched rim show an initial increase (FT/FT* decreases), followed by a decrease in F_T towards the grain center where the same value as the unpolished grain is obtained. Further polishing decreases the values significantly since the depleted rim now constitutes the majority of the grain volume left. Grains with depleted rims show a more complicated F_T response to polishing. Very thin rims do not have a mentionable effect until a large portion of the grain is polished away. With increasing rim widths, the deviation from F_T towards lower FT* becomes more pronounced and outpaces the effects of enriched rims. A rather wide range of values indicates that any attempt to use a standard F_T-correction for modified grain shapes would only be valid if one can be certain that the grain was polished very closely to its half-width and the parent concentrations are in fact symmetrical. In the case of wide and depleted rims, these model results show that most of the variation is in fact around the center of the grain. Although not explicitly shown in these plots, even grains with homogenous parent concentrations could require a correction exceeding ~5% if not polished close to their half-width.

3.4.3 F_T calculated from depth profiles

Ongoing improvement of detection limits and hardware in LA-ICPMS has made accurate measurement of parent nuclide concentrations increasingly reachable. A very common and effective way to determine zonation patterns is depth profiling where concentrations are continuously measured while “drilling” through the grain. Assuming symmetric growth zonation, the measurement of concentration over time (= depth) can simply be converted to a three-dimensional grid and F_T calculated subsequently. This approach does not require any modification to the grain before laser ablation but only provides a one-dimensional representation of the zonation pattern. The *FT-Calculator* includes an option to import the results from depth profiling and based on user-defined concentration bins and grain shape, automatically generates the zoned grain matrix. This was used by Bargnesi et al. (2013, submitted) to correct for high-U rims in zircons. Fig. 3.13 illustrates how the measurements are processed and shows the final zoned grain for.

3.4.4 Inclusions

Inclusions are the single most important reason why apatite (U-Th)/He thermochronology can be very time-consuming. Contrary to zircon, where inclusions are the norm rather than the exception but do not constitute a severe problem because of the high parent concentrations in the host grain, a significant amount of time is spent to select inclusion free apatites. Vermeesch (2007) conducted a theoretical analysis on the effect of inclusions on F_T using cumulative distribution functions (CDF's) to simulate varying numbers of inclusions with changing host/inclusion concentration ratios. One of the outcomes of this investigation was that a larger number of inclusions can effectively re-distribute He within the host grain resulting in a pseudo-homogenous daughter distribution yielding similar F_T compared to the same grain with no inclusions. Furthermore, he could show that apatites with small randomly distributed inclusions yielded reproducible ages when completely dissolved in HF avoiding "parentless" He.

Using similar input parameters as Vermeesch (2007), the *FT-Calculator* is used to test the influence of inclusions on actual grain geometries. For a single grain dimension (80 x 120 μm), which represents the lower end of the recommended apatite size, a number of inclusions (n = 1, 2, 4, 10, 20, 50, and 100) with varying sizes (w = 1, 3, and 6 μm) and concentration gradients (C_I/C_H = 10, 20, 30, 40, 50, 60, 70, 80, 90, 100) are randomly created and F_T calculated. Fig. 3.14 shows the normalized He distribution for a subset (C_I/C_H = 100) of the individual model runs. The results for all 210 model runs are shown in Fig. 3.15 where the inclusion activity, the ratio of He production from inclusions divided by the total He production, is plotted against the inclusion-free (FT) divided by inclusion-bearing (FT*) values. Even for the highest concentration gradient, F_T values for grains with very small inclusions are within 1% of the value for the homogenous grain. In instances where apatites have larger inclusions, their position is critical and F_T values tend to show a more significant deviation from the base case.

3.4.5 He-Implantation ("Bad Neighborhood")

Significant contribution of He caused by implantation from nearby high-U/Th phases has the potential to produce over-dispersed and inaccurate He-ages (e.g. Spencer et al., 2004). In an attempt to explain the high variability in rutile He ages from samples collected from cores of the Continental Deep Drilling project (KTB), Wolfe (unpublished M.S. thesis, 2009) conducted in-depth analysis on polished thin sections using secondary electron microscopy (SEM). Besides the large scatter in the dataset, rutile He ages younger than zircon and titanite He ages from the same samples are in disagreement with the proposed closure temperature of ~210-235°C derived from laboratory diffusion experiments. These values are higher than the closure temperatures for the other two phases, therefore rutile He ages should be older than zircon and titanite He ages assuming similar grain sizes and homogenous parent distribution. SEM analysis revealed that many of the rutile grains were either surrounded or adjacent to titanite formed as a result of rutile breakdown during retrograde metamorphosis. Based on this analysis, Wolfe determined a representative titanite rim width of 0-5 μm for the rutile population. As an additional complication, the titanite rims are not or only partially preserved after standard mechanical grain separation, which adds the problem of measuring "parentless" He during (U-Th)/He analysis. Using isotope concentrations from published titanite analysis (Stockli and Farley, 2004) as a proxy for the parent concentration of the titanite rims, a 5-75 fold increase in the effective uranium concentration (eU=[U]+0.2299*[Th]+0.0051*[Sm]) from rutile core to titanite rim is suggested. As a function of rim width, concentration gradient, and rim preservation, three possible scenarios are identified by Wolfe. (1) rutile grains that never had a titanite rim will give a correct age, (2) rutile grains with preserved rims will give ages that are too young because of increased He ejection out of the rim, and (3) rutile grains that lost their rims during mechanical separation will yield ages that are too old because of He implantation and "parentless" He measurement. In an attempt to correct the raw ages, Wolfe first converted the grain measurements to spheres with equivalent spherical radius (ESR). Following, different rim widths and concentrations were modeled with the forward modeling tool within HeMP using published thermal histories for the KTB drill hole. Actual F_T values were calculated from the He diffusion profile summing over parts of the profile only.

Here, a similar exercise is undertaken using a tetragonal prism instead of converting the grain dimensions to spheres with equivalent spherical radius. Based on the average U/Th ratios and eU (rutile, pers. comm., Wolfe; titanite, Stockli and Farley, 2004) the rim concentrations are adjusted accordingly to give the proposed range of eU (5-75 times the core concentration). Proportionate distribution of U and Th based on the U/Th ratios of rutile and titanite is important because of the significantly different stopping distances of these two isotopes. 40 models with rim widths of 1-5 μm and varying concentration ratios are run. A subset of the model results illustrating the severe redistribution of He is shown in Fig. 3.16. For all different concentration gradients and rim widths, the grains show elevated He concentrations within ~10-20 μm of the grain edge and a maximum relative accumulation of He at the corners of the grain. F_T is calculated for all possible scenarios of rim removal during mineral separation and the results are shown in Fig. 3.17 for each concentration gradient.

3.5 DISCUSSION

Although the chosen approach to calculate F_T based on a three-dimensional grid might not be as elegant or efficient as others (Farley, 1999; Farley and Stockli, 2002; Hourigan et al., 2005; Ketcham et al., 2011), the gridding has been proven advantageous for following reasons. First, there is no requirement for symmetrical zoning but the user can define zones of different geometries that can be shifted in all three dimensions within the grain or can model grains with micro-inclusions dispersed in a host grain. Second, having these matrices on hand, one can calculate the F_T for grains that have been modified by polishing or mechanical abrasion by simply summing over portions of the output grids (M_{HeP}, M_{HeD}) prior to dividing them. The additional option to create "Library" files for any grain shape and size of interest can dramatically decrease computational time if the user is only interested in bulk F_T and the final He distribution is not a requirement. Additionally, it has to be noted that the creation of the ejection spheres is not based on a random Monte-Carlo simulation, which has the advantage that repeated modeling runs will give the exact same result.

Results from modeling a variety of unzoned grain geometries show that HeMP can accurately recreate the results obtained from calculations using parametric equations (Farley et al., 1996; Farley and Stockli, 2002; Ketcham et al., 2011) with the limitation that smaller grains will yield higher deviations from the parametrically calculated F_T as a function of the decreasing number of cells. Furthermore, comparison with the work done by Hourigan et al. (2005) proves that the approach used in this study yields reliable results for zoned crystals as well.

From the analysis of the Shillong apatite dataset, it becomes apparent that Sm cannot be neglected in the calculation of F_T and the raw He age. Besides the very high Sm concentrations in some of the samples, the other interesting fact about this dataset is that some of the published mean He ages (Biswas et al., 2007) are similar or even older than the corresponding apatite fission track (AFT) ages. At the time of this publication, Sm was included in the He age calculation but F_T was calculated using Farley (2002). Such a mismatch between AHe and AFT has been documented from other sources (e.g. Belton et al., 2004; Hendriks and Redfield, 2005;

Hansen and Reiners, 2006; Green et al., 2006; Danisik et al., 2008; Glotzbach et al., 2008; Persano et al., 2009; Kohn et al., 2009) and has caused discussions about the reliability of the (U-Th)/He technique. Although independent modeling using the recently developed radiation damage accumulation and annealing model (RDAAM, Flowers et al., 2009) confirms that He ages can be similar or older than AFT ages, this study shows that proper incorporation of Sm into the age and F_T equations can result in significantly younger ages by itself. So far, the results presented the impact of Sm on individual aliquots but in (U/Th)/He dating it is common practice to combine aliquots and report the mean age and standard deviations as the result. Table 3.1 lists the mean He ages and standard deviations calculated with and without Sm as well as the published AFT ages. All mean ages show some degree of improvement towards younger ages although not as dramatic as some of the aliquot analysis would suggest. A decrease in the standard deviation for all but two samples might suggest that in fact the insufficient incorporation of Sm in the F_T calculation contributed to the relative large scatter of aliquot ages. Given that the spread is still much larger than the 2σ uncertainty of 6% determined from analysis of lab standards, one could argue that the parent distribution is not homogenous and zonation is responsible for the high variability in the data. Overall, this analysis proves that Sm should not be neglected and needs to be measured and incorporated into the age and F_T calculation to avoid results that are shifted towards incorrect, older ages.

Grain shape modifications during sedimentary transport can be one of the most critical factors influenced the final He age in sedimentary studies. Contrary to analysis of magmatic samples, the outer parts of the grain are lost and therefore not accessible to further analysis. As shown above, assuming that the remaining grain has an F_T value equal to 1 is only valid for homogenous parent distributions and abrasion exceeding the maximum stopping distance.

Although this assumption might be the best available, the *FT-Calculator* offers the tools to investigate the range of possible F_T values for estimated initial grain dimensions and parent concentration patterns. A very important outcome of the abrasion modeling is that manual abrasion of grains prior to (U-Th)/He analysis to remove the outer ~20 μm and artificially set the F_T to 1 can, depending on the zonation pattern, potentially introduce larger errors compared to calculation of F_T based on the full grain

As suggested by Vermeesch (2007), inclusions do not represent as a dramatic problem in apatite (U/Th)/He analysis as often put forward to explain large scatter in He ages. From the limited number of model runs done in this study it has to be concluded that even a very large number of small inclusions do not significantly affect F_T. Although values can exceed 6%, it is more than unlikely that grains with that many inclusions of considerable size are used for analysis. The vast majority of model runs yield results within 1% of the F_T value obtained from the same apatite grain with no inclusions. For practical purposes, the analyst has several options to avoid introducing large uncertainties in the age calculation based on erroneous F_T values. First and foremost, only inclusion free grains should be analyzed but if the sample quality is insufficient then grains with small inclusions should be selected preferentially. Inclusions as big as 6 μm are visible on standard binoculars and the analyst should not have any problems to discard grains that do not meet that criterion. Secondly, instead of using single grain aliquots, several grains should be combined into a single aliquot to achieve a better statistical distribution of inclusions and yield F_T values close to the homogenous parent concentration case. If inclusions are not randomly distributed but aligned with self-similar growth zonation then He will be re-distributed similarly to the zonation cases already discussed in detail and such grains should be avoided as well. In agreement with Vermeesch (2007), personal experience has shown that apatite dissolution following the zircon procedure (HF dissolution step) led to better inter-aliquot reproducibility. Advances in computer-generated tomography (CT) scanning (Herman et al., 2007) have added the opportunity to calculate F_T based on the actual grain geometry, which might show some deviation from the perfect, idiomorphic shape. Furthermore, the density contrast measured by the X-ray allows detection of inclusions within the resolution limits of this technique (2-3 μm, Stockli pers. comm.). Still, the parent distribution cannot be assessed with this technique and must be determined with other techniques or estimated by back-calculating from bulk parent concentrations using the known volume fraction of the inclusions. In this case, the *FT-Calculator* can greatly improve knowledge of the uncertainty attached to the F_T value. Based on the CT scan output, a “Library” file can be created and subsequently a large number of F_T values quickly calculated using ranges of host and inclusion parent concentrations.

As a unique case of inhomogeneous parent concentration, the rutile KTB sample analysis proved that in some instances a more elaborate study of the entire rock framework has to be undertaken. F_T values of > 10 for grains with the highest rim/core concentration gradient (X = 75), rim width (5 μm), and which have lost their titanite rim during mineral separation, demonstrate that the standard approach to correct for He ejection is insufficient.

Depth-profiling can be a very efficient technique to obtain knowledge of the zonation patterns in grains and the *FT-Calculator* accommodates the analysis of the effect on FT with an easy-to-use graphical user interface. The downside is that the concentration profile only allows a one-dimensional assessment of parent distribution. Farley et al. (2011) employed two-dimensional concentration mapping on polished sections of apatites to improve the characterization of the parent distribution. Concentration maps obtained from transverses parallel and perpendicular to the c-axis were transformed to a cylindrical geometry and F_T calculated.

Ratios of resulting F_T versus values calculated assuming homogeneous parent distribution ranged from 0.91 to 1.06 illustrating the variability that can be encountered within a single sample. An advantage of polishing grains over depth-profiling is that cathodoluminescence (CL) analysis prior to laser ablation can give an additional qualitative measure of element distributions (e.g. Jolivet et al., 2003). With the *FT-Calculator* on hand, both techniques can be exploited. Initial depth profiling can be followed up with polishing and CL imaging and/or two-dimensional laser-ablation mapping. Afterwards the grain can be re-measured and analyzed while an accurate F_T can be modeled using the imposed zonation pattern and parent concentrations. If desired, one even has the opportunity to take samples already analyzed by standard LA-ICPMS and conduct (U-Th)/He thermochronology using this new software package to calculate F_T. Because polishing is of no concern and can be corrected for with the presented workflow, sedimentary samples should be subjected to the more conventional dating approach (LA-ICPMS on polished thin sections instead on whole grains mounted on tape) where additional information about the grain interior can be gathered. Finally, as clearly demonstrated by the results in Fig. 3.10, laser ablation does not affect F_T sufficiently to justify additional correction. Nevertheless, the *FT-Calculator* has the capability to do so and might be utilized for other cases not studied here.

Parent isotope zonation and inclusions have varying effects on the F_T correction factor but even more importantly, they could significantly influence the degree of diffusive loss of He out of the grain. Zonation patterns that effectively re-distribute He towards the grain edge will cause over-proportionate He loss leading to apparent ages that are too young. Using geometric conversion functions (e.g. Ketcham et al., 2011), the grain geometry and zonation pattern can be transformed to an equivalent sphere. Forward modeling utilizing the other modules within HeMP can then be used to address the affect of zonation on the closure temperature and the diffusion profile. Investigating this topic, Gautheron et al. (2010) presented a Monte-Carlo based algorithm that used actual grain geometries and Brownian motion theory to track He from production to final resting place after diffusion.

3.6 CONCLUSION

The F_T correction is a simple but very critical step in (U-Th)/He thermochronology and a necessity to calculate accurate He ages. Current practice is using a single value derived from parametric equations directly as a correction for the raw age (Farley et al., 1996) or within the age equation (Ketcham et al., 2011). The final uncertainty on a single aliquot He age is determined by the reproducibility of standards, which in all cases exceeds the analytical precision of parent/daughter concentration measurements. The underlying assumption is that the dispersion in standard ages is capturing the natural variability within the standard population and serves as a best estimate for analysis of other samples. Unfortunately, this comparison only holds true for samples that are cooled quickly, in other cases the uncertainties might be significantly higher because of combined effects of ejection and diffusion of He. Therefore, an independent estimation of age uncertainties for each sample set is favorable.

The best-case scenario would be a complete decoupling of uncertainties related to analytical errors from uncertainties in the F_T calculation. As a result, both errors could be rigorously propagated throughout the age equation leading to an improved representation of the uncertainties around the calculated ages. In routine (U-Th)/He analysis this is difficult to accomplish because each analyzed grain would have to undergo additional analysis to characterize its exact geometry, zonation pattern, and inclusion distribution. Nevertheless, the *FT-Calculator* provides all the necessary tools to be able to calculate an accurate F_T using auxiliary data. Although the current version includes a wide variety of tools to model F_T, future versions could provide methods that are even more accurate. Especially the CT-scanning technique could bolster analysis because measurement uncertainties would be eliminated and the effects of inclusions could be modeled with greater confidence. Sedimentary samples are particularly problematic because the geometry of the grain changes while He is ejected continuously throughout the post-cooling history of the sample. As of now, the *FT-Calculator* ignores this circumstance but could be adapted to incorporate multi-stage modeling.

CHAPTER 3: REFERENCES CITED

Belton, D. X., Kohn, B. P., and Gleadow, A. J. W., 2004a, Quantifying "excess helium": some of the issues and assumptions in combined (U–Th)/He and fission track analysis: In: Andressien, P. (Ed.), 10th International Fission track Dating Conference. Amsterdam, p. 18.

Belton, D. X., Lorencak, M., Carter, T. J., Norman, M., Kohn, B. P., and Gleadow, A. J. W., 2004b, Samarium in apatite: contributions to radiogenic helium and the effect on (U–Th)/He thermochronology: In: Andressien, P. (Ed.), 10th International Fission track Dating Conference. Amsterdam, p. 40.

Biswas, S., Coutand, I., Grujic, D., Hager, C., Stöckli, D., and Grasemann, B., 2007, Exhumation and uplift of the Shillong plateau and its influence on the eastern Himalayas: New constraints from apatite and zircon (U-Th-[Sm])/He and apatite fission track analyses: Tectonics, v. 26, no. 6, p. TC6013.

Boyce, J. W., and Hodges, K. V., 2005, U and Th zoning in Cerro de Mercado (Durango, Mexico) fluorapatite: Insights regarding the impact of recoil redistribution of radiogenic ^{4}He on (U-Th)/He thermochronology: Chemical Geology, v. 219, p. 261-274.

Boyce, J. W., Hodges, K. V., King, D., Crowley, J. L., Jercinovic, M., Chatterjee, N., Bowring, S. A., and Searle, M., 2009, Improved confidence in (U-Th)/He thermochronology using the laser microprobe: An example from a Pleistocene leucogranite, Nanga Parbat, Pakistan: Geochem. Geophys. Geosyst., v. 10.

Boyce, J. W., Hodges, K. V., Olszewski, W. J., Jercinovic, M. J., Carpenter, B. D., and Reiners, P. W., 2006, Laser microprobe (U-Th)/He geochronology: Geochimica et Cosmochimica Acta, v. 70, no. 12, p. 3031-3039.

Corfu, F., Hanchar, J. M., Hoskin, P. W. O., and Kinny, P., 2003, Atlas of Zircon Textures: Reviews in Mineralogy and Geochemistry, v. 53, no. 1, p. 469-500.

Danišík, M., Sachsenhofer, R. F., Privalov, V. A., Panova, E. A., Frisch, W., and Spiegel, C., 2008, Low-temperature thermal evolution of the Azov Massif (Ukrainian Shield–Ukraine) - Implications for interpreting (U–Th)/He and fission track ages from cratons: Tectonophysics, v. 456, no. 3–4, p. 171-179.

Emmel, B., Jacobs, J., Crowhurst, P., Austegard, A., and Schwarz-Schampera, U., 2008, Apatite single-grain (U-Th)/He data from Heimefrontfjella, East Antarctica: Indications for differential exhumation related to glacial loading?: Tectonics, v. 27, no. 6, p. TC6010.

Emmel, B., Jacobs, J., Crowhurst, P., and Daszinnies, M., 2007, Combined apatite fission-track and single grain apatite (U–Th)/He ages from basement rocks of central Dronning Maud Land (East Antarctica)—Possible identification of thermally overprinted crustal segments?: Earth and Planetary Science Letters, v. 264, no. 1, p. 72-88.

Farley, K. A., 2002, (U-Th)/He dating; techniques, calibrations, and applications: Reviews in Mineralogy and Geochemistry, v. 47, p. 819-843.

Farley, K. A., Kohn, B. P., and Pillans, B., 2002, The effects of secular disequilibrium on (U-Th)/He systematics and dating of Quaternary volcanic zircon and apatite: Earth and Planetary Science Letters, v. 201, no. 1, p. 117-125.

Farley, K. A., and Stockli, D. F., 2002, (U-Th)/He Dating of Phosphates: Apatite, Monazite, and Xenotime: Reviews in Mineralogy and Geochemistry, v. 48, no. 1, p. 559-577.

Farley, K. A., Wolf, R. A., and Silver, L. T., 1996, The effects of long alpha-stopping distances on (U-Th)/he ages: Geochimica et Cosmochimica Acta, v. 60, p. 4223-4229.

Fitzgerald, P. G., Baldwin, S. L., Webb, L. E., and O'Sullivan, P. B., 2006, Interpretation of (U–Th)/He single grain ages from slowly cooled crustal terranes: A case study from the Transantarctic Mountains of southern Victoria Land: Chemical Geology, v. 225, no. 1–2, p. 91-120.

Flowers, R. M., Ketcham, R. A., Shuster, D. L., and Farley, K. A., 2009, Apatite (U-Th)/He thermochronometry using a radiation damage accumulation and annealing model: Geochimica et Cosmochimica Acta, v. 73, no. 8, p. 2347-2365.

Gautheron, C., and Tassan-Got, L., 2010, A Monte Carlo approach to diffusion applied to noble gas/helium thermochronology: Chemical Geology, v. 273, no. 3–4, p. 212-224.

Glotzbach, C., Reinecker, J., Danišík, M., Rahn, M., Frisch, W., and Spiegel, C., 2008, Neogene exhumation history of the Mont Blanc massif, western Alps: Tectonics, v. 27, no. 4, p. TC4011.

Hansen, K., and Reiners, P. W., 2006, Low temperature thermochronology of the southern East Greenland continental margin: Evidence from apatite (U-Th)/He and fission track analysis and implications for intermethod calibration: Lithos, v. 92, no. 1-2, p. 117-136.

Hendriks, B. W. H., and Redfield, T. F., 2005, Apatite fission track and (U-Th)/He data from Fennoscandia: An example of underestimation of fission track annealing in apatite: Earth and Planetary Science Letters, v. 236, no. 1–2, p. 443-458.

Herman, F., Braun, J., Senden, T. J., and Dunlap, W. J., 2007, (U-Th)/He thermochronometry: Mapping 3D geometry using micro-X-ray tomography and solving the associated production-diffusion equation: Chemical Geology, v. 242, no. 1-2, p. 126-136.

Hourigan, J., K., Reiners, P. W., and Brandon, M., T., 2005, U-Th zonation-dependent alpha-ejection in (U-Th)/He chronometry: Geochimica et Cosmochimica Acta, v. 69, no. 13, p. 3349-3365.

House, M. A., Farley, K. A., and Stockli, D., 2000, Helium chronometry of apatite and titanite using Nd-YAG laser heating: Earth and Planetary Science Letters, v. 183, no. 3-4, p. 365-368.

Jolivet, M., Dempster, T., and Cox, R., 2003, Distribution of U and Th in apatites: implications for U-Th/He thermochronology: Comptes Rendus Geosciences, v. 335, p. 899-906.

Ketcham, R. A., Gautheron, C., and Tassan-Got, L., 2011, Accounting for long alpha-particle stopping distances in (U–Th–Sm)/He geochronology: Refinement of the baseline case: Geochimica et Cosmochimica Acta, v. 75, no. 24, p. 7779-7791.

Kohn, B., Lorencak, M., Gleadow, A., Kohlmann, A., Raza, A., Osadetz, K., and Sorjonen-Ward, P., 2009, Low-temperature thermochronology of the eastern Fennoscandia Shield and radiation enhanced annealing revisited: Geological Society of London Special Publication, v. 324.

Min, K., Farley, K. A., Renne, P. R., and Marti, K., 2003, Single grain (U–Th)/He ages from phosphates in Acapulco meteorite and implications for thermal history: Earth and Planetary Science Letters, v. 209, no. 3, p. 323-336.

Persano, C., Swift, D. A., Stuart, F. M., and Olive, V., 2009, Reproducibility of old apatite (U-Th)/He ages: an example from East Greenland: EGU General Assembly 2009, held 19-24 April, 2009 in Vienna, p. 10247.

Rahl, J. M., Reiners, P. W., Campbell, I. H., Nicolescu, S., and Allen, C. M., 2003, Combined single-grain (U-Th)/He and U/Pb dating of detrital zircons from the Navajo Sandstone, Utah: Geology, v. 31, no. 9, p. 761-764.

Reiners, P. W., 2005, Zircon (U-Th)/He Thermochronometry: Reviews in Mineralogy and Geochemistry, v. 58, no. 1, p. 151-179.

Spencer, A. S., Kohn, B. P., Gleadow, A. J. W., Norman, M., Belton, D. X., and Carter, T. J., 2004, The importance of residing in a good neighbourhood: rechecking the rules of the game for apatite (U–Th)/He thermochronology: In: Andressien, P. (Ed.), 10th International Fission track Dating Conference. Amsterdam, p. 20.

Spiegel, C., Kohn, B., Belton, D., Berner, Z., and Gleadow, A., 2009, Apatite (U–Th–Sm)/He thermochronology of rapidly cooled samples: The effect of He implantation: Earth and Planetary Science Letters, v. 285, no. 1–2, p. 105-114.

Stockli, D., F., and Farley, K. A., 2004, Empirical constraints on the titanite (U-Th)/He partial retention zone from the KTB drill hole: Chemical Geology, v. 207, p. 223-236.

Vermeesch, P., Seward, D., Latkoczy, C., Wipf, M., Günther, D., and Baur, H., 2007, [alpha]-Emitting mineral inclusions in apatite, their effect on (U-Th)/He ages, and how to reduce it: Geochimica et Cosmochimica Acta, v. 71, no. 7, p. 1737-1746.

Wolfe, M., 2009, He diffusion in rutile and calibration of rutile (U–Th)/He thermochronology on the KTB ultra-deep borehole: Unpublished MS, The University of Kansas, Lawrence, Kansas.

Ziegler, J. F., and Biersack, J. P., 2008, SRIM-2008, Stopping Power and Range of Ions in Matter: v05 ed. SRIM Co., Chester, Maryland.

Ziegler, J. F., Biersack, J. P., and Ziegler, M. D., 2008, SRIM-2008 software package: available online at www.srim.org.

CHAPTER 3: FIGURES AND TABLES

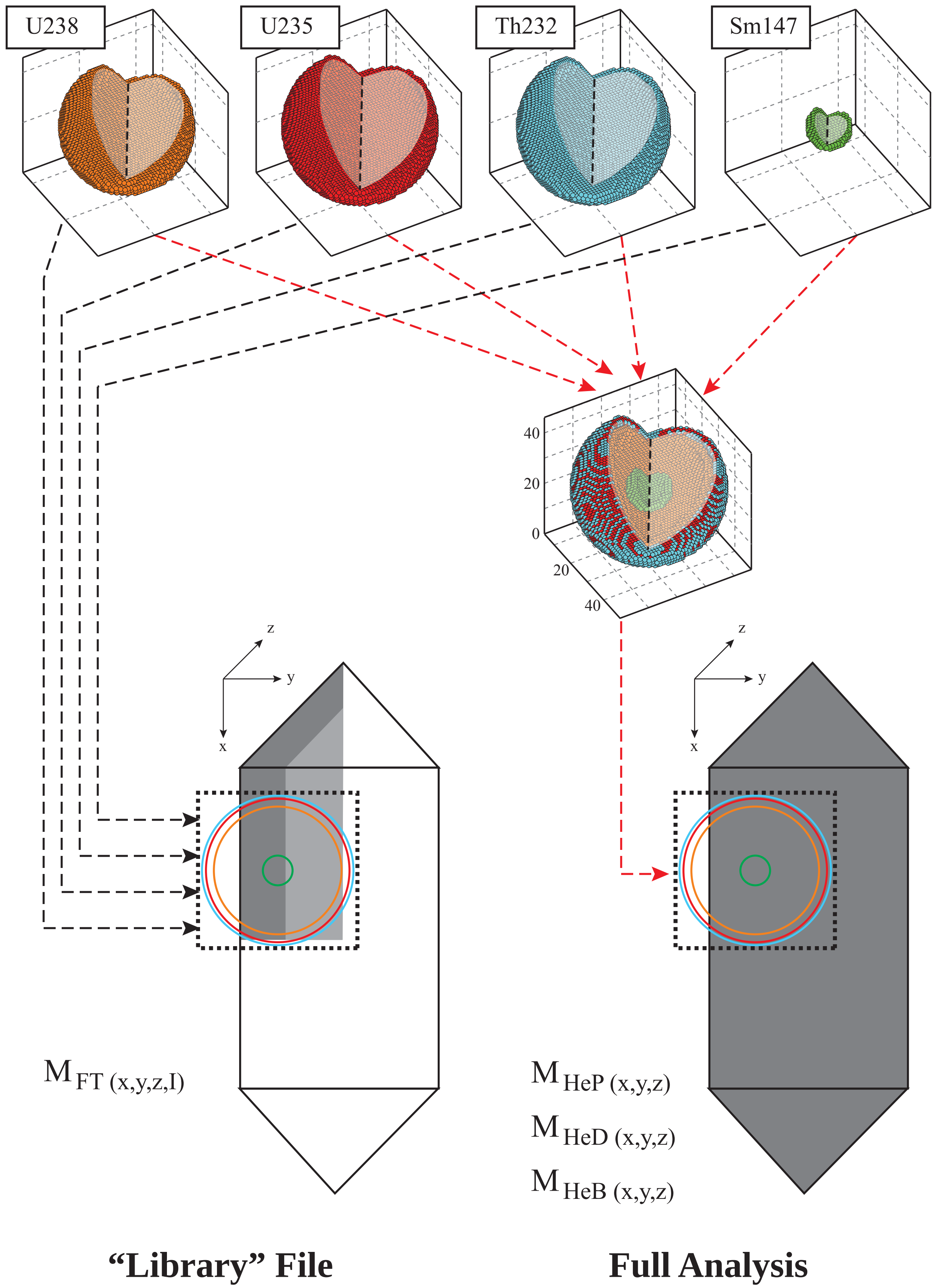
U238
U235
Th232
Sm147
40
20
0
20
40
z
y
x
z
y
x
M FT (x,y,z,I)
M HeP (x,y,z)
M HeD (x,y,z)
M HeB (x,y,z)
“Library” File
Full Analysis

Figure 3.1: Illustration of the two model approaches and outputs available in the *FT-Calculator*. On top, the individual ejection spheres for each isotope which are combined and moved through the entire 3D grain grid (dark-grey shaded area) during the full analysis. Each node (x, y, z) in the He distribution matrix (M_{HeD}) contains the sum of all He particles ejected from surrounding nodes. Contrary, during creation of the "Library" file, each individual ejection sphere is moved through a reduced 3D grain grid (dark-grey shaded area) and each node has the value of the local F_T for each isotope (I). Light-grey shaded area (not to scale!) marks the portion of the grid that does not need to be analyzed because FT in the interior of the grain equals 1.

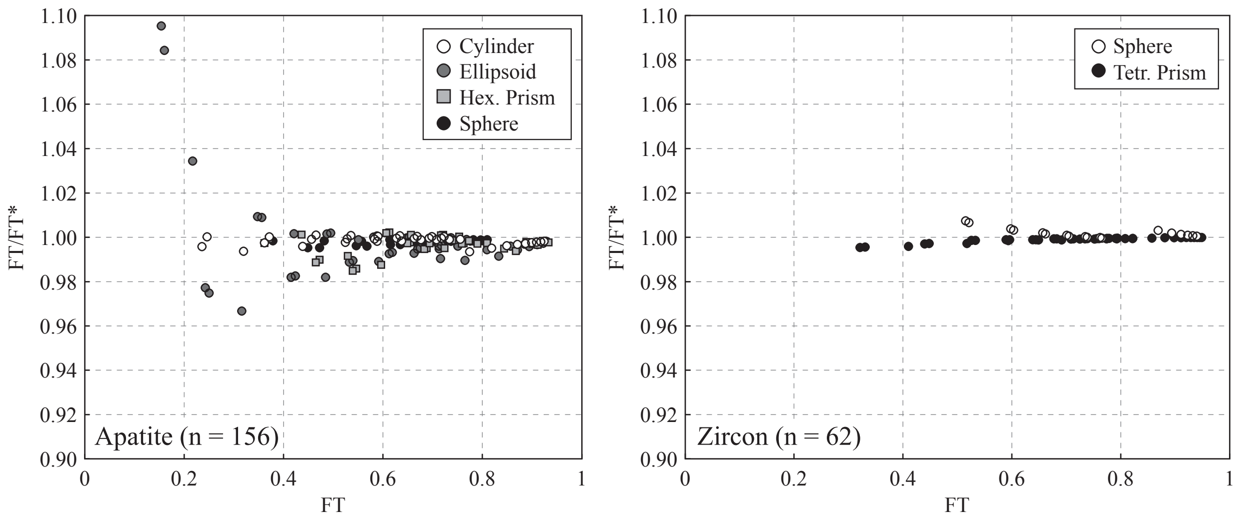
Cylinder
Ellipsoid
Hex. Prism
Sphere
Apatite (n = 156)
FT/FT*
FT
Sphere
Tetr. Prism
Zircon (n = 62)
FT/FT*
FT

Figure 3.2: Comparative plots of F_T obtained from the *FT-Calculator* (FT) versus F_T calculated with the equations provided by Ketcham et al. (2011, FT*) for a variety of grain geometries.

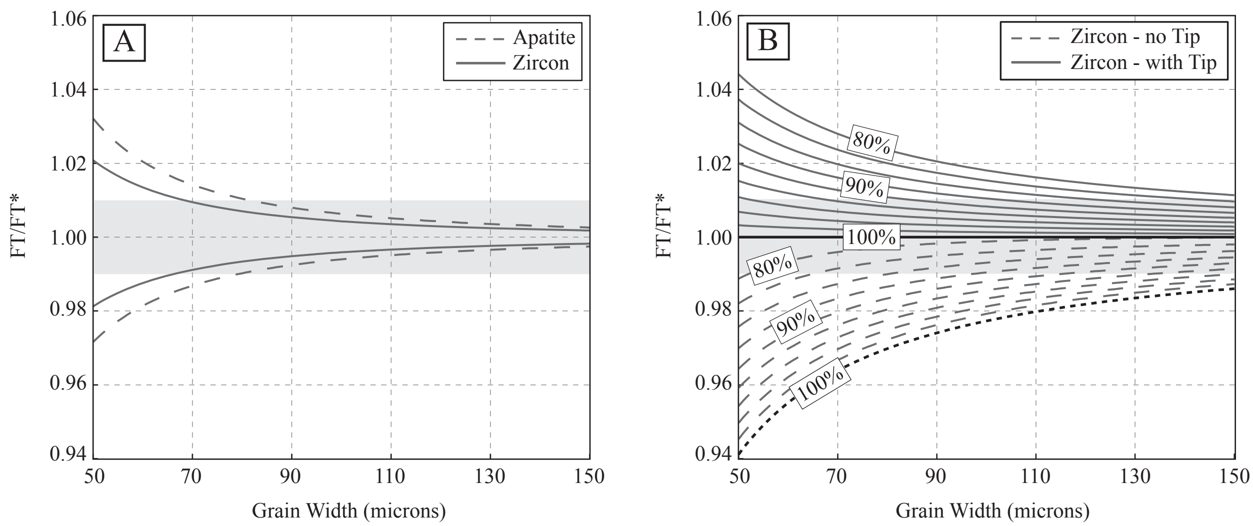
A
Apatite
Zircon
FT/FT*
Grain Width (microns)
1.06
1.04
1.02
1.00
0.98
0.96
0.94
50
70
90
110
130
150
B
Zircon - no Tip
Zircon - with Tip
80%
90%
100%
80%
90%
100%
FT/FT*
Grain Width (microns)

Figure 3.3: A) True F_T value (FT) divided by F_T correction factor (FT*) based on inaccurate measurement of grain dimensions plotted against grain widths. B) Effect on FT from insufficient capture of full three-dimensional grain shape for a range of zircon widths.

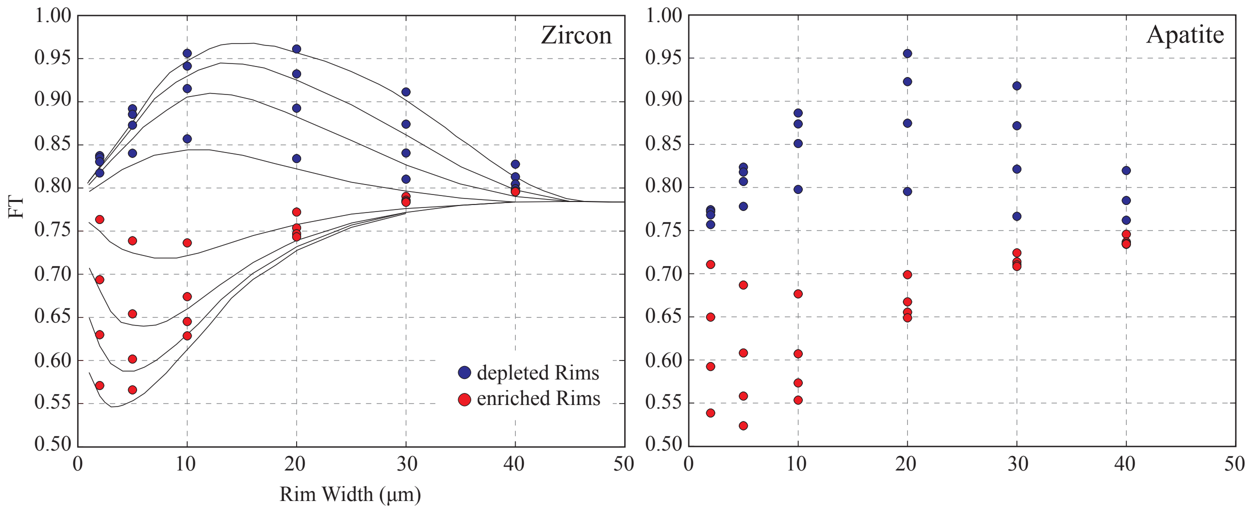
Zircon
Apatite
FT
Rim Width (µm)
depleted Rims
enriched Rims
1.00
0.95
0.90
0.85
0.80
0.75
0.70
0.65
0.60
0.55
0.50
0
10
20
30
40
50

Figure 3.4: F_T dependence on rim width and concentration gradient for a zircon grain of given dimension shown on the left. Circles represent the results from the *FT-Calculator* superimposed on Hourigan et al. (2005) analysis (lines). On the right, results for hexagonal prism geometry using the same input parameters.

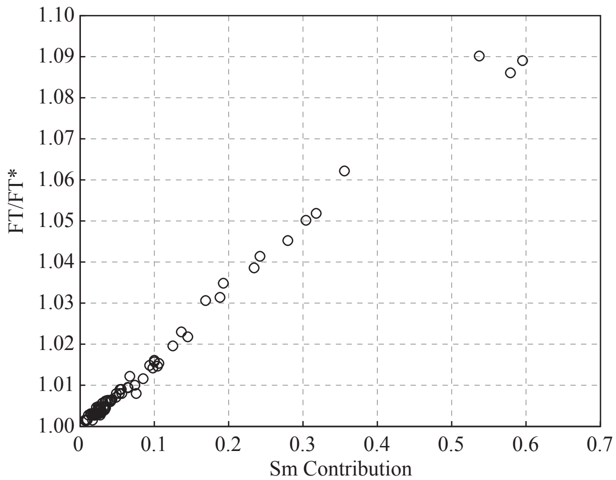
FT/FT*
Sm Contribution
1.10
1.09
1.08
1.07
1.06
1.05
1.04
1.03
1.02
1.01
1.00
0
0.1
0.2
0.3
0.4
0.5
0.6
0.7

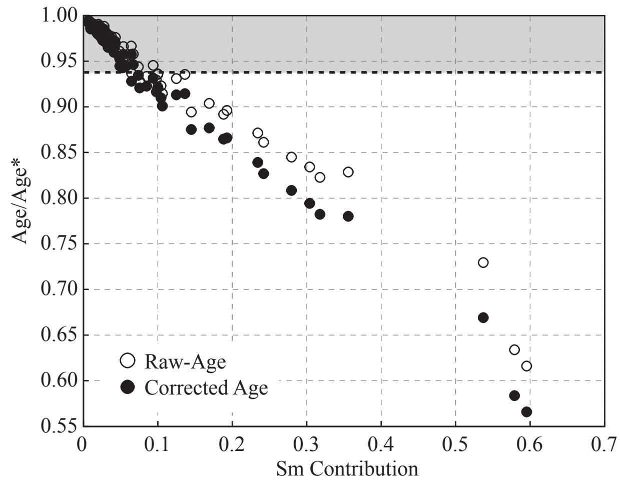
Age/Age*
Sm Contribution
Raw-Age
Corrected Age
1.00
0.95
0.90
0.85
0.80
0.75
0.70
0.65
0.60
0.55
0
0.1
0.2
0.3
0.4
0.5
0.6
0.7

Figure 3.5: Effect of Sm contribution on F_T for Shillong apatites shown on the left. Ratio of He ages (raw and corrected) ignoring Sm and incorporating Sm plotted against Sm contribution on the right. Grey-shaded area marks the accepted uncertainty range ($2\sigma \leq 6\%$) of apatite (U/Th)/He dating.

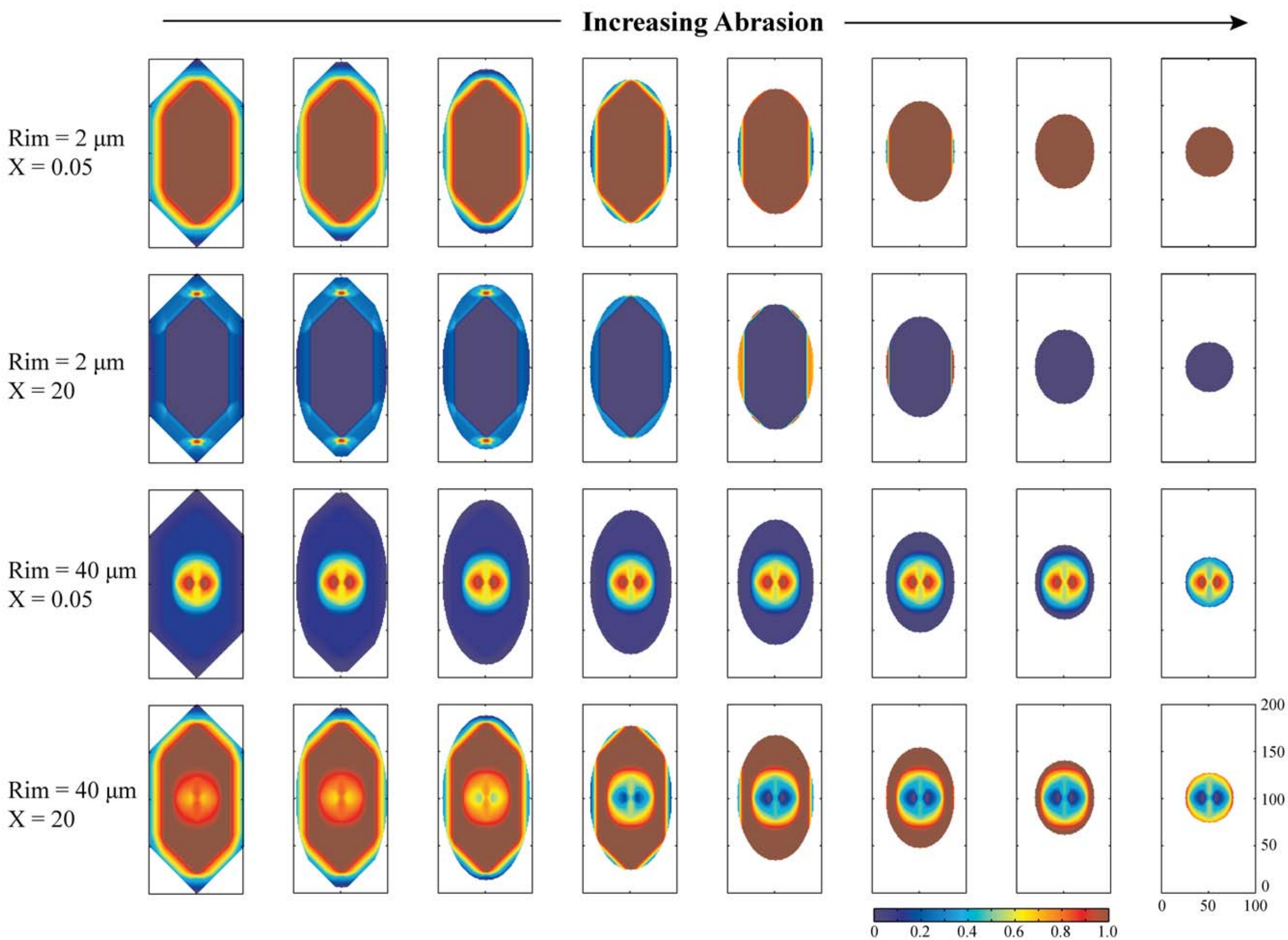
Increasing Abrasion
Rim = 2 µm
X = 0.05
Rim = 2 µm
X = 20
Rim = 40 µm
X = 0.05
Rim = 40 µm
X = 20
200
150
100
50
0
0
50
100
0
0.2
0.4
0.6
0.8
1.0

Figure 3.6: Examples of abrasion using an ellipsoidal mask that progressively decreases to a spherical geometry. Normalized He distribution is shown for maximum and minimum rim width and concentration gradients of zircon grains with tetragonal geometry and pyramidal tips.

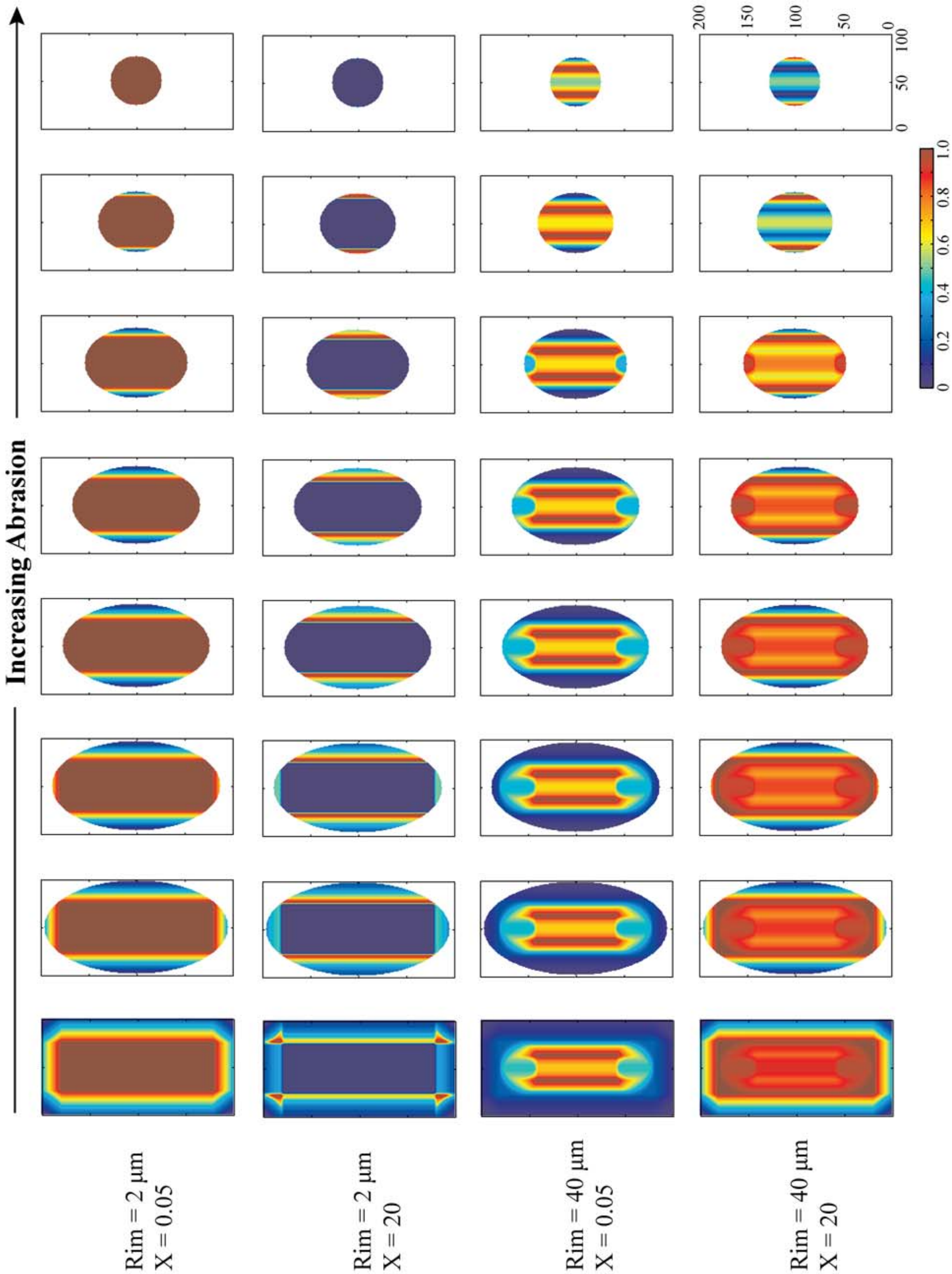

Increasing Abrasion
Rim = 2 µm
X = 0.05
Rim = 2 µm
X = 20
Rim = 40 µm
X = 0.05
Rim = 40 µm
X = 20
0
0.2
0.4
0.6
0.8
1.0
0
50
100
0
50
100
150
200

Figure 3.7: Examples of abrasion using an ellipsoidal mask that progressively decreases to a spherical geometry. Normalized He distribution is shown for maximum and minimum rim width and concentration gradients of apatite grains with hexagonal prism shape.

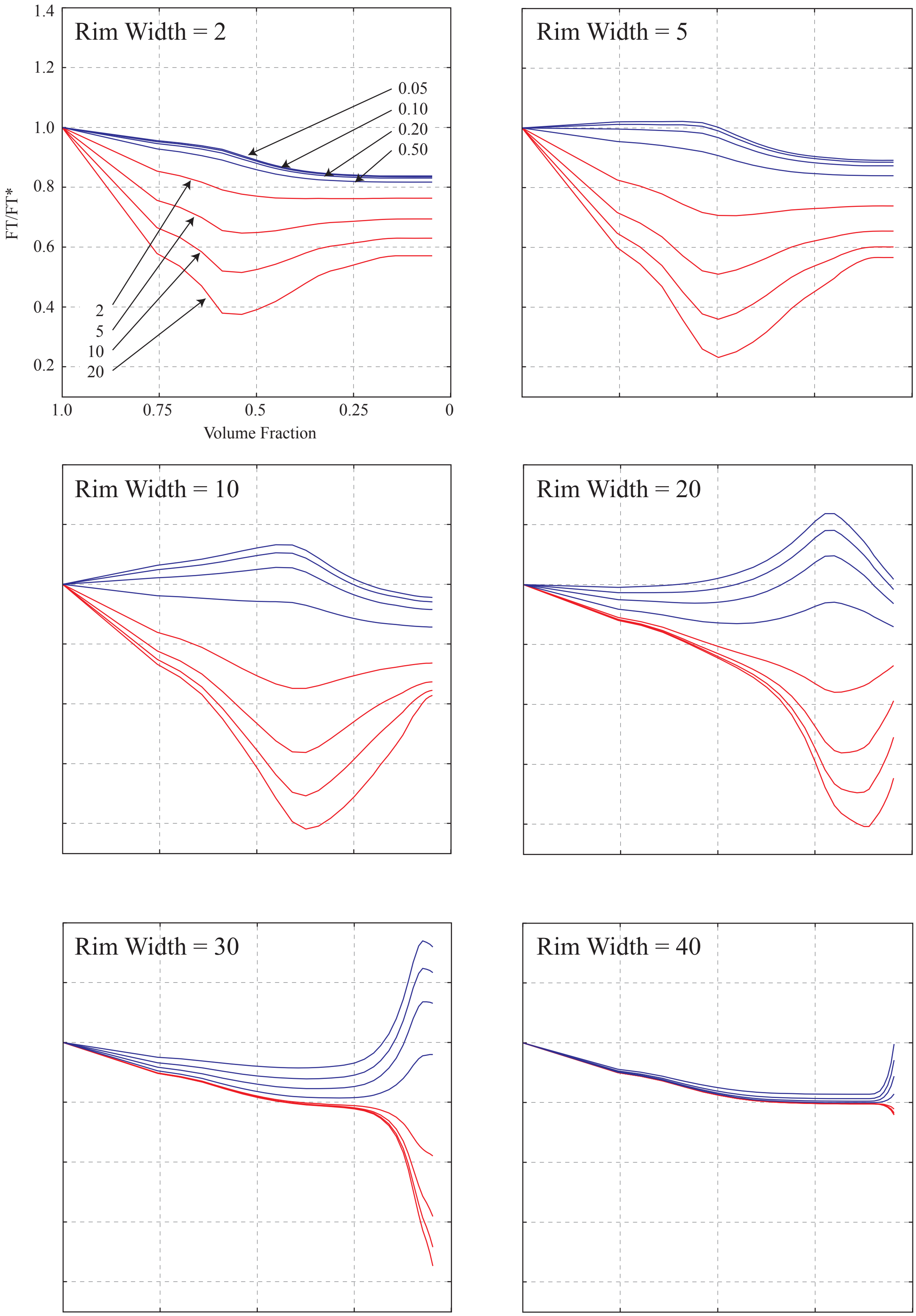

Rim Width = 2
Rim Width = 5
Rim Width = 10
Rim Width = 20
Rim Width = 30
Rim Width = 40
FT/FT*
Volume Fraction
1.4
1.2
1.0
0.8
0.6
0.4
0.2
1.0
0.75
0.5
0.25
0
0.05
0.10
0.20
0.50
2
5
10
20

Figure 3.8: Original F_T (FT) divided by F_T after abrasion (FT*) plotted against the volume fraction remaining after abrasion for zircon with different rim widths. Blue and red lines highlight model runs with depleted and enriched rims respectively.

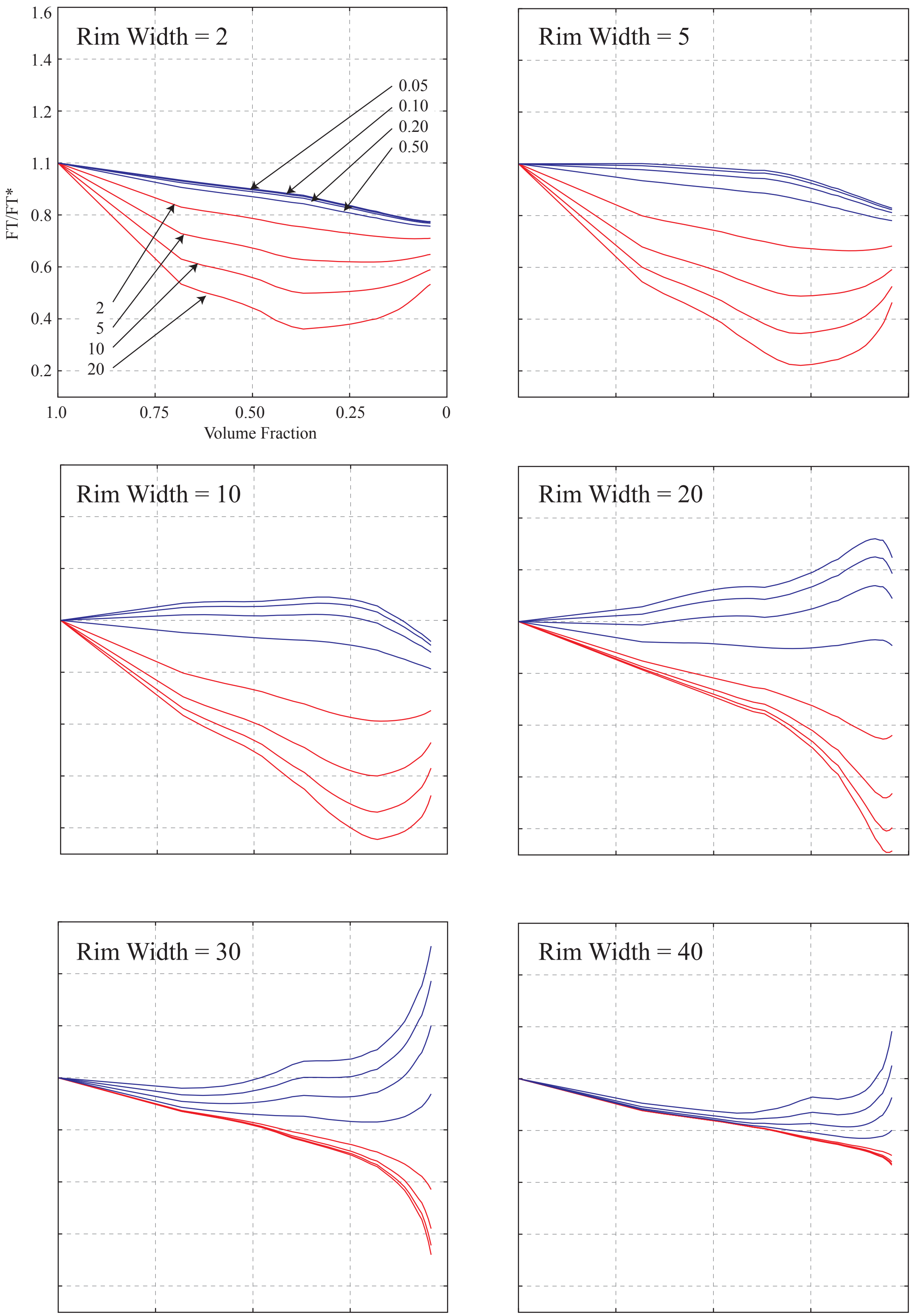
Rim Width = 2
Rim Width = 5
Rim Width = 10
Rim Width = 20
Rim Width = 30
Rim Width = 40
FT/FT*
Volume Fraction
1.6
1.4
1.2
1.1
0.8
0.6
0.4
0.2
1.0
0.75
0.50
0.25
0
0.05
0.10
0.20
0.50
2
5
10
20

Figure 3.9: Original F_T (FT) divided by F_T after abrasion (FT*) plotted against the volume fraction remaining after abrasion for apatite grains with different rim widths. Blue and red lines highlight model runs with depleted and enriched rims respectively.

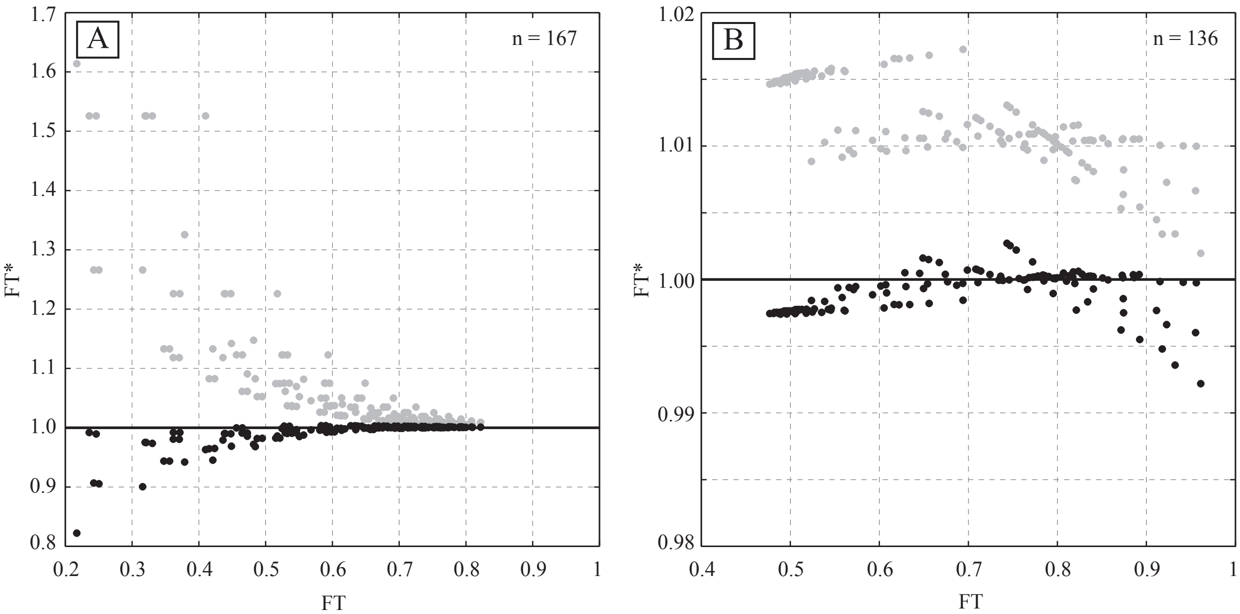
A
n = 167
FT*
FT
1.7
1.6
1.5
1.4
1.3
1.2
1.1
1.0
0.9
0.8
0.2
0.3
0.4
0.5
0.6
0.7
0.8
0.9
1
B
n = 136
1.02
1.01
1.00
0.99
0.98
0.4

Figure 3.10: F_T ratios (FT/FT*) for grains with A) homogenous parent concentrations and various geometries and dimensions and B) zoned apatite and zircon with fixed size but changing rim width and concentrations plotted against F_T of unmodified grains (FT). Grey circles indicate the ratio based on laser ablation after He degassing, black circles the common practice of laser ablation before He analysis.

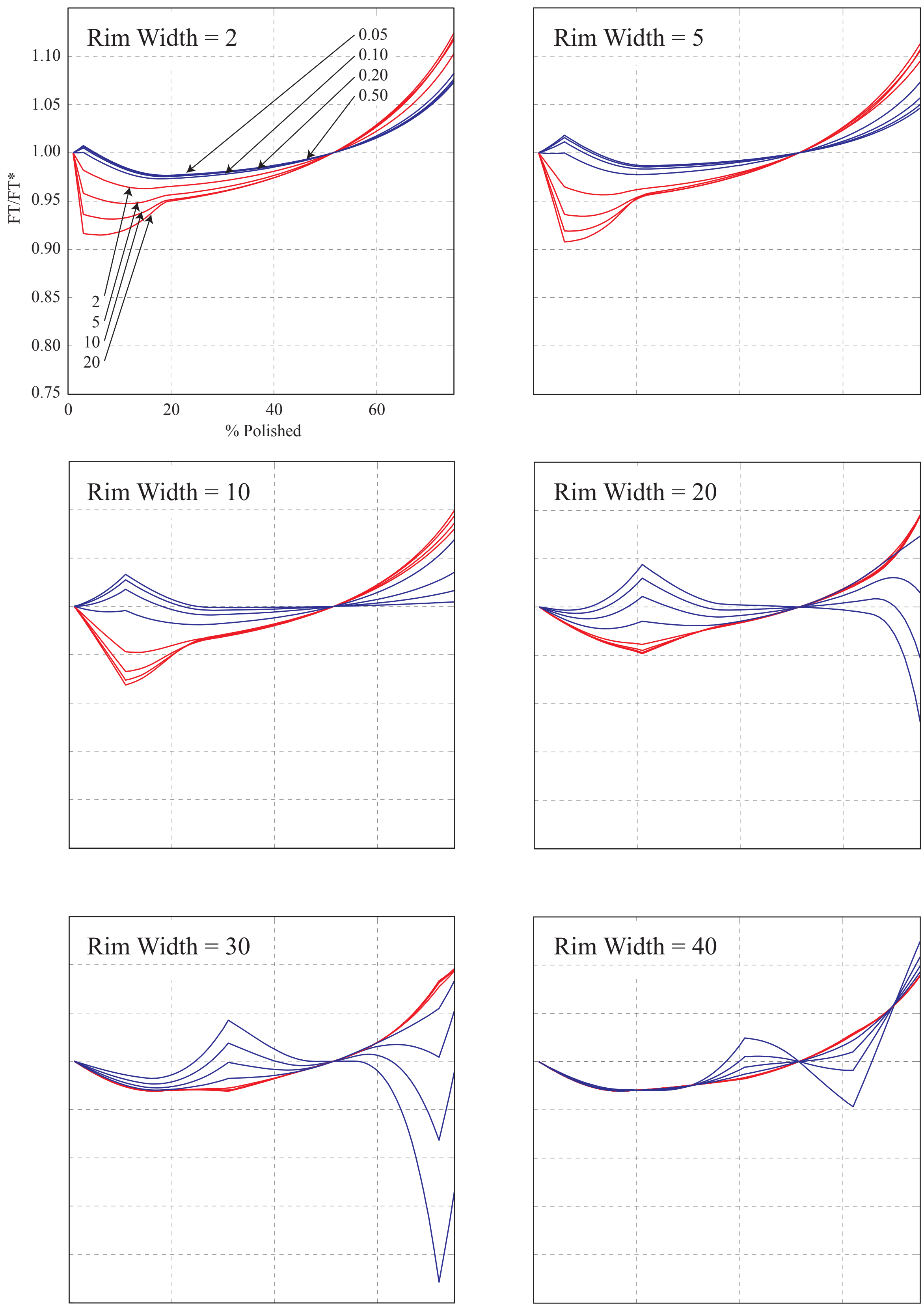

Rim Width = 2
0.05
0.10
0.20
0.50
1.10
1.05
1.00
0.95
0.90
0.85
0.80
0.75
FT/FT*
2
5
10
20
0
20
40
60
% Polished
Rim Width = 5
Rim Width = 10
Rim Width = 20
Rim Width = 30
Rim Width = 40

Figure 3.11: Original F_T divided by F_T after polishing (FT/FT*) plotted against the width fraction of abrasion for zircon grains with different rim widths. Blue and red lines highlight model runs with depleted and enriched rims respectively.

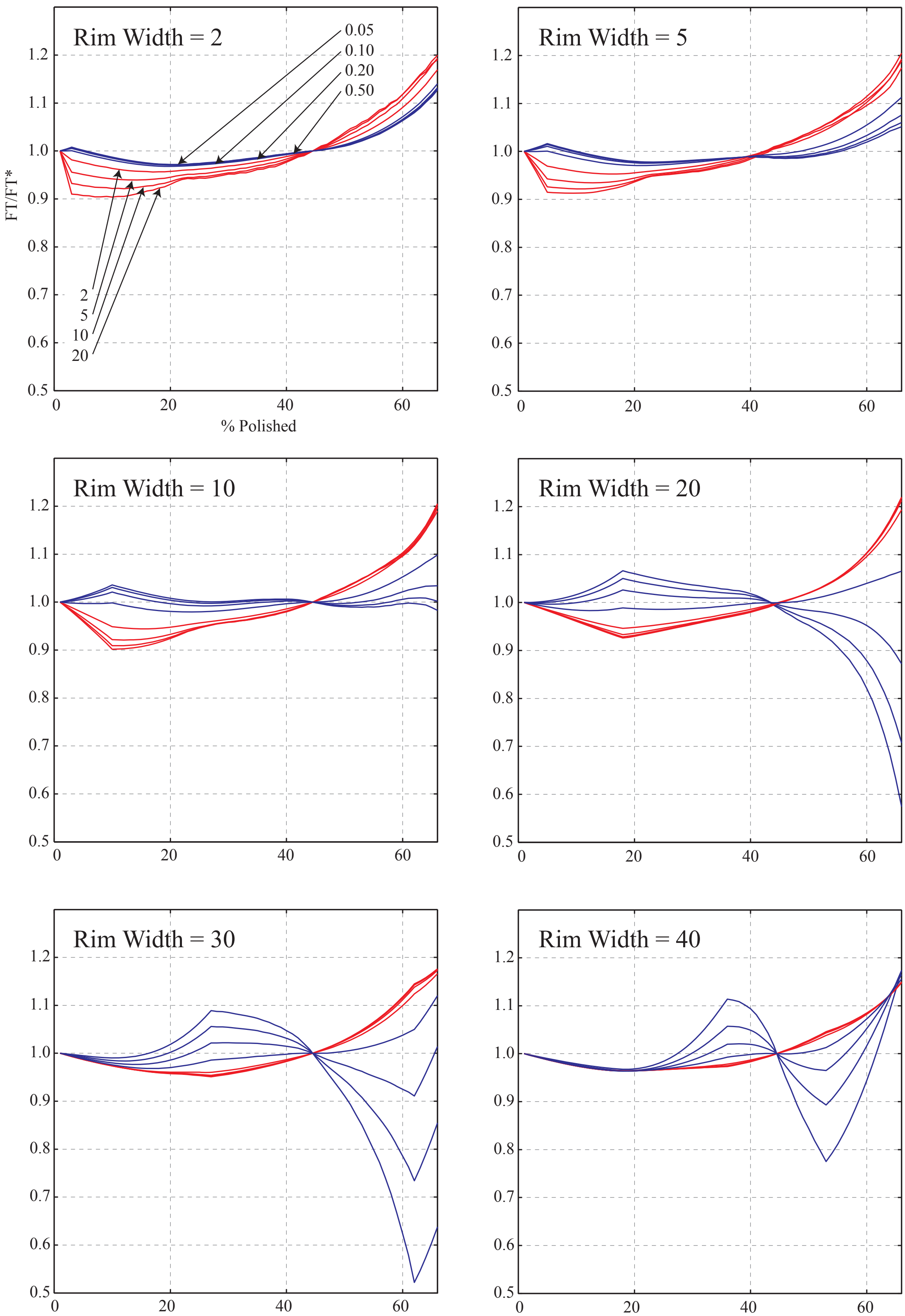
Rim Width = 2
Rim Width = 5
Rim Width = 10
Rim Width = 20
Rim Width = 30
Rim Width = 40
FT/FT*
% Polished
0.05
0.10
0.20
0.50
2
5
10
20

Figure 3.12: Original F_T divided by F_T after polishing (FT/FT*) plotted against the width fraction of abrasion for apatite grains with different rim widths. Blue and red lines highlight model runs with depleted and enriched rims respectively.

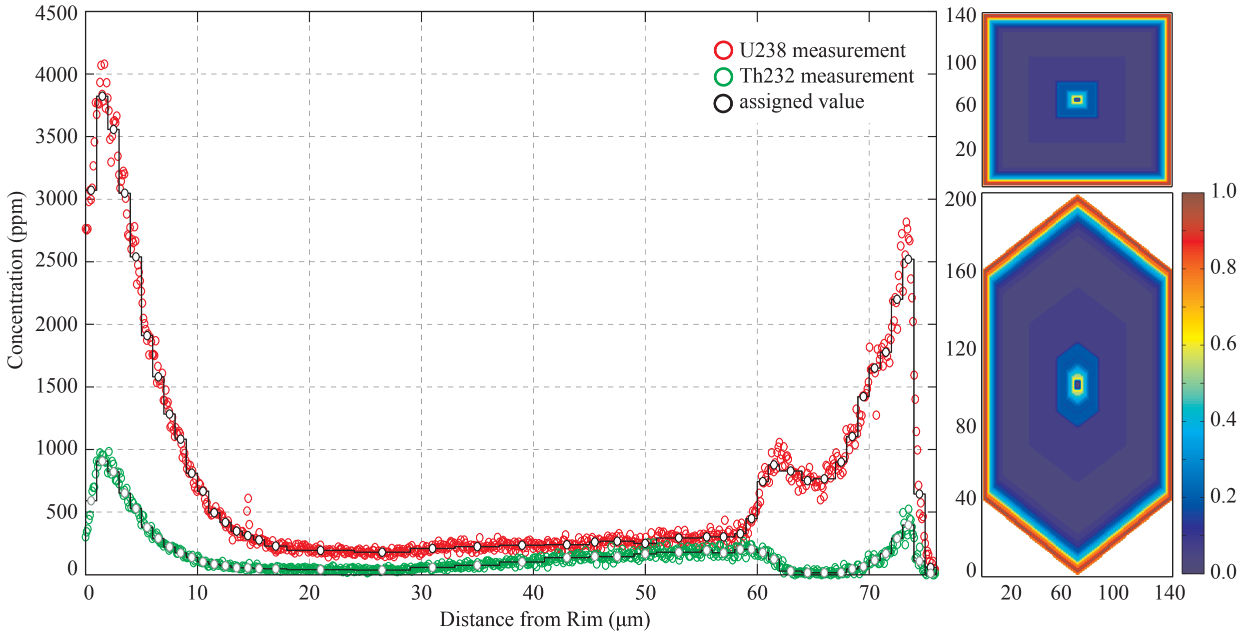

U238 measurement
Th232 measurement
assigned value
Concentration (ppm)
Distance from Rim (μm)
4500
4000
3500
3000
2500
2000
1500
1000
500
0
0
10
20
30
40
50
60
70
140
100
60
20
200
160
120
80
40
0
20
60
100
140
1.0
0.8
0.6
0.4
0.2
0.0

Figure 3.13: Analysis of parent concentrations using data from LA-ICPMS depth profiling. Left-hand side shows the raw data of uranium and thorium measurements plotted against ablation depth. Black stair-step lines and white circles indicate the binning of the data into discrete zones using user-defined limits (100 ppm in this example). On the right the final zonation pattern contoured by the normalized production.

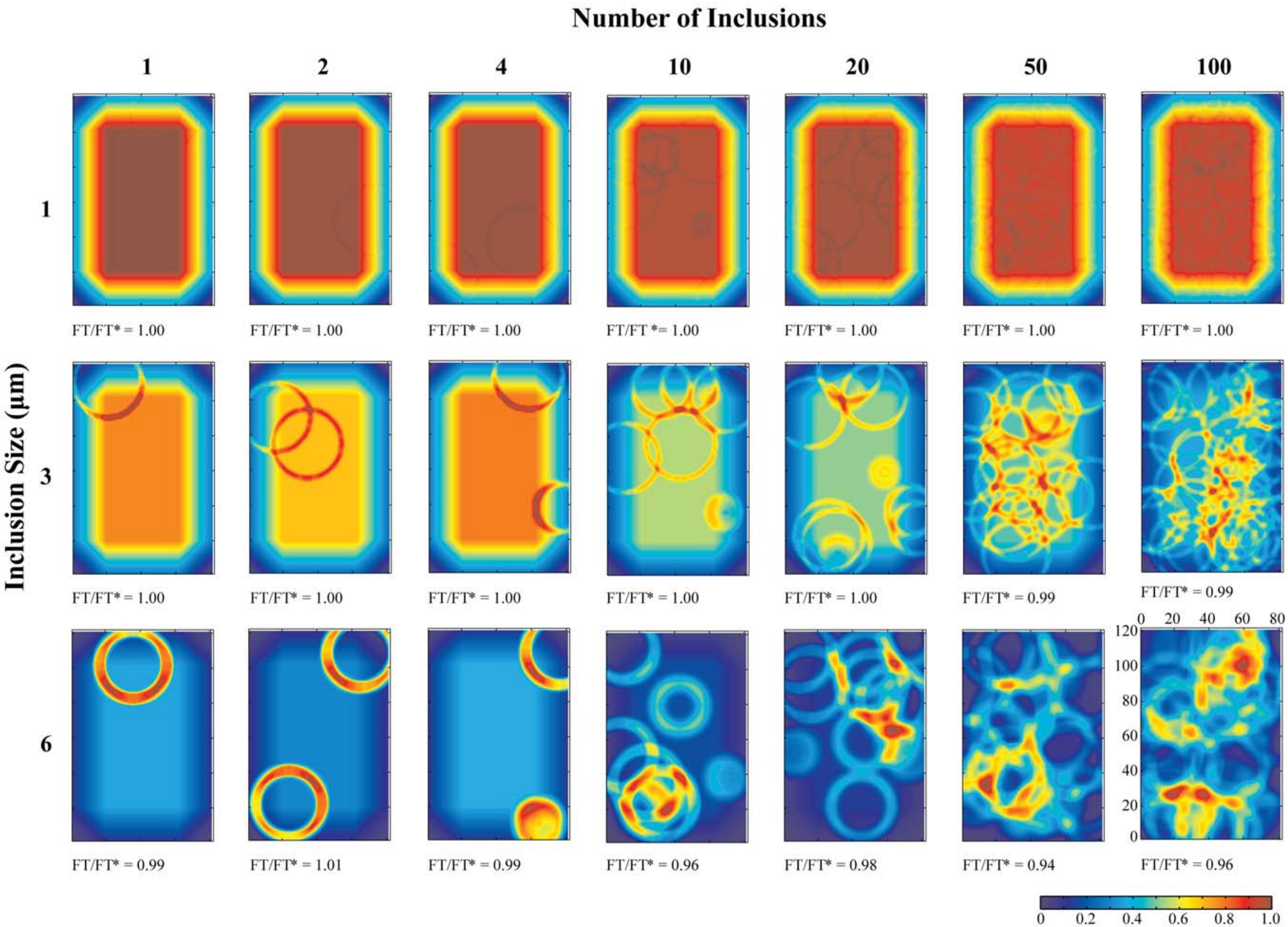

Number of Inclusions
1
2
4
10
20
50
100
Inclusion Size (μm)
1
3
6
FT/FT* = 1.00
FT/FT* = 1.00
FT/FT* = 1.00
FT/FT *= 1.00
FT/FT* = 1.00
FT/FT* = 1.00
FT/FT* = 1.00
FT/FT* = 1.00
FT/FT* = 1.00
FT/FT* = 1.00
FT/FT* = 1.00
FT/FT* = 1.00
FT/FT* = 0.99
FT/FT* = 0.99
FT/FT* = 0.99
FT/FT* = 1.01
FT/FT* = 0.99
FT/FT* = 0.96
FT/FT* = 0.98
FT/FT* = 0.94
FT/FT* = 0.96
0 20 40 60 80
120 100 80 60 40 20 0
0 0.2 0.4 0.6 0.8 1.0

Figure 3.14: Contour plots of normalized He distribution for a subset of the inclusion model runs. Top to bottom: size of inclusions increase, left to right: increasing number of inclusions. Shown results are based on inclusion concentrations (C_I) 100 times greater than the concentration at each node in the host grain (C).

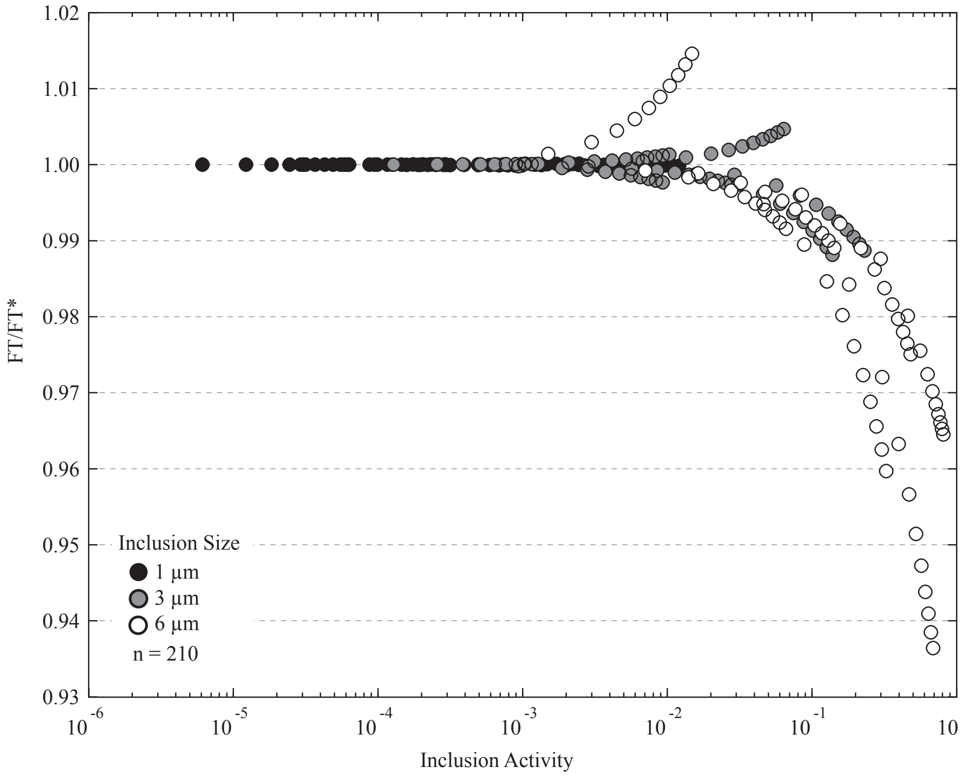
1.02
1.01
1.00
0.99
0.98
0.97
0.96
0.95
0.94
0.93
FT/FT*
Inclusion Size
1 µm
3 µm
6 µm
n = 210
10 -6
10 -5
10 -4
10 -3
10 -2
10 -1
10 0
Inclusion Activity

Figure 3.15: Ratio of F_T for homogenous parent distribution (FT) and F_T for inclusion case (FT*) plotted against inclusion activity for all model runs grouped by inclusion size. Note logarithmic scale on x-axis.

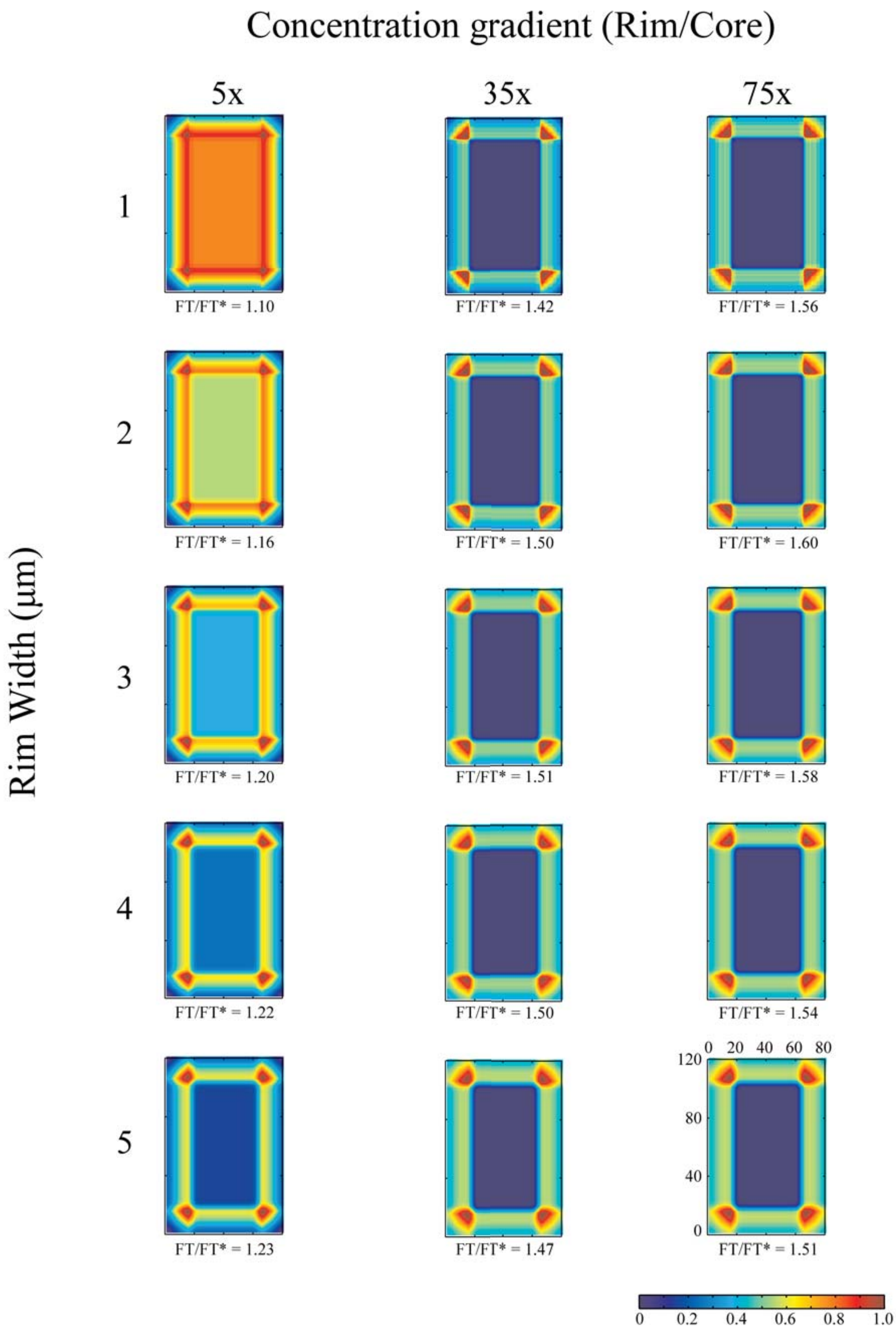
Concentration gradient (Rim/Core)
5x
35x
75x
Rim Width (µm)
1
2
3
4
5
FT/FT* = 1.10
FT/FT* = 1.42
FT/FT* = 1.56
FT/FT* = 1.16
FT/FT* = 1.50
FT/FT* = 1.60
FT/FT* = 1.20
FT/FT* = 1.51
FT/FT* = 1.58
FT/FT* = 1.22
FT/FT* = 1.50
FT/FT* = 1.54
FT/FT* = 1.23
FT/FT* = 1.47
FT/FT* = 1.51
0 20 40 60 80
120
80
40
0
0 0.2 0.4 0.6 0.8 1.0

Figure 3.16: Normalized He distribution contour plots for a subset of the rutile model runs. FT/FT* equals the F_T value for homogenous parent concentration divided by F_T for the shown rim widths and concentration gradients.

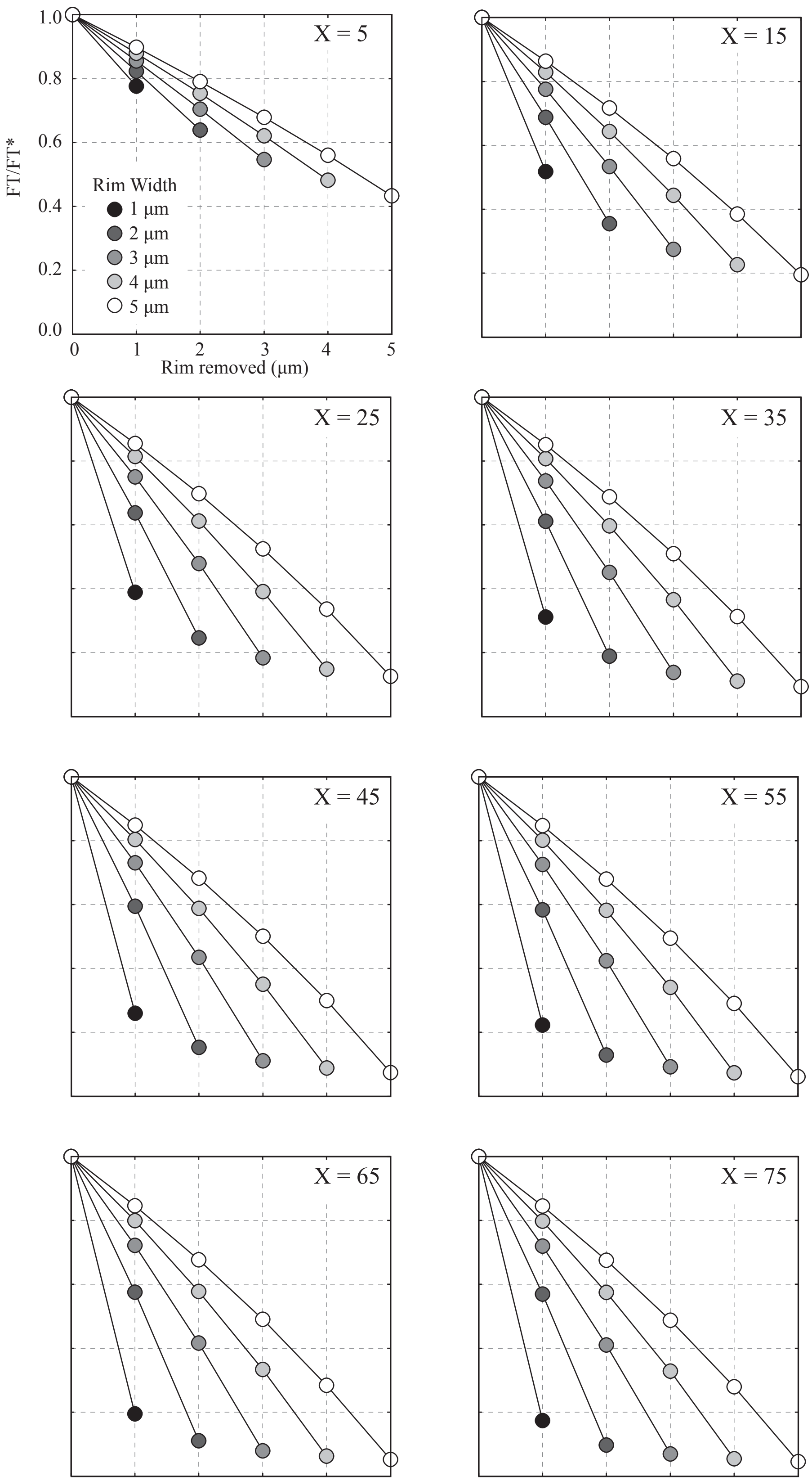

X = 5
X = 15
X = 25
X = 35
X = 45
X = 55
X = 65
X = 75
FT/FT*
Rim Width
1 µm
2 µm
3 µm
4 µm
5 µm
Rim removed (µm)
0.0
0.2
0.4
0.6
0.8
1.0
0
1
2
3
4
5

Figure 3.17: Results for all rutile model runs for each rim/core concentration gradient. In this case FT/FT* equals the F_T value for the zoned, full-size grain divided by F_T for grains that partially or fully lost the titanite rim during mineral separation.

Table 3.1: Comparison of Shillong apatite He ages with apatite fission track results

Sample	Sm excluded			Sm included			dHeAge	dStDev	AFT (Ma)	± 1σ (Ma)
	HeAge (Ma)	± 6% (Ma)	StDev	HeAge (Ma)	± 6% (Ma)	StDev				
GP15S11	11.4	0.7	2.7	10.3	0.6	2.6	0.90	0.99	12.8	1.1
GP13S9	13.0	0.8	3.5	10.2	0.6	2.4	0.78	0.70	10.6	0.9
GP13/14S10	14.1	0.8	3.9	13.8	0.8	3.9	0.98	1.01	8.6	0.6
GP11S8	14.2	0.9	3.3	12.7	0.8	3.2	0.89	0.96	9.7	1.0
GP15/16	16.5	1.0	4.7	15.9	1.0	4.7	0.97	0.98	11.6	0.8
GP9S6	24.6	1.5	9.9	20.0	1.2	9.2	0.81	0.92	26.9	1.7
GP7S10	34.6	2.1	11.8	32.5	2.0	11.4	0.94	0.97		
GP6GN3.2	84.3	5.1	34.9	82.6	5.0	34.2	0.98	0.98	76.6	2.5
GP6GN3.3	99.2	6.0	30.6	97.0	5.8	29.8	0.98	0.97	101.1	5.5
GP6GN3.1	102.1	6.1	9.3	99.8	6.0	9.6	0.98	1.03	75.0	2.7
GP6GN3	113.1	6.8	6.5	110.9	6.7	6.2	0.98	0.95	98.6	3.4
GP5GN2	149.3	9.0	20.3	145.9	8.8	19.7	0.98	0.97		

He ages are mean ages from aliquot analysis. Reported uncertainties are 6% (2σ) errors based on reproducibility of apatite standards as well as the standard deviation from aliquot analysis. dHeAge and dStDev are the differences between results including/excluding Sm expressed as fractions. AFT is the apatite fission track age with 1σ error.

Page intentionally left blank

CHAPTER 4:

Improvement of (U-Th)/He data analysis.

Part 2: Thermal history recovery from single and multi-thermochronometer (U-Th)/He data and data arrays

Abstract

The (U-Th)/He methodology offers the lowest closure temperatures in standard thermochronological investigations and is therefore best suited to gain insights into the latest phases of tectonic processes. Although it has to potential as a true geochronometer, its main application is in deciphering the thermal evolution of upper crustal rocks. Since the early beginnings of (U-Th)/He technique, much attention has been directed to quantitative analysis of the diffusion characteristics of a variety of mineral phases which subsequently allowed for recovery of thermal histories through modeling. Refinements of, and additions to these efforts led to growing number of algorithms and modeling packages that enabled the scientific community to improve their knowledge of areas of interest. As the technique evolved so did the sampling strategy and sample arrays instead of single samples have proven to be most effective to determine thermal histories of crustal sections. Single sample modeling is still a valuable tool that should precede other modeling attempts because it provides vital clues about the quality of the obtained He ages and can direct towards more advanced analysis if the results are inconclusive. Furthermore, it provides initial constraints for subsequent sample array modeling. The advantage of sample arrays is the extended thermal sensitivity of the combined samples which can result in well constrained thermal histories even from a dataset with only a single

phase available. Multi-phase analyses from sample arrays have the potential to directly constrain the paleo-geothermal gradient prior to the event of interest.

4.1 INTRODUCTION

With the proliferation of thermochronometric techniques, increasing effort has been invested into the development of modeling tools that support quantitative analysis of the data. The scope of these efforts grew with the range of applications. What started as “simple” programs to test the sensitivity of the (U-Th)/He system, forward model (U-Th)/He ages based on a given thermal path, or compare laboratory derived diffusion kinetics with real-world datasets, quickly evolved into more complex tools that aim to explain the time-temperature (t-T) history of single samples or sample arrays. To date, this progression culminates in the effort to understand and recreate the evolution of a three-dimensional landscape, spatially as well as temporally, and test these models against low-T thermochronology datasets. An overview of available software packages is given by Ehlers et al. (2005) and a brief description of critical issues, modeling approaches and tools dealing with the (U-Th)/He dating technique is provided in subsequent sections.

(U-Th)/He thermochronology is based on the production of α-particles (^{4}He nucleus, called He hereafter) through the decay of U, Th, and Sm parent isotopes. The high energy involved in this process causes the He to travel a certain distance (~20 μm) through the crystal lattice before it reaches its resting point. In the worst-case scenario, He is actually expelled out of the host grain if the decaying parent is close to the grain boundary. To account for this loss, Farley et al. (1996) introduced a correction factor based on the size and shape of apatite and zircon grains (F_T correction factor). Thermally activated He diffusion counteracts the accumulation of He within the mineral grain until a temperature is reached where He is retained quantitatively. At this point the geologic clock starts and analysis of parent/daughter concentrations will yield a He age that corresponds to the time of cooling through a specific temperature (or temperature range) called the closure temperature (T_C). The temperature sensitivity of the (U-Th)/He system was first explored in the laboratory using step-wise heating experiments to determine diffusivities (D_0) and activation energies (E_a) for different mineral phases (Zeitler et al., 1987; Lippolt et al., 1994; Wolf et al., 1996b; Warnock et al., 1997; Reiners and Farley, 1999). Based on the results, nominal closure temperatures (T_C) and partial retention zones (HePRZ), the temperature range at which the crystal retains only a certain percentage of the produced He (10-90%) during isothermal holding, were derived using equations provided by Dodson (1973, 1979). For apatite and zircon, the two most commonly used minerals in (U-Th)/He dating, the HePRZ's are 55-80°C (Farley, 2000) and 145-190°C (Reiners et al., 2004) respectively. A useful graphical user interface (GUI) called CLOSURE that calculates closure temperatures and HePRZ's for a variety of thermochronometers was developed by Brandon et al. (1998). Besides providing kinematic parameters for He diffusion, the stepwise heating experiments also indicated that the diffusion domain was the grain itself and diffusivities scale with the physical grain size. As demonstrated by Farley (2000) and Reiners and Farley (2001), He ages from individual mineral grains from a single sample who experienced the same thermal history will be older for larger grains (higher T_C) and younger for smaller grains (lower T_C).

An increasing number of apatite He ages (AHe) from samples that have been analyzed by apatite fission-track (AFT) dating revealed unexpected results, similar or even older ages of AHe compared to AFT. At first, this seemed discouraging but investigations by Shuster et al. (2006, 2009) and subsequently Flowers et al. (2009) culminated in what is known now as the radiation damage accumulation and annealing model (RDAAM). Based on natural samples and irradiation experiments, they could show that grain lattice defects caused by radiation damage increased the diffusivity in apatite significantly. The effective uranium concentration (eU= [U]+0.2299*[Th]+0.0051*[Sm]) was used as a proxy for radiation damage and similar to the grain size effect, analysis of grains of comparable size resulted in older AHe ages for minerals with higher eU and vice versa. Additionally, closure temperatures in the vicinity of the AFT annealing temperature (>100°C; Laslett et al., 1987; Green, 1988; Ketcham et al., 1999) were reported, proving the possibility of equal or older AHe ages compared to AFT. One advantage of fission track dating is that it offers direct insight in the thermal history of the analyzed grain by means of its track length distribution besides the FT age derived from the number of tracks. The He diffusion profile across a mineral grain would give similar insight into the t-T path but this information is not captured in traditional (U-Th)/He analysis which represents a total gas age. More advanced $^3He/^4He$ analysis would be necessary to access this valuable information (e.g. Shuster and Farley, 2003).

The majority of currently available He modeling tools convert the geometric shape of the mineral grain (e.g. hexagonal prism for apatite) into a sphere with equivalent surface-to-volume ratio (e.g. Ketcham, 2005) or equivalent F_T correction factor (Ketcham et al., 2011). Furthermore, diffusion of He out of the grain is assumed to be homogenous in all directions reducing the mathematics to a one-dimensional problem of He diffusion along the spherical radius. Recent studies show that diffusion is in fact not isotropic along the crystallographic axes (Cherniak et al., 2009; Bengston et al., 2012) but for faster computation, the above simplification is used within HeMP.

Relative low T_C and the concept that an exhumed HePRZ reveals insight into the thermal evolution of a fault block, initiated the use of the (U-Th)/He technique as a powerful investigative tool of slip along normal faults. Traditional age versus elevation plots allow limited, qualitative description of the t-T history and do not provide sufficient information about the statistical uncertainties. Solving the production-diffusion equation for He as a function of time and temperature was the critical task to accomplish in order to be able to successfully model He ages with robust and computationally efficient programs. Wolf et al. (1998) as well as Ketcham (2005) utilized a finite-difference method (Crank-Nicolson algorithm) that allowed computation of diffusion along a single dimension, an efficient method to model spheres. HeFTy (Ketcham, 2005) is a widely used stand-alone application that allows forward and inverse modeling of single/multi-phase samples/thermochronometers including options for parent zonation. Meesters and Dunai (2002a, b) solved the problem of diffusion along a spherical radius as well as simple geometric shapes (finite/infinite cylinders, rectangular blocks) with decomposition into eigenmodes. Parent zonation for a binary case (core-rim of different concentrations) is included. A standalone tool for forward modeling of He ages called DECOMP (Dunai et al., 2003) is available. The latest development in this category is provided by Gautheron and Tassan-Got (2010) who used a Monte-Carlo approach to simulate diffusion represented by Brownian motion. Their algorithm is applicable to any crystal shape and parent zonation and provides fast and robust results.

Depending on the geologic question, sample arrays from boreholes or vertical transect rather than single samples might be better suited to recover the thermal history. Because the software packages discussed so far were not capable of modeling several samples connected through their spatial location at once, other solutions had to be found. Gallagher et al. (2005) jointly modeled a synthetic apatite fission track dataset by simply applying a geothermal gradient to the vertical sample suite. Their results showed that this approach yielded a much better defined thermal history than the solutions from the single sample modeling. Additionally, they were able to better constrain paleo-temperature gradients directly from the model runs.

The described software tools produce one-dimensional solutions, meaning that samples are treated independent of their locations on/in the earth's surface/interior, or simply depending on one variable (z) in the case of vertical transects. Changes in temperature are accomplished by linear segments along a t-T path and transient geothermal gradients based on exhumation/burial are not accounted for. For many applications, these simplifications are justified, the models run with a few well known input parameter, and yield geologic meaningful results within reasonable time. In order to understand the effect of erosion, exhumation rates, and fault localization on an evolving landscape more complex algorithms and an increasing number of variables must be applied. PECUBE, a finite-element code that solves the transient three-dimensional heat transport equation in a crustal block undergoing uplift and erosion was developed by Braun et al. (2003) to test predicted He ages against sample ages. To-date, this algorithm is the most sophisticated but also requires substantial computational power.

Availability, shortfalls in flexibility and capabilities, as well as computational intensity of some applications initiated the need for a customized He-Modeling package. Using MATLAB© (Mathworks, the, 1996), a powerful technical programming language, the goal was to 1) create a versatile, flexible and extendable code to investigate many challenging problems in (U-Th)/He thermochronology like alpha-ejection correction and thermal modeling, 2) improve quantitative analysis of (U-Th)/He data produced in the laboratory, 3) distribute an easy-to-use Graphical User Interface (GUI) to the broader scientific community, and 4) be able to quickly demonstrate concepts of He diffusion in minerals in introductory and advanced thermochronology lectures and labs.

4.2 SOFTWARE OVERVIEW, ALGORITHMS, AND VALIDATION

Starting HeMP opens the *Main Menu* GUI, which lists all available modules and provides a preview and short description of the capabilities of each of them. In summary, this software package enables the user to (i) calculate the F_T-correction factor for mineral grains (not discussed here), (ii) forward model He ages based on pre-defined t-T paths, and (iii) inverse model He ages calculated from randomly created t-T paths. Fig. 4.1 provides an overview of the different modules including their input requirements as well as some of the available graphical representations of the model results. To allow for quick setup or changes of parameter sets, Excel© spreadsheets utilized by each module proved to be exceptionally versatile import media. All modules utilize the same mineral data import table, which organizes individual samples in different sheets and their corresponding mineral phases in columns, ensuring flexible cross-module compatibility. Results are saved as *.mat files that can be loaded either within the modules or in separate graphing GUI's. To keep track of the input files and chosen run parameters, a log-file is created at the end of each model run. All modules contain an option to export graphs in a variety of file formats for subsequent processing in standard software packages.

In order to calculate model ages from these t-T paths and extract solutions that fit the observed data, HeMP follows the same approach described in detail by Ketcham (2005) and used in HeFTy©. A short overview of the underlying calculations is provided in this section.

First, the grain measurements and its geometry (e.g. zircon = tetragonal prism + pyramidal terminations) are used to calculate the surface-to-volume ratio (S/V) of the geometric body and transform it into a sphere of equivalent radius (a):

$$a = \frac{3}{S/V}$$

This approximation, which is supported by Farley et al. (1996) and Meesters and Dunai (2002) who showed that the effects of He-ejection due to long alpha stopping distances are proportional to the S/V of a variety of mineral geometries encountered in (U-Th)/He dating, has the advantage of simplifying the He-diffusion to an easily manageable one-dimensional problem. The grain radius is subdivided into a closely spaced grid (512 nodes) where each node (i) represents the position of parent nuclides and their concentrations. Following these initial geometric conversions and gridding operations, the t-T path is subdivided into discrete intervals (n) following the rules that the individual interval cannot exceed a temperature range greater than 3.5°C and has to be shorter than 1% of the overall thermal history. This ensures accurate results while keeping computational time within reasonable limits.

It is crucial to keep track of how much He is produced as well as how much He is diffusing out of the grain during each interval (n) to be able to calculate a final model age for a given thermal history. Because of the long stopping distances of He particles traveling through the grain, an effective He production ($A_{eff,i}$) for each node has to be calculated to account for loss of ^4He due to ejection beyond the sphere radius. This is accomplished with following equation (see Ketcham, 2005):

$$A_{eff,i,I} = \frac{\int_{X_i-S_I}^{X_i+S_I} A(X')dX}{\int_{X_i-S_I}^{X_i+S_I} dX}$$

where X_i is the radial position of the node, X' is the radial position of the shell edge relative to the spherical grain, S_I is the average stopping distance for parent isotope I (given in Farley et al., 1996), and A is the uncorrected He production. Using this in the general He generation equation:

$$^4He_i = 8A_{eff,i,238}\left(e^{\lambda_{238}t_2}-e^{\lambda_{238}t_1}\right)+7A_{eff,i,235}\left(e^{\lambda_{235}t_2}-e^{\lambda_{235}t_1}\right)$$
$$+ 6A_{eff,i,232}\left(e^{\lambda_{232}t_2}-e^{\lambda_{232}t_1}\right)+1A_{eff,i,147}\left(e^{\lambda_{147}t_2}-e^{\lambda_{147}t_1}\right)$$

the amount of He produced at each node (i) in the sphere during each interval (n) bounded by t_1 and t_2 can be calculated. For each of these intervals the He production at each radial node is calculated assuming that all He is produced instantaneously at t_1. Optional modeling of parent isotope zonation can be easily incorporated by assigning different values to the radial nodes through a separate user-defined zoning input table. Now that the He in-growth at each t-T interval is established, the task on hand is to solve the He diffusion/accumulation equation that provides the amount of He retained in the mineral grain at the end of each t-T interval. This is accomplished using the Crank-Nicolson finite difference solution for diffusion in a sphere (e.g., Press et al., 1988):

$$\frac{u_i^{n+1} - u_i^n}{\Delta t} = \frac{D}{2}\,\frac{\left(u_{i+1}^{n+1} - 2u_i^{n+1} + u_{i-1}^{n+1}\right)+\left(u_{i+1}^{n} - 2u_i^{n} + u_{i-1}^{n}\right)}{\Delta a^2}+A_{eff,i}*a$$

where u is the substitution of the He concentration multiplied by the radius, i subscript refers to the nodes along the radius, and n superscript to the interval number along the t-T path. D denotes the diffusivity which is treated differently based on the chosen model run setup. HeMP includes the option to use the Radiation Damage Accumulation and Annealing Model (RDAAM) for apatite (Flowers et al., 2009) and if the user checks this option then D is calculated as:

$$\frac{D}{a^2} = \frac{\frac{D_{oL}}{a^2} * e^{-E_L/RT}}{\left(k_o * v_{rd} * e^{E_{trap}/RT}\right) + 1}$$

where E_{trap} is the activation energy associated with the radiation damage traps; subscript 'L' for diffusivity and activation energy is used to differentiate these quantities that were obtained from diffusion in undamaged crystals from the values used in the conventional Arrhenius equation; k_o is the radiation damage density scaled by v_{rd}. Given that the values for E_{trap}, D_{oL}, and other factors were derived empirically, these inputs must be hard-coded. For all other mineral phases and the case that the RDAAM option is not checked, diffusivities are calculated using the standard equation:

$$\frac{D}{a^2} = \frac{D_o}{a^2} * e^{-E/RT}$$

If not stated otherwise, all following model run results are based on the RDAAM model.

Summation along the diffusion profile at present time, given by the final He concentration along the nodes, and multiplying by the volume of the sphere gives the final amount of He retained within the spherical geometry. Simply dividing this quantity by the effective He production rate ($^4HeP_{eff}$) yields the He model age:

$$\text{Age} = \frac{\left[{}^4He\right]}{\sum {}^4HeP_{eff,i}}$$

where

$$^{4}HeP_{eff,i} = 8A_{eff,i,238}\lambda_{238} + 7A_{eff,i,235}\lambda_{235} + 6A_{eff,i,232}\lambda_{232} + 1A_{eff,i,147}\lambda_{147}$$

Another important value, the F_T correction factor, can be calculated directly from the ejection corrected He production rate as follows:

$$F_T = \frac{\sum {}^{4}HeP_{eff,i}}{\sum {}^{4}HeP_i}$$

where $^{4}HeP_i$ is the uncorrected He production rate. Testing the fit of model ages against the sample ages obtained in the laboratory is accomplished with a “Goodness of Fit (GOF)” criteria used by Ketcham et al. (2000):

$$\mathrm{GOF} = 1 - \int_{\tau_{meas}-|\tau_{meas}-\tau_{mod}|}^{\tau_{meas}+|\tau_{meas}-\tau_{mod}|} \frac{1}{\sigma\sqrt{2\pi}} e^{-(x-\tau_{meas})^2/2\sigma_{meas}^2}\, dx$$

where τ refers to the modeled and measured He ages, and σ to the uncertainty around the measured age. Based on the merit function of Ketcham et al. (2000), a calculated model age is defined as an acceptable solution if GOF > 0.05, and as a good solution if GOF > 0.5.

4.2.1 Forward modeling

In the *Single Sample(s)* module a single thermal history serves as the basis for subsequent creation of additional t-T paths constraint by three parameters, the (i) number of desired t-T paths, (ii) T-offset, and (iii) t-offset for individual t-T paths. The offsets can be adjusted individually for each initial node, which enables the user to simulate converging/diverging isotherms as expected during rapid exhumation/slow burial. Graphical outputs include the He age evolution, final He concentration profiles, final He ages, and the representation of t-T paths that match GOF criteria. These results can be plotted for any given number of t-T paths and samples. Proving its versatility and user-friendliness, the *Single Sample(s)* module was utilized extensively to validate HeMP against the HeFTy software to ensure correct and reproducible results before applying it to the datasets discussed in later sections. A variety of synthetic apatite and zircon samples were forward modeled on the basis of four generic t-T histories (see Fig. 4.2) that simulated 1) linear cooling, 2) very rapid cooling, 3) slow cooling through the He partial retention zone (HePRZ), and 4) linear reheating followed by linear cooling. Each of these t-T histories was modeled starting at t = 100, 50, and 10 Ma to evaluate if the choice of interval lengths (n) scales properly. The models were run using kinetic parameters from Farley (2000; Durango model, apatite), Flowers et al. (2009; RDAAM model, apatite), and Reiners et al. (2004; zircon). As shown in Fig. 4.2, the majority of the model ages are well within 5% of the results obtained from HeFTy, providing confidence that the model results are sufficiently accurate (within the uncertainty of the (U-Th)/He technique). Table C.1 in Appendix C lists the results for each t-T history and analyzed sample. To demonstrate the sensitivity of AHe ages as a function of varying kinetic parameters, 10 apatite grains ranging in size from 30-120 μm equivalent spherical radii with constant parent concentrations and 10 apatites of equal size (a = 50 μm) with eU ranging from 30-120 ppm were modeled using the *Single Samples(s)* module. Fig. 4.3 shows the AHe age evolution from 100 Ma to present for both synthetic samples based on the thermal histories shown in Fig. 4.2. Fast and moderate cooling (Fig. 4.3 t-T history 1, 2) show much less dispersion in final AHe ages than t-T paths that spend considerable time within the apatite HePRZ (Fig. 4.3 t-T history 3) or pass through the apatite HePRZ during reheating and again during subsequent exhumation (Fig. 4.3 t-T history 4). Additionally, the forward modeling approach was used to demonstrate the utilization of vertical sample spacing as shown in Fig. 4.4. This model run illustrates cooling of a 2 km thick crustal section represented by eleven samples spaced by 200 meters. Based on the assumption of a constant geothermal gradient of 25°C/km, the temperature difference between the top and bottom sample equals 50°C. The resulting age versus depth (temperature) plot shows predicted AHe ages for each sample as a function of eU (dashed, grey lines) as well as a hypothetical result (black, solid line). The drastic increase in the apparent AHe age along the hypothetical sample array between 0.8-1.0 km could easily be misinterpreted as e.g. a fault zone although changes in e.g. lithology accompanied with different parent isotope concentrations could explain the complexity in the AHe versus depth relationship.

In the *Sample Array* module, offset t-T paths are generated based on a range of user-defined thermal gradients and sample elevation data, simulating the thermal conditions for each sample at depth. T-offsets are simply calculated using the elevation difference between samples and a single (or a range of) geothermal gradient(s), an approach already applied by Gallagher et al. (2005). Fig. 4.5 illustrates this concept with geothermal gradients of 23°C (solid black lines) and 39°C (dashed grey lines) applied to a synthetic dataset consisting of apatite and zircon He ages. The resulting model ages from this family of t-T paths are then compared to the corresponding samples and good/acceptable solutions are obtained if a user-defined number of model ages match the sample ages. In this example, a geothermal gradient somewhere between 23-39°C is most likely to fit the majority of the data. Once created, the user can interactively change the t-T paths and model ages and GOF's are calculated on the fly. This module has been proven to be of great value to quickly test thermal histories for a sample suite from a vertical transect and provided guidance for the choice of initial constraints for subsequent inverse modeling.

4.2.2 Inverse modeling

The *Single Sample(s)* module is a more or less exact replica of HeFTy©. It randomly generates single t-T paths based on initial user constraints and model ages are compared to sample ages by GOF algorithm. The model run can be set to stop after a total number of t-T paths are analyzed, or a number of acceptable/good solutions for each sample are reached. Currently, the software does not allow more than 100,000 iterations, which in general should be more than sufficient especially for the *Single Sample(s)* modeling. An advantage of HeMP is that the algorithm does not require all aliquots to fit a certain t-T history but continuously tracks results based on the maximum number of fitting aliquots. The additional merit of this approach lies in the capability to see which aliquots do not fit any thermal histories, which is helpful in identifying outliers. It is common practice to discard results from apatite with high re-extracts during degassing and/or atypical U/Th ratios, both cases indicative of possible inclusions. Additionally, there is always the temptation to ignore ages that are significantly older or younger than other results. Prior to the introduction of RDAAM, it was easier to make this decision because theoretically smaller grains should always yield younger ages than larger grains based on the finding that the diffusion domain is the grain itself. With the introduced dependency of the diffusion coefficient on eU, this straightforward relationship is no longer valid and it has become much more difficult to determine if an unusually high or low age is in fact an outlier or just the result of the combination of size, eU, and the thermal history of the sample.

Using the same approach as the *Sample Array* forward model to create offset thermal histories for each sample from a vertical transect, the *Sample Array* inverse model conversely relies on the random generation of initial t-T paths that pass through user-defined areas in t-T space. Calculation of model ages and their fit with regards to the obtained sample ages follows the same procedures as described for the equivalent forward model. HeMP saves each t-T path that produces acceptable/good fits for each individual geothermal gradient, which can be subsequently displayed in a separate graphing GUI. Furthermore, this GUI includes the option to plot time vs. exhumation rate, time vs. cumulative exhumation, and age distribution graphs.

4.3 THERMAL HISTORY RECOVERY

In this section, the range of approaches to derive continuous thermal histories is demonstrated by means of a variety of datasets collected from outcrops or sampled from boreholes. As discussed and graphically shown earlier, 1) variations in grain size and eU (apatite only), 2) differences in kinetic parameters (Do, Ea) between mineral phases, and 3) vertical sample spacing can be used to extract geologic meaningful thermal histories. Any range in size, eU, or kinetic parameters results in a change of the closure temperature of the (U-Th)/He system potentially extending the thermal sensitivity of the sample set at hand. Collecting samples from different elevations and conjoint modeling offers the benefit of analyzing samples that are at any point in time at different temperatures. Even if all the samples share the exact kinetic parameters, this approach will give increased control over the thermal history. As shown in Fig. 4.3, the spread in He ages is also highly dependent on the cooling rate and time spent within the HePRZ. Even large intra-sample heterogeneity will yield very similar aliquot ages if the sample cooled quickly. The opposite is true for samples that spent a significant time within the HePRZ where slight differences in the diffusion kinetics will affect the individual aliquot ages dramatically. All presented results are from the available modules in HeMP, demonstrating its great versatility and give proof of HeMP's capabilities to gain insight into the thermal history of a given dataset.

4.3.1 Single Sample / Single Phase

4.3.1.1 Cajon Pass (CA, U.S.A) – Borehole Samples

The first dataset discussed is from a borehole on the Cajon Pass (California) that penetrated sandstones and underlying granitic basement rocks. Four samples were collected from present borehole temperatures of 48°C (CJ-12), 62°C (CJ-16), 70°C (CJ-18), and 84°C (CJ-23). From each sample, up to twelve single apatite grains with a wide range of grain sizes (equivalent spherical radii of ~20-100 µm) were handpicked and analyzed. An overview of the data is given Fig. 4.7 showing a series of key cross-plots. Sample CJ-12, and to a lesser degree CJ-16, shows a wide spread of AHe ages and a positive correlation with grain size indicating slow monotonic cooling through the apatite HePRZ or a re-heating event as demonstrated earlier (compare with Fig. 4.3). Because samples CJ-16, CJ-18 and CJ-23 are currently at temperatures well within the apatite HePRZ, a correlation with grain size is either overprinted by ongoing diffusive loss of He, or these samples have been rapidly exhumed from temperatures above the apatite HePRZ and have not had the chance to establish such a relationship. Except for CJ-18, none of the samples show a clear positive correlation of AHe age with eU which makes this dataset well suited to investigate the grain size-dependant sensitivity of the (U-Th)/He system. Based on the emplacement age of ~80 Ma for the latest plutonic event, the model run was set to start at 80 Ma at an elevated temperature of 500°C. Additional t-T constraints allowed for cooling to temperatures below the apatite HePRZ (<40°C) and subsequent re-heating to a maximum temperature of 150°C. The final temperature constraint was given by the current borehole temperature at the sample location with an additional uncertainty of ±5°C. This setup ensured that all scenarios including monotonic cooling and cooling followed by re-heating followed by cooling, were accounted for. Results from the model runs are displayed in Fig. 4.8. Within the maximum number of fitting aliquots, HeMP differentiates the combinations that are represented by shades of grey in the individual plots.

7 out of 11 aliquots from CJ-12 yield common acceptable solutions that indicate cooling below ~50°C shortly after 60 Ma followed by an extensive period of isothermal holding and/or very slow cooling past 20 Ma. Both aliquot combinations require re-heating to current borehole temperatures but the timing of this event is not well constrained. For CJ-16, only 4 of the total 12 aliquots match a common t-T path and numerous aliquot combinations result in non-unique solutions. CJ-18 yields acceptable fits for 3 out of 4 aliquots and the early thermal history of this sample is clearly unconstrained. After ~30 Ma, re-heating from > 50°C to present borehole temperatures is the most likely scenario for this sample. The bottom-most (CJ-23) shows a comparable thermal evolution as the top-most sample (CJ-12) with a similar timing of re-heating although it has to be noted that only 3 out of 12 aliquots are matched. In general, samples CJ-12 and CJ-18 yield the more reliable results from these model runs but at this point it is rather unclear how exactly the crustal section sampled from the borehole thermally evolved through time.

4.3.1.2 Shillong Plateau (India) – Surface Samples

The second dataset is from the Shillong Plateau, a pop-up structure located in the foreland of the Indian Himalayas. Biswas et al. (2007) analyzed surface samples from the exposed granitic basement using apatite/zircon (U-Th)/He and apatite fission track (AFT) dating techniques. Age information from AFT together with auxiliary geological evidence from the sedimentary record was used to model the evolution of this crustal block with HeFTy. Sensitive within ~60-100°C (apatite partial annealing zone PAZ, e.g. Green et al., 1989), this technique complements the apatite (U-Th)/He system towards higher temperatures. For an in-depth review of analytical techniques, model setup, and results see Biswas et al. (2007).

Several aspects of this dataset are quite interesting. First, apatites exhibit a wide range of Sm concentrations, some of them exceeding 1000 ppm, which is rather unusual. In combination with low U concentrations of generally less than 50 ppm, this would result in AHe ages that are more than 40% too young if the He contribution from ^{147}Sm would not be included (see Chapter 3). Furthermore, the calculation of the effective spontaneous track density ($e\rho_s$), a critical parameter in the RDAAM equations, would consequently lead to erroneous results as well. Fig. 4.9 shows plots of eU versus AHe ages for Group 1, collected in the northern part, and Group 2, collected in the central and southern part of the Shillong plateau. Group 1 apatites show a Cretaceous cooling signal based on AHe, AFT, and a positive correlation between eU and He age. Although there is a much wider range and generally higher values of eU for Group 2 apatites, the ages appear to be unaffected and cluster around 10 Ma. This fundamental difference, and the fact that all samples originate from Paleo-Proterozoic granitic rocks unconformably overlain by Late Cretaceous continental sediments, already implies that the rocks of Group 2 must have re-entered temperatures that partially reset the apatite ages and allowed for annealing of accumulated He radiation damage prior 10 Ma. This event is clearly captured in the Tertiary rock record that shows shallow marine on top of Cretaceous continental sediments. On the other hand, Proterozoic ZHe cooling ages throughout the entire plateau indicate that re-heating during this tertiary burial event was not extensive enough to reset the geologic clock in zircon, therefore putting an upper limit of ~150°C (lower bound of zircon HePRZ) on the peak temperature. Based on their modeling of the AFT data, Biswas et al. (2007) suggested that exhumation of the northern part of the plateau (Group 1 samples) started between 25-3 Ma from temperatures of 20-70°C. In contrast, the southern part of the plateau (Group 2 samples) experienced greater burial to temperatures ranging from 100-160°C followed by a more pronounced exhumation event at ~15-9 Ma. At the time of Biswas et al.'s (2007) work, the RDAAM model was not available and given the striking relationship between eU and apatite He ages it seems straightforward to re-model this dataset and evaluate if the (U-Th)/He results alone can be used to arrive at equal or similar results.

Group 1 and Group 2 apatites were analyzed with the *Single Sample(s)* inverse modeling module using identical t-T constraints. An initial constraint at 190-200 Ma and 140-160°C was followed by a constraint at 60-80 Ma and 10-40°C to honor the Cretaceous exhumation manifested in the sedimentary record. A large box spanning 5-55 Ma and 10-160°C ensured that the model run was not limited to re-heating but could yield t-T paths that represented slow cooling or even isothermal holding throughout the Tertiary.

Fig. 4.10 and Fig. 4.11 show the resulting t-T paths for Group 1 and 2 apatites collected in the northern part of the plateau. All samples, except GP13/14S10, were analyzed using 6 aliquots and the individual plots show the results for the maximum number of aliquots that yielded acceptable solutions after 100,000 trials. Where available, the black dashed lines mark the boundaries of the acceptable solutions modeled by Biswas et al. (2006) with HeFTy on basis of their AFT dating. For Group 1 apatites, 2-5 out of 6 aliquots resulted in matching thermal histories. Sample GP6GN3.1 only has 2 aliquots that yield acceptable fits and the four combinations exhibit a wide range of possible thermal histories for this sample. Surprisingly, the maximum number of fitting aliquots (5) for sample GP5GN2 does not result in the \best-constrained thermal history. Overall, the results indicate that, after exhumation to the near-surface during the Cretaceous either very slow cooling or re-heating to temperatures of ~80°C could explain the AHe ages. Although these initial results were valuable and provided answers to very high-level questions about the evolution of the Shillong plateau, the somewhat poor performance of the number of aliquots that fit the same thermal history was in need of improvement. In a second model run, the errors of the AHe ages were increased for selected samples from 6% to 10% (2σ) to allow more aliquots to fit. Fig. 4.11 shows the results for Group 1 apatites. Sample GP6GN3.1 shows the most improved definition of the thermal history although only one more aliquot is added, followed by Sample GP6GN3 where now all 6 instead of 4 aliquots could be matched. Sample GP6GN3.3 now shows a slightly wider range of possible thermal histories as a consequence of the greater errors. Compared to the AFT results, the maximum temperature reached after exhumation in the Cretaceous is lower and rapid cooling starts consistently earlier.

Results from Group 2 apatites are telling a different story as shown in Fig. 4.15. As anticipated, the re-heating event is much more pronounced and exceeds ~100°C in most cases. Indicated by the randomness of the t-T segments prior 80 Ma, any record of this part of the thermal history is completely erased by the Tertiary re-heating event. Most samples show t-T paths that reach the limit of the constraint at 160°C followed by rapid exhumation to current surface temperatures. GP9S6 shows a somewhat similar evolution but re-heating does not exceed 80°C. Comparable t-T evolutions are shown by aliquot combination 1-2-3-6 in sample GP11S8 and to a lesser degree in sample GP13/14S10.

4.3.2 Single Sample / Multi Phase

4.3.2.1 Xainze Rift (Tibet) – Vertical Transect Samples

Sampled along a normal fault bounded triangular facet in the center of the N-S trending Xainze rift (S-Tibet), this transect spans a vertical relief of ~450 m covered by seven samples. ZHe ages show an overall trend from older ages at the top (~32 Ma) to younger ages at the bottom of the transect (~22 Ma), whereas apatite analysis yielded almost elevation invariant AHe ages around 10 Ma. From the He age versus elevation plot (see Fig. 4.11), a first order thermal history starting with slow cooling through the zircon HePRZ during Oligocene time followed by rapid exhumation through the apatite HePRZ in the middle/late Miocene can be inferred. In the best case scenario, a clear inflection point in the apatite data would directly mark the onset of rapid uplift along the normal fault but probably a consequence of the limited vertical sample spacing, this information is not readily available.

The *Single Sample(s)* inverse modeling module was used to gain insight into the t-T evolution of each individual sample. Not able to utilize the vertical sample spacing, this module as well as HeFTy, only considered the apatite/zircon pair for each sample to find t-T paths that matched the corresponding He ages. In order to show as unbiased results as possible, only one initial constraint spanning 80-60 Ma and 300-350°C was given as starting point. Otherwise, the model was able to explore the entire t-T space with the limitation of monotonic cooling. It is common practice in (U-Th)/He dating to report the mean age and standard deviation in addition to the individual aliquot ages to assess the reproducibility of the sample analysis. For comparison, this dataset was modeled using the mean ages as well as the individual aliquot ages for each mineral phase. The run with mean ages was terminated after 500 acceptable solutions have been found for each sample. Fig. 4.13 shows the good (dark grey) and acceptable (light grey) t-T paths for each individual sample. At a first glance, the results look relatively indistinguishable from each other except for somewhat steeper gradients in the 25-10 Ma interval for the two lowermost samples (05XID73, 05XID74). All samples exhibit an obvious convergence of good/acceptable solutions at ~170°C and ~60°C, which is not surprising given that these temperatures lie within the corresponding HePRZ's near the nominal closure temperature of the zircon and apatite system. Outside this area, t-T paths quickly diverge resulting in a "braid-like" geometry. To improve on these initial results, another model run using the individual aliquot ages (up to 13 apatite and zircon analysis) was performed. Fig. 4.14 shows the acceptable fits for the given aliquot combinations after 100,000 iterations. Compared to the results for the mean ages, much less and better defined thermal histories emerge. Still, the divergence between the temperatures sensitive to the apatite and zircon thermochronometers is prominent and results in very dissimilar thermal histories. In summary, the *Single Sample(s)* module provides a wide range of possible cooling scenarios for each sample and a common thermal history for the entire fault block is still out of reach.

4.3.3 Sample Array / Single Phase

Conquering the shortcomings of the *Single Sample(s)* module led to the development of one of the cornerstones of the HeMP software, the *Sample Array* inverse modeling module. The Tibet dataset demonstrates that looking at a single sample only provides a snapshot at a single point in space and especially without utilizing intra-sample variability in diffusion kinetics (aliquot versus mean age model runs) the result is ambiguous. Being able to combine spatially distributed samples should improve the understanding of the t-T evolution significantly. As a reminder, this module randomly generates initial t-T paths, which subsequently are offset to higher temperatures using sample elevations and user-defined geothermal gradients. In order to achieve a sufficient number of solutions it is recommended to add additional constraints to better steer the random t-T path generator. In the following examples, this is either done using the results from the single sample modeling or additional constraints from other sources.

4.3.3.1 KTB (Germany) – Borehole Samples

The Continental Deep Drilling Project (KTB) sample suite originated from a 9 km deep cored section through the earth's crust below Germany. Still one of the best available datasets in (U-Th)/He dating, ZHe analysis by Wolfe and Stockli (2010) proved the postulated zircon HePRZ (145-190°C, Reiners et al., 2004). Based on other thermochronometers, Wagner et al. (1997) and later Stockli and Farley (2004) derived thermal histories for the four fault blocks encountered in that section. Given the well studied nature of this dataset it is well suited to test if HeMP can derive the same or similar t-T histories as suggested previously.

Wolfe and Stockli (2010) revisited the rock record of the KTB project in Germany and analyzed X samples (XX aliquots) from 0-9 km depth encompassing down-hole temperatures of 7-265ºC at an average geothermal gradient of ~27.5ºC/km (Clauser et al., 1997). The goal of this study was to gain insight into the diffusion kinetics of zircons by i) evaluating the ZHe ages as a function of depth and thermal history, and ii) conducting laboratory based diffusion experiments to determine activation energy (E_a) and diffusivity (D_o) of selected samples. Details about the dataset, lab procedures, model setup, and other pertinent information not addressed here are available through the above reference. Mean ages (28) and standard deviations of single grain zircon analysis were used to model the t-T evolution of this crustal section with the *Sample*

Array module. The t-T evolution for Block A shown in Wolfe and Stockli (2010) served as guidance for one of the initial model constraints set at 50-120 Ma and 50-300ºC and the model run allowed for six outliers. Fig. 4.15 presents the result for geothermal gradients ranging from 20-40ºC/km in 1ºC intervals where darker lines represent lower geothermal gradients. The black dashed line indicates the thermal history for fault block “A” derived by Wagner et al. (1997) and later Stockli and Farley (2004).

4.3.3.2 Cajon Pass (CA, U.S.A) – Borehole Samples

As a result of the analysis strategy using many aliquots with a wide range of grain sizes, the thermal history for sample CJ-12 from the Cajon Pass could be constrained to some extent already. Adding the other samples and model the entire dataset including the vertical sample spacing could potentially improve the result. Basically, the *Sample Array* module should filter the acceptable solutions from the *Single Sample* model run of sample CJ-12 and arrive at a subset of t-T paths whose parallel offsets also fit the sample ages collected at greater depths. To keep computational time to a minimum and ensure a number of fitting thermal histories, the first model run (Fig. 4.19A) utilized the mean ages from the subset of aliquots that yielded acceptable fits in the previous *Single Sample* models. Instead of the nominal 6% error, two standard deviations around the mean served as input for the uncertainty to cover the entire age range. In excess of 1,400 solutions for the best fitting geothermal gradients (28-30°C, highlighted in blue) proof that this approach did not improve on the previous results. Besides the already established re-heating, a cooling event ~5 Ma seems to be necessary to fit the entire sample set. In order to get a better definition of the t-T paths, more control on the temperature sensitivity needs to be added from the samples. The top-most sample (CJ-12) shows the best behaved age versus size relationship and the widest range of ages, therefore this sample should affect the results the most. Subsequently, a hybrid run using the youngest and oldest aliquots from sample CJ-12 that fit both combinations (Aliquot 4 and 10) together with the mean ages from the remaining samples was run. The much tighter constraints used in this run are based on an intermediate run (not shown) with the initial, larger constraints that led to only a few acceptable solutions. This approach of course takes some of the resolution gained by the single aliquot analysis away but many modeling tries, with this and other datasets, showed that it seems to be impossible to yield fits during multi-aliquot/multi-sample analysis. The final result is shown in Fig. 4.19B clearly illustrating the improved definition of the thermal history of this crustal section. After cooling to temperatures below 50°C, slow re-heating to a maximum temperature of ~65°C between 10-5 Ma is followed by cooling to the present down hole temperature.

4.3.4 Sample Array / Multi Phase

4.3.4.1 Xainze Rift (Tibet) – Vertical Transect Samples

Unlike the *Cajon Pass* samples, this dataset comprises apatite and zircons grains of similar size, which limits the temperature sensitivity within each system. The t-T paths obtained from earlier modeling are simply based on the spread in closure temperature ranges between apatite and zircon. Using the mean AHe and ZHe ages and standard deviations of the single aliquot analysis, the vertical transect from Tibet was subsequently modeled with the *Sample Array* module. Based on the findings from the *Single Sample* model runs, two additional constraints at 40-20 Ma (220-130°C) and 15-5 Ma (100-20°C) were added to provide more guidance for the random t-T path generator without jeopardizing the integrity of the results. A range of geothermal gradients from 15-50°C in 2°C increments and a total number of 100,000 iterations complete the model setup and the resulting solutions are shown in Fig. 4.17. As obvious from this figure, the model allowed for one sample outlier (mean apatite ages of 05XID73 did not fit the resulting thermal histories). Based on this approach, a transition from moderate to fast cooling at ~10 Ma becomes apparent.

4.4 DISCUSSION

4.4.1 Case Studies

The Cajon Pass sample modeling demonstrates how variations in grain size can be utilized to increase the thermal sensitivity of the dataset without analyzing other mineral phases or using a completely different low-T thermochronological technique. The *Single Sample* modeling yields a set of thermal histories that seems consistent throughout independent sample analysis (except CJ-16). Within the context of the vertical sample spacing, which has not been considered during this initial analysis, an important inter-sample mismatch becomes apparent. Sample CJ-23 exhibits thermal histories that suggest cooling to or even below the temperatures seen by the top-most sample CJ-12. Following the logic that any sample below another one must reside at higher temperatures at all times, this result has to be incorrect assuming that there is no localized heat source (e.g. dyke emplacement or fluid percolation around fault zones). Utilizing the vertical sample spacing in the *Sample Array* module, HeMP is able to improve on the previous results and yield thermal histories that are consistent with all samples. After initial cooling, slow re-heating to peak temperatures of ~65°C at 10-5 Ma and subsequent cooling to present-day conditions is considered the final, best estimate of the t-T evolution of this dataset. Potential improvements of the results could be accomplished by analyzing samples in between CJ-12 and CJ-16 and/or using AFT to constrain the higher temperature thermal sensitivity of samples CJ-

16, CJ-18, and CJ-23. On the other hand, ZHe analyses would not add much of additional value because the majority of the t-T history evolves below the sensitivity of this system (~190-150°C).

The Shillong samples probably represent the least constraint dataset in terms of temperature sensitivity control. The samples were collected over great distances, no vertical transect was available, and only a single mineral phase (apatite) was subjected to modeling. On an aliquot basis, none of the samples showed positive correlations of He age with neither grain size nor eU. Group 1 apatites, seen as one population, exhibit some positive correlation of He age with eU for aliquots with eU exceeding ~50 ppm (Fig. 4.8). The comparison of acceptable fits from HeMP with the AFT modeling in HeFTy (Fig. 4.9-4.13) reveals some agreement as well as differences in the obtained results. For Group 1 apatites, the Cretaceous cooling signal is generally better constraint but slightly older than what has been modeled with AFT data. As a result and contrary to the AFT model runs, some of the acceptable t-T paths require very little or no re-heating to fit the aliquot ages. The maximum temperatures reached during burial are in good agreement with the AFT results. Group 2 apatites yield virtually identical results from both techniques. Although HeMP produces less acceptable solutions, the rapid cooling event past 20 Ma as well as re-heating to temperatures in excess of 100°C is clearly captured. Going back to the earlier discussion, thermal histories characterized by high cooling rates are less sensitive to differences in diffusion kinetics, which explains why the results from two very different techniques converge at the same solution. On the other hand, prolonged residence in the low-T portion of the HePRZ as suggested by the AFT modeling will affect the apatite He system much more than the AFT system. Which solution is more favorable is up for discussion because on one hand the AFT technique offers age together with track length information, on the other hand its low-T sensitivity is limited to ~60°C. Modeling these systems together would most certainly narrow the range of possible thermal histories. The zircon He ages are much too old to add any additional insight to the Tertiary evolution of the Shillong plateau, nevertheless they provided the important constraint that peak temperatures during re-heating were not sufficiently high enough to re-set the ZHe system.

The KTB model result shows a very similar t-T evolution than what was proposed by Wagner et al. (1997) and later Stockli and Farley (2004) although the initiation of rapid cooling happens slightly earlier ranging from ~100-80 Ma. Based on the quite large standard deviation of the aliquot analysis, this result is not surprising. A potential increase in resolution could be obtained by adding more zircon aliquots, which hopefully would decrease the standard deviation, or adding another higher temperature system like the titanite (U-Th)/He thermochronometer. Including AHe analysis would not be useful to refine this tectonic event but most certainly improve the later stages of the thermal evolution after the main pulse of exhumation. As a common factor of uncertainty, zircon analysis is challenged by the usually unknown and most likely heterogeneous parent nuclide distribution, which greatly affects diffusion and F_T-correction factor.

Comparing the results from the modeling of the Xainze transect, it again becomes apparent that linking individual samples enhances the model results. A variety of approaches ranging from *Single Sample* modeling based on mean ages, *Single Sample* modeling based on individual aliquot ages, and using mean ages in the *Sample Array* module were presented and progressively led to a narrower range of possible thermal histories. While numerous good and acceptable fits for individual samples cover a larger, not well-constrained area in t-T space as demonstrated in Fig. 2.15, the *Sample Array* module yields a much tighter area of realizable t-T evolutions. The rapid cooling event indicated by elevation invariant apatite ages is now clearly constrained at ~10 Ma. Because of the thermal history generation algorithm, which offsets an initial t-T according to sample elevation and geothermal gradient, the result of the *Sample Array* module resembles the thermal evolution for the top-most sample obtained through the *Single Sample* modeling run. The practical consequence of this is that only the top-most, not all samples, can be modeled initially to refine the model constraints for subsequent *Sample Array* runs.

4.4.2 HeMP – Capabilities, Lessons Learned, Best Practices

Intensive testing on different datasets, synthetic and real world, proved that HeMP is capable of delivering reliable results while being a very versatile tool to analyze them in various ways. An unprecedented wealth of options to present the raw data, model them and graphically display the results in different ways empowers the user to investigate the dataset in detail. Deviations in model ages between HeMP and HeFTy (see Fig. 4.2) are primarily attributed to differences in the t-T interval setup and unknown precision of hard-coded constant values and their conversions. Although HeMP applies the same rule as outlined by Ketcham (2000) and subdivides the t-T path into smaller intervals not exceeding 3.5°C, it is not clear how the duration of each interval in the case of very slow cooling is defined. As designed, the entire He production for each individual t-T interval is added instantaneously at the beginning of the interval and as a result, different setups will certainly produce slightly different model ages. Based on internal testing, HeMP uses the rule that each interval should be no longer than 1% of the overall t-T path, which ensures accurate results while keeping computational time within acceptable limits.

Forward modeling is a powerful tool to gain insight into the sensitivity of input parameters. They run relatively quickly and can be used to assess the effects of grain size, parent nuclide concentrations (eU), and diffusion parameters (D_o, E_a) on model ages. This adds great value not only to scientists who strive to explore their data, but also to teachers who would like to demonstrate simple concepts of He-diffusion in a classroom setting. Able to create a number of thermal histories offset from each other by user-defined inputs greatly aids in analysis of vertically spaced samples.

HeMP's inverse modeling options, can be used to recover thermal histories from a given dataset while also providing the range of uncertainties. The *Single Sample* modeling should be the starting point of each analysis for several reasons. First, it has been shown that only modeling the data will provide additional confidence if age dispersion is caused by much different diffusion kinetics (size, eU) or other factors like zonation or inclusions need to be considered. This is impressively documented by sample GP9S6 (Fig. 4.10B) where three aliquots separated by ~50 Myrs yield thermal histories consistent with other samples of this group. Second, the initial modeling provides additional constraints for subsequent *Sample Array* analysis increasing the chance to find matching t-T paths.

Although very powerful, the user has to be aware that the t-T path offsets during modeling of sample arrays are based on a range of fixed geothermal gradients. Given the impact of exhumation/burial rates together with the related transient shape of the earth surface on the thermal field around the collected samples, this approach is an oversimplification. In nature, isotherms will be compressed during periods of rapid exhumation, conversely extended during times of fast burial. Furthermore, topographic effects can have significant influence on the geometry as well as the geothermal gradient especially for very low-T thermochronometers like apatite (Mantelow,…). These effects are obviously not accounted for in the current version of the algorithm and their impact on the model results has to be evaluated on a case by case basis. As mentioned earlier, the forward modeling tool in HeMP can help to understand the effects of diverging/converging t-T paths on the model ages. Offsetting this additional complication to some extent is the fact that model ages become more insensitive to the geothermal gradient with increasing exhumation rates because the samples move quickly through the HePRZ. For slow cooling/heating rates on the other hand, in can be assumed that the geothermal gradient is in steady-state equilibrium and the simplification of a fixed T-offset is valid again. In this case, the model results also allow direct inferences of the geothermal gradient.

Ongoing improvements of laboratory equipment (e.g. noble gas extraction lines, ICPMS) led to increased detection limits and nowadays the analysis of low concentration single apatite grains is no longer a problem. As a consequence, the use of multi-grain aliquots to obtain sufficient amounts of parent and daughter products is not required and should be avoided. In (U-Th)/He thermochronology, common lab procedure is to hand-select several grains of equal size and combine them into one aliquot and only reproducible analysis of three or more aliquots from the same sample are considered a reliable He age. Keeping in mind the effect of kinetic variability (e.g. grain size, eU) on the final He age as a function of the thermal history (see Fig. 4.3), the dogma of striving towards reproducibility might have to be reconsidered. Instead, selecting single grains from different populations to obtain as much irreproducibility as possible could narrow the range of acceptable thermal histories significantly. This is especially important if no other mineral phase, no offset sample (vertical spacing) or other thermochronometer is available and/or the sample spent considerable time in the HePRZ. In this context, the Cajon Pass borehole with its heterogeneous lithologies presents an interesting case for a thought experiment related to sampling strategy. Assuming that apatites from two adjacent lithologies might have very different parent concentrations, one could sample above and below the contact and combine the samples into a single “pseudo” sample. Given the short distance, the thermal evolution has to be the same but the temperature sensitivity of the sample has potentially been extended because of a wider range in eU. As discussed earlier, it has been impossible during this study to yield fitting thermal histories for the vertical transect and borehole datasets utilizing all aliquot ages within the *Sample Array* module. Using the mean ages or a hybrid approach has been successful but the drawback is clearly the loss of the intra-sample thermal sensitivity. In summary, modeling has been proven a very iterative process supported by HeMP’s exceptional user-friendly layout and cross-functionality.

Finally, the rationale behind using larger errors on some repeat runs needs further explanation. The error assigned to an individual aliquot analysis (2σ of 6% for apatite and 8% for zircon) is based on the reproducibility of standards. Analyzing chards of big, gem-quality Durango apatite crystals and idiomorph zircon crystals from the Fish Canyon tuff is a widely accepted way of monitoring the reliability of the measurements and general lab procedures. Unfortunately, both are not representative for the majority of natural samples because Durango apatite does not require a F_T-correction, is basically free of inclusions and as well as Fish Canyon tuff zircons was cooled almost instantaneously. Parent nuclide zonation is the rule rather than the exception in zircons and occurs in apatites probably more often than desired as suggested by LA-ICPMS measurements and observed track density distributions during AFT dating. As special case of inhomogeneous distribution of parent isotopes are inclusions, which add the additional complication that they might not dissolve during standard apatite procedures resulting in a “parentless” He contribution. Both of these cases have significant impact on the F_T correction factor, which directly affects the final He age. Fitzgerald et al. (2006) provides a comprehensive compilation of factors that contribute to variations in intra-sample AHe ages. Given the merit of additional control points, it seems tempting to increase aliquot errors to yield better constraint t-T paths. If the uncertainties become unreasonable, the user should consult other techniques (e.g. depth profiling, SEM analysis, CT scanning) to either back up the inclusion problem, or determine the severity of zoning which then could be incorporated in subsequent model runs. The Shillong dataset has been challenging because of poor quality apatite, mostly related to inclusions. Although, great care was taken to pick inclusion-free mineral grains, the possibility of analysis of grains with undetected micro-inclusion could not be excluded. Relaxing the errors on the individual analysis in order to increase the number of fitting aliquots seems to be a valid approach and in this case justified by the observations.

Experience shows that modeling of (U-Th)/He data is usually done after all the samples have been collected and analyzed and probably more often than desired, one would like to go back to the field to collect another sample because of inconclusive results. Using remote sensing techniques as an analogy, HeMP offers a variety of tools to improve sampling and analysis strategies before going to the field, which might save time and money for unnecessary analysis. Taking the vertical relief of a transect of interest together with a number of hypothesized thermal histories, one could forward model the age versus elevation relationships and specifically target elevations where the results show characteristic patterns (e.g. inflection points). During sample analysis, iterative modeling of the growing number of available He ages could be used to limit the effort to samples that characterize the thermal history sufficiently therefore, avoiding over-analysis that would not add any improvements. Keeping in mind the dependency of a He ages on grain size and eU (unfortunately this cannot be verified before the analysis) the grain selection and number of aliquots strategy could be optimized on the go. As the thermochronometer with the lowest T-sensitivity used routinely, the apatite (U-Th/He) technique is capable of answering a variety of geologic questions as presented in the case studies. Deployed at the beginning of the analysis process, spending time and money on other techniques might be avoided if the dataset is capable of recovering the sought after information. On the other hand, the results from AHe analysis can help to address which other low-T system is capable of filling the gaps in a weakly constrained thermal history and pin-point existing samples or other sample locations for additional thermochronological analysis.

On a final note, the user has to be aware at all times that the models are based on simplifications (e.g. diffusion in a sphere) and that a naturally occurring process that evolves over millions of years is modeled in minutes or hours using discrete time intervals that compress a considerable amount of time into a single mathematical operation. Furthermore, and most importantly, the results can only be as good as the input and modeling will yield a range of possible outcomes. In the end and it is up to the user's responsibility to carefully evaluate the results and the assumptions that went into the model before drawing final conclusions.

4.5 CONCLUSIONS

(U-Th)/He thermochronology has been applied to answer critical questions in many tectonic settings and has proven itself as a valuable technique to access the late-stage history of an evolving landscape. Quantitative analysis of the data to derive meaningful thermal histories has become a standard approach and a variety of software packages is available to extract this information. The new tool presented here combines many different modules ranging from calculation of F_T to several forward and inverse modeling modules. The *Sample Array* module has proven to be of great value to derive thermal histories from vertical transects or boreholes samples where independent sample analysis fails to sufficiently constrain the thermal history.

HeMP's capability to graphically present input as well as output data in many different ways enables the user to dissect the results in detail and examine their viability. A single input table that can be quickly adjusted to test different input parameters (e.g. diffusion coefficients, activation energies, stopping distances,…) paired with an exceptional user-friendly surface makes HeMP a very versatile and easy to use platform for advanced analysis of (U-Th)/He data.

Based on a wealth of experience with multiple datasets from different tectonic settings, is has become apparent that sample selection is key to successfully gain insight into the thermal history. Quickly cooled samples are less sensitive to intra-sample kinetic variations and as a result might require other thermochronometers (e.g. zircon additional to apatite analysis) or even another technique (e.g. AFT) to broaden the thermal sensitivity of the sample. Slowly cooled samples on the other hand might be already sufficiently constrained by single-thermochronometer analysis with favorable spreads in kinetic parameters.

CHAPTER 4: REFERENCES CITED

Bengtson, A., Ewing, R. C., and Becker, U., 2012, He diffusion and closure temperatures in apatite and zircon: A density functional theory investigation: Geochimica et Cosmochimica Acta, v. 86, no. 0, p. 228-238.

Biswas, S., Coutand, I., Grujic, D., Hager, C., Stöckli, D., and Grasemann, B., 2007, Exhumation and uplift of the Shillong plateau and its influence on the eastern Himalayas: New constraints from apatite and zircon (U-Th-[Sm])/He and apatite fission track analyses: Tectonics, v. 26, no. 6, p. TC6013.

Brandon, M. T., Roden-Tice, M. K., and Garver, J. I., 1998, Late Cenozoic exhumation of the Cascadia accretionary wedge in the Olympic Mountains, northwest Washington State: Geological Society of America Bulletin, v. 110, no. 8, p. 985-1009.

Braun, J., 2003, Pecube: a new finite-element code to solve the 3D heat transport equation including the effects of a time-varying, finite amplitude surface topography: Computers & Geosciences, v. 29, no. 6, p. 787-794.

Cherniak, D. J., Watson, E. B., and Thomas, J. B., 2009, Diffusion of helium in zircon and apatite: Chemical Geology, v. 268, no. 1-2, p. 155-166.

Clauser, C., Giese, P., Huenges, E., Kohl, T., Lehmann, H., Rybach, L., Šafanda, J., Wilhelm, H., Windloff, K., and Zoth, G., 1997, The thermal regime of the crystalline continental crust: Implications from the KTB: Journal of Geophysical Research: Solid Earth, v. 102, no. B8, p. 18417-18441.

Dodson, M. H., 1973, Closure temperature in cooling geochronological and petrological systems: Contributions to Mineralogy and Petrology, v. 40, p. 259-274.

Dodson, M. H., 1979, Archaean Geochronology, *in* Jäger, E., and Hunziker, J., eds., Lectures in Isotope Geology, Springer Berlin Heidelberg, p. 207-214.

Dunai, T. J., Bikker, A., and Meesters, A. G. C., 2003, Decomp: a user friendly forward modeling program for (U-Th)/He low-temperature geochronology: EGS - AGU - EUG Joint Assembly, Abstracts from the meeting held in Nice, France, 6 - 11 April 2003, abstract #14076.

Ehlers, T. A., Chaudhri, T., Kumar, S., Fuller, C. W., Willett, S. D., Ketcham, R. A., Brandon, M. T., Belton, D. X., Kohn, B. P., Gleadow, A. J. W., Dunai, T. J., and Fu, F. Q., 2005, Computational Tools for Low-Temperature Thermochronometer Interpretation: Reviews in Mineralogy and Geochemistry, v. 58, no. 1, p. 589-622.

Farley, K. A., 2000, Helium diffusion from apatite; general behavior as illustrated by Durango fluorapatite: Journal of Geophysical Research, v. 105, no. B2, p. 2903-2914.

Farley, K. A., Wolf, R. A., and Silver, L. T., 1996, The effects of long alpha-stopping distances on (U-Th)/he ages: Geochimica et Cosmochimica Acta, v. 60, p. 4223-4229.

Fitzgerald, P. G., Baldwin, S. L., Webb, L. E., and O'Sullivan, P. B., 2006, Interpretation of (U–Th)/He single grain ages from slowly cooled crustal terranes: A case study from the Transantarctic Mountains of southern Victoria Land: Chemical Geology, v. 225, no. 1–2, p. 91-120.

Flowers, R. M., Ketcham, R. A., Shuster, D. L., and Farley, K. A., 2009, Apatite (U-Th)/He thermochronometry using a radiation damage accumulation and annealing model: Geochimica et Cosmochimica Acta, v. 73, no. 8, p. 2347-2365.

Gallagher, K., Stephenson, J., Brown, R., Holmes, C., and Fitzgerald, P., 2005, Low temperature thermochronology and modeling strategies for multiple samples 1: Vertical profiles: Earth and Planetary Science Letters, v. 237, no. 1-2, p. 193-208.

Gautheron, C., and Tassan-Got, L., 2010, A Monte Carlo approach to diffusion applied to noble gas/helium thermochronology: Chemical Geology, v. 273, no. 3–4, p. 212-224.

Green, P. F., 1988, The relationship between track shortening and fission track age reduction in apatite: combined influences of inherent instability, annealing anisotropy, length bias and system calibration: Earth and Planetary Science Letters, v. 89, no. 3–4, p. 335-352.

Green, P. F., Duddy, I. R., Laslett, G. M., Hegarty, K. A., Gleadow, A. J. W., and Lovering, J. F., 1989, Thermal annealing of fission tracks in apatite 4. Quantitative modelling techniques and extension to geological timescales: Chemical Geology: Isotope Geoscience section, v. 79, no. 2, p. 155-182.

Ketcham, R. A., 2005, Forward and Inverse Modeling of Low-Temperature Thermochronometry Data: Reviews in Mineralogy and Geochemistry, v. 58, no. 1, p. 275-314.

Ketcham, R. A., Donelick, R. A., and Carlson, W. D., 1999, Variability of apatite fission-track annealing kinetics: III. Extrapolation to geological time scales: American Mineralogist, v. 84, p. 1235-1255.

Ketcham, R. A., Donelick, R. A., and Donelick, M. B., 2000, AFTSolve: A program for multi-kinetic modeling of apatite fission-track data: Geological Materials Research, v. 2, no. 1, p. 1-32.

Ketcham, R. A., Gautheron, C., and Tassan-Got, L., 2011, Accounting for long alpha-particle stopping distances in (U–Th–Sm)/He geochronology: Refinement of the baseline case: Geochimica et Cosmochimica Acta, v. 75, no. 24, p. 7779-7791.

Laslett, G. M., Green, P. F., Duddy, I. R., and Gleadow, A. J. W., 1987, Thermal annealing of fission tracks in apatite 2. A quantitative analysis: Chemical Geology: Isotope Geoscience section, v. 65, no. 1, p. 1-13.

Lippolt, H. J., Leitz, M., Wernicke, R. S., and Hagedorn, B., 1994, (Uranium + thorium)/helium dating of apatite: experience with samples from different geochemical environments: Chemical Geology, v. 112, no. 1–2, p. 179-191.

Meesters, A. G. C. A., and Dunai, T., J., 2002a, Solving the production-diffusion equation for finite diffusion domains of various shapes Part l. Implications for low-temperature (U-Th)/He thermochronology: Chemical Geology, v. 186, p. 333-344.

Meesters, A. G. C. A., and Dunai, T., J., 2002b, Solving the production-diffusion equation for finite diffusion domains of various shapes Part ll. Application to cases with alpha-ejection and nonhomogeneous distribution of the source: Chemical Geology, v. 186, p. 347-363.

Reiners, P. W., and Farley, K. A., 1999, Helium diffusion and (U-Th)/He thermochronometry of titanite: Geochimica et Cosmochimica Acta, v. 63, no. 22, p. 3845-3859.

Reiners, P. W., and Farley, K. A., 2001, Influence of crystal size on apatite (U-Th)/He thermochronology: an example from the Bighorn Mountains, Wyoming: Earth and Planetary Science Letters, v. 188, p. 413-420.

Reiners, P. W., Spell, T. L., Nicolescu, S., and Zanetti, K. A., 2004, Zircon (U-Th)/He thermochronometry: He diffusion and comparisons with 40Ar/39Ar dating: Geochimica et Cosmochimica Acta, v. 68, no. 8, p. 1857-1887.

Shuster, D. L., and Farley, K. A., 2003, $^{4}He/^{3}He$ thermochronometry: Earth and Planetary Science Letters, v. 217, p. 1-17.

Shuster, D. L., and Farley, K. A., 2009, The influence of artificial radiation damage and thermal annealing on helium diffusion kinetics in apatite: Geochimica et Cosmochimica Acta, v. 73, no. 1, p. 183-196.

Shuster, D. L., Farley, K. A., Sisterson, J., M., and Burnett, D., S., 2003, Quantifying the diffusion kinetics and spatial distributions of radiogenic ^{4}He in minerals containing proton-induced ^{3}He: Earth and Planetary Science Letters, v. 217, p. 19-32.

Shuster, D. L., Flowers, R. M., and Farley, K. A., 2006, The influence of natural radiation damage on helium diffusion kinetics in apatite: Earth and Planetary Science Letters, v. 249, no. 3-4, p. 148-161.

Stockli, D., F., and Farley, K. A., 2004, Empirical constraints on the titanite (U-Th)/He partial retention zone from the KTB drill hole: Chemical Geology, v. 207, p. 223-236.

Wagner, G. A., Coyle, D. A., Duyster, J., Henjes-Kunst, F., Peterek, A., Schröder, B., Stöckhert, B., Wemmer, K., Zulauf, G., Ahrendt, H., Bischoff, R., Hejl, E., Jacobs, J., Menzel, D., Lal, N., Van den haute, P., Vercoutere, C., and Welzel, B., 1997, Post-Variscan thermal and tectonic evolution of the KTB site and its surroundings: Journal of Geophysical Research: Solid Earth, v. 102, no. B8, p. 18221-18232.

Warnock, A. C., Zeitler, P. K., Wolf, R. A., and Bergman, S. C., 1997, An evaluation of low-temperature apatite (U-Th)/He thermochronometry: Geochimica et Cosmochimica Acta, v. 61, no. 24, p. 5371-5377.

Wolf, R. A., Farley, K. A., and Kass, D. M., 1998, Modeling of the temperature sensitivity of the apatite (U-Th)/He thermochronometer: Chemical Geology, v. 148, no. 1-2, p. 105-114.

Wolf, R. A., Farley, K. A., and Silver, L. T., 1996, Helium diffusion and low-temperature thermochronometry of apatite: Geochimica et Cosmochimica Acta, v. 60, no. 21, p. 4231-4240.

Wolfe, M. R., and Stockli, D. F., 2010, Zircon (U-Th)/He thermochronometry in the KTB drill hole, Germany, and its implications for bulk He diffusion kinetics in zircon: Earth and Planetary Science Letters, v. 295, no. 1-2, p. 69-82.

Zeitler, P. K., Herczeg, A. L., McDougall, I., and Honda, M., 1987, U-Th-He dating of apatite: A potential thermochronometer: Geochimica et Cosmochimica Acta, v. 51, no. 10, p. 2865-2868.

CHAPTER 4: FIGURES AND TABLES

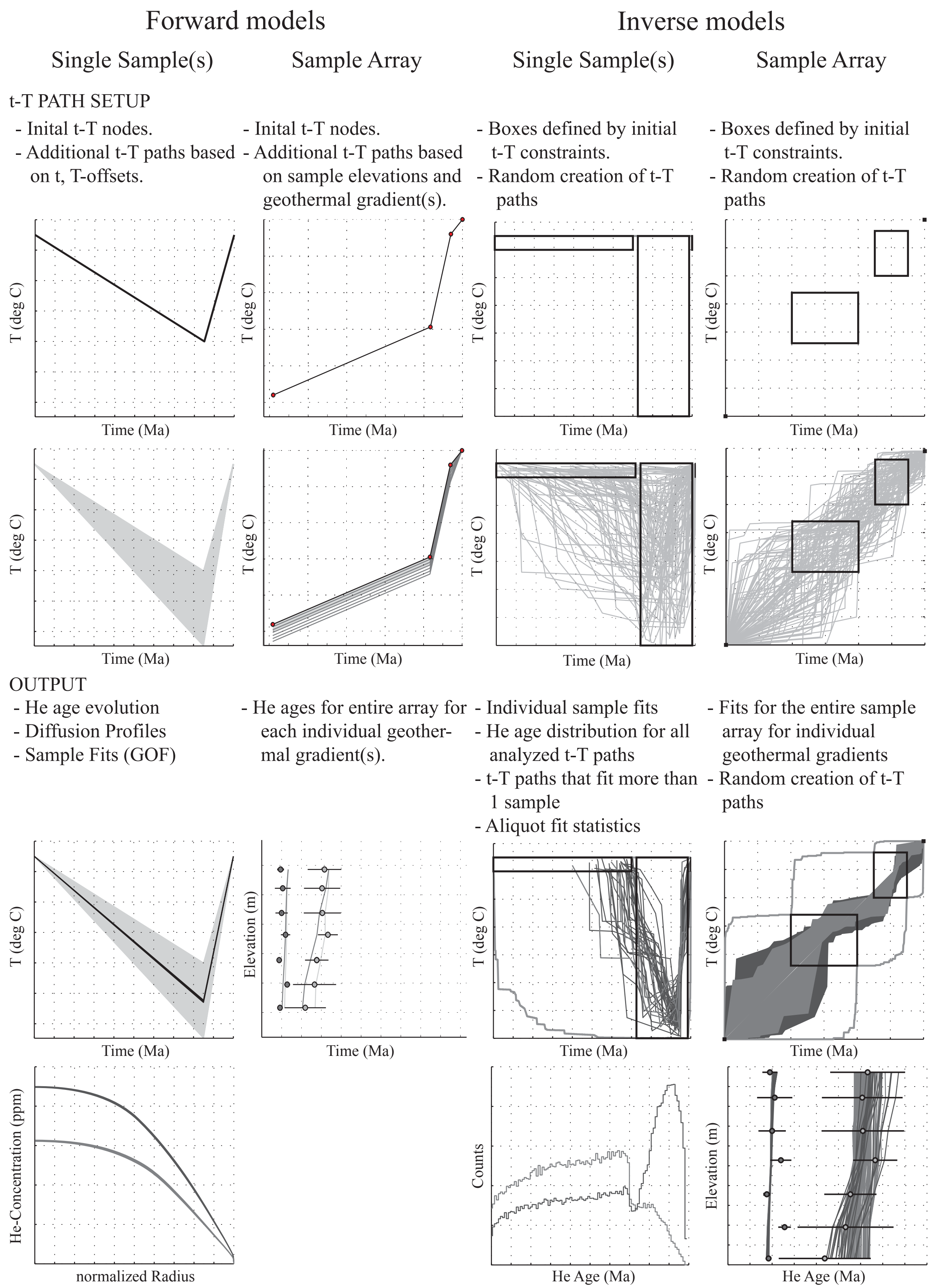

Forward models
Inverse models
Single Sample(s)
Sample Array
Single Sample(s)
Sample Array
t-T PATH SETUP
- Inital t-T nodes.
- Additional t-T paths based on t, T-offsets.
- Inital t-T nodes.
- Additional t-T paths based on sample elevations and geothermal gradient(s).
- Boxes defined by initial t-T constraints.
- Random creation of t-T paths
- Boxes defined by initial t-T constraints.
- Random creation of t-T paths
T (deg C)
Time (Ma)
OUTPUT
- He age evolution
- Diffusion Profiles
- Sample Fits (GOF)
- He ages for entire array for each individual geothermal gradient(s).
- Individual sample fits
- He age distribution for all analyzed t-T paths
- t-T paths that fit more than 1 sample
- Aliquot fit statistics
- Fits for the entire sample array for individual geothermal gradients
- Random creation of t-T paths
Elevation (m)
He-Concentration (ppm)
normalized Radius
Counts
He Age (Ma)

Figure 4.1: Overview of model setup, input requirements, and some examples of available outputs for the various He-modeling modules

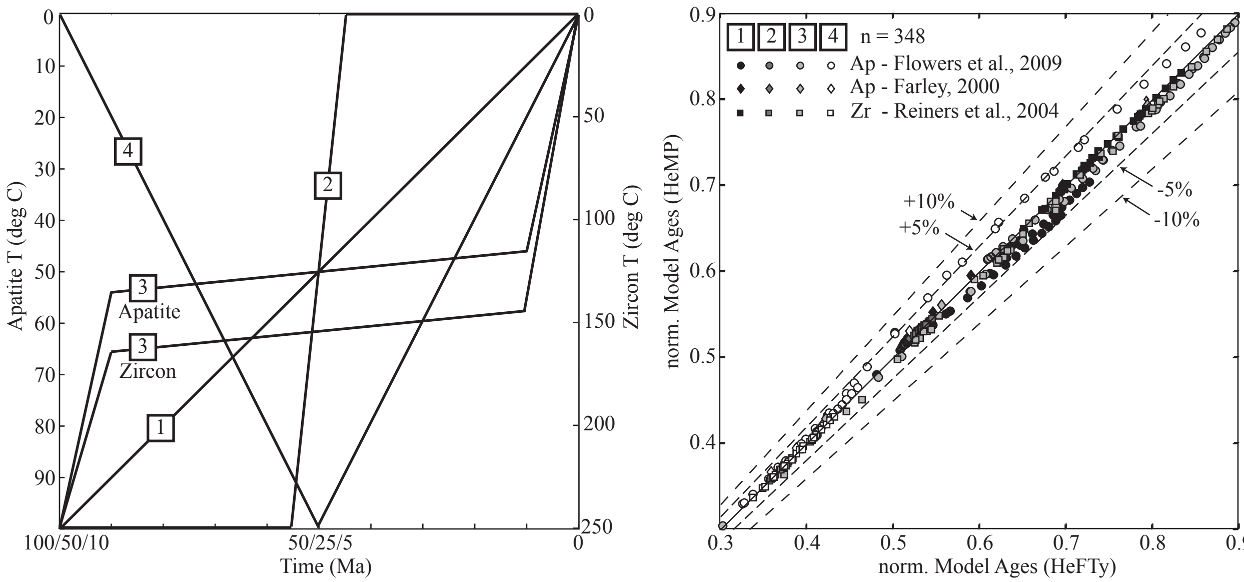
Apatite T (deg C)
Zircon T (deg C)
Time (Ma)
100/50/10
50/25/5
Apatite
Zircon
1
2
3
4
n = 348
Ap - Flowers et al., 2009
Ap - Farley, 2000
Zr - Reiners et al., 2004
+10%
+5%
-5%
-10%
norm. Model Ages (HeMP)
norm. Model Ages (HeFTy)

Figure 4.2: Test scenarios to compare HeFTy model ages with results obtained from the *Single Sample(s)* forward modeling module. Left-hand graph shows thermals histories used for testing. Right-hand graph shows the normalized model ages plotted against the normalized model ages obtained from HeFTy. Shades of grey indicate the t-T path, and type of symbols the kinetic model used for generating model ages. Dashed lines mark 5 and 10% deviations from the HeFTy age.

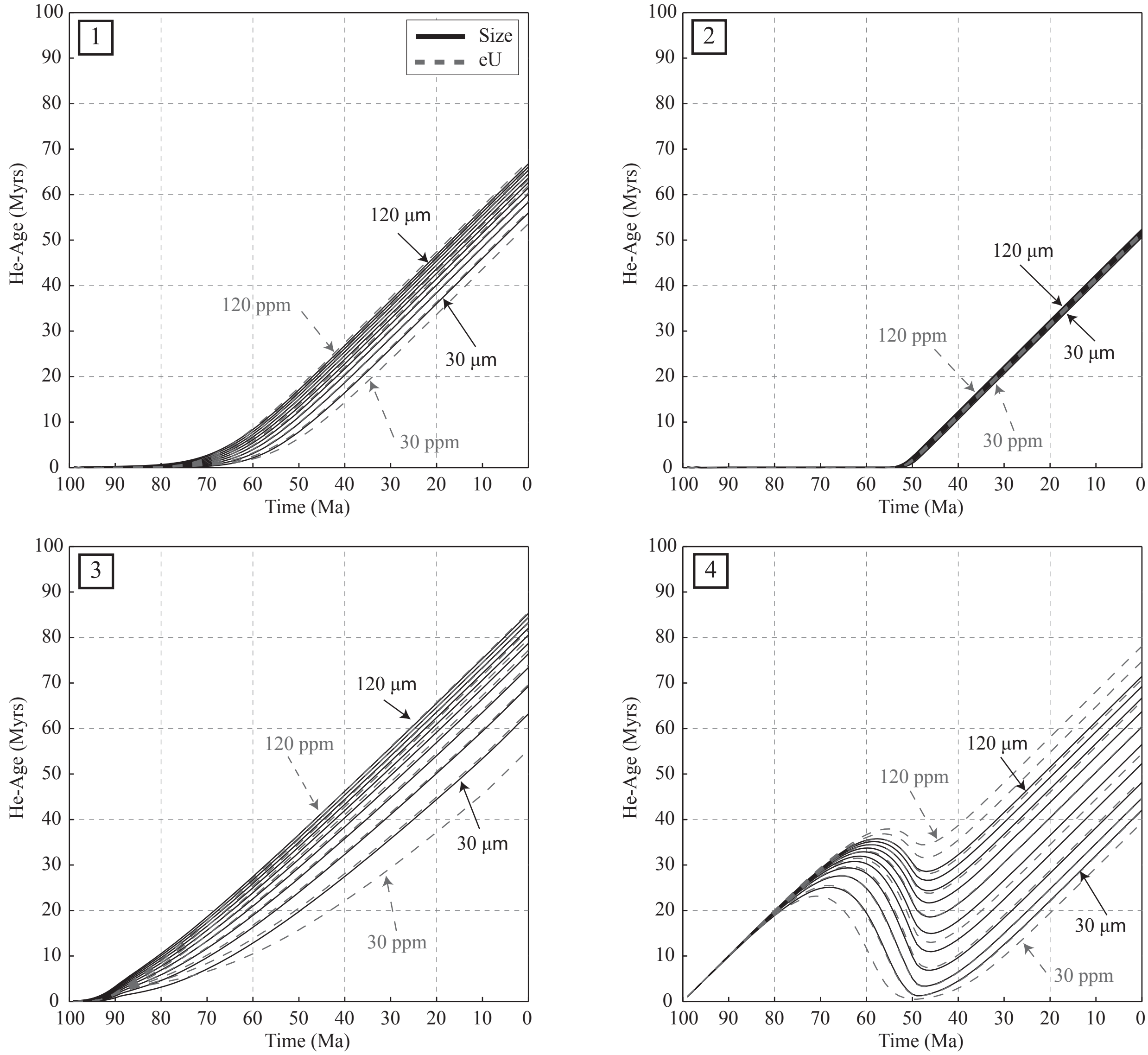
1
Size
eU
120 µm
120 ppm
30 µm
30 ppm
2
120 µm
120 ppm
30 µm
30 ppm
3
120 µm
120 ppm
30 µm
30 ppm
4
120 µm
120 ppm
30 µm
30 ppm
He-Age (Myrs)
Time (Ma)

Figure 4.3: He age evolution plots for 10 apatite grains with varying a) grain size (solid black lines) and b) eU (dashed grey lines) based on the four generic t-T paths used earlier. Note that an age difference of almost 40 myrs is realizable if the sample underwent burial and subsequent exhumation (t-T history 4) and eU ranges from 30-120 ppm.

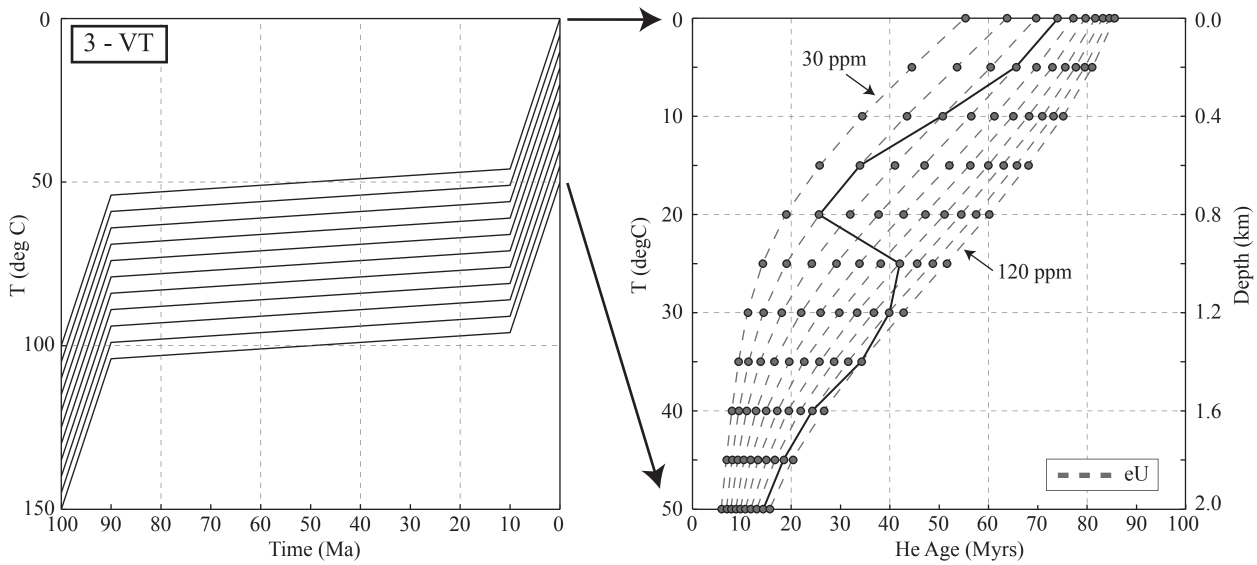
3 - VT
T (deg C)
Time (Ma)
30 ppm
120 ppm
eU
T (degC)
He Age (Myrs)
Depth (km)

Figure 4.4: t-T History 3 used to illustrate the prediction of He ages based on vertical sample spacing and eU. Left-hand graph: Suite of thermal histories based on a geothermal gradient of 25°C/km representing t-T histories for 11 samples spaced by 200 m. Right-hand graph: Dashed grey lines connect AHe ages based on equal eU and show the predicted decrease in ages towards greater depths (higher T). Black solid line represents the AHe ages from a hypothetical sample suite collected from e.g. a cored borehole section. Even a very simple thermal history can produce complicated age vs. depth relationships if the diffusion kinetics are dissimilar.

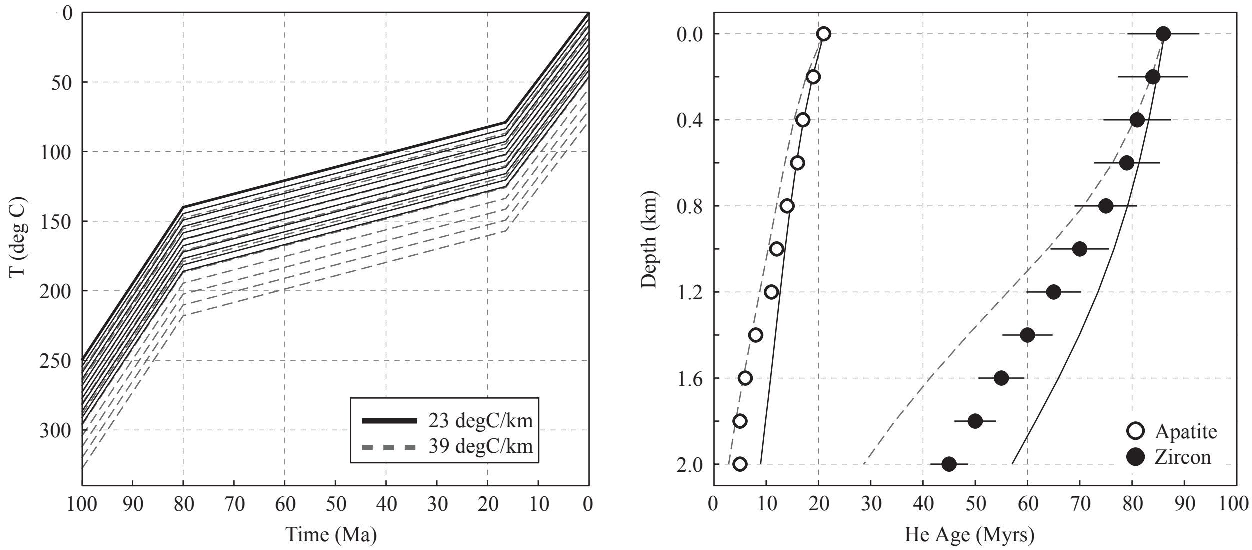
T (deg C)
Time (Ma)
23 degC/km
39 degC/km
Depth (km)
He Age (Myrs)
Apatite
Zircon

Figure 4.5: Example of the *Sample Array* forward modeling module. Left-hand graph: An initial thermal history (bold black line) is offset with a geothermal gradient of 23°C/km (solid black lines) and 39°C/km (dashed grey lines). Right-hand graph: He age versus depth plot for a synthetic dataset of 11 samples with apatite and zircon analysis. Predicted model ages for a geothermal gradient of 39°C/km are too young (dashed grey lines) and too old for 23°C/km (solid black lines). Based on this user-defined thermal history, a geothermal gradient in between might fit the data.

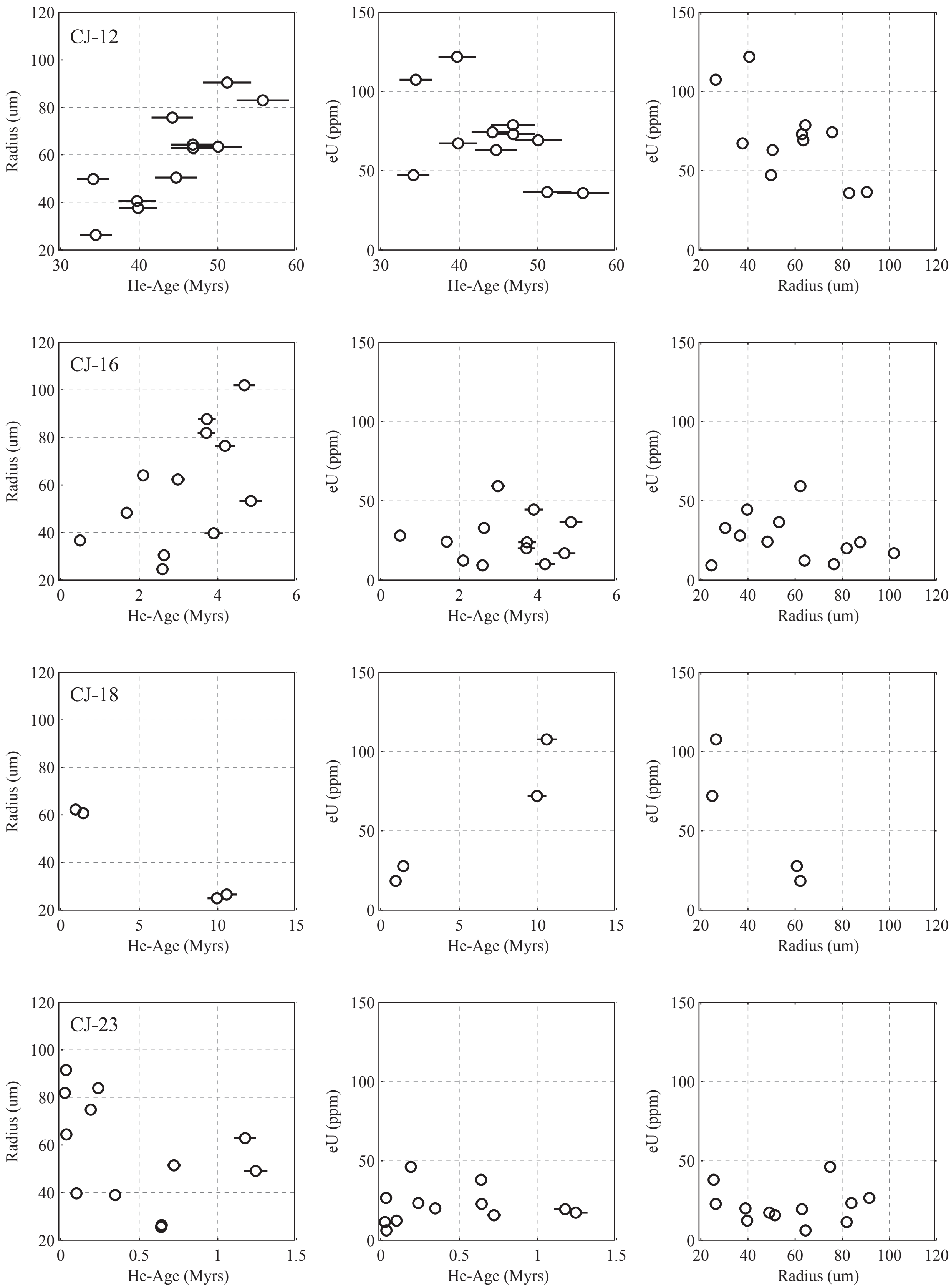
CJ-12
CJ-16
CJ-18
CJ-23
Radius (um)
eU (ppm)
He-Age (Myrs)
Radius (um)

Figure 4.6: Cross plots for Cajon Pass samples showing the relationships between He age, grain size, and eU.

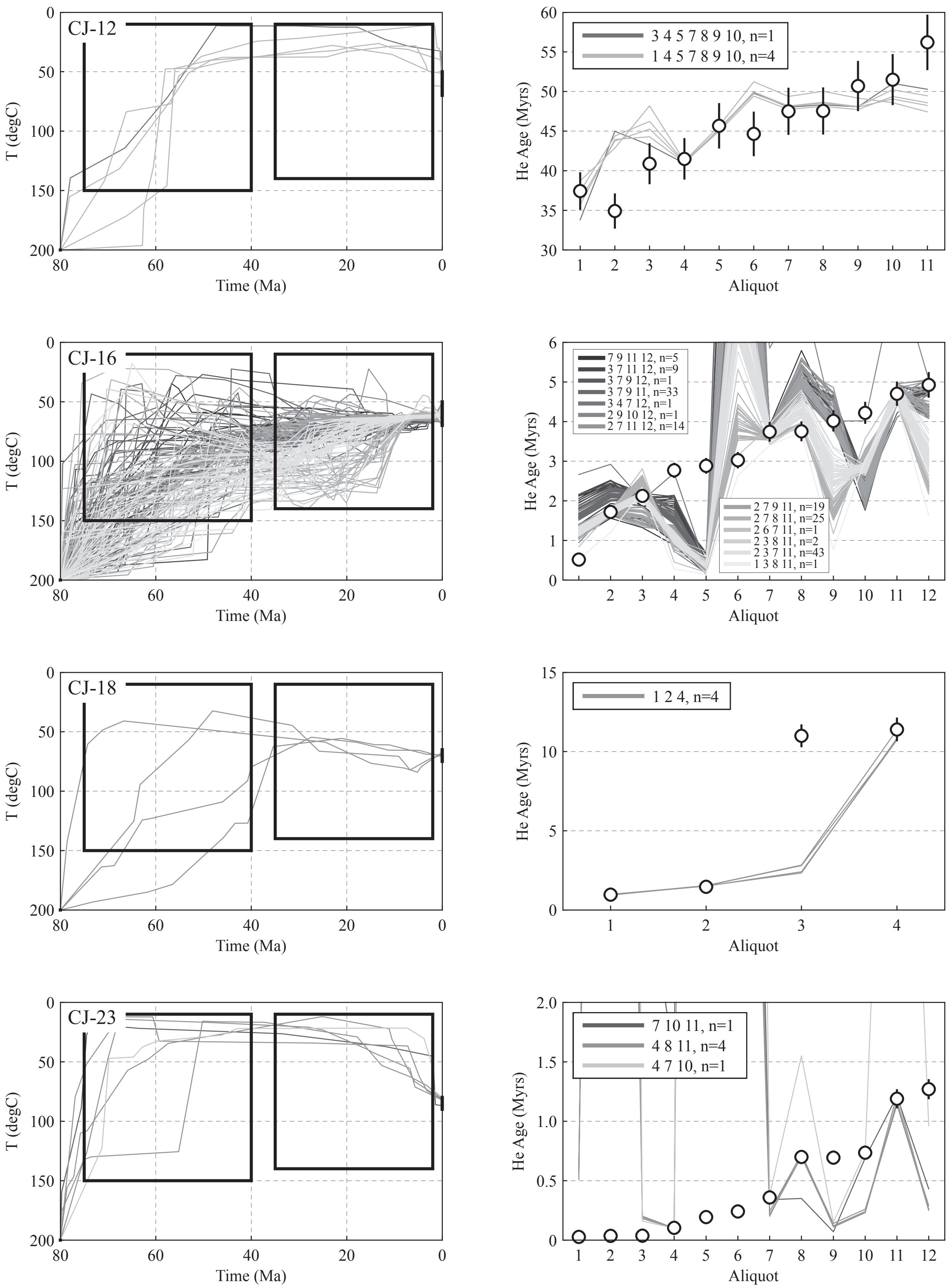
CJ-12
T (degC)
Time (Ma)
3 4 5 7 8 9 10, n=1
1 4 5 7 8 9 10, n=4
He Age (Myrs)
Aliquot
CJ-16
T (degC)
Time (Ma)
7 9 11 12, n=5
3 7 11 12, n=9
3 7 9 12, n=1
3 7 9 11, n=33
3 4 7 12, n=1
2 9 10 12, n=1
2 7 11 12, n=14
2 7 9 11, n=19
2 7 8 11, n=25
2 6 7 11, n=1
2 3 8 11, n=2
2 3 7 11, n=43
1 3 8 11, n=1
He Age (Myrs)
Aliquot
CJ-18
T (degC)
Time (Ma)
1 2 4, n=4
He Age (Myrs)
Aliquot
CJ-23
T (degC)
Time (Ma)
7 10 11, n=1
4 8 11, n=4
4 7 10, n=1
He Age (Myrs)
Aliquot

Figure 4.7: Results from inverse modeling of individual Cajon Pass samples. Left column shows resulting acceptable t-T paths, right column the model (lines) and sample (circles) ages. Error bars, where visible, indicate 6% (2σ) uncertainty. Aliquot combinations that resulted in fitting thermal histories are highlighted by different shades of grey.

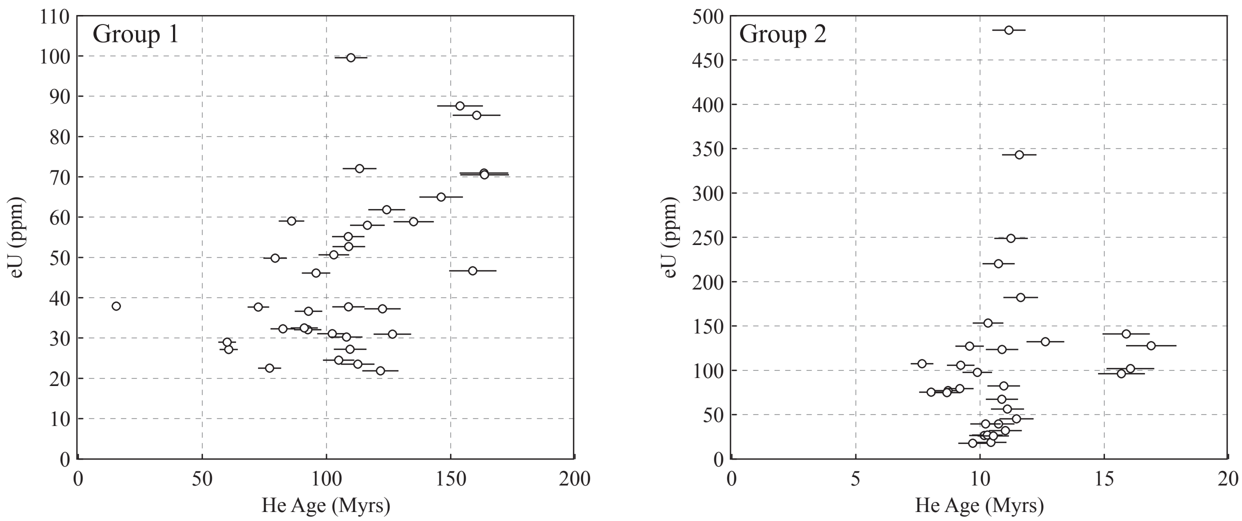
Group 1
eU (ppm)
He Age (Myrs)
Group 2
eU (ppm)
He Age (Myrs)

Figure 4.8: Effective Uranium concentration (eU) plotted against He ages for the two populations of Shillong Plateau samples. Note the positive correlation for Group 1 above 50 ppm.

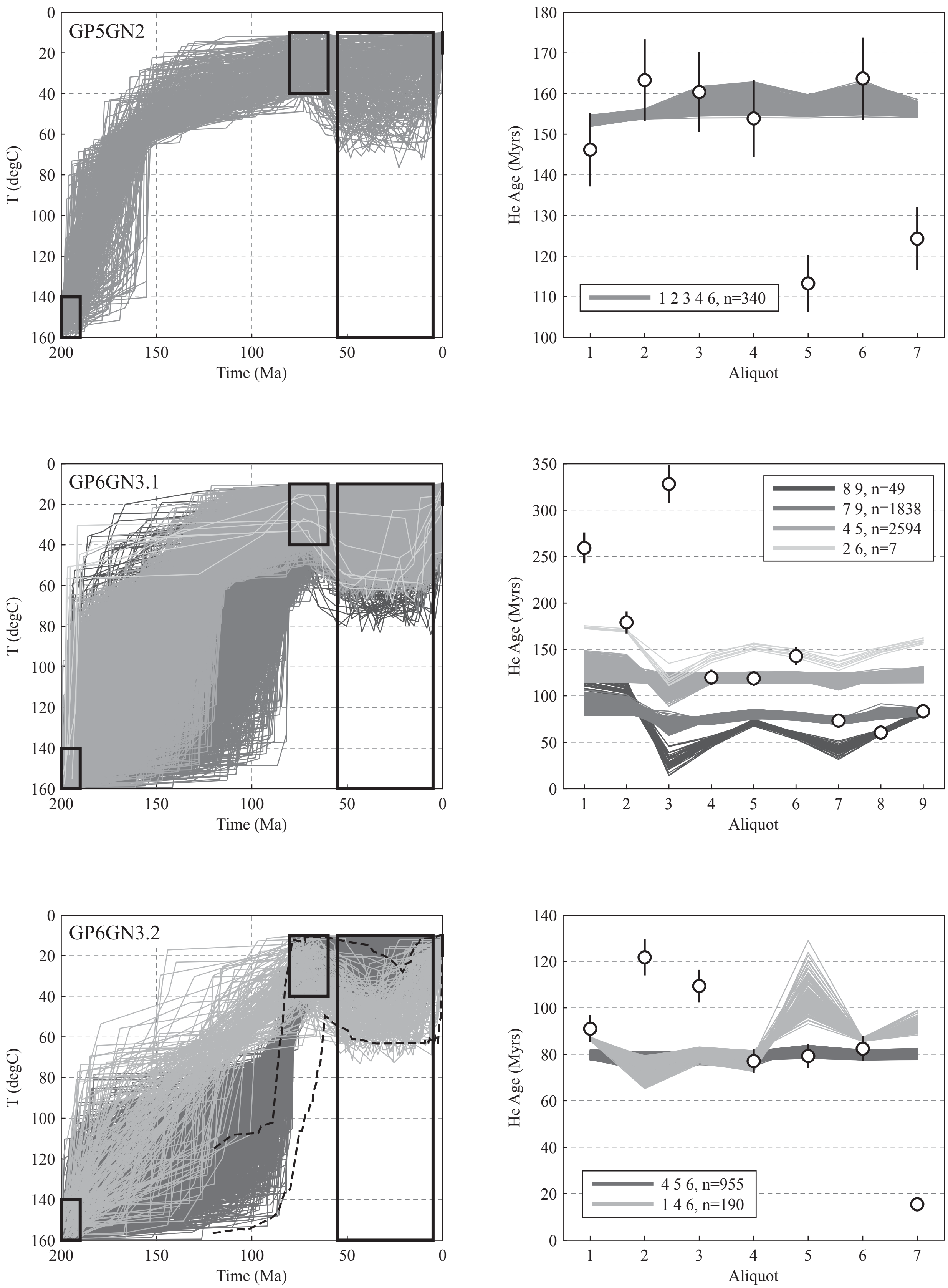
GP5GN2
T (degC)
Time (Ma)
He Age (Myrs)
Aliquot
1 2 3 4 6, n=340
GP6GN3.1
T (degC)
Time (Ma)
8 9, n=49
7 9, n=1838
4 5, n=2594
2 6, n=7
He Age (Myrs)
Aliquot
GP6GN3.2
T (degC)
Time (Ma)
4 5 6, n=955
1 4 6, n=190
He Age (Myrs)
Aliquot

Figure 4.9: Results of Single Sample inverse modeling of Shillong apatites for Group 1. Left column shows resulting acceptable t-T paths, right column the model (lines) and sample (circles) ages. Error bars, where visible, indicate 6% (2σ) uncertainty. Aliquot combinations that resulted in fitting thermal histories are highlighted by different shades of grey. Dashed black lines outline the acceptable solutions from independent AFT analysis (Biswas et al., 2006).

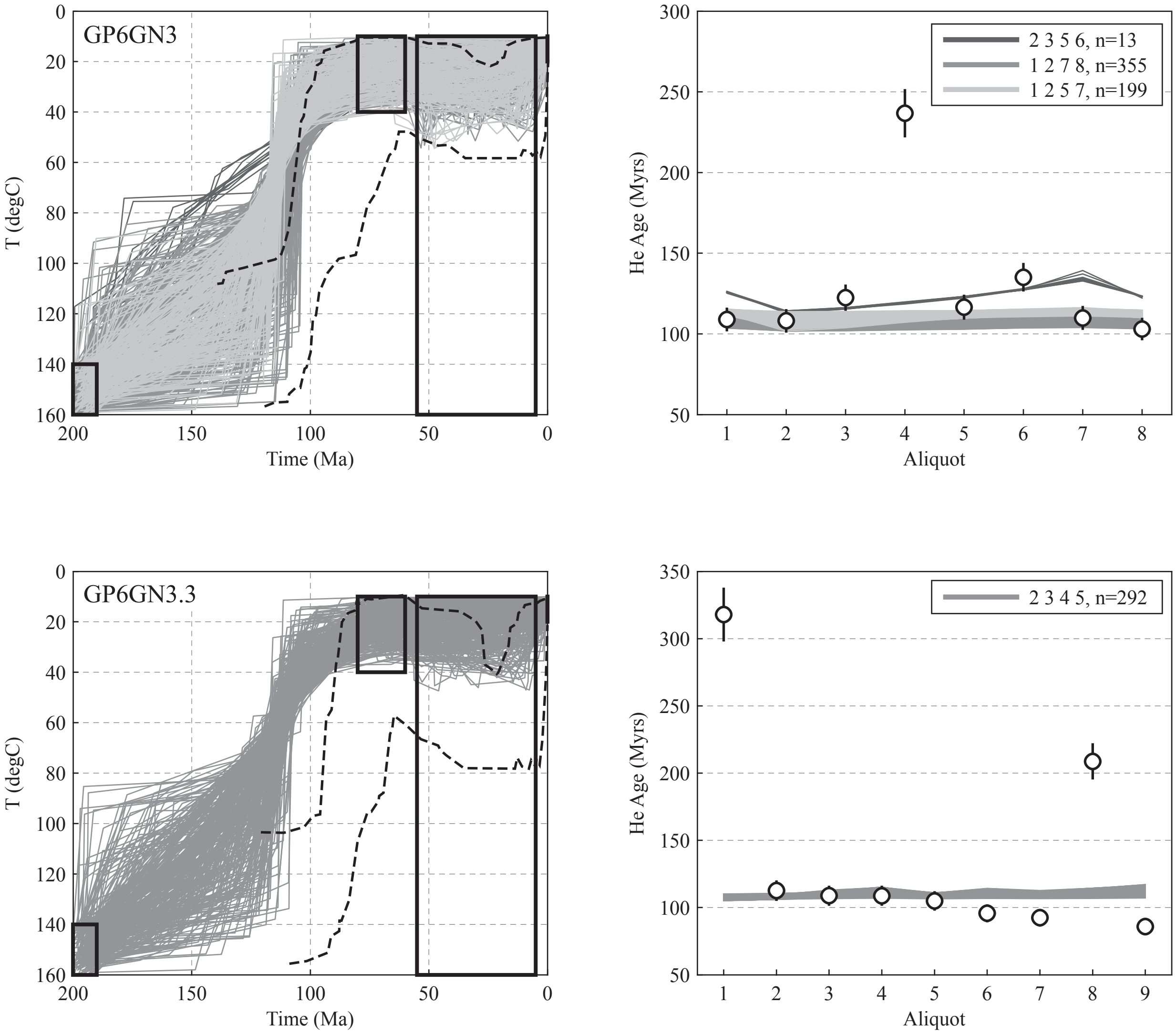
GP6GN3
T (degC)
Time (Ma)
He Age (Myrs)
Aliquot
2 3 5 6, n=13
1 2 7 8, n=355
1 2 5 7, n=199
GP6GN3.3
T (degC)
Time (Ma)
He Age (Myrs)
Aliquot
2 3 4 5, n=292

Figure 4.10: Results of Single Sample inverse modeling of Shillong apatites for Group 1; continued.

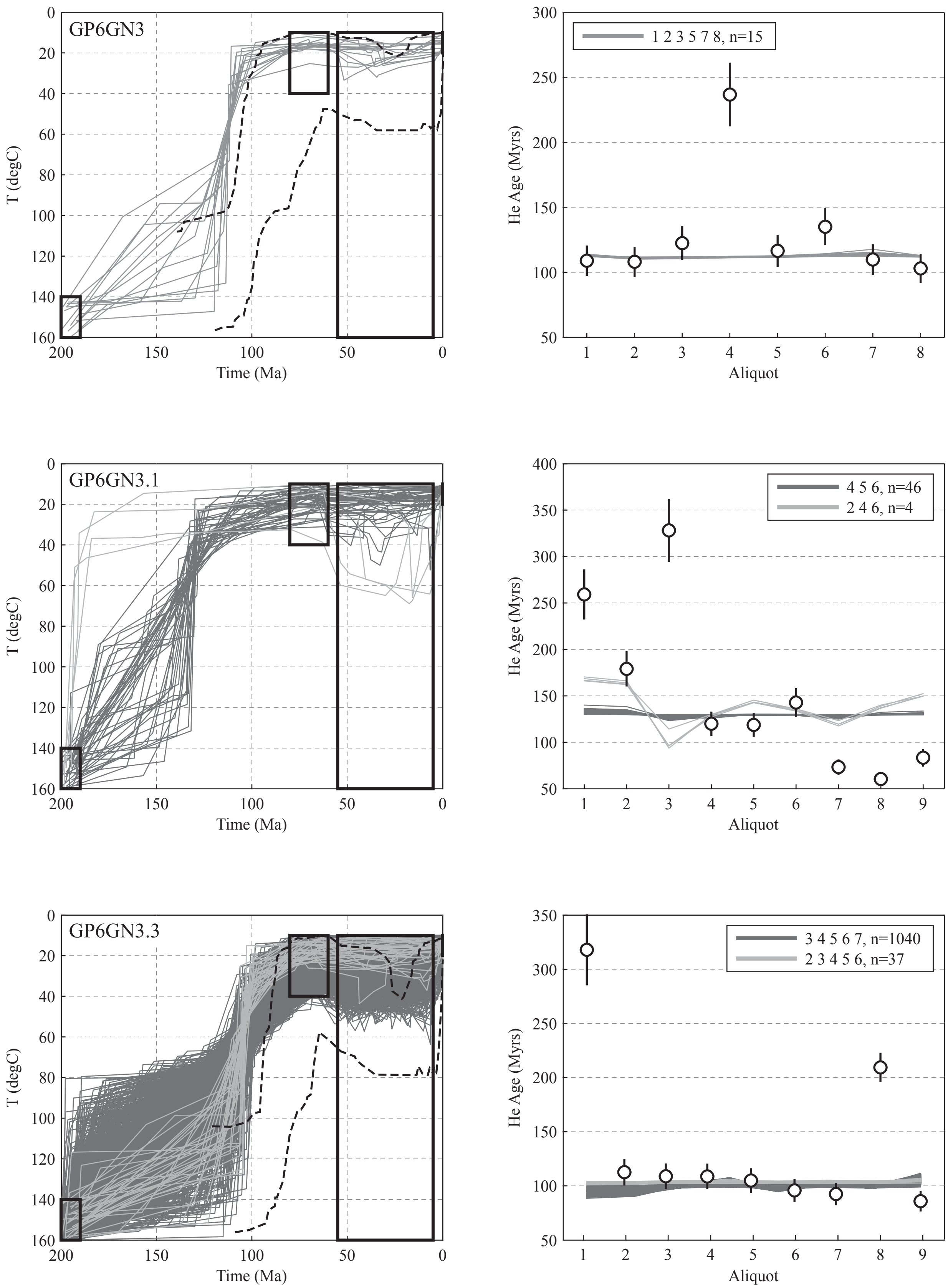
GP6GN3
T (degC)
Time (Ma)
1 2 3 5 7 8, n=15
He Age (Myrs)
Aliquot
GP6GN3.1
T (degC)
Time (Ma)
4 5 6, n=46
2 4 6, n=4
He Age (Myrs)
Aliquot
GP6GN3.3
T (degC)
Time (Ma)
3 4 5 6 7, n=1040
2 3 4 5 6, n=37
He Age (Myrs)
Aliquot

Figure 4.11: Results of Single Sample inverse modeling of Shillong apatites for Group 1 using larger uncertainties (10%).

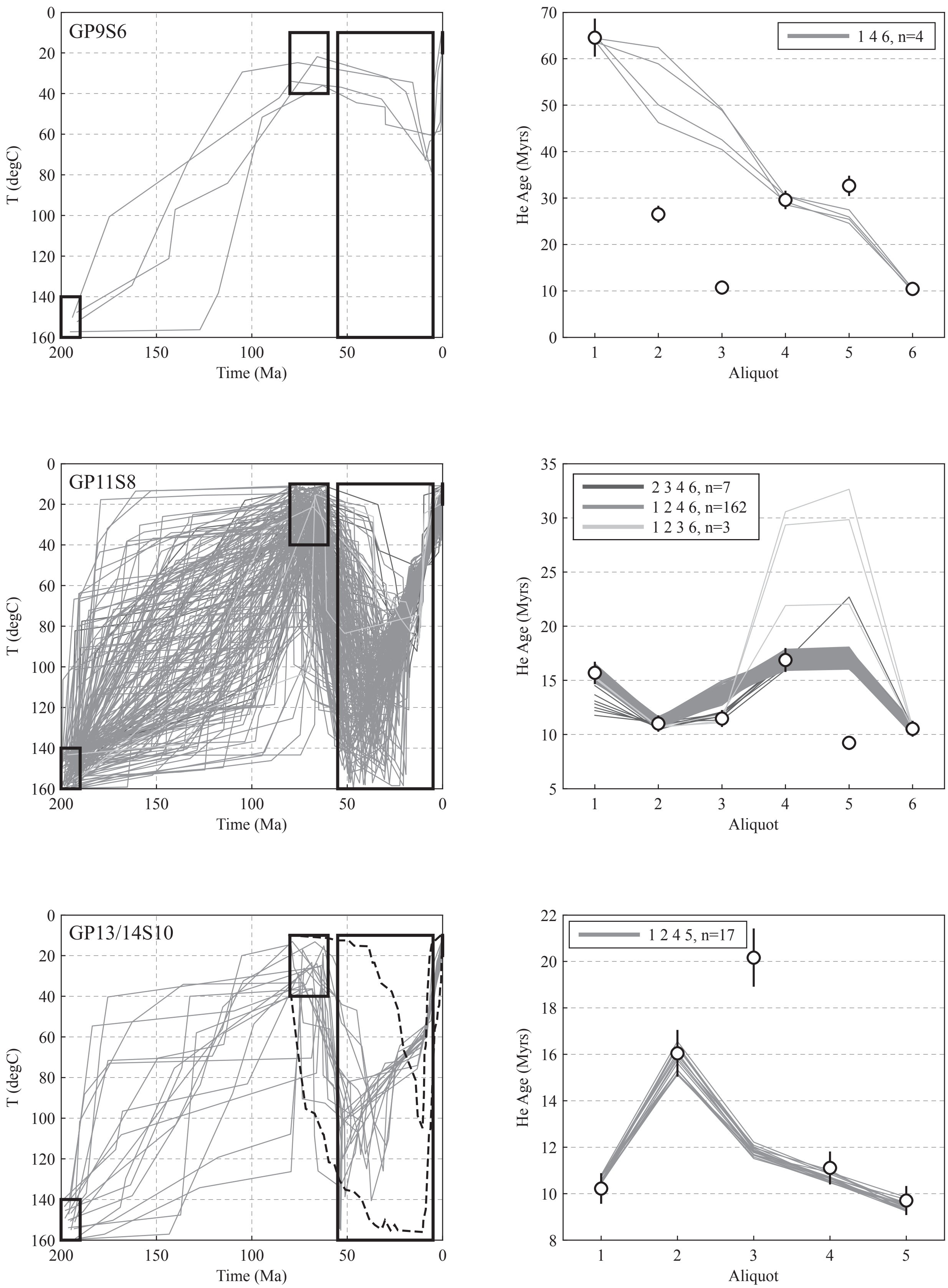
GP9S6
T (degC)
Time (Ma)
He Age (Myrs)
Aliquot
1 4 6, n=4
GP11S8
T (degC)
Time (Ma)
He Age (Myrs)
Aliquot
2 3 4 6, n=7
1 2 4 6, n=162
1 2 3 6, n=3
GP13/14S10
T (degC)
Time (Ma)
He Age (Myrs)
Aliquot
1 2 4 5, n=17

Figure 4.12: Results of Single Sample inverse modeling of Shillong apatites for Group 2. Left column shows resulting acceptable t-T paths, right column the model (lines) and sample (circles) ages. Error bars, where visible, indicate 6% (2σ) uncertainty. Aliquot combinations that resulted in fitting thermal histories are highlighted by different shades of grey. Dashed black lines outline the acceptable solutions from independent AFT analysis (Biswas et al., 2006).

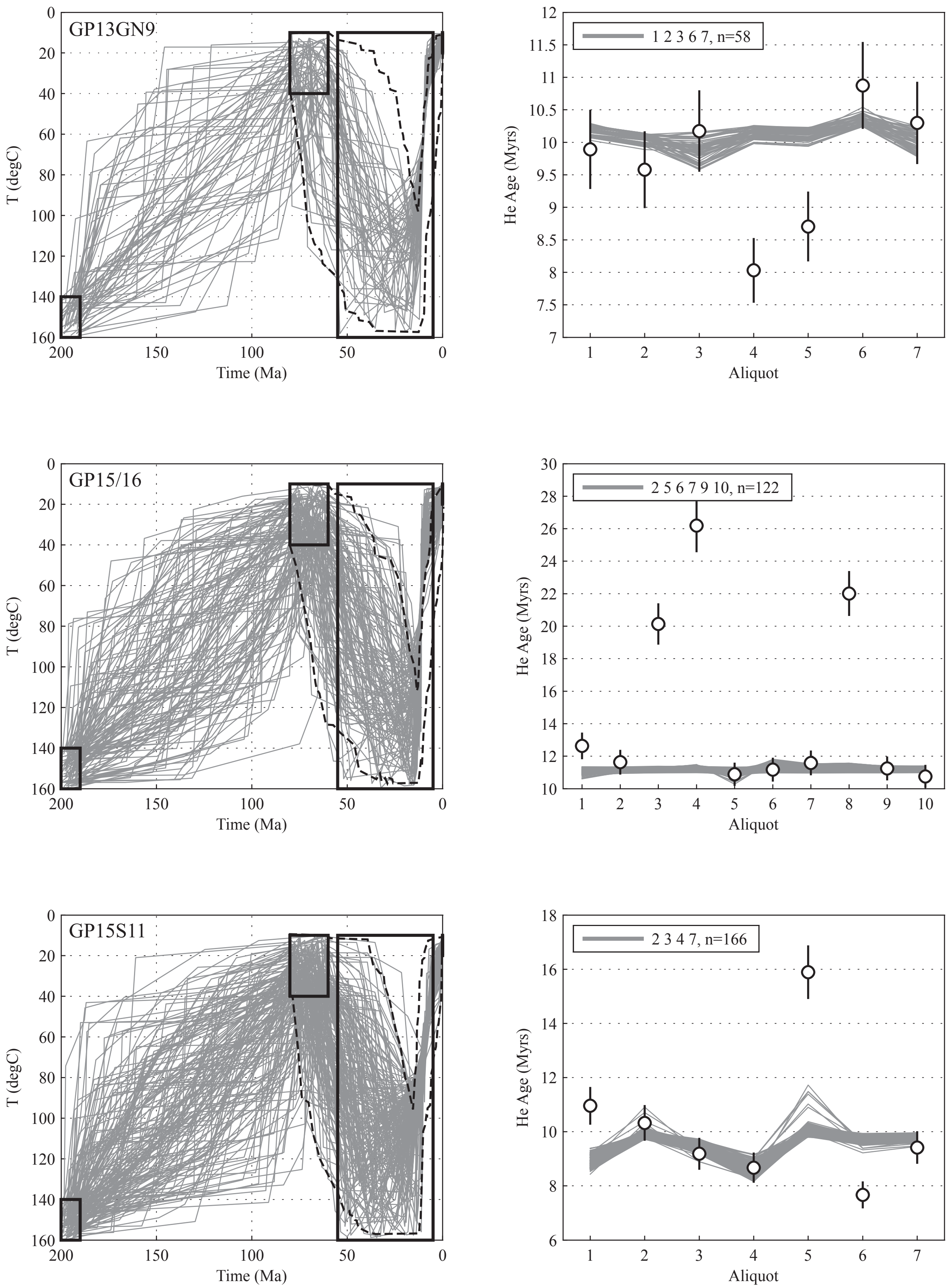
GP13GN9
T (degC)
Time (Ma)
1 2 3 6 7, n=58
He Age (Myrs)
Aliquot
GP15/16
T (degC)
Time (Ma)
2 5 6 7 9 10, n=122
He Age (Myrs)
Aliquot
GP15S11
T (degC)
Time (Ma)
2 3 4 7, n=166
He Age (Myrs)
Aliquot

Figure 4.13: Results of Single Sample inverse modeling of Shillong apatites for Group 2; continued.

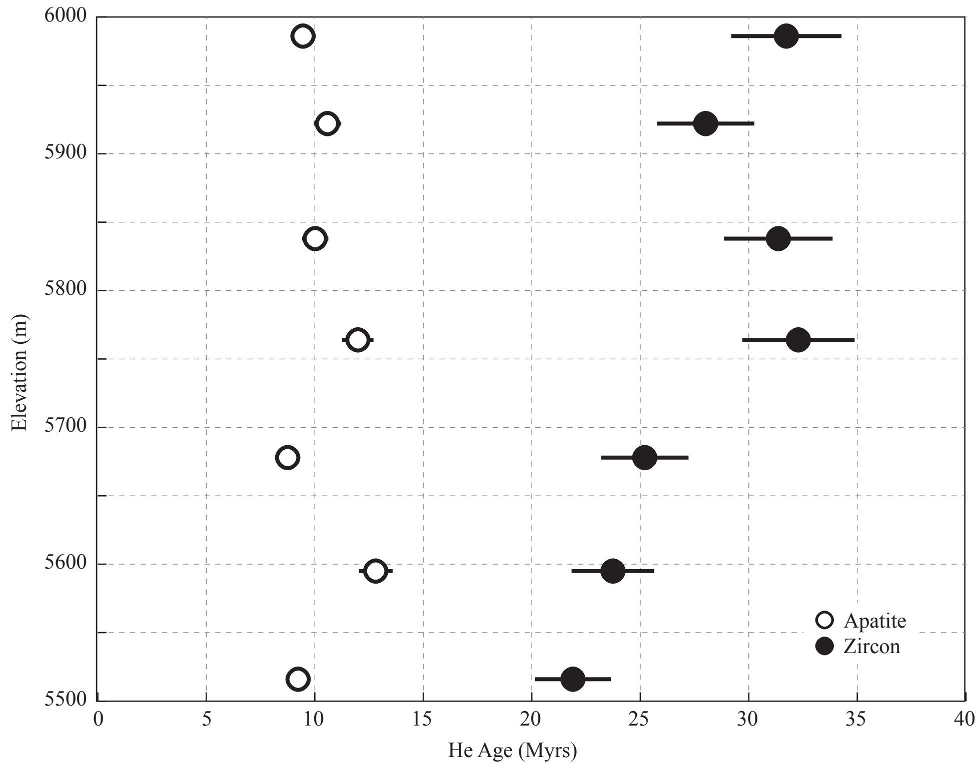
6000
5900
5800
5700
5600
5500
Elevation (m)
0
5
10
15
20
25
30
35
40
He Age (Myrs)
Apatite
Zircon

Figure 4.14: Mean He ages for apatite (white circles) / zircon (black circles) pairs of a vertical transect collected in Tibet plotted against sample elevations. Error bars indicate the 2σ uncertainty based on the standard deviation of the aliquot analysis.

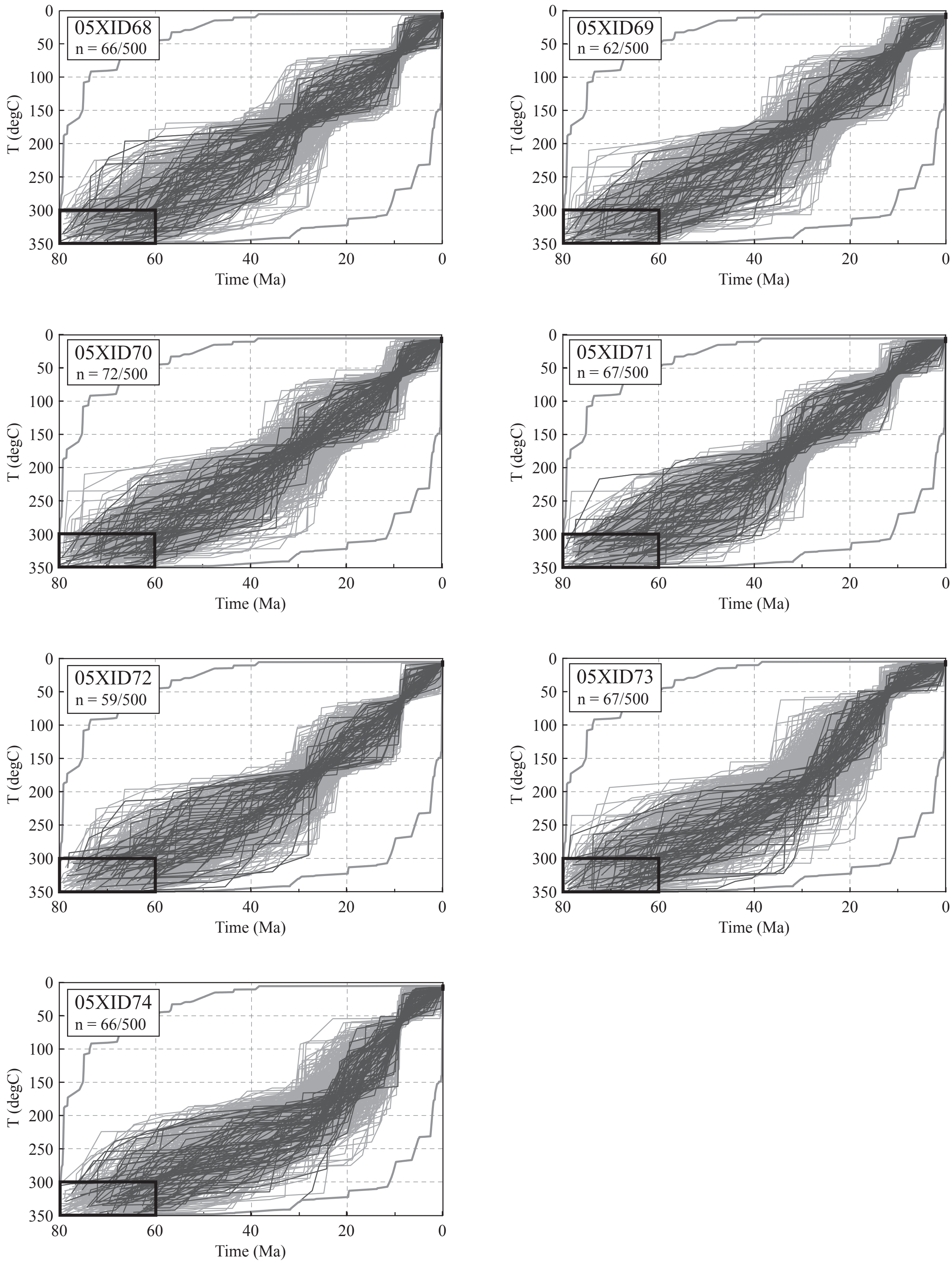
05XID68
n = 66/500
05XID69
n = 62/500
05XID70
n = 72/500
05XID71
n = 67/500
05XID72
n = 59/500
05XID73
n = 67/500
05XID74
n = 66/500
T (degC)
Time (Ma)
0
50
100
150
200
250
300
350
80
60
40
20
0

Figure 4.15: Results of Single Sample inverse modeling of the Tibet samples based on the mean ages. Acceptable fits are shown in light grey, good fit solutions in dark grey.

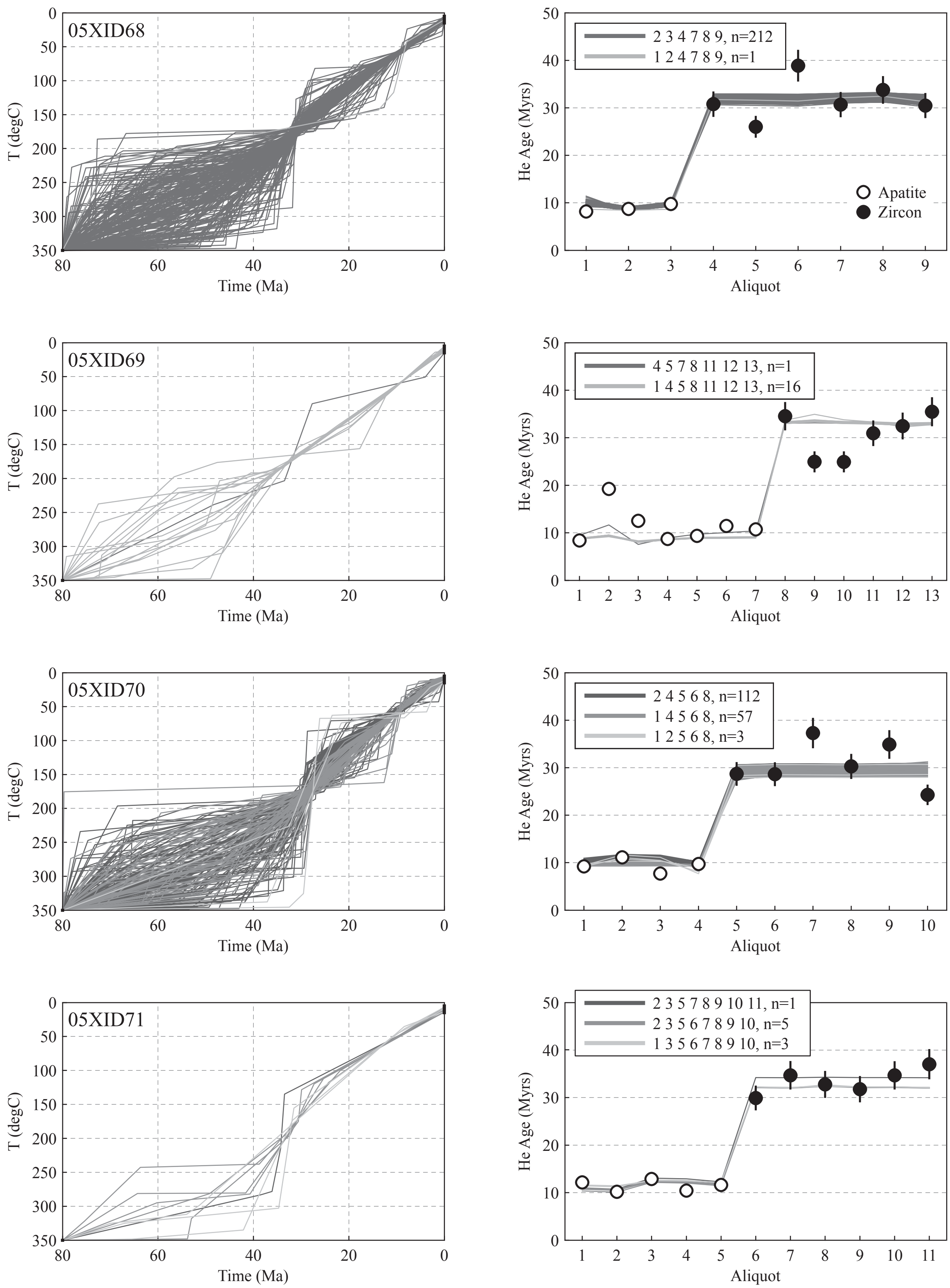
05XID68
T (degC)
Time (Ma)
He Age (Myrs)
Aliquot
2 3 4 7 8 9, n=212
1 2 4 7 8 9, n=1
Apatite
Zircon
05XID69
4 5 7 8 11 12 13, n=1
1 4 5 8 11 12 13, n=16
05XID70
2 4 5 6 8, n=112
1 4 5 6 8, n=57
1 2 5 6 8, n=3
05XID71
2 3 5 7 8 9 10 11, n=1
2 3 5 6 7 8 9 10, n=5
1 3 5 6 7 8 9 10, n=3

Figure 4.16: Acceptable solutions after inverse modeling of the Tibet samples based on individual aliquot ages. Left column shows resulting acceptable t-T paths, right column the model (lines) and sample (circles) ages. Error bars, where visible, indicate 6% (2σ) uncertainty. Aliquot combinations that resulted in fitting thermal histories are highlighted by different shades of grey. White circles correspond to apatite, black circles to zircon aliquots.

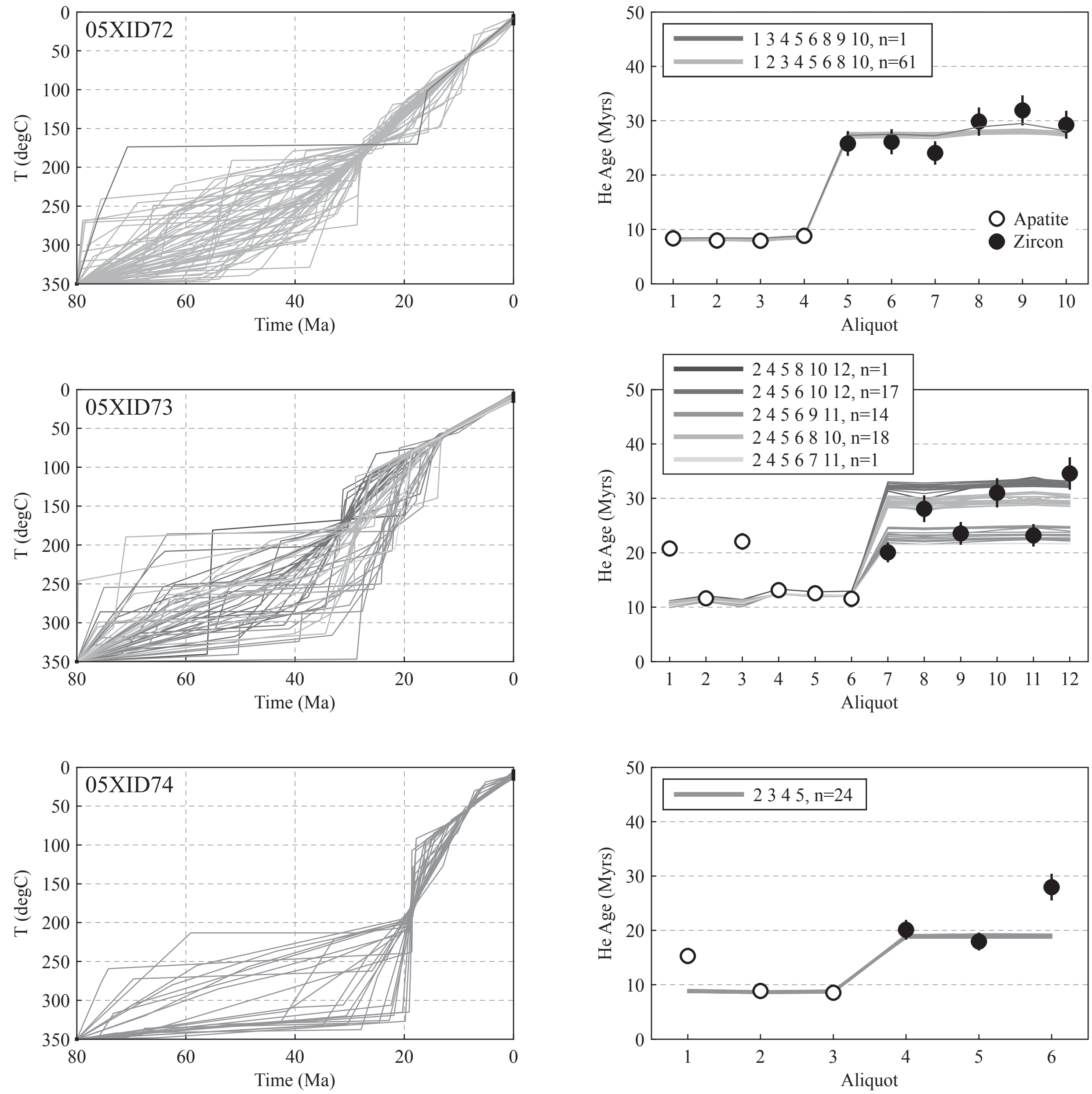
05XID72
T (degC)
Time (Ma)
He Age (Myrs)
Aliquot
1 3 4 5 6 8 9 10, n=1
1 2 3 4 5 6 8 10, n=61
Apatite
Zircon
05XID73
T (degC)
Time (Ma)
He Age (Myrs)
Aliquot
2 4 5 8 10 12, n=1
2 4 5 6 10 12, n=17
2 4 5 6 9 11, n=14
2 4 5 6 8 10, n=18
2 4 5 6 7 11, n=1
05XID74
T (degC)
Time (Ma)
He Age (Myrs)
Aliquot
2 3 4 5, n=24

Figure 4.17: Acceptable solutions after inverse modeling of the Tibet samples based on individual aliquot ages; continued.

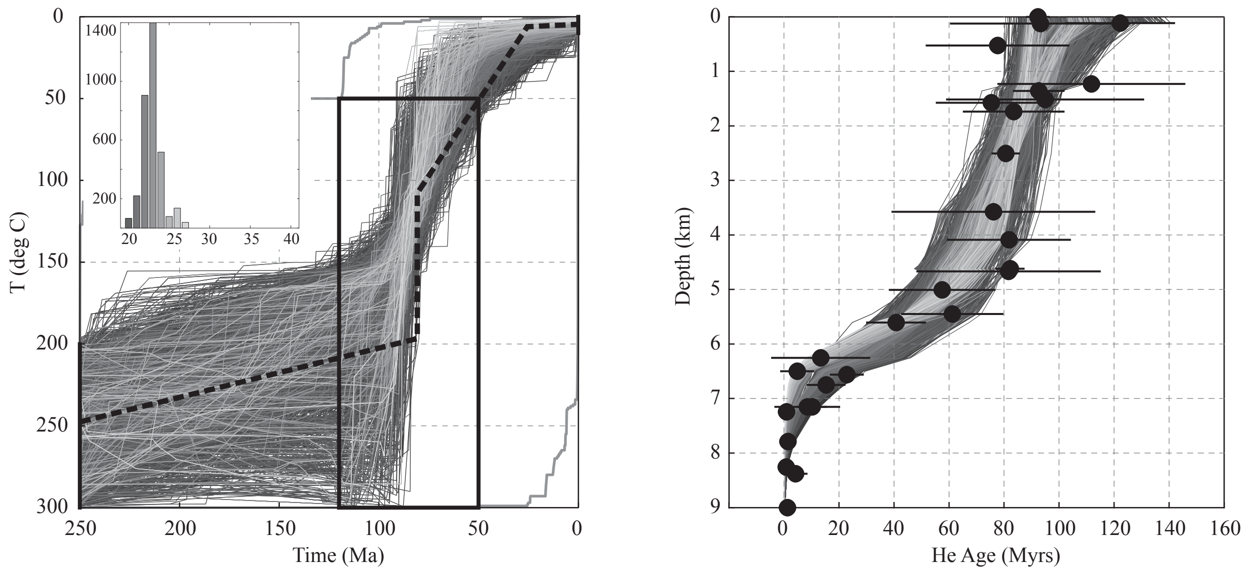

T (deg C)
Time (Ma)
Depth (km)
He Age (Myrs)

Figure 4.18: KTB samples samples modeled with the *Sample Array* module. Left side shows t-T paths yielding acceptable solutions. Black dashed line corresponds to the proposed thermal history from Wagner et al. (1997) and later Stockli and Farley (2004). Right side shows the model ages (lines) and mean of zircon aliquot analysis (black circles). Error bars indicate the 2σ uncertainty based on the standard deviation of the aliquot analysis. Shades of grey depict individual geothermal gradients used as input. Inset shows distribution of number of fits per geothermal gradient.

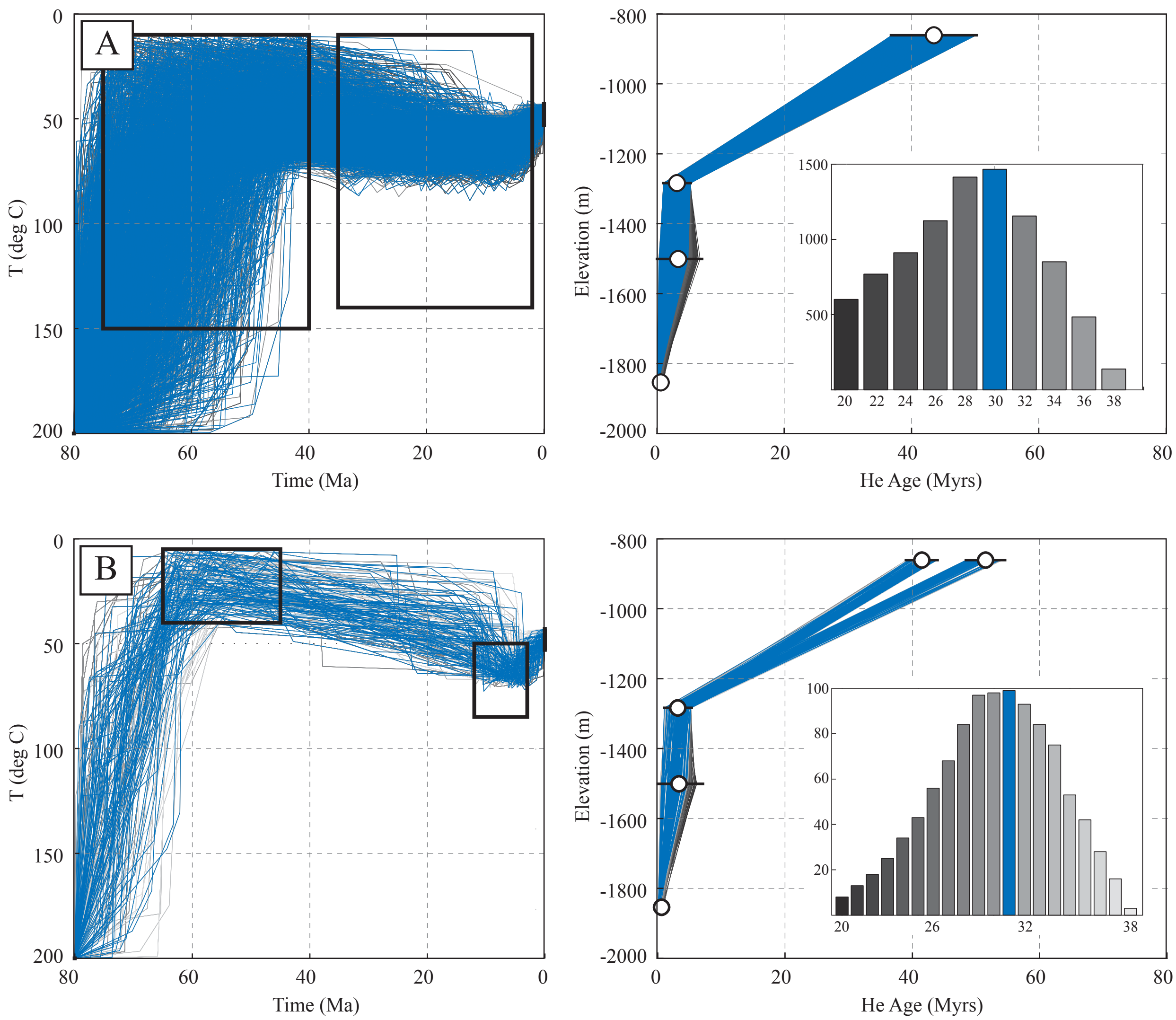
A
B
T (deg C)
Time (Ma)
Elevation (m)
He Age (Myrs)

Figure 4.19: Cajon Pass samples modeled with the *Sample Array* module. A) Acceptable solutions based on initial model run using mean aliquot ages for the entire transect. Best fitting geothermal gradient (30°C/km) is highlighted in blue. B) Final results from modeling oldest and youngest fitting aliquot from sample CJ-12 together with mean ages from the other samples. Inset shows distribution of number of fits per geothermal gradient.

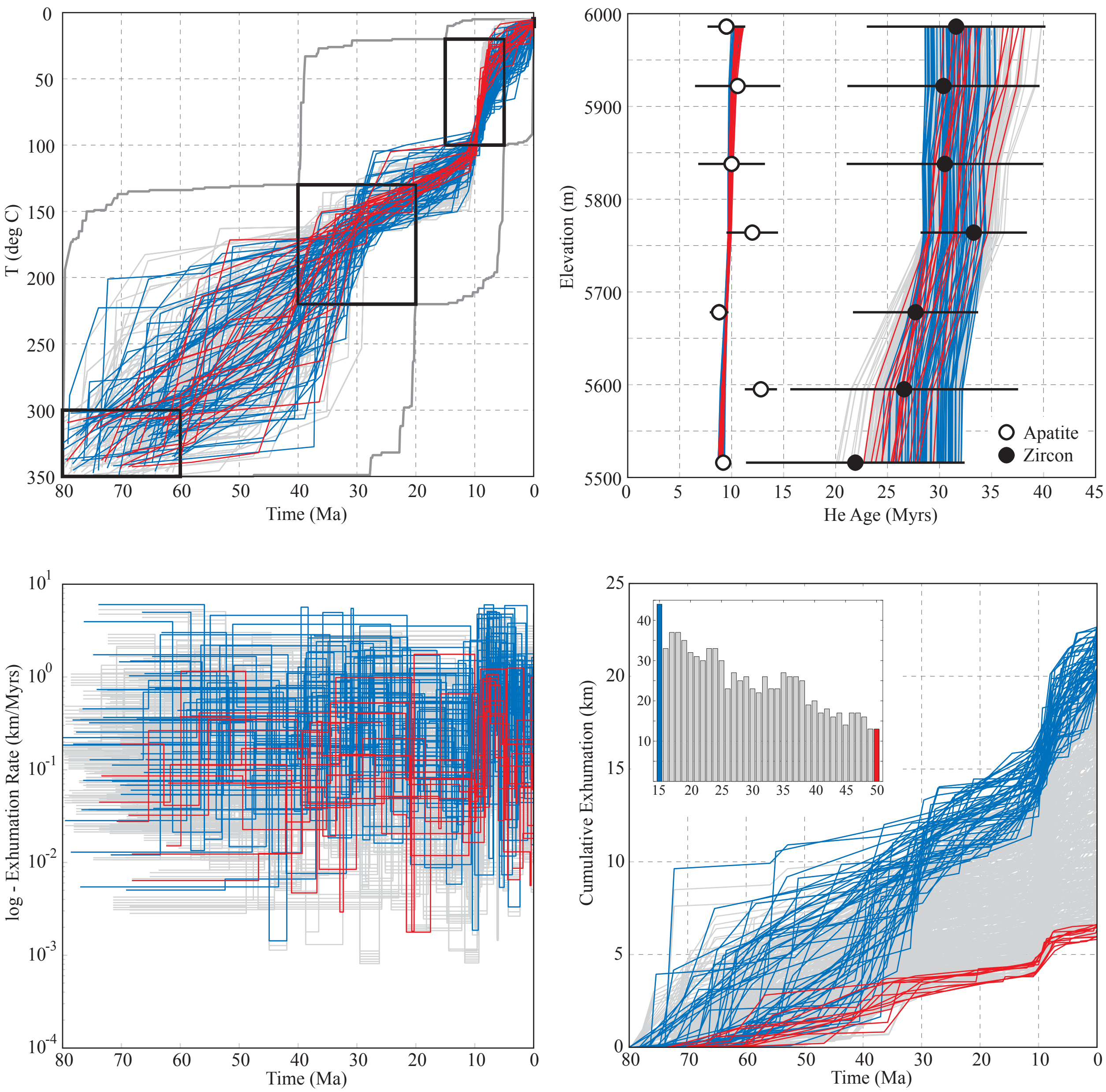
T (deg C)
Time (Ma)
Elevation (m)
He Age (Myrs)
Apatite
Zircon
log - Exhumation Rate (km/Myrs)
Time (Ma)
Cumulative Exhumation (km)
Time (Ma)

Figure 4.20: Vertical transect (VT-D) from Tibet modeled with the *Sample Array* module. Additional to standard plots, the exhumation rate and cumulative exhumation over time are displayed. Blue lines correspond to the lowest geothermal gradient (15°C/km), red lines to the highest geothermal gradient (50°C/km). Inset shows distribution of number of fits per geothermal gradient.

Page intentionally left blank

APPENDIX A

Table A.1: U-Pb (zircon) geochronologic analyses by LA-ICPMS

Analysis	U	206Pb	U/Th	Isotopic ratios				Apparent ages (Ma)						Best age	±
	(ppm)	204Pb		207Pb* 235U	± (%)	206Pb* 238U	± (%)	206Pb* 238U	± (Ma)	207Pb* 235U	± (Ma)	206Pb* 207Pb*	± (Ma)	(Ma)	(Ma)
02PX05-01	762.4	480.3	2.2	0.070	5.190	0.010	1.564	63.3	1.0	68.5	3.4	253.5	113.9	63.3	1.0
02PX05-02	172.9	3691.6	1.0	0.145	6.129	0.010	3.580	66.7	2.4	137.2	7.9	1639.8	92.4	66.7	2.4
02PX05-03	297.3	7838.1	0.9	0.108	5.614	0.010	2.258	65.2	1.5	103.9	5.5	1116.0	102.6	65.2	1.5
02PX05-04	587.9	2352.3	2.0	0.084	5.051	0.010	3.298	63.9	2.1	82.2	4.0	653.4	82.1	63.9	2.1
02PX05-05	314.7	1137.6	1.8	0.103	7.255	0.010	2.666	65.0	1.7	99.6	6.9	1033.7	136.5	65.0	1.7
02PX05-06	507.5	617.6	0.7	0.079	5.289	0.010	2.669	62.3	1.7	77.5	3.9	577.1	99.3	62.3	1.7
02PX05-07	301.6	2140.1	1.9	0.102	8.209	0.010	1.933	65.1	1.3	98.9	7.7	1015.1	161.9	65.1	1.3
02PX05-08	656.8	13518.5	1.3	0.088	6.988	0.010	2.110	63.7	1.3	85.3	5.7	741.5	141.0	63.7	1.3
02PX05-09	234.7	1893.1	1.6	0.108	7.524	0.010	5.114	63.9	3.3	103.9	7.4	1159.6	109.5	63.9	3.3
02PX05-10	668.9	6030.2	1.5	0.082	3.387	0.010	2.011	65.3	1.3	79.7	2.6	536.4	59.7	65.3	1.3
02PX05-11	359.9	1043.6	1.7	0.093	10.226	0.010	2.307	65.9	1.5	90.8	8.9	806.6	209.0	65.9	1.5
02PX05-12	1287.0	4468.3	0.7	0.063	3.506	0.010	1.653	61.6	1.0	62.3	2.1	90.4	73.3	61.6	1.0
02PX05-13	508.4	3578.6	1.1	0.088	5.108	0.010	3.327	66.6	2.2	86.1	4.2	664.9	83.0	66.6	2.2
02PX05-14	192.7	2843.3	0.7	0.123	12.595	0.010	4.521	63.0	2.8	117.9	14.0	1443.7	224.7	63.0	2.8
02PX05-15	1095.1	3258.3	0.7	0.064	5.574	0.010	1.883	62.4	1.2	63.3	3.4	97.8	124.2	62.4	1.2
02PX05-16	603.8	3115.7	1.6	0.081	7.367	0.010	1.966	63.5	1.2	79.1	5.6	581.7	154.4	63.5	1.2
02PX05-17	1007.6	5831.1	2.2	0.076	6.808	0.010	3.252	63.2	2.0	74.2	4.9	444.5	133.1	63.2	2.0
02PX05-18	294.3	2011.6	1.1	0.104	14.194	0.010	2.131	66.6	1.4	100.4	13.6	1002.9	286.2	66.6	1.4
02PX05-19	810.5	2921.1	1.4	0.081	21.802	0.010	3.249	62.3	2.0	79.1	16.6	620.8	470.2	62.3	2.0
02PX05-20	222.9	861.4	1.1	0.126	13.646	0.010	5.288	64.5	3.4	120.9	15.6	1450.2	240.4	64.5	3.4
02PX05-21	753.2	12917.8	2.6	0.084	4.830	0.010	3.300	64.7	2.1	81.8	3.8	613.5	76.2	64.7	2.1
02PX05-22	212.8	1370.4	2.3	0.106	13.003	0.010	2.825	64.8	1.8	102.4	12.7	1098.9	254.9	64.8	1.8
02PX05-23	359.4	1899.3	1.2	0.089	7.173	0.010	1.823	63.8	1.2	86.6	6.0	773.7	146.1	63.8	1.2
02PX05-24	326.6	1968.1	1.2	0.098	6.850	0.010	3.559	65.3	2.3	94.6	6.2	913.2	120.6	65.3	2.3
04GB01-01	207.5	2325.0	1.5	0.044	26.222	0.007	4.490	47.3	2.1	44.0	11.3	-128.6	647.4	47.3	2.1
04GB01-02	146.3	2136.0	1.4	0.032	46.103	0.008	9.170	48.4	4.4	32.0	14.5	-1080.3	1422.7	48.4	4.4
04GB01-03	206.3	2820.0	0.8	0.051	22.707	0.008	5.230	48.9	2.5	50.5	11.2	126.9	525.6	48.9	2.5
04GB01-05	122.9	2142.0	1.6	0.048	######	0.007	3.350	46.7	1.6	47.2	81.0	71.3	0.0	46.7	1.6
04GB01-06	178.1	3672.0	1.0	0.053	44.526	0.007	8.360	46.0	3.8	52.6	22.8	365.7	1032.3	46.0	3.8
04GB01-07	221.5	1710.0	1.7	0.034	29.513	0.007	3.350	46.2	1.5	34.2	9.9	-747.5	836.8	46.2	1.5
04GB01-08	115.3	462.0	1.0	0.158	27.971	0.008	9.840	54.0	5.3	149.1	38.8	2181.2	464.4	54.0	5.3
04GB01-09	183.9	1689.0	1.0	0.069	21.759	0.007	6.630	47.8	3.2	67.6	14.2	840.8	435.8	47.8	3.2

Table A.1: continued

Analysis	U (ppm)	206Pb 204Pb	U/Th	Isotopic ratios 207Pb* 235U	± (%)	206Pb* 238U	± (%)	Apparent ages (Ma) 206Pb* 238U	± (Ma)	207Pb* 235U	± (Ma)	206Pb* 207Pb*	± (Ma)	Best age (Ma)	± (Ma)
04GB01-10	347.7	3000.0	0.9	0.056	11.593	0.008	2.560	49.0	1.3	55.2	6.2	330.7	257.2	49.0	1.3
04GB01-11	295.7	1722.0	1.0	0.056	37.820	0.007	5.280	43.6	2.3	55.7	20.5	610.8	837.3	43.6	2.3
04GB01-12	248.6	1689.0	0.8	0.063	29.779	0.007	5.340	46.2	2.5	62.5	18.1	741.4	632.5	46.2	2.5
04GB01-14	486.0	1632.0	0.6	0.068	18.817	0.007	6.030	48.1	2.9	66.7	12.2	800.8	376.2	48.1	2.9
04GB01-15	118.6	1584.0	1.3	0.053	44.535	0.007	5.290	46.6	2.5	52.6	22.8	334.2	1050.6	46.6	2.5
04GB01-16	205.0	1491.0	1.1	0.043	17.668	0.008	2.610	49.4	1.3	42.6	7.4	-323.7	451.6	49.4	1.3
04GB01-17	208.0	2304.0	1.3	0.048	81.746	0.007	4.300	45.5	1.9	47.5	37.9	149.3	2392.1	45.5	1.9
04GB01-18	337.7	3510.0	2.9	0.046	26.185	0.007	4.520	42.6	1.9	45.2	11.6	185.0	609.5	42.6	1.9
04GB01-19	166.5	1995.0	1.5	0.055	50.415	0.007	3.900	44.1	1.7	54.4	26.7	534.6	1173.5	44.1	1.7
04GB01-20	206.7	594.0	1.1	0.122	12.658	0.009	2.650	55.4	1.5	116.5	13.9	1664.2	230.0	55.4	1.5
04GB01-21	99.8	1140.0	1.7	0.032	65.537	0.007	9.140	44.4	4.0	32.2	20.8	-809.1	2042.2	44.4	4.0
04GB01-22	231.8	939.0	1.9	0.061	34.863	0.007	6.030	46.8	2.8	59.9	20.3	619.3	762.2	46.8	2.8
04GB01-23	259.2	1950.0	2.1	0.036	36.355	0.008	5.880	48.3	2.8	36.2	12.9	-709.0	1024.9	48.3	2.8
04GB01-25	194.0	1359.0	1.3	0.072	31.836	0.007	5.340	46.6	2.5	70.9	21.8	997.8	653.4	46.6	2.5
04GB01-26	215.6	2142.0	1.0	0.064	21.617	0.008	2.900	52.2	1.5	63.3	13.3	503.6	476.4	52.2	1.5
04GB01-27	247.4	1398.0	1.6	0.062	30.602	0.006	8.870	41.0	3.6	61.5	18.3	956.4	611.5	41.0	3.6
04GB01-28	253.2	2133.0	0.8	0.060	26.605	0.007	4.800	48.0	2.3	58.8	15.2	525.2	582.9	48.0	2.3
04GB01-29	336.5	5952.0	0.8	0.038	25.617	0.008	6.610	48.9	3.2	37.9	9.5	-618.3	683.8	48.9	3.2
04GB01-30	212.8	1011.0	0.9	0.076	18.583	0.008	1.810	52.5	0.9	74.3	13.3	845.8	387.8	52.5	0.9
04GB02-01	255.1	2496.0	1.1	0.048	19.892	0.007	4.370	48.1	2.1	48.0	9.3	42.8	467.7	48.1	2.1
04GB02-02	642.3	3414.0	1.6	0.057	16.611	0.007	3.950	48.2	1.9	56.2	9.1	413.1	362.8	48.2	1.9
04GB02-03	274.4	1383.0	1.3	0.047	23.180	0.006	3.200	40.6	1.3	46.5	10.5	364.3	523.8	40.6	1.3
04GB02-04	573.5	1533.0	1.8	0.063	15.948	0.007	1.700	46.1	0.8	61.6	9.5	714.7	338.8	46.1	0.8
04GB02-05	189.2	1311.0	1.5	0.046	35.058	0.007	3.450	44.6	1.5	45.9	15.7	112.0	846.3	44.6	1.5
04GB02-06	223.7	1971.0	0.7	0.032	37.444	0.008	9.040	48.7	4.4	32.4	11.9	-1056.9	1120.2	48.7	4.4
04GB02-07	241.8	1257.0	1.6	0.052	24.520	0.008	3.260	49.7	1.6	51.1	12.2	117.0	580.5	49.7	1.6
04GB02-08	248.9	1383.0	1.1	0.073	11.853	0.008	3.240	51.3	1.7	71.8	8.2	824.3	238.7	51.3	1.7
04GB02-09	201.8	750.0	1.1	0.069	41.569	0.008	8.660	49.1	4.2	67.3	27.1	777.3	891.1	49.1	4.2
04GB02-11	213.6	3387.0	0.9	0.046	35.576	0.007	6.950	45.0	3.1	46.1	16.0	102.9	847.8	45.0	3.1
04GB02-12	293.1	3414.0	1.0	0.048	31.629	0.008	2.790	48.2	1.3	47.3	14.6	-1.6	776.4	48.2	1.3
04GB02-13	322.6	2967.0	1.6	0.033	71.906	0.008	1.890	50.2	0.9	33.0	23.3	-1095.9	2480.0	50.2	0.9
04GB02-14	279.5	2205.0	1.4	0.036	25.144	0.007	6.020	45.5	2.7	35.5	8.8	-601.7	671.9	45.5	2.7

Table A.1: continued

Analysis	U	206Pb	U/Th	Isotopic ratios				Apparent ages (Ma)						Best age	±
	(ppm)	204Pb		207Pb* 235U	± (%)	206Pb* 238U	± (%)	206Pb* 238U	± (Ma)	207Pb* 235U	± (Ma)	206Pb* 207Pb*	± (Ma)	(Ma)	(Ma)
04GB02-15	245.1	1440.0	1.0	0.056	28.160	0.007	5.610	47.3	2.6	55.5	15.2	428.7	626.0	47.3	2.6
04GB02-17	214.4	2109.0	1.2	0.031	42.829	0.006	4.890	41.5	2.0	31.2	13.2	-705.2	1228.9	41.5	2.0
04GB02-20	130.1	1224.0	1.5	0.063	38.918	0.007	4.470	46.9	2.1	61.8	23.4	686.7	855.9	46.9	2.1
04GB02-22	446.0	492.0	0.9	0.230	30.552	0.008	5.620	50.9	2.9	210.4	58.1	2909.0	499.6	50.9	2.9
04GB02-24	238.6	2328.0	1.0	0.052	49.122	0.007	4.490	47.1	2.1	51.7	24.8	270.5	1189.1	47.1	2.1
04GB02-25	389.8	2793.0	1.1	0.054	21.585	0.008	5.370	49.4	2.6	53.2	11.2	229.5	487.5	49.4	2.6
04GB03-01	132.7	1530.0	1.2	0.047	35.906	0.007	5.990	47.0	2.8	47.1	16.5	55.0	868.5	47.0	2.8
04GB03-02	231.8	1746.0	1.4	0.054	13.682	0.008	1.330	50.4	0.7	53.7	7.2	204.5	317.2	50.4	0.7
04GB03-03	177.4	1752.0	1.0	0.041	15.981	0.007	2.980	45.9	1.4	40.9	6.4	-248.6	399.2	45.9	1.4
04GB03-04	404.8	3375.0	1.4	0.047	9.791	0.008	1.410	51.2	0.7	46.6	4.5	-183.3	242.4	51.2	0.7
04GB03-05	576.2	4857.0	1.0	0.050	10.415	0.008	0.910	51.6	0.5	49.9	5.1	-32.2	252.2	51.6	0.5
04GB03-06	317.1	2595.0	1.2	0.051	19.698	0.008	4.620	50.9	2.3	50.2	9.7	16.2	463.7	50.9	2.3
04GB03-07	364.3	3645.0	1.3	0.045	11.304	0.008	1.550	49.2	0.8	44.8	5.0	-181.8	280.3	49.2	0.8
04GB03-08	85.6	762.0	1.1	0.072	55.925	0.008	8.300	51.4	4.3	70.4	38.0	774.1	1264.2	51.4	4.3
04GB03-09	995.6	8418.0	1.2	0.053	5.083	0.008	0.970	50.7	0.5	52.2	2.6	121.0	117.6	50.7	0.5
04GB03-10	356.0	3066.0	0.9	0.054	13.610	0.008	2.100	51.3	1.1	53.0	7.0	132.4	317.4	51.3	1.1
04GB03-11	825.7	10497.0	1.4	0.065	5.267	0.010	3.210	63.7	2.0	63.8	3.3	68.8	99.4	63.7	2.0
04GB03-12	460.1	3465.0	0.6	0.049	7.103	0.008	2.140	50.6	1.1	48.2	3.3	-68.4	165.6	50.6	1.1
04GB03-13	386.6	4134.0	1.3	0.052	8.199	0.009	2.130	55.2	1.2	51.8	4.1	-102.6	194.9	55.2	1.2
04GB03-14	842.4	9342.0	1.7	0.059	2.945	0.009	0.720	60.0	0.4	58.6	1.7	-0.1	68.8	60.0	0.4
04GB03-15	266.4	1872.0	1.2	0.066	23.784	0.008	3.060	52.4	1.6	65.1	15.0	562.5	520.5	52.4	1.6
04GB03-16	565.5	9549.0	1.3	0.051	14.176	0.008	1.930	52.8	1.0	50.6	7.0	-55.2	343.5	52.8	1.0
04GB03-17	281.5	2928.0	1.2	0.050	19.550	0.008	2.360	50.8	1.2	49.7	9.5	-6.5	472.1	50.8	1.2
04GB03-18	411.2	3363.0	1.1	0.046	12.274	0.008	1.350	51.1	0.7	45.2	5.4	-253.9	309.9	51.1	0.7
04GB03-19	589.2	2562.0	0.7	0.060	8.119	0.008	1.730	50.3	0.9	58.9	4.6	423.3	177.3	50.3	0.9
04GB03-20	627.2	6387.0	0.8	0.054	9.582	0.008	0.980	53.7	0.5	53.7	5.0	57.2	227.7	53.7	0.5
04GB03-21	2005.7	3384.0	0.3	0.070	20.767	0.009	1.920	54.6	1.0	68.6	13.8	588.7	453.0	54.6	1.0
04GB03-22	333.6	3201.0	1.3	0.052	13.959	0.008	2.780	52.7	1.5	51.7	7.0	3.9	330.8	52.7	1.5
04GB03-23	312.7	2670.0	1.0	0.064	33.069	0.008	5.490	50.4	2.8	62.9	20.2	570.2	727.6	50.4	2.8
04GB03-24	211.1	1989.0	1.1	0.050	16.933	0.008	4.020	53.3	2.1	49.3	8.2	-138.3	409.5	53.3	2.1
04GB03-25	180.4	1440.0	0.8	0.039	20.562	0.007	3.470	47.7	1.6	38.9	7.8	-473.7	541.1	47.7	1.6
04GB03-26	294.5	2343.0	1.0	0.043	13.382	0.008	1.970	48.9	1.0	43.1	5.7	-268.1	337.3	48.9	1.0

Table A.1: continued

Analysis	U	206Pb	U/Th	Isotopic ratios				Apparent ages (Ma)						Best age	±
	(ppm)	204Pb		207Pb*/235U	± (%)	206Pb*/238U	± (%)	206Pb*/238U	± (Ma)	207Pb*/235U	± (Ma)	206Pb*/207Pb*	± (Ma)	(Ma)	(Ma)
04GB03-27	312.7	2940.0	1.1	0.045	11.660	0.008	2.970	49.6	1.5	44.4	5.1	-226.8	284.7	49.6	1.5
04GB03-28	420.2	3414.0	0.8	0.049	7.832	0.008	2.280	52.2	1.2	48.6	3.7	-127.5	185.3	52.2	1.2
04GB04-01	161.4	17700.0	1.2	0.625	3.420	0.081	2.200	500.1	10.6	493.2	13.4	461.6	58.1	500.1	10.6
04GB04-02	229.9	120765.0	2.0	11.622	6.365	0.450	5.650	2396.9	113.1	2574.4	59.6	2717.3	48.3	2717.3	48.3
04GB04-03	600.7	91068.0	2.6	0.864	2.891	0.103	1.550	629.1	9.3	632.5	13.6	644.6	52.5	629.1	9.3
04GB04-04	136.8	18663.0	2.0	0.669	3.616	0.085	1.750	525.3	8.8	520.1	14.7	497.3	69.7	525.3	8.8
04GB04-05	71.0	41088.0	1.0	8.322	3.924	0.381	1.560	2081.3	27.7	2266.7	35.6	2438.4	61.0	2438.4	61.0
04GB04-06	88.6	9414.0	56.6	0.691	3.516	0.086	2.370	532.8	12.1	533.5	14.6	536.4	56.9	532.8	12.1
04GB04-07	89.2	14556.0	2.2	0.841	5.313	0.098	1.500	599.8	8.6	619.9	24.7	693.8	108.7	599.8	8.6
04GB04-08	250.8	109071.0	2.1	2.643	3.495	0.221	1.450	1289.1	16.9	1312.7	25.8	1351.3	61.4	1351.3	61.4
04GB04-09	310.5	48909.0	1.7	0.753	4.714	0.092	0.830	565.2	4.5	569.8	20.6	588.3	100.7	565.2	4.5
04GB04-10	170.8	120600.0	2.0	8.583	2.780	0.396	0.740	2151.7	13.5	2294.7	25.3	2424.6	45.5	2424.6	45.5
04GB04-11	354.5	127923.0	2.0	1.509	2.826	0.158	1.490	944.6	13.1	934.0	17.3	909.2	49.4	909.2	49.4
04GB04-12	298.0	85023.0	3.3	2.039	2.823	0.186	1.310	1098.0	13.2	1128.7	19.2	1188.2	49.4	1188.2	49.4
04GB04-13	112.6	19458.0	1.0	1.208	2.224	0.133	1.270	802.4	9.6	804.3	12.4	809.7	38.2	802.4	9.6
04GB04-14	523.8	68214.0	2.1	0.987	2.426	0.114	1.000	694.1	6.6	697.0	12.2	706.4	47.0	694.1	6.6
04GB04-15	732.5	99408.0	1.9	1.618	1.567	0.162	0.640	968.6	5.8	977.2	9.8	996.6	29.1	996.6	29.1
04GB04-16	270.0	58557.0	0.8	0.862	2.790	0.101	1.500	619.2	8.9	631.1	13.1	673.8	50.3	619.2	8.9
04GB04-17	128.8	79755.0	3.2	22.226	2.266	0.603	0.500	3043.4	12.1	3193.7	22.0	3289.4	34.7	3289.4	34.7
04GB04-18	92.1	58674.0	1.9	20.542	3.151	0.549	0.900	2820.8	20.6	3117.2	30.5	3314.2	47.3	3314.2	47.3
04GB04-19	296.7	85956.0	0.9	1.954	2.797	0.186	1.620	1101.3	16.4	1099.7	18.8	1096.4	45.6	1096.4	45.6
04GB04-21	144.9	70311.0	1.7	3.922	2.874	0.285	1.580	1618.4	22.6	1618.3	23.3	1618.2	44.7	1618.2	44.7
04GB04-22	282.9	57906.0	1.7	1.507	4.068	0.150	2.800	903.5	23.6	933.1	24.8	1003.7	59.9	1003.7	59.9
04GB04-23	122.8	25527.0	0.8	0.724	4.206	0.091	1.280	559.2	6.9	552.9	17.9	527.2	87.9	559.2	6.9
04GB04-25	304.1	61797.0	5.4	1.928	2.102	0.183	1.540	1085.8	15.4	1090.7	14.1	1100.6	28.6	1100.6	28.6
04GB04-26	243.1	47856.0	3.9	1.605	2.005	0.161	0.860	961.8	7.7	972.3	12.5	996.2	36.8	996.2	36.8
04GB04-27	299.7	46440.0	0.9	1.873	1.860	0.180	1.420	1067.4	14.0	1071.6	12.3	1080.3	24.1	1080.3	24.1
04GB04-28	208.8	35679.0	2.2	1.141	1.872	0.116	1.130	708.7	7.6	773.1	10.1	963.9	30.5	708.7	7.6
04GB04-29	231.5	33306.0	2.6	0.831	1.699	0.100	0.770	616.2	4.5	614.2	7.8	607.0	32.8	616.2	4.5
04GB04-30	187.7	21285.0	3.2	0.827	1.909	0.099	0.500	609.8	2.9	611.8	8.8	619.4	39.8	609.8	2.9
04GB04-31	293.3	51513.0	2.9	2.778	3.620	0.222	1.730	1292.5	20.3	1349.7	27.0	1441.4	60.6	1441.4	60.6
04GB04-32	56.7	20751.0	0.6	10.265	2.322	0.460	0.610	2439.5	12.4	2459.0	21.5	2475.1	37.8	2475.1	37.8

Table A.1: continued

Analysis	U	206Pb	U/Th	Isotopic ratios				Apparent ages (Ma)						Best age	±
	(ppm)	204Pb		207Pb* 235U	± (%)	206Pb* 238U	± (%)	206Pb* 238U	± (Ma)	207Pb* 235U	± (Ma)	206Pb* 207Pb*	± (Ma)	(Ma)	(Ma)
04GB04-33	308.8	54324.0	14.9	1.416	2.186	0.149	2.070	895.5	17.3	895.7	13.0	896.1	14.5	896.1	14.5
04GB04-34	516.7	65274.0	9.6	0.766	1.582	0.093	0.500	573.3	2.7	577.3	7.0	593.1	32.5	573.3	2.7
04GB04-35	289.0	56808.0	1.9	1.246	1.812	0.135	0.500	817.0	3.8	821.8	10.2	834.9	36.3	817.0	3.8
04GB04-36	280.8	47535.0	3.9	1.528	2.698	0.158	0.850	943.0	7.5	941.8	16.6	938.9	52.5	938.9	52.5
04GB04-37	62.1	14817.0	1.5	2.093	2.109	0.196	0.650	1152.5	6.9	1146.4	14.5	1134.9	39.9	1134.9	39.9
04GB04-38	143.2	30099.0	2.2	2.889	1.668	0.202	0.840	1186.4	9.1	1379.1	12.6	1691.3	26.6	1691.3	26.6
04GB04-39	138.7	10275.0	0.2	0.871	23.823	0.092	1.610	569.8	8.8	635.9	113.0	878.4	498.6	569.8	8.8
04GB04-40	466.0	161601.0	2.8	9.458	1.750	0.430	0.850	2304.0	16.5	2383.5	16.1	2452.2	25.9	2452.2	25.9
04GB04-41	599.5	59409.0	1.3	0.805	2.028	0.097	1.540	599.6	8.8	599.5	9.2	599.1	28.6	599.6	8.8
04GB04-42	363.0	47007.0	4.0	1.009	2.613	0.113	1.680	689.2	11.0	708.1	13.3	768.7	42.2	689.2	11.0
04GB04-43	103.0	6294.0	232.2	0.702	3.668	0.085	1.070	527.4	5.4	540.1	15.4	594.3	76.0	527.4	5.4
04GB04-44	135.0	41952.0	1.3	3.030	2.250	0.236	1.630	1365.9	20.1	1415.3	17.2	1490.4	29.4	1490.4	29.4
04GB04-45	395.8	69738.0	5.0	1.604	2.190	0.160	1.380	956.3	12.3	971.8	13.7	1007.0	34.5	1007.0	34.5
04QT02-01	105.9	3060.0	0.9	0.106	22.187	0.017	3.590	109.0	3.9	102.4	21.6	-50.8	538.3	109.0	3.9
04QT02-02	210.7	3432.0	1.0	0.115	17.660	0.017	3.390	110.6	3.7	110.2	18.4	102.6	412.4	110.6	3.7
04QT02-03	232.0	8376.0	1.5	0.139	11.102	0.019	2.830	121.5	3.4	132.4	13.8	333.1	244.0	121.5	3.4
04QT02-04	5984.8	28392.0	0.4	0.130	3.660	0.019	2.470	122.1	3.0	124.2	4.3	166.0	63.1	122.1	3.0
04QT02-05	216.6	2517.0	1.3	0.112	8.178	0.018	1.650	115.1	1.9	107.5	8.3	-57.3	195.4	115.1	1.9
04QT02-06	352.8	26145.0	3.6	0.697	2.996	0.078	2.340	484.3	10.9	537.1	12.5	768.3	39.4	484.3	10.9
04QT02-08	290.2	7242.0	1.7	0.120	9.501	0.019	3.710	122.1	4.5	115.0	10.3	-29.6	212.3	122.1	4.5
04QT02-09	214.9	4230.0	1.2	0.124	13.820	0.018	4.050	117.1	4.7	118.4	15.4	143.8	311.2	117.1	4.7
04QT02-10	126.9	873.0	0.8	0.182	28.184	0.019	6.820	123.9	8.4	169.9	44.1	870.0	577.0	123.9	8.4
04QT02-11	113.3	4296.0	0.9	0.100	30.734	0.017	6.090	111.1	6.7	97.2	28.5	-231.9	774.3	111.1	6.7
04QT02-12	173.5	5418.0	1.2	0.109	14.011	0.017	2.590	105.7	2.7	105.2	14.0	95.8	327.3	105.7	2.7
04QT02-13	184.7	2742.0	1.1	0.103	24.208	0.017	7.600	106.4	8.0	99.2	22.9	-70.5	567.9	106.4	8.0
04QT02-14	329.7	6978.0	1.0	0.130	11.383	0.019	1.670	120.2	2.0	123.9	13.3	195.9	262.4	120.2	2.0
04QT02-15	705.0	12891.0	1.1	0.122	6.458	0.019	1.090	123.1	1.3	116.8	7.1	-10.6	153.9	123.1	1.3
04QT02-16	128.6	3465.0	1.1	0.143	22.238	0.018	6.790	116.7	7.9	135.6	28.2	480.2	472.7	116.7	7.9
04QT02-18	164.6	4266.0	1.3	0.115	23.477	0.019	1.950	118.4	2.3	110.4	24.6	-58.3	576.9	118.4	2.3
04QT02-19	138.9	4416.0	1.2	0.114	12.301	0.018	3.190	112.9	3.6	109.6	12.8	37.1	285.2	112.9	3.6
04QT02-20	198.3	13266.0	2.9	1.395	7.334	0.076	6.060	472.5	27.6	886.9	43.4	2138.6	72.3	472.5	27.6
04QT02-21	106.0	3720.0	1.1	0.103	44.332	0.017	5.150	109.0	5.6	99.6	42.1	-118.9	1134.8	109.0	5.6

Table A.1: continued

Analysis	U	206Pb	U/Th	Isotopic ratios				Apparent ages (Ma)						Best age	±
	(ppm)	204Pb		207Pb* 235U	± (%)	206Pb* 238U	± (%)	206Pb* 238U	± (Ma)	207Pb* 235U	± (Ma)	206Pb* 207Pb*	± (Ma)	(Ma)	(Ma)
04QT02-22	245.4	5145.0	1.0	0.110	14.200	0.018	3.650	117.8	4.3	105.8	14.3	-158.5	342.4	117.8	4.3
04QT02-23	194.1	4794.0	0.9	0.109	20.771	0.018	5.340	112.5	6.0	105.1	20.7	-60.3	493.6	112.5	6.0
04QT02-24	344.1	6861.0	1.5	0.124	11.484	0.018	1.480	112.2	1.6	118.6	12.9	247.4	262.9	112.2	1.6
04QT02-26	218.0	3561.0	1.3	0.106	18.924	0.018	2.060	112.9	2.3	101.9	18.4	-147.5	470.0	112.9	2.3
04QT02-27	216.9	657.0	1.1	0.279	41.814	0.018	4.780	115.4	5.5	250.1	93.0	1834.6	790.0	115.4	5.5
04QT02-28	179.8	4140.0	1.4	0.127	21.002	0.020	5.730	126.6	7.2	121.6	24.1	24.3	489.0	126.6	7.2
04QT02-29	147.2	2613.0	1.3	0.132	37.013	0.019	4.890	118.7	5.7	125.9	43.9	265.2	868.6	118.7	5.7
04QT02-30	440.0	8397.0	1.4	0.115	6.600	0.018	1.750	115.6	2.0	110.4	6.9	-0.6	153.5	115.6	2.0
04QT02-31	275.9	4269.0	1.1	0.123	12.049	0.019	3.840	120.0	4.6	117.8	13.4	72.7	272.3	120.0	4.6
04QT02-32	152.4	5655.0	1.4	0.102	21.485	0.019	2.900	119.7	3.4	98.3	20.1	-394.8	559.8	119.7	3.4
04QT02-33	162.0	3027.0	1.3	0.122	17.551	0.018	0.880	118.0	1.0	116.7	19.4	90.3	418.1	118.0	1.0
04QT03-01	300.1	7317.0	1.1	0.112	9.964	0.018	1.140	111.9	1.3	107.6	10.2	12.3	238.5	111.9	1.3
04QT03-03	604.8	13659.0	0.9	0.115	3.947	0.018	0.740	113.0	0.8	110.4	4.1	54.2	92.5	113.0	0.8
04QT03-04	683.5	324.0	1.3	0.520	16.185	0.019	1.710	123.7	2.1	425.5	56.3	2783.1	265.6	123.7	2.1
04QT03-05	632.4	13878.0	1.1	0.121	3.915	0.018	1.320	114.7	1.5	116.1	4.3	144.6	86.5	114.7	1.5
04QT03-06	171.4	4008.0	1.7	0.107	12.404	0.018	1.180	115.4	1.3	102.8	12.1	-181.6	309.2	115.4	1.3
04QT03-07	481.6	12210.0	1.7	0.129	3.149	0.019	0.500	122.0	0.6	123.1	3.6	143.8	73.0	122.0	0.6
04QT03-08	993.1	25392.0	1.1	0.118	4.399	0.018	0.960	112.1	1.1	113.2	4.7	136.5	100.9	112.1	1.1
04QT03-09	203.4	1125.0	1.6	0.183	9.479	0.019	2.290	118.6	2.7	171.0	14.9	975.8	187.9	118.6	2.7
04QT03-10	842.1	9135.0	0.9	0.128	3.896	0.018	0.810	116.6	0.9	122.2	4.5	232.9	88.0	116.6	0.9
04QT03-11	1011.7	24987.0	0.9	0.122	2.139	0.019	0.830	118.5	1.0	116.5	2.4	74.8	46.8	118.5	1.0
04QT03-12	2964.6	2793.0	1.5	0.184	19.228	0.019	0.500	124.0	0.6	171.4	30.3	888.2	400.7	124.0	0.6
04QT03-13	150.0	7200.0	2.1	0.102	24.076	0.017	4.420	110.0	4.8	98.2	22.5	-180.3	597.7	110.0	4.8
04QT03-14	516.9	11286.0	1.2	0.130	11.689	0.018	1.000	116.3	1.2	124.2	13.7	278.4	267.4	116.3	1.2
04QT03-15	1834.6	28851.0	0.5	0.127	3.264	0.019	0.520	120.1	0.6	121.2	3.7	142.2	75.7	120.1	0.6
04QT03-16	1246.6	2214.0	0.5	0.186	21.420	0.019	1.770	124.4	2.2	173.3	34.1	906.6	444.6	124.4	2.2
04QT03-17	1293.7	23037.0	0.8	0.123	2.132	0.018	1.150	116.5	1.3	117.8	2.4	144.2	42.1	116.5	1.3
04QT03-18	4175.4	7368.0	1.9	0.155	7.659	0.020	1.660	129.0	2.1	146.4	10.4	439.4	166.6	129.0	2.1
04QT03-19	517.3	10404.0	0.9	0.122	7.456	0.019	1.800	119.4	2.1	116.6	8.2	61.4	172.6	119.4	2.1
04QT03-20	307.6	6528.0	1.1	0.160	18.066	0.019	3.280	120.7	3.9	150.7	25.3	653.3	384.0	120.7	3.9
04QT03-21	1894.1	24078.0	0.4	0.132	1.635	0.019	1.180	123.9	1.4	125.6	1.9	157.0	26.5	123.9	1.4
04QT03-22	3286.0	19059.0	2.8	0.131	4.568	0.019	1.120	118.9	1.3	125.1	5.4	244.5	102.0	118.9	1.3

Table A.1: continued

Analysis	U	206Pb	U/Th	Isotopic ratios				Apparent ages (Ma)						Best age	±
	(ppm)	204Pb		207Pb* 235U	± (%)	206Pb* 238U	± (%)	206Pb* 238U	± (Ma)	207Pb* 235U	± (Ma)	206Pb* 207Pb*	± (Ma)	(Ma)	(Ma)
04QT03-23	526.5	1392.0	0.5	0.265	49.389	0.020	2.050	127.9	2.6	238.9	105.5	1547.6	993.6	127.9	2.6
04QT03-24	1266.0	11340.0	0.9	0.125	4.604	0.018	1.970	114.7	2.2	119.5	5.2	216.6	96.4	114.7	2.2
04QT03-25	482.8	2415.0	1.1	0.231	49.895	0.017	4.760	110.8	5.2	211.3	95.4	1563.1	999.2	110.8	5.2
04QT03-26	141.0	3399.0	1.5	0.102	19.337	0.018	2.790	113.0	3.1	98.9	18.2	-228.6	485.8	113.0	3.1
04QT03-27	483.8	12087.0	1.0	0.128	4.963	0.019	1.310	119.4	1.6	122.6	5.7	184.0	111.6	119.4	1.6
04QT03-28	528.7	9306.0	1.1	0.125	5.074	0.019	1.050	120.8	1.3	119.2	5.7	87.3	117.8	120.8	1.3
04QT03-29	727.8	22290.0	0.9	0.123	3.478	0.019	1.350	120.3	1.6	117.8	3.9	68.2	76.3	120.3	1.6
04QT03-30	2435.0	5499.0	1.7	0.143	4.106	0.019	1.440	120.1	1.7	136.0	5.2	423.9	85.8	120.1	1.7
04XI03-01	1206.0	11031.0	1.7	0.117	3.858	0.017	0.590	111.4	0.7	112.7	4.1	140.6	89.5	111.4	0.7
04XI03-02	869.4	8706.0	2.9	0.115	4.149	0.017	2.090	111.1	2.3	110.3	4.3	93.6	84.9	111.1	2.3
04XI03-03	854.3	864.0	1.3	0.244	24.221	0.018	3.600	113.9	4.1	221.3	48.2	1607.3	453.2	113.9	4.1
04XI03-04	2104.6	25065.0	1.0	0.116	2.610	0.017	1.140	109.9	1.2	111.4	2.8	143.9	55.1	109.9	1.2
04XI03-05	763.2	3192.0	1.6	0.136	7.809	0.018	1.400	116.6	1.6	129.8	9.5	378.8	173.0	116.6	1.6
04XI03-06	862.0	10290.0	1.3	0.111	8.915	0.017	4.390	108.6	4.7	106.8	9.0	67.0	184.9	108.6	4.7
04XI03-07	1374.0	17745.0	1.4	0.118	2.939	0.018	0.500	113.2	0.6	113.7	3.2	123.3	68.3	113.2	0.6
04XI03-08	1479.2	14226.0	1.6	0.118	2.556	0.018	1.720	112.6	1.9	112.9	2.7	119.9	44.5	112.6	1.9
04XI03-09	1463.9	81399.0	1.2	2.566	1.575	0.194	0.660	1141.4	6.9	1290.9	11.5	1549.0	26.9	1549.0	26.9
04XI03-11	1124.9	18594.0	1.6	0.122	2.316	0.018	0.630	114.1	0.7	117.0	2.6	175.8	52.0	114.1	0.7
04XI03-12	889.9	10680.0	1.6	0.119	9.006	0.018	0.870	112.8	1.0	113.9	9.7	137.4	210.9	112.8	1.0
04XI03-13	1207.6	13959.0	1.3	0.111	4.737	0.017	1.460	110.1	1.6	106.9	4.8	36.3	107.9	110.1	1.6
04XI03-14	139.8	1980.0	1.7	0.123	19.596	0.017	3.610	110.3	3.9	117.4	21.7	264.3	445.7	110.3	3.9
04XI03-15	951.7	12207.0	1.6	0.118	5.934	0.018	1.440	112.6	1.6	113.2	6.4	126.2	135.6	112.6	1.6
04XI03-16	1009.0	12189.0	1.3	0.120	3.610	0.018	0.910	116.0	1.0	114.7	3.9	87.3	82.9	116.0	1.0
04XI03-17	1165.6	12801.0	1.2	0.123	2.415	0.019	1.020	119.3	1.2	117.6	2.7	82.8	51.9	119.3	1.2
04XI03-18	1010.0	8046.0	1.7	0.127	4.846	0.018	2.130	113.7	2.4	121.1	5.5	268.3	99.9	113.7	2.4
04XI03-19	997.2	8976.0	1.2	0.126	5.480	0.018	0.600	115.6	0.7	120.3	6.2	215.3	126.2	115.6	0.7
04XI03-20	158.8	2349.0	1.2	0.110	23.374	0.016	8.880	105.5	9.3	105.9	23.5	114.6	515.3	105.5	9.3
04XI03-21	1539.2	14991.0	1.0	0.120	2.479	0.017	1.190	111.4	1.3	115.4	2.7	200.7	50.5	111.4	1.3
04XI03-22	662.6	1392.0	2.0	0.179	5.981	0.018	0.500	115.3	0.6	167.5	9.2	988.4	121.4	115.3	0.6
04XI03-23	1054.3	12939.0	1.4	0.115	4.337	0.018	0.500	114.2	0.6	110.8	4.6	37.0	103.1	114.2	0.6
04XI03-24	997.4	12879.0	1.1	0.113	5.668	0.017	1.600	110.6	1.8	108.4	5.8	60.7	129.7	110.6	1.8
04XI03-25	1075.8	15432.0	1.3	0.121	3.536	0.018	1.880	112.0	2.1	115.7	3.9	192.9	69.7	112.0	2.1

Table A.1: continued

Analysis	U	206Pb	U/Th	Isotopic ratios				Apparent ages (Ma)						Best age	±
	(ppm)	204Pb		207Pb* 235U	± (%)	206Pb* 238U	± (%)	206Pb* 238U	± (Ma)	207Pb* 235U	± (Ma)	206Pb* 207Pb*	± (Ma)	(Ma)	(Ma)
04XI03-26	1154.0	8751.0	1.3	0.115	2.988	0.017	1.220	106.8	1.3	110.2	3.1	182.5	63.6	106.8	1.3
04XI03-27	917.3	12537.0	1.3	0.113	4.597	0.017	2.000	111.2	2.2	108.9	4.7	59.7	98.7	111.2	2.2
04XI03-28	989.3	10290.0	1.2	0.115	4.709	0.017	0.500	111.5	0.6	110.3	4.9	83.1	111.2	111.5	0.6
04XI18-01	93.6	2875.2	0.9	0.333	8.259	0.021	5.024	134.4	6.7	292.0	21.0	1875.9	118.3	134.4	6.7
04XI18-02	107.1	3680.9	1.2	0.324	7.187	0.021	3.570	133.0	4.7	285.0	17.9	1843.6	113.0	133.0	4.7
04XI18-04	82.5	2568.4	1.1	0.334	8.785	0.021	4.748	131.9	6.2	292.8	22.3	1914.9	132.8	131.9	6.2
04XI18-05	188.9	7658.5	1.1	0.216	3.937	0.021	2.176	132.9	2.9	198.8	7.1	1075.8	65.9	132.9	2.9
04XI18-06	400.3	8559.7	1.7	0.194	5.560	0.023	3.494	146.3	5.1	179.8	9.2	645.9	93.0	146.3	5.1
04XI18-07	156.1	1731.3	1.8	0.273	7.068	0.021	4.026	131.2	5.2	245.0	15.4	1552.9	109.2	131.2	5.2
04XI18-08	37.1	1499.4	1.3	0.437	16.549	0.021	8.905	136.8	12.1	368.1	51.1	2320.8	240.4	136.8	12.1
04XI18-09	960.6	6430.0	1.2	0.140	5.683	0.020	1.549	126.7	1.9	132.8	7.1	243.5	126.0	126.7	1.9
04XI18-10	135.2	3073.0	1.1	0.237	3.935	0.020	2.598	130.4	3.4	215.8	7.6	1293.3	57.5	130.4	3.4
04XI18-11	221.4	4800.7	1.5	0.195	4.968	0.020	1.466	126.9	1.8	180.9	8.2	961.4	97.0	126.9	1.8
04XI18-12	326.1	1050.1	1.0	0.124	24.804	0.020	5.861	127.6	7.4	118.4	27.7	-63.0	595.3	127.6	7.4
04XI18-13	96.9	1886.6	1.0	0.272	8.228	0.020	4.181	127.4	5.3	244.2	17.9	1601.7	132.4	127.4	5.3
04XI18-14	241.6	11314.4	1.5	0.191	5.085	0.020	2.299	128.7	2.9	177.1	8.3	883.7	93.8	128.7	2.9
04XI18-15	69.6	4036.7	1.4	0.360	16.760	0.022	9.796	142.7	13.8	312.4	45.1	1906.7	245.4	142.7	13.8
04XI18-16	125.9	795.4	0.9	0.211	18.859	0.020	5.069	127.0	6.4	194.7	33.4	1123.1	365.1	127.0	6.4
04XI18-17	157.8	3210.6	1.1	0.218	7.807	0.021	1.577	131.7	2.1	199.8	14.2	1105.9	153.0	131.7	2.1
04XI18-18	119.7	733.0	1.2	0.203	20.367	0.020	6.773	128.3	8.6	188.1	35.0	1026.1	392.0	128.3	8.6
04XI18-19	240.2	6679.4	1.2	0.197	18.578	0.020	5.833	125.0	7.2	182.3	31.0	1009.0	360.4	125.0	7.2
04XI18-20	265.6	8016.3	0.6	0.166	3.290	0.020	2.147	126.9	2.7	156.0	4.8	623.0	53.8	126.9	2.7
04XI18-21	107.7	1948.4	1.2	0.242	9.397	0.021	2.465	130.9	3.2	220.5	18.6	1332.9	175.8	130.9	3.2
04XI18-22	634.6	8718.4	1.0	0.151	7.052	0.020	5.047	130.7	6.5	142.6	9.4	345.5	111.5	130.7	6.5
04XI18-23	128.3	968.2	1.3	0.196	17.033	0.020	4.019	125.6	5.0	182.0	28.4	996.7	338.5	125.6	5.0
04XI18-24	144.6	3292.3	1.2	0.235	7.182	0.020	4.115	126.1	5.1	214.4	13.9	1345.2	113.8	126.1	5.1
04XI18-25	296.4	463.0	1.4	0.092	46.850	0.019	4.348	123.8	5.3	89.3	40.1	-758.1	1374.1	123.8	5.3
04XI19-01	180.2	1344.6	0.5	0.124	9.969	0.010	6.051	64.8	3.9	118.9	11.2	1409.1	151.9	64.8	3.9
04XI19-02	126.9	837.5	1.1	0.194	22.316	0.010	9.164	67.0	6.1	180.4	36.9	2163.1	358.8	67.0	6.1
04XI19-03	198.5	1518.6	0.5	0.134	12.083	0.010	3.735	65.0	2.4	128.0	14.5	1550.6	216.5	65.0	2.4
04XI19-04	239.1	1280.4	0.6	0.113	10.178	0.010	2.984	64.5	1.9	108.3	10.5	1225.1	191.6	64.5	1.9

Table A.1: continued

Analysis	U	206Pb	U/Th	Isotopic ratios				Apparent ages (Ma)						Best age	±
	(ppm)	204Pb		207Pb*/235U	± (%)	206Pb*/238U	± (%)	206Pb*/238U	± (Ma)	207Pb*/235U	± (Ma)	206Pb*/207Pb*	± (Ma)	(Ma)	(Ma)
04XI19-05	5503.8	15593.7	1.0	0.072	2.360	0.011	1.210	69.9	0.8	70.5	1.6	89.9	48.0	69.9	0.8
04XI19-06	3888.3	8222.6	1.7	0.069	1.814	0.010	1.123	65.9	0.7	67.3	1.2	118.1	33.6	65.9	0.7
04XI19-07	198.1	1630.1	0.8	0.135	9.381	0.011	3.067	68.7	2.1	128.4	11.3	1452.0	169.0	68.7	2.1
04XI19-08	2499.1	1529.7	1.6	0.063	2.814	0.010	1.283	62.8	0.8	61.9	1.7	26.8	60.1	62.8	0.8
04XI19-09	257.3	1506.0	0.6	0.109	9.768	0.010	3.332	64.0	2.1	104.8	9.7	1173.3	182.1	64.0	2.1
04XI19-10	346.2	2676.0	0.6	0.097	7.301	0.010	2.614	63.2	1.6	94.1	6.6	970.3	139.2	63.2	1.6
04XI19-11	478.3	3930.4	0.6	0.089	6.275	0.010	2.520	63.8	1.6	86.7	5.2	774.4	121.0	63.8	1.6
04XI19-13	196.4	1354.1	0.7	0.106	14.267	0.010	4.608	64.8	3.0	102.7	13.9	1106.8	271.0	64.8	3.0
04XI19-14	157.4	752.1	0.9	0.151	10.266	0.010	5.968	67.3	4.0	143.2	13.7	1709.7	154.0	67.3	4.0
04XI19-15	157.1	2546.2	0.5	0.133	16.929	0.010	7.133	66.1	4.7	126.9	20.2	1501.7	291.9	66.1	4.7
04XI19-16	203.7	109.7	0.7	0.009	98.780	0.009	20.104	57.6	11.5	8.6	8.5	0.0	1449.5	57.6	11.5
04XI19-17	4017.1	35143.5	1.8	0.067	1.436	0.010	1.000	63.1	0.6	65.5	0.9	153.4	24.1	63.1	0.6
04XI19-18	152.6	846.0	0.8	0.128	15.098	0.010	5.893	64.1	3.8	122.7	17.5	1492.7	264.4	64.1	3.8
04XI19-19	6086.9	33228.6	1.8	0.067	1.496	0.010	1.000	64.3	0.6	65.7	1.0	115.4	26.2	64.3	0.6
04XI19-20	338.0	5821.3	0.8	0.103	8.991	0.010	3.786	63.8	2.4	99.6	8.5	1070.7	164.1	63.8	2.4
04XI19-21	221.5	1860.7	0.7	0.126	8.523	0.010	4.042	65.4	2.6	120.9	9.7	1424.2	143.5	65.4	2.6
04XI19-22	328.7	2317.6	1.1	0.103	3.821	0.010	1.750	63.8	1.1	99.9	3.6	1078.5	68.2	63.8	1.1
04XI19-23	6312.7	40119.1	1.4	0.066	1.604	0.010	1.000	63.5	0.6	64.9	1.0	116.7	29.6	63.5	0.6
04XI19-24	3326.0	3827.9	2.2	0.063	7.447	0.010	1.164	63.3	0.7	61.7	4.5	3.1	177.4	63.3	0.7
04XI20-01	186.4	33330.0	1.0	0.667	2.500	0.082	1.800	508.2	8.8	519.1	10.2	567.3	37.8	508.2	8.8
04XI20-02	107.2	32589.0	1.0	2.086	1.773	0.195	0.500	1149.6	5.3	1144.4	12.2	1134.3	33.9	1134.3	33.9
04XI20-03	146.1	35235.0	1.1	2.125	1.470	0.196	0.500	1153.9	5.3	1157.0	10.2	1162.9	27.4	1162.9	27.4
04XI20-04	172.2	32760.0	2.0	0.724	1.934	0.090	0.960	556.0	5.1	552.8	8.2	540.0	36.7	556.0	5.1
04XI20-05	538.6	51504.0	2.9	0.695	1.483	0.085	0.590	528.5	3.0	535.5	6.2	565.4	29.6	528.5	3.0
04XI20-06	155.3	44274.0	1.9	3.519	1.902	0.265	1.230	1517.5	16.6	1531.5	15.0	1551.0	27.2	1551.0	27.2
04XI20-07	420.9	108678.0	2.8	3.351	1.334	0.254	0.860	1460.6	11.2	1493.0	10.4	1539.4	19.2	1539.4	19.2
04XI20-08	373.8	58704.0	2.4	3.197	6.252	0.218	3.920	1272.6	45.3	1456.5	48.4	1736.0	89.4	1736.0	89.4
04XI20-09	167.2	20565.0	1.2	2.636	1.839	0.218	0.580	1272.4	6.7	1310.7	13.5	1373.9	33.6	1373.9	33.6
04XI20-10	322.9	48714.0	2.2	2.882	3.467	0.237	2.530	1372.4	31.3	1377.1	26.1	1384.5	45.5	1384.5	45.5
04XI20-11	131.5	77094.0	5.0	7.304	2.743	0.368	2.670	2017.7	46.3	2149.3	24.5	2277.5	10.9	2277.5	10.9
04XI20-12	126.5	73416.0	1.8	11.280	2.353	0.485	0.580	2549.8	12.2	2546.6	21.9	2544.0	38.2	2544.0	38.2
04XI20-13	60.4	19170.0	0.6	2.064	2.508	0.192	0.690	1131.6	7.2	1137.1	17.2	1147.7	47.9	1147.7	47.9

Table A.1: continued

Analysis	U	206Pb	U/Th	Isotopic ratios				Apparent ages (Ma)						Best age	±
	(ppm)	204Pb		207Pb* 235U	± (%)	206Pb* 238U	± (%)	206Pb* 238U	± (Ma)	207Pb* 235U	± (Ma)	206Pb* 207Pb*	± (Ma)	(Ma)	(Ma)
04XI20-14	59.5	30513.0	2.4	10.823	1.785	0.399	0.680	2165.8	12.5	2508.0	16.6	2798.1	27.0	2798.1	27.0
04XI20-15	83.6	8751.0	0.8	2.136	3.069	0.193	0.780	1137.6	8.1	1160.7	21.2	1204.0	58.5	1204.0	58.5
04XI20-16	417.1	38922.0	3.9	0.876	3.056	0.102	0.830	625.0	4.9	639.0	14.5	688.7	62.8	625.0	4.9
04XI20-17	380.0	156957.0	1.5	4.262	1.981	0.289	1.450	1634.2	20.9	1686.1	16.3	1751.4	24.7	1751.4	24.7
04XI20-18	280.9	45261.0	6.0	1.572	1.218	0.160	0.870	955.4	7.7	959.4	7.6	968.3	17.4	968.3	17.4
04XI20-19	130.9	72372.0	0.5	11.820	1.047	0.475	0.500	2505.8	10.4	2590.2	9.8	2657.0	15.3	2657.0	15.3
04XI20-21	371.2	47397.0	5.6	1.290	2.177	0.132	0.730	797.2	5.5	841.4	12.5	960.2	41.9	960.2	41.9
04XI20-22	389.3	48324.0	1.5	0.639	3.653	0.080	1.010	497.0	4.8	501.8	14.5	523.4	77.0	497.0	4.8
04XI20-23	89.0	21567.0	0.9	2.172	2.608	0.200	1.020	1175.6	11.0	1172.3	18.1	1166.2	47.5	1166.2	47.5
04XI20-24	105.1	60201.0	1.8	13.423	3.162	0.483	1.630	2540.1	34.2	2709.9	29.9	2839.1	44.2	2839.1	44.2
04XI20-25	138.3	113454.0	1.5	14.630	2.608	0.526	1.560	2725.6	34.7	2791.5	24.8	2839.5	34.1	2839.5	34.1
04XI20-26	92.5	4152.0	0.5	0.759	8.445	0.082	0.810	510.6	4.0	573.7	37.0	832.0	175.5	510.6	4.0
04XI20-27	247.1	29334.0	0.9	0.652	3.326	0.080	1.090	494.6	5.2	509.6	13.3	577.6	68.3	494.6	5.2
04XI20-28	174.6	24324.0	1.3	2.685	2.626	0.224	0.890	1304.9	10.5	1324.3	19.4	1355.8	47.6	1355.8	47.6
04XI20-29	182.1	71457.0	2.2	1.572	3.659	0.155	1.400	927.5	12.1	959.3	22.7	1033.2	68.3	1033.2	68.3
04XI20-31	117.3	36927.0	1.6	3.687	2.330	0.268	1.290	1532.7	17.6	1568.5	18.6	1617.0	36.1	1617.0	36.1
04XI20-32	179.6	82068.0	2.2	6.539	2.885	0.316	2.550	1768.4	39.4	2051.1	25.4	2348.7	23.1	2348.7	23.1
04XI20-33	180.9	100065.0	1.0	12.886	1.366	0.504	0.670	2629.3	14.5	2671.3	12.9	2703.3	19.6	2703.3	19.6
04XI20-34	142.5	23100.0	1.0	0.953	2.392	0.110	1.080	673.5	6.9	679.8	11.9	700.4	45.5	673.5	6.9
04XI20-35	116.1	29070.0	1.2	1.735	4.383	0.164	4.190	980.0	38.1	1021.6	28.2	1111.8	25.7	1111.8	25.7
04XI21-01	287.0	4101.0	0.7	0.059	17.900	0.010	2.380	64.8	1.5	58.5	10.2	-191.9	446.7	64.8	1.5
04XI21-02	519.1	4743.0	0.5	0.061	7.642	0.010	2.180	62.5	1.4	60.5	4.5	-17.0	177.3	62.5	1.4
04XI21-03	226.2	1755.0	0.9	0.070	36.407	0.011	3.020	67.9	2.0	68.4	24.1	87.4	886.2	67.9	2.0
04XI21-05	237.4	2502.0	0.7	0.053	19.591	0.008	6.060	52.4	3.2	52.7	10.1	66.1	446.8	52.4	3.2
04XI21-06	305.9	3150.0	0.7	0.055	14.933	0.010	1.400	61.7	0.9	53.9	7.8	-278.8	380.1	61.7	0.9
04XI21-07	260.7	3171.0	0.6	0.047	24.516	0.009	7.470	57.5	4.3	46.9	11.2	-468.9	624.5	57.5	4.3
04XI21-08	326.7	2460.0	0.7	0.068	18.028	0.010	1.240	66.2	0.8	66.7	11.6	83.5	429.7	66.2	0.8
04XI21-09	822.2	5856.0	0.5	0.062	7.401	0.010	2.680	63.4	1.7	61.3	4.4	-19.1	167.0	63.4	1.7
04XI21-10	162.5	1062.0	1.0	0.087	23.790	0.010	2.530	63.6	1.6	84.7	19.3	728.7	508.0	63.6	1.6
04XI21-11	208.7	1695.0	0.7	0.061	19.113	0.010	6.480	62.3	4.0	59.7	11.1	-40.1	439.7	62.3	4.0
04XI21-12	127.2	1425.0	0.9	0.046	######	0.008	9.310	50.5	4.7	45.3	61.6	-221.7	1612.8	50.5	4.7
04XI21-13	108.9	1002.0	1.1	0.064	42.195	0.010	5.750	65.3	3.7	63.4	25.9	-10.3	1050.6	65.3	3.7

Table A.1: continued

Analysis	U	206Pb	U/Th	Isotopic ratios				Apparent ages (Ma)						Best age	±
	(ppm)	204Pb		207Pb* 235U	± (%)	206Pb* 238U	± (%)	206Pb* 238U	± (Ma)	207Pb* 235U	± (Ma)	206Pb* 207Pb*	± (Ma)	(Ma)	(Ma)
04XI21-14	520.3	4842.0	0.6	0.066	6.083	0.011	0.500	67.5	0.3	64.9	3.8	-31.8	147.1	67.5	0.3
04XI21-15	496.8	5370.0	0.6	0.063	10.248	0.010	1.180	65.5	0.8	62.1	6.2	-67.8	249.1	65.5	0.8
04XI21-16	188.4	2949.0	0.8	0.058	15.079	0.010	1.680	65.8	1.1	57.7	8.5	-265.0	382.1	65.8	1.1
04XI21-17	263.5	2562.0	0.8	0.067	9.858	0.010	2.820	65.6	1.8	66.1	6.3	84.5	224.5	65.6	1.8
04XI21-18	270.0	2751.0	0.7	0.071	21.047	0.010	2.920	61.4	1.8	69.9	14.2	371.6	473.9	61.4	1.8
04XI21-19	276.3	921.0	0.7	0.074	14.052	0.011	0.540	68.7	0.4	72.9	9.9	213.2	326.7	68.7	0.4
04XI21-20	185.3	2292.0	0.7	0.070	25.136	0.010	2.110	64.0	1.3	69.0	16.8	244.1	585.1	64.0	1.3
04XI21-21	1636.0	13569.0	0.8	0.068	4.969	0.010	0.500	65.8	0.3	67.2	3.2	117.5	116.6	65.8	0.3
04XI21-22	345.5	3099.0	0.9	0.058	10.423	0.010	2.160	62.5	1.3	57.6	5.8	-144.5	253.3	62.5	1.3
04XI21-23	370.9	3051.0	0.6	0.062	7.240	0.010	1.450	65.2	0.9	61.2	4.3	-93.6	174.2	65.2	0.9
04XI21-24	531.6	12930.0	1.5	0.136	3.786	0.021	1.150	131.0	1.5	129.5	4.6	102.0	85.3	131.0	1.5
04XI21-25	276.3	7620.0	0.9	0.130	5.108	0.020	0.960	129.2	1.2	123.9	6.0	23.7	120.4	129.2	1.2
04XI21-26	200.1	2730.0	0.9	0.058	16.426	0.010	5.480	62.7	3.4	57.3	9.2	-160.4	386.9	62.7	3.4
04XI21-27	283.6	2508.0	0.6	0.064	13.459	0.010	1.950	62.3	1.2	62.7	8.2	79.3	317.4	62.3	1.2
04XI21-28	412.7	3789.0	0.6	0.057	12.241	0.010	2.410	62.4	1.5	56.0	6.7	-211.2	302.2	62.4	1.5
04XI36-01	43.3	2553.0	2.3	0.122	55.340	0.013	8.980	80.5	7.2	117.1	61.3	943.2	1214.3	80.5	7.2
04XI36-01	77.7	1161.0	1.4	0.082	34.182	0.017	2.360	108.6	2.5	79.6	26.2	-724.4	974.7	108.6	2.5
04XI36-02	82.8	1875.0	1.2	0.093	48.428	0.019	3.010	118.4	3.5	90.3	41.9	-599.6	1383.0	118.4	3.5
04XI36-03	210.4	4473.0	1.2	0.119	12.878	0.018	3.880	116.5	4.5	113.9	13.9	60.0	293.6	116.5	4.5
04XI36-04	235.3	6048.0	1.1	0.123	8.279	0.018	3.820	117.9	4.5	118.0	9.2	121.7	173.2	117.9	4.5
04XI36-05	149.5	2394.0	0.9	0.127	21.372	0.020	1.970	126.6	2.5	121.2	24.4	16.6	516.3	126.6	2.5
04XI36-06	139.6	2970.0	0.7	0.111	23.813	0.019	3.210	120.1	3.8	106.9	24.2	-179.4	595.7	120.1	3.8
04XI36-07	95.1	2763.0	1.2	0.150	17.603	0.018	6.550	114.0	7.4	141.7	23.3	633.9	353.9	114.0	7.4
04XI36-08	114.6	2844.0	1.1	0.145	32.720	0.019	3.660	122.6	4.4	137.6	42.1	403.5	746.1	122.6	4.4
04XI36-09	89.5	2037.0	1.0	0.115	34.031	0.019	4.890	119.5	5.8	110.3	35.6	-84.9	845.8	119.5	5.8
04XI36-10	140.9	3981.0	1.2	0.114	15.895	0.019	1.730	121.4	2.1	109.5	16.5	-143.7	393.6	121.4	2.1
04XI36-11	214.5	3519.0	0.6	0.151	12.305	0.020	3.400	128.0	4.3	142.9	16.4	398.2	265.9	128.0	4.3
04XI36-12	110.2	2685.0	1.7	0.133	13.264	0.018	2.630	115.6	3.0	127.1	15.8	346.9	295.1	115.6	3.0
04XI36-13	140.1	4230.0	1.1	0.119	18.629	0.018	3.770	116.7	4.4	114.6	20.2	69.9	437.1	116.7	4.4
04XI36-15	119.6	3228.0	1.1	0.098	29.891	0.020	2.480	127.4	3.1	95.1	27.1	-655.9	834.3	127.4	3.1
04XI36-16	191.1	3852.0	0.9	0.114	14.181	0.018	6.710	114.4	7.6	109.8	14.8	10.5	301.5	114.4	7.6
04XI36-17	177.2	3945.0	0.9	0.123	11.464	0.020	3.060	129.6	3.9	118.2	12.8	-106.9	272.5	129.6	3.9

Table A.1: continued

Analysis	U	206Pb	U/Th	Isotopic ratios				Apparent ages (Ma)						Best age	±
	(ppm)	204Pb		207Pb* 235U	± (%)	206Pb* 238U	± (%)	206Pb* 238U	± (Ma)	207Pb* 235U	± (Ma)	206Pb* 207Pb*	± (Ma)	(Ma)	(Ma)
04XI36-18	201.7	6819.0	1.1	0.106	18.126	0.017	3.870	109.7	4.2	102.1	17.6	-72.5	435.6	109.7	4.2
04XI36-20	223.9	744.0	1.0	0.318	35.932	0.021	2.190	131.1	2.8	280.6	88.3	1838.9	672.8	131.1	2.8
04XI36-21	320.5	11388.0	1.6	0.134	9.213	0.021	3.370	135.5	4.5	127.7	11.1	-14.6	207.6	135.5	4.5
04XI36-23	96.0	5973.0	0.9	0.118	29.782	0.016	5.790	99.9	5.7	113.4	32.0	406.8	666.7	99.9	5.7
04XI36-24	126.4	3366.0	0.8	0.134	13.692	0.019	3.530	120.6	4.2	127.4	16.4	255.8	305.2	120.6	4.2
04XI36-25	116.7	2346.0	1.2	0.096	31.503	0.018	4.730	118.0	5.5	93.1	28.0	-505.9	847.0	118.0	5.5
04XI36-27	400.5	6618.0	0.8	0.131	7.345	0.019	3.050	123.9	3.7	125.0	8.6	146.3	156.9	123.9	3.7
04XI36-29	356.3	4248.0	1.2	0.127	14.517	0.019	1.470	122.3	1.8	121.7	16.7	110.8	342.5	122.3	1.8
04XI36-30	136.1	2532.0	1.3	0.159	20.928	0.020	6.230	124.7	7.7	149.9	29.2	570.7	438.7	124.7	7.7
04XI36-31	1668.5	37704.0	1.2	0.138	2.771	0.021	0.770	131.8	1.0	131.5	3.4	125.2	62.7	131.8	1.0
04XI36-32	75.0	534.0	0.8	0.342	75.002	0.017	8.090	107.9	8.7	298.5	196.4	2309.6	647.7	107.9	8.7
04XI92-01	213.1	5706.4	1.9	0.115	9.588	0.009	5.904	57.0	3.3	110.9	10.1	1513.7	142.8	57.0	3.3
04XI92-02	363.3	4016.4	1.3	0.086	6.405	0.009	3.862	56.0	2.2	83.7	5.1	968.4	104.3	56.0	2.2
04XI92-03	241.6	5093.7	1.4	0.115	8.710	0.009	3.768	56.4	2.1	110.2	9.1	1520.1	148.3	56.4	2.1
04XI92-04	360.7	7681.4	1.2	0.089	6.046	0.008	2.951	53.7	1.6	86.7	5.0	1127.9	105.2	53.7	1.6
04XI92-05	348.5	2564.2	1.9	0.086	8.362	0.008	2.808	53.6	1.5	83.9	6.7	1062.4	158.7	53.6	1.5
04XI92-06	301.5	10009.1	1.5	0.084	9.921	0.008	2.553	53.3	1.4	81.6	7.8	1015.0	194.7	53.3	1.4
04XI92-07	217.1	5646.5	1.9	0.105	7.163	0.008	2.757	53.6	1.5	101.5	6.9	1453.8	125.9	53.6	1.5
04XI92-08	234.2	4908.8	1.3	0.114	7.498	0.009	3.565	54.8	1.9	109.2	7.8	1556.1	123.9	54.8	1.9
04XI92-09	234.7	2331.8	1.8	0.095	11.987	0.008	3.204	53.2	1.7	91.8	10.5	1267.6	226.2	53.2	1.7
04XI92-10	549.5	990.9	1.1	0.110	14.234	0.009	5.197	55.7	2.9	106.2	14.4	1469.7	252.7	55.7	2.9
04XI92-11	221.0	1264.3	1.8	0.098	16.368	0.008	4.989	54.0	2.7	95.4	14.9	1314.3	304.2	54.0	2.7
04XI92-12	241.2	10493.9	1.4	0.101	11.089	0.009	4.897	55.6	2.7	97.8	10.3	1307.5	193.6	55.6	2.7
04XI92-13	288.9	766.3	1.7	0.071	21.636	0.008	3.266	54.4	1.8	69.5	14.5	624.3	466.1	54.4	1.8
04XI92-14	443.3	2383.5	1.3	0.078	8.164	0.009	2.517	55.8	1.4	76.2	6.0	775.6	163.6	55.8	1.4
04XI92-15	317.4	758.1	1.2	0.059	25.486	0.009	3.961	54.7	2.2	58.0	14.4	197.5	593.2	54.7	2.2
04XI92-16	500.2	4932.1	1.5	0.077	9.455	0.008	2.260	53.8	1.2	75.5	6.9	830.0	191.8	53.8	1.2
04XI92-17	312.7	746.4	1.7	0.072	21.746	0.009	4.129	54.7	2.2	70.4	14.8	642.8	463.8	54.7	2.2
04XI92-18	109.8	1353.1	1.7	0.160	12.695	0.008	6.279	52.8	3.3	151.0	17.8	2244.1	191.4	52.8	3.3
04XI92-19	459.6	5601.1	1.6	0.083	7.167	0.009	2.592	55.0	1.4	81.1	5.6	939.2	137.1	55.0	1.4
04XI92-20	555.6	3095.9	1.5	0.071	8.209	0.009	2.375	54.8	1.3	69.6	5.5	613.2	170.0	54.8	1.3
04XI92-21	326.1	2189.9	1.7	0.080	12.694	0.008	2.879	53.9	1.5	78.6	9.6	914.0	255.3	53.9	1.5

Table A.1: continued

Analysis	U	206Pb	U/Th	Isotopic ratios				Apparent ages (Ma)						Best age	±
	(ppm)	204Pb		207Pb* 235U	± (%)	206Pb* 238U	± (%)	206Pb* 238U	± (Ma)	207Pb* 235U	± (Ma)	206Pb* 207Pb*	± (Ma)	(Ma)	(Ma)
04XI92-22	132.3	1631.3	1.7	0.142	11.722	0.009	9.308	56.8	5.3	134.7	14.8	1898.7	128.2	56.8	5.3
04XI92-23	286.7	2729.8	1.7	0.095	8.108	0.008	3.073	53.2	1.6	92.1	7.1	1271.9	146.6	53.2	1.6
04XI92-24	317.2	3940.2	1.9	0.094	10.381	0.009	4.510	58.3	2.6	91.6	9.1	1078.0	188.1	58.3	2.6
04XI92-25	349.0	4492.2	1.8	0.090	9.784	0.009	3.778	55.6	2.1	87.2	8.2	1069.6	181.7	55.6	2.1
04XIA01-01	293.7	6177.5	0.6	0.221	13.468	0.021	2.001	134.5	2.7	202.6	24.7	1093.9	267.8	134.5	2.7
04XIA01-02	1733.2	16231.8	1.5	0.146	1.965	0.021	1.055	133.5	1.4	138.7	2.5	229.0	38.3	133.5	1.4
04XIA01-03	174.3	7632.1	0.6	0.261	8.450	0.021	5.354	136.5	7.2	235.3	17.8	1390.8	125.6	136.5	7.2
04XIA01-04	108.7	4931.7	0.7	0.340	6.675	0.022	2.958	141.7	4.1	297.5	17.2	1816.9	108.7	141.7	4.1
04XIA01-05	255.4	5964.1	0.7	0.209	10.279	0.021	3.024	132.3	4.0	192.8	18.0	1017.1	199.5	132.3	4.0
04XIA01-06	1231.8	8236.5	1.7	0.157	4.067	0.022	3.136	138.8	4.3	147.6	5.6	292.3	59.1	138.8	4.3
04XIA01-07	2123.2	2616.1	1.9	0.175	13.284	0.021	3.207	132.7	4.2	163.7	20.1	639.0	278.3	132.7	4.2
04XIA01-08	2877.1	115754.1	2.0	0.144	2.351	0.021	2.125	136.0	2.9	136.4	3.0	143.3	23.6	136.0	2.9
04XIA01-09	826.6	19269.3	1.2	0.155	2.806	0.021	1.577	132.6	2.1	146.2	3.8	372.8	52.2	132.6	2.1
04XIA01-10	630.1	17798.3	1.0	0.166	3.073	0.021	1.750	136.3	2.4	156.0	4.4	466.6	56.0	136.3	2.4
04XIA01-11	2900.7	35024.5	1.5	0.135	2.420	0.020	1.874	130.4	2.4	128.3	2.9	89.3	36.3	130.4	2.4
04XIA01-12	90.9	2301.1	0.5	0.328	4.901	0.021	3.498	132.6	4.6	288.3	12.3	1873.7	61.9	132.6	4.6
04XIA01-13	485.6	5533.5	1.7	0.184	8.541	0.021	2.345	136.3	3.2	171.7	13.5	692.0	175.4	136.3	3.2
04XIA01-14	2104.8	20607.7	2.1	0.146	3.076	0.021	2.428	132.4	3.2	138.2	4.0	239.2	43.5	132.4	3.2
04XIA01-15	1909.2	11691.2	0.7	0.144	16.896	0.020	5.255	127.2	6.6	136.4	21.6	299.0	368.4	127.2	6.6
04XIA01-16	2499.2	33940.2	1.3	0.139	5.150	0.020	2.292	127.6	2.9	132.5	6.4	220.3	106.8	127.6	2.9
04XIA01-17	341.2	9997.8	1.8	0.201	10.137	0.021	3.082	134.6	4.1	186.0	17.2	900.5	199.6	134.6	4.1
04XIA01-18	783.2	17969.0	1.3	0.156	4.338	0.021	2.597	132.3	3.4	146.8	5.9	388.2	78.0	132.3	3.4
04XIA01-19	1393.0	17015.0	2.2	0.143	1.994	0.021	1.692	134.7	2.3	135.4	2.5	148.4	24.8	134.7	2.3
04XIA01-20	1148.6	28468.2	1.4	0.148	2.060	0.021	1.000	131.3	1.3	139.9	2.7	288.0	41.2	131.3	1.3
04XIA01-21	649.7	10707.3	1.0	0.172	6.722	0.020	1.099	130.2	1.4	161.0	10.0	640.8	142.8	130.2	1.4
04XIA01-22	347.0	1095.2	1.0	0.145	18.697	0.020	2.468	128.8	3.1	137.7	24.1	294.3	426.3	128.8	3.1
04XIA01-23	197.3	5499.5	0.6	0.229	7.315	0.022	3.446	137.5	4.7	209.4	13.8	1122.7	128.8	137.5	4.7
04XIA01-24	153.8	2720.0	0.9	0.264	6.797	0.022	3.133	140.7	4.4	238.2	14.4	1358.6	116.4	140.7	4.4
05GB05-01	562.4	17859.0	0.7	0.230	3.888	0.034	1.430	213.3	3.0	209.9	7.4	172.4	84.4	213.3	3.0
05GB05-02	649.0	1980.0	1.5	0.269	3.740	0.029	1.070	183.2	1.9	241.8	8.0	857.9	74.4	183.2	1.9
05GB05-03	623.7	3897.0	2.7	0.277	11.888	0.034	2.740	213.6	5.8	247.9	26.2	586.9	251.8	213.6	5.8

Table A.1: continued

Analysis	U (ppm)	206Pb/204Pb	U/Th	Isotopic ratios: 207Pb*/235U	± (%)	206Pb*/238U	± (%)	Apparent ages (Ma): 206Pb*/238U	± (Ma)	207Pb*/235U	± (Ma)	206Pb*/207Pb*	± (Ma)	Best age (Ma)	± (Ma)
05GB05-05	1012.0	12051.0	0.9	0.233	2.044	0.033	0.980	206.8	2.0	212.9	3.9	281.2	41.1	206.8	2.0
05GB05-06	2009.5	2277.0	0.8	0.307	14.132	0.032	3.530	203.2	7.1	271.5	33.7	911.1	283.0	203.2	7.1
05GB05-07	540.8	116649.0	1.5	3.610	2.595	0.265	2.110	1513.7	28.5	1551.7	20.6	1603.8	28.2	1603.8	28.2
05GB05-08	2388.2	1791.0	3.1	0.285	7.928	0.028	4.470	178.3	7.9	254.2	17.8	1029.5	132.5	178.3	7.9
05GB05-09	2478.6	4881.0	0.8	0.321	30.821	0.034	1.000	212.5	2.1	282.3	76.1	909.9	649.3	212.5	2.1
05GB05-10	2854.8	4542.0	2.4	0.238	2.927	0.029	2.210	186.9	4.1	216.7	5.7	554.5	41.9	186.9	4.1
05XI52-01	358.4	1520.2	1.0	0.084	5.051	0.009	2.299	59.4	1.4	81.8	4.0	796.7	94.3	59.4	1.4
05XI52-02	228.7	859.4	0.8	0.116	9.700	0.010	5.655	62.2	3.5	111.9	10.3	1363.2	152.0	62.2	3.5
05XI52-03	3554.5	10365.3	1.2	0.063	3.444	0.010	2.393	61.8	1.5	61.6	2.1	53.6	59.1	61.8	1.5
05XI52-04	239.8	1380.1	1.0	0.130	29.176	0.010	7.725	64.9	5.0	124.1	34.1	1490.5	543.7	64.9	5.0
05XI52-05	196.2	955.4	0.9	0.107	12.668	0.009	7.917	59.4	4.7	103.5	12.5	1292.8	192.8	59.4	4.7
05XI52-06	185.7	188.2	0.9	0.128	19.752	0.010	5.717	66.0	3.8	122.5	22.8	1434.3	363.9	66.0	3.8
05XI52-07	242.4	675.6	1.1	0.102	21.819	0.010	6.182	64.2	3.9	98.6	20.5	1039.1	427.0	64.2	3.9
05XI52-08	297.1	1451.4	1.3	0.113	9.456	0.010	3.792	63.1	2.4	109.1	9.8	1284.9	169.0	63.1	2.4
05XI52-09	711.5	5526.2	1.0	0.077	4.136	0.009	1.630	59.4	1.0	75.2	3.0	610.7	82.2	59.4	1.0
05XI52-10	346.5	1984.0	1.2	0.095	7.402	0.009	2.623	60.7	1.6	92.6	6.5	1019.2	140.3	60.7	1.6
05XI52-11	229.9	1501.4	0.9	0.095	8.956	0.010	4.712	61.6	2.9	92.1	7.9	977.9	155.4	61.6	2.9
05XI52-12	304.6	2226.5	0.9	0.102	6.995	0.010	2.153	61.7	1.3	98.3	6.6	1111.9	133.0	61.7	1.3
05XI52-13	171.7	822.4	1.2	0.151	26.465	0.009	6.046	60.6	3.6	143.0	35.3	1899.2	471.5	60.6	3.6
05XI52-14	338.3	802.0	0.9	0.166	29.812	0.010	9.152	66.1	6.0	156.0	43.1	1908.7	520.6	66.1	6.0
05XI52-15	256.1	1853.2	0.9	0.104	9.821	0.010	3.894	63.4	2.5	100.2	9.4	1099.3	180.7	63.4	2.5
05XI52-16	182.9	3756.9	0.7	0.145	11.970	0.010	6.260	63.4	4.0	137.3	15.4	1735.6	187.6	63.4	4.0
05XI52-17	581.4	3507.2	0.8	0.082	8.718	0.009	1.945	58.7	1.1	79.7	6.7	765.9	179.3	58.7	1.1
05XI52-18	187.4	2306.7	1.1	0.129	8.660	0.009	3.605	60.5	2.2	123.4	10.1	1612.9	146.9	60.5	2.2
05XI52-19	183.4	1280.3	0.9	0.113	15.261	0.009	3.649	59.8	2.2	108.3	15.7	1372.8	286.6	59.8	2.2
05XI52-20	181.3	2670.1	0.8	0.115	8.171	0.010	3.386	62.3	2.1	110.6	8.6	1337.8	144.0	62.3	2.1
05XI52-21	182.4	640.0	0.8	0.097	26.269	0.009	4.949	60.2	3.0	94.3	23.7	1073.6	526.7	60.2	3.0
05XI52-22	146.5	1340.3	1.0	0.159	5.545	0.010	2.400	64.7	1.5	149.6	7.7	1867.8	90.2	64.7	1.5
05XI52-23	320.7	1906.5	0.9	0.103	10.946	0.009	4.888	59.3	2.9	99.1	10.3	1207.2	193.3	59.3	2.9
05XI52-24	288.4	2688.6	1.0	0.105	8.005	0.009	5.343	60.2	3.2	101.6	7.7	1231.1	117.1	60.2	3.2
05XI52-25	218.5	4011.5	0.9	0.125	10.027	0.010	5.307	61.8	3.3	120.0	11.4	1517.7	160.8	61.8	3.3

Table A.1: continued

Analysis	U	206Pb	U/Th	Isotopic ratios				Apparent ages (Ma)						Best age	±
	(ppm)	204Pb		207Pb* 235U	± (%)	206Pb* 238U	± (%)	206Pb* 238U	± (Ma)	207Pb* 235U	± (Ma)	206Pb* 207Pb*	± (Ma)	(Ma)	(Ma)
05XI63-01	2140.1	15950.3	3.3	0.062	4.143	0.009	2.444	60.1	1.5	60.7	2.4	86.4	79.3	60.1	1.5
05XI63-02	197.1	2156.2	0.7	0.116	9.642	0.010	3.345	61.4	2.0	111.2	10.2	1376.5	174.2	61.4	2.0
05XI63-03	275.9	3730.0	0.9	0.100	8.964	0.009	3.478	59.6	2.1	96.6	8.3	1144.1	164.5	59.6	2.1
05XI63-04	3862.4	27967.9	2.2	0.062	4.183	0.010	1.849	61.1	1.1	61.4	2.5	71.9	89.2	61.1	1.1
05XI63-05	164.4	1738.3	1.0	0.112	14.294	0.010	3.710	61.9	2.3	107.7	14.6	1295.6	269.7	61.9	2.3
05XI63-06	1840.4	8699.7	1.9	0.069	3.562	0.010	2.116	63.0	1.3	67.9	2.3	242.5	66.0	63.0	1.3
05XI63-07	308.2	1528.2	0.8	0.084	11.276	0.010	5.763	62.0	3.6	81.9	8.9	710.7	206.5	62.0	3.6
05XI63-08	3366.9	10083.3	1.0	0.060	5.035	0.009	2.029	59.0	1.2	59.3	2.9	73.0	109.6	59.0	1.2
05XI63-09	209.0	2602.9	0.9	0.111	16.046	0.010	7.247	61.1	4.4	106.6	16.2	1299.0	279.7	61.1	4.4
05XI63-10	181.9	2105.1	1.5	0.111	11.974	0.010	5.251	62.4	3.3	106.8	12.1	1261.5	210.9	62.4	3.3
05XI63-11	476.0	2524.5	1.8	0.076	6.913	0.009	5.869	60.5	3.5	74.7	5.0	557.3	79.7	60.5	3.5
05XI63-12	1120.3	2724.6	0.5	0.063	4.353	0.009	1.255	59.1	0.7	62.1	2.6	181.9	97.2	59.1	0.7
05XI63-13	148.1	1150.7	0.9	0.113	9.833	0.009	6.984	57.5	4.0	108.3	10.1	1448.9	131.9	57.5	4.0
05XI63-14	181.8	2114.4	1.0	0.111	9.953	0.010	6.078	63.4	3.8	106.5	10.1	1224.6	155.1	63.4	3.8
05XI63-15	472.7	2167.4	1.6	0.084	14.091	0.009	1.943	59.2	1.1	81.5	11.0	795.8	294.0	59.2	1.1
05XI63-16	1219.4	6237.4	2.2	0.071	6.651	0.009	2.677	60.0	1.6	69.2	4.4	399.5	136.5	60.0	1.6
05XI63-17	159.2	882.0	0.9	0.116	12.364	0.009	6.409	58.8	3.7	111.0	13.0	1457.6	201.6	58.8	3.7
05XI63-18	207.0	1139.7	1.2	0.090	10.913	0.010	6.407	62.6	4.0	87.5	9.1	835.3	184.4	62.6	4.0
05XI63-19	261.0	1316.8	1.1	0.082	11.195	0.009	3.899	59.7	2.3	79.8	8.6	732.0	222.9	59.7	2.3
05XI63-21	422.9	1997.9	1.0	0.085	9.614	0.010	4.786	63.2	3.0	83.2	7.7	704.8	177.7	63.2	3.0
05XI63-22	542.3	997.8	1.1	0.067	29.907	0.009	7.327	60.3	4.4	65.9	19.1	275.3	676.9	60.3	4.4
05XI63-23	521.0	3753.3	1.4	0.068	7.036	0.009	3.710	57.9	2.1	66.9	4.6	399.2	134.1	57.9	2.1
05XI63-24	1907.6	6986.3	0.8	0.062	3.681	0.010	2.476	61.7	1.5	60.7	2.2	23.2	65.4	61.7	1.5
05XI63-25	364.6	407.8	1.4	0.043	49.070	0.009	5.218	58.3	3.0	42.9	20.6	-756.4	1443.9	58.3	3.0
05XI67-01	644.0	4962.8	3.5	0.078	4.575	0.009	2.075	57.3	1.2	76.3	3.4	720.4	86.6	57.3	1.2
05XI67-02	390.2	8405.7	1.0	0.084	7.415	0.009	2.976	54.7	1.6	81.9	5.8	972.7	138.7	54.7	1.6
05XI67-03	358.6	3818.1	1.1	0.083	7.009	0.008	2.455	54.0	1.3	81.2	5.5	978.9	133.9	54.0	1.3
05XI67-04	1068.4	7140.2	1.0	0.061	3.189	0.008	2.323	52.4	1.2	59.8	1.9	367.7	49.2	52.4	1.2
05XI67-05	380.4	3617.7	1.1	0.085	6.734	0.008	4.843	54.3	2.6	82.7	5.3	1006.7	95.0	54.3	2.6
05XI67-06	375.6	776.8	0.8	0.074	21.136	0.008	3.401	53.8	1.8	72.5	14.8	746.3	445.4	53.8	1.8
05XI67-07	2483.3	9986.5	0.7	0.054	2.821	0.008	1.293	51.9	0.7	53.3	1.5	115.3	59.1	51.9	0.7
05XI67-08	1562.1	671.4	1.0	0.062	3.945	0.008	1.647	51.5	0.8	61.0	2.3	451.9	79.6	51.5	0.8

Table A.1: continued

Analysis	U	206Pb	U/Th	Isotopic ratios				Apparent ages (Ma)						Best age	±
	(ppm)	204Pb		207Pb*/235U	± (%)	206Pb*/238U	± (%)	206Pb*/238U	± (Ma)	207Pb*/235U	± (Ma)	206Pb*/207Pb*	± (Ma)	(Ma)	(Ma)
05XI67-09	367.5	593.4	0.7	0.063	27.195	0.008	4.279	51.3	2.2	62.4	16.5	510.2	600.3	51.3	2.2
05XI67-10	5664.0	8362.5	2.4	0.068	4.603	0.009	3.911	59.0	2.3	66.4	3.0	343.3	54.9	59.0	2.3
05XI67-11	323.6	4167.3	1.2	0.095	8.337	0.008	3.258	54.1	1.8	91.7	7.3	1230.0	150.8	54.1	1.8
05XI67-12	251.0	26420.1	1.1	0.111	6.796	0.008	4.816	54.2	2.6	107.1	6.9	1538.5	90.3	54.2	2.6
05XI67-13	1778.7	520.0	1.0	0.058	7.967	0.008	1.822	52.9	1.0	57.7	4.5	261.3	178.3	52.9	1.0
05XI67-14	300.6	2542.1	0.7	0.080	9.628	0.008	4.404	52.8	2.3	78.2	7.2	946.4	175.6	52.8	2.3
05XI67-15	1893.4	6149.1	1.0	0.059	7.173	0.008	2.527	52.3	1.3	58.3	4.1	313.3	152.9	52.3	1.3
05XI67-16	324.6	1642.4	0.8	0.082	6.447	0.008	2.387	52.3	1.2	79.7	4.9	1005.0	121.6	52.3	1.2
05XI67-17	413.1	1405.7	0.9	0.081	14.375	0.008	6.278	53.2	3.3	79.0	10.9	952.3	265.6	53.2	3.3
05XI67-18	392.1	2905.8	1.2	0.082	6.626	0.009	2.320	55.3	1.3	79.9	5.1	895.2	128.2	55.3	1.3
05XI67-19	3432.6	14270.6	1.2	0.054	2.731	0.008	1.708	51.8	0.9	53.5	1.4	130.8	50.1	51.8	0.9
05XI67-20	271.2	1536.0	1.2	0.091	10.589	0.008	4.357	52.4	2.3	88.2	8.9	1210.3	190.4	52.4	2.3
05XI67-21	972.4	6692.0	1.2	0.070	16.768	0.008	5.460	53.1	2.9	68.6	11.1	651.1	342.3	53.1	2.9
05XI67-22	458.8	3890.4	1.4	0.088	10.746	0.009	2.601	55.1	1.4	85.2	8.8	1042.5	210.9	55.1	1.4
05XI67-23	487.0	3409.1	0.8	0.079	8.378	0.008	2.049	54.0	1.1	77.2	6.2	871.5	168.5	54.0	1.1
05XI67-24	347.1	5830.5	0.8	0.095	9.308	0.009	2.294	54.9	1.3	91.8	8.2	1204.0	178.1	54.9	1.3
05XI67-25	1774.0	12382.1	1.0	0.057	3.357	0.008	2.537	53.0	1.3	56.2	1.8	196.5	51.1	53.0	1.3
05XI75-06	788.8	1686.0	0.8	0.017	27.131	0.002	3.730	13.8	0.5	17.4	4.7	549.7	596.7	13.8	0.5
05XI75-07	1770.4	3924.0	1.1	0.015	18.447	0.002	1.840	15.1	0.3	15.4	2.8	66.4	440.1	15.1	0.3
05XI75-08	2245.0	7200.0	0.6	0.015	17.117	0.002	2.050	15.4	0.3	14.7	2.5	-95.4	419.7	15.4	0.3
05XI75-09	586.6	1311.0	0.5	0.014	######	0.002	9.100	13.7	1.2	13.7	38.0	12.5	0.0	13.7	1.2
05XI75-10	7975.2	12858.0	1.7	0.016	4.425	0.002	2.110	16.0	0.3	15.8	0.7	-10.2	93.9	16.0	0.3
05XI75-11	783.9	2265.0	1.1	0.019	33.808	0.003	5.000	21.6	1.1	18.9	6.3	-311.8	877.2	21.6	1.1
05XI75-14	219.9	504.0	0.6	0.016	46.464	0.003	3.860	16.4	0.6	15.9	7.3	-46.7	1183.5	16.4	0.6
05XI75-15	6053.7	16515.0	0.6	0.016	3.032	0.002	1.440	15.6	0.2	15.6	0.5	19.6	64.1	15.6	0.2
05XI75-16	1850.9	1968.0	0.5	0.019	3.741	0.003	0.700	16.8	0.1	19.2	0.7	329.1	83.4	16.8	0.1
05XI75-17	883.4	2652.0	0.6	0.014	15.675	0.002	2.720	15.3	0.4	14.5	2.3	-106.3	381.6	15.3	0.4
05XI75-18	1086.1	2268.0	0.3	0.014	18.536	0.002	2.150	15.0	0.3	14.0	2.6	-147.4	459.8	15.0	0.3
05XI75-19	2471.4	8184.0	0.5	0.017	4.599	0.003	2.130	16.2	0.3	17.0	0.8	128.4	96.0	16.2	0.3
05XI75-20	1006.0	2304.0	0.3	0.013	14.473	0.002	3.950	15.1	0.6	13.4	1.9	-284.1	356.1	15.1	0.6
05XI75-22	1665.3	4722.0	2.2	0.018	7.786	0.003	1.940	19.0	0.4	18.0	1.4	-117.9	186.1	19.0	0.4
05XI75-23	2633.3	2838.0	0.4	0.017	7.529	0.002	2.220	15.6	0.3	17.3	1.3	267.4	165.2	15.6	0.3

Table A.1: continued

Analysis	U (ppm)	206Pb/204Pb	U/Th	Isotopic ratios: 207Pb*/235U	± (%)	206Pb*/238U	± (%)	Apparent ages (Ma): 206Pb*/238U	± (Ma)	207Pb*/235U	± (Ma)	206Pb*/207Pb*	± (Ma)	Best age (Ma)	± (Ma)
05XI75-25	518.2	6492.0	1.2	0.066	6.591	0.010	0.550	63.3	0.3	65.1	4.2	132.5	154.6	63.3	0.3
05XI75-26	501.4	5043.0	1.6	0.043	9.822	0.007	6.120	42.7	2.6	42.9	4.1	56.3	183.4	42.7	2.6
05XI75-27	1366.1	2028.0	0.5	0.022	38.558	0.002	6.840	14.8	1.0	22.5	8.6	956.1	804.6	14.8	1.0
05XI75-28	688.7	4836.0	0.9	0.045	8.540	0.007	4.410	44.1	1.9	45.1	3.8	101.9	173.1	44.1	1.9
05XI75-29	610.7	1371.0	0.5	0.018	21.363	0.002	1.480	15.8	0.2	17.7	3.7	281.3	492.6	15.8	0.2
05XI75-30	706.8	6483.0	3.0	0.046	5.892	0.007	2.370	44.0	1.0	45.9	2.6	145.8	126.6	44.0	1.0
05XI75-31	608.0	2433.0	1.5	0.018	18.867	0.003	4.860	19.9	1.0	18.6	3.5	-154.3	455.9	19.9	1.0
05XI75-32	908.2	5979.0	1.1	0.040	11.727	0.006	6.830	41.6	2.8	40.1	4.6	-47.7	232.3	41.6	2.8
05XI75-33	502.3	1815.0	0.4	0.008	48.851	0.002	3.110	13.8	0.4	8.2	4.0	-1415.4	1669.4	13.8	0.4
05XI75-35	1893.0	3234.0	0.3	0.016	8.687	0.002	2.370	15.0	0.4	15.7	1.4	118.2	197.3	15.0	0.4
05XI75-37	194.0	3453.0	0.8	0.060	17.758	0.011	2.740	69.8	1.9	58.8	10.2	-367.8	457.4	69.8	1.9
05XI75-39	532.3	4371.0	1.2	0.053	11.164	0.008	1.330	50.1	0.7	52.6	5.7	167.3	259.6	50.1	0.7
05XI79-01	7402.3	14955.0	4.7	0.213	4.235	0.029	2.010	183.9	3.6	196.2	7.6	347.0	84.3	183.9	3.6
05XI79-02	812.4	39036.0	2.8	0.233	4.707	0.032	1.070	204.5	2.2	212.7	9.0	304.7	104.5	204.5	2.2
05XI79-03	5962.9	132894.0	2.5	0.254	2.472	0.036	0.500	226.2	1.1	230.0	5.1	268.5	55.5	226.2	1.1
05XI79-04	5054.1	47106.0	6.4	0.251	1.859	0.035	0.900	220.4	2.0	227.6	3.8	302.5	37.1	220.4	2.0
05XI79-05	5593.8	90771.0	6.4	0.210	2.202	0.029	1.400	187.3	2.6	193.9	3.9	274.8	38.9	187.3	2.6
05XI79-06	5635.2	1950.0	4.8	0.254	4.843	0.026	2.150	164.5	3.5	229.9	10.0	966.8	88.6	164.5	3.5
05XI79-07	7629.9	39963.0	15.9	0.232	2.272	0.032	1.890	204.7	3.8	212.0	4.3	293.7	28.8	204.7	3.8
05XI79-08	1688.3	13563.0	2.5	0.260	3.682	0.035	1.720	220.4	3.7	234.6	7.7	379.1	73.2	220.4	3.7
05XI79-09	7396.5	173073.0	13.4	0.221	2.596	0.031	0.830	199.7	1.6	202.4	4.8	233.1	56.8	199.7	1.6
05XI79-10	2957.2	94665.0	3.1	0.222	4.369	0.032	1.270	200.9	2.5	203.7	8.1	236.5	96.5	200.9	2.5
05XI79-11	5642.8	71625.0	6.9	0.217	1.584	0.031	0.680	194.0	1.3	199.6	2.9	265.6	32.8	194.0	1.3
05XI79-12	6798.5	8253.0	4.4	0.246	3.909	0.032	2.440	200.2	4.8	223.4	7.8	475.4	67.6	200.2	4.8
05XI79-13	6369.1	9126.0	7.2	0.256	2.329	0.033	0.740	211.5	1.5	231.6	4.8	440.3	49.1	211.5	1.5
05XI79-14	1059.7	61662.0	1.8	0.227	3.017	0.033	1.260	209.3	2.6	208.0	5.7	193.7	63.7	209.3	2.6
05XI79-15	4205.2	6063.0	10.1	0.283	10.447	0.035	2.020	222.6	4.4	253.1	23.4	545.9	224.5	222.6	4.4
05XI79-16	1379.0	5100.0	2.9	0.262	6.584	0.033	1.610	208.0	3.3	236.3	13.9	528.9	140.0	208.0	3.3
05XI79-17	3776.6	188550.0	2.9	0.227	1.969	0.033	0.840	206.5	1.7	207.6	3.7	220.3	41.2	206.5	1.7
05XI79-18	2608.7	149721.0	7.8	0.244	3.161	0.035	2.250	220.2	4.9	221.4	6.3	234.5	51.3	220.2	4.9
05XI79-19	5106.8	145896.0	7.4	0.244	2.862	0.035	1.730	219.1	3.7	221.9	5.7	251.7	52.5	219.1	3.7
05XI79-20	8688.0	15831.0	13.4	0.237	4.248	0.032	2.300	202.5	4.6	216.4	8.3	370.4	80.5	202.5	4.6

Table A.1: continued

Analysis	U	206Pb	U/Th	Isotopic ratios				Apparent ages (Ma)						Best age	±
	(ppm)	204Pb		207Pb* 235U	± (%)	206Pb* 238U	± (%)	206Pb* 238U	± (Ma)	207Pb* 235U	± (Ma)	206Pb* 207Pb*	± (Ma)	(Ma)	(Ma)
05XI79-21	2254.1	28122.0	4.4	0.224	6.243	0.031	1.530	194.7	2.9	205.4	11.6	329.4	137.4	194.7	2.9
05XI79-22	2455.6	45330.0	4.2	0.250	3.574	0.033	1.490	211.4	3.1	226.8	7.3	389.4	73.0	211.4	3.1
05XI79-23	6965.8	10545.0	7.6	0.246	5.224	0.033	2.830	208.1	5.8	223.0	10.5	383.1	98.7	208.1	5.8
05XI79-24	4699.8	15168.0	3.1	0.254	12.997	0.029	4.500	187.2	8.3	230.1	26.8	694.6	260.8	187.2	8.3
05XI79-25	2287.0	5742.0	1.9	0.243	4.152	0.031	3.490	197.9	6.8	220.6	8.2	469.5	49.8	197.9	6.8
05XI79-26	5902.8	1467.0	7.1	0.333	20.677	0.028	2.690	179.5	4.8	292.0	52.5	1328.2	401.0	179.5	4.8
05XI79-27	6011.5	4395.0	11.3	0.259	3.551	0.032	2.050	201.0	4.1	233.5	7.4	574.1	63.1	201.0	4.1
05XI79-28	2077.4	49593.0	1.5	0.224	2.082	0.032	0.610	202.6	1.2	204.9	3.9	231.3	46.0	202.6	1.2
05XI79-29	7115.0	32127.0	15.9	0.246	2.152	0.034	1.080	216.2	2.3	223.0	4.3	295.8	42.5	216.2	2.3
05XI79-30	1397.0	120129.0	1.9	0.237	2.256	0.033	1.480	208.7	3.0	215.8	4.4	293.9	38.9	208.7	3.0
05XI90-01	150.8	326.9	1.5	0.180	11.637	0.008	5.850	50.8	3.0	167.9	18.0	2507.3	169.7	50.8	3.0
05XI90-02	485.6	868.2	2.8	0.088	9.656	0.008	5.696	51.2	2.9	85.4	7.9	1194.8	154.1	51.2	2.9
05XI90-03	425.4	1454.1	1.4	0.080	7.876	0.008	3.390	51.2	1.7	78.0	5.9	1003.4	144.5	51.2	1.7
05XI90-05	100.4	629.4	1.6	0.180	12.452	0.007	7.932	47.6	3.8	167.7	19.3	2614.2	160.2	47.6	3.8
05XI90-06	424.3	2607.7	1.8	0.080	4.367	0.008	2.536	50.6	1.3	78.1	3.3	1031.5	71.9	50.6	1.3
05XI90-07	178.2	1523.5	1.3	0.111	9.850	0.008	7.443	49.0	3.6	106.9	10.0	1722.2	118.6	49.0	3.6
05XI90-08	185.1	447.7	1.5	0.093	24.779	0.008	9.888	52.0	5.1	89.9	21.3	1265.2	449.5	52.0	5.1
05XI90-09	370.6	526.0	3.5	0.088	22.770	0.008	9.663	48.7	4.7	85.3	18.6	1288.3	405.6	48.7	4.7
05XI90-10	249.6	1123.6	1.6	0.090	12.958	0.008	3.911	49.7	1.9	87.6	10.9	1304.6	240.8	49.7	1.9
05XI90-11	212.6	596.7	1.2	0.090	6.355	0.008	3.235	49.0	1.6	87.7	5.3	1330.6	105.9	49.0	1.6
05XI90-12	121.6	222.4	2.0	0.143	15.834	0.007	9.445	46.4	4.4	135.8	20.1	2271.7	220.0	46.4	4.4
05XI90-13	209.6	1755.5	1.3	0.105	9.239	0.008	4.610	52.6	2.4	101.1	8.9	1481.7	152.0	52.6	2.4
05XI90-14	338.8	1261.1	1.8	0.084	13.197	0.007	3.427	47.3	1.6	82.1	10.4	1269.7	249.7	47.3	1.6
05XI90-15	330.8	662.6	2.0	0.052	25.065	0.008	4.396	48.5	2.1	51.7	12.6	199.6	580.8	48.5	2.1
05XI90-16	143.6	9881.2	1.4	0.151	9.086	0.008	4.163	50.3	2.1	142.4	12.1	2220.5	140.2	50.3	2.1
05XI90-17	156.2	691.5	1.5	0.113	11.827	0.008	5.608	51.3	2.9	108.7	12.2	1668.8	193.1	51.3	2.9
05XI90-18	138.8	942.1	1.5	0.116	16.527	0.008	7.212	49.3	3.5	111.3	17.4	1788.2	272.5	49.3	3.5
05XI90-19	108.3	321.1	1.7	0.108	24.543	0.008	6.795	52.3	3.5	104.3	24.3	1553.5	449.2	52.3	3.5
05XI90-20	818.0	5287.8	2.6	0.068	8.863	0.008	3.542	53.3	1.9	67.2	5.8	594.6	176.3	53.3	1.9
05XI90-21	158.9	349.0	2.3	0.079	15.214	0.008	6.573	50.3	3.3	77.3	11.3	1018.3	279.1	50.3	3.3
05XI90-22	214.1	1268.8	1.8	0.097	7.891	0.008	6.352	50.4	3.2	93.7	7.1	1413.1	89.6	50.4	3.2
05XI90-23	128.2	896.9	1.6	0.135	14.390	0.008	6.912	50.0	3.4	128.2	17.3	2032.5	224.3	50.0	3.4

Table A.1: continued

Analysis	U (ppm)	206Pb 204Pb	U/Th	Isotopic ratios 207Pb* 235U	± (%)	206Pb* 238U	± (%)	Apparent ages (Ma) 206Pb* 238U	± (Ma)	207Pb* 235U	± (Ma)	206Pb* 207Pb*	± (Ma)	Best age (Ma)	± (Ma)
05XI90-24	386.4	1516.8	1.3	0.074	8.575	0.008	3.304	49.0	1.6	72.6	6.0	942.5	162.4	49.0	1.6
05XI90-25	173.5	1246.4	1.5	0.120	10.190	0.008	8.126	49.4	4.0	115.3	11.1	1852.0	111.3	49.4	4.0
05XI91-01	394.3	665.8	4.2	0.055	25.417	0.007	3.518	46.9	1.6	54.1	13.4	382.7	573.9	46.9	1.6
05XI91-02	148.7	944.8	1.0	0.128	13.800	0.008	9.008	50.7	4.6	122.3	15.9	1918.7	188.0	50.7	4.6
05XI91-03	278.2	927.4	1.2	0.084	11.838	0.008	5.447	52.8	2.9	82.0	9.3	1047.0	212.5	52.8	2.9
05XI91-04	183.9	910.7	0.8	0.111	7.827	0.008	3.104	51.9	1.6	107.0	7.9	1618.1	133.9	51.9	1.6
05XI91-05	153.2	580.4	1.3	0.100	23.847	0.008	4.038	53.7	2.2	97.2	22.1	1361.2	459.2	53.7	2.2
05XI91-06	213.3	1619.8	1.0	0.109	10.251	0.008	3.935	51.3	2.0	105.2	10.2	1606.3	176.9	51.3	2.0
05XI91-07	129.4	2405.1	1.1	0.138	14.912	0.008	9.335	52.3	4.9	131.2	18.3	1996.1	207.4	52.3	4.9
05XI91-08	280.8	3918.6	1.1	0.113	21.592	0.008	8.948	53.9	4.8	108.9	22.3	1582.0	371.2	53.9	4.8
05XI91-09	262.8	526.5	1.2	0.097	22.514	0.008	9.031	53.2	4.8	94.4	20.3	1323.1	403.8	53.2	4.8
05XI91-10	779.2	3525.8	3.5	0.089	27.291	0.008	6.404	50.0	3.2	86.5	22.6	1267.4	527.2	50.0	3.2
05XI91-11	428.4	2916.0	1.3	0.093	27.910	0.008	7.612	49.9	3.8	90.2	24.1	1353.0	527.6	49.9	3.8
05XI91-12	148.8	1942.0	1.5	0.130	14.978	0.008	9.622	54.4	5.2	124.0	17.5	1818.5	209.1	54.4	5.2
05XI91-13	117.4	789.6	1.2	0.136	9.451	0.008	4.912	52.8	2.6	129.5	11.5	1957.6	144.4	52.8	2.6
05XI91-14	136.9	1755.9	1.5	0.131	13.576	0.008	7.540	51.7	3.9	125.0	16.0	1925.0	203.0	51.7	3.9
05XI91-15	221.6	787.0	1.3	0.099	16.238	0.008	6.018	51.7	3.1	96.3	14.9	1417.5	290.0	51.7	3.1
05XI91-17	1144.8	16151.9	7.7	0.071	4.621	0.008	1.706	50.3	0.9	69.9	3.1	807.7	89.9	50.3	0.9
05XI91-18	145.1	892.0	1.0	0.136	12.731	0.008	5.613	51.7	2.9	129.9	15.5	1999.2	203.7	51.7	2.9
05XI91-19	225.0	1175.9	0.9	0.105	7.174	0.008	5.773	49.5	2.8	101.5	6.9	1604.7	79.5	49.5	2.8
05XI91-20	206.6	4421.6	1.0	0.123	11.959	0.008	3.997	52.8	2.1	117.9	13.3	1776.6	206.3	52.8	2.1
05XI91-21	229.2	3655.9	1.5	0.115	10.833	0.008	4.965	53.1	2.6	110.6	11.4	1640.0	179.1	53.1	2.6
05XI91-22	233.6	917.3	1.1	0.100	25.009	0.008	4.979	51.8	2.6	96.7	23.1	1421.9	475.5	51.8	2.6
05XI91-23	619.9	3773.1	0.9	0.078	10.643	0.008	2.987	50.7	1.5	76.4	7.8	980.2	208.6	50.7	1.5
05XI91-24	141.6	1214.3	1.1	0.129	9.698	0.008	7.008	53.3	3.7	123.0	11.2	1841.2	121.5	53.3	3.7
05XI91-25	368.5	2126.5	2.7	0.106	21.278	0.008	3.899	50.3	2.0	102.6	20.8	1593.8	395.1	50.3	2.0
05XI94-01	323.3	1910.0	1.1	0.095	15.140	0.009	3.513	55.2	1.9	92.1	13.3	1198.6	291.9	55.2	1.9
05XI94-02	255.2	1721.2	1.3	0.103	10.234	0.008	4.188	52.3	2.2	99.5	9.7	1459.3	177.9	52.3	2.2
05XI94-03	386.2	1550.3	1.5	0.093	12.606	0.009	4.298	56.7	2.4	90.7	10.9	1114.7	237.4	56.7	2.4
05XI94-04	224.4	2570.0	1.2	0.109	9.052	0.009	2.408	54.7	1.3	105.3	9.1	1488.6	165.6	54.7	1.3
05XI94-05	365.1	309.2	1.2	0.046	52.189	0.008	6.694	52.0	3.5	45.9	23.4	-261.8	1397.3	52.0	3.5

Table A.1: continued

Analysis	U	206Pb	U/Th	Isotopic ratios				Apparent ages (Ma)						Best age	±
	(ppm)	204Pb		207Pb* 235U	± (%)	206Pb* 238U	± (%)	206Pb* 238U	± (Ma)	207Pb* 235U	± (Ma)	206Pb* 207Pb*	± (Ma)	(Ma)	(Ma)
05XI94-06	393.8	2902.2	1.4	0.091	6.963	0.009	2.996	55.4	1.7	88.6	5.9	1112.1	125.6	55.4	1.7
05XI94-07	203.8	457.0	1.4	0.089	29.839	0.008	6.165	53.2	3.3	86.2	24.7	1134.6	593.6	53.2	3.3
05XI94-08	282.0	907.9	1.3	0.113	11.284	0.008	4.559	53.7	2.4	109.0	11.7	1593.2	193.3	53.7	2.4
05XI94-09	197.0	728.6	1.4	0.115	17.207	0.009	3.124	60.3	1.9	110.6	18.0	1399.3	326.7	60.3	1.9
05XI94-10	315.2	4343.1	1.1	0.106	9.815	0.009	3.467	54.6	1.9	102.2	9.5	1432.0	175.6	54.6	1.9
05XI94-11	225.2	446.9	1.3	0.150	18.190	0.009	4.831	60.7	2.9	142.1	24.1	1883.7	318.4	60.7	2.9
05XI94-12	174.4	948.1	1.2	0.140	8.739	0.009	5.240	57.6	3.0	132.9	10.9	1847.6	126.7	57.6	3.0
05XI94-13	249.5	1285.2	1.2	0.096	10.420	0.008	2.655	53.8	1.4	92.8	9.2	1265.5	197.3	53.8	1.4
05XI94-14	335.7	229.8	1.1	0.029	71.191	0.008	9.625	53.5	5.1	29.1	20.4	-1721.0	2786.1	53.5	5.1
05XI94-15	279.3	3832.2	1.6	0.103	9.127	0.009	2.085	56.0	1.2	99.8	8.7	1333.6	172.2	56.0	1.2
05XI94-16	286.0	3412.4	1.7	0.108	8.419	0.009	5.906	56.3	3.3	104.4	8.4	1415.3	114.8	56.3	3.3
05XI94-17	297.3	1135.9	1.1	0.111	18.070	0.008	4.441	54.2	2.4	107.2	18.4	1540.3	332.0	54.2	2.4
05XI94-18	395.2	1984.8	1.5	0.094	11.233	0.009	1.855	55.4	1.0	91.1	9.8	1167.5	220.1	55.4	1.0
05XI94-19	207.1	510.0	1.2	0.114	18.272	0.009	6.000	55.8	3.3	109.8	19.0	1532.5	327.4	55.8	3.3
05XI94-20	235.7	1811.5	1.2	0.116	9.211	0.009	4.982	57.8	2.9	111.5	9.7	1498.1	146.7	57.8	2.9
05XI94-22	197.0	2523.3	1.5	0.133	7.561	0.009	2.604	56.6	1.5	126.8	9.0	1790.9	129.5	56.6	1.5
05XI94-23	247.1	3432.8	1.5	0.116	16.128	0.009	3.073	55.8	1.7	111.2	17.0	1558.9	298.9	55.8	1.7
05XI94-24	234.0	3066.2	1.2	0.108	10.277	0.008	5.196	54.4	2.8	104.5	10.2	1482.5	168.4	54.4	2.8
05XI94-25	273.7	2791.7	1.2	0.099	9.945	0.009	3.340	56.2	1.9	96.1	9.1	1250.5	183.7	56.2	1.9
05XIB41-01	312.6	337.0	1.1	0.127	8.480	0.010	3.557	66.0	2.3	121.5	9.7	1416.6	147.4	66.0	2.3
05XIB41-02	263.7	896.9	1.0	0.106	15.151	0.010	4.728	63.3	3.0	101.9	14.7	1136.5	287.8	63.3	3.0
05XIB41-03	5745.6	6369.0	1.6	0.064	1.743	0.010	1.000	63.7	0.6	63.0	1.1	35.1	34.2	63.7	0.6
05XIB41-04	152.6	564.6	0.7	0.177	14.039	0.010	7.849	65.1	5.1	165.7	21.5	2053.1	206.3	65.1	5.1
05XIB41-05	259.5	988.8	0.6	0.110	6.497	0.010	2.854	64.6	1.8	106.4	6.6	1185.1	115.4	64.6	1.8
05XIB41-06	315.0	1658.4	0.7	0.100	5.909	0.010	2.891	61.7	1.8	96.4	5.4	1072.9	103.6	61.7	1.8
05XIB41-07	8442.5	28309.0	1.6	0.063	1.501	0.010	1.064	61.7	0.7	61.9	0.9	69.2	25.2	61.7	0.7
05XIB41-08	119.3	962.7	1.0	0.198	7.717	0.010	5.585	62.4	3.5	183.0	12.9	2315.4	91.4	62.4	3.5
05XIB41-09	650.6	3356.5	0.9	0.075	4.556	0.009	1.934	60.7	1.2	73.8	3.2	521.8	90.5	60.7	1.2
05XIB41-10	347.2	1284.2	0.8	0.112	19.490	0.010	5.195	65.6	3.4	107.9	20.0	1184.7	374.4	65.6	3.4
05XIB41-11	431.1	3279.3	0.6	0.091	5.306	0.009	2.782	60.9	1.7	88.7	4.5	922.5	92.9	60.9	1.7
05XIB41-12	209.2	1245.4	1.0	0.126	21.657	0.010	5.655	63.7	3.6	120.8	24.7	1474.5	401.1	63.7	3.6
05XIB41-13	5653.3	52016.8	1.3	0.063	1.960	0.010	1.027	61.6	0.6	62.5	1.2	95.7	39.5	61.6	0.6

Table A.1: continued

Analysis	U	206Pb	U/Th	Isotopic ratios				Apparent ages (Ma)						Best age	±
	(ppm)	204Pb		207Pb* 235U	± (%)	206Pb* 238U	± (%)	206Pb* 238U	± (Ma)	207Pb* 235U	± (Ma)	206Pb* 207Pb*	± (Ma)	(Ma)	(Ma)
05XIB41-14	162.1	1585.4	0.7	0.140	7.455	0.010	4.773	63.0	3.0	133.3	9.3	1689.4	105.7	63.0	3.0
05XIB41-15	5666.2	11946.3	2.0	0.069	9.086	0.010	3.197	64.2	2.0	68.0	6.0	205.7	197.6	64.2	2.0
05XIB41-16	204.2	1413.0	1.2	0.117	8.412	0.010	3.818	61.3	2.3	112.4	9.0	1402.2	143.8	61.3	2.3
05XIB41-17	179.8	1485.5	1.2	0.136	12.537	0.009	9.190	60.2	5.5	129.9	15.3	1723.4	156.9	60.2	5.5
05XIB41-18	589.9	2668.0	0.5	0.072	6.259	0.009	3.977	60.3	2.4	70.8	4.3	442.4	107.6	60.3	2.4
05XIB41-19	191.4	2078.3	1.6	0.133	10.399	0.009	5.466	60.9	3.3	126.8	12.4	1654.0	164.3	60.9	3.3
05XIB41-20	191.9	1255.4	1.0	0.109	13.188	0.009	4.976	59.6	3.0	105.4	13.2	1325.2	237.4	59.6	3.0
05XIB41-21	1231.5	2722.2	1.9	0.067	8.171	0.010	1.458	61.6	0.9	65.5	5.2	210.4	186.6	61.6	0.9
05XIB41-22	447.7	3355.9	0.4	0.082	13.536	0.010	4.126	61.5	2.5	80.2	10.4	680.0	276.5	61.5	2.5
05XIB41-23	1167.1	1192.4	0.7	0.070	14.079	0.010	6.357	63.8	4.0	68.3	9.3	230.7	291.1	63.8	4.0
05XIB41-24	517.9	3459.1	0.6	0.074	5.970	0.009	2.712	59.0	1.6	72.1	4.2	530.0	116.6	59.0	1.6
05XIB41-25	135.2	1458.8	1.2	0.176	9.228	0.010	5.037	65.2	3.3	164.3	14.0	2032.3	137.0	65.2	3.3
05XIB48-01	2792.3	11739.4	1.7	0.062	2.789	0.010	2.356	61.4	1.4	61.1	1.7	47.8	35.7	61.4	1.4
05XIB48-02	3026.1	6993.3	1.8	0.066	3.962	0.010	1.737	63.0	1.1	65.0	2.5	138.5	83.7	63.0	1.1
05XIB48-04	3030.8	2088.1	1.3	0.083	20.373	0.010	1.916	63.3	1.2	81.2	15.9	647.0	439.9	63.3	1.2
05XIB48-05	3511.6	27839.8	1.8	0.063	1.681	0.010	1.272	61.8	0.8	62.0	1.0	70.1	26.2	61.8	0.8
05XIB48-06	557.1	7589.0	1.7	0.098	13.578	0.010	3.517	66.4	2.3	95.1	12.3	892.2	271.9	66.4	2.3
05XIB48-07	174.8	1634.5	0.8	0.131	8.750	0.010	7.258	62.9	4.5	125.1	10.3	1566.4	91.6	62.9	4.5
05XIB48-08	163.6	1910.2	0.8	0.161	11.989	0.010	4.656	63.4	2.9	151.1	16.8	1921.9	198.7	63.4	2.9
05XIB48-09	93.3	2428.8	0.8	0.245	12.855	0.010	7.833	65.5	5.1	222.6	25.7	2598.2	170.4	65.5	5.1
05XIB48-10	4325.9	4267.2	1.7	0.063	2.612	0.010	2.235	61.7	1.4	62.5	1.6	94.1	32.0	61.7	1.4
05XIB48-12	195.7	768.4	0.5	0.136	13.245	0.010	2.591	65.4	1.7	129.9	16.1	1567.8	244.4	65.4	1.7
05XIB48-13	3700.7	28325.6	1.7	0.064	1.910	0.009	1.210	60.7	0.7	62.6	1.2	137.5	34.7	60.7	0.7
05XIB48-14	136.5	1539.7	1.2	0.189	7.966	0.010	5.502	66.1	3.6	176.0	12.9	2141.1	100.8	66.1	3.6
05XIB48-15	245.7	3704.7	0.5	0.113	10.910	0.010	4.374	61.8	2.7	109.1	11.3	1325.7	194.0	61.8	2.7
05XIB48-16	278.6	370.0	0.5	0.106	11.851	0.010	3.571	61.8	2.2	102.7	11.6	1201.0	223.4	61.8	2.2
05XIB48-17	319.3	2204.1	0.7	0.097	4.301	0.010	1.467	63.2	0.9	94.1	3.9	973.8	82.5	63.2	0.9
05XIB48-18	3827.9	27889.7	1.5	0.063	2.391	0.010	1.940	61.5	1.2	62.4	1.4	96.8	33.1	61.5	1.2
05XIB48-19	3385.9	2195.3	1.6	0.066	13.536	0.010	2.480	62.4	1.5	65.3	8.6	172.1	311.8	62.4	1.5
05XIB48-20	1636.3	3909.8	0.7	0.068	3.511	0.010	1.096	61.4	0.7	67.2	2.3	278.3	76.4	61.4	0.7
05XIB48-21	2306.9	19096.7	1.7	0.066	2.476	0.010	1.626	62.3	1.0	64.7	1.6	154.7	43.7	62.3	1.0
05XIB48-22	562.5	2454.3	1.1	0.078	8.994	0.010	1.279	62.6	0.8	76.7	6.6	542.7	195.0	62.6	0.8

Table A.1: continued

Analysis	U (ppm)	206Pb/204Pb	U/Th	Isotopic ratios: 207Pb*/235U	± (%)	206Pb*/238U	± (%)	Apparent ages (Ma): 206Pb*/238U	± (Ma)	207Pb*/235U	± (Ma)	206Pb*/207Pb*	± (Ma)	Best age (Ma)	± (Ma)
05XIB48-23	5288.9	10102.1	1.4	0.063	2.245	0.010	1.908	61.7	1.2	61.7	1.3	61.5	28.2	61.7	1.2
05XIB48-24	4320.1	13749.6	1.1	0.064	1.921	0.010	1.595	62.6	1.0	63.2	1.2	88.1	25.4	62.6	1.0
05XID68-01	611.8	7935.4	1.8	0.152	1.923	0.020	1.000	130.6	1.3	143.4	2.6	361.2	37.1	130.6	1.3
05XID68-02	61.3	2097.0	1.0	0.443	9.404	0.022	7.444	139.8	10.3	372.2	29.3	2305.0	98.8	139.8	10.3
05XID68-03	187.2	5641.4	1.0	0.194	8.514	0.021	3.633	132.5	4.8	180.4	14.1	865.9	159.9	132.5	4.8
05XID68-04	490.8	14290.8	1.3	0.160	3.436	0.020	2.351	130.7	3.0	150.9	4.8	481.3	55.4	130.7	3.0
05XID68-05	245.7	3904.5	1.0	0.170	8.316	0.021	3.659	131.6	4.8	159.3	12.3	592.5	162.1	131.6	4.8
05XID68-06	1833.5	24794.7	1.9	0.129	5.950	0.020	2.973	125.7	3.7	123.5	6.9	82.3	122.4	125.7	3.7
05XID68-07	677.0	14514.3	1.1	0.146	2.876	0.020	1.936	128.8	2.5	138.8	3.7	312.9	48.4	128.8	2.5
05XID68-08	625.7	7067.6	1.2	0.137	3.661	0.020	1.518	125.6	1.9	130.4	4.5	219.4	77.1	125.6	1.9
05XID68-09	362.4	4442.7	1.6	0.164	13.646	0.020	3.909	125.7	4.9	154.0	19.5	615.6	283.4	125.7	4.9
05XID68-10	633.1	19646.7	1.5	0.152	4.003	0.020	2.566	127.9	3.3	143.5	5.4	409.2	68.7	127.9	3.3
05XID68-11	93.9	2497.0	0.9	0.271	5.757	0.020	3.745	129.8	4.8	243.7	12.5	1562.0	82.0	129.8	4.8
05XID68-12	260.8	4208.4	1.5	0.181	4.725	0.021	2.665	134.4	3.5	168.8	7.3	683.2	83.3	134.4	3.5
05XID68-13	235.5	2001.0	0.7	0.165	7.282	0.020	1.330	125.4	1.7	155.4	10.5	642.5	154.1	125.4	1.7
05XID68-14	236.6	6947.5	1.2	0.185	12.185	0.020	2.920	126.2	3.6	172.1	19.3	861.4	246.3	126.2	3.6
05XID68-15	244.7	15422.8	1.5	0.192	5.397	0.022	4.427	137.3	6.0	178.5	8.8	766.8	65.0	137.3	6.0
05XID68-16	816.4	10120.3	1.6	0.136	6.907	0.020	4.432	130.5	5.7	129.5	8.4	111.8	125.1	130.5	5.7
05XID68-17	151.4	2373.1	0.8	0.211	6.052	0.022	2.286	138.7	3.1	194.4	10.7	939.5	114.9	138.7	3.1
05XID68-18	280.1	916.7	0.5	0.216	17.281	0.020	4.282	127.7	5.4	198.9	31.2	1158.5	334.3	127.7	5.4
05XID68-19	706.2	4811.0	2.3	0.150	6.291	0.021	1.445	131.0	1.9	141.9	8.3	328.4	139.1	131.0	1.9
05XID68-20	857.7	5815.0	1.5	0.145	11.337	0.021	8.760	131.4	11.4	137.5	14.6	244.3	166.0	131.4	11.4
05XID68-21	279.1	9177.8	1.1	0.188	9.212	0.020	3.631	128.5	4.6	174.5	14.8	854.8	176.1	128.5	4.6
05XID68-22	443.6	10537.8	1.5	0.159	8.059	0.020	3.586	128.8	4.6	149.8	11.2	496.7	159.2	128.8	4.6
05XID68-23	810.4	17879.9	1.2	0.144	4.005	0.020	2.425	128.2	3.1	136.5	5.1	282.6	73.0	128.2	3.1
05XID68-24	772.4	8466.4	1.9	0.165	20.837	0.020	5.625	128.0	7.1	155.1	30.0	592.4	439.0	128.0	7.1
05XIE82-02	1344.7	3738.4	0.9	0.043	10.408	0.006	6.029	38.1	2.3	42.5	4.3	302.2	193.7	38.1	2.3
05XIE82-03	1303.2	1921.5	2.3	0.022	11.448	0.002	1.977	13.7	0.3	22.2	2.5	1078.4	227.0	13.7	0.3
05XIE82-05	271.4	1107.5	1.5	0.107	9.535	0.007	6.404	48.0	3.1	102.9	9.3	1686.2	130.5	48.0	3.1
05XIE82-06	640.1	412.6	1.1	0.066	3.887	0.007	2.682	46.1	1.2	65.4	2.5	842.7	58.5	46.1	1.2
05XIE82-07	990.1	2180.9	0.8	0.055	4.589	0.006	1.924	41.6	0.8	54.0	2.4	646.7	89.5	41.6	0.8

Table A.1: continued

				Isotopic ratios				Apparent ages (Ma)							
Analysis	U (ppm)	206Pb 204Pb	U/Th	207Pb* 235U	± (%)	206Pb* 238U	± (%)	206Pb* 238U	± (Ma)	207Pb* 235U	± (Ma)	206Pb* 207Pb*	± (Ma)	Best age (Ma)	± (Ma)
05XIE82-08	1537.1	11261.0	1.7	0.053	3.841	0.007	2.506	44.3	1.1	52.1	1.9	423.9	64.9	44.3	1.1
05XIE82-09	1256.5	3785.9	1.6	0.025	8.104	0.002	3.493	14.2	0.5	25.1	2.0	1247.2	143.4	14.2	0.5
05XIE82-10	526.3	22816.5	1.2	0.042	10.586	0.002	5.467	15.2	0.8	42.0	4.4	2094.8	159.6	15.2	0.8
05XIE82-13	442.6	5145.3	1.0	0.085	5.182	0.007	2.184	47.6	1.0	82.6	4.1	1267.2	91.8	47.6	1.0
05XIE82-15	1093.3	2199.5	1.7	0.027	9.909	0.002	4.740	14.4	0.7	26.7	2.6	1348.8	168.3	14.4	0.7
05XIE82-16	772.0	3415.4	1.7	0.060	8.658	0.006	6.387	40.3	2.6	58.7	4.9	895.4	120.7	40.3	2.6
05XIE82-18	619.8	1232.5	1.3	0.038	7.515	0.002	5.250	15.5	0.8	37.6	2.8	1859.5	97.2	15.5	0.8
05XIE82-19	480.4	1098.8	1.1	0.069	17.384	0.008	8.100	48.7	3.9	67.9	11.4	811.2	323.5	48.7	3.9
05XIE82-20	705.9	840.3	3.7	0.031	14.462	0.002	5.006	14.1	0.7	31.1	4.4	1679.9	251.8	14.1	0.7
05XIE82-23	380.9	1442.1	1.2	0.053	10.928	0.003	8.708	17.1	1.5	52.7	5.6	2293.1	113.7	17.1	1.5
05XIE82-24	675.1	2690.0	2.0	0.056	8.994	0.005	8.255	30.9	2.5	55.1	4.8	1295.6	69.4	30.9	2.5
05XIE82-25	197.6	786.2	1.1	0.112	16.377	0.007	9.138	47.2	4.3	107.7	16.7	1806.7	248.2	47.2	4.3
05XIE82-26	558.5	2290.1	1.1	0.070	13.919	0.008	3.599	49.2	1.8	68.6	9.2	809.6	282.5	49.2	1.8
05XIE82-27	8373.3	12454.0	8.2	0.016	5.712	0.002	2.983	13.8	0.4	16.0	0.9	367.9	109.8	13.8	0.4
05XIE82-28	1496.4	3737.7	1.6	0.022	8.264	0.002	3.173	14.4	0.5	22.0	1.8	968.2	155.9	14.4	0.5
05XIE87-01	400.0	2113.7	4.6	0.047	11.926	0.002	5.659	13.4	0.8	47.1	5.5	2507.4	177.1	13.4	0.8
05XIE87-02	275.2	549.1	5.4	0.053	12.820	0.002	8.711	14.6	1.3	52.1	6.5	2541.3	158.1	14.6	1.3
05XIE87-03	1796.7	12287.7	16.6	0.036	19.895	0.004	2.728	25.5	0.7	35.5	6.9	780.5	418.0	25.5	0.7
05XIE87-04	837.9	1448.0	2.8	0.030	12.554	0.003	4.934	19.6	1.0	29.6	3.7	942.3	237.3	19.6	1.0
05XIE87-07	1030.2	4569.2	2.2	0.021	9.762	0.002	2.666	13.2	0.4	20.8	2.0	1022.2	190.5	13.2	0.4
05XIE87-08	1233.1	6636.5	3.7	0.042	10.007	0.005	9.742	33.6	3.3	41.5	4.1	524.5	50.1	33.6	3.3
05XIE87-09	358.5	4650.7	0.4	0.071	6.372	0.006	4.366	38.2	1.7	69.8	4.3	1355.7	89.6	38.2	1.7
05XIE87-10	1284.8	18562.5	1.3	0.045	4.790	0.006	3.362	39.6	1.3	44.5	2.1	319.3	77.6	39.6	1.3
05XIE87-12	1210.3	1677.9	3.4	0.019	5.597	0.002	2.890	12.5	0.4	19.6	1.1	1007.1	97.3	12.5	0.4
05XIE87-13	1266.9	11283.7	3.0	0.070	3.452	0.010	1.565	61.6	1.0	68.5	2.3	316.6	70.0	61.6	1.0
05XIE87-14	538.9	1741.3	1.5	0.055	10.304	0.007	2.399	44.8	1.1	54.0	5.4	482.6	221.8	44.8	1.1
05XIE87-15	915.9	1628.5	2.4	0.024	13.692	0.002	8.550	12.5	1.1	23.8	3.2	1404.2	205.4	12.5	1.1
05XIE87-16	1257.2	3446.0	3.4	0.018	6.738	0.002	4.714	13.2	0.6	18.6	1.2	790.5	101.1	13.2	0.6
05XIE87-17	363.2	948.3	1.3	0.046	22.624	0.002	8.390	14.5	1.2	45.2	10.0	2302.0	365.3	14.5	1.2
05XIE87-18	743.8	678.1	2.6	0.021	21.490	0.002	5.441	13.0	0.7	20.7	4.4	1041.7	424.0	13.0	0.7
05XIE87-19	675.4	1340.7	2.4	0.027	9.222	0.002	4.766	12.8	0.6	27.5	2.5	1625.9	147.1	12.8	0.6
05XIE87-20	180.3	1215.1	1.2	0.096	9.875	0.007	4.859	44.1	2.1	93.3	8.8	1656.6	159.5	44.1	2.1

Table A.2: Overview of complied literature data from the Lhasa terrane and Himalayas

Sample	Terrane	Location	Lithology	Latitude (dd)	Longitude (dd)	Quadrant	Age (Ma)
NDG-01	Lhasa Terrane		Gabbro	32.8374	78.8555	Q2	122.0
NDG-02	Lhasa Terrane		Gabbro	32.8541	78.8210	Q2	122.0
NDG-03	Lhasa Terrane		Gabbro	32.8678	78.8067	Q2	122.0
NDG-04	Lhasa Terrane		Gabbro	32.8773	78.7942	Q2	122.0
NDG-05	Lhasa Terrane		Gabbro	32.8922	78.7823	Q2	122.0
NDG-06	Lhasa Terrane		Gabbro	32.9296	78.7502	Q2	122.0
NDG-07	Lhasa Terrane		Gabbro	32.9409	78.7199	Q2	122.0
NDG-08	Lhasa Terrane		Gabbro	32.9576	78.6871	Q2	122.0
NDG-09	Lhasa Terrane		Gabbro	32.9832	78.6526	Q2	122.0
NDV-01	Lhasa Terrane		Volcanic rock (mafic)	32.8844	78.8382	Q2	122.0
NDV-04	Lhasa Terrane		Volcanic rock (mafic)	32.9142	78.8073	Q2	122.0
NDV-05	Lhasa Terrane		Volcanic rock (mafic)	32.9594	78.7276	Q2	122.0
NDV-1S	Lhasa Terrane		Volcanic rock (mafic)	32.9968	78.6717	Q2	122.0
NDV-2S	Lhasa Terrane		Volcanic rock (mafic)	33.0230	78.6384	Q2	122.0
NDV-3S	Lhasa Terrane		Volcanic rock (mafic)	33.0498	78.6175	Q2	122.0
NDV-4S	Lhasa Terrane		Volcanic rock (mafic)	33.0718	78.6027	Q2	122.0
NN-13	Lhasa Terrane		Gabbro	33.2074	78.4516	Q2	122.0
NN-14	Lhasa Terrane		Gabbro	33.1848	78.4682	Q2	122.0
NN-15	Lhasa Terrane		Gabbro	33.1610	78.4879	Q2	122.0
NN-19	Lhasa Terrane		Gabbro	33.1426	78.5063	Q2	122.0
NV-01	Lhasa Terrane		Volcanic rock (felsic)	32.9385	78.8103	Q2	122.0
NV-02	Lhasa Terrane		Volcanic rock (felsic)	32.9653	78.7722	Q2	122.0
NV-03	Lhasa Terrane		Volcanic rock (felsic)	32.9939	78.7127	Q2	122.0
NV-04	Lhasa Terrane		Volcanic rock (felsic)	33.0563	78.6574	Q2	122.0
NV-05	Lhasa Terrane		Volcanic rock (felsic)	33.0700	78.6395	Q2	122.0
NV-06	Lhasa Terrane		Volcanic rock (felsic)	33.0867	78.6259	Q2	122.0
NV-07	Lhasa Terrane		Volcanic rock (felsic)	33.1158	78.5866	Q2	122.0
NV-08	Lhasa Terrane		Volcanic rock (felsic)	33.1283	78.5551	Q2	122.0
NV-09	Lhasa Terrane		Volcanic rock (felsic)	33.1670	78.5093	Q2	122.0
NV-10	Lhasa Terrane		Volcanic rock (felsic)	33.1908	78.4867	Q2	122.0
NV-11	Lhasa Terrane		Volcanic rock (felsic)				122.0
93BG1	Himalayas	Zanskar	Leucogranite (Tur)	33.5245	76.9718	Q2	19.5
93G18	Himalayas	Zanskar	Leucogranite (Tur)	33.5245	76.9718	Q2	19.5
93G2	Himalayas	Zanskar	Leucogranite (Bt)	33.5245	76.9718	Q2	19.5

Sample data continued

Sample	87Sr/86Sr(i)	eNd(t)	206Pb/ 204Pb(t)	207Pb/ 204Pb(t)	208Pb/ 204Pb(t)	*UPR	**ADK	Source
NDG-01						No	No	Ahmad et al. (2008)
NDG-02						No	No	Ahmad et al. (2008)
NDG-03						No	No	Ahmad et al. (2008)
NDG-04						No	No	Ahmad et al. (2008)
NDG-05	0.7043	7.4				No	No	Ahmad et al. (2008)
NDG-06	0.7044	7.6				No	No	Ahmad et al. (2008)
NDG-07	0.7055	7.6				No	No	Ahmad et al. (2008)
NDG-08	0.7044	9.8				No	No	Ahmad et al. (2008)
NDG-09	0.7047	7.2				No	No	Ahmad et al. (2008)
NDV-01						No	No	Ahmad et al. (2008)
NDV-04						No	No	Ahmad et al. (2008)
NDV-05	0.7056	7.7				No	No	Ahmad et al. (2008)
NDV-1S	0.7054	8.0				No	No	Ahmad et al. (2008)
NDV-2S						No	No	Ahmad et al. (2008)
NDV-3S						No	No	Ahmad et al. (2008)
NDV-4S						No	No	Ahmad et al. (2008)
NN-13	0.7031	7.2				No	No	Ahmad et al. (2008)
NN-14	0.7034	7.4				No	No	Ahmad et al. (2008)
NN-15	0.7034	7.5				No	No	Ahmad et al. (2008)
NN-19	0.7034	7.1				No	No	Ahmad et al. (2008)
NV-01						No	No	Ahmad et al. (2008)
NV-02	0.7060	8.0				No	No	Ahmad et al. (2008)
NV-03						No	No	Ahmad et al. (2008)
NV-04	0.7063	8.0				No	No	Ahmad et al. (2008)
NV-05	0.7064	7.6				No	No	Ahmad et al. (2008)
NV-06						No	No	Ahmad et al. (2008)
NV-07						No	No	Ahmad et al. (2008)
NV-08	0.7074	2.4				No	No	Ahmad et al. (2008)
NV-09	0.7065	7.7				No	No	Ahmad et al. (2008)
NV-10	0.7064	7.7				No	No	Ahmad et al. (2008)
NV-11						No	No	Ahmad et al. (2008)
93BG1						No	No	Ayres et al. (1997)
93G18						No	No	Ayres et al. (1997)
93G2						No	No	Ayres et al. (1997)

Table A.2: continued

Sample	Terrane	Location	Lithology	Latitude (dd)	Longitude (dd)	Quadrant	Age (Ma)
93G8	Himalayas	Zanskar	Leucogranite (Bt)	33.5245	76.9718	Q2	19.5
93ZP3	Himalayas	Zanskar	Leucogranite (Tur)	33.5245	76.9718	Q2	19.5
MA88.1	Himalayas	Zanskar	Leucogranite (Bt)	33.5245	76.9718	Q2	19.5
MA97.3	Himalayas	Zanskar	Leucogranite (Tur)	33.5245	76.9718	Q2	19.5
MN14	Himalayas	Zanskar	Leucogranite (Bt)	33.5245	76.9718	Q2	19.5
PAN2	Himalayas	Zanskar	Metasediment	33.5245	76.9718	Q2	500.0
PAN3	Himalayas	Zanskar	Metasediment	33.5245	76.9718	Q2	500.0
BC-01	Lhasa Terrane		Granite	29.6723	96.2623	Q6	117.8
BC-02	Lhasa Terrane		Granite	29.7371	96.1212	Q6	113.0
BC-03	Lhasa Terrane		Granite	29.8111	95.8830	Q6	115.8
BM-02	Lhasa Terrane		Granite	29.8042	95.6933	Q6	115.3
BM-03	Lhasa Terrane		Granite	29.7741	95.6956	Q6	63.1
BT-07-02	Lhasa Terrane		Granite	29.9661	94.8329	Q6	40.0
BT-17-01	Lhasa Terrane		Granite	30.0493	95.2331	Q6	21.0
BT-19	Lhasa Terrane		Granite	29.8967	93.7575	Q6	16.4
BT-20E	Lhasa Terrane		Granite	29.8643	94.1206	Q6	49.5
BT-33	Lhasa Terrane		Granite	30.1858	94.9440	Q6	21.0
BT-4-01	Lhasa Terrane		Granite	29.6030	94.4791	Q6	26.0
IG-15a	Himalayas		Granite	29.5451	94.9023	Q6	6.2
IG-16	Himalayas		Granite	29.4226	94.9185	Q6	4.3
IG-18	Himalayas		Granite	29.4572	94.9347	Q6	2.9
IG-2d	Himalayas		Granite	29.7186	94.9255	Q6	14.0
IG-4	Himalayas		Granite	29.6908	94.9093	Q6	3.0
IG-6b	Himalayas		Granite	29.6376	94.9185	Q6	9.7
NB-120-02	Lhasa Terrane		Granite	29.8065	94.3172	Q6	52.1
NB-159-02	Lhasa Terrane		Granite	29.7463	94.6965	Q6	65.7
NB-35-02	Lhasa Terrane		Granite	30.0031	94.7196	Q6	
158a	Lhasa Terrane		Xenolith (micaceous)	29.3306	87.0109	Q4	14.4
158f	Lhasa Terrane		Granulite (mafic)	29.3306	87.0109	Q4	
158g	Lhasa Terrane		Granulite (felsic)	29.3306	87.0109	Q4	16.8
158m	Lhasa Terrane		Xenolith (ultramafic)	29.3306	87.0109	Q4	
158o	Lhasa Terrane		Granulite (mafic)	29.3306	87.0109	Q4	
158p	Lhasa Terrane		Xenolith (ultramafic)	29.3306	87.0109	Q4	15.6
DG01-2	Lhasa Terrane	Xainza	Rhyolite	31.3341	88.9174	Q4	114.0

Sample data continued

Sample	87Sr/86Sr(i)	eNd(t)	206Pb/ 204Pb(t)	207Pb/ 204Pb(t)	208Pb/ 204Pb(t)	*UPR	**ADK	Source
93G8						No	No	Ayres et al. (1997)
93ZP3						No	No	Ayres et al. (1997)
MA88.1						No	No	Ayres et al. (1997)
MA97.3						No	No	Ayres et al. (1997)
MN14						No	No	Ayres et al. (1997)
PAN2						No	No	Ayres et al. (1997)
PAN3						N.D.	N.D.	Ayres et al. (1997)
BC-01						N.D.	N.D.	Booth et al. (2004)
BC-02						N.D.	N.D.	Booth et al. (2004)
BC-03						N.D.	N.D.	Booth et al. (2004)
BM-02						N.D.	N.D.	Booth et al. (2004)
BM-03						N.D.	N.D.	Booth et al. (2004)
BT-07-02						N.D.	N.D.	Booth et al. (2004)
BT-17-01						N.D.	N.D.	Booth et al. (2004)
BT-19						N.D.	N.D.	Booth et al. (2004)
BT-20E						N.D.	N.D.	Booth et al. (2004)
BT-33						N.D.	N.D.	Booth et al. (2004)
BT-4-01						N.D.	N.D.	Booth et al. (2004)
IG-15a						N.D.	N.D.	Booth et al. (2004)
IG-16						N.D.	N.D.	Booth et al. (2004)
IG-18						N.D.	N.D.	Booth et al. (2004)
IG-2d						N.D.	N.D.	Booth et al. (2004)
IG-4						N.D.	N.D.	Booth et al. (2004)
IG-6b						N.D.	N.D.	Booth et al. (2004)
NB-120-02						N.D.	N.D.	Booth et al. (2004)
NB-159-02						N.D.	N.D.	Booth et al. (2004)
NB-35-02						N.D.	N.D.	Booth et al. (2004)
158a						Yes	No	Chan et al. (2009)
158f						No	No	Chan et al. (2009)
158g						No	No	Chan et al. (2009)
158m						No	No	Chan et al. (2009)
158o						No	No	Chan et al. (2009)
158p						No	No	Chan et al. (2009)
DG01-2						No	No	Chen et al. (2013)

Table A.2: continued

Sample	Terrane	Location	Lithology	Latitude (dd)	Longitude (dd)	Quadrant	Age (Ma)
DG02-1	Lhasa Terrane	Xainza	Rhyolite	31.3303	88.9134	Q4	114.0
DG03-1	Lhasa Terrane	Xainza	Rhyolite	31.3202	88.9032	Q4	114.0
GRC03-1	Lhasa Terrane	Xainza	Basalt	31.2220	88.1080	Q4	114.0
SZ01-2	Lhasa Terrane	Xainza	Dacite	30.7624	88.9205	Q4	114.0
SZ02-1	Lhasa Terrane	Xainza	Andesite	30.7628	88.9105	Q4	114.0
SZ03-1	Lhasa Terrane	Xainza	Andesite	30.7652	88.9152	Q4	114.0
SZ04-1	Lhasa Terrane	Xainza	Andesite	30.7600	88.9168	Q4	114.0
SZ04-2	Lhasa Terrane	Xainza	Andesite	30.7567	88.9206	Q4	114.0
SZ05-1	Lhasa Terrane	Xainza	Dacite	30.7654	88.9070	Q4	114.0
SZ05-2	Lhasa Terrane	Xainza	Dacite	30.7729	88.9059	Q4	114.0
SZ05-2R	Lhasa Terrane	Xainza	Dacite	30.7683	88.9104	Q4	114.0
SZ09-1	Lhasa Terrane	Xainza	Basalt	30.8847	88.6585	Q4	114.0
SZ10-2	Lhasa Terrane	Xainza	Dacite	30.8987	88.6561	Q4	114.0
SZ11-1	Lhasa Terrane	Xainza	Basalt	30.8919	88.6562	Q4	114.0
SZ12-1	Lhasa Terrane	Xainza	Basalt	30.9150	88.6450	Q4	114.0
SZ12-2	Lhasa Terrane	Xainza	Basalt	30.9111	88.6562	Q4	114.0
SZ12-3	Lhasa Terrane	Xainza	Basalt	30.9080	88.6480	Q4	114.0
ET014C	Lhasa Terrane	Bomi-Ranwu	Granite	30.1100	95.0700	Q6	58.7
ET103B	Lhasa Terrane	Bomi-Ranwu	Orthogneiss (granitic)	29.9542	95.3845	Q6	118.6
ET104A	Lhasa Terrane	Bomi-Ranwu	Granite	29.5075	96.6044	Q6	114.8
ET106A	Lhasa Terrane	Bomi-Ranwu	Granite	29.3855	96.8690	Q6	122.5
ET113B	Lhasa Terrane	Chayu-Shama	Granite	28.5616	97.0852	Q6	59.1
ET115E	Lhasa Terrane	Chayu-Shama	Orthogneiss (granitic)	28.5991	97.2496	Q6	133.1
ET116A	Lhasa Terrane	Chayu-Shama	Granite	28.6724	97.4698	Q6	132.6
ET117B	Lhasa Terrane	Bomi-Ranwu	Granite	29.3213	97.1343	Q6	116.9
ET120B	Lhasa Terrane	Bomi-Ranwu	Granite	29.7417	96.0209	Q6	109.0
ET122E	Lhasa Terrane	Bomi-Ranwu	Granite	29.7649	95.6971	Q6	66.1
ET125B	Lhasa Terrane	Bomi-Ranwu	Orthogneiss (granitic)	29.7565	95.7163	Q6	125.1
ET207A	Lhasa Terrane	Chayu-Shama	Granite	28.5639	97.0865	Q6	56.5
ET210A	Lhasa Terrane	Chayu-Shama	Orthogneiss (granitic)	28.6191	97.3661	Q6	130.4
ET215A	Lhasa Terrane	Chayu-Shama	Granite	28.9849	97.4034	Q6	132.9
ET218A	Lhasa Terrane	Bomi-Ranwu	Granite	29.3855	96.8683	Q6	122.5
ET219A	Lhasa Terrane	Bomi-Ranwu	Granite	29.3922	96.8515	Q6	125.0
ET223A	Lhasa Terrane	Basu-Ranwu	Granite	29.8690	96.6869	Q6	197.7

Sample data continued

Sample	87Sr/86Sr(i)	eNd(t)	206Pb/ 204Pb(t)	207Pb/ 204Pb(t)	208Pb/ 204Pb(t)	*UPR	**ADK	Source
DG02-1						No	No	Chen et al. (2013)
DG03-1						No	No	Chen et al. (2013)
GRC03-1		-3.5				No	No	Chen et al. (2013)
SZ01-2						No	No	Chen et al. (2013)
SZ02-1	0.7209	-13.6				No	No	Chen et al. (2013)
SZ03-1						No	No	Chen et al. (2013)
SZ04-1	0.7218	-13.0				No	No	Chen et al. (2013)
SZ04-2						No	No	Chen et al. (2013)
SZ05-1						No	No	Chen et al. (2013)
SZ05-2	0.7123	-9.4				No	No	Chen et al. (2013)
SZ05-2R						No	No	Chen et al. (2013)
SZ09-1	0.7182	-2.3				No	No	Chen et al. (2013)
SZ10-2						No	No	Chen et al. (2013)
SZ11-1	0.7083	-0.1				No	No	Chen et al. (2013)
SZ12-1	0.7077	0.6				No	No	Chen et al. (2013)
SZ12-2	0.7070	-0.9				No	No	Chen et al. (2013)
SZ12-3	0.7088	-0.1				No	No	Chen et al. (2013)
ET014C						N.D.	N.D.	Chiu et al. (2009)
ET103B						N.D.	N.D.	Chiu et al. (2009)
ET104A						N.D.	N.D.	Chiu et al. (2009)
ET106A						N.D.	N.D.	Chiu et al. (2009)
ET113B						N.D.	N.D.	Chiu et al. (2009)
ET115E						N.D.	N.D.	Chiu et al. (2009)
ET116A						N.D.	N.D.	Chiu et al. (2009)
ET117B						N.D.	N.D.	Chiu et al. (2009)
ET120B						N.D.	N.D.	Chiu et al. (2009)
ET122E						N.D.	N.D.	Chiu et al. (2009)
ET125B						N.D.	N.D.	Chiu et al. (2009)
ET207A						N.D.	N.D.	Chiu et al. (2009)
ET210A						N.D.	N.D.	Chiu et al. (2009)
ET215A						N.D.	N.D.	Chiu et al. (2009)
ET218A						N.D.	N.D.	Chiu et al. (2009)
ET219A						N.D.	N.D.	Chiu et al. (2009)
ET223A						N.D.	N.D.	Chiu et al. (2009)

Table A.2: continued

Sample	Terrane	Location	Lithology	Latitude (dd)	Longitude (dd)	Quadrant	Age (Ma)
ET224A	Lhasa Terrane	Basu-Ranwu	Granite	29.9001	96.6820	Q6	130.0
ET225A	Lhasa Terrane	Basu-Ranwu	Granodiorite	30.0058	96.6893	Q6	124.0
ET226A	Lhasa Terrane	Basu-Ranwu	Granodiorite	30.0321	96.7252	Q6	125.3
ET227A	Lhasa Terrane	Basu-Ranwu	Granite	30.0383	96.7868	Q6	122.7
ET227C	Lhasa Terrane	Basu-Ranwu	Andesite	30.0383	96.7868	Q6	127.6
ET234A	Lhasa Terrane	Basu-Ranwu	Granite	29.7649	96.7096	Q6	114.8
ET234C	Lhasa Terrane	Basu-Ranwu	Enclave	29.7649	96.7096	Q6	115.7
ET023	Lhasa Terrane	Jiama	Adakite (plug)	29.6100	91.6000	Q5	17.0
ET025B	Lhasa Terrane	Jiama	Adakite (plug)	26.6900	91.7500	Q5	15.0
ET025E	Lhasa Terrane	Jiama	Adakite (dike)	26.6900	91.7500	Q5	13.2
ET026C	Lhasa Terrane	Nanmu	Adakite (plug)	29.4800	90.8700	Q5	16.6
ET026D	Lhasa Terrane	Nanmu	Adakite (dike)	29.4800	90.8700	Q5	16.4
T016	Lhasa Terrane	Linzhi	Adakite (plug)	29.5700	94.5800	Q6	26.2
T041D	Lhasa Terrane	Xigaze	Adakite (dike)	29.3600	88.8100	Q4	15.0
T065C	Lhasa Terrane	Majiang	Adakite (dike)	29.7400	89.8800	Q5	13.0
T081	Lhasa Terrane	Xigaze	Adakite (dike)	29.3200	88.8500	Q4	18.4
ST107A	Lhasa Terrane	Yaja-Zedong	Adakite	29.2700	91.8900	Q5	30.3
ST107B	Lhasa Terrane	Yaja-Zedong	Adakite	29.2700	91.8900	Q5	31.0
T060B	Lhasa Terrane		Adakite	29.5200	90.0400	Q5	15.1
Coulon_T380	Lhasa Terrane	Gyantso	Andesite	31.7733	90.8708	Q5	
T248	Lhasa Terrane	Linzhu	Andesite	30.0974	91.2090	Q5	49.2
T286	Lhasa Terrane	Yangbajain	Trachyte	30.2937	90.8337	Q5	50.0
T301	Lhasa Terrane	NE Maquiang	Ignimbrite	30.0428	90.2446	Q5	12.2
T31	Lhasa Terrane	NW Lhasa	Dike (andesitic)	29.9796	90.7486	Q5	90.0
T323	Lhasa Terrane	SW Maquiang	Ignimbrite	29.9294	90.0591	Q5	10.5
T324	Lhasa Terrane	SW Maquiang	Andesite	29.9359	90.0700	Q5	10.1
T328	Lhasa Terrane	SW Maquiang	Andesite	29.9425	90.0853	Q5	14.4
T398	Lhasa Terrane	E Gyantso	Dacite	31.3936	91.0017	Q5	85.0
T468	Lhasa Terrane	Daqin	Rhyolite	30.5948	90.1224	Q5	74.3
T486	Lhasa Terrane	Barda	Rhyolite	31.6140	91.4359	Q5	112.3
T492	Lhasa Terrane	Barda	Dacite	31.6183	91.4621	Q5	89.0
T54	Lhasa Terrane	Nagqu	Andesite	31.4874	92.0457	Q5	101.5
T8284	Lhasa Terrane	Xainxa	Rhyolite	30.9722	88.6844	Q4	114.4
AY06-29-06-8A1	Himalayas	Qiongjie	Sandstone	28.9713	91.6595	Q5	210.0

Sample data continued

Sample	87Sr/86Sr(i)	eNd(t)	206Pb/ 204Pb(t)	207Pb/ 204Pb(t)	208Pb/ 204Pb(t)	*UPR	**ADK	Source
ET224A						N.D.	N.D.	Chiu et al. (2009)
ET225A						N.D.	N.D.	Chiu et al. (2009)
ET226A						N.D.	N.D.	Chiu et al. (2009)
ET227A						N.D.	N.D.	Chiu et al. (2009)
ET227C						N.D.	N.D.	Chiu et al. (2009)
ET234A						N.D.	N.D.	Chiu et al. (2009)
ET234C						N.D.	N.D.	Chiu et al. (2009)
ET023						No	Yes	Chung et al. (2003)
ET025B						No	No	Chung et al. (2003)
ET025E						No	Yes	Chung et al. (2003)
ET026C						No	Yes	Chung et al. (2003)
ET026D						No	Yes	Chung et al. (2003)
T016						No	Yes	Chung et al. (2003)
T041D						No	No	Chung et al. (2003)
T065C						No	Yes	Chung et al. (2003)
T081						No	Yes	Chung et al. (2003)
ST107A						N.D.	N.D.	Chung et al. (2009)
ST107B						N.D.	N.D.	Chung et al. (2009)
T060B						N.D.	N.D.	Chung et al. (2009)
Coulon_T380						N.D.	N.D.	Coulon et al. (1986)
T248						N.D.	N.D.	Coulon et al. (1986)
T286						N.D.	N.D.	Coulon et al. (1986)
T301						N.D.	N.D.	Coulon et al. (1986)
T31						N.D.	N.D.	Coulon et al. (1986)
T323						N.D.	N.D.	Coulon et al. (1986)
T324						N.D.	N.D.	Coulon et al. (1986)
T328						N.D.	N.D.	Coulon et al. (1986)
T398						N.D.	N.D.	Coulon et al. (1986)
T468						N.D.	N.D.	Coulon et al. (1986)
T486						N.D.	N.D.	Coulon et al. (1986)
T492						N.D.	N.D.	Coulon et al. (1986)
T54						N.D.	N.D.	Coulon et al. (1986)
T8284						N.D.	N.D.	Coulon et al. (1986)
AY06-29-06-8A1		-6.3				N.D.	N.D.	Dai et al. (2008)

Table A.2: continued

Sample	Terrane	Location	Lithology	Latitude (dd)	Longitude (dd)	Quadrant	Age (Ma)
AY06-29-06-8B1	Himalayas	Qiongjie	Siltstone	28.9713	91.6595	Q5	210.0
AY06-29-06-9A2	Himalayas	Qiongjie	Phyllite	28.9500	91.6488	Q5	210.0
AY07-01-06-23	Himalayas	Lhakang	Slate	28.2601	91.2283	Q5	130.0
AY07-01-06-5A4	Himalayas	Lhakang	Metapelite	28.1734	91.2361	Q5	130.0
AY07-01-06-5B4	Himalayas	Lhakang	Quartz Arenite	28.1734	91.2361	Q5	130.0
AY07-02-06-45	Himalayas	Lhakang	Phyllite	28.1212	91.0968	Q5	130.0
AY07-02-06-6A6	Himalayas	Lhakang	Phyllite	28.2191	91.0085	Q5	130.0
AY07-02-06-6B6	Himalayas	Lhakang	Phyllite	28.2191	91.0085	Q5	130.0
AY07-03-06-17	Himalayas	Rangkazi	Metagreywacke	29.0928	90.3934	Q5	210.0
202-20	Lhasa Terrane	Nyanqentanglha	Granitoid	30.0758	90.5172	Q5	52.8
202-22	Lhasa Terrane	Nyanqentanglha	Granitoid	30.0758	90.5172	Q5	53.9
202-33	Lhasa Terrane	Nyanqentanglha	Granitoid	30.0758	90.5172	Q5	51.8
99-5-11-1a	Lhasa Terrane	Nyanqentanglha	Granitoid	30.2502	90.3115	Q5	87.9
99-5-11-2	Lhasa Terrane	Nyanqentanglha	Granitoid	30.2302	90.3434	Q5	11.9
99-5-16-2a	Lhasa Terrane	Nyanqentanglha	Granitoid	30.3744	90.7614	Q5	
99-5-2-1a	Lhasa Terrane	Nyanqentanglha	Granitoid				53.9
99-5-4-2	Lhasa Terrane	Nyanqentanglha	Granitoid	29.9695	90.2499	Q5	21.7
99-5-4-3	Lhasa Terrane	Nyanqentanglha	Granitoid	29.9766	90.2519	Q5	
99-5-5-4c	Lhasa Terrane	Nyanqentanglha					
99-5-5-4d	Lhasa Terrane	Nyanqentanglha	Granitoid	29.9055	90.0980	Q5	54.8
99-5-7-2a	Lhasa Terrane	Nyanqentanglha	Granitoid	29.9285	90.1416	Q5	
99-5-7-2b	Lhasa Terrane	Nyanqentanglha	Granitoid	29.9285	90.1416	Q5	
99-5-7-3b	Lhasa Terrane	Nyanqentanglha	Granitoid	29.9310	90.1303	Q5	130.0
99-5-9-3	Lhasa Terrane	Nyanqentanglha	Granitoid	30.1465	90.4768	Q5	13.0
99-5-9-4	Lhasa Terrane	Nyanqentanglha	Granitoid	30.1523	90.4571	Q5	
99-5-9-4a	Lhasa Terrane	Nyanqentanglha	Granitoid	30.1523	90.4571	Q5	60.9
99-7-26-1	Lhasa Terrane	Nyanqentanglha	Granitoid	30.5303	90.7649	Q5	
99-7-26-1b	Lhasa Terrane	Nyanqentanglha	Granitoid	30.5303	90.7649	Q5	212.7
99-7-26-2	Lhasa Terrane	Nyanqentanglha	Granitoid	30.5393	90.7678	Q5	
99-7-26-3	Lhasa Terrane	Nyanqentanglha	Granitoid	30.5564	90.8124	Q5	
99-7-27-1	Lhasa Terrane	Nyanqentanglha	Granitoid	30.6010	90.7656	Q5	
99-7-27-2	Lhasa Terrane	Nyanqentanglha	Granitoid	30.5852	90.7630	Q5	
99-7-27-3c	Lhasa Terrane	Nyanqentanglha	dike				
99-7-27-4	Lhasa Terrane	Nyanqentanglha	Granitoid	30.5929	90.7540	Q5	

Sample data continued

Sample	87Sr/86Sr(i)	eNd(t)	206Pb/204Pb(t)	207Pb/204Pb(t)	208Pb/204Pb(t)	*UPR	**ADK	Source
AY06-29-06-8B1		-5.8				N.D.	N.D.	Dai et al. (2008)
AY06-29-06-9A2		-7.3				N.D.	N.D.	Dai et al. (2008)
AY07-01-06-23		-15.4				N.D.	N.D.	Dai et al. (2008)
AY07-01-06-5A4		-15.2				N.D.	N.D.	Dai et al. (2008)
AY07-01-06-5B4		-16.1				N.D.	N.D.	Dai et al. (2008)
AY07-02-06-45		-6.4				N.D.	N.D.	Dai et al. (2008)
AY07-02-06-6A6		-16.6				N.D.	N.D.	Dai et al. (2008)
AY07-02-06-6B6		-15.3				N.D.	N.D.	Dai et al. (2008)
AY07-03-06-17		-3.5				N.D.	N.D.	Dai et al. (2008)
202-20						No	No	D'Andrea Kapp et al. (2005)
202-22						No	No	D'Andrea Kapp et al. (2005)
202-33						No	No	D'Andrea Kapp et al. (2005)
99-5-11-1a	0.7072	-5.7				No	Yes	D'Andrea Kapp et al. (2005)
99-5-11-2	0.7089					No	No	D'Andrea Kapp et al. (2005)
99-5-16-2a						N.D.	N.D.	D'Andrea Kapp et al. (2005)
99-5-2-1a	0.7071	-4.1				N.D.	N.D.	D'Andrea Kapp et al. (2005)
99-5-4-2	0.7091					No	No	D'Andrea Kapp et al. (2005)
99-5-4-3						N.D.	N.D.	D'Andrea Kapp et al. (2005)
99-5-5-4c						N.D.	N.D.	D'Andrea Kapp et al. (2005)
99-5-5-4d	0.7063	-3.6				No	No	D'Andrea Kapp et al. (2005)
99-5-7-2a	0.7022					No	No	D'Andrea Kapp et al. (2005)
99-5-7-2b						N.D.	N.D.	D'Andrea Kapp et al. (2005)
99-5-7-3b	0.7034	-7.7				No	No	D'Andrea Kapp et al. (2005)
99-5-9-3	0.7070	-4.4				No	No	D'Andrea Kapp et al. (2005)
99-5-9-4						N.D.	N.D.	D'Andrea Kapp et al. (2005)
99-5-9-4a	0.7187	-11.6				No	No	D'Andrea Kapp et al. (2005)
99-7-26-1						N.D.	N.D.	D'Andrea Kapp et al. (2005)
99-7-26-1b	0.7111					No	No	D'Andrea Kapp et al. (2005)
99-7-26-2						N.D.	N.D.	D'Andrea Kapp et al. (2005)
99-7-26-3						N.D.	N.D.	D'Andrea Kapp et al. (2005)
99-7-27-1						N.D.	N.D.	D'Andrea Kapp et al. (2005)
99-7-27-2						N.D.	N.D.	D'Andrea Kapp et al. (2005)
99-7-27-3c						N.D.	N.D.	D'Andrea Kapp et al. (2005)
99-7-27-4						N.D.	N.D.	D'Andrea Kapp et al. (2005)

Table A.2: continued

Sample	Terrane	Location	Lithology	Latitude (dd)	Longitude (dd)	Quadrant	Age (Ma)
BD-1	Lhasa Terrane	Nyanqentanglha	Granitoid	30.2870	90.6204	Q5	
BD-2	Lhasa Terrane	Nyanqentanglha	Granitoid	30.2876	90.6143	Q5	
BD-3	Lhasa Terrane	Nyanqentanglha	Granitoid	30.2915	90.6020	Q5	19.6
BD-5	Lhasa Terrane	Nyanqentanglha	Granitoid	30.2925	90.5962	Q5	
BD-7	Lhasa Terrane	Nyanqentanglha	Granitoid	30.2918	90.5791	Q5	8.6
BD-8	Lhasa Terrane	Nyanqentanglha	Granitoid	30.2938	90.5694	Q5	9.1
BS 4	Lhasa Terrane	Nyanqentanglha	Granitoid	30.2960	90.5536	Q5	10.3
BS 5	Lhasa Terrane	Nyanqentanglha	Granitoid	30.2963	90.5346	Q5	
BS 6	Lhasa Terrane	Nyanqentanglha	Granitoid	30.3012	90.5194	Q5	
BS 7	Lhasa Terrane	Nyanqentanglha	Granitoid	30.3150	90.4977	Q5	21.0
GL-1	Lhasa Terrane	Nyanqentanglha	Granitoid	30.2596	90.2453	Q5	140.5
GL-11	Lhasa Terrane	Nyanqentanglha	Granitoid	30.2983	90.1978	Q5	126.3
GL-12	Lhasa Terrane	Nyanqentanglha	Granitoid	30.3153	90.2076	Q5	125.0
GL-3	Lhasa Terrane	Nyanqentanglha	Granitoid	30.2660	90.2330	Q5	
GL-4	Lhasa Terrane	Nyanqentanglha	Granitoid	30.2660	90.2285	Q5	
LM-1-02	Lhasa Terrane	Nyanqentanglha	Granitoid	30.4832	90.8999	Q5	
ND-1	Lhasa Terrane	Nyanqentanglha	Granitoid	30.3692	90.3264	Q5	
ND-13	Lhasa Terrane	Nyanqentanglha	Granitoid	30.3641	90.3996	Q5	
ND-14	Lhasa Terrane	Nyanqentanglha	Granitoid	30.3550	90.3980	Q5	58.4
ND-15	Lhasa Terrane	Nyanqentanglha	Granitoid	30.3870	90.3696	Q5	53.5
ND-19	Lhasa Terrane	Nyanqentanglha	Granitoid	30.3641	90.2105	Q5	
ND-20	Lhasa Terrane	Nyanqentanglha	Granitoid	30.3589	90.2092	Q5	
ND-22	Lhasa Terrane	Nyanqentanglha	Granitoid	30.3411	90.2670	Q5	66.5
ND-3	Lhasa Terrane	Nyanqentanglha	Granitoid	30.3599	90.3290	Q5	35.4
ND-4	Lhasa Terrane	Nyanqentanglha	Granitoid	30.3570	90.3415	Q5	20.0
ND-7	Lhasa Terrane	Nyanqentanglha	Granitoid	30.5745	90.6116	Q5	
ND-9	Lhasa Terrane	Nyanqentanglha	Granitoid	30.3802	90.3693	Q5	53.3
QC11a	Lhasa Terrane	Nyanqentanglha	Granulite				
QC12b-a	Lhasa Terrane	Nyanqentanglha	Orthogneiss				
QC14	Lhasa Terrane	Nyanqentanglha	Granitoid	30.3108	90.5523	Q5	18.2
QC17	Lhasa Terrane	Nyanqentanglha	Granitoid	30.2921	90.5882	Q5	20.6
QC18	Lhasa Terrane	Nyanqentanglha	Granitoid	30.2847	90.6053	Q5	21.9
QC19	Lhasa Terrane	Nyanqentanglha	Granitoid	30.2776	90.6069	Q5	22.1
QC2	Lhasa Terrane	Nyanqentanglha	Granitoid	30.2173	90.3492	Q5	16.8

Sample data continued

Sample	87Sr/86Sr(i)	eNd(t)	206Pb/ 204Pb(t)	207Pb/ 204Pb(t)	208Pb/ 204Pb(t)	*UPR	**ADK	Source
BD-1						N.D.	N.D.	D'Andrea Kapp et al. (2005)
BD-2						N.D.	N.D.	D'Andrea Kapp et al. (2005)
BD-3	0.7115	-7.0				No	No	D'Andrea Kapp et al. (2005)
BD-5						N.D.	N.D.	D'Andrea Kapp et al. (2005)
BD-7	0.7074	-7.0				No	No	D'Andrea Kapp et al. (2005)
BD-8	0.7132	-8.4				No	No	D'Andrea Kapp et al. (2005)
BS 4						N.D.	N.D.	D'Andrea Kapp et al. (2005)
BS 5						N.D.	N.D.	D'Andrea Kapp et al. (2005)
BS 6						N.D.	N.D.	D'Andrea Kapp et al. (2005)
BS 7						N.D.	N.D.	D'Andrea Kapp et al. (2005)
GL-1						No	No	D'Andrea Kapp et al. (2005)
GL-11						No	No	D'Andrea Kapp et al. (2005)
GL-12						No	No	D'Andrea Kapp et al. (2005)
GL-3						N.D.	N.D.	D'Andrea Kapp et al. (2005)
GL-4						N.D.	N.D.	D'Andrea Kapp et al. (2005)
LM-1-02						N.D.	N.D.	D'Andrea Kapp et al. (2005)
ND-1						N.D.	N.D.	D'Andrea Kapp et al. (2005)
ND-13						No	No	D'Andrea Kapp et al. (2005)
ND-14						No	No	D'Andrea Kapp et al. (2005)
ND-15						No	No	D'Andrea Kapp et al. (2005)
ND-19						N.D.	N.D.	D'Andrea Kapp et al. (2005)
ND-20						N.D.	N.D.	D'Andrea Kapp et al. (2005)
ND-22						No	No	D'Andrea Kapp et al. (2005)
ND-3						No	No	D'Andrea Kapp et al. (2005)
ND-4	0.6915					No	No	D'Andrea Kapp et al. (2005)
ND-7						N.D.	N.D.	D'Andrea Kapp et al. (2005)
ND-9						No	No	D'Andrea Kapp et al. (2005)
QC11a		-15.2				N.D.	N.D.	D'Andrea Kapp et al. (2005)
QC12b-a		-7.6				N.D.	N.D.	D'Andrea Kapp et al. (2005)
QC14	0.7068	-5.2				No	No	D'Andrea Kapp et al. (2005)
QC17	0.7084	-6.2				No	No	D'Andrea Kapp et al. (2005)
QC18	0.7086	-7.6				No	No	D'Andrea Kapp et al. (2005)
QC19	0.7067	-6.4				No	No	D'Andrea Kapp et al. (2005)
QC2	0.7119	-7.4				No	No	D'Andrea Kapp et al. (2005)

Table A.2: continued

Sample	Terrane	Location	Lithology	Latitude (dd)	Longitude (dd)	Quadrant	Age (Ma)
QC3b	Lhasa Terrane	Nyanqentanglha	Orthogneiss				
QC4	Lhasa Terrane	Nyanqentanglha	Granitoid	30.1750	90.4257	Q5	8.7
QC5	Lhasa Terrane	Nyanqentanglha	Granitoid	30.1343	90.4593	Q5	10.8
QC7	Lhasa Terrane	Nyanqentanglha	Granite (Bt)				
QC8	Lhasa Terrane	Nyanqentanglha	Granodiorite				
SD7	Lhasa Terrane	Nyanqentanglha	Granitoid	30.0079	90.2548	Q5	
SD8	Lhasa Terrane	Nyanqentanglha	Granitoid	30.0166	90.2483	Q5	
SD9	Lhasa Terrane	Nyanqentanglha	Granitoid	30.0111	90.2538	Q5	
YD-11	Lhasa Terrane	Nyanqentanglha	Granitoid	30.0629	90.5710	Q5	53.3
YD-13	Lhasa Terrane	Nyanqentanglha	Granitoid				52.5
YD-15	Lhasa Terrane	Nyanqentanglha	Granitoid	30.0978	90.5516	Q5	
YD-19	Lhasa Terrane	Nyanqentanglha	Granitoid	30.5755	90.6207	Q5	
YD-20	Lhasa Terrane	Nyanqentanglha	Granitoid	30.2960	90.6314	Q5	24.8
YD-32	Lhasa Terrane	Nyanqentanglha	Granitoid	30.0800	90.5920	Q5	
YD-33	Lhasa Terrane	Nyanqentanglha	Granitoid	30.0636	90.5836	Q5	52.0
YD-35	Lhasa Terrane	Nyanqentanglha	Granitoid	30.0660	90.3251	Q5	8.3
YD-37	Lhasa Terrane	Nyanqentanglha	Granitoid	30.0455	90.5168	Q5	65.6
YD-7	Lhasa Terrane	Nyanqentanglha	Granitoid	30.0265	90.6013	Q5	53.9
YD-8	Lhasa Terrane	Nyanqentanglha	Granitoid	30.0394	90.5939	Q5	54.1
98T57	Lhasa Terrane	Yulinshan	Tephriphonolite	31.0768	86.5248	Q4	30.0
99T132	Lhasa Terrane	Chazi	Phonotephrite	30.0660	86.7790	Q4	13.3
99T134	Lhasa Terrane	Chazi	Trachyte	30.1445	86.5248	Q4	11.5
99T145	Lhasa Terrane	Chazi	Trachyte	30.0017	86.4849	Q4	8.2
99T152	Lhasa Terrane	Chazi	Trachyte	30.0175	86.5320	Q4	11.5
99T154	Lhasa Terrane	Chazi	Trachyandesite	30.0517	86.5163	Q4	13.1
99T53	Lhasa Terrane	Wenbu	Trachyte	31.0953	86.5263	Q4	22.7
99T56	Lhasa Terrane	Wenbu	Phonolite	31.0996	86.5420	Q4	22.7
99T57	Lhasa Terrane	Wenbu	Trachyte	31.0768	86.5248	Q4	22.7
99T60	Lhasa Terrane	Wenbu	Phonolite	31.0739	86.5434	Q4	22.9
99T62	Lhasa Terrane	Wenbu	Trachyte	31.0882	86.5577	Q4	22.5
CHZ-1	Lhasa Terrane	Chazi	Lava (ultrapotassic)	30.0406	86.5303	Q4	11.5
CHZ-10	Lhasa Terrane	Chazi	Lava (ultrapotassic)	30.0406	86.5303	Q4	11.5
CHZ-11	Lhasa Terrane	Chazi	Lava (ultrapotassic)	30.0406	86.5303	Q4	11.5
CHZ-12	Lhasa Terrane	Chazi	Lava (ultrapotassic)	30.0406	86.5303	Q4	11.5

Sample data continued

Sample	87Sr/86Sr(i)	eNd(t)	206Pb/ 204Pb(t)	207Pb/ 204Pb(t)	208Pb/ 204Pb(t)	*UPR	**ADK	Source
QC3b		-19.3				N.D.	N.D.	D'Andrea Kapp et al. (2005)
QC4	0.7497	-7.6				No	No	D'Andrea Kapp et al. (2005)
QC5	0.7215	-11.9				No	No	D'Andrea Kapp et al. (2005)
QC7		-7.4				N.D.	N.D.	D'Andrea Kapp et al. (2005)
QC8		-6.4				N.D.	N.D.	D'Andrea Kapp et al. (2005)
SD7						N.D.	N.D.	D'Andrea Kapp et al. (2005)
SD8						N.D.	N.D.	D'Andrea Kapp et al. (2005)
SD9						N.D.	N.D.	D'Andrea Kapp et al. (2005)
YD-11						No	No	D'Andrea Kapp et al. (2005)
YD-13						No	No	D'Andrea Kapp et al. (2005)
YD-15						N.D.	N.D.	D'Andrea Kapp et al. (2005)
YD-19						N.D.	N.D.	D'Andrea Kapp et al. (2005)
YD-20						N.D.	N.D.	D'Andrea Kapp et al. (2005)
YD-32						N.D.	N.D.	D'Andrea Kapp et al. (2005)
YD-33						No	No	D'Andrea Kapp et al. (2005)
YD-35						N.D.	N.D.	D'Andrea Kapp et al. (2005)
YD-37						No	No	D'Andrea Kapp et al. (2005)
YD-7						No	No	D'Andrea Kapp et al. (2005)
YD-8						No	No	D'Andrea Kapp et al. (2005)
98T57	0.7091	-9.1	19.0	15.7	39.4	No	No	Ding et al. (2003)
99T132	0.7201	-12.9	18.8	15.7	39.4	Yes	No	Ding et al. (2003)
99T134	0.7182	-12.2	18.8	15.7	39.5	No	No	Ding et al. (2003)
99T145	0.7178	-12.7	18.9	15.7	39.6	No	No	Ding et al. (2003)
99T152	0.7193	-14.5	18.9	15.8	39.5	Yes	No	Ding et al. (2003)
99T154	0.7165	-13.7	18.9	15.8	39.6	Yes	No	Ding et al. (2003)
99T53	0.7219	-15.0	18.5	15.8	39.5	No	No	Ding et al. (2003)
99T56	0.7218	-14.9	18.9	15.7	39.3	Yes	No	Ding et al. (2003)
99T57	0.7240	-15.1	18.4	15.7	39.3	Yes	No	Ding et al. (2003)
99T60	0.7183	-14.8	18.4	15.7	39.3	Yes	No	Ding et al. (2003)
99T62	0.7202	-14.8	18.5	15.7	39.4	Yes	No	Ding et al. (2003)
CHZ-1	0.7363	-15.6	18.8	15.7	39.5	Yes	No	Gao et al. (2007b)
CHZ-10	0.7363	-15.8	18.8	15.7	39.6	Yes	No	Gao et al. (2007b)
CHZ-11			18.8	15.7	39.6	Yes	No	Gao et al. (2007b)
CHZ-12	0.7362	-16.0	18.8	15.7	39.7	Yes	No	Gao et al. (2007b)

Table A.2: continued

Sample	Terrane	Location	Lithology	Latitude (dd)	Longitude (dd)	Quadrant	Age (Ma)
CHZ-2	Lhasa Terrane	Chazi	Lava (ultrapotassic)	30.0406	86.5303	Q4	11.5
CHZ-3	Lhasa Terrane	Chazi	Lava (ultrapotassic)	30.0406	86.5303	Q4	11.5
CHZ-4	Lhasa Terrane	Chazi	Lava (ultrapotassic)	30.0406	86.5303	Q4	11.5
CHZ-5	Lhasa Terrane	Chazi	Lava (ultrapotassic)	30.0406	86.5303	Q4	11.5
CHZ-6	Lhasa Terrane	Chazi	Lava (ultrapotassic)	30.0406	86.5303	Q4	11.5
CHZ-7	Lhasa Terrane	Chazi	Lava (ultrapotassic)	30.0406	86.5303	Q4	11.5
CHZ-8	Lhasa Terrane	Chazi	Lava (ultrapotassic)	30.0406	86.5303	Q4	11.5
CHZ-9	Lhasa Terrane	Chazi	Lava (ultrapotassic)	30.0406	86.5303	Q4	11.5
Tl/03	Lhasa Terrane	Mibale	Lava (ultrapotassic)	30.8500	86.6572	Q4	19.0
Tl/06	Lhasa Terrane	Mibale	Lava (potassic)	30.8500	86.6572	Q4	19.0
Tl/08	Lhasa Terrane	Mibale	Lava (ultrapotassic)	30.8500	86.6572	Q4	19.0
Tl/10	Lhasa Terrane	Mibale	Lava (ultrapotassic)	30.8500	86.6572	Q4	19.0
Tl/11	Lhasa Terrane	Mibale	Lava (ultrapotassic)	30.8500	86.6572	Q4	19.0
Tl/13	Lhasa Terrane	Mibale	Lava (ultrapotassic)	30.8500	86.6572	Q4	19.0
Tl/17	Lhasa Terrane	Mibale	Lava (ultrapotassic)	30.8500	86.6572	Q4	19.0
Tl/18	Lhasa Terrane	Mibale	Lava (ultrapotassic)	30.8500	86.6572	Q4	19.0
Tl/59	Lhasa Terrane	Mibale	Lava (potassic)	30.8500	86.6572	Q4	19.0
DZ-01	Lhasa Terrane	Dazi	Basalt	29.6724	91.6684	Q5	40.0
DZ-02	Lhasa Terrane	Dazi	Picrite	29.6724	91.6684	Q5	40.0
DZ-03	Lhasa Terrane	Dazi	Basalt	29.6724	91.6684	Q5	40.0
DZ-05	Lhasa Terrane	Dazi	Basalt	29.6724	91.6684	Q5	40.0
DZ-07	Lhasa Terrane	Dazi	Basalt	29.6724	91.6684	Q5	40.0
DZ-10	Lhasa Terrane	Dazi	Basalt	29.6724	91.6684	Q5	40.0
DZ-11	Lhasa Terrane	Dazi	Picrite	29.6724	91.6684	Q5	40.0
DZ-13	Lhasa Terrane	Dazi	Basalt	29.6724	91.6684	Q5	40.0
DZ-14	Lhasa Terrane	Dazi	Basalt	29.6724	91.6684	Q5	40.0
DZ-16	Lhasa Terrane	Dazi	Basalt	29.6724	91.6684	Q5	40.0
DZ-17	Lhasa Terrane	Dazi	Basalt	29.6724	91.6684	Q5	40.0
DZ-18	Lhasa Terrane	Dazi	Basalt	29.6724	91.6684	Q5	40.0
DZ-19	Lhasa Terrane	Dazi	Basaltic Andesite	29.6724	91.6684	Q5	40.0
DZ-20	Lhasa Terrane	Dazi	Basalt	29.6724	91.6684	Q5	40.0
DZ-21	Lhasa Terrane	Dazi	Basalt	29.6724	91.6684	Q5	40.0
DZ-22	Lhasa Terrane	Dazi	Basalt	29.6724	91.6684	Q5	40.0
DZ-23	Lhasa Terrane	Dazi	Basaltic Andesite	29.6724	91.6684	Q5	40.0

Sample data continued

Sample	87Sr/86Sr(i)	eNd(t)	206Pb/204Pb(t)	207Pb/204Pb(t)	208Pb/204Pb(t)	*UPR	**ADK	Source
CHZ-2			18.8	15.7	39.7	Yes	No	Gao et al. (2007b)
CHZ-3			18.9	15.7	39.7	Yes	No	Gao et al. (2007b)
CHZ-4			18.9	15.7	39.8	Yes	No	Gao et al. (2007b)
CHZ-5	0.7308	-15.8	18.9	15.7	39.6	Yes	No	Gao et al. (2007b)
CHZ-6			18.9	15.8	39.9	Yes	No	Gao et al. (2007b)
CHZ-7			18.8	15.7	39.6	Yes	No	Gao et al. (2007b)
CHZ-8	0.7309	-15.8	18.8	15.7	39.6	Yes	No	Gao et al. (2007b)
CHZ-9			18.8	15.7	39.6	Yes	No	Gao et al. (2007b)
Tl/03	0.7195	-13.3	18.6	15.8	39.7	Yes	No	Gao et al. (2007b)
Tl/06	0.7195	-13.6	18.6	15.8	39.8	No	No	Gao et al. (2007b)
Tl/08	0.7191	-15.4	18.5	15.8	39.7	Yes	No	Gao et al. (2007b)
Tl/10	0.7187	-13.9	18.5	15.8	40.1	Yes	No	Gao et al. (2007b)
Tl/11	0.7182	-14.1	18.5	15.8	39.7	Yes	No	Gao et al. (2007b)
Tl/13	0.7166	-13.4	18.5	15.8	39.6	Yes	No	Gao et al. (2007b)
Tl/17	0.7258	-16.4	18.6	15.8	39.9	Yes	No	Gao et al. (2007b)
Tl/18	0.7191	-16.0	18.5	15.8	39.8	Yes	No	Gao et al. (2007b)
Tl/59	0.7178	-13.2	18.5	15.8	39.7	No	No	Gao et al. (2007b)
DZ-01						No	No	Gao et al. (2008)
DZ-02						No	No	Gao et al. (2008)
DZ-03						No	No	Gao et al. (2008)
DZ-05						No	No	Gao et al. (2008)
DZ-07						No	No	Gao et al. (2008)
DZ-10						No	No	Gao et al. (2008)
DZ-11						No	No	Gao et al. (2008)
DZ-13						No	No	Gao et al. (2008)
DZ-14						No	No	Gao et al. (2008)
DZ-16						No	No	Gao et al. (2008)
DZ-17						No	No	Gao et al. (2008)
DZ-18						No	No	Gao et al. (2008)
DZ-19						No	No	Gao et al. (2008)
DZ-20						No	No	Gao et al. (2008)
DZ-21						No	No	Gao et al. (2008)
DZ-22						No	No	Gao et al. (2008)
DZ-23						No	No	Gao et al. (2008)

Table A.2: continued

Sample	Terrane	Location	Lithology	Latitude (dd)	Longitude (dd)	Quadrant	Age (Ma)
DZ-28	Lhasa Terrane	Dazi	Basaltic Andesite	29.6724	91.6684	Q5	40.0
L012	Lhasa Terrane	Dazi	Unknown	29.6724	91.6684	Q5	40.0
L014	Lhasa Terrane	Dazi	Unknown	29.6724	91.6684	Q5	40.0
LKA-01	Lhasa Terrane	Dazi	Basaltic Andesite	29.6724	91.6684	Q5	40.0
LKA-02	Lhasa Terrane	Dazi	Basaltic Andesite	29.6724	91.6684	Q5	40.0
LKA-03	Lhasa Terrane	Dazi	Basaltic Andesite	29.6724	91.6684	Q5	40.0
LKA-04	Lhasa Terrane	Dazi	Basalt	29.6724	91.6684	Q5	40.0
LKA-05	Lhasa Terrane	Dazi	Basalt	29.6724	91.6684	Q5	40.0
LKA-06	Lhasa Terrane	Dazi	Lava (altered)	29.6724	91.6684	Q5	40.0
LKA-07	Lhasa Terrane	Dazi	Lava (altered)	29.6724	91.6684	Q5	40.0
LKA-08	Lhasa Terrane	Dazi	Lava (altered)	29.6724	91.6684	Q5	40.0
LKA-09	Lhasa Terrane	Dazi	Lava (altered)	29.6724	91.6684	Q5	40.0
LKA-11	Lhasa Terrane	Dazi	Lava (altered)	29.6724	91.6684	Q5	40.0
LKA-12	Lhasa Terrane	Dazi	Lava (altered)	29.6724	91.6684	Q5	40.0
LKA-13	Lhasa Terrane	Dazi	Lava (altered)	29.6724	91.6684	Q5	40.0
LKA-14	Lhasa Terrane	Dazi	Basalt	29.6724	91.6684	Q5	40.0
LKA-15	Lhasa Terrane	Dazi	Basalt	29.6724	91.6684	Q5	40.0
LKA-16	Lhasa Terrane	Dazi	Basalt	29.6724	91.6684	Q5	40.0
LKA-17	Lhasa Terrane	Dazi	Lava (altered)	29.6724	91.6684	Q5	40.0
LKA-19	Lhasa Terrane	Dazi	Lava (altered)	29.6724	91.6684	Q5	40.0
LKA-22	Lhasa Terrane	Dazi	Lava (altered)	29.6724	91.6684	Q5	40.0
LKA-24	Lhasa Terrane	Dazi	Lava (altered)	29.6724	91.6684	Q5	40.0
ML18-1	Lhasa Terrane	Wolong	Gabbro	29.0205	93.2187	Q5	38.0
ML18-10	Lhasa Terrane	Wolong	Granodiorite	29.0205	93.2187	Q5	38.0
ML18-2	Lhasa Terrane	Wolong	Granite	29.0205	93.2187	Q5	37.4
ML18-3	Lhasa Terrane	Wolong	Granodiorite	29.0205	93.2187	Q5	38.0
ML18-4	Lhasa Terrane	Wolong	Syenodiorite	29.0205	93.2187	Q5	38.5
ML18-5	Lhasa Terrane	Wolong	Syenodiorite	29.0205	93.2187	Q5	38.0
ML18-6	Lhasa Terrane	Wolong	Syenite	29.0205	93.2187	Q5	38.0
ML18-7	Lhasa Terrane	Wolong	Granodiorite	29.0205	93.2187	Q5	38.0
ML18-8	Lhasa Terrane	Wolong	Syenite	29.0205	93.2187	Q5	38.0
ML18-9	Lhasa Terrane	Wolong	Granite	29.0205	93.2187	Q5	38.0
1-Lt	Himalayas	Manaslu	Leucogranite (Bt, Ms, Tur)	28.5340	84.5821	Q4	24.0
2-Lmt	Himalayas	Manaslu	Leucogranite (Bt, Ms, Tur)	28.5340	84.5821	Q4	24.0

Sample data continued

Sample	87Sr/86Sr(i)	eNd(t)	206Pb/ 204Pb(t)	207Pb/ 204Pb(t)	208Pb/ 204Pb(t)	*UPR	**ADK	Source
DZ-28						No	No	Gao et al. (2008)
L012	0.7049	4.7	18.5	15.6	38.7	N.D.	N.D.	Gao et al. (2008)
L014	0.7047	4.7	18.5	15.6	38.7	N.D.	N.D.	Gao et al. (2008)
LKA-01	0.7045	4.7	18.6	15.6	38.6	No	No	Gao et al. (2008)
LKA-02			18.5	15.6	38.5	No	No	Gao et al. (2008)
LKA-03			18.6	15.6	38.6	No	No	Gao et al. (2008)
LKA-04	0.7062	3.6	18.4	15.6	38.5	No	No	Gao et al. (2008)
LKA-05	0.7058	4.8	18.3	15.6	38.4	No	No	Gao et al. (2008)
LKA-06			18.5	15.6	38.7	No	No	Gao et al. (2008)
LKA-07	0.7057	5.2	18.5	15.6	38.7	No	No	Gao et al. (2008)
LKA-08			18.5	15.6	38.7	No	No	Gao et al. (2008)
LKA-09			18.5	15.6	38.7	No	No	Gao et al. (2008)
LKA-11	0.7059	4.5	18.6	15.6	38.8	No	No	Gao et al. (2008)
LKA-12	0.7044	4.1	18.7	15.6	38.9	No	No	Gao et al. (2008)
LKA-13	0.7053	4.2	18.5	15.6	38.7	No	No	Gao et al. (2008)
LKA-14	0.7056	4.1	18.6	15.6	38.8	No	No	Gao et al. (2008)
LKA-15	0.7056	4.9	18.6	15.6	38.8	No	No	Gao et al. (2008)
LKA-16	0.7056	4.8	18.6	15.6	38.7	No	No	Gao et al. (2008)
LKA-17	0.7053	4.8	18.5	15.6	38.7	Yes	No	Gao et al. (2008)
LKA-19			18.6	15.6	38.8	No	No	Gao et al. (2008)
LKA-22						Yes	No	Gao et al. (2008)
LKA-24						Yes	No	Gao et al. (2008)
ML18-1	0.7054	-2.6				No	No	Guan et al. (2012)
ML18-10	0.7055	-2.3				No	Yes	Guan et al. (2012)
ML18-2						No	Yes	Guan et al. (2012)
ML18-3	0.7053	-1.6				No	Yes	Guan et al. (2012)
ML18-4	0.7053	-1.4				No	No	Guan et al. (2012)
ML18-5	0.7055	-2.7				No	No	Guan et al. (2012)
ML18-6	0.7054	-1.8				Yes	No	Guan et al. (2012)
ML18-7	0.7055	-2.0				No	Yes	Guan et al. (2012)
ML18-8						No	Yes	Guan et al. (2012)
ML18-9						No	Yes	Guan et al. (2012)
1-Lt						No	No	Guillot et al. (1995)
2-Lmt						No	No	Guillot et al. (1995)

Table A.2: continued

Sample	Terrane	Location	Lithology	Latitude (dd)	Longitude (dd)	Quadrant	Age (Ma)
3-L2m	Himalayas	Manaslu	Leucogranite (Bt, Ms, Tur)	28.5340	84.5821	Q4	24.0
G006	Lhasa Terrane	Nanmu	Adakite	29.5000	90.9000	Q5	16.3
G016	Lhasa Terrane	Jiama	Adakite	29.8000	91.8000	Q5	15.1
G019	Lhasa Terrane	Jiama	Adakite	29.8000	91.8000	Q5	15.1
G025	Lhasa Terrane	Linzhi	Adakite	29.6000	94.6000	Q6	26.2
G09	Lhasa Terrane	Wuyu	Adakite	29.4000	89.4000	Q5	14.2
GUO37	Lhasa Terrane	Xigaze	Adakite	29.3000	88.8000	Q4	17.2
GUO48	Lhasa Terrane	Daggyai	Adakite	29.6000	85.6000	Q4	18.5
GUO51	Lhasa Terrane	Gegar	Adakite	31.5000	81.8000	Q3	17.0
GUO62	Lhasa Terrane	Gegar	Adakite	31.5000	81.8000	Q3	17.0
ZF09	Lhasa Terrane	Shiquanhe	Adakite	33.5000	80.2000	Q2	22.5
ZFG17	Lhasa Terrane	Majiang	Adakite	29.7000	89.9000	Q5	12.4
AP052904-A	Lhasa Terrane	Amdo	Syenite (Qz, porphyritic)	31.7700	92.2900	Q5	177.9
AP060604-A	Lhasa Terrane	Amdo	Syenite (Qz, porphyritic)	31.9600	92.1600	Q5	179.5
AP061504-B	Lhasa Terrane	Amdo	Granite (Bt, porphyritic)	32.1900	91.7000	Q5	175.1
AP061604-B	Lhasa Terrane	Amdo	Granite (Bt)	32.1100	91.7100	Q5	174.1
AP062104-A	Lhasa Terrane	Amdo	Granite (Alkali-Fsp)	32.0700	92.2700	Q5	171.9
JG061504-7	Lhasa Terrane	Amdo	Granodiorite (Bt, Hbl)	32.2000	91.7100	Q5	183.0
JG062004-4	Lhasa Terrane	Amdo	Syenite (Qz, porphyritic)	31.9300	92.2400	Q5	170.8
JG062204-1	Lhasa Terrane	Amdo	Granodiorite (Bt, Hbl)	32.1200	92.3600	Q5	177.8
PK97-6-4-3A	Lhasa Terrane	Amdo	Orthogneiss	32.1100	91.7100	Q5	852.0
G10	Lhasa Terrane	Lhasa	Monzogranite (Bt)	29.4739	90.8447	Q5	41.4
G100	Lhasa Terrane		Granite (Bt)	31.5548	90.9355	Q5	123.0
G100A	Lhasa Terrane		Granite (Bt)	31.5548	90.9355	Q5	123.0
G100C	Lhasa Terrane		Granite (Bt)	31.5548	90.9355	Q5	123.0
G100E	Lhasa Terrane		Granite (Bt)	31.5548	90.9355	Q5	123.0
G101	Lhasa Terrane		Granodiorite (Hbl, Bt)	31.5878	90.9066	Q5	44.0
G101A	Lhasa Terrane		Granodiorite (Hbl, Bt)	31.5878	90.9066	Q5	44.0
G101C	Lhasa Terrane		Granodiorite (Hbl, Bt)	31.5878	90.9066	Q5	44.0
G101E	Lhasa Terrane		Granodiorite (Hbl, Bt)	31.5878	90.9066	Q5	44.0
G101G	Lhasa Terrane		Granodiorite (Hbl, Bt)	31.5878	90.9066	Q5	44.0
G117	Lhasa Terrane		Amphibolite	31.7447	91.7407	Q5	
G117A	Lhasa Terrane		Amphibolite	31.7447	91.7407	Q5	
G117B	Lhasa Terrane		Amphibolite	31.7447	91.7407	Q5	

Sample data continued

Sample	87Sr/86Sr(i)	eNd(t)	206Pb/ 204Pb(t)	207Pb/ 204Pb(t)	208Pb/ 204Pb(t)	*UPR	**ADK	Source
3-L2m						No	No	Guillot et al. (1995)
G006	0.7047	-0.3	18.2	15.5	38.1	No	No	Guo et al. (2007)
G016	0.7074	-2.1	18.7	15.7	38.7	No	Yes	Guo et al. (2007)
G019	0.7076	-1.5	18.7	15.7	38.8	No	Yes	Guo et al. (2007)
G025	0.7054	-1.9	18.4	15.6	38.5	No	Yes	Guo et al. (2007)
G09	0.7058	-0.6	18.3	15.6	38.1	No	Yes	Guo et al. (2007)
GUO37	0.7066	-2.1	18.5	15.6	38.4	No	Yes	Guo et al. (2007)
GUO48	0.7067	-9.1	18.5	15.6	39.1	No	Yes	Guo et al. (2007)
GUO51	0.7090	-7.2	18.2	15.6	38.3	No	Yes	Guo et al. (2007)
GUO62	0.7072	-5.1	18.2	15.6	38.2	No	Yes	Guo et al. (2007)
ZF09	0.7080	-7.3	18.3	15.6	38.3	No	Yes	Guo et al. (2007)
ZFG17	0.7047	3.4	18.3	15.5	38.2	No	Yes	Guo et al. (2007)
AP052904-A						N.D.	N.D.	Gyunn et al. (2006)
AP060604-A						N.D.	N.D.	Gyunn et al. (2006)
AP061504-B						N.D.	N.D.	Gyunn et al. (2006)
AP061604-B						N.D.	N.D.	Gyunn et al. (2006)
AP062104-A						N.D.	N.D.	Gyunn et al. (2006)
JG061504-7						N.D.	N.D.	Gyunn et al. (2006)
JG062004-4						N.D.	N.D.	Gyunn et al. (2006)
JG062204-1						N.D.	N.D.	Gyunn et al. (2006)
PK97-6-4-3A						N.D.	N.D.	Gyunn et al. (2006)
G10	0.7050	3.5				No	No	Harris et al. (1988a)
G100						N.D.	N.D.	Harris et al. (1988a)
G100A						No	No	Harris et al. (1988a)
G100C						No	No	Harris et al. (1988a)
G100E						No	No	Harris et al. (1988a)
G101						N.D.	N.D.	Harris et al. (1988a)
G101A						No	No	Harris et al. (1988a)
G101C						No	No	Harris et al. (1988a)
G101E						No	No	Harris et al. (1988a)
G101G						No	No	Harris et al. (1988a)
G117						N.D.	N.D.	Harris et al. (1988a)
G117A						No	No	Harris et al. (1988a)
G117B						No	No	Harris et al. (1988a)

Table A.2: continued

Sample	Terrane	Location	Lithology	Latitude (dd)	Longitude (dd)	Quadrant	Age (Ma)
G118	Lhasa Terrane		Orthogneiss (Bt)	31.7282	91.7530	Q5	531.0
G118A	Lhasa Terrane	Amdo	Orthogneiss (tonalitic)	31.7282	91.7530	Q5	531.0
G118C	Lhasa Terrane		Orthogneiss (tonalitic)	31.7282	91.7530	Q5	531.0
G118D	Lhasa Terrane	Amdo	Orthogneiss (tonalitic)	31.7282	91.7530	Q5	531.0
G118G	Lhasa Terrane		Orthogneiss (tonalitic)	31.7282	91.7530	Q5	531.0
G12	Lhasa Terrane	Lhasa	Granodiorite	29.5977	91.1874	Q5	
G120	Lhasa Terrane		Unknown	32.0130	91.7076	Q5	
G120A	Lhasa Terrane		Unknown	32.0130	91.7076	Q5	
G121	Lhasa Terrane		Unknown	32.0626	91.6952	Q5	
G121B	Lhasa Terrane		Unknown	32.0626	91.6952	Q5	
G124	Lhasa Terrane		Granodiorite (Hbl, Bt)	32.1452	91.7200	Q5	
G124A	Lhasa Terrane	Nyainrong-Amdo	Granodiorite (Hbl, Bt)	32.1452	91.7200	Q5	
G124C	Lhasa Terrane		Granodiorite (Hbl, Bt)	32.1452	91.7200	Q5	
G125	Lhasa Terrane		Unknown	32.1658	91.7241	Q5	
G125A	Lhasa Terrane		Unknown	32.1658	91.7241	Q5	
G15	Lhasa Terrane	Dagze	Tonalite	29.5895	91.2659	Q5	
G15A	Lhasa Terrane	Dagze	Tonalite	29.5895	91.2659	Q5	56.0
G20	Lhasa Terrane	Yangbajain	Granite (Bt)	30.1262	90.5474	Q5	
G26	Lhasa Terrane	Yangbajain	Granite (Bt, Hbl)	30.0767	90.5598	Q5	28.7
G38	Lhasa Terrane		Orthogneiss (granitic)	29.9776	90.0561	Q5	
G38E	Lhasa Terrane		Orthogneiss (granitic)	29.9776	90.0561	Q5	
G4	Lhasa Terrane	Quxu	Monzodiorite	29.3417	90.6589	Q5	
G40	Lhasa Terrane		Orthogneiss (granitic)	30.2047	90.4153	Q5	
G41	Lhasa Terrane		Orthogneiss (granitic)	30.3533	90.6176	Q5	
G41B	Lhasa Terrane		Orthogneiss (granitic)	30.3533	90.6176	Q5	
G42	Lhasa Terrane		Orthogneiss (granitic)	30.3409	90.5887	Q5	
G42A	Lhasa Terrane	Nyainqentanglha	Orthogneiss (granitic)	30.3409	90.5887	Q5	
G42B	Lhasa Terrane		Granite (Bt)	30.3409	90.5887	Q5	
G5	Lhasa Terrane	Quxu	Monzodiorite	29.3913	90.7332	Q5	
G57	Lhasa Terrane		Unknown	32.0296	92.3228	Q5	
G57A	Lhasa Terrane		Unknown	32.0296	92.3228	Q5	
G60	Lhasa Terrane		Granite (Hbl, Bt)	32.0337	92.2815	Q5	
G60A	Lhasa Terrane		Granite (Hbl, Bt)	32.0337	92.2815	Q5	
G61	Lhasa Terrane		Granite (Hbl, Bt)	32.0048	92.2774	Q5	

Sample data continued

Sample	87Sr/86Sr(i)	eNd(t)	206Pb/ 204Pb(t)	207Pb/ 204Pb(t)	208Pb/ 204Pb(t)	*UPR	**ADK	Source
G118						N.D.	N.D.	Harris et al. (1988a)
G118A	0.7326	-3.4				No	No	Harris et al. (1988a)
G118C						No	No	Harris et al. (1988a)
G118D	0.7379	-6.3				No	No	Harris et al. (1988a)
G118G						No	No	Harris et al. (1988a)
G12						No	No	Harris et al. (1988a)
G120						N.D.	N.D.	Harris et al. (1988a)
G120A						No	No	Harris et al. (1988a)
G121						N.D.	N.D.	Harris et al. (1988a)
G121B						No	No	Harris et al. (1988a)
G124						N.D.	N.D.	Harris et al. (1988a)
G124A						No	No	Harris et al. (1988a)
G124C						No	No	Harris et al. (1988a)
G125						N.D.	N.D.	Harris et al. (1988a)
G125A						No	No	Harris et al. (1988a)
G15						N.D.	N.D.	Harris et al. (1988a)
G15A	0.7045	3.1				No	No	Harris et al. (1988a)
G20						No	No	Harris et al. (1988a)
G26	0.7090	-5.8				No	No	Harris et al. (1988a)
G38						N.D.	N.D.	Harris et al. (1988a)
G38E						No	No	Harris et al. (1988a)
G4						No	No	Harris et al. (1988a)
G40						No	No	Harris et al. (1988a)
G41						N.D.	N.D.	Harris et al. (1988a)
G41B						No	No	Harris et al. (1988a)
G42						N.D.	N.D.	Harris et al. (1988a)
G42A						No	No	Harris et al. (1988a)
G42B						No	No	Harris et al. (1988a)
G5						No	No	Harris et al. (1988a)
G57						N.D.	N.D.	Harris et al. (1988a)
G57A						No	No	Harris et al. (1988a)
G60						N.D.	N.D.	Harris et al. (1988a)
G60A						No	No	Harris et al. (1988a)
G61						N.D.	N.D.	Harris et al. (1988a)

Table A.2: continued

Sample	Terrane	Location	Lithology	Latitude (dd)	Longitude (dd)	Quadrant	Age (Ma)
G61A	Lhasa Terrane		Granite (Hbl, Bt)	32.0048	92.2774	Q5	
G64	Lhasa Terrane		Granite (Bt, porphyritic)	31.9552	92.1783	Q5	
G64A	Lhasa Terrane	Nyainrong-Amdo	Granite (Bt, porphyritic)	31.9552	92.1783	Q5	
G64C	Lhasa Terrane		Granite (Bt, porphyritic)	31.9552	92.1783	Q5	
G66	Lhasa Terrane		Unknown	31.1956	90.7787	Q5	
G66A	Lhasa Terrane		Unknown	31.1956	90.7787	Q5	
G67	Lhasa Terrane		Granite (Bt)	31.1543	90.6507	Q5	
G67A	Lhasa Terrane		Granite (Bt)	31.1543	90.6507	Q5	
G68	Lhasa Terrane		Tonalite (Bt)	31.3896	90.2089	Q5	28.7
G68A	Lhasa Terrane	Baingoin	Tonalite	31.3896	90.2089	Q5	
G68B	Lhasa Terrane		Tonalite	31.3896	90.2089	Q5	
G69	Lhasa Terrane		Granite (Bt, Ms, Tur)	31.3937	90.2502	Q5	
G69A	Lhasa Terrane		Granite (Bt, Ms, Tur)	31.3937	90.2502	Q5	
G69C	Lhasa Terrane		Granite (Bt, Ms, Tur)	31.3937	90.2502	Q5	
G71	Lhasa Terrane	Baingoin	Granite (Bt, Ms, Tur)	31.4268	90.0809	Q5	121.0
S70C	Lhasa Terrane	Nyainqentanglha	Orthogneiss (granitic)	30.2047	90.4153	Q5	50.0
S70D	Lhasa Terrane	Nyainqentanglha	Granite (Bt)	30.2047	90.4153	Q5	50.0
X45	Lhasa Terrane		Granodiorite	31.0469	90.5516	Q5	
N-9	Lhasa Terrane		Granodiorite	29.3300	92.2217	Q5	48.9
NM-1	Lhasa Terrane	Yaja	Granodiorite	29.2700	91.9033	Q5	30.4
NM-2	Lhasa Terrane	Yaja	Granodiorite	29.2700	91.9033	Q5	30.4
NM-3	Lhasa Terrane	Yaja	Granodiorite	29.2650	91.9033	Q5	30.4
NM-4	Lhasa Terrane	Yaja	Granodiorite	29.2633	91.9017	Q5	30.4
NM-5	Lhasa Terrane	Yaja	Granodiorite	29.2617	91.8983	Q5	30.4
NM-6	Lhasa Terrane	Yaja	Granodiorite	29.2600	91.8967	Q5	30.4
NM-7	Lhasa Terrane	Yaja	Granodiorite	29.2567	91.8933	Q5	30.4
YANS 10	Lhasa Terrane	Kangagang	Granodiorite	29.2917	92.1467	Q5	42.5
YANS 2	Lhasa Terrane	Kangagang	Granodiorite	30.5364	92.1867	Q5	42.5
YANS 4	Lhasa Terrane	Kangagang	Granodiorite	30.5361	92.1633	Q5	42.5
YANS 5	Lhasa Terrane	Kangagang	Granodiorite	29.3000	92.1567	Q5	42.5
ZH-1-94	Lhasa Terrane	Yaja	Granodiorite	29.2650	91.8800	Q5	30.4
ZH-3-92	Lhasa Terrane	Yaja	Granodiorite	29.2650	91.8800	Q5	30.4
SH522021	Lhasa Terrane	Linzhou	Dike (felsic)	29.9283	91.3533	Q5	51.7
SH530022	Lhasa Terrane	Linzhou	Rhyolite	29.9550	91.2167	Q5	68.7

Sample data continued

Sample	87Sr/86Sr(i)	eNd(t)	206Pb/ 204Pb(t)	207Pb/ 204Pb(t)	208Pb/ 204Pb(t)	*UPR	**ADK	Source
G61A						No	No	Harris et al. (1988a)
G64						N.D.	N.D.	Harris et al. (1988a)
G64A						No	No	Harris et al. (1988a)
G64C						No	No	Harris et al. (1988a)
G66						N.D.	N.D.	Harris et al. (1988a)
G66A						No	No	Harris et al. (1988a)
G67						N.D.	N.D.	Harris et al. (1988a)
G67A						No	No	Harris et al. (1988a)
G68	0.7086	-9.3				No	No	Harris et al. (1988a)
G68A						No	No	Harris et al. (1988a)
G68B						No	No	Harris et al. (1988a)
G69						N.D.	N.D.	Harris et al. (1988a)
G69A						No	No	Harris et al. (1988a)
G69C						No	No	Harris et al. (1988a)
G71	0.7211	-6.0				No	No	Harris et al. (1988a)
S70C	0.7139	-6.9				No	No	Harris et al. (1988a)
S70D	0.7084	-6.2				No	No	Harris et al. (1988a)
X45						No	No	Harris et al. (1988a)
N-9						N.D.	N.D.	Harrison et al. (2000)
NM-1						No	Yes	Harrison et al. (2000)
NM-2						No	Yes	Harrison et al. (2000)
NM-3						No	Yes	Harrison et al. (2000)
NM-4						No	Yes	Harrison et al. (2000)
NM-5						No	Yes	Harrison et al. (2000)
NM-6						No	Yes	Harrison et al. (2000)
NM-7						No	Yes	Harrison et al. (2000)
YANS 10						N.D.	N.D.	Harrison et al. (2000)
YANS 2						No	No	Harrison et al. (2000)
YANS 4						No	No	Harrison et al. (2000)
YANS 5						N.D.	N.D.	Harrison et al. (2000)
ZH-1-94						No	Yes	Harrison et al. (2000)
ZH-3-92						No	No	Harrison et al. (2000)
SH522021						N.D.	N.D.	He et al. (2007)
SH530022						N.D.	N.D.	He et al. (2007)

Table A.2: continued

Sample	Terrane	Location	Lithology	Latitude (dd)	Longitude (dd)	Quadrant	Age (Ma)
SH712032	Lhasa Terrane	Linzhou	Granite	30.0650	91.1350	Q5	51.9
SH728032	Lhasa Terrane	Linzhou	Dike (felsic)	29.9500	91.1967	Q5	52.0
SH823034	Lhasa Terrane	Linzhou	Tuff (felsic)	30.0033	91.1483	Q5	47.1
SH830034	Lhasa Terrane	Linzhou	Tuff (rhyolitic)	29.9450	91.1317	Q5	62.6
SH831031	Lhasa Terrane	Linzhou	Tuff (felsic)	29.9883	91.1417	Q5	53.9
DC-31	Lhasa Terrane	Bangoin	Granite	31.4667	89.9214	Q5	117.5
DC-33	Lhasa Terrane	Bangoin	Granite	31.3723	90.0154	Q5	111.6
H-23	Lhasa Terrane	Bangoin	Granite	31.4225	89.8043	Q5	117.0
H-24	Lhasa Terrane	Bangoin	Granite	31.4431	89.8056	Q5	114.1
H-29	Lhasa Terrane	Bangoin	Granite	31.4431	89.8983	Q5	111.7
H-30	Lhasa Terrane	Bangoin	Granite	31.4680	89.8961	Q5	112.8
H-31	Lhasa Terrane	Bangoin	Granite	31.4787	89.9193	Q5	114.1
Cj-02	Lhasa Terrane	Nimu	Adakite	29.4331	90.1625	Q5	16.0
Cj-20	Lhasa Terrane	Nimu	Adakite	29.4331	90.1625	Q5	16.0
Cj-22	Lhasa Terrane	Nimu	Adakite	29.4331	90.1625	Q5	16.0
CZK051-26	Lhasa Terrane	Chongjiang	Adakite	29.5956	90.0128	Q5	15.6
CZK051-470	Lhasa Terrane	Chongjiang	Adakite	29.5956	90.0128	Q5	14.5
Dzl-01	Lhasa Terrane	Lakange	Adakite	29.5732	91.3839	Q5	13.4
Dzl-05	Lhasa Terrane	Lakange	Adakite	29.5732	91.3839	Q5	13.4
Dzl-06	Lhasa Terrane	Lakange	Adakite	29.5732	91.3839	Q5	13.4
Dzl-07	Lhasa Terrane	Lakange	Adakite	29.5732	91.3839	Q5	13.4
Hou_2004_1	Lhasa Terrane	Jiama	Granite (porphyritic)	29.7205	91.7362	Q5	15.9
Hou_2004_10	Lhasa Terrane	Chongjiang	Diorite (porphyritic)	29.5956	90.0128	Q5	14.5
Hou_2004_11	Lhasa Terrane	Chongjiang	Granite (porphyritic)	29.5956	90.0128	Q5	13.5
Hou_2004_12	Lhasa Terrane	Chongjiang	Granite (porphyritic)	29.5956	90.0128	Q5	12.2
Hou_2004_13	Lhasa Terrane	Chongjiang	Granite (porphyritic)	29.5956	90.0128	Q5	12.2
Hou_2004_14	Lhasa Terrane	Tinggong	Granite (porphyritic)	29.5476	90.0577	Q5	16.5
Hou_2004_15	Lhasa Terrane	Maquiang	Ignimbrite	29.9626	90.1147	Q5	15.8
Hou_2004_16	Lhasa Terrane	Maquiang	Ignimbrite	29.9626	90.1147	Q5	14.2
Hou_2004_17	Lhasa Terrane	Maquiang	Ignimbrite	29.9626	90.1147	Q5	12.9
Hou_2004_18	Lhasa Terrane	Maquiang	Ignimbrite	29.9626	90.1147	Q5	10.5
Hou_2004_19	Lhasa Terrane	Maquiang	Ignimbrite	29.9626	90.1147	Q5	10.1
Hou_2004_2	Lhasa Terrane	Qulong	Granite (porphyritic)	29.6116	91.5921	Q5	15.9
Hou_2004_20	Lhasa Terrane	Gazacun	Ignimbrite	29.6476	89.6391	Q5	13.6

Sample data continued

Sample	87Sr/86Sr(i)	eNd(t)	206Pb/ 204Pb(t)	207Pb/ 204Pb(t)	208Pb/ 204Pb(t)	*UPR	**ADK	Source
SH712032						N.D.	N.D.	He et al. (2007)
SH728032						N.D.	N.D.	He et al. (2007)
SH823034						N.D.	N.D.	He et al. (2007)
SH830034						N.D.	N.D.	He et al. (2007)
SH831031						N.D.	N.D.	He et al. (2007)
DC-31						N.D.	N.D.	Hetzel et al. (2011)
DC-33						N.D.	N.D.	Hetzel et al. (2011)
H-23						N.D.	N.D.	Hetzel et al. (2011)
H-24						N.D.	N.D.	Hetzel et al. (2011)
H-29						N.D.	N.D.	Hetzel et al. (2011)
H-30						N.D.	N.D.	Hetzel et al. (2011)
H-31						N.D.	N.D.	Hetzel et al. (2011)
Cj-02	0.7050	0.9	18.5	15.6	38.7	No	No	Hou et al. (2004)
Cj-20	0.7052	-2.3	18.4	15.6	38.6	No	No	Hou et al. (2004)
Cj-22	0.7051	-1.3	18.4	15.6	38.5	No	No	Hou et al. (2004)
CZK051-26						N.D.	N.D.	Hou et al. (2004)
CZK051-470						N.D.	N.D.	Hou et al. (2004)
Dzl-01	0.7052	0.6	18.4	15.5	38.5	No	No	Hou et al. (2004)
Dzl-05	0.7050	1.8	18.4	15.5	38.4	No	Yes	Hou et al. (2004)
Dzl-06	0.7050	0.8	18.5	15.6	38.6	No	Yes	Hou et al. (2004)
Dzl-07	0.7047	2.0				No	Yes	Hou et al. (2004)
Hou_2004_1						N.D.	N.D.	Hou et al. (2004)
Hou_2004_10						N.D.	N.D.	Hou et al. (2004)
Hou_2004_11						N.D.	N.D.	Hou et al. (2004)
Hou_2004_12						N.D.	N.D.	Hou et al. (2004)
Hou_2004_13						N.D.	N.D.	Hou et al. (2004)
Hou_2004_14						N.D.	N.D.	Hou et al. (2004)
Hou_2004_15						N.D.	N.D.	Hou et al. (2004)
Hou_2004_16						N.D.	N.D.	Hou et al. (2004)
Hou_2004_17						N.D.	N.D.	Hou et al. (2004)
Hou_2004_18						N.D.	N.D.	Hou et al. (2004)
Hou_2004_19						N.D.	N.D.	Hou et al. (2004)
Hou_2004_2						N.D.	N.D.	Hou et al. (2004)
Hou_2004_20						N.D.	N.D.	Hou et al. (2004)

Table A.2: continued

Sample	Terrane	Location	Lithology	Latitude (dd)	Longitude (dd)	Quadrant	Age (Ma)
Hou_2004_21	Lhasa Terrane	Gazacun	Ignimbrite	29.6476	89.6391	Q5	12.0
Hou_2004_22	Lhasa Terrane	S Gegar	Dacite, Rhyolite	31.5167	81.8667	Q3	16.2
Hou_2004_23	Lhasa Terrane	S Gegar	Dacite, Rhyolite	31.5167	81.8667	Q3	17.7
Hou_2004_24	Himalayas	SE Barga	Dacite, Rhyolite	30.8540	81.4268	Q3	16.7
Hou_2004_25	Himalayas	SE Barga	Dacite, Rhyolite	30.8540	81.4268	Q3	17.0
Hou_2004_26	Himalayas	SE Barga	Dacite, Rhyolite	30.8540	81.4268	Q3	17.0
Hou_2004_3	Lhasa Terrane	Lakang'e	Granite (porphyritic)	29.5732	91.3839	Q5	14.9
Hou_2004_4	Lhasa Terrane	Nanmu	Granite (porphyritic)	29.4771	90.8297	Q5	13.4
Hou_2004_5	Lhasa Terrane	Tinggong	Granite (porphyritic)	29.5476	90.0577	Q5	17.6
Hou_2004_6	Lhasa Terrane	Chongjiang	Monzonite (Qz, porphyritic)	29.5956	90.0128	Q5	13.4
Hou_2004_7	Lhasa Terrane	Dongga	Monzonite (Qz, porphyritic)	29.4130	88.3759	Q4	12.5
Hou_2004_8	Lhasa Terrane	Nanmu	Granite (porphyritic)	29.5245	90.9339	Q5	16.0
Hou_2004_9	Lhasa Terrane	Chongjiang	Monzonite (porphyritic)	29.5956	90.0128	Q5	15.6
Jm-16	Lhasa Terrane	Jiama	Adakite	29.7205	91.7362	Q5	15.9
Jm-21	Lhasa Terrane	Jiama	Adakite	29.7205	91.7362	Q5	
Jm-23	Lhasa Terrane	Jiama	Adakite	29.7205	91.7362	Q5	15.9
Jm-7	Lhasa Terrane	Jiama	Adakite	29.7205	91.7362	Q5	
Jmy-01	Lhasa Terrane	Jiama	Adakite	29.7205	91.7362	Q5	15.9
Jmy-04	Lhasa Terrane	Jiama	Adakite	29.7205	91.7362	Q5	15.9
Jmy-07	Lhasa Terrane	Jiama	Adakite	29.7205	91.7362	Q5	15.9
Ng-16	Lhasa Terrane	Nanmu	Adakite	29.5245	90.9339	Q5	16.0
Ng-18	Lhasa Terrane	Nanmu	Adakite	29.5245	90.9339	Q5	16.0
Nmy-01	Lhasa Terrane	Nanmu	Adakite	29.5245	90.9339	Q5	
Nmy-02	Lhasa Terrane	Nanmu	Adakite	29.5245	90.9339	Q5	
Nmy-04	Lhasa Terrane	Nanmu	Adakite	29.5245	90.9339	Q5	16.0
Nmy-05	Lhasa Terrane	Nanmu	Adakite	29.5245	90.9339	Q5	
Nmy-07	Lhasa Terrane	Nanmu	Adakite	29.5245	90.9339	Q5	16.0
Nt-03	Lhasa Terrane	Nimu	Adakite	29.4331	90.1625	Q5	16.0
Nt-05	Lhasa Terrane	Nimu	Adakite	29.4331	90.1625	Q5	
Nt-07	Lhasa Terrane	Nimu	Adakite	29.4331	90.1625	Q5	
Nt-08	Lhasa Terrane	Nimu	Adakite	29.4331	90.1625	Q5	16.0
Nt-10	Lhasa Terrane	Nimu	Adakite	29.4331	90.1625	Q5	16.0
Nt-12	Lhasa Terrane	Nimu	Adakite	29.4331	90.1625	Q5	
Nt-31	Lhasa Terrane	Nimu	Adakite	29.4331	90.1625	Q5	

Sample data continued

Sample	87Sr/86Sr(i)	eNd(t)	206Pb/ 204Pb(t)	207Pb/ 204Pb(t)	208Pb/ 204Pb(t)	*UPR	**ADK	Source
Hou_2004_21						N.D.	N.D.	Hou et al. (2004)
Hou_2004_22						N.D.	N.D.	Hou et al. (2004)
Hou_2004_23						N.D.	N.D.	Hou et al. (2004)
Hou_2004_24						N.D.	N.D.	Hou et al. (2004)
Hou_2004_25						N.D.	N.D.	Hou et al. (2004)
Hou_2004_26						N.D.	N.D.	Hou et al. (2004)
Hou_2004_3						N.D.	N.D.	Hou et al. (2004)
Hou_2004_4						N.D.	N.D.	Hou et al. (2004)
Hou_2004_5						N.D.	N.D.	Hou et al. (2004)
Hou_2004_6						N.D.	N.D.	Hou et al. (2004)
Hou_2004_7						N.D.	N.D.	Hou et al. (2004)
Hou_2004_8						N.D.	N.D.	Hou et al. (2004)
Hou_2004_9						N.D.	N.D.	Hou et al. (2004)
Jm-16	0.7069	-1.5	18.6	15.6	38.9	No	No	Hou et al. (2004)
Jm-21						No	Yes	Hou et al. (2004)
Jm-23	0.7062	-1.3				No	No	Hou et al. (2004)
Jm-7						No	No	Hou et al. (2004)
Jmy-01	0.7068	-2.3	18.6	15.6	38.9	No	No	Hou et al. (2004)
Jmy-04	0.7065	-6.2	18.7	15.6	39.0	No	No	Hou et al. (2004)
Jmy-07	0.7064	-2.1	18.6	15.6	38.9	No	No	Hou et al. (2004)
Ng-16	0.7050	-3.3	18.4	15.6	38.5	No	Yes	Hou et al. (2004)
Ng-18	0.7048	1.4	18.4	15.6	38.5	No	Yes	Hou et al. (2004)
Nmy-01						No	Yes	Hou et al. (2004)
Nmy-02						No	No	Hou et al. (2004)
Nmy-04	0.7051	2.2	18.2	15.5	39.0	No	Yes	Hou et al. (2004)
Nmy-05						No	Yes	Hou et al. (2004)
Nmy-07	0.7048	5.5	18.4	15.6	38.9	No	Yes	Hou et al. (2004)
Nt-03	0.7054	-0.1	18.4	15.6	38.6	No	Yes	Hou et al. (2004)
Nt-05						No	No	Hou et al. (2004)
Nt-07						No	Yes	Hou et al. (2004)
Nt-08	0.7056	-2.3	18.4	15.6	38.6	No	Yes	Hou et al. (2004)
Nt-10	0.7059	-1.3	18.4	15.6	38.7	No	Yes	Hou et al. (2004)
Nt-12						No	Yes	Hou et al. (2004)
Nt-31						No	No	Hou et al. (2004)

Table A.2: continued

Sample	Terrane	Location	Lithology	Latitude (dd)	Longitude (dd)	Quadrant	Age (Ma)
Nty-01	Lhasa Terrane	Nanmu	Adakite	29.5245	90.9339	Q5	
Nty-04	Lhasa Terrane	Nanmu	Adakite	29.5245	90.9339	Q5	
Nty-05	Lhasa Terrane	Nanmu	Adakite	29.5245	90.9339	Q5	
Nty-08	Lhasa Terrane	Nanmu	Adakite	29.5245	90.9339	Q5	
Nty-11	Lhasa Terrane	Nanmu	Adakite	29.5245	90.9339	Q5	
PI-18	Lhasa Terrane	Nanmu	Adakite	29.5245	90.9339	Q5	16.0
PI-28	Lhasa Terrane	Nanmu	Adakite	29.5245	90.9339	Q5	16.0
QZK001	Lhasa Terrane	Qulong	Adakite	29.6337	91.2955	Q5	17.7
0317-01	Himalayas	Dala	Granite	28.6472	92.2260	Q5	44.6
0317-02	Himalayas	Dala	Granite	28.6472	92.2260	Q5	44.6
0317-03	Himalayas	Dala	Granite	28.6472	92.2260	Q5	44.6
0317-04	Himalayas	Dala	Granite	28.6472	92.2260	Q5	44.6
0317-05	Himalayas	Dala	Granite	28.6472	92.2260	Q5	44.6
0317-06	Himalayas	Dala	Granite	28.6472	92.2260	Q5	44.6
0389-10	Himalayas	Quedang	Granite	28.5130	92.3059	Q5	46.3
0389-11	Himalayas	Quedang	Granite	28.5130	92.3059	Q5	46.3
0389-12	Himalayas	Quedang	Granite	28.5130	92.3059	Q5	46.3
0389-17	Himalayas	Yardoi	Amphibolite	28.8299	91.9555	Q5	
0389-6	Himalayas	Quedang	Granite	28.5130	92.3059	Q5	46.3
0389-7	Himalayas	Quedang	Granite	28.5130	92.3059	Q5	46.3
0389-8	Himalayas	Quedang	Granite	28.5130	92.3059	Q5	46.3
0389-9	Himalayas	Quedang	Granite	28.5130	92.3059	Q5	46.3
cb-154	Himalayas	Dala	Granite	28.6472	92.2260	Q5	44.6
cb-167	Himalayas	Dala	Granite	28.6472	92.2260	Q5	44.6
cb-168	Himalayas	Dala	Granite	28.6472	92.2260	Q5	44.6
cb-172	Himalayas	Dala	Granite	28.6472	92.2260	Q5	44.6
cb-178	Himalayas	Dala	Granite	28.6472	92.2260	Q5	44.6
cb-189	Himalayas	Dala	Granite	28.6472	92.2260	Q5	44.6
cb-193	Himalayas	Dala	Granite	28.6472	92.2260	Q5	44.6
cb-206	Himalayas	Quedang	Granite	28.5130	92.3059	Q5	46.3
cb-207	Himalayas	Quedang	Granite	28.5130	92.3059	Q5	46.3
cb-208	Himalayas	Quedang	Granite	28.5130	92.3059	Q5	46.3
cb-209	Himalayas	Quedang	Granite	28.5130	92.3059	Q5	46.3
cb-210	Himalayas	Quedang	Granite	28.5130	92.3059	Q5	46.3

Sample data continued

Sample	87Sr/86Sr(i)	eNd(t)	206Pb/ 204Pb(t)	207Pb/ 204Pb(t)	208Pb/ 204Pb(t)	*UPR	**ADK	Source
Nty-01						No	No	Hou et al. (2004)
Nty-04						No	No	Hou et al. (2004)
Nty-05						No	Yes	Hou et al. (2004)
Nty-08						No	No	Hou et al. (2004)
Nty-11						No	No	Hou et al. (2004)
PI-18	0.7049	1.6	18.4	15.6	38.6	No	Yes	Hou et al. (2004)
PI-28	0.7051	0.5	18.4	15.6	38.6	No	Yes	Hou et al. (2004)
QZK001						N.D.	N.D.	Hou et al. (2004)
0317-01	0.7176	-12.3				N.D.	N.D.	Hou et al. (2012)
0317-02	0.7179	-9.2				N.D.	N.D.	Hou et al. (2012)
0317-03	0.7178	-12.2				N.D.	N.D.	Hou et al. (2012)
0317-04	0.7178	-12.4				N.D.	N.D.	Hou et al. (2012)
0317-05	0.7177	-12.3				N.D.	N.D.	Hou et al. (2012)
0317-06	0.7178	-12.1				N.D.	N.D.	Hou et al. (2012)
0389-10	0.7159	-11.0				N.D.	N.D.	Hou et al. (2012)
0389-11	0.7162	-11.0				N.D.	N.D.	Hou et al. (2012)
0389-12	0.7163	-11.2				N.D.	N.D.	Hou et al. (2012)
0389-17	0.7334	-15.6				N.D.	N.D.	Hou et al. (2012)
0389-6	0.7151	-10.0				N.D.	N.D.	Hou et al. (2012)
0389-7	0.7160	-11.1				N.D.	N.D.	Hou et al. (2012)
0389-8	0.7158	-10.9				N.D.	N.D.	Hou et al. (2012)
0389-9	0.7156	-11.0				N.D.	N.D.	Hou et al. (2012)
cb-154						No	No	Hou et al. (2012)
cb-167	0.7178	-12.6				No	No	Hou et al. (2012)
cb-168						No	No	Hou et al. (2012)
cb-172	0.7179	-12.4				No	No	Hou et al. (2012)
cb-178						No	No	Hou et al. (2012)
cb-189	0.7176	-12.5				No	No	Hou et al. (2012)
cb-193	0.7181	-12.6				No	No	Hou et al. (2012)
cb-206						No	No	Hou et al. (2012)
cb-207	0.7165	-11.8				No	No	Hou et al. (2012)
cb-208	0.7159	-11.6				No	No	Hou et al. (2012)
cb-209	0.7158	-11.3				No	No	Hou et al. (2012)
cb-210	0.7154	-11.3				No	No	Hou et al. (2012)

Table A.2: continued

Sample	Terrane	Location	Lithology	Latitude (dd)	Longitude (dd)	Quadrant	Age (Ma)
cb-211	Himalayas	Quedang	Granite	28.5130	92.3059	Q5	46.3
cb-212-1	Himalayas	Quedang	Granite	28.5130	92.3059	Q5	46.3
cb-213-2	Himalayas	Quedang	Granite	28.5130	92.3059	Q5	46.3
cb-31	Lhasa Terrane	Zedong	Granodiorite	29.2918	91.8059	Q5	29.8
cb-33	Lhasa Terrane	Zedong	Granodiorite	29.2918	91.8059	Q5	29.8
cb-34	Lhasa Terrane	Zedong	Granodiorite	29.2918	91.8059	Q5	29.8
cb-35	Lhasa Terrane	Zedong	Granodiorite	29.2918	91.8059	Q5	29.8
cb-36	Lhasa Terrane	Zedong	Granodiorite	29.2918	91.8059	Q5	29.8
cb-37	Lhasa Terrane	Zedong	Granodiorite	29.2918	91.8059	Q5	29.8
cb-38	Lhasa Terrane	Zedong	Granodiorite	29.2918	91.8059	Q5	29.8
cb-77	Himalayas	Quedang	Granite	28.5130	92.3059	Q5	46.3
cb-77-1	Himalayas	Quedang	Granite	28.5130	92.3059	Q5	46.3
cb-77-2	Himalayas	Quedang	Granite	28.5130	92.3059	Q5	46.3
cb-77-3	Himalayas	Quedang	Granite	28.5130	92.3059	Q5	46.3
cb-78	Himalayas	Quedang	Granite	28.5130	92.3059	Q5	46.3
cb-79	Himalayas	Quedang	Granite	28.5130	92.3059	Q5	46.3
CMD-1	Lhasa Terrane	Zedong	Granodiorite	29.2918	91.8059	Q5	29.8
CMD-10	Lhasa Terrane	Zedong	Granodiorite	29.2918	91.8059	Q5	29.8
CMD-16-1	Lhasa Terrane	Zedong	Granodiorite	29.2918	91.8059	Q5	29.8
CMD-17	Lhasa Terrane	Zedong	Granodiorite	29.2918	91.8059	Q5	29.8
CMD-18	Lhasa Terrane	Zedong	Granodiorite	29.2918	91.8059	Q5	29.8
CMD-19	Lhasa Terrane	Zedong	Granodiorite	29.2918	91.8059	Q5	29.8
CMD-20	Lhasa Terrane	Zedong	Granodiorite	29.2918	91.8059	Q5	29.8
CMD-21	Lhasa Terrane	Zedong	Granodiorite	29.2918	91.8059	Q5	29.8
CMD-30	Lhasa Terrane	Zedong	Granodiorite	29.2918	91.8059	Q5	29.8
CMD-31	Lhasa Terrane	Zedong	Granodiorite	29.2918	91.8059	Q5	29.8
CMD-32	Lhasa Terrane	Zedong	Granodiorite	29.2918	91.8059	Q5	29.8
CMD-33	Lhasa Terrane	Zedong	Granodiorite	29.2918	91.8059	Q5	29.8
CMD-36	Lhasa Terrane	Zedong	Granodiorite	29.2918	91.8059	Q5	29.8
CMD-37	Lhasa Terrane	Zedong	Granodiorite	29.2918	91.8059	Q5	29.8
T0319-6	Himalayas	Yardoi	Granite	28.8299	91.9555	Q5	42.6
T0319-7	Himalayas	Yardoi	Granite	28.8299	91.9555	Q5	42.6
T0319-8	Himalayas	Yardoi	Granite	28.8299	91.9555	Q5	42.6
T0319-9	Himalayas	Yardoi	Granite	28.8299	91.9555	Q5	42.6

Sample data continued

Sample	87Sr/86Sr(i)	eNd(t)	206Pb/ 204Pb(t)	207Pb/ 204Pb(t)	208Pb/ 204Pb(t)	*UPR	**ADK	Source
cb-211	0.7131	-10.6				No	Yes	Hou et al. (2012)
cb-212-1	0.7158	-9.0				N.D.	N.D.	Hou et al. (2012)
cb-213-2						No	No	Hou et al. (2012)
cb-31						No	No	Hou et al. (2012)
cb-33						No	No	Hou et al. (2012)
cb-34	0.7064	-3.2				No	No	Hou et al. (2012)
cb-35						No	No	Hou et al. (2012)
cb-36	0.7062	-3.4				No	No	Hou et al. (2012)
cb-37						No	Yes	Hou et al. (2012)
cb-38	0.7066	-3.3				No	No	Hou et al. (2012)
cb-77	0.7158	-11.4				No	No	Hou et al. (2012)
cb-77-1						No	No	Hou et al. (2012)
cb-77-2						No	No	Hou et al. (2012)
cb-77-3						No	No	Hou et al. (2012)
cb-78	0.7159	-11.6				No	No	Hou et al. (2012)
cb-79	0.7161	-11.5				No	No	Hou et al. (2012)
CMD-1						No	Yes	Hou et al. (2012)
CMD-10	0.7062	-3.2				No	Yes	Hou et al. (2012)
CMD-16-1						No	Yes	Hou et al. (2012)
CMD-17	0.7063	-3.4				No	Yes	Hou et al. (2012)
CMD-18						No	Yes	Hou et al. (2012)
CMD-19						No	Yes	Hou et al. (2012)
CMD-20	0.7061	-2.5				No	Yes	Hou et al. (2012)
CMD-21						No	No	Hou et al. (2012)
CMD-30						No	Yes	Hou et al. (2012)
CMD-31						No	Yes	Hou et al. (2012)
CMD-32	0.7062	-3.1				No	Yes	Hou et al. (2012)
CMD-33	0.7062	-3.2				No	Yes	Hou et al. (2012)
CMD-36						No	No	Hou et al. (2012)
CMD-37						No	No	Hou et al. (2012)
T0319-6						No	No	Hou et al. (2012)
T0319-7						No	No	Hou et al. (2012)
T0319-8						No	No	Hou et al. (2012)
T0319-9						No	No	Hou et al. (2012)

Table A.2: continued

Sample	Terrane	Location	Lithology	Latitude (dd)	Longitude (dd)	Quadrant	Age (Ma)
T0320-6	Himalayas	Yardoi	Granite	28.8299	91.9555	Q5	42.6
YX-10	Himalayas	Yangxiong	Granite (Bt,Ms)	28.4085	92.5255	Q5	46.5
YX-11	Himalayas	Yangxiong	Granite (Bt,Ms)	28.4085	92.5255	Q5	46.5
YX-12	Himalayas	Yangxiong	Granite (Bt,Ms)	28.4085	92.5255	Q5	46.5
YX-13	Himalayas	Yangxiong	Granite (Bt,Ms)	28.4085	92.5255	Q5	46.5
YX-14	Himalayas	Yangxiong	Granite (Bt,Ms)	28.4085	92.5255	Q5	46.5
06FW101	Lhasa Terrane	N Lhasa	Monzogranite (Bt)	29.6867	91.1117	Q5	64.7
06FW104	Lhasa Terrane	N Lhasa	Monzogranite (Bt)	29.6753	91.0756	Q5	64.4
06FW105	Lhasa Terrane	Yangda	Monzogranite (Bt)	29.6817	90.9319	Q5	55.2
06FW108	Lhasa Terrane	N Gurong	Granodiorite (Bt, Hbl)	29.7589	90.7756	Q5	56.8
06FW110	Lhasa Terrane	Zhongduiguo	Monzogranite (Bt)	29.7375	90.8331	Q5	54.3
06FW111	Lhasa Terrane	Caina	Monzogranite (Bt, Hbl)	29.4433	90.9564	Q5	50.6
06FW112	Lhasa Terrane	N Caina	Granodiorite (Bt, Hbl)	29.4906	90.9611	Q5	53.4
06FW114	Lhasa Terrane	NorthE Caina	Granodiorite (Bt, Hbl)	29.5308	90.9931	Q5	86.4
06FW118	Lhasa Terrane	Niedang	Monzogranite (Bt)	29.4992	90.9386	Q5	51.0
06FW119	Lhasa Terrane	Niedang	Granodiorite (Bt)	29.4992	90.9386	Q5	51.2
06FW120	Lhasa Terrane	Niedang	Enclave (dioritic)	29.4992	90.9386	Q5	50.3
06FW121	Lhasa Terrane	Niedang	Dike (granitic)	29.4992	90.9386	Q5	51.1
06FW123	Lhasa Terrane	Nanmu Copper	Monzogranite (Bt)	29.5217	90.8106	Q5	17.0
06FW124	Lhasa Terrane	Nanmu Copper	Granite (porphyritic)	29.5217	90.8106	Q5	15.3
06FW125	Lhasa Terrane	E Nanmu Copper	Monzogranite (Bt, Hbl)	29.5172	90.8247	Q5	17.7
06FW126	Lhasa Terrane	Nanmu Power Station	Granodiorite (Hbl)	29.4817	90.8739	Q5	55.3
06FW127	Lhasa Terrane	Nanmu Power Station	Dike (granitic)	29.4817	90.8739	Q5	49.5
06FW128	Lhasa Terrane	Nanmu Power Station	Dike (doleritic)	29.4817	90.8739	Q5	49.9
06FW129	Lhasa Terrane	Nanmu	Granodiorite (Bt, Hbl)	29.4639	90.8967	Q5	52.9
06FW131	Lhasa Terrane	Jiangcun	Orthogneiss (tonalitic)	29.4078	90.9058	Q5	44.0
06FW133	Lhasa Terrane	Galashan tunnel	Monzonite (Bt, Hbl)	29.3336	90.8656	Q5	47.1
06FW134	Lhasa Terrane	Galashan tunnel	Monzogranite (Bt)	29.3606	90.8756	Q5	41.9
06FW139	Lhasa Terrane	E Quxu	Monzonite (Qz)	29.3831	90.7156	Q5	41.5
06FW140	Lhasa Terrane	Badi	Monzogranite (Bt)	29.4725	90.7156	Q5	43.7
06FW142	Lhasa Terrane	Baijin	Monzogranite (Bt)	29.4392	90.7108	Q5	21.3
06FW146	Lhasa Terrane	Qupu	Gabbro	29.4028	90.7175	Q5	56.9
06FW147	Lhasa Terrane	NW Quxu	Granodiorite (Bt)	29.3675	90.7244	Q5	51.5
06FW148	Lhasa Terrane	NW Quxu	Dike (syenogranitic)	29.3675	90.7244	Q5	51.3

Sample data continued

Sample	87Sr/86Sr(i)	eNd(t)	206Pb/ 204Pb(t)	207Pb/ 204Pb(t)	208Pb/ 204Pb(t)	*UPR	**ADK	Source
T0320-6						No	Yes	Hou et al. (2012)
YX-10	0.7175	-12.9				No	No	Hou et al. (2012)
YX-11	0.7175	-13.0				No	No	Hou et al. (2012)
YX-12						No	No	Hou et al. (2012)
YX-13						No	No	Hou et al. (2012)
YX-14						No	No	Hou et al. (2012)
06FW101						No	No	Ji et al. (2009)
06FW104						No	No	Ji et al. (2009)
06FW105						No	No	Ji et al. (2009)
06FW108						No	No	Ji et al. (2009)
06FW110						No	No	Ji et al. (2009)
06FW111						No	No	Ji et al. (2009)
06FW112						No	No	Ji et al. (2009)
06FW114						N.D.	N.D.	Ji et al. (2009)
06FW118						No	No	Ji et al. (2009)
06FW119						No	Yes	Ji et al. (2009)
06FW120						No	No	Ji et al. (2009)
06FW121						No	No	Ji et al. (2009)
06FW123						N.D.	N.D.	Ji et al. (2009)
06FW124						N.D.	N.D.	Ji et al. (2009)
06FW125						N.D.	N.D.	Ji et al. (2009)
06FW126						No	No	Ji et al. (2009)
06FW127						No	No	Ji et al. (2009)
06FW128						No	No	Ji et al. (2009)
06FW129						No	No	Ji et al. (2009)
06FW131						No	Yes	Ji et al. (2009)
06FW133						No	Yes	Ji et al. (2009)
06FW134						No	No	Ji et al. (2009)
06FW139						No	Yes	Ji et al. (2009)
06FW140						No	No	Ji et al. (2009)
06FW142						N.D.	N.D.	Ji et al. (2009)
06FW146						No	No	Ji et al. (2009)
06FW147						No	No	Ji et al. (2009)
06FW148						No	No	Ji et al. (2009)

Table A.2: continued

Sample	Terrane	Location	Lithology	Latitude (dd)	Longitude (dd)	Quadrant	Age (Ma)
06FW151	Lhasa Terrane	W Quxu	Diorite	29.3575	90.7167	Q5	55.5
06FW152-2	Lhasa Terrane	E Qulin	Diorite	29.4014	90.1789	Q5	57.3
06FW154	Lhasa Terrane	Angang	Monzogranite (Bt)	29.5781	90.2742	Q5	51.3
06FW155	Lhasa Terrane	Angang Power Station	Monzogranite (Bt)	29.5425	90.2731	Q5	61.1
06FW156	Lhasa Terrane	Kongdonglang	Monzogranite (Bt)	29.4994	90.2711	Q5	55.4
06FW157	Lhasa Terrane	NW Qulin	Monzogranite	29.4136	90.2233	Q5	32.5
06FW158	Lhasa Terrane	SW Nymo	Monzogranite (Bt)	29.5208	90.0419	Q5	14.9
06FW159	Lhasa Terrane	Chongjiang Copper	Monzogranite	29.6069	89.9839	Q5	15.3
06FW160	Lhasa Terrane	Chongjiang Copper	Granite (porphyritic)	29.6069	89.9839	Q5	13.7
06FW161	Lhasa Terrane	Chongjiang Copper	Diorite (porphyritic)	29.6069	89.9839	Q5	13.5
06FW162	Lhasa Terrane	Numa	Granodiorite	29.5389	89.6225	Q5	50.9
06FW163	Lhasa Terrane	Numa	Monzogranite	29.5389	89.6225	Q5	48.2
06FW164	Lhasa Terrane	Numa	Monzogranite	29.5219	89.6233	Q5	184.9
06FW165	Lhasa Terrane	N Numa	Orthogneiss (granodioritic)	29.5033	89.6311	Q5	194.0
06FW166	Lhasa Terrane	N Numa	Orthogneiss (monzogranitic)	29.5033	89.6311	Q5	205.3
06FW167	Lhasa Terrane	W Numa	Monzogranite	29.4397	89.6319	Q5	155.9
06FW168	Lhasa Terrane	W Numa	Diorite (Hbl)	29.4397	89.6319	Q5	174.2
06FW169	Lhasa Terrane	W Numa	Dike (syenogranitic)	29.4397	89.6319	Q5	151.8
06FW170	Lhasa Terrane	N Dazhuqu	Diorite (Bt, Hbl)	29.3928	89.6283	Q5	108.6
06FW174	Lhasa Terrane	Karu	Diorite (Hbl)	29.3511	90.0969	Q5	50.2
06FW175	Lhasa Terrane	Karu	Diorite (Qz, Hbl)	29.3489	90.0672	Q5	52.6
06FW176	Lhasa Terrane	Nymo	Diorite (Hbl)	29.3347	90.2492	Q5	53.6
08FW51	Lhasa Terrane	SE Lhasa	Granodiorite	29.6370	91.1640	Q5	64.5
09FW41	Lhasa Terrane	Cuijiu	Monzogranite	29.4190	92.7380	Q5	56.1
09FW42	Lhasa Terrane	Cuijiu	Monzogranite	29.4070	92.7450	Q5	50.7
09FW43	Lhasa Terrane	Cuijiu	Monzogranite	29.4070	92.7450	Q5	42.0
09FW50	Lhasa Terrane	N Jiacha	Granodiorite	29.2390	92.6970	Q5	50.2
SR01-1	Lhasa Terrane	Sangri	Granodiorite	29.2880	92.0960	Q5	45.4
SR02-1	Lhasa Terrane	Sangri	Granite	29.2880	92.1190	Q5	37.7
SR03-1	Lhasa Terrane	Zangga	Granodiorite	29.2670	92.2170	Q5	59.8
SR04-1	Lhasa Terrane	Woka	Granodiorite	29.3160	92.2370	Q5	42.1
07TB33a-1	Lhasa Terrane	Kelu	Monzonite (adakitic)	29.3500	91.4125	Q5	91.3
07TB33a-2	Lhasa Terrane	Kelu	Diorite (adakitic)	29.3500	91.4125	Q5	91.6
07TB33b-1	Lhasa Terrane	Kelu	Monzonite (adakitic)	29.3500	91.4125	Q5	91.6

Sample data continued

Sample	87Sr/86Sr(i)	eNd(t)	206Pb/ 204Pb(t)	207Pb/ 204Pb(t)	208Pb/ 204Pb(t)	*UPR	**ADK	Source
06FW151						No	No	Ji et al. (2009)
06FW152-2						No	No	Ji et al. (2009)
06FW154						No	No	Ji et al. (2009)
06FW155						No	No	Ji et al. (2009)
06FW156						No	No	Ji et al. (2009)
06FW157						N.D.	N.D.	Ji et al. (2009)
06FW158						N.D.	N.D.	Ji et al. (2009)
06FW159						N.D.	N.D.	Ji et al. (2009)
06FW160						N.D.	N.D.	Ji et al. (2009)
06FW161						N.D.	N.D.	Ji et al. (2009)
06FW162						No	No	Ji et al. (2009)
06FW163						No	No	Ji et al. (2009)
06FW164						N.D.	N.D.	Ji et al. (2009)
06FW165						N.D.	N.D.	Ji et al. (2009)
06FW166						N.D.	N.D.	Ji et al. (2009)
06FW167						N.D.	N.D.	Ji et al. (2009)
06FW168						N.D.	N.D.	Ji et al. (2009)
06FW169						N.D.	N.D.	Ji et al. (2009)
06FW170						N.D.	N.D.	Ji et al. (2009)
06FW174						No	No	Ji et al. (2009)
06FW175						No	No	Ji et al. (2009)
06FW176						No	No	Ji et al. (2009)
08FW51						No	No	Ji et al. (2012)
09FW41						No	No	Ji et al. (2012)
09FW42						No	No	Ji et al. (2012)
09FW43						No	No	Ji et al. (2012)
09FW50						No	Yes	Ji et al. (2012)
SR01-1						No	No	Ji et al. (2012)
SR02-1						No	No	Ji et al. (2012)
SR03-1						No	No	Ji et al. (2012)
SR04-1						No	No	Ji et al. (2012)
07TB33a-1	0.7038	3.4				No	No	Jiang et al. (2012)
07TB33a-2	0.7040	3.0				No	No	Jiang et al. (2012)
07TB33b-1						No	No	Jiang et al. (2012)

Table A.2: continued

Sample	Terrane	Location	Lithology	Latitude (dd)	Longitude (dd)	Quadrant	Age (Ma)
07TB33b-2	Lhasa Terrane	Kelu	Monzonite (adakitic)	29.3500	91.4125	Q5	93.3
07TB33c-1	Lhasa Terrane	Kelu	Diorite (adakitic)	29.3500	91.4125	Q5	91.6
07TB33d	Lhasa Terrane	Kelu	Diorite (adakitic)	29.3500	91.4125	Q5	90.3
07TB33e	Lhasa Terrane	Kelu	Monzonite (adakitic)	29.3500	91.4125	Q5	91.6
T5D1	Himalayas	SE Nyonno Ri	Orthogneiss	28.1481	87.6391	Q4	
T5D10	Himalayas	SE Nyonno Ri	Gneiss (migmatitic, Grt)	28.1562	87.6460	Q4	
T5D19	Himalayas	STDSZ S Dinggye	Micaschist (Grt, Sil)	28.1846	87.7810	Q4	
T5D22	Himalayas	S Nyonno Ri	Orthogneiss (migmatitic)	28.1586	87.6165	Q4	12.9
T5D26	Himalayas	S Nyonno Ri	Pegmatite	28.1601	87.6111	Q4	9.8
T5D33	Himalayas	E Sangkar Ri	Paragneiss (Grt, Sil)	28.3173	87.7160	Q4	10.8
T5D39	Himalayas	E Sangkar Ri	Paragneiss (Grt, Sil)	28.3169	87.7397	Q4	13.1
T5D40	Himalayas	north Dinggye	Granite (Bt, Ms)	28.4094	87.7533	Q4	
T5D5	Himalayas	SE Nyonno Ri	Dike (leucocratic)	28.1437	87.6466	Q4	11.1
T5D6	Himalayas	SE Nyonno Ri	Orthogneiss	28.1437	87.6466	Q4	13.1
T7A10	Himalayas	upper Arun gorges	Orthogneiss	28.2701	87.3993	Q4	8.5
T7A14	Himalayas	upper Arun gorges	Orthogneiss (micro-granitic)	28.2695	87.3969	Q4	6.2
T7A19	Himalayas	Arun south gorges	Mylonite	28.0932	87.3674	Q4	23.5
T7A20	Himalayas	Arun south gorges	Orthogneiss	28.0947	87.3664	Q4	
T7A33	Himalayas	W Tanghyu valley	Gneiss	28.2349	87.3832	Q4	10.9
T7A48	Himalayas	north flank	Quartz Cataclasite	28.3415	87.5134	Q4	12.2
97-7-16-2pk	Lhasa Terrane	Longzi La	Volcanic rock	32.4963	80.2025	Q2	22.5
97-7-3-3bpk	Lhasa Terrane	Longzi La	Granite	32.4963	80.2025	Q2	126.0
6-4-98-3d	Lhasa Terrane	S Gaize	Volcanic Rock	32.2593	84.0714	Q3	109.0
6-6-98-2	Lhasa Terrane	SE Gaize	Volcanic Rock	32.2479	84.3041	Q3	110.0
7-27-98-1	Lhasa Terrane	N Siling Co	Volcanic Rock	32.0456	88.5924	Q4	42.7
1DC367	Lhasa Terrane	Nima	Tuff (reworked)	31.8100	87.6700	Q4	24.9
1DC82	Lhasa Terrane	Nima	Tuff (reworked)	31.8200	87.6700	Q4	25.8
2NM170	Lhasa Terrane	Nima	Tuff (reworked)	31.7500	87.1000	Q4	25.3
3MC13	Lhasa Terrane	Nima	Tuff	31.7200	87.5200	Q4	99.0
6-11-04-2	Lhasa Terrane	Nima	Sandstone	31.7100	87.5300	Q4	97.0
6-11-04-4	Lhasa Terrane	Nima	Sandstone	31.7500	87.5200	Q4	106.0
7-11-05-2	Lhasa Terrane	Nima	Sandstone	31.7600	87.5200	Q4	125.0
7-14-98-2	Lhasa Terrane	Puzuo	Granite	31.9000	87.1700	Q4	124.0
8-13-03-1	Lhasa Terrane	Nima	Tuff (reworked)	31.8100	87.4700	Q4	23.5

Sample data continued

Sample	87Sr/86Sr(i)	eNd(t)	206Pb/ 204Pb(t)	207Pb/ 204Pb(t)	208Pb/ 204Pb(t)	*UPR	**ADK	Source
07TB33b-2	0.7038	3.7				No	No	Jiang et al. (2012)
07TB33c-1						No	No	Jiang et al. (2012)
07TB33d	0.7041	4.4				No	No	Jiang et al. (2012)
07TB33e	0.7039	3.9				No	No	Jiang et al. (2012)
T5D1						N.D.	N.D.	Kali et al. (2010)
T5D10						N.D.	N.D.	Kali et al. (2010)
T5D19						N.D.	N.D.	Kali et al. (2010)
T5D22						N.D.	N.D.	Kali et al. (2010)
T5D26						N.D.	N.D.	Kali et al. (2010)
T5D33						N.D.	N.D.	Kali et al. (2010)
T5D39						N.D.	N.D.	Kali et al. (2010)
T5D40						N.D.	N.D.	Kali et al. (2010)
T5D5						N.D.	N.D.	Kali et al. (2010)
T5D6						N.D.	N.D.	Kali et al. (2010)
T7A10						N.D.	N.D.	Kali et al. (2010)
T7A14						N.D.	N.D.	Kali et al. (2010)
T7A19						N.D.	N.D.	Kali et al. (2010)
T7A20						N.D.	N.D.	Kali et al. (2010)
T7A33						N.D.	N.D.	Kali et al. (2010)
T7A48						N.D.	N.D.	Kali et al. (2010)
97-7-16-2pk						N.D.	N.D.	Kapp et al. (2003a)
97-7-3-3bpk						N.D.	N.D.	Kapp et al. (2003a)
6-4-98-3d						N.D.	N.D.	Kapp et al. (2005)
6-6-98-2						N.D.	N.D.	Kapp et al. (2005)
7-27-98-1						N.D.	N.D.	Kapp et al. (2005)
1DC367						N.D.	N.D.	Kapp et al. (2007)
1DC82						N.D.	N.D.	Kapp et al. (2007)
2NM170						N.D.	N.D.	Kapp et al. (2007)
3MC13						N.D.	N.D.	Kapp et al. (2007)
6-11-04-2						N.D.	N.D.	Kapp et al. (2007)
6-11-04-4						N.D.	N.D.	Kapp et al. (2007)
7-11-05-2						N.D.	N.D.	Kapp et al. (2007)
7-14-98-2						N.D.	N.D.	Kapp et al. (2007)
8-13-03-1						N.D.	N.D.	Kapp et al. (2007)

Table A.2: continued

Sample	Terrane	Location	Lithology	Latitude (dd)	Longitude (dd)	Quadrant	Age (Ma)
8-6-03-1	Lhasa Terrane	Nima	Tuff (reworked)	31.7700	87.1000	Q4	26.0
8-6-03-2	Lhasa Terrane	Nima	Tuff (reworked)	31.7700	87.1000	Q4	26.1
6-11-05-1B	Lhasa Terrane	Lunggar rift	Orthogneiss (leucogranitic)	31.6104	83.5384	Q3	15.2
6-15-05-3	Lhasa Terrane	Lunggar rift	Granite (Bt)	31.4794	83.5695	Q3	21.7
6-7-05-2	Lhasa Terrane	Lunggar rift	Orthogneiss (leucogranitic)	31.5787	83.5385	Q3	8.9
6-7-05-3	Lhasa Terrane	Lunggar rift	Orthogneiss (leucogranitic)	31.5784	83.5397	Q3	9.0
6-9-05-2	Lhasa Terrane	Lunggar rift	Granite	31.8157	83.6575	Q3	152.0
Khan_1	Lhasa Terrane	Teru Volcanic Field	Unknown	36.1800	72.7300	Q1	64.8
Khan_103	Lhasa Terrane		Unknown	36.1600	73.0800	Q1	
Khan_104	Lhasa Terrane		Unknown	36.2500	73.7400	Q1	
Khan_106	Lhasa Terrane		Unknown	36.1000	73.5700	Q1	
Khan_108	Lhasa Terrane		Unknown				
Khan_111	Lhasa Terrane		Unknown				
Khan_16	Lhasa Terrane		Unknown	36.1800	73.0500	Q1	
Khan_17	Lhasa Terrane		Unknown	36.1800	73.0500	Q1	
Khan_18	Lhasa Terrane		Unknown	36.1700	73.0700	Q1	
Khan_2	Lhasa Terrane	Teru Volcanic Field	Unknown	36.1900	72.7300	Q1	63.1
Khan_20	Lhasa Terrane	Shunji Pluton	Unknown	36.2100	73.2800	Q1	64.5
Khan_33	Lhasa Terrane		Unknown	36.1500	73.0900	Q1	
Khan_34	Lhasa Terrane		Unknown	36.1500	73.1000	Q1	
Khan_38	Lhasa Terrane		Unknown	36.2400	73.4300	Q1	
Khan_41	Lhasa Terrane		Unknown	36.1800	73.1800	Q1	
Khan_47	Lhasa Terrane		Unknown	36.1900	73.2500	Q1	
Khan_52	Lhasa Terrane		Unknown	36.3100	73.3800	Q1	
Khan_59	Lhasa Terrane		Unknown	36.2500	73.3400	Q1	
Khan_61	Lhasa Terrane		Unknown	36.2500	73.4200	Q1	
Khan_63	Lhasa Terrane		Unknown	36.3900	73.3200	Q1	
Khan_67	Lhasa Terrane		Unknown	36.2300	73.5400	Q1	
Khan_69	Lhasa Terrane		Unknown	36.3500	73.3400	Q1	
Khan_70	Lhasa Terrane		Unknown	36.3500	73.3400	Q1	
Khan_72	Lhasa Terrane		Unknown	36.2500	73.6900	Q1	
Khan_76	Lhasa Terrane		Unknown	36.1800	72.7600	Q1	
Khan_8	Lhasa Terrane	Pingal Pluton	Unknown	36.1300	73.1600	Q1	
Khan_9	Lhasa Terrane	Teru Volcanic Field	Unknown	36.1800	72.8000	Q1	64.9

Sample data continued

Sample	87Sr/86Sr(i)	eNd(t)	206Pb/ 204Pb(t)	207Pb/ 204Pb(t)	208Pb/ 204Pb(t)	*UPR	**ADK	Source
8-6-03-1						N.D.	N.D.	Kapp et al. (2007)
8-6-03-2						N.D.	N.D.	Kapp et al. (2007)
6-11-05-1B						N.D.	N.D.	Kapp et al. (2008)
6-15-05-3						N.D.	N.D.	Kapp et al. (2008)
6-7-05-2						N.D.	N.D.	Kapp et al. (2008)
6-7-05-3						N.D.	N.D.	Kapp et al. (2008)
6-9-05-2						N.D.	N.D.	Kapp et al. (2008)
Khan_1	0.7041	4.2	18.5	15.6	38.6	No	No	Khan et al. (2009)
Khan_103	0.7043	5.8	18.6	15.5	38.7	No	No	Khan et al. (2009)
Khan_104	0.7042	5.7	18.6	15.5	38.6	No	No	Khan et al. (2009)
Khan_106	0.7041	5.9	18.6	15.5	38.5	No	No	Khan et al. (2009)
Khan_108	0.7041	6.3	18.6	15.5	38.5	No	No	Khan et al. (2009)
Khan_111	0.7048	4.3	18.6	15.5	38.7	No	No	Khan et al. (2009)
Khan_16	0.7045	5.6	18.7	15.6	38.7	No	No	Khan et al. (2009)
Khan_17	0.7045	5.4	18.5	15.6	38.6	No	No	Khan et al. (2009)
Khan_18	0.7049	5.5	18.6	15.6	38.7	No	No	Khan et al. (2009)
Khan_2	0.7048	4.3	18.4	15.6	38.7	No	No	Khan et al. (2009)
Khan_20	0.7052	4.3	18.5	15.6	38.7	No	No	Khan et al. (2009)
Khan_33	0.7047	4.0	18.4	15.6	38.4	No	No	Khan et al. (2009)
Khan_34	0.7043	4.1	18.4	15.6	38.4	No	No	Khan et al. (2009)
Khan_38	0.7052	4.2	18.6	15.6	38.8	No	No	Khan et al. (2009)
Khan_41	0.7038	5.2	18.4	15.6	38.4	No	No	Khan et al. (2009)
Khan_47	0.7039		18.3	15.5	38.1	No	No	Khan et al. (2009)
Khan_52	0.7045	3.2	18.7	15.6	38.8	No	No	Khan et al. (2009)
Khan_59	0.7043	5.8	18.4	15.5	38.3	No	No	Khan et al. (2009)
Khan_61	0.7043	3.2	18.5	15.5	38.3	No	No	Khan et al. (2009)
Khan_63	0.7041	4.9	18.6	15.6	38.7	No	No	Khan et al. (2009)
Khan_67	0.7049	3.5	18.7	15.5	38.7	No	No	Khan et al. (2009)
Khan_69	0.7042	5.3	18.4	15.5	38.2	No	No	Khan et al. (2009)
Khan_70	0.7044	6.4	18.3	15.5	38.2	No	No	Khan et al. (2009)
Khan_72	0.7042	6.1	18.4	15.5	38.2	No	No	Khan et al. (2009)
Khan_76	0.7041	6.4	18.2	15.5	38.0	No	No	Khan et al. (2009)
Khan_8	0.7046	1.9	18.6	15.6	38.9	No	No	Khan et al. (2009)
Khan_9	0.7041	4.3	18.5	15.6	38.7	No	No	Khan et al. (2009)

Table A.2: continued

Sample	Terrane	Location	Lithology	Latitude (dd)	Longitude (dd)	Quadrant	Age (Ma)
Khan_96	Lhasa Terrane		Unknown	36.2500	73.7300	Q1	
Khan_99	Lhasa Terrane		Unknown	36.2600	73.7400	Q1	
BD-19	Lhasa Terrane	Linzhou	Rhyolite	30.1600	91.2500	Q5	49.2
D-3	Lhasa Terrane	Linzhou	Andesite	30.1600	91.2500	Q5	64.5
ET022A	Lhasa Terrane	Qulong	Rhyolite	29.5200	91.5100	Q5	87.2
Lee_N-9	Lhasa Terrane	Linzhou	Andesite	30.1600	91.2500	Q5	
LZ-1	Lhasa Terrane	Linzhou	Ignimbrite	30.1600	91.2500	Q5	48.7
LZ9913	Lhasa Terrane	Linzhou	Andesite	30.1600	91.2500	Q5	61.5
M-01	Lhasa Terrane	Maqu	Andesite	33.9988	102.0721	Q5	59.8
P-6-1	Lhasa Terrane	Linzhou	Rhyolite	30.1600	91.2500	Q5	48.1
ST053	Lhasa Terrane	Linzhou	Dacite	30.1100	91.2800	Q5	47.1
ST055A	Lhasa Terrane	Linzhou	Rhyolite	30.1600	91.2500	Q5	49.3
ST055C	Lhasa Terrane	Linzhou	Basaltic Andesite	30.1600	91.2500	Q5	43.8
ST057A	Lhasa Terrane	Linzhou	Andesite	30.2900	91.4100	Q5	46.5
ST059A	Lhasa Terrane	Linzhou	Dacite	30.2300	91.3600	Q5	48.8
ST060C	Lhasa Terrane	Linzhou	Dacite	30.2000	91.3400	Q5	48.7
ST062	Lhasa Terrane	Linzhou	Dacite	30.2700	91.2400	Q5	48.5
T006B1	Lhasa Terrane	Jinda	Basaltic Andesite	29.9900	93.0400	Q5	45.7
T036D	Lhasa Terrane		Unknown				
T038F	Lhasa Terrane	N Sangsang	Dacite	29.6500	86.7000	Q4	47.7
T038G	Lhasa Terrane	N Sangsang	Dacite	29.6500	86.7000	Q4	45.1
T040A	Lhasa Terrane		Unknown				
T041F	Lhasa Terrane	Xigaze	Basaltic Andesite	29.3600	88.8100	Q4	49.3
T047	Lhasa Terrane	Nanmulin	Basalt	29.6700	89.0800	Q4	44.0
T054A	Lhasa Terrane		Unknown				
T065A	Lhasa Terrane	Majiang	Rhyolite	29.7400	89.8800	Q5	48.6
T065B	Lhasa Terrane	Majiang	Rhyolite	29.7400	89.8800	Q5	
T068	Lhasa Terrane	Majiang	Rhyolite	29.7300	89.9800	Q5	47.8
T078B	Lhasa Terrane	Lhasa-NE	Dacite	29.9100	91.2300	Q5	97.3
T083C	Lhasa Terrane	W Lhasa	Basalt	29.7700	90.7800	Q5	43.2
T105A	Lhasa Terrane	NE Majiang	Andesite	29.9000	90.1300	Q5	53.0
T131A	Lhasa Terrane	N Comai	Rhyolite	30.6500	87.0600	Q4	112.0
T136A	Lhasa Terrane	Comai	Rhyolite	30.5100	87.0600	Q4	59.9
T139	Lhasa Terrane	Bangduo	Rhyolite	31.3500	85.9000	Q4	85.8

Sample data continued

Sample	87Sr/86Sr(i)	eNd(t)	206Pb/ 204Pb(t)	207Pb/ 204Pb(t)	208Pb/ 204Pb(t)	*UPR	**ADK	Source
Khan_96	0.7049	3.9	18.7	15.6	38.9	No	No	Khan et al. (2009)
Khan_99	0.7051	1.1	18.7	15.6	39.0	No	No	Khan et al. (2009)
BD-19						N.D.	N.D.	Lee et al. (2009)
D-3						N.D.	N.D.	Lee et al. (2009)
ET022A						N.D.	N.D.	Lee et al. (2009)
Lee_N-9						N.D.	N.D.	Lee et al. (2009)
LZ-1						N.D.	N.D.	Lee et al. (2009)
LZ9913						N.D.	N.D.	Lee et al. (2009)
M-01						N.D.	N.D.	Lee et al. (2009)
P-6-1						N.D.	N.D.	Lee et al. (2009)
ST053						N.D.	N.D.	Lee et al. (2009)
ST055A						N.D.	N.D.	Lee et al. (2009)
ST055C						No	No	Lee et al. (2009)
ST057A						No	No	Lee et al. (2009)
ST059A						N.D.	N.D.	Lee et al. (2009)
ST060C						No	No	Lee et al. (2009)
ST062						N.D.	N.D.	Lee et al. (2009)
T006B1						N.D.	N.D.	Lee et al. (2009)
T036D						No	No	Lee et al. (2009)
T038F						N.D.	N.D.	Lee et al. (2009)
T038G						N.D.	N.D.	Lee et al. (2009)
T040A						No	No	Lee et al. (2009)
T041F						No	No	Lee et al. (2009)
T047						No	No	Lee et al. (2009)
T054A						No	No	Lee et al. (2009)
T065A						No	No	Lee et al. (2009)
T065B						No	No	Lee et al. (2009)
T068						N.D.	N.D.	Lee et al. (2009)
T078B						N.D.	N.D.	Lee et al. (2009)
T083C						N.D.	N.D.	Lee et al. (2009)
T105A						N.D.	N.D.	Lee et al. (2009)
T131A						N.D.	N.D.	Lee et al. (2009)
T136A						N.D.	N.D.	Lee et al. (2009)
T139						N.D.	N.D.	Lee et al. (2009)

Table A.2: continued

Sample	Terrane	Location	Lithology	Latitude (dd)	Longitude (dd)	Quadrant	Age (Ma)
T140B	Lhasa Terrane	Bangduo	Andesite	31.3400	85.8800	Q4	106.0
T142	Lhasa Terrane	Coqin	Dacite	30.9800	85.1300	Q4	71.1
T151	Lhasa Terrane	NW Dajiaco	Basalt	30.2300	85.3200	Q4	53.9
T155	Lhasa Terrane	Dajiaco	Dacite	29.9000	85.7400	Q4	48.9
T169A	Lhasa Terrane	Namuco	Rhyolite	30.8500	91.1400	Q5	110.0
T233A	Lhasa Terrane	Linzhou	Breccia	30.1600	91.2500	Q5	62.5
T235C	Lhasa Terrane	Linzhou	Ignimbrite	30.1600	91.2500	Q5	56.4
TE087/93	Lhasa Terrane	SW Jarga	Dacite	31.4878	82.6548	Q3	44.8
XGS 93	Lhasa Terrane	Lhasa-Yangbajing	Ignimbrite				56.2
XT 59	Lhasa Terrane	Linzhou	Andesite	30.1600	91.2500	Q5	59.3
Y-5	Lhasa Terrane	Yangying	Rhyolite				52.9
T5D19b	Himalayas	STDSZ S Dinggye	Micaschist (Grt, Sil)	28.1846	87.7810	Q4	15.2
T5D20	Himalayas	STDSZ S Dinggye	Orthogneiss (leucogranitic)	28.1846	87.7810	Q4	14.2
T5D21	Himalayas	STDSZ S Dinggye	Leucogranite	28.1846	87.7810	Q4	13.6
73-164	Lhasa Terrane	E Transhimalaya	Granite	28.4644	97.1726	Q6	
73-540	Lhasa Terrane	E Transhimalaya	Granite				
73-720	Lhasa Terrane	E Transhimalaya	Granodiorite	29.8985	95.5393	Q6	
73-721	Lhasa Terrane	E Transhimalaya	Granodiorite	29.8719	95.5606	Q6	
73-73	Lhasa Terrane	E Transhimalaya	Granite	28.6449	97.4913	Q6	128.0
73-750	Lhasa Terrane	E Transhimalaya	Gabbro	29.8108	95.7810	Q6	
ET103A	Lhasa Terrane	E Transhimalaya	Orthogneiss (granitic)	29.9542	95.3845	Q6	119.0
ET104B	Lhasa Terrane	E Transhimalaya	Granite	29.5075	96.6044	Q6	115.0
ET105A	Lhasa Terrane	E Transhimalaya	Granite	29.5003	96.6066	Q6	120.0
ET105B	Lhasa Terrane	E Transhimalaya	Granite	29.5003	96.6066	Q6	120.0
ET105C	Lhasa Terrane	E Transhimalaya	Granite	29.5003	96.6066	Q6	
ET105D	Lhasa Terrane	E Transhimalaya	Granite	29.5003	96.6066	Q6	
ET105E	Lhasa Terrane	E Transhimalaya	Granite	29.5003	96.6066	Q6	
ET105F	Lhasa Terrane	E Transhimalaya	Granite	29.5003	96.6066	Q6	
ET105G	Lhasa Terrane	E Transhimalaya	Enclave	29.5003	96.6066	Q6	120.0
ET106A2	Lhasa Terrane	E Transhimalaya	Granite	29.3855	96.8690	Q6	123.0
ET107A	Lhasa Terrane	E Transhimalaya	Granite	29.3721	96.9119	Q6	120.0
ET108B	Lhasa Terrane	E Transhimalaya	Granite	28.4731	97.0499	Q6	
ET111B	Lhasa Terrane	E Transhimalaya	Granite	28.5193	97.0800	Q6	
ET113A	Lhasa Terrane	E Transhimalaya	Granite	28.5616	97.0852	Q6	59.0

Sample data continued

Sample	87Sr/86Sr(i)	eNd(t)	206Pb/ 204Pb(t)	207Pb/ 204Pb(t)	208Pb/ 204Pb(t)	*UPR	**ADK	Source
T140B						N.D.	N.D.	Lee et al. (2009)
T142						N.D.	N.D.	Lee et al. (2009)
T151						N.D.	N.D.	Lee et al. (2009)
T155						N.D.	N.D.	Lee et al. (2009)
T169A						N.D.	N.D.	Lee et al. (2009)
T233A						N.D.	N.D.	Lee et al. (2009)
T235C						N.D.	N.D.	Lee et al. (2009)
TE087/93						N.D.	N.D.	Lee et al. (2009)
XGS 93						N.D.	N.D.	Lee et al. (2009)
XT 59						N.D.	N.D.	Lee et al. (2009)
Y-5						N.D.	N.D.	Lee et al. (2009)
T5D19b						N.D.	N.D.	Leloup et al. (2010)
T5D20						N.D.	N.D.	Leloup et al. (2010)
T5D21						N.D.	N.D.	Leloup et al. (2010)
73-164						No	No	Lin et al. (2012)
73-540						No	No	Lin et al. (2012)
73-720						No	No	Lin et al. (2012)
73-721						No	No	Lin et al. (2012)
73-73	0.7449	-12.7				No	No	Lin et al. (2012)
73-750						No	No	Lin et al. (2012)
ET103A	0.7118	-10.6				No	No	Lin et al. (2012)
ET104B	0.7089	-7.1				No	No	Lin et al. (2012)
ET105A	0.7106	-7.8				No	No	Lin et al. (2012)
ET105B	0.7022	-7.4				No	No	Lin et al. (2012)
ET105C						No	No	Lin et al. (2012)
ET105D						No	No	Lin et al. (2012)
ET105E						No	No	Lin et al. (2012)
ET105F						No	No	Lin et al. (2012)
ET105G	0.7052	-4.3				No	No	Lin et al. (2012)
ET106A2	0.5927	-11.3				No	No	Lin et al. (2012)
ET107A	0.7156	-6.1				No	No	Lin et al. (2012)
ET108B						No	No	Lin et al. (2012)
ET111B						No	No	Lin et al. (2012)
ET113A	0.7139	-10.5				No	No	Lin et al. (2012)

Table A.2: continued

Sample	Terrane	Location	Lithology	Latitude (dd)	Longitude (dd)	Quadrant	Age (Ma)
ET115F1	Lhasa Terrane	E Transhimalaya	Orthogneiss (granitic)	28.5991	97.2496	Q6	133.0
ET115F2	Lhasa Terrane	E Transhimalaya	Orthogneiss (granitic)	28.5991	97.2496	Q6	
ET116B	Lhasa Terrane	E Transhimalaya	Granite	28.6724	97.4698	Q6	133.0
ET117A	Lhasa Terrane	E Transhimalaya	Granite	29.3213	97.1343	Q6	117.0
ET117C	Lhasa Terrane	E Transhimalaya	Granite	29.3213	97.1343	Q6	
ET119A	Lhasa Terrane	E Transhimalaya	Enclave	29.5074	96.7540	Q6	120.0
ET120A	Lhasa Terrane	E Transhimalaya	Granite	29.7417	96.0209	Q6	109.0
ET120C	Lhasa Terrane	E Transhimalaya	Enclave	29.7417	96.0209	Q6	109.0
ET120D	Lhasa Terrane	E Transhimalaya	Enclave	29.7417	96.0209	Q6	109.0
ET120E	Lhasa Terrane	E Transhimalaya	Enclave	29.7417	96.0209	Q6	109.0
ET122A	Lhasa Terrane	E Transhimalaya	Gabbroic diorite	29.7649	95.6971	Q6	66.0
ET122B	Lhasa Terrane	E Transhimalaya	Granite	29.7649	95.6971	Q6	
ET122D	Lhasa Terrane	E Transhimalaya	Granite	29.7649	95.6971	Q6	
ET124C	Lhasa Terrane	E Transhimalaya	Granite	29.7568	95.7080	Q6	
ET124D	Lhasa Terrane	E Transhimalaya	Enclave	29.7568	95.7080	Q6	
ET125A	Lhasa Terrane	E Transhimalaya	Orthogneiss (granitic)	29.7565	95.7163	Q6	125.0
ET203B	Lhasa Terrane	E Transhimalaya	Granite	28.4539	97.0314	Q6	60.0
ET203D	Lhasa Terrane	E Transhimalaya	Granite	28.4539	97.0314	Q6	60.0
ET219B2	Lhasa Terrane	E Transhimalaya	Granite	29.3922	96.8515	Q6	125.0
ET220B	Lhasa Terrane	E Transhimalaya	Granite	29.3922	96.8515	Q6	125.0
ET221B	Lhasa Terrane	E Transhimalaya	Granite	29.3922	96.8515	Q6	125.0
ET222B	Lhasa Terrane	E Transhimalaya	Granite	29.3922	96.8515	Q6	125.0
RAW11	Lhasa Terrane	Ranwu	Andesite	29.3555	96.7704	Q6	120.0
RAW12	Lhasa Terrane	Ranwu	Basaltic Andesite	29.3634	96.7717	Q6	120.0
RAW13	Lhasa Terrane	Ranwu	Andesite	29.3697	96.7729	Q6	120.0
RAW15	Lhasa Terrane	Ranwu	Basaltic Andesite	29.3751	96.7742	Q6	120.0
RAW17	Lhasa Terrane	Ranwu	Dacite	29.3810	96.7759	Q6	120.0
RAW20	Lhasa Terrane	Ranwu	Basaltic Andesite	29.3848	96.7766	Q6	120.0
RAW22	Lhasa Terrane	Ranwu	Basaltic Andesite	29.3913	96.7778	Q6	120.0
RAW24	Lhasa Terrane	Ranwu	Basaltic Andesite	29.3956	96.7782	Q6	120.0
RAW25	Lhasa Terrane	Ranwu	Basalt	29.4020	96.7792	Q6	120.0
RAW26	Lhasa Terrane	Ranwu	Basaltic Andesite	29.4069	96.7802	Q6	120.0
RAW29	Lhasa Terrane	Ranwu	Basaltic Andesite	29.4157	96.7808	Q6	120.0
RAW30	Lhasa Terrane	Ranwu	Basalt	29.4117	96.7804	Q6	120.0

Sample data continued

Sample	87Sr/86Sr(i)	eNd(t)	206Pb/204Pb(t)	207Pb/204Pb(t)	208Pb/204Pb(t)	*UPR	**ADK	Source
ET115F1	0.7181	-9.5				No	No	Lin et al. (2012)
ET115F2						No	No	Lin et al. (2012)
ET116B	0.7274	-7.9				No	No	Lin et al. (2012)
ET117A	0.7101	-7.1				No	No	Lin et al. (2012)
ET117C						No	No	Lin et al. (2012)
ET119A	0.7055					No	No	Lin et al. (2012)
ET120A	0.7029	-3.6				No	No	Lin et al. (2012)
ET120C	0.7058	-2.6				No	No	Lin et al. (2012)
ET120D	0.7058	-1.7				No	No	Lin et al. (2012)
ET120E	0.7053	-2.8				No	No	Lin et al. (2012)
ET122A	0.7115	-4.0				No	No	Lin et al. (2012)
ET122B						No	No	Lin et al. (2012)
ET122D						No	No	Lin et al. (2012)
ET124C						No	Yes	Lin et al. (2012)
ET124D						No	No	Lin et al. (2012)
ET125A	0.7179	-12.6				No	No	Lin et al. (2012)
ET203B	0.7056	-1.5				No	No	Lin et al. (2012)
ET203D	0.7045	-1.7				No	No	Lin et al. (2012)
ET219B2	0.6027	-11.4				No	No	Lin et al. (2012)
ET220B	0.6309	-10.6				No	No	Lin et al. (2012)
ET221B	0.5925	-10.7				No	No	Lin et al. (2012)
ET222B	0.5906	-10.6				No	No	Lin et al. (2012)
RAW11	0.7064	-0.5				No	No	Lin et al. (2012)
RAW12	0.7066	0.0				No	No	Lin et al. (2012)
RAW13	0.7072	-3.6				No	No	Lin et al. (2012)
RAW15	0.7063	0.4				No	No	Lin et al. (2012)
RAW17	0.7051	-6.0				No	No	Lin et al. (2012)
RAW20	0.7064	0.1				No	No	Lin et al. (2012)
RAW22	0.7053	-0.1				No	No	Lin et al. (2012)
RAW24	0.7053	1.7				No	No	Lin et al. (2012)
RAW25	0.7054	3.0				No	No	Lin et al. (2012)
RAW26	0.7058	-0.1				No	No	Lin et al. (2012)
RAW29	0.7057	-0.1				No	No	Lin et al. (2012)
RAW30	0.7060	0.2				No	No	Lin et al. (2012)

Table A.2: continued

Sample	Terrane	Location	Lithology	Latitude (dd)	Longitude (dd)	Quadrant	Age (Ma)
YZS-1	Lhasa Terrane	Xigaze IYSZ	Basalt	29.2669	88.8814	Q4	110.0
YZS-11	Lhasa Terrane	Xigaze IYSZ	Basalt	29.2669	88.8814	Q4	110.0
YZS-2	Lhasa Terrane	Xigaze IYSZ	Basalt	29.2669	88.8814	Q4	110.0
YZS-3	Lhasa Terrane	Xigaze IYSZ	Basalt	29.2669	88.8814	Q4	110.0
YZS-6	Lhasa Terrane	Xigaze IYSZ	Basalt	29.2669	88.8814	Q4	110.0
YZS-7	Lhasa Terrane	Xigaze IYSZ	Basalt	29.2669	88.8814	Q4	110.0
MB12-1	Lhasa Terrane	Mamba	Granodiorite	30.0753	92.1541	Q5	88.0
MB12-1R	Lhasa Terrane	Mamba	Granodiorite	30.0753	92.1541	Q5	88.0
MB12-3	Lhasa Terrane	Mamba	Granodiorite	30.0753	92.1541	Q5	88.0
MB12-5	Lhasa Terrane	Mamba	Granodiorite	30.0753	92.1541	Q5	88.0
MB12-7	Lhasa Terrane	Mamba	Granodiorite	30.0753	92.1541	Q5	88.0
MB12-8	Lhasa Terrane	Mamba	Granodiorite	30.0753	92.1541	Q5	88.0
MB12-9	Lhasa Terrane	Mamba	Granodiorite	30.0753	92.1541	Q5	88.0
MB13-2	Lhasa Terrane	Mamba	Enclave (dioritic)	30.0731	92.1541	Q5	87.2
MB13-2R	Lhasa Terrane	Mamba	Enclave (dioritic)	30.0731	92.1541	Q5	87.2
MB13-3	Lhasa Terrane	Mamba	Enclave (gabbroic)	30.0731	92.1541	Q5	87.2
MB14-2	Lhasa Terrane	Mamba	Enclave (dioritic)	30.0338	92.0969	Q5	85.2
MB14-2R	Lhasa Terrane	Mamba	Enclave (dioritic)	30.0338	92.0969	Q5	87.2
MB14-4	Lhasa Terrane	Mamba	Granodiorite	30.0338	92.0969	Q5	83.7
MB14-5	Lhasa Terrane	Mamba	Enclave (dioritic)	30.0338	92.0969	Q5	87.2
MB16-1	Lhasa Terrane	Mamba	Granodiorite	30.0338	92.0969	Q5	87.2
MB17-1	Lhasa Terrane	Mamba	Granodiorite	30.0338	92.0969	Q5	87.2
TE005/93	Lhasa Terrane		Xenolith (pegmatite)				
TE007/93	Lhasa Terrane	S Xungba	Volcanic rock (silicic potassic)	31.8585	81.9061	Q3	
TE008/93	Lhasa Terrane	S Xungba	Volcanic rock (ultrapotassic)	31.8585	81.9061	Q3	
TE009/93	Lhasa Terrane	S Xungba	Volcanic rock (ultrapotassic)	31.8585	81.9061	Q3	
TE011/93	Lhasa Terrane	S Xungba	Volcanic rock (ultrapotassic)	31.8585	81.9061	Q3	21.0
TE012/93	Lhasa Terrane	S Xungba	Volcanic rock (ultrapotassic)	31.8585	81.9061	Q3	
TE019/93	Lhasa Terrane	SE Xungba	Granodiorite (Hbl)	31.7999	82.0664	Q3	91.5
TE025/93	Lhasa Terrane	S Xungba	Volcanic rock (silicic potassic)	31.8585	81.9061	Q3	22.8
TE047/93	Lhasa Terrane	S Gregar	Volcanic rock (calc-alkaline)				17.7
TE117/93	Lhasa Terrane	E Jarga	Volcanic rock (ultrapotassic)	31.4878	82.6548	Q3	18.5
TE118/93	Lhasa Terrane	E Jarga	Volcanic rock (ultrapotassic)	31.4878	82.6548	Q3	15.5
TE119/93	Lhasa Terrane	S Xungba	Volcanic rock (silicic potassic)	31.8585	81.9061	Q3	

Sample data continued

Sample	87Sr/86Sr(i)	eNd(t)	206Pb/ 204Pb(t)	207Pb/ 204Pb(t)	208Pb/ 204Pb(t)	*UPR	**ADK	Source
YZS 1	0.7040	8.4	17.5	15.4	37.4	N.D.	N.D.	Mahoney et al. (1998)
YZS 11	0.7039	8.2	17.4	15.4	37.3	N.D.	N.D.	Mahoney et al. (1998)
YZS 2	0.7041	8.2	17.5	15.4	37.3	N.D.	N.D.	Mahoney et al. (1998)
YZS 3	0.7041	8.5	17.5	15.4	37.4	N.D.	N.D.	Mahoney et al. (1998)
YZS 6	0.7039	8.0	17.5	15.4	37.3	N.D.	N.D.	Mahoney et al. (1998)
YZS 7	0.7039	8.1	17.4	15.4	37.3	N.D.	N.D.	Mahoney et al. (1998)
MB12-1	0.7067	-4.1				No	No	Meng et al. (2010)
MB12-1R						N.D.	N.D.	Meng et al. (2013)
MB12-3	0.7067	-4.3				No	No	Meng et al. (2013)
MB12-5						No	Yes	Meng et al. (2013)
MB12-7						No	Yes	Meng et al. (2013)
MB12-8	0.7067	-4.3				No	No	Meng et al. (2013)
MB12-9						No	Yes	Meng et al. (2013)
MB13-2						No	No	Meng et al. (2013)
MB13-2R						No	No	Meng et al. (2013)
MB13-3	0.7073	-4.0				No	No	Meng et al. (2013)
MB14-2	0.7067	-3.6				No	No	Meng et al. (2013)
MB14-2R						N.D.	N.D.	Meng et al. (2013)
MB14-4	0.7067	-4.4				No	No	Meng et al. (2013)
MB14-5						No	No	Meng et al. (2013)
MB16-1	0.7066	-5.7				No	Yes	Meng et al. (2013)
MB17-1						No	Yes	Meng et al. (2013)
TE005/93	0.7197	-4.4				N.D.	N.D.	Miller et al. (1999)
TE007/93						No	No	Miller et al. (1999)
TE008/93						Yes	No	Miller et al. (1999)
TE009/93						N.D.	N.D.	Miller et al. (1999)
TE011/93	0.7218	-13.7				Yes	No	Miller et al. (1999)
TE012/93						N.D.	N.D.	Miller et al. (1999)
TE019/93	0.7092	-2.6				N.D.	N.D.	Miller et al. (1999)
TE025/93	0.7376	-13.1	18.7	15.8	39.5	No	No	Miller et al. (1999)
TE047/93	0.7093	-9.5				No	No	Miller et al. (1999)
TE117/93	0.7193					Yes	No	Miller et al. (1999)
TE118/93	0.7194	-14.3	18.5	15.7	39.6	Yes	No	Miller et al. (1999)
TE119/93						N.D.	N.D.	Miller et al. (1999)

Table A.2: continued

Sample	Terrane	Location	Lithology	Latitude (dd)	Longitude (dd)	Quadrant	Age (Ma)
TE122/93	Lhasa Terrane	S Xungba	Volcanic rock (silicic potassic)	31.8585	81.9061	Q3	
TE124/93	Lhasa Terrane	S Xungba	Volcanic rock (ultrapotassic)	31.8585	81.9061	Q3	
TE125/93	Lhasa Terrane	S Xungba	Volcanic rock (ultrapotassic)	31.8585	81.9061	Q3	23.0
TE126/93	Lhasa Terrane	S Xungba	Volcanic rock (ultrapotassic)	31.8585	81.9061	Q3	23.0
TE127/93	Lhasa Terrane	S Xungba	Volcanic rock (ultrapotassic)	31.8585	81.9061	Q3	
TE131/93	Lhasa Terrane	S Xungba	Volcanic rock (ultrapotassic)	31.8585	81.9061	Q3	
TE134/93	Lhasa Terrane	S Xungba	Volcanic rock (ultrapotassic)	31.8585	81.9061	Q3	
TE136/93	Lhasa Terrane	S Xungba	Volcanic rock (silicic potassic)	31.8585	81.9061	Q3	18.0
TE137/93	Lhasa Terrane	S Xungba	Volcanic rock (ultrapotassic)	31.8585	81.9061	Q3	18.0
TE138/93	Lhasa Terrane	S Xungba	Volcanic rock (ultrapotassic)	31.8585	81.9061	Q3	18.1
TE148/93	Lhasa Terrane	S Bongba	Volcanic rock (silicic potassic)	31.9693	81.2440	Q3	23.3
TE149/93	Lhasa Terrane	S Bongba	Volcanic rock (silicic potassic)	31.9693	81.2440	Q3	
TE150/93	Lhasa Terrane	S Bongba	Volcanic rock (silicic potassic)	31.9693	81.2440	Q3	25.4
TE153/93	Lhasa Terrane	S Bongba	Volcanic rock (silicic potassic)	31.9693	81.2440	Q3	25.0
TE154/93	Lhasa Terrane	S Bongba	Volcanic rock (silicic potassic)	31.9693	81.2440	Q3	25.0
TE189/93	Himalayas	Manasarowar	Volcanic rock (calc-alkaline)	30.6692	81.4920	Q3	17.0
TE192/93	Himalayas	Manasarowar	Volcanic rock (calc-alkaline)	30.6692	81.4920	Q3	17.0
TE193/93	Himalayas	Manasarowar	Volcanic rock (calc-alkaline)	30.6692	81.4920	Q3	
TE194/93	Himalayas	Manasarowar	Volcanic rock (calc-alkaline)	30.6692	81.4920	Q3	16.7
TE197/93	Himalayas	Manasarowar	Volcanic rock (calc-alkaline)	30.6692	81.4920	Q3	
TE198/93	Himalayas	Manasarowar	Volcanic rock (calc-alkaline)	30.6692	81.4920	Q3	
CM028/93	Lhasa Terrane	SW Labru	Dike (rhyolithic)	31.8510	80.1310	Q2	37.0
CM045/93	Lhasa Terrane	S Labru	Granodiorite (Hbl)	31.8771	80.1870	Q2	120.0
CM048/93	Lhasa Terrane	SW Labru	Dike (dacitic)	31.8510	80.1310	Q2	37.0
CM051/93	Lhasa Terrane	SW Labru	Dike (dacitic)	31.8510	80.1310	Q2	37.0
CM060/93	Lhasa Terrane	SW Labru	Dike (rhyolithic)	31.8510	80.1310	Q2	37.0
CM068/93	Lhasa Terrane	SW Labru		31.8566	80.1515	Q2	
CM070/93	Lhasa Terrane	S Labru	Gabbro (Hbl)	31.8696	80.1814	Q2	120.0
CM104/93	Lhasa Terrane	Kailas Molasse	Rhyolite	31.0455	81.3037	Q3	
CM106/93	Lhasa Terrane	E Kailas	Granodiorite (Hbl)	31.0775	81.3280	Q3	120.0
CM108/93	Lhasa Terrane	E Kailas	Enclave (mafic)	31.0775	81.3429	Q3	120.0
HF086/93	Lhasa Terrane	E Bamba	Granite (Bt)	32.1950	82.2528	Q3	120.0
HF090/93	Lhasa Terrane	W Gegyai	Granodiorite (Hbl)	32.3881	81.1211	Q3	120.0
HF091/93	Lhasa Terrane	SE Gar	Syenite	32.4079	79.9074	Q2	64.0

Sample data continued

Sample	87Sr/86Sr(i)	eNd(t)	206Pb/ 204Pb(t)	207Pb/ 204Pb(t)	208Pb/ 204Pb(t)	*UPR	**ADK	Source
TE122/93						N.D.	N.D.	Miller et al. (1999)
TE124/93						N.D.	N.D.	Miller et al. (1999)
TE125/93	0.7193	-11.9				Yes	No	Miller et al. (1999)
TE126/93	0.7200	-12.7	18.5	15.7	39.4	Yes	No	Miller et al. (1999)
TE127/93	0.7069	-8.0				Yes	No	Miller et al. (1999)
TE131/93						Yes	No	Miller et al. (1999)
TE134/93						N.D.	N.D.	Miller et al. (1999)
TE136/93	0.7176					No	Yes	Miller et al. (1999)
TE137/93	0.7218	-13.8	18.5	15.7	39.8	Yes	No	Miller et al. (1999)
TE138/93	0.7173	-13.3	18.4	15.7	39.6	Yes	No	Miller et al. (1999)
TE148/93						No	Yes	Miller et al. (1999)
TE149/93						N.D.	N.D.	Miller et al. (1999)
TE150/93	0.7324	-14.5	18.6	15.7	39.1	No	Yes	Miller et al. (1999)
TE153/93	0.7327	-13.1				No	No	Miller et al. (1999)
TE154/93	0.7325					No	Yes	Miller et al. (1999)
TE189/93	0.7090	-7.7				No	Yes	Miller et al. (1999)
TE192/93	0.7097	-7.1				No	No	Miller et al. (1999)
TE193/93						N.D.	N.D.	Miller et al. (1999)
TE194/93	0.7095	-8.1				N.D.	N.D.	Miller et al. (1999)
TE197/93						N.D.	N.D.	Miller et al. (1999)
TE198/93	0.7091	-7.1				N.D.	N.D.	Miller et al. (1999)
CM028/93	0.7305					N.D.	N.D.	Miller et al. (2000)
CM045/93	0.7104					No	Yes	Miller et al. (2000)
CM048/93	0.7085					N.D.	N.D.	Miller et al. (2000)
CM051/93	0.7088					N.D.	N.D.	Miller et al. (2000)
CM060/93	0.7353					N.D.	N.D.	Miller et al. (2000)
CM068/93						N.D.	N.D.	Miller et al. (2000)
CM070/93	0.7046	0.5				No	No	Miller et al. (2000)
CM104/93						N.D.	N.D.	Miller et al. (2000)
CM106/93	0.7051					N.D.	N.D.	Miller et al. (2000)
CM108/93	0.7074	-1.3				No	No	Miller et al. (2000)
HF086/93	0.7087					N.D.	N.D.	Miller et al. (2000)
HF090/93	0.7141					N.D.	N.D.	Miller et al. (2000)
HF091/93	0.7035	0.4				N.D.	N.D.	Miller et al. (2000)

Table A.2: continued

Sample	Terrane	Location	Lithology	Latitude (dd)	Longitude (dd)	Quadrant	Age (Ma)
HF092/93	Lhasa Terrane	SE Gar	Syenite	32.4079	79.9074	Q2	64.0
HF095/93	Lhasa Terrane	SE Gar	Trachyte	32.3967	79.9074	Q2	64.0
HF107/93	Lhasa Terrane	S Jarga	Granodiorite (Hbl)	31.3019	82.1130	Q3	120.0
HF185/93	Lhasa Terrane	W Kailas	Granodiorite (Hbl)	31.0906	81.3298	Q3	120.0
HF187/93	Lhasa Terrane	W Kailas	Enclave (mafic)	31.0906	81.3298	Q3	119.0
HF189/93	Lhasa Terrane	NW Kailas	Dike (aplitic)	31.0906	81.3298	Q3	40.0
HF191/91	Lhasa Terrane	NW Kailas	Granite (Bt)	31.0906	81.3298	Q3	120.0
HF193/93	Lhasa Terrane	NW Kailas	Granite (Hbl)	31.0906	81.3298	Q3	120.0
HF194/93	Lhasa Terrane	NW Kailas	Dike (aplitic)	31.0906	81.3298	Q3	40.0
HF196/93	Lhasa Terrane	NW Kailas	Dike (aplitic)	31.0906	81.3298	Q3	40.0
HF197/93	Lhasa Terrane	NW Kailas	Granodiorite (Hbl)	31.0906	81.3298	Q3	119.0
HF198/93	Lhasa Terrane	NW Kailas	Leucogranite	31.0906	81.3298	Q3	120.0
HF200/93	Lhasa Terrane	NW Kailas	Granite (Bt)	31.0906	81.3298	Q3	120.0
HF202/93	Lhasa Terrane	E Kailas	Granodiorite (Hbl)	31.0906	81.3298	Q3	120.0
HF203/93	Lhasa Terrane	E Kailas	Enclave (mafic)	31.0906	81.3447	Q3	120.0
TE026/93	Lhasa Terrane	SSE Xungba	Basalt	31.7720	82.0627	Q3	120.0
TE028/93	Lhasa Terrane	SSE Xungba		31.7701	82.0776	Q3	
TE059/93	Lhasa Terrane	NE Indus	Dacite				
TE060/93	Lhasa Terrane	Indus source	Leucogranite	31.2080	81.4584	Q3	40.0
TE073/93	Lhasa Terrane	S Bongba	Basalt	31.9693	81.2440	Q3	
TE078/93	Lhasa Terrane			31.4902	82.1652	Q3	
TE082/93	Lhasa Terrane	W Jarga	Basaltic Andesite	31.5181	82.1559	Q3	120.0
TE085/93	Lhasa Terrane			31.5181	82.1726	Q3	
TE086/93	Lhasa Terrane	SW Jarga	Andesite	31.3504	82.0888	Q3	55.0
TE091/93	Lhasa Terrane	SW Jarga	Andesite	31.3504	82.0888	Q3	
TE092/93	Lhasa Terrane	SW Jarga	Andesite	31.3504	82.0888	Q3	55.0
TE105/93	Lhasa Terrane	SW Jarga	Rhyolite	31.3392	82.0888	Q3	55.0
TE107/93	Lhasa Terrane	S Jarga		31.3019	82.1130	Q3	
TE110/93	Lhasa Terrane	E Jarga	Andesite	31.4417	82.4261	Q3	55.0
TE114/93	Lhasa Terrane	E Jarga	Andesite	31.4417	82.4261	Q3	54.1
TE187/93	Lhasa Terrane	SW Jarga	Dacite	31.3504	82.0888	Q3	45.0
Miller_2001_1	Himalayas	Kaplas	Granite	32.9414	75.6143	Q2	552.0
Miller_2001_10	Himalayas	Mandi	Granodiorite	31.5430	77.0095	Q2	507.0
Miller_2001_11	Himalayas	Manikaran	Granite	32.0264	77.3468	Q2	467.0

Sample data continued

Sample	87Sr/86Sr(i)	eNd(t)	206Pb/ 204Pb(t)	207Pb/ 204Pb(t)	208Pb/ 204Pb(t)	*UPR	**ADK	Source
HF092/93	0.7036					No	No	Miller et al. (2000)
HF095/93	0.7035	0.7				No	No	Miller et al. (2000)
HF107/93	0.7038					N.D.	N.D.	Miller et al. (2000)
HF185/93	0.7044					N.D.	N.D.	Miller et al. (2000)
HF187/93	0.7048	-0.9				N.D.	N.D.	Miller et al. (2000)
HF189/93	0.7113					N.D.	N.D.	Miller et al. (2000)
HF191/91	0.7088	-5.9				N.D.	N.D.	Miller et al. (2000)
HF193/93	0.7050					N.D.	N.D.	Miller et al. (2000)
HF194/93	0.7089					N.D.	N.D.	Miller et al. (2000)
HF196/93	0.7190					N.D.	N.D.	Miller et al. (2000)
HF197/93	0.7049	-0.8				No	No	Miller et al. (2000)
HF198/93	0.7097					N.D.	N.D.	Miller et al. (2000)
HF200/93	0.7089					N.D.	N.D.	Miller et al. (2000)
HF202/93	0.7046					N.D.	N.D.	Miller et al. (2000)
HF203/93	0.7048					N.D.	N.D.	Miller et al. (2000)
TE026/93	0.7078	-7.8				N.D.	N.D.	Miller et al. (2000)
TE028/93						N.D.	N.D.	Miller et al. (2000)
TE059/93						No	Yes	Miller et al. (2000)
TE060/93	0.7108					N.D.	N.D.	Miller et al. (2000)
TE073/93						No	No	Miller et al. (2000)
TE078/93						N.D.	N.D.	Miller et al. (2000)
TE082/93	0.7055	0.2				No	No	Miller et al. (2000)
TE085/93						N.D.	N.D.	Miller et al. (2000)
TE086/93	0.7081	-6.1				No	No	Miller et al. (2000)
TE091/93						N.D.	N.D.	Miller et al. (2000)
TE092/93	0.7060					N.D.	N.D.	Miller et al. (2000)
TE105/93	0.7046					N.D.	N.D.	Miller et al. (2000)
TE107/93						N.D.	N.D.	Miller et al. (2000)
TE110/93	0.7061					No	No	Miller et al. (2000)
TE114/93	0.7053	-2.5				N.D.	N.D.	Miller et al. (2000)
TE187/93	0.7058					N.D.	N.D.	Miller et al. (2000)
Miller_2001_1						N.D.	N.D.	Miller et al. (2001)
Miller_2001_10						N.D.	N.D.	Miller et al. (2001)
Miller_2001_11						N.D.	N.D.	Miller et al. (2001)

Table A.2: continued

Sample	Terrane	Location	Lithology	Latitude (dd)	Longitude (dd)	Quadrant	Age (Ma)
Miller_2001_12	Himalayas	Kullu	Granite	31.9568	77.1114	Q2	495.0
Miller_2001_13	Himalayas	Kinnaur Kailash	Orthogneiss	31.6324	78.3760	Q2	453.0
Miller_2001_14	Himalayas	Hante	Granite				489.0
Miller_2001_15	Himalayas	Miyar	Granite				549.0
Miller_2001_16	Himalayas	Nyimaling	Unknown	32.8850	78.1301	Q2	460.0
Miller_2001_17	Himalayas	Khadrala	Unknown				460.0
Miller_2001_18	Himalayas	Champawat	Unknown	29.3402	80.0924	Q3	560.0
Miller_2001_19	Himalayas	Dadeldhura	Unknown	29.2174	80.5018	Q3	470.0
Miller_2001_2	Himalayas	Kinnaur Kailash	Granite	31.6324	78.3760	Q2	488.0
Miller_2001_20	Himalayas	Simchar	Unknown				466.0
Miller_2001_21	Himalayas	Formation III	Unknown				513.0
Miller_2001_22	Himalayas	Kangmar	Granite	28.6517	89.6660	Q5	485.0
Miller_2001_23	Himalayas	Kangmar	Granite	28.6517	89.6660	Q5	484.0
Miller_2001_24	Himalayas	Mandi	Granodiorite	31.5430	77.0095	Q2	496.0
Miller_2001_3	Himalayas	Miyar	Granite				479.0
Miller_2001_4	Himalayas	Rupshu	Granite				483.0
Miller_2001_5	Himalayas	Tso Morari	Granite	32.9030	78.3159	Q2	479.0
Miller_2001_6	Himalayas	Tso Morari	Granite	32.9030	78.3159	Q2	479.0
Miller_2001_7	Himalayas	Palung	Orthogneiss				470.0
Miller_2001_8	Himalayas	Kangmar	Granite	28.6517	89.6660	Q5	562.0
Miller_2001_9	Himalayas	Mansehra	Granite				516.0
HB06/97	Himalayas	Kinnaur Kailas	Leucogranite	31.6324	78.3760	Q2	488.0
HB18/97	Himalayas	Kinnaur Kailas	Granite (Bt, Ms)	31.6324	78.3760	Q2	488.0
HB25/97	Himalayas	Kinnaur Kailas	Granitoid	31.6324	78.3760	Q2	488.0
HB26/97	Himalayas	Kinnaur Kailas	Granitoid	31.6324	78.3760	Q2	488.0
HF01/91	Himalayas	Hanuman Tibba	Granite (Bt)	32.2550	77.0670	Q2	500.0
HF05/92	Himalayas	Chandra	Granite (Bt, Ms)	32.2454	77.5268	Q2	500.0
HF06/92	Himalayas	Chandra	Granite (Bt, Ms)	32.2454	77.5268	Q2	500.0
HF07/92	Himalayas	Chandra	Granite (Bt, Ms)	32.2454	77.5268	Q2	500.0
HF08/92	Himalayas	Chandra	Granite (Bt, Ms)	32.2454	77.5268	Q2	500.0
HF09/92	Himalayas	Chandra	Granite (Bt, Ms)	32.2454	77.5268	Q2	500.0
HF10/92	Himalayas	Chandra	Leucogranite	32.2454	77.5268	Q2	500.0
HF11/92	Himalayas	Chandra	Leucogranite	32.2454	77.5268	Q2	500.0
HF13/92	Himalayas	Chandra	Granite (Bt)	32.2454	77.5268	Q2	500.0

Sample data continued

Sample	87Sr/86Sr(i)	eNd(t)	206Pb/ 204Pb(t)	207Pb/ 204Pb(t)	208Pb/ 204Pb(t)	*UPR	**ADK	Source
Miller_2001_12						N.D.	N.D.	Miller et al. (2001)
Miller_2001_13						N.D.	N.D.	Miller et al. (2001)
Miller_2001_14						N.D.	N.D.	Miller et al. (2001)
Miller_2001_15						N.D.	N.D.	Miller et al. (2001)
Miller_2001_16						N.D.	N.D.	Miller et al. (2001)
Miller_2001_17						N.D.	N.D.	Miller et al. (2001)
Miller_2001_18						N.D.	N.D.	Miller et al. (2001)
Miller_2001_19						N.D.	N.D.	Miller et al. (2001)
Miller_2001_2						N.D.	N.D.	Miller et al. (2001)
Miller_2001_20						N.D.	N.D.	Miller et al. (2001)
Miller_2001_21						N.D.	N.D.	Miller et al. (2001)
Miller_2001_22						N.D.	N.D.	Miller et al. (2001)
Miller_2001_23						N.D.	N.D.	Miller et al. (2001)
Miller_2001_24						N.D.	N.D.	Miller et al. (2001)
Miller_2001_3						N.D.	N.D.	Miller et al. (2001)
Miller_2001_4						N.D.	N.D.	Miller et al. (2001)
Miller_2001_5						N.D.	N.D.	Miller et al. (2001)
Miller_2001_6						N.D.	N.D.	Miller et al. (2001)
Miller_2001_7						N.D.	N.D.	Miller et al. (2001)
Miller_2001_8						N.D.	N.D.	Miller et al. (2001)
Miller_2001_9						N.D.	N.D.	Miller et al. (2001)
HB06/97	0.8939	-13.1				No	No	Miller et al. (2001)
HB18/97	0.7177	-7.8				No	No	Miller et al. (2001)
HB25/97						No	No	Miller et al. (2001)
HB26/97						No	No	Miller et al. (2001)
HF01/91	0.7424					N.D.	N.D.	Miller et al. (2001)
HF05/92	0.8285	-8.9				No	No	Miller et al. (2001)
HF06/92	0.8413					N.D.	N.D.	Miller et al. (2001)
HF07/92	0.7986					N.D.	N.D.	Miller et al. (2001)
HF08/92	0.8887					N.D.	N.D.	Miller et al. (2001)
HF09/92	0.8085					N.D.	N.D.	Miller et al. (2001)
HF10/92	1.3843					N.D.	N.D.	Miller et al. (2001)
HF11/92	1.0333					N.D.	N.D.	Miller et al. (2001)
HF13/92	0.8248					N.D.	N.D.	Miller et al. (2001)

Table A.2: continued

Sample	Terrane	Location	Lithology	Latitude (dd)	Longitude (dd)	Quadrant	Age (Ma)
HF142/90	Himalayas	Kaplas	Granite (Bt, Ms)	32.9414	75.6143	Q2	553.2
HF143/90	Himalayas	Kaplas	Granite (Bt, Ms)	32.9414	75.6143	Q2	553.2
HF144/90	Himalayas	Kaplas	Granite (Bt, Ms)	32.9414	75.6143	Q2	553.2
HF145/90	Himalayas	Kaplas	Granite (Bt, Ms)	32.9414	75.6143	Q2	553.2
HF15/92	Himalayas	Chandra	Granite (Bt, Ms)	32.2454	77.5268	Q2	500.0
HF16/92	Himalayas	Chandra	Granite (Bt)	32.2454	77.5268	Q2	500.0
HF17/92	Himalayas	Chandra	Granite (Bt, Ms)	32.2454	77.5268	Q2	500.0
HF18/92	Himalayas	Chandra	Granite (Bt)	32.2454	77.5268	Q2	500.0
HF22/92	Himalayas	Chandra	Granite (Bt, Ms)	32.2454	77.5268	Q2	500.0
HF29/92	Himalayas	Kinnaur Kailas	Granite (Bt, Ms)	31.6324	78.3760	Q2	488.0
HF30/92	Himalayas	Kinnaur Kailas	Granite (Bt, Ms)	31.6324	78.3760	Q2	488.0
HF31/92	Himalayas	Kinnaur Kailas	Granite (Bt)	31.6324	78.3760	Q2	488.0
HF32/92	Himalayas	Kinnaur Kailas	Leucogranite	31.6324	78.3760	Q2	488.0
HF59/91	Himalayas	Mandi	Mafic pillow	31.5430	77.0095	Q2	496.0
HF61/91	Himalayas	Mandi	Mafic pillow	31.5430	77.0095	Q2	496.0
HF63/91	Himalayas	Mandi	Granite (Bt)	31.5430	77.0095	Q2	496.0
HF64/91	Himalayas	Mandi	Granodiorite	31.5430	77.0095	Q2	496.0
HF66b/91	Himalayas	Mandi	Mafic pillow	31.5430	77.0095	Q2	496.0
HF67/91	Himalayas	Mandi	Granite (Bt, Ms)	31.5430	77.0095	Q2	496.0
HF68/91	Himalayas	Nyimaling	Granite (Bt, Ms)	32.8850	78.1301	Q2	460.0
HF69/91	Himalayas	Nyimaling	Granite (Bt, Ms)	32.8850	78.1301	Q2	460.0
HF70/91	Himalayas	Nyimaling	Granite (Bt, Ms, Grt)	32.8850	78.1301	Q2	460.0
HF73/91	Himalayas	Nyimaling	Granite (Crd)	32.8850	78.1301	Q2	460.0
HF89/90	Himalayas	Mandi	Diorite	31.5430	77.0095	Q2	496.0
HF92/90	Himalayas	Mandi	Mafic pillow	31.5430	77.0095	Q2	496.0
HF94/90	Himalayas	Mandi	Diorite (Qz)	31.5430	77.0095	Q2	496.0
HF95/90	Himalayas	Mandi	Mafic pillow	31.5430	77.0095	Q2	496.0
HF98/90	Himalayas	Baragran	Granitoid	32.1342	77.1458	Q2	
KAW883	Himalayas	Mandi	Granite (Bt, Ms)	31.5430	77.0095	Q2	496.0
PG9136	Himalayas	Kaplas	Granite (Bt, Ms)	32.9414	75.6143	Q2	553.2
PG9137	Himalayas	Kaplas	Granite (Bt, Ms)	32.9414	75.6143	Q2	553.2
PG9180	Himalayas	Kaplas	Granite (Bt, Ms)	32.9414	75.6143	Q2	553.2
T41	Himalayas	Jaspa	Granite (Ms)	32.7658	77.0095	Q2	496.0
WAP2069	Himalayas	NW Tindi	Metasediment				500.0

Sample data continued

Sample	87Sr/86Sr(i)	eNd(t)	206Pb/ 204Pb(t)	207Pb/ 204Pb(t)	208Pb/ 204Pb(t)	*UPR	**ADK	Source
HF142/90	0.7884					N.D.	N.D.	Miller et al. (2001)
HF143/90	0.7631					No	No	Miller et al. (2001)
HF144/90	0.7083	-8.7				No	No	Miller et al. (2001)
HF145/90	0.8979					N.D.	N.D.	Miller et al. (2001)
HF15/92	0.9382					N.D.	N.D.	Miller et al. (2001)
HF16/92	0.7909					N.D.	N.D.	Miller et al. (2001)
HF17/92	0.8696					N.D.	N.D.	Miller et al. (2001)
HF18/92	0.7769					N.D.	N.D.	Miller et al. (2001)
HF22/92	0.8276					N.D.	N.D.	Miller et al. (2001)
HF29/92	0.7644					N.D.	N.D.	Miller et al. (2001)
HF30/92	0.7524					N.D.	N.D.	Miller et al. (2001)
HF31/92	0.7476					N.D.	N.D.	Miller et al. (2001)
HF32/92	0.8216					N.D.	N.D.	Miller et al. (2001)
HF59/91	0.7035	1.0				No	No	Miller et al. (2001)
HF61/91	0.7041	0.5				No	No	Miller et al. (2001)
HF63/91	0.7152	-9.1				No	No	Miller et al. (2001)
HF64/91	0.7131					No	No	Miller et al. (2001)
HF66b/91	0.7053	-2.8				No	No	Miller et al. (2001)
HF67/91	1.1758	-10.3				No	No	Miller et al. (2001)
HF68/91	0.7959					N.D.	N.D.	Miller et al. (2001)
HF69/91	0.9036					N.D.	N.D.	Miller et al. (2001)
HF70/91	0.8216					N.D.	N.D.	Miller et al. (2001)
HF73/91		-9.3				No	No	Miller et al. (2001)
HF89/90	0.7135					N.D.	N.D.	Miller et al. (2001)
HF92/90	0.7052					N.D.	N.D.	Miller et al. (2001)
HF94/90	0.7086					No	No	Miller et al. (2001)
HF95/90	0.7056					No	No	Miller et al. (2001)
HF98/90						No	No	Miller et al. (2001)
KAW883	1.2130	-10.4				No	No	Miller et al. (2001)
PG9136	0.8691					N.D.	N.D.	Miller et al. (2001)
PG9137	0.8629					N.D.	N.D.	Miller et al. (2001)
PG9180	0.7695					N.D.	N.D.	Miller et al. (2001)
T41	0.7116	-10.1				N.D.	N.D.	Miller et al. (2001)
WAP2069	0.7327	-8.7				N.D.	N.D.	Miller et al. (2001)

Table A.2: continued

Sample	Terrane	Location	Lithology	Latitude (dd)	Longitude (dd)	Quadrant	Age (Ma)
WAP2070	Himalayas	Miyar Valley	Metasediment				500.0
WAP2071	Himalayas	Dhali	Metasediment				500.0
WAP2072	Himalayas	Mashobra	Metasediment				500.0
WAP2073	Himalayas	NE Marwa	Metasediment				500.0
WAP2074	Himalayas	E Udaipur	Metasediment				500.0
WAP2075	Himalayas	Khanderghat	Metasediment				500.0
WAP2076	Himalayas	Naldera	Metasediment				500.0
WAP25	Himalayas	Hanuman Tibba	Granite (Bt)	32.2550	77.0670	Q2	500.0
WAP28	Himalayas	Chamba	Granite (Bt, Ms)	32.5558	76.1261	Q2	
BD-103	Lhasa Terrane	U. Pana Fm.	Ignimbrite (rhyolitic)	30.0107	91.1403	Q5	46.5
BD-106	Lhasa Terrane	U. Pana Fm.	Ignimbrite (rhyolitic)	30.0103	91.1403	Q5	46.5
BD-114	Lhasa Terrane	U. Pana Fm.	Tuff (rhyolitic)	30.0375	91.1405	Q5	43.9
BD-123	Lhasa Terrane	L. Dianzhong Fm.	Andesite	29.9168	91.0513	Q5	62.5
BD-145	Lhasa Terrane	L. Dianzhong Fm.	Andesite	29.9532	91.1987	Q5	62.5
BD-151	Lhasa Terrane	L. Dianzhong Fm.	Andesite	29.9675	91.2077	Q5	62.5
BD-160	Lhasa Terrane	L. Dianzhong Fm.	Trachyandesite	29.9725	91.1760	Q5	62.5
BD-27	Lhasa Terrane	L. Dianzhong Fm.	Andesite	29.9672	91.0975	Q5	62.5
BD-55	Lhasa Terrane	M. Nianbo Fm.	Tuff (rhyolitic)	29.9788	91.1713	Q5	54.0
BD-58	Lhasa Terrane		Diabase	29.9803	91.1710	Q5	
BD-65	Lhasa Terrane	M. Nianbo Fm.	Trachybasalt	29.9842	91.1700	Q5	54.0
BD-77	Lhasa Terrane	U. Pana Fm.	Tuff (rhyolitic)	29.9750	91.1410	Q5	46.5
D-15	Lhasa Terrane	L. Dianzhong Fm.	Andesite	29.9642	91.1888	Q5	60.6
D-2	Lhasa Terrane	L. Dianzhong Fm.	Trachyandesite	29.9520	91.1980	Q5	62.5
L060	Lhasa Terrane	M. Nianbo Fm.	Tuff (rhyolitic)	29.9770	91.1933	Q5	54.0
L-1108	Lhasa Terrane	L. Dianzhong Fm.	Basaltic Andesite				62.5
LZ9910	Lhasa Terrane	M. Nianbo Fm.	Trachyandesite	29.9648	91.1253	Q5	54.0
LZ9912	Lhasa Terrane	Mafic Dykes	Diabase	29.9648	91.1253	Q5	
LZ9916	Lhasa Terrane	U. Pana Fm.	Tuff (rhyolitic)	30.0087	91.1503	Q5	46.5
LZ9917	Lhasa Terrane	U. Pana Fm.	Tuff (rhyolitic)	30.0087	91.1503	Q5	46.5
LZ9921	Lhasa Terrane	M. Nianbo Fm.	Ignimbrite (rhyolitic)	29.9808	91.1858	Q5	54.0
LZ994	Lhasa Terrane	M. Nianbo Fm.	Rhyolite (brecciated)	29.9648	91.1253	Q5	54.0
P-1	Lhasa Terrane	U. Pana Fm.	Ignimbrite (rhyolitic)	29.9863	91.1500	Q5	46.5
GMH 1	Himalayas	Gurla Mandhata	Schist	30.3994	81.2605	Q3	9.0
GMH 2	Himalayas	Gurla Mandhata	Gneiss	30.3912	81.1984	Q3	9.0

Sample data continued

Sample	87Sr/86Sr(i)	eNd(t)	206Pb/ 204Pb(t)	207Pb/ 204Pb(t)	208Pb/ 204Pb(t)	*UPR	**ADK	Source
WAP2070	0.7257	-13.6				N.D.	N.D.	Miller et al. (2001)
WAP2071	0.7172	-10.2				N.D.	N.D.	Miller et al. (2001)
WAP2072	0.7265	-9.7				N.D.	N.D.	Miller et al. (2001)
WAP2073	0.7238	-6.8				N.D.	N.D.	Miller et al. (2001)
WAP2074	0.7275	-14.0				N.D.	N.D.	Miller et al. (2001)
WAP2075	0.7363	-12.5				N.D.	N.D.	Miller et al. (2001)
WAP2076	0.7165	-9.8				N.D.	N.D.	Miller et al. (2001)
WAP25	0.7220	-9.2				No	No	Miller et al. (2001)
WAP28	0.8059					N.D.	N.D.	Miller et al. (2001)
BD-103						No	No	Mo et al. (2008)
BD-106	0.7047	-0.9				N.D.	N.D.	Mo et al. (2008)
BD-114	0.7057	-1.9				N.D.	N.D.	Mo et al. (2008)
BD-123	0.7063	0.8				N.D.	N.D.	Mo et al. (2008)
BD-145						No	No	Mo et al. (2008)
BD-151						No	No	Mo et al. (2008)
BD-160						No	No	Mo et al. (2008)
BD-27	0.7061	-2.6				N.D.	N.D.	Mo et al. (2008)
BD-55	0.7076	0.6				No	No	Mo et al. (2008)
BD-58						No	No	Mo et al. (2008)
BD-65						No	No	Mo et al. (2008)
BD-77						No	No	Mo et al. (2008)
D-15						No	No	Mo et al. (2008)
D-2	0.7058	-0.4				No	No	Mo et al. (2008)
L060						No	No	Mo et al. (2008)
L-1108	0.7046	9.2				N.D.	N.D.	Mo et al. (2008)
LZ9910	0.7074	2.3				N.D.	N.D.	Mo et al. (2008)
LZ9912						No	No	Mo et al. (2008)
LZ9916						No	No	Mo et al. (2008)
LZ9917						No	No	Mo et al. (2008)
LZ9921	0.7070	-0.2				No	No	Mo et al. (2008)
LZ994						No	No	Mo et al. (2008)
P-1	0.7047	-3.0				No	No	Mo et al. (2008)
GMH 1	0.7564	-10.5				N.D.	N.D.	Murphy et al. (2007)
GMH 2	0.7500	-17.6				N.D.	N.D.	Murphy et al. (2007)

Table A.2: continued

Sample	Terrane	Location	Lithology	Latitude (dd)	Longitude (dd)	Quadrant	Age (Ma)
GMH 3	Himalayas	Gurla Mandhata	Gneiss	30.4002	81.2518	Q3	9.0
GMH 4	Himalayas	Gurla Mandhata	Migmatite	30.4002	81.3260	Q3	9.0
GMH 5	Himalayas	Gurla Mandhata	Migmatite	30.4036	81.3165	Q3	9.0
GMH 6	Himalayas	Gurla Mandhata	Migmatite	30.4010	81.3107	Q3	9.0
GMH 7	Himalayas	Gurla Mandhata	Migmatite	30.3957	81.2948	Q3	9.0
GMH 8	Himalayas	Gurla Mandhata	Sill (granitic)	30.1877	80.2883	Q3	9.0
GMH 9	Himalayas	Gurla Mandhata	Sill (granitic)	30.3976	81.2700	Q3	9.0
Nomade_2004_1	Lhasa Terrane	Jiama	Lava	31.2450	90.4876	Q5	17.0
Nomade_2004_10	Himalayas	Manasarowar	Lava	30.6692	81.4920	Q3	17.0
Nomade_2004_11	Himalayas	Manasarowar	Lava	30.6692	81.4920	Q3	16.7
Nomade_2004_12	Lhasa Terrane	Zabuye	Lava	31.4454	84.0534	Q3	16.2
Nomade_2004_13	Lhasa Terrane	Zabuye	Lava	31.4454	84.0534	Q3	16.2
Nomade_2004_14	Lhasa Terrane	Zabuye	Lava	31.4454	84.0534	Q3	16.1
Nomade_2004_15	Lhasa Terrane	Zabuye	Lava	31.4454	84.0534	Q3	16.1
Nomade_2004_16	Lhasa Terrane	Dajia Co	Dike	29.8428	85.7317	Q4	18.3
Nomade_2004_17	Lhasa Terrane	Dajia Co	Dike	29.8428	85.7317	Q4	18.3
Nomade_2004_18	Lhasa Terrane	Wenbu	Lava	31.0739	86.5434	Q4	22.9
Nomade_2004_19	Lhasa Terrane	Chazi	Lava	30.1174	86.4536	Q4	13.1
Nomade_2004_2	Lhasa Terrane	Jiama	Lava	31.2450	90.4876	Q5	15.0
Nomade_2004_20	Lhasa Terrane	Chazi	Lava	30.1174	86.4536	Q4	8.2
Nomade_2004_21	Lhasa Terrane	Pabbai Zong	Dike	29.4543	86.9341	Q4	14.8
Nomade_2004_22	Lhasa Terrane	Pabbai Zong	Dike	29.4543	86.9341	Q4	14.8
Nomade_2004_23	Lhasa Terrane	Pabbai Zong	Xenolith	29.4543	86.9341	Q4	14.8
Nomade_2004_24	Lhasa Terrane	Pabbai Zong	Dike	29.4543	86.9341	Q4	14.8
Nomade_2004_25	Lhasa Terrane	Xigaze	Sill, Dike	29.2669	88.8814	Q4	18.3
Nomade_2004_26	Lhasa Terrane	Xigaze	Dike	29.2669	88.8814	Q4	15.1
Nomade_2004_27	Lhasa Terrane	Xigaze	Dike	29.2669	88.8814	Q4	18.4
Nomade_2004_28	Lhasa Terrane	Namling	Lava	29.6757	89.1030	Q4	14.0
Nomade_2004_29	Lhasa Terrane	Namling	Lava	29.6757	89.1030	Q4	15.3
Nomade_2004_3	Lhasa Terrane	Linzhi	Lava	29.5700	94.5800	Q6	26.2
Nomade_2004_30	Lhasa Terrane	Namling	Lava	29.6757	89.1030	Q4	15.0
Nomade_2004_31	Lhasa Terrane	Namling	Lava	29.6757	89.1030	Q4	15.1
Nomade_2004_32	Lhasa Terrane	Majiang	Lava	31.7603	81.4427	Q3	10.5
Nomade_2004_33	Lhasa Terrane	Majiang	Lava	31.7603	81.4427	Q3	10.1

Sample data continued

Sample	87Sr/86Sr(i)	eNd(t)	206Pb/ 204Pb(t)	207Pb/ 204Pb(t)	208Pb/ 204Pb(t)	*UPR	**ADK	Source
GMH 3	0.7573	-14.4				N.D.	N.D.	Murphy et al. (2007)
GMH 4	0.9051	-22.8				N.D.	N.D.	Murphy et al. (2007)
GMH 5	0.9840	-21.3				N.D.	N.D.	Murphy et al. (2007)
GMH 6	0.8115	-23.0				N.D.	N.D.	Murphy et al. (2007)
GMH 7	0.8011	-23.4				N.D.	N.D.	Murphy et al. (2007)
GMH 8	0.7602	-14.0				N.D.	N.D.	Murphy et al. (2007)
GMH 9	0.8907	-21.3				N.D.	N.D.	Murphy et al. (2007)
Nomade_2004_1						N.D.	N.D.	Nomade et al. (2004)
Nomade_2004_10						N.D.	N.D.	Nomade et al. (2004)
Nomade_2004_11						N.D.	N.D.	Nomade et al. (2004)
Nomade_2004_12						N.D.	N.D.	Nomade et al. (2004)
Nomade_2004_13						N.D.	N.D.	Nomade et al. (2004)
Nomade_2004_14						N.D.	N.D.	Nomade et al. (2004)
Nomade_2004_15						N.D.	N.D.	Nomade et al. (2004)
Nomade_2004_16						N.D.	N.D.	Nomade et al. (2004)
Nomade_2004_17						N.D.	N.D.	Nomade et al. (2004)
Nomade_2004_18						N.D.	N.D.	Nomade et al. (2004)
Nomade_2004_19						N.D.	N.D.	Nomade et al. (2004)
Nomade_2004_2						N.D.	N.D.	Nomade et al. (2004)
Nomade_2004_20						N.D.	N.D.	Nomade et al. (2004)
Nomade_2004_21						N.D.	N.D.	Nomade et al. (2004)
Nomade_2004_22						N.D.	N.D.	Nomade et al. (2004)
Nomade_2004_23						N.D.	N.D.	Nomade et al. (2004)
Nomade_2004_24						N.D.	N.D.	Nomade et al. (2004)
Nomade_2004_25						N.D.	N.D.	Nomade et al. (2004)
Nomade_2004_26						N.D.	N.D.	Nomade et al. (2004)
Nomade_2004_27						N.D.	N.D.	Nomade et al. (2004)
Nomade_2004_28						N.D.	N.D.	Nomade et al. (2004)
Nomade_2004_29						N.D.	N.D.	Nomade et al. (2004)
Nomade_2004_3						N.D.	N.D.	Nomade et al. (2004)
Nomade_2004_30						N.D.	N.D.	Nomade et al. (2004)
Nomade_2004_31						N.D.	N.D.	Nomade et al. (2004)
Nomade_2004_32						N.D.	N.D.	Nomade et al. (2004)
Nomade_2004_33						N.D.	N.D.	Nomade et al. (2004)

Table A.2: continued

Sample	Terrane	Location	Lithology	Latitude (dd)	Longitude (dd)	Quadrant	Age (Ma)
Nomade_2004_34	Lhasa Terrane	Majiang	Lava	31.7603	81.4427	Q3	12.9
Nomade_2004_35	Lhasa Terrane	Majiang	Lava	31.7603	81.4427	Q3	10.7
Nomade_2004_36	Lhasa Terrane	Majiang	Lava	31.7603	81.4427	Q3	10.7
Nomade_2004_37	Lhasa Terrane	Nanmu	Dike	29.5245	90.9339	Q5	16.4
Nomade_2004_38	Lhasa Terrane	Nanmu	Lava	29.5245	90.9339	Q5	16.7
Nomade_2004_39	Lhasa Terrane	Jiama	Lava	31.2450	90.4876	Q5	12.9
Nomade_2004_4	Lhasa Terrane	Shiquanhe	Lava	32.5041	80.1006	Q2	22.6
Nomade_2004_40	Lhasa Terrane	Jiama	Lava	31.2450	90.4876	Q5	15.2
Nomade_2004_5	Lhasa Terrane	Xungba	Lava	31.8585	81.9061	Q3	23.0
Nomade_2004_6	Lhasa Terrane	Jarga	Dike	31.4878	82.6548	Q3	18.5
Nomade_2004_7	Lhasa Terrane	Xungba	Dike	31.8585	81.9061	Q3	18.1
Nomade_2004_8	Lhasa Terrane	Xungba	Lava	31.8585	81.9061	Q3	22.8
Nomade_2004_9	Lhasa Terrane	Gegar	Lava	31.5167	81.8667	Q3	17.7
Y2	Lhasa Terrane	Yangying	Trachyandesite	29.7194	90.3716	Q5	10.6
Y4	Lhasa Terrane	Yangying	Trachyandesite	29.7414	90.3667	Q5	10.9
ZB1	Lhasa Terrane	Zabuye Salt Lake	Trachyandesite	32.4083	84.3005	Q3	16.2
ZB10	Lhasa Terrane	Zabuye Salt Lake	Trachyandesite	32.4083	84.3005	Q3	16.1
ZB12	Lhasa Terrane	Zabuye Salt Lake	Trachyandesite	32.4083	84.3005	Q3	16.1
ZB4	Lhasa Terrane	Zabuye Salt Lake	Trachyandesite	32.4083	84.3005	Q3	16.1
LT-10	Himalayas	Langtang	Metasediment	28.1473	85.3171	Q4	
LT-18	Himalayas	Langtang	Metasediment	28.1585	85.3145	Q4	
LT-19	Himalayas	Langtang	Metasediment	28.1575	85.3153	Q4	
LT-20	Himalayas	Langtang	Metasediment	28.1617	85.3193	Q4	
LT-21	Himalayas	Langtang	Metasediment	28.1593	85.3659	Q4	
LT-22	Himalayas	Langtang	Metasediment	28.1591	85.3766	Q4	
LT-24	Himalayas	Langtang	Metasediment	28.1575	85.3864	Q4	
LT-29	Himalayas	Langtang	Metasediment	28.1903	85.4446	Q4	925.6
LT-33	Himalayas	Langtang	Metasediment	28.1471	85.3417	Q4	
LT-34	Himalayas	Langtang	Metasediment	28.1519	85.3353	Q4	698.7
LT-4	Himalayas	Langtang	Metasediment	28.1279	85.3019	Q4	1709.5
LT-6	Himalayas	Langtang	Metasediment	28.1359	85.3075	Q4	
LT-7	Himalayas	Langtang	Metasediment	28.1372	85.3086	Q4	
LT-8	Himalayas	Langtang	Metasediment	28.1383	85.3097	Q4	1738.9
B29a	Himalayas		Quartzite	27.2720	91.2478	Q5	

Sample data continued

Sample	87Sr/86Sr(i)	eNd(t)	206Pb/ 204Pb(t)	207Pb/ 204Pb(t)	208Pb/ 204Pb(t)	*UPR	**ADK	Source
Nomade_2004_34						N.D.	N.D.	Nomade et al. (2004)
Nomade_2004_35						N.D.	N.D.	Nomade et al. (2004)
Nomade_2004_36						N.D.	N.D.	Nomade et al. (2004)
Nomade_2004_37						N.D.	N.D.	Nomade et al. (2004)
Nomade_2004_38						N.D.	N.D.	Nomade et al. (2004)
Nomade_2004_39						N.D.	N.D.	Nomade et al. (2004)
Nomade_2004_4						N.D.	N.D.	Nomade et al. (2004)
Nomade_2004_40						N.D.	N.D.	Nomade et al. (2004)
Nomade_2004_5						N.D.	N.D.	Nomade et al. (2004)
Nomade_2004_6						N.D.	N.D.	Nomade et al. (2004)
Nomade_2004_7						N.D.	N.D.	Nomade et al. (2004)
Nomade_2004_8						N.D.	N.D.	Nomade et al. (2004)
Nomade_2004_9						N.D.	N.D.	Nomade et al. (2004)
Y2						N.D.	N.D.	Nomade et al. (2004)
Y4						N.D.	N.D.	Nomade et al. (2004)
ZB1	0.7097	-8.6	18.8	15.8	39.6	Yes	No	Nomade et al. (2004)
ZB10	0.7094	-7.4	18.8	15.7	39.5	Yes	No	Nomade et al. (2004)
ZB12	0.7105	-7.7				Yes	No	Nomade et al. (2004)
ZB4	0.7095	-7.9				Yes	No	Nomade et al. (2004)
LT-10		-25.3				N.D.	N.D.	Parrish et al. (1996)
LT-18		-25.9				N.D.	N.D.	Parrish et al. (1996)
LT-19		-23.5				N.D.	N.D.	Parrish et al. (1996)
LT-20		-21.4				N.D.	N.D.	Parrish et al. (1996)
LT-21		-15.6				N.D.	N.D.	Parrish et al. (1996)
LT-22		-14.6				N.D.	N.D.	Parrish et al. (1996)
LT-24		-15.8				N.D.	N.D.	Parrish et al. (1996)
LT-29		-18.5				N.D.	N.D.	Parrish et al. (1996)
LT-33		-16.3				N.D.	N.D.	Parrish et al. (1996)
LT-34		-17.5				N.D.	N.D.	Parrish et al. (1996)
LT-4		-24.8				N.D.	N.D.	Parrish et al. (1996)
LT-6		-24.9				N.D.	N.D.	Parrish et al. (1996)
LT-7		-23.4				N.D.	N.D.	Parrish et al. (1996)
LT-8						N.D.	N.D.	Parrish et al. (1996)
B29a	0.9182	-21.0				No	No	Richards et al. (2006)

Table A.2: continued

Sample	Terrane	Location	Lithology	Latitude (dd)	Longitude (dd)	Quadrant	Age (Ma)
B29b	Himalayas		Phyllite	27.2720	91.2478	Q5	
B36a	Himalayas		Phyllite	27.2652	91.3970	Q5	
B39	Himalayas		Schist (Ky)	27.3385	91.5460	Q5	
B41	Himalayas		Gneiss (Bt)	27.4322	91.5697	Q5	
B45	Himalayas		Gneiss (Bt)	27.5838	91.4982	Q5	
B50	Himalayas		Schist (Sill)	27.3473	91.6180	Q5	
B51	Himalayas		Schist (Mica)	27.3470	91.6270	Q5	
B68	Himalayas		Gneiss (Bt)	27.2368	91.5520	Q5	
B71b	Himalayas		Quartzite	27.2982	91.4747	Q5	
B75	Himalayas	Daling-Shumar Group	Quartzite	27.2683	91.3957	Q5	2500.0
B81	Himalayas		Phyllite (Grt)	27.4568	90.3678	Q5	
B83	Himalayas		Schist (Grt)	27.5152	90.2957	Q5	
B85b	Himalayas		Schist (Grt)	27.3900	89.5873	Q5	
B87	Himalayas		Gneiss (Bt)	27.4972	89.3542	Q5	
B88b	Himalayas		Schist (Grt)	27.3147	89.5487	Q5	
Bh10b	Himalayas		Schist (Grt)	27.3148	89.5457	Q5	
Bh12	Himalayas		Schist (Grt)	27.9175	89.4742	Q5	
Bh13	Himalayas		Phyllite	26.9012	89.4500	Q5	
Bh3	Himalayas		Gneiss (Bt,Sill)	27.8662	89.7258	Q5	
Bh6	Himalayas		Gneiss (Bt)	27.6293	89.8205	Q5	
RP109	Himalayas	Daling-Shumar Group	Rhyolite	27.2801	91.3629	Q5	1840.0
RP69	Himalayas	Takhtsang Formation	Orthogneiss	27.6322	91.5955	Q5	825.0
RP71	Himalayas	HHC	Quartzite	27.5461	91.5955	Q5	1400.0
Sanchez_2013	Lhasa Terrane	Lopukangri	Granite	29.9167	84.4667	Q4	38.4
XGS 10	Lhasa Terrane	Qushui	Granodiorite	29.4663	90.8621	Q5	41.4
XGS 95	Lhasa Terrane	Lhasa	Granite	29.6592	91.1450	Q5	53.0
XR-494	Lhasa Terrane	Qushui	Granodiorite	29.4567	90.8437	Q5	41.7
XT-135	Lhasa Terrane	Dazhuka	Diorite				67.0
XT-144	Lhasa Terrane	Dazhuka	Diorite	29.3932	89.6750	Q5	93.4
XT-145	Lhasa Terrane	Dazhuka	Diorite	29.3882	89.6922	Q5	94.2
SLW NMT-02	Lhasa Terrane	Lunggar rift	Orthogneiss (leucogranitic)	31.0736	83.4050	Q3	20.4
SLW SFTR-02	Lhasa Terrane	Lunggar rift	Orthogneiss (leucogranitic)	30.9919	83.4145	Q3	62.9
YH01-1	Lhasa Terrane	Yanhu	Basalt	32.2691	82.5451	Q3	110.0
YH02-1	Lhasa Terrane	Yanhu	Basalt	32.2656	82.5556	Q3	108.9

Sample data continued

Sample	87Sr/86Sr(i)	eNd(t)	206Pb/ 204Pb(t)	207Pb/ 204Pb(t)	208Pb/ 204Pb(t)	*UPR	**ADK	Source
B29b	0.8803	-20.9				No	No	Richards et al. (2006)
B36a	0.9714	-21.6				No	No	Richards et al. (2006)
B39	0.8362	-11.6				No	No	Richards et al. (2006)
B41	0.7753	-10.2				No	No	Richards et al. (2006)
B45	0.7535	-10.2				No	No	Richards et al. (2006)
B50	0.7751	-10.3				No	No	Richards et al. (2006)
B51	0.8368	-11.5				No	No	Richards et al. (2006)
B68	0.7645	-10.5				No	No	Richards et al. (2006)
B71b	0.9206	-12.8				No	No	Richards et al. (2006)
B75	1.0590	-20.4				No	No	Richards et al. (2006)
B81	0.8005	-9.1				No	No	Richards et al. (2006)
B83	0.7278	-7.4				No	No	Richards et al. (2006)
B85b	0.7896	-11.4				No	No	Richards et al. (2006)
B87	0.7439	-11.6				No	No	Richards et al. (2006)
B88b	0.7598	-9.5				No	No	Richards et al. (2006)
Bh10b		-12.1				N.D.	N.D.	Richards et al. (2006)
Bh12		-11.9				N.D.	N.D.	Richards et al. (2006)
Bh13		-25.6				N.D.	N.D.	Richards et al. (2006)
Bh3		-7.5				N.D.	N.D.	Richards et al. (2006)
Bh6		-10.3				N.D.	N.D.	Richards et al. (2006)
RP109						N.D.	N.D.	Richards et al. (2006)
RP69						N.D.	N.D.	Richards et al. (2006)
RP71						N.D.	N.D.	Richards et al. (2006)
Sanchez_2013						N.D.	N.D.	Sanchez et al. (2013)
XGS 10						N.D.	N.D.	Schaerer et al. (1984)
XGS 95						N.D.	N.D.	Schaerer et al. (1984)
XR-494						N.D.	N.D.	Schaerer et al. (1984)
XT-135						N.D.	N.D.	Schaerer et al. (1984)
XT-144						N.D.	N.D.	Schaerer et al. (1984)
XT-145						N.D.	N.D.	Schaerer et al. (1984)
SLW NMT-02						N.D.	N.D.	Styron et al. (2013)
SLW SFTR-02						N.D.	N.D.	Styron et al. (2013)
YH01-1	0.7062	-0.6				No	No	Sui et al. (2013)
YH02-1	0.7060	2.1				No	No	Sui et al. (2013)

Table A.2: continued

Sample	Terrane	Location	Lithology	Latitude (dd)	Longitude (dd)	Quadrant	Age (Ma)
YH02-2	Lhasa Terrane	Yanhu	Rhyolite	32.2639	82.5532	Q3	
YH03-1	Lhasa Terrane	Yanhu	Rhyolite	32.2743	82.5550	Q3	
YH10-2	Lhasa Terrane	Yanhu	Diorite	32.3635	82.5718	Q3	109.7
YH10-3	Lhasa Terrane	Yanhu	Enclave (dioritic)	32.3635	82.5758	Q3	
YH10-4	Lhasa Terrane	Yanhu	Diorite	32.3589	82.5724	Q3	
YH10-6	Lhasa Terrane	Yanhu	Enclave (dioritic)	32.3589	82.5758	Q3	110.4
YH22-1	Lhasa Terrane	Yanhu	Basalt	32.3473	82.4402	Q3	
YH22-2	Lhasa Terrane	Yanhu	Basalt	32.3473	82.4455	Q3	111.8
YH22-3	Lhasa Terrane	Yanhu	Rhyolite	32.3427	82.4402	Q3	
82109PK1	Lhasa Terrane	Lunggar rift	Intrusion (Qz, Fsp)	31.6635	83.6636	Q3	152.0
82209PK1	Lhasa Terrane	Lunggar rift	Granodiorite	31.7281	83.5730	Q3	152.3
82309PK1	Lhasa Terrane	Lunggar rift	Granite (Bt)	31.5789	83.5356	Q3	13.3
82309PK2	Lhasa Terrane	Lunggar rift	Leucogranite	31.5787	83.5315	Q3	14.1
82309PK3	Lhasa Terrane	Lunggar rift	Orthogneiss (leucogranitic)	31.5787	83.5256	Q3	14.4
82309PK4	Lhasa Terrane	Lunggar rift	Orthogneiss (leucogranitic)	31.5797	83.5184	Q3	14.9
82309PK5	Lhasa Terrane	Lunggar rift	Orthogneiss (leucogranitic)	31.5800	83.5101	Q3	14.5
82409PK1	Lhasa Terrane	Lunggar rift	Tuff (rhyolitic)	31.9557	83.7586	Q3	111.0
82409PK2	Lhasa Terrane	Lunggar rift	Rhyolite (porphyritic)	31.9557	83.7586	Q3	145.5
82609PK1	Lhasa Terrane	Lunggar rift	Orthogneiss (granitic)	31.5241	83.5318	Q3	13.8
82609PK4	Lhasa Terrane	Lunggar rift	Leucogranite	31.5266	83.5191	Q3	13.2
82609PK5	Lhasa Terrane	Lunggar rift	Granite (Bt)	31.5347	83.5229	Q3	13.0
82609PK6	Lhasa Terrane	Lunggar rift	Granite (Bt, weakly deformed)	31.5317	83.5207	Q3	13.1
82709PK2	Lhasa Terrane	Lunggar rift	Orthogneiss (Bt, granitic)	31.4349	83.5640	Q3	123.8
82709PK3	Lhasa Terrane	Lunggar rift	Granodiorite	31.6014	83.2795	Q3	154.4
82809PK1	Lhasa Terrane	Lunggar rift	Volcanic Rock	31.4820	83.5470	Q3	126.7
82909PK1	Lhasa Terrane	Lunggar rift	Volcanic rock (Qz, San)	31.8780	83.7042	Q3	144.2
82909PK2	Lhasa Terrane	Lunggar rift	Volcanic rock (Qz, Pl)	31.8041	83.7928	Q3	145.9
RG-13	Lhasa Terrane	Daah-Hanu	Tonalite				52.5
RG-14	Lhasa Terrane	Daah-Hanu	Tonalite				53.4
RG-16	Lhasa Terrane	Chang La	Granodiorite	34.0544	77.9427	Q2	57.6
RG-20	Lhasa Terrane	Daah-Hanu	Granodiorite				45.3
RG-6	Lhasa Terrane	Hundar	Granite	34.5947	77.4643	Q2	66.1
C32	Lhasa Terrane	N Ayilari	Dike (leucocratic)	32.3882	79.7237	Q2	22.7
C43	Lhasa Terrane	N Ayilari	Gneiss (leucocratic)	32.3230	79.7404	Q2	

Sample data continued

Sample	87Sr/86Sr(i)	eNd(t)	206Pb/ 204Pb(t)	207Pb/ 204Pb(t)	208Pb/ 204Pb(t)	*UPR	**ADK	Source
YH02-2						No	No	Sui et al. (2013)
YH03-1						No	No	Sui et al. (2013)
YH10-2	0.7042	3.6				No	Yes	Sui et al. (2013)
YH10-3		4.0				No	No	Sui et al. (2013)
YH10-4		3.5				No	Yes	Sui et al. (2013)
YH10-6	0.7042	3.4				No	No	Sui et al. (2013)
YH22-1						No	No	Sui et al. (2013)
YH22-2	0.7063	0.6				No	No	Sui et al. (2013)
YH22-3						No	No	Sui et al. (2013)
82109PK1						N.D.	N.D.	Sundell et al. (2013)
82209PK1						N.D.	N.D.	Sundell et al. (2013)
82309PK1						N.D.	N.D.	Sundell et al. (2013)
82309PK2						N.D.	N.D.	Sundell et al. (2013)
82309PK3						N.D.	N.D.	Sundell et al. (2013)
82309PK4						N.D.	N.D.	Sundell et al. (2013)
82309PK5						N.D.	N.D.	Sundell et al. (2013)
82409PK1						N.D.	N.D.	Sundell et al. (2013)
82409PK2						N.D.	N.D.	Sundell et al. (2013)
82609PK1						N.D.	N.D.	Sundell et al. (2013)
82609PK4						N.D.	N.D.	Sundell et al. (2013)
82609PK5						N.D.	N.D.	Sundell et al. (2013)
82609PK6						N.D.	N.D.	Sundell et al. (2013)
82709PK2						N.D.	N.D.	Sundell et al. (2013)
82709PK3						N.D.	N.D.	Sundell et al. (2013)
82809PK1						N.D.	N.D.	Sundell et al. (2013)
82909PK1						N.D.	N.D.	Sundell et al. (2013)
82909PK2						N.D.	N.D.	Sundell et al. (2013)
RG-13						No	No	Upadhyay et al. (2008)
RG-14						No	No	Upadhyay et al. (2008)
RG-16						No	No	Upadhyay et al. (2008)
RG-20						No	Yes	Upadhyay et al. (2008)
RG-6						No	No	Upadhyay et al. (2008)
C32						N.D.	N.D.	Valli et al. (2008)
C43						N.D.	N.D.	Valli et al. (2008)

Table A.2: continued

Sample	Terrane	Location	Lithology	Latitude (dd)	Longitude (dd)	Quadrant	Age (Ma)
K2P30	Lhasa Terrane	Labhar Kangri	Granite	30.4831	83.0395	Q3	21.1
L89	Lhasa Terrane	N Ayilari	Migmatite	32.4457	79.5602	Q2	23.4
P18	Lhasa Terrane	N Ayilari	Gneiss (Bt,Ms)	32.3914	79.7264	Q2	23.3
P20	Lhasa Terrane	N Ayilari	Gneiss (Bt)	32.3887	79.7244	Q2	21.7
P34	Lhasa Terrane	N Ayilari	Gneiss (mylonitic,leucocratic)	32.4168	79.7017	Q2	
8-18-03-1	Lhasa Terrane	Xiagangjiang Range	Tuff	31.5400	85.2300	Q4	123.0
8-18-03-2	Lhasa Terrane	Xiagangjiang Range	Tuff	31.5400	85.2300	Q4	113.0
JG081203-2	Lhasa Terrane	Xiagangjiang Range	Tuff	31.4700	85.1400	Q4	131.0
JG081203-4	Lhasa Terrane	Xiagangjiang Range	Tuff	31.4700	85.1400	Q4	131.0
JG082103-1	Lhasa Terrane	Xiagangjiang Range	Granite (Bt)	31.5100	85.0800	Q4	159.0
JG082103-2	Lhasa Terrane	Xiagangjiang Range	Granite (Bt)	31.5200	85.0800	Q4	138.0
JG082103-3	Lhasa Terrane	Xiagangjiang Range	Granite (Bt)	31.5200	85.0900	Q4	153.0
JG082603-1	Lhasa Terrane	Xiagangjiang Range	Granite (Bt)	31.5300	85.0700	Q4	143.0
JV081603-1	Lhasa Terrane	Xiagangjiang Range	Tuff	31.4000	85.1200	Q4	130.0
KK3	Lhasa Terrane	Namru	Granite (Chl)	31.8424	80.0696	Q2	65.7
KK4	Lhasa Terrane	Namru	Orthogneiss (Bt,Hbl, granitic)	31.8659	80.1078	Q2	48.0
KK5	Lhasa Terrane	Namru	Orthogneiss (granitic)	31.8682	80.1108	Q2	49.2
KK6	Lhasa Terrane	Namru	Orthogneiss (Bt,Hbl, granitic)	31.8718	80.1139	Q2	11.7
KK9	Lhasa Terrane	Namru	Orthogneiss (granitic)	31.8794	80.1228	Q2	48.6
71-1	Lhasa Terrane	Langxian	Granodiorite	29.0400	93.1600	Q5	103.0
ET021D	Lhasa Terrane	Qulong	Granite	29.6900	91.6300	Q5	64.6
ET021E	Lhasa Terrane	Qulong	Diorite	29.6900	91.6300	Q5	64.0
ET026I	Lhasa Terrane	Quxu/Nanmu	Granodiorite	29.4800	90.8700	Q5	46.4
ST042F	Lhasa Terrane	Xietongmen	Granodiorite	29.4500	88.2300	Q4	50.7
ST043A	Lhasa Terrane	Xietongmen	Granodiorite	29.4500	88.2300	Q4	50.4
ST104A	Lhasa Terrane	Zedong	Granodiorite	29.2700	91.8100	Q5	60.1
ST117A	Lhasa Terrane	Sangri	Granite	29.2500	92.1900	Q5	60.5
ST124A	Lhasa Terrane	Sangyi	Granodiorite	29.3000	91.4400	Q5	89.3
ST126A	Lhasa Terrane	Sangyi	Diorite	29.3000	91.4600	Q5	95.0
ST129A	Lhasa Terrane	Dazhuka	Diorite	29.3900	89.6300	Q5	94.1
ST141A	Lhasa Terrane	Xigaze Nanmulin	Gabbro	29.4000	89.0900	Q4	90.5
ST143A	Lhasa Terrane	Dazhuka-Nimu	Diorite	29.3100	89.8100	Q5	84.8
ST144A	Lhasa Terrane	Dazhuka-Nimu	Diorite	29.3200	89.9400	Q5	85.2
ST147A	Lhasa Terrane	Nimu	Diorite	29.4000	90.1800	Q5	50.6

Sample data continued

Sample	87Sr/86Sr(i)	eNd(t)	206Pb/ 204Pb(t)	207Pb/ 204Pb(t)	208Pb/ 204Pb(t)	*UPR	**ADK	Source
K2P30						N.D.	N.D.	Valli et al. (2008)
L89						N.D.	N.D.	Valli et al. (2008)
P18						N.D.	N.D.	Valli et al. (2008)
P20						N.D.	N.D.	Valli et al. (2008)
P34						N.D.	N.D.	Valli et al. (2008)
8-18-03-1						N.D.	N.D.	Volkmer et al. (2007)
8-18-03-2						N.D.	N.D.	Volkmer et al. (2007)
JG081203-2						N.D.	N.D.	Volkmer et al. (2007)
JG081203-4						N.D.	N.D.	Volkmer et al. (2007)
JG082103-1						N.D.	N.D.	Volkmer et al. (2007)
JG082103-2						N.D.	N.D.	Volkmer et al. (2007)
JG082103-3						N.D.	N.D.	Volkmer et al. (2007)
JG082603-1						N.D.	N.D.	Volkmer et al. (2007)
JV081603-1						N.D.	N.D.	Volkmer et al. (2007)
KK3						N.D.	N.D.	Wang et al. (2009)
KK4						N.D.	N.D.	Wang et al. (2009)
KK5						N.D.	N.D.	Wang et al. (2009)
KK6						N.D.	N.D.	Wang et al. (2009)
KK9						N.D.	N.D.	Wang et al. (2009)
71-1						N.D.	N.D.	Wen et al. (2008)
ET021D						N.D.	N.D.	Wen et al. (2008)
ET021E						N.D.	N.D.	Wen et al. (2008)
ET026I						N.D.	N.D.	Wen et al. (2008)
ST042F						N.D.	N.D.	Wen et al. (2008)
ST043A						N.D.	N.D.	Wen et al. (2008)
ST104A						N.D.	N.D.	Wen et al. (2008)
ST117A						N.D.	N.D.	Wen et al. (2008)
ST124A						N.D.	N.D.	Wen et al. (2008)
ST126A						N.D.	N.D.	Wen et al. (2008)
ST129A						N.D.	N.D.	Wen et al. (2008)
ST141A						N.D.	N.D.	Wen et al. (2008)
ST143A						N.D.	N.D.	Wen et al. (2008)
ST144A						N.D.	N.D.	Wen et al. (2008)
ST147A						N.D.	N.D.	Wen et al. (2008)

Table A.2: continued

Sample	Terrane	Location	Lithology	Latitude (dd)	Longitude (dd)	Quadrant	Age (Ma)
ST152A	Lhasa Terrane	Quxu Bridge	Gabbro	29.3300	90.6900	Q5	52.7
T036E	Lhasa Terrane	Nimu-Quxu	Diorite	29.3200	90.3100	Q5	102.2
T044E	Lhasa Terrane	Nanmulin	Gabbro	29.4900	89.0800	Q4	48.3
T076	Lhasa Terrane	Lhasa	Granite	29.6700	91.2200	Q5	59.3
T153	Lhasa Terrane	Cuoqin-Dajia Co	Diorite	30.1300	85.4100	Q4	49.9
T201A	Lhasa Terrane	Quxu	Enclave (gabbroic)	29.3500	90.7300	Q5	50.0
T201B	Lhasa Terrane	Quxu	Granodiorite	29.3500	90.7300	Q5	50.7
T228A	Lhasa Terrane	Baiba	Granite	29.7600	94.0100	Q6	55.0
T024	Lhasa Terrane	Lilong	Granodiorite	29.1400	93.7500	Q5	80.4
T026	Lhasa Terrane	Langxian	Granodiorite	29.1200	93.4400	Q5	82.7
T027	Lhasa Terrane	Langxian	Granodiorite	29.0000	93.3200	Q5	82.7
T212	Lhasa Terrane	Langxian	Granodiorite	29.0000	93.3100	Q5	82.7
T213	Lhasa Terrane	Langxian	Granodiorite	29.0400	93.3400	Q5	82.7
T215	Lhasa Terrane	Langxian	Granodiorite	29.1000	93.4100	Q5	82.7
T216A	Lhasa Terrane	Lilong	Granodiorite	29.1700	93.6100	Q5	80.4
T217	Lhasa Terrane	Lilong	Granodiorite	29.1400	93.6400	Q5	80.4
T218B	Lhasa Terrane	Lilong	Granodiorite	29.1400	93.7500	Q5	80.4
JPT14.2	Lhasa Terrane	Daggyai Tso	Dike (dacitic)	29.8428	85.7317	Q4	19.3
JPT7	Lhasa Terrane	Pabbai Zong	Dike (ultrapotassic)	29.4543	86.9341	Q4	18.3
T11B	Lhasa Terrane	Daggyai Tso	Dike (dacitic)	29.8428	85.7317	Q4	17.3
T2A	Lhasa Terrane	Pabbai Zong	Dike (ultrapotassic)	29.4543	86.9341	Q4	13.8
T3B	Lhasa Terrane	Pabbai Zong	Xenolith (ultrapotassic)	29.4543	86.9341	Q4	13.8
T4A	Lhasa Terrane	Pabbai Zong	Dike (ultrapotassic)	29.4543	86.9341	Q4	
T5A	Lhasa Terrane	Pabbai Zong	Dike (ultrapotassic)	29.4543	86.9341	Q4	13.3
ZC-05	Lhasa Terrane	Xigaze	Gabbro	29.2669	88.8814	Q4	110.0
ZC-186	Lhasa Terrane	Xigaze	Basaltic Andesite	29.2669	88.8814	Q4	110.0
ZC-192	Lhasa Terrane	Xigaze	Gabbro	29.2669	88.8814	Q4	110.0
ZC-206	Lhasa Terrane	Xigaze	Gabbro (cumulate)	29.2669	88.8814	Q4	110.0
ZC-232	Lhasa Terrane	Xigaze	Basalt	29.2669	88.8814	Q4	110.0
GL-22	Lhasa Terrane	Lushui	Dike (basaltic)	26.0011	98.6824	QX	41.8
GL-24	Lhasa Terrane	Lushui	Dike (basaltic)	26.0011	98.6824	QX	41.8
GL-8	Lhasa Terrane	Lushui	Dike (basaltic)	26.0011	98.6824	QX	41.8
GLS 16	Lhasa Terrane	Lushui	Dike (basaltic)	26.0011	98.6824	QX	41.8
GLS 21	Lhasa Terrane	Lushui	Dike (basaltic)	26.0011	98.6824	QX	41.8

Sample data continued

Sample	87Sr/86Sr(i)	eNd(t)	206Pb/ 204Pb(t)	207Pb/ 204Pb(t)	208Pb/ 204Pb(t)	*UPR	**ADK	Source
ST152A						N.D.	N.D.	Wen et al. (2008)
T036E						N.D.	N.D.	Wen et al. (2008)
T044E						N.D.	N.D.	Wen et al. (2008)
T076						N.D.	N.D.	Wen et al. (2008)
T153						N.D.	N.D.	Wen et al. (2008)
T201A						N.D.	N.D.	Wen et al. (2008)
T201B						N.D.	N.D.	Wen et al. (2008)
T228A						N.D.	N.D.	Wen et al. (2008)
T024						No	Yes	Wen et al. (2008)
T026						No	Yes	Wen et al. (2008)
T027						No	Yes	Wen et al. (2008)
T212						No	Yes	Wen et al. (2008)
T213						No	Yes	Wen et al. (2008)
T215						No	Yes	Wen et al. (2008)
T216A						No	Yes	Wen et al. (2008)
T217						No	Yes	Wen et al. (2008)
T218B						No	Yes	Wen et al. (2008)
JPT14.2	0.7069	-7.2				No	Yes	Williams et al. (2001)
JPT7						N.D.	N.D.	Williams et al. (2001)
T11B	0.7069	-10.6				No	Yes	Williams et al. (2001)
T2A	0.7399	-17.4				Yes	No	Williams et al. (2001)
T3B	0.7122	-14.7				Yes	No	Williams et al. (2001)
T4A	0.7117	-12.7				Yes	No	Williams et al. (2001)
T5A	0.7106	-14.0				Yes	No	Williams et al. (2001)
ZC-05	0.7030	9.2	17.4	15.4	37.3	No	No	Xu et al. (2004)
ZC-186	0.7046	8.7				No	No	Xu et al. (2004)
ZC-192	0.7034	9.1	17.5	15.4	37.3	No	No	Xu et al. (2004)
ZC-206	0.7038	9.0	17.1	15.4	36.9	No	No	Xu et al. (2004)
ZC-232	0.7045	9.1				No	No	Xu et al. (2004)
GL-22						No	No	Xu et al. (2008)
GL-24						No	No	Xu et al. (2008)
GL-8						No	No	Xu et al. (2008)
GLS 16						No	No	Xu et al. (2008)
GLS 21						No	No	Xu et al. (2008)

Table A.2: continued

Sample	Terrane	Location	Lithology	Latitude (dd)	Longitude (dd)	Quadrant	Age (Ma)
GLS 27	Lhasa Terrane	Lushui	Dike (basaltic)	26.0011	98.6824	QX	41.8
TL-2	Lhasa Terrane	Lianghe	Dike (basaltic)	24.6963	98.3658	QX	39.7
TL-3	Lhasa Terrane	Lianghe	Dike (basaltic)	24.6963	98.3658	QX	39.7
TL-4	Lhasa Terrane	Lianghe	Dike (basaltic)	24.6963	98.3658	QX	39.7
TL-7	Lhasa Terrane	Lianghe	Dike (basaltic)	24.6963	98.3658	QX	39.7
T339	Lhasa Terrane	Chongjiang	Granite (porphyritic)	29.5458	90.0212	Q5	14.6
T358	Lhasa Terrane	Tingong	Granite (porphyritic)	29.5871	90.0543	Q5	14.2
T379	Lhasa Terrane	Pagu	Granodiorite	29.5458	90.0212	Q5	14.2
T380	Lhasa Terrane	Pagu	Granodiorite	29.5871	90.0543	Q5	90.4
T381	Lhasa Terrane	Pagu	Granodiorite	29.6181	89.9840	Q5	14.0
T399	Lhasa Terrane	Nanmuqie	Granite (porphyritic)	29.4982	88.3962	Q4	14.3
T400	Lhasa Terrane	Nanmuqie	Granite (porphyritic)	29.5520	88.2825	Q4	14.2
T401	Lhasa Terrane	Nanmuqie	Granite	29.7442	88.3218	Q4	14.2
T402	Lhasa Terrane	Nanmuqie	Granite	29.8269	88.3610	Q4	14.2
T403	Lhasa Terrane	Nanmuqie	Granite	29.7442	88.3218	Q4	14.4
T404	Lhasa Terrane	Nanmuqie	Granite	29.8269	88.3610	Q4	14.2
T604	Lhasa Terrane	E Syntaxis	Granulite (mafic)				
T605	Lhasa Terrane	E Syntaxis	Granulite (mafic)				
T606	Lhasa Terrane	E Syntaxis	Granulite (mafic)				
T607	Lhasa Terrane	E Syntaxis	Granulite (mafic)				
T608	Lhasa Terrane	E Syntaxis	Granulite (mafic)				
0319-02	Himalayas	Yardoi	Gneiss (Bt,Grt)	28.8299	91.9555	Q5	
0319-03	Himalayas	Yardoi	Gneiss (Bt,Grt)	28.8299	91.9555	Q5	
0319-06	Himalayas	Yardoi	Leucogranite	28.8299	91.9555	Q5	42.6
0319-07	Himalayas	Yardoi	Gneiss (Bt,Grt)	28.8299	91.9555	Q5	
0321-011	Himalayas	Yardoi	Gneiss (Grt,Gr)	28.8299	91.9555	Q5	
0321-021	Himalayas	Yardoi	Gneiss (Ms,Grt)	28.8299	91.9555	Q5	
0321-031	Himalayas	Yardoi	Leucogranite	28.8299	91.9555	Q5	35.3
0321-041	Himalayas	Yardoi	Leucogranite	28.8299	91.9555	Q5	42.6
0321-07	Himalayas	Yardoi	Leucogranite	28.8299	91.9555	Q5	42.6
0321-08	Himalayas	Yardoi	Amphibolite (Grt)	28.8299	91.9555	Q5	42.6
0321-09	Himalayas	Yardoi	Amphibolite (Grt)	28.8299	91.9555	Q5	42.6
0321-12	Himalayas	Yardoi	Gneiss (Bt,Grt)	28.8299	91.9555	Q5	
0322-01	Himalayas	Yardoi	Leucogranite	28.8299	91.9555	Q5	42.6

Sample data continued

Sample	87Sr/86Sr(i)	eNd(t)	206Pb/ 204Pb(t)	207Pb/ 204Pb(t)	208Pb/ 204Pb(t)	*UPR	**ADK	Source
GLS 27						No	No	Xu et al. (2008)
TL-2						No	No	Xu et al. (2008)
TL-3						No	No	Xu et al. (2008)
TL-4						No	No	Xu et al. (2008)
TL-7						No	No	Xu et al. (2008)
T339						No	Yes	Xu et al. (2010)
T358	0.7056	-2.4				No	Yes	Xu et al. (2010)
T379	0.7062	-4.0				No	Yes	Xu et al. (2010)
T380	0.7060	-3.8				No	Yes	Xu et al. (2010)
T381	0.7060	-3.5				No	Yes	Xu et al. (2010)
T399	0.7068	-5.8				No	Yes	Xu et al. (2010)
T400	0.7068	-5.5				No	Yes	Xu et al. (2010)
T401	0.7082	-8.1				No	Yes	Xu et al. (2010)
T402						No	No	Xu et al. (2010)
T403	0.7064	-5.2				No	No	Xu et al. (2010)
T404	0.7076	-7.4				No	No	Xu et al. (2010)
T604						N.D.	N.D.	Xu et al. (2010)
T605						N.D.	N.D.	Xu et al. (2010)
T606						N.D.	N.D.	Xu et al. (2010)
T607						N.D.	N.D.	Xu et al. (2010)
T608						N.D.	N.D.	Xu et al. (2010)
0319-02	0.9551	-14.0				N.D.	N.D.	Zeng et al. (2009)
0319-03	0.8747	-16.6				N.D.	N.D.	Zeng et al. (2009)
0319-06	0.7155	-11.5				No	No	Zeng et al. (2009)
0319-07	0.8581	-11.3				N.D.	N.D.	Zeng et al. (2009)
0321-011	0.7193	-6.9				N.D.	N.D.	Zeng et al. (2009)
0321-021	0.9222	-15.3				N.D.	N.D.	Zeng et al. (2009)
0321-031	0.7175	-11.6				No	No	Zeng et al. (2009)
0321-041	0.7186	-10.4				No	No	Zeng et al. (2009)
0321-07	0.7193	-9.9				No	No	Zeng et al. (2009)
0321-08	0.7121	-4.6				No	No	Zeng et al. (2009)
0321-09	0.7127	-4.4				No	No	Zeng et al. (2009)
0321-12	0.9041	-15.4				No	No	Zeng et al. (2009)
0322-01	0.7156	-10.4				No	No	Zeng et al. (2009)

Table A.2: continued

Sample	Terrane	Location	Lithology	Latitude (dd)	Longitude (dd)	Quadrant	Age (Ma)
0322-04	Himalayas	Yardoi	Leucogranite	28.8299	91.9555	Q5	42.6
0323-01	Himalayas	Yardoi	Leucogranite	28.8299	91.9555	Q5	42.6
0323-02	Himalayas	Yardoi	Leucogranite	28.8299	91.9555	Q5	42.6
0323-03	Himalayas	Yardoi	Leucogranite	28.8299	91.9555	Q5	42.6
0323-04	Himalayas	Yardoi	Leucogranite	28.8299	91.9555	Q5	42.6
T0317-01	Himalayas	Dala	Granite	28.6472	92.2260	Q5	44.1
T0317-02	Himalayas	Dala	Granite	28.6472	92.2260	Q5	44.1
T0317-03	Himalayas	Dala	Granite	28.6472	92.2260	Q5	44.1
T0317-04	Himalayas	Dala	Granite	28.6472	92.2260	Q5	44.1
T0317-05	Himalayas	Dala	Granite	28.6472	92.2260	Q5	44.1
T0317-06	Himalayas	Dala	Granite	28.6472	92.2260	Q5	44.1
T0319-06	Himalayas	Yardoi	Granite (Bt,Ms)	28.8299	91.9555	Q5	42.6
T0319-07	Himalayas	Yardoi	Granite (Bt,Ms)	28.8299	91.9555	Q5	42.6
T0319-08	Himalayas	Yardoi	Granite (Bt,Ms)	28.8299	91.9555	Q5	42.6
T0319-09	Himalayas	Yardoi	Granite (Bt,Ms)	28.8299	91.9555	Q5	42.6
T0319-10	Himalayas	Yardoi	Granite (Bt,Ms)	28.8299	91.9555	Q5	42.6
T0319-11	Himalayas	Yardoi	Granite (Bt,Ms)	28.8299	91.9555	Q5	42.6
T0319-12	Himalayas	Yardoi	Granite (Bt,Ms)	28.8299	91.9555	Q5	42.6
T0320-06	Himalayas	Yardoi	Granite (Bt,Ms)	28.8299	91.9555	Q5	42.6
T0321-08	Himalayas	Yardoi	Amphibolite	28.8299	91.9555	Q5	
T0321-09	Himalayas	Yardoi	Amphibolite	28.8299	91.9555	Q5	
T0389-0	Himalayas	Quedang	Granite	28.5130	92.3059	Q5	42.8
T0389-10	Himalayas	Quedang	Granite	28.5130	92.3059	Q5	42.8
T0389-11	Himalayas	Quedang	Granite	28.5130	92.3059	Q5	42.8
T0389-12	Himalayas	Quedang	Granite	28.5130	92.3059	Q5	42.8
T0389-17	Himalayas	Yardoi	Amphibolite	28.8299	91.9555	Q5	
T0389-4	Himalayas	Quedang	Granite	28.5130	92.3059	Q5	42.8
T0389-5	Himalayas	Quedang	Granite	28.5130	92.3059	Q5	42.8
T0389-6	Himalayas	Quedang	Granite	28.5130	92.3059	Q5	42.8
T0389-7	Himalayas	Quedang	Granite	28.5130	92.3059	Q5	42.8
T0389-8	Himalayas	Quedang	Granite	28.5130	92.3059	Q5	42.8
T0389-9	Himalayas	Quedang	Granite	28.5130	92.3059	Q5	42.8
T0392-0	Himalayas	Yardoi	Orthogneiss	28.8299	91.9555	Q5	42.6
T0392-1	Himalayas	Yardoi	Orthogneiss	28.8299	91.9555	Q5	42.6

Sample data continued

Sample	87Sr/86Sr(i)	eNd(t)	206Pb/ 204Pb(t)	207Pb/ 204Pb(t)	208Pb/ 204Pb(t)	*UPR	**ADK	Source
0322-04	0.7150	-10.4				No	No	Zeng et al. (2009)
0323-01	0.7133	-9.1				No	No	Zeng et al. (2009)
0323-02	0.7160	-13.7				N.D.	N.D.	Zeng et al. (2009)
0323-03	0.7144	-8.9				No	No	Zeng et al. (2009)
0323-04	0.7143	-9.3				No	No	Zeng et al. (2009)
T0317-01	0.7176	-12.3				No	No	Zeng et al. (2011)
T0317-02	0.7179	-9.2				No	Yes	Zeng et al. (2011)
T0317-03	0.7178	-12.2				No	Yes	Zeng et al. (2011)
T0317-04	0.7178	-12.4				No	No	Zeng et al. (2011)
T0317-05	0.7177	-12.3				No	No	Zeng et al. (2011)
T0317-06	0.7178	-12.2				No	Yes	Zeng et al. (2011)
T0319-06	0.7154	-11.4				No	No	Zeng et al. (2011)
T0319-07	0.7159	-13.3				No	No	Zeng et al. (2011)
T0319-08	0.7188	-9.8				No	No	Zeng et al. (2011)
T0319-09						No	No	Zeng et al. (2011)
T0319-10						No	No	Zeng et al. (2011)
T0319-11						No	No	Zeng et al. (2011)
T0319-12						No	No	Zeng et al. (2011)
T0320-06	0.7119	-14.9				No	Yes	Zeng et al. (2011)
T0321-08	0.7121	-4.5				N.D.	N.D.	Zeng et al. (2011)
T0321-09	0.7127	-4.3				N.D.	N.D.	Zeng et al. (2011)
T0389-0						No	No	Zeng et al. (2011)
T0389-10						No	No	Zeng et al. (2011)
T0389-11	0.7162	-11.0				No	No	Zeng et al. (2011)
T0389-12	0.7163	-11.2				No	No	Zeng et al. (2011)
T0389-17	0.7334	-15.6				N.D.	N.D.	Zeng et al. (2011)
T0389-4	0.7156	-11.2				No	No	Zeng et al. (2011)
T0389-5	0.7151	-10.1				No	No	Zeng et al. (2011)
T0389-6	0.7160	-11.1				No	No	Zeng et al. (2011)
T0389-7	0.7158	-10.8				No	No	Zeng et al. (2011)
T0389-8	0.7156	-11.1				No	No	Zeng et al. (2011)
T0389-9	0.7159	-10.9				No	No	Zeng et al. (2011)
T0392-0	0.8295	-15.3				N.D.	N.D.	Zeng et al. (2011)
T0392-1	0.9616	-11.7				N.D.	N.D.	Zeng et al. (2011)

Table A.2: continued

Sample	Terrane	Location	Lithology	Latitude (dd)	Longitude (dd)	Quadrant	Age (Ma)
T0392-3	Himalayas	Yardoi	Orthogneiss	28.8299	91.9555	Q5	42.6
T0394-1	Himalayas	Yardoi	Amphibolite	28.8299	91.9555	Q5	
T0394-10	Himalayas	Yardoi	Amphibolite	28.8299	91.9555	Q5	
T0394-21	Himalayas	Yardoi	Amphibolite	28.8299	91.9555	Q5	
T0394-6	Himalayas	Yardoi	Amphibolite	28.8299	91.9555	Q5	
T0394-8	Himalayas	Yardoi	Amphibolite	28.8299	91.9555	Q5	
T0395-01	Himalayas	Yardoi	Orthogneiss	28.8299	91.9555	Q5	42.6
T0395-03	Himalayas	Yardoi	Orthogneiss	28.8299	91.9555	Q5	42.6
T100	Himalayas	Kuday	Granite (Bt, Ms, Grt)	28.9273	88.3927	Q4	27.5
T101	Himalayas	Kuday	Granite (Bt, Ms, Grt)	28.9273	88.3927	Q4	27.5
T104	Himalayas	Kuday	Granite (Bt, Ms, Grt)	28.9273	88.3927	Q4	27.5
T105	Himalayas	Kuday	Granite (Bt, Ms, Grt)	28.9273	88.3927	Q4	27.5
T107	Himalayas	Kuday	Migmatite (Bt,Ms,Grt)	28.9273	88.3927	Q4	27.5
T110	Himalayas	Kouwu	Granite (Bt, Ms)	28.7708	88.1235	Q4	14.4
T111	Himalayas	Kouwu	Granite (Bt, Ms)	28.7708	88.1235	Q4	14.4
T113	Himalayas	Kouwu	Granite (Bt, Ms)	28.7708	88.1235	Q4	14.4
T114	Himalayas	Kouwu	Granite (Bt, Ms)	28.7708	88.1235	Q4	14.4
T117	Himalayas	Mabja	Granite (Bt, Ms, And)	28.7255	87.9254	Q4	9.8
T118	Himalayas	Mabja	Granite (Bt, Ms, Tur)	28.7255	87.9254	Q4	9.8
T120	Himalayas	Mabja	Granite (Bt,Ms)	28.7255	87.9254	Q4	9.8
T121	Himalayas	Mabja	Granite (Bt,Ms)	28.7255	87.9254	Q4	9.8
T125	Himalayas	Kangmar	Schist (Bt,Ms)	28.6517	89.6660	Q5	
T129	Himalayas	Kangmar	Schist (Bt,Ms)	28.6517	89.6660	Q5	
T135	Himalayas	Kangmar	Schist (Bt,Ms,Grt,St)	28.6517	89.6660	Q5	
T136	Himalayas	Kangmar	Gneiss (Bt)	28.6517	89.6660	Q5	
T137	Himalayas	Kangmar	Schist (Bt,Ms,Grt,St)	28.6517	89.6660	Q5	
T71	Himalayas	Kangmar	Gneiss (Bt)	28.6517	89.6660	Q5	
T72	Himalayas	Kangmar	Gneiss (Bt)	28.6517	89.6660	Q5	
T73	Himalayas	Lhagoi Kangri	Granite (Bt)	28.7595	87.6228	Q4	15.1
T74	Himalayas	Lhagoi Kangri	Granite (Bt,Ms)	28.7595	87.6228	Q4	15.1
T75	Himalayas	Lhagoi Kangri	Granite (Bt,Ms)	28.7595	87.6228	Q4	15.1
T76	Himalayas	Dingge	Leucogranite (Bt,Ms)	28.3671	87.7672	Q4	
T77	Himalayas	Dingge	Leucogranite (Ms)	28.3671	87.7672	Q4	
T78	Himalayas	Dingge	Leucogranite (Bt,Ms)	28.3671	87.7672	Q4	

Sample data continued

Sample	87Sr/86Sr(i)	eNd(t)	206Pb/ 204Pb(t)	207Pb/ 204Pb(t)	208Pb/ 204Pb(t)	*UPR	**ADK	Source
T0392-3	0.9694	-11.5				N.D.	N.D.	Zeng et al. (2011)
T0394-1	0.7140	-6.4				N.D.	N.D.	Zeng et al. (2011)
T0394-10	0.7127	1.6				N.D.	N.D.	Zeng et al. (2011)
T0394-21	0.7115	1.9				N.D.	N.D.	Zeng et al. (2011)
T0394-6	0.7109	-12.0				N.D.	N.D.	Zeng et al. (2011)
T0394-8	0.7148	-7.7				N.D.	N.D.	Zeng et al. (2011)
T0395-01	1.1604	-7.5				N.D.	N.D.	Zeng et al. (2011)
T0395-03	1.2030	-10.1				N.D.	N.D.	Zeng et al. (2011)
T100	0.7660	-13.7				No	No	Zhang et al. (2004)
T101	0.7715	-13.4				No	No	Zhang et al. (2004)
T104	0.7852	-13.8				No	No	Zhang et al. (2004)
T105	0.7831	-13.1				No	No	Zhang et al. (2004)
T107	0.7485	-17.7				N.D.	N.D.	Zhang et al. (2004)
T110	0.7385	-13.7				No	No	Zhang et al. (2004)
T111	0.7384	-14.1				No	No	Zhang et al. (2004)
T113	0.7377	-13.5				No	No	Zhang et al. (2004)
T114	0.7373	-13.3				No	No	Zhang et al. (2004)
T117						No	No	Zhang et al. (2004)
T118	0.8533	-19.3				No	No	Zhang et al. (2004)
T120	0.8532	-18.3				No	No	Zhang et al. (2004)
T121	0.8547	-19.0				No	No	Zhang et al. (2004)
T125	0.7903	-16.1				N.D.	N.D.	Zhang et al. (2004)
T129						N.D.	N.D.	Zhang et al. (2004)
T135	0.7787	-14.7				N.D.	N.D.	Zhang et al. (2004)
T136	0.7801	-12.2				No	No	Zhang et al. (2004)
T137	0.7703	-14.5				N.D.	N.D.	Zhang et al. (2004)
T71	0.7728	-11.6				No	No	Zhang et al. (2004)
T72	0.7731	-10.6				No	No	Zhang et al. (2004)
T73	0.7406	-14.1				No	No	Zhang et al. (2004)
T74	0.7407	-12.5				No	No	Zhang et al. (2004)
T75	0.7413	-13.6				No	No	Zhang et al. (2004)
T76	0.7796	-12.0				No	No	Zhang et al. (2004)
T77	0.7711	-14.9				No	No	Zhang et al. (2004)
T78		-15.5				N.D.	N.D.	Zhang et al. (2004)

Table A.2: continued

Sample	Terrane	Location	Lithology	Latitude (dd)	Longitude (dd)	Quadrant	Age (Ma)
T97-26	Himalayas	Yadon	Leucogranite (Bt,Ms)	28.1417	89.4960	Q5	
T97-57	Himalayas	Yadon	Leucogranite (Bt,Ms)	28.1417	89.4960	Q5	
T97-61	Himalayas	Kangmar	Gneiss (Bt)	28.6517	89.6660	Q5	
T519	Lhasa Terrane	Bayi	Granite	29.6846	94.3303	Q6	22.0
T520	Lhasa Terrane	Bayi	Granite	29.6846	94.3303	Q6	22.0
T521	Lhasa Terrane	Bayi	Granite	29.6846	94.3303	Q6	22.0
T522	Lhasa Terrane	Bayi	Granite	29.6846	94.3303	Q6	22.0
T523	Lhasa Terrane	Bayi	Granite	29.6846	94.3303	Q6	22.0
T524	Lhasa Terrane	Bayi	Granite	29.6846	94.3303	Q6	22.0
T529	Lhasa Terrane	Confluence	Granite	29.4681	94.4324	Q6	49.1
T529/2	Lhasa Terrane	Confluence	Granite	29.4681	94.4324	Q6	49.1
T600	Himalayas	Zhibai	Gneiss	29.6208	94.9348	Q6	
T602	Himalayas	Zhibai	Gneiss	29.6208	94.9348	Q6	
T603	Himalayas	Zhibai	Gneiss	29.6208	94.9348	Q6	
T611	Himalayas	Duoxiongla	Migmatite	29.4611	94.9305	Q6	
T612	Himalayas	Duoxiongla	Migmatite	29.4611	94.9305	Q6	
T613	Himalayas	Duoxiongla	Migmatite	29.4611	94.9305	Q6	
T614	Himalayas	Duoxiongla	Migmatite	29.4611	94.9305	Q6	
T616	Himalayas	Duoxiongla	Migmatite	29.4611	94.9305	Q6	
T617	Himalayas	Zhibai	Gneiss	29.6208	94.9348	Q6	
T618	Himalayas	Zhibai	Gneiss	29.6208	94.9348	Q6	
T632	Lhasa Terrane	Lunan	Granite	29.5989	94.5745	Q6	25.4
T633	Lhasa Terrane	Lunan	Granite	29.5989	94.5745	Q6	25.4
T634	Lhasa Terrane	Lunan	Granite	29.5989	94.5745	Q6	25.4
T636	Lhasa Terrane	Lunan	Granite	29.5989	94.5745	Q6	25.4
T637	Lhasa Terrane	Lunan	Granite	29.5989	94.5745	Q6	25.4
T638	Lhasa Terrane	Lunan	Granite	29.5989	94.5745	Q6	25.4
T525	Lhasa Terrane	Nyingchi	Gneiss	29.6526	94.3588	Q6	
T527	Lhasa Terrane	Nyingchi	Gneiss	29.6526	94.3588	Q6	
T528	Lhasa Terrane	Nyingchi	Gneiss	29.6526	94.3588	Q6	
CQ01	Lhasa Terrane	Gongmutang	Basaltic Trachyandesite	30.8150	84.4383	Q4	16.1
CQ02	Lhasa Terrane	Gongmutang	Trachyandesite	30.8150	84.4400	Q4	16.6
CQ03	Lhasa Terrane	Gongmutang	Basaltic Trachyandesite	30.8167	84.4400	Q4	
D9103	Lhasa Terrane	Gongmutang	Trachyandesite	30.8000	84.4333	Q4	

Sample data continued

Sample	87Sr/86Sr(i)	eNd(t)	206Pb/ 204Pb(t)	207Pb/ 204Pb(t)	208Pb/ 204Pb(t)	*UPR	**ADK	Source
T97-26	0.7729	-16.3				No	No	Zhang et al. (2004)
T97-57	0.7608	-14.6				No	No	Zhang et al. (2004)
T97-61	0.7731	-11.1				No	No	Zhang et al. (2004)
T519	0.7065	-4.1				No	No	Zhang et al. (2010)
T520	0.7064	-4.1				No	No	Zhang et al. (2010)
T521	0.7065	-3.9				No	No	Zhang et al. (2010)
T522	0.7065	-4.1				No	No	Zhang et al. (2010)
T523	0.7065	-4.2				No	No	Zhang et al. (2010)
T524	0.7065	-4.1				No	No	Zhang et al. (2010)
T529	0.7069	-4.3				No	No	Zhang et al. (2010)
T529/2						N.D.	N.D.	Zhang et al. (2010)
T600	0.7684	-10.2				N.D.	N.D.	Zhang et al. (2010)
T602	0.7522	-13.0				N.D.	N.D.	Zhang et al. (2010)
T603	0.7616	-15.7				N.D.	N.D.	Zhang et al. (2010)
T611	0.9859	-17.5				N.D.	N.D.	Zhang et al. (2010)
T612	0.8474	-17.4				N.D.	N.D.	Zhang et al. (2010)
T613	0.8048	-16.0				N.D.	N.D.	Zhang et al. (2010)
T614	0.7458	-20.0				N.D.	N.D.	Zhang et al. (2010)
T616	0.8318	-17.0				N.D.	N.D.	Zhang et al. (2010)
T617	0.8074	-18.0				N.D.	N.D.	Zhang et al. (2010)
T618	0.7942	-13.6				N.D.	N.D.	Zhang et al. (2010)
T632						No	Yes	Zhang et al. (2010)
T633						No	No	Zhang et al. (2010)
T634	0.7060	-3.2				No	Yes	Zhang et al. (2010)
T636	0.7070	-4.8				No	Yes	Zhang et al. (2010)
T637	0.7060	-2.6				No	Yes	Zhang et al. (2010)
T638	0.7062	-3.3				No	Yes	Zhang et al. (2010)
T525	0.7276	-13.5				N.D.	N.D.	Zhang et al. (2010)
T527	0.7131	-11.5				N.D.	N.D.	Zhang et al. (2010)
T528	0.7325	-15.1				N.D.	N.D.	Zhang et al. (2010)
CQ01	0.7206	-14.2	18.7	15.8	39.9	Yes	No	Zhao et al (2009)
CQ02	0.7140	-12.6	19.3	15.8	40.2	Yes	No	Zhao et al (2009)
CQ03	0.7233	-14.5	18.7	15.8	39.8	Yes	No	Zhao et al (2009)
D9103	0.7164	-11.8	19.0	15.8	39.9	Yes	No	Zhao et al (2009)

Table A.2: continued

Sample	Terrane	Location	Lithology	Latitude (dd)	Longitude (dd)	Quadrant	Age (Ma)
DR01-1	Lhasa Terrane	Dangreyong	Trachyte	30.9433	86.3917	Q4	13.4
DR01-2	Lhasa Terrane	Dangreyong	Trachyte	30.9433	86.3917	Q4	13.7
DR03	Lhasa Terrane	Dangreyong	Trachyte	30.9433	86.3917	Q4	14.2
DR04	Lhasa Terrane	Dangreyong	Trachyte	30.9433	86.3917	Q4	13.5
GGP-7	Lhasa Terrane	Gongmutang	Tephrite	30.8000	84.4333	Q4	
SL0618	Lhasa Terrane	Sailipu	Trachyandesite	31.2967	82.9750	Q3	
SL0619	Lhasa Terrane	Sailipu	Trachyandesite	31.2967	82.9750	Q3	
SL0620	Lhasa Terrane	Sailipu	Trachyandesite	31.2967	82.9750	Q3	
SL0621	Lhasa Terrane	Sailipu	Trachyandesite	31.2967	82.9750	Q3	
SL0622	Lhasa Terrane	Sailipu	Trachyandesite	31.2967	82.9750	Q3	
SL0623	Lhasa Terrane	Sailipu	Trachyandesite	31.2967	82.9750	Q3	
SL0624	Lhasa Terrane	Sailipu	Trachyandesite	31.2967	82.9750	Q3	
SL0625	Lhasa Terrane	Sailipu	Trachyandesite	31.2967	82.9750	Q3	
SL0628	Lhasa Terrane	Sailipu	Trachyandesite	31.2967	82.9750	Q3	17.7
SL0630	Lhasa Terrane	Sailipu	Trachyandesite	31.2967	82.9750	Q3	
SL0631	Lhasa Terrane	Sailipu	Trachyandesite	31.2967	82.9750	Q3	
XR01-1	Lhasa Terrane	Xuru lake	Trachyte	30.0717	86.5133	Q4	
XR01-3	Lhasa Terrane	Xuru lake	Basaltic Trachyandesite	30.0717	86.5133	Q4	11.5
XR02-1	Lhasa Terrane	Xuru lake	Tephriphonolite	30.0400	86.5267	Q4	
Z8030-18	Lhasa Terrane	Dangreyong	Trachyandesite	31.8500	86.6567	Q4	13.2
Z8030-5	Lhasa Terrane	Dangreyong	Trachyte	31.8500	86.6567	Q4	13.5
ZB11	Lhasa Terrane	Zabuye	Trachyandesite	31.4017	84.3000	Q3	
ZB14	Lhasa Terrane	Zabuye	Trachyandesite	31.4017	84.3000	Q3	
ZB16	Lhasa Terrane	Zabuye	Trachyandesite	31.4017	84.3000	Q3	
ZB18	Lhasa Terrane	Zabuye	Trachyandesite	31.4033	84.3017	Q3	
ZB20	Lhasa Terrane	Zabuye	Trachyandesite	31.4033	84.3017	Q3	
ZB21	Lhasa Terrane	Zabuye	Trachyandesite	31.4617	84.3883	Q3	27.1
ZB22	Lhasa Terrane	Zabuye	Trachyandesite	31.4617	84.3883	Q3	
ZB3	Lhasa Terrane	Zabuye	Trachyandesite	31.4017	84.3000	Q3	
ZB6	Lhasa Terrane	Zabuye	Trachyandesite	31.4017	84.3000	Q3	
ZB8	Lhasa Terrane	Zabuye	Trachyandesite	31.4013	84.3000	Q3	
ZB9	Lhasa Terrane	Zabuye	Trachyandesite	31.4017	84.3000	Q3	
GZ-11	Lhasa Terrane	Wuyu Basin	Granite (porphyritic)	29.6476	89.6391	Q5	15.0
GZ-12	Lhasa Terrane	Wuyu Basin	Trachyte	29.6476	89.6391	Q5	15.0

Sample data continued

Sample	87Sr/86Sr(i)	eNd(t)	206Pb/ 204Pb(t)	207Pb/ 204Pb(t)	208Pb/ 204Pb(t)	*UPR	**ADK	Source
DR01-1	0.7159	-12.4	18.5	15.8	39.5	No	No	Zhao et al (2009)
DR01-2	0.7158	-12.3	18.5	15.7	39.4	No	No	Zhao et al (2009)
DR03	0.7163	-12.6	18.5	15.8	39.5	No	No	Zhao et al (2009)
DR04						No	No	Zhao et al (2009)
GGP-7	0.7151	-10.6	18.4	15.7	39.5	Yes	No	Zhao et al (2009)
SL0618	0.7148	-14.7	18.6	15.7	39.6	Yes	No	Zhao et al (2009)
SL0619						Yes	No	Zhao et al (2009)
SL0620	0.7141	-14.4	18.6	15.7	39.6	Yes	No	Zhao et al (2009)
SL0621	0.7159	-14.7	18.6	15.7	39.6	Yes	No	Zhao et al (2009)
SL0622	0.7147	-14.5	18.6	15.7	39.6	Yes	No	Zhao et al (2009)
SL0623	0.7152	-14.9	18.7	15.7	39.6	Yes	No	Zhao et al (2009)
SL0624	0.7138	-14.8	18.6	15.7	39.6	Yes	No	Zhao et al (2009)
SL0625	0.7126	-14.0	18.7	15.8	39.7	Yes	No	Zhao et al (2009)
SL0628						No	No	Zhao et al (2009)
SL0630						Yes	No	Zhao et al (2009)
SL0631	0.7131	-14.2	18.6	15.7	39.6	Yes	No	Zhao et al (2009)
XR01-1	0.7164	-12.7	18.9	15.8	39.6	Yes	No	Zhao et al (2009)
XR01-3	0.7115	-14.8	18.7	15.8	39.8	Yes	No	Zhao et al (2009)
XR02-1	0.7323	-14.0	18.8	15.8	39.8	Yes	No	Zhao et al (2009)
Z8030-18	0.7165	-13.5				Yes	No	Zhao et al (2009)
Z8030-5	0.7150	-13.5	18.5	15.8	39.6	Yes	No	Zhao et al (2009)
ZB11	0.7107	-7.5				Yes	No	Zhao et al (2009)
ZB14	0.7100	-8.3	18.8	15.7	39.5	No	No	Zhao et al (2009)
ZB16	0.7102	-7.5				No	No	Zhao et al (2009)
ZB18	0.7100	-7.8	18.9	15.8	39.7	Yes	No	Zhao et al (2009)
ZB20	0.7100	-7.7	18.8	15.7	39.5	Yes	No	Zhao et al (2009)
ZB21	0.7080	-9.6	19.0	15.8	39.9	No	No	Zhao et al (2009)
ZB22	0.7059	-9.3	18.9	15.8	39.9	No	No	Zhao et al (2009)
ZB3	0.7094	-8.2	18.8	15.7	39.5	No	No	Zhao et al (2009)
ZB6	0.7097	-8.2				No	No	Zhao et al (2009)
ZB8	0.7096	-7.6				Yes	No	Zhao et al (2009)
ZB9	0.7094	-7.7				Yes	No	Zhao et al (2009)
GZ-11	0.7104		18.6	15.6	39.2	No	No	Zhao et al. (2001)
GZ-12	0.7067		18.5	15.6	38.8	No	No	Zhao et al. (2001)

Table A.2: continued

Sample	Terrane	Location	Lithology	Latitude (dd)	Longitude (dd)	Quadrant	Age (Ma)
GZ-14	Lhasa Terrane	Wuyu Basin	Trachyte	29.6476	89.6391	Q5	15.0
GZ-3	Lhasa Terrane	Wuyu Basin	Granite (porphyritic)	29.6476	89.6391	Q5	15.0
GZ-5	Lhasa Terrane	Wuyu Basin	Trachyte	29.6476	89.6391	Q5	15.0
GZ-6	Lhasa Terrane	Wuyu Basin	Granite (porphyritic)	29.6966	89.5761	Q5	11.2
GZ-7	Lhasa Terrane	Wuyu Basin	Basaltic Trachyte	29.6476	89.6391	Q5	15.0
GZ-8	Lhasa Terrane	Wuyu Basin	Granite (porphyritic)	29.6476	89.6391	Q5	15.0
GZ-9	Lhasa Terrane	Wuyu Basin	Trachyte	29.6476	89.6391	Q5	15.0
ZLY01	Lhasa Terrane	Zhuomo Copper Deposit	Granite (Bt, porphyritic)	29.6563	87.4662	Q4	15.6
ZLY02	Lhasa Terrane	Zhuomo Copper Deposit	Granite (Bt, porphyritic)	29.6544	87.4639	Q4	13.9
ZLY03	Lhasa Terrane	Zhuomo Copper Deposit	Granite (Bt, porphyritic)	29.6574	87.4628	Q4	14.0
ZLY04	Lhasa Terrane	Zhuomo Copper Deposit	Granite (Bt, porphyritic)	29.6586	87.4650	Q4	13.8
GZ-10	Lhasa Terrane	Wuyu	Dacite (porphyritic)	29.6821	89.7027	Q5	15.5
GZ-15	Lhasa Terrane	Wuyu	Dacite (porphyritic)	29.6901	89.5769	Q5	13.0
GZ-16	Lhasa Terrane	Wuyu	Trachyte (porphyritic)	29.6858	89.5761	Q5	13.6
GZ-18	Lhasa Terrane	Wuyu	Trachyandesite (porphyritic)	29.6818	89.5766	Q5	12.6
Y-1-1	Lhasa Terrane	Yangying	Rhyolite	29.7025	90.3423	Q5	11.4
Y-2	Lhasa Terrane	Yangying	Trachyte (porphyritic)	29.7194	90.3716	Q5	10.7
Y-3	Lhasa Terrane	Yangying	Trachyte (porphyritic)	29.7570	90.3749	Q5	11.1
Y-4	Lhasa Terrane	Yangying	Rhyolite	29.7414	90.3667	Q5	10.3
CMN04-2	Lhasa Terrane	N Bangdo	Rhyolite	31.3508	85.9082	Q4	125.0
DX13-1	Lhasa Terrane	N Daxiong	Dacite	31.5013	85.1787	Q4	121.0
DX19-1	Lhasa Terrane	E Dawa Tso	Monzogranite	31.2818	85.1262	Q4	107.0
DX2-1	Lhasa Terrane	NW Daxiong	Dacite	31.4585	84.9347	Q4	130.0
DX21-1	Lhasa Terrane	SW Coqen	Rhyolite	30.0000	85.1170	Q4	111.0
DXL1-3	Lhasa Terrane	N Daxiong	Rhyolite	31.6552	85.1950	Q4	112.0
GB-8	Lhasa Terrane	W Nixiong	Granodiorite	30.7593	85.5375	Q4	116.0
GJ0611	Lhasa Terrane	E Xiongba	Rhyolite	32.0403	82.2007	Q3	143.0
GJ0612	Lhasa Terrane	E Xiongba	Rhyolite	32.0403	82.2007	Q3	129.0
GJ0613	Lhasa Terrane	E Xiongba	Rhyolite	32.0403	82.2007	Q3	139.0
NX5-2	Lhasa Terrane	W Nixiong	Granodiorite	30.7610	85.5308	Q4	109.0
NX5-3	Lhasa Terrane	W Nixiong	Diorite	30.7610	85.5308	Q4	108.0
SQ0666	Lhasa Terrane	S Gar	Andesite	32.3433	80.0263	Q2	102.0
SZ08-1	Lhasa Terrane	SE Shenza	Diorite	30.7728	88.8438	Q4	111.0
SZ08-3	Lhasa Terrane	SE Shenza	Granodiorite	30.7728	88.8438	Q4	113.0

Sample data continued

Sample	87Sr/86Sr(i)	eNd(t)	206Pb/ 204Pb(t)	207Pb/ 204Pb(t)	208Pb/ 204Pb(t)	*UPR	**ADK	Source
GZ-14	0.7057		18.5	15.5	38.7	No	No	Zhao et al. (2001)
GZ-3	0.7095		18.5	15.6	39.0	No	No	Zhao et al. (2001)
GZ-5	0.7072		18.5	15.6	38.8	No	No	Zhao et al. (2001)
GZ-6	0.7100		18.5	15.6	39.0	No	No	Zhao et al. (2001)
GZ-7	0.7070		18.5	15.6	39.1	No	No	Zhao et al. (2001)
GZ-8	0.7080		18.5	15.6	39.0	No	No	Zhao et al. (2001)
GZ-9	0.7061		18.6	15.6	38.8	No	No	Zhao et al. (2001)
ZLY01						N.D.	N.D.	Zheng et al. (2007)
ZLY02						N.D.	N.D.	Zheng et al. (2007)
ZLY03						N.D.	N.D.	Zheng et al. (2007)
ZLY04						N.D.	N.D.	Zheng et al. (2007)
GZ-10	0.7066	3.8				No	Yes	Zhou et al. (2010)
GZ-15	0.7066	3.7				No	Yes	Zhou et al. (2010)
GZ-16						No	No	Zhou et al. (2010)
GZ-18						No	No	Zhou et al. (2010)
Y-1-1	0.7122	8.0				No	No	Zhou et al. (2010)
Y-2	0.7122	8.2				No	No	Zhou et al. (2010)
Y-3	0.7108	6.3				No	Yes	Zhou et al. (2010)
Y-4	0.7112	7.7				No	No	Zhou et al. (2010)
CMN04-2						N.D.	N.D.	Zhu et al. (2009)
DX13-1	0.7146	-10.7				No	No	Zhu et al. (2009)
DX19-1	0.7076	-4.6				No	No	Zhu et al. (2009)
DX2-1	0.7141	-10.5				No	No	Zhu et al. (2009)
DX21-1	0.7082	-8.3				No	No	Zhu et al. (2009)
DXL1-3	0.7073	-5.9				No	No	Zhu et al. (2009)
GB-8	0.7156	-7.8				No	No	Zhu et al. (2009)
GJ0611						N.D.	N.D.	Zhu et al. (2009)
GJ0612						N.D.	N.D.	Zhu et al. (2009)
GJ0613						N.D.	N.D.	Zhu et al. (2009)
NX5-2	0.7095	-8.1				No	No	Zhu et al. (2009)
NX5-3	0.7088	-7.8				No	No	Zhu et al. (2009)
SQ0666						N.D.	N.D.	Zhu et al. (2009)
SZ08-1						N.D.	N.D.	Zhu et al. (2009)
SZ08-3						N.D.	N.D.	Zhu et al. (2009)

Table A.2: continued

Sample	Terrane	Location	Lithology	Latitude (dd)	Longitude (dd)	Quadrant	Age (Ma)
SZ39	Lhasa Terrane	Eyang	Granite (porphyritic)	30.8285	87.9307	Q4	125.0
SZ43	Lhasa Terrane	Eyang	Rhyolite	30.8323	87.9303	Q4	129.0
SZ48	Lhasa Terrane	Eyang	Andesite	30.8410	87.9303	Q4	111.0
SZ52	Lhasa Terrane	Eyang	Dacite	30.8410	87.9303	Q4	107.0
CY1-01	Lhasa Terrane	Zayu Pluton	Monzogranite	28.6203	97.1791	Q6	129.1
CY1-02	Lhasa Terrane	Zayu Pluton	Monzogranite	28.6135	97.1955	Q6	128.8
CY1-02R	Lhasa Terrane	Zayu Pluton	Monzogranite	28.6217	97.2092	Q6	128.8
CY1-1	Lhasa Terrane	Zayu Pluton	Monzogranite	28.6449	97.1518	Q6	128.8
CY2-1	Lhasa Terrane	Zayu Pluton	Monzogranite	28.6408	97.1655	Q6	128.8
CY3-1	Lhasa Terrane	Zayu Pluton	Monzogranite	28.6367	97.1791	Q6	128.8
CY4-1	Lhasa Terrane	Zayu Pluton	Monzogranite	28.6299	97.1928	Q6	128.8
CY6-1	Lhasa Terrane	Zayu Pluton	Monzogranite	28.6258	97.1655	Q6	128.5
GBJD-1	Lhasa Terrane	Jiangda	Granite	29.9959	93.0385	Q5	
GBJD-2	Lhasa Terrane	Jiangda	Granite	29.9959	93.0417	Q5	
GBJD-3	Lhasa Terrane	Jiangda	Granite	29.9931	93.0406	Q5	
PK01-1	Lhasa Terrane	Pikang	Granite	29.9771	93.1032	Q5	263.0
PK01-2	Lhasa Terrane	Pikang	Granite	29.9767	93.1056	Q5	263.0
PK01-3	Lhasa Terrane	Pikang	Granite	29.9750	93.1081	Q5	263.0
PK01-4	Lhasa Terrane	Pikang	Granite	29.9725	93.1073	Q5	263.0
PK01-5	Lhasa Terrane	Pikang	Granite	29.9742	93.1045	Q5	263.0
PK01-6	Lhasa Terrane	Pikang	Granite	29.9742	93.1045	Q5	263.0
MM02-2	Lhasa Terrane	Mamen	Andesite (adakitic)	29.2535	91.9755	Q5	136.5
MM02-3	Lhasa Terrane	Mamen	Andesite (adakitic)	29.2535	91.9755	Q5	136.5
MM02-4	Lhasa Terrane	Mamen	Andesite (adakitic)	29.2535	91.9755	Q5	136.5
MM02-5	Lhasa Terrane	Mamen	Andesite (adakitic)	29.2535	91.9755	Q5	136.5
MM02-6	Lhasa Terrane	Mamen	Andesite (adakitic)	29.2535	91.9755	Q5	136.5
T203A	Lhasa Terrane	Mamen	Andesite (adakitic)	29.2535	91.9755	Q5	136.5
YH01-2	Lhasa Terrane	Yanhu	Rhyolite	32.2656	82.5451	Q3	109.0
YH22-4	Lhasa Terrane	Yanhu	Rhyolite	32.3432	82.4437	Q3	110.6
08CQ02	Lhasa Terrane	S Lhasa subterrane	Syenogranite	29.6251	85.7434	Q4	43.9
08CQ03	Lhasa Terrane	S Lhasa subterrane	Monzogranite	29.7814	85.7581	Q4	51.9
08CQ09	Lhasa Terrane	S Lhasa subterrane	Granodiorite (porphyritic)	29.8953	85.7409	Q4	50.0
08CQ13	Lhasa Terrane	S Lhasa subterrane	Diorite	30.1369	85.4088	Q4	51.5
08CQ35	Lhasa Terrane	Cent. Lhasa subterrane	Monzogranite	30.9391	84.5714	Q4	122.6

Sample data continued

Sample	87Sr/86Sr(i)	eNd(t)	206Pb/ 204Pb(t)	207Pb/ 204Pb(t)	208Pb/ 204Pb(t)	*UPR	**ADK	Source
SZ39	0.7180	-13.7				No	No	Zhu et al. (2009)
SZ43	0.7209	-13.1				No	No	Zhu et al. (2009)
SZ48	0.7148	-9.9				No	No	Zhu et al. (2009)
SZ52	0.7138	-10.4				No	No	Zhu et al. (2009)
CY1-01	0.7179	-10.9				No	No	Zhu et al. (2009)
CY1-02						No	No	Zhu et al. (2009)
CY1-02R						No	No	Zhu et al. (2009)
CY1-1	0.7173	-9.2				No	No	Zhu et al. (2009)
CY2-1						No	No	Zhu et al. (2009)
CY3-1	0.7120	-7.6				No	No	Zhu et al. (2009)
CY4-1	0.7162	-9.3				No	No	Zhu et al. (2009)
CY6-1	0.7167	-9.5				No	No	Zhu et al. (2009)
GBJD-1						No	No	Zhu et al. (2009)
GBJD-2						No	No	Zhu et al. (2009)
GBJD-3						No	No	Zhu et al. (2009)
PK01-1	0.7096	-6.0				No	No	Zhu et al. (2009)
PK01-2	0.7091	-6.2				No	No	Zhu et al. (2009)
PK01-3	0.7093	-6.1				No	No	Zhu et al. (2009)
PK01-4	0.7088	-6.1				No	No	Zhu et al. (2009)
PK01-5	0.7082	-6.1				No	No	Zhu et al. (2009)
PK01-6	0.7088	-6.4				No	No	Zhu et al. (2009)
MM02-2	0.7051	3.7	18.6	15.6	38.7	No	No	Zhu et al. (2009a)
MM02-3	0.7041	5.8	18.4	15.6	38.4	No	No	Zhu et al. (2009a)
MM02-4	0.7047	4.0	18.5	15.6	38.7	No	No	Zhu et al. (2009a)
MM02-5						No	No	Zhu et al. (2009a)
MM02-6	0.7046	3.9	18.5	15.6	38.7	No	No	Zhu et al. (2009a)
T203A						No	No	Zhu et al. (2009a)
YH01-2	0.7072	0.9				No	No	Zhu et al. (2010)
YH22-4	0.7050	0.1				No	No	Zhu et al. (2010)
08CQ02						N.D.	N.D.	Zhu et al. (2011)
08CQ03						N.D.	N.D.	Zhu et al. (2011)
08CQ09						N.D.	N.D.	Zhu et al. (2011)
08CQ13						N.D.	N.D.	Zhu et al. (2011)
08CQ35						N.D.	N.D.	Zhu et al. (2011)

Table A.2: continued

Sample	Terrane	Location	Lithology	Latitude (dd)	Longitude (dd)	Quadrant	Age (Ma)
08DX17	Lhasa Terrane	Nyainrong	Monzogranite	30.7560	91.5828	Q5	193.6
08DX21	Lhasa Terrane	N Lhasa subterrane	Syenogranite	31.0477	91.6908	Q5	110.7
08YR07	Lhasa Terrane	Cent. Lhasa subterrane	Rhyolite	31.8030	82.1401	Q3	146.1
08YR09	Lhasa Terrane	Cent. Lhasa subterrane	Dacite	31.7900	82.1404	Q3	159.8
08YR11	Lhasa Terrane	Cent. Lhasa subterrane	Tonalite	31.7302	82.1530	Q3	134.3
08YR14	Lhasa Terrane	Cent. Lhasa subterrane	Breccia (rhyolitic)	31.6922	82.1666	Q3	133.8
08YR16	Lhasa Terrane	Cent. Lhasa subterrane	Rhyolite	31.6803	82.1758	Q3	142.9
08YR27	Lhasa Terrane	S Lhasa subterrane	Rhyolite	31.0603	82.1938	Q3	80.6
08YR28	Lhasa Terrane	S Lhasa subterrane	Andesite	31.0087	82.1594	Q3	50.8
08YR29	Lhasa Terrane	S Lhasa subterrane	Dacite	30.9688	82.1830	Q3	61.2
08YR30	Lhasa Terrane	S Lhasa subterrane	Monzogranite	30.8988	82.1524	Q3	54.2
DG01-1	Lhasa Terrane	N Lhasa subterrane	Rhyolite	31.3545	88.9300	Q4	115.7
DG05-1	Lhasa Terrane	N Lhasa subterrane	Dacite	31.3283	88.9148	Q4	114.3
GRC02-1	Lhasa Terrane	S Geren Tso	Dacite	31.0663	88.2068	Q4	114.0
GRC03-2	Lhasa Terrane	S Geren Tso	Dacite	31.2262	88.1268	Q4	113.8
JD08-1	Lhasa Terrane	Cent. Lhasa subterrane	Monzogranite	29.9990	93.0775	Q5	182.9
JD12-1	Lhasa Terrane	Cent. Lhasa subterrane	Granodiorite	30.0208	92.9615	Q5	193.2
MB01-1	Lhasa Terrane	Cent. Lhasa subterrane	Tonalite	30.1536	92.3235	Q5	154.0
MB05-7	Lhasa Terrane	Cent. Lhasa subterrane	Monzogranite	30.1011	92.3260	Q5	129.9
MB09-1	Lhasa Terrane	Cent. Lhasa subterrane	Granodiorite	30.1007	92.2295	Q5	210.2
MB22-1	Lhasa Terrane	Cent. Lhasa subterrane	Syenogranite	29.9847	91.9060	Q5	194.9
MD01-1	Lhasa Terrane	Cent. Lhasa subterrane	Syenogranite	30.6459	85.1304	Q4	152.9
ML01-1	Lhasa Terrane	S Lhasa subterrane	Tonalite	29.0061	93.3151	Q5	84.2
ML06-1	Lhasa Terrane	S Lhasa subterrane	Granodiorite	29.0572	93.3802	Q5	79.3
ML11-1	Lhasa Terrane	S Lhasa subterrane	Monzogranite	29.1132	93.4520	Q5	82.2
ML31-1	Lhasa Terrane	S Lhasa subterrane	Monzogranite	29.6061	93.3213	Q5	191.9
ML38-5	Lhasa Terrane	S Lhasa subterrane	Syenogranite	29.6245	93.3070	Q5	203.2
ML45-1	Lhasa Terrane	S Lhasa subterrane	Granodiorite	29.6823	93.3122	Q5	201.3
NM01-1	Lhasa Terrane	N Lhasa subterrane	Dacite	31.8438	87.0875	Q4	111.9
NML01-1	Lhasa Terrane	S Lhasa subterrane	Diorite	29.4408	89.0945	Q4	87.7
NML03-1	Lhasa Terrane	S Lhasa subterrane	Diorite	29.6225	89.0607	Q4	62.4
NML05-1	Lhasa Terrane	Cent. Lhasa subterrane	Granite (Bt, Ms)	30.0847	89.1167	Q4	206.0
NML06-1	Lhasa Terrane	Cent. Lhasa subterrane	Granite (Bt, Ms)	30.1090	89.1577	Q4	206.5
NQ09-1	Lhasa Terrane	N Lhasa subterrane	Monzogranite	31.7662	92.6234	Q5	110.7

Sample data continued

Sample	87Sr/86Sr(i)	eNd(t)	206Pb/204Pb(t)	207Pb/204Pb(t)	208Pb/204Pb(t)	*UPR	**ADK	Source
08DX17						N.D.	N.D.	Zhu et al. (2011)
08DX21						N.D.	N.D.	Zhu et al. (2011)
08YR07						N.D.	N.D.	Zhu et al. (2011)
08YR09						N.D.	N.D.	Zhu et al. (2011)
08YR11						N.D.	N.D.	Zhu et al. (2011)
08YR14						N.D.	N.D.	Zhu et al. (2011)
08YR16						N.D.	N.D.	Zhu et al. (2011)
08YR27						N.D.	N.D.	Zhu et al. (2011)
08YR28						N.D.	N.D.	Zhu et al. (2011)
08YR29						N.D.	N.D.	Zhu et al. (2011)
08YR30						N.D.	N.D.	Zhu et al. (2011)
DG01-1						No	No	Zhu et al. (2011)
DG05-1						No	No	Zhu et al. (2011)
GRC02-1						No	No	Zhu et al. (2011)
GRC03-2						No	No	Zhu et al. (2011)
JD08-1						N.D.	N.D.	Zhu et al. (2011)
JD12-1						N.D.	N.D.	Zhu et al. (2011)
MB01-1						N.D.	N.D.	Zhu et al. (2011)
MB05-7						N.D.	N.D.	Zhu et al. (2011)
MB09-1						N.D.	N.D.	Zhu et al. (2011)
MB22-1						N.D.	N.D.	Zhu et al. (2011)
MD01-1						N.D.	N.D.	Zhu et al. (2011)
ML01-1						N.D.	N.D.	Zhu et al. (2011)
ML06-1						No	Yes	Zhu et al. (2011)
ML11-1						N.D.	N.D.	Zhu et al. (2011)
ML31-1						N.D.	N.D.	Zhu et al. (2011)
ML38-5						N.D.	N.D.	Zhu et al. (2011)
ML45-1						N.D.	N.D.	Zhu et al. (2011)
NM01-1						N.D.	N.D.	Zhu et al. (2011)
NML01-1						N.D.	N.D.	Zhu et al. (2011)
NML03-1						N.D.	N.D.	Zhu et al. (2011)
NML05-1						N.D.	N.D.	Zhu et al. (2011)
NML06-1						N.D.	N.D.	Zhu et al. (2011)
NQ09-1						N.D.	N.D.	Zhu et al. (2011)

Table A.2: continued

Sample	Terrane	Location	Lithology	Latitude (dd)	Longitude (dd)	Quadrant	Age (Ma)
NQ12-10	Lhasa Terrane	N Lhasa subterrane	Andesite	31.4801	92.1072	Q5	110.8
NQ16-1	Lhasa Terrane	Nyainrong	Monzogranite	31.7893	92.0683	Q5	117.5
NR04-1	Lhasa Terrane	Nyainrong	Granodiorite	32.1085	92.2916	Q5	185.7
NR13-3	Lhasa Terrane	Nyainrong	Granodiorite	32.0687	92.2136	Q5	174.9
NR15-1	Lhasa Terrane	Nyainrong	Granodiorite	32.0114	92.1904	Q5	184.5
NR18-1	Lhasa Terrane	Nyainrong	Granodiorite (porphyritic)	31.9459	92.1555	Q5	110.4
RGZ01-1	Lhasa Terrane	S Lhasa subterrane	Diorite	29.2653	90.4117	Q5	87.4
SB01-2	Lhasa Terrane	N Lhasa subterrane	Monzogranite	30.9933	92.5557	Q5	118.4
ST134A	Lhasa Terrane	S Lhasa subterrane	Granodiorite	29.5200	89.6200	Q5	188.1
SZ01-1	Lhasa Terrane	SE Shenza	Dacite	30.7563	88.9223	Q4	116.7
SZ07-1	Lhasa Terrane	SE Shenza	Dacite	30.7660	88.9013	Q4	110.9
SZ10-1	Lhasa Terrane	S Shenza	Dacite	30.8900	88.6623	Q4	112.1
YH04-2	Lhasa Terrane	N Lhasa subterrane	Andesite	32.2847	82.5476	Q3	116.7
YH06-3	Lhasa Terrane	N Lhasa subterrane	Andesite	32.2995	82.5528	Q3	131.2
YH15-1	Lhasa Terrane	N Lhasa subterrane	Monzogranite	32.5010	82.4454	Q3	110.1
ZGP06-1	Lhasa Terrane	N Lhasa subterrane	Dacite	31.5382	87.4995	Q4	91.0

*UPR - ultrapotassic rock; **ADK - Adakite. 'N.D.' - no wholE rock geochemistry data available

Sample data continued

Sample	87Sr/86Sr(i)	eNd(t)	206Pb/ 204Pb(t)	207Pb/ 204Pb(t)	208Pb/ 204Pb(t)	*UPR	**ADK	Source
NQ12-10						N.D.	N.D.	Zhu et al. (2011)
NQ16-1						N.D.	N.D.	Zhu et al. (2011)
NR04-1						N.D.	N.D.	Zhu et al. (2011)
NR13-3						N.D.	N.D.	Zhu et al. (2011)
NR15-1						N.D.	N.D.	Zhu et al. (2011)
NR18-1						N.D.	N.D.	Zhu et al. (2011)
RGZ01-1						N.D.	N.D.	Zhu et al. (2011)
SB01-2						N.D.	N.D.	Zhu et al. (2011)
ST134A						N.D.	N.D.	Zhu et al. (2011)
SZ01-1	0.7132	-9.4				No	No	Zhu et al. (2011)
SZ07-1	0.7141	-9.3				No	No	Zhu et al. (2011)
SZ10-1	0.7147	-9.1				No	No	Zhu et al. (2011)
YH04-2						N.D.	N.D.	Zhu et al. (2011)
YH06-3						N.D.	N.D.	Zhu et al. (2011)
YH15-1						N.D.	N.D.	Zhu et al. (2011)
ZGP06-1						N.D.	N.D.	Zhu et al. (2011)

Table A.3: Whole rock geochemistry (XRF - Major elements) for Lhasa terrane and Himalayan literature samples. All measurements reported in wt %

Sample	SiO2	TiO2	Al2O3	Fe2O3	FeO	MnO	MgO
NDG-01	48.90	0.44	15.00	7.30		0.11	12.20
NDG-02	49.10	0.49	14.90	5.80		0.10	11.90
NDG-03	51.20	0.58	15.10	6.70		0.13	9.90
NDG-04	51.80	0.70	14.00	11.70		0.15	8.10
NDG-05	48.60	0.13	14.30	5.70		0.06	14.80
NDG-06	47.10	0.16	15.40	10.30		0.16	14.80
NDG-07	49.50	0.13	15.40	3.30		0.03	15.00
NDG-08	46.80	0.16	15.40	11.00		0.18	14.50
NDG-09	49.80	0.13	14.40	3.20		0.04	11.40
NDV-01	66.87	0.60	14.21	8.07		0.15	2.21
NDV-04	50.22	0.82	14.19	9.43		0.19	11.16
NDV-05	50.92	0.83	14.31	12.63		0.22	7.93
NDV-1S	52.65	1.87	14.10	13.79		0.13	5.54
NDV-2S	57.89	0.79	14.43	10.60		0.18	4.30
NDV-3S	52.55	0.78	13.73	10.47		0.18	8.32
NDV-4S	53.42	1.19	14.36	11.13		0.17	5.12
NN-13	46.40	0.13	14.40	5.90		0.09	14.30
NN-14	46.50	0.23	14.50	6.60		0.10	13.00
NN-15	46.50	0.10	15.50	5.80		0.10	14.10
NN-19	45.10	0.19	13.70	6.30		0.13	15.40
NV-01	67.36	0.45	11.98	6.89		0.12	4.40
NV-02	68.69	0.42	11.42	6.93		0.09	3.92
NV-03	65.56	0.44	12.06	7.89		0.10	4.39
NV-04	66.96	0.45	11.99	7.07		0.11	4.82
NV-05	66.23	0.45	11.98	7.42		0.11	5.36
NV-06	65.54	0.49	12.36	7.38		0.12	4.59
NV-07	65.34	0.46	12.31	7.54		0.12	4.83
NV-08	66.27	0.49	12.38	6.85		0.12	7.05
NV-09	67.03	0.45	12.24	6.74		0.12	3.89
NV-10	66.37	0.46	12.23	7.05		0.12	4.22
NV-11	65.27	0.48	12.52	7.34		0.13	4.43
93BG1	74.15	0.03	14.90	0.48		0.01	0.08
93G18	74.43	0.06	14.69	0.82		0.03	0.11
93G2	73.42	0.13	15.23	1.51		0.03	0.29
93G8	73.12	0.13	15.13	1.64		0.04	0.24
93ZP3	74.62	0.04	14.64	0.76		0.06	0.09
MA88.1	73.38	0.15	15.31	1.20		0.02	0.25
MA97.3	73.85	0.08	15.05	0.90		0.02	0.18
MN14	74.88	0.14	14.01	1.28		0.03	0.19
PAN2	66.85	0.75	16.80	6.45		0.14	1.86
158a	37.90	4.80	19.00		13.50	0.10	14.80
158f	57.80	0.30	18.00		5.30	0.00	4.40
158g	74.10	0.00	14.30		1.40	0.00	0.60
158m	45.60	2.00	16.90		9.40	0.10	8.70
158o	66.50	0.10	17.30		3.40	0.10	1.80
158p	43.60	1.70	15.40		13.90	0.20	10.80
DG01-1	75.08	0.23	13.39	2.70		0.03	0.12
DG01-2	75.99	0.25	13.30	2.29		0.01	0.15

Sample data continued

Sample	CaO	Na2O	K2O	P2O5	LOI	Total	Source
NDG-01	12.50	2.12	0.77	0.05	2.23	101.57	Ahmad et al. (2008)
NDG-02	13.80	1.80	0.88	0.05	3.00	101.84	Ahmad et al. (2008)
NDG-03	12.10	2.58	1.22	0.08	2.85	102.37	Ahmad et al. (2008)
NDG-04	9.50	3.48	0.14	0.07	3.20	102.76	Ahmad et al. (2008)
NDG-05	14.70	1.02	0.02	0.02	2.35	101.60	Ahmad et al. (2008)
NDG-06	12.60	0.81	0.04	0.03	1.20	102.60	Ahmad et al. (2008)
NDG-07	14.00	1.55	0.06	0.03	2.83	101.80	Ahmad et al. (2008)
NDG-08	12.00	0.90	0.05	0.02	1.30	102.37	Ahmad et al. (2008)
NDG-09	16.70	1.45	0.21	0.04	2.65	99.96	Ahmad et al. (2008)
NDV-01	1.71	4.79	0.10	0.10	2.96	101.76	Ahmad et al. (2008)
NDV-04	7.88	3.63	0.05	0.08	4.06	100.07	Ahmad et al. (2008)
NDV-05	6.58	4.44	0.04	0.08	3.12	101.11	Ahmad et al. (2008)
NDV-1S	6.28	4.81	0.16	0.17	2.09	101.58	Ahmad et al. (2008)
NDV-2S	4.46	4.34	0.45	0.09	1.83	99.37	Ahmad et al. (2008)
NDV-3S	8.48	3.39	0.07	0.08	3.24	101.30	Ahmad et al. (2008)
NDV-4S	7.28	3.83	0.04	0.13	3.36	100.03	Ahmad et al. (2008)
NN-13	16.10	0.85	0.02	0.03	1.73	99.97	Ahmad et al. (2008)
NN-14	14.50	1.31	0.04	0.04	2.78	99.57	Ahmad et al. (2008)
NN-15	14.30	1.19	0.10	0.04	2.90	100.48	Ahmad et al. (2008)
NN-19	14.20	1.29	0.02	0.03	3.80	100.13	Ahmad et al. (2008)
NV-01	2.57	4.39	0.20	0.07	2.13	100.55	Ahmad et al. (2008)
NV-02	2.80	3.95	0.12	0.07	2.24	100.67	Ahmad et al. (2008)
NV-03	2.44	4.52	0.33	0.08	1.56	99.38	Ahmad et al. (2008)
NV-04	2.02	4.87	0.11	0.07	2.11	100.58	Ahmad et al. (2008)
NV-05	1.60	3.92	0.11	0.08	2.36	99.61	Ahmad et al. (2008)
NV-06	2.18	4.75	0.10	0.08	2.13	99.72	Ahmad et al. (2008)
NV-07	2.12	4.71	0.12	0.07	1.80	99.43	Ahmad et al. (2008)
NV-08	2.08	4.19	0.98	0.09	2.13	102.62	Ahmad et al. (2008)
NV-09	2.14	4.36	0.11	0.07	3.00	100.14	Ahmad et al. (2008)
NV-10	2.64	4.40	0.09	0.07	2.60	100.26	Ahmad et al. (2008)
NV-11	2.69	4.39	0.09	0.08	2.43	99.84	Ahmad et al. (2008)
93BG1	0.48	5.02	3.78	0.11	0.50	99.54	Ayres et al. (1997)
93G18	0.54	4.69	3.87	0.22	0.61	100.07	Ayres et al. (1997)
93G2	0.65	4.08	4.12	0.18	0.66	100.30	Ayres et al. (1997)
93G8	0.69	3.55	4.29	0.18	0.80	99.80	Ayres et al. (1997)
93ZP3	0.55	4.40	4.06	0.17	0.58	99.97	Ayres et al. (1997)
MA88.1	0.86	4.11	3.74	0.20	0.95	100.15	Ayres et al. (1997)
MA97.3	0.62	4.30	4.27	0.19	0.82	100.25	Ayres et al. (1997)
MN14	0.79	2.47	6.14	0.17	0.37	100.47	Ayres et al. (1997)
PAN2	0.50	0.69	3.85	0.09	2.10	100.07	Ayres et al. (1997)
158a	0.20	0.30	9.40			100.00	Chan et al. (2009)
158f	8.80	4.60	0.80			100.00	Chan et al. (2009)
158g	2.20	3.10	4.20			99.90	Chan et al. (2009)
158m	13.20	2.10	1.80			99.80	Chan et al. (2009)
158o	4.90	4.70	1.30			100.10	Chan et al. (2009)
158p	11.40	1.10	1.90			100.00	Chan et al. (2009)
DG01-1	0.21	3.52	4.60	0.04	0.96	99.92	Chen et al. (2013)
DG01-2	0.16	3.64	4.49	0.03	1.17	100.31	Chen et al. (2013)

Table A.3: continued

Sample	SiO2	TiO2	Al2O3	Fe2O3	FeO	MnO	MgO
DG02-1	76.86	0.20	13.24	1.60		0.01	0.09
DG03-1	75.70	0.39	14.96	0.42		0.01	0.18
DG05-1	68.74	0.64	14.08	5.67		0.09	0.95
GRC02-1	66.05	0.58	15.52	5.31		0.08	2.63
GRC03-1	50.84	1.80	16.85	12.10		0.19	4.73
GRC03-2	67.42	0.56	15.46	4.63		0.07	1.67
SZ01-1	67.38	0.64	13.72	5.53		0.10	1.61
SZ01-2	66.49	0.71	14.59	6.49		0.11	2.04
SZ02-1	60.51	0.85	16.47	7.61		0.13	3.23
SZ03-1	60.55	0.88	16.44	7.68		0.12	4.00
SZ04-1	60.62	0.86	16.49	7.67		0.13	3.74
SZ04-2	61.11	0.86	16.37	7.51		0.14	3.66
SZ05-1	65.12	0.69	15.57	5.90		0.08	2.72
SZ05-2	66.15	0.64	15.53	4.77		0.10	3.00
SZ05-2R	66.21	0.64	15.56	4.79		0.11	3.00
SZ06-2	64.87	0.66	15.67	5.70		0.10	2.58
SZ07-1	64.91	0.67	15.79	6.13		0.08	1.64
SZ09-1	49.15	1.46	17.56	10.23		0.16	6.42
SZ10-1	65.85	0.70	15.61	6.51		0.08	2.64
SZ10-2	66.81	0.69	15.30	5.49		0.11	3.12
SZ11-1	49.08	1.33	17.02	10.68		0.17	6.43
SZ12-1	50.03	1.52	17.44	10.54		0.13	8.21
SZ12-2	47.66	1.66	17.18	11.47		0.16	8.25
SZ12-3	49.46	1.45	17.50	10.87		0.13	8.81
ET023	65.27	0.53	16.81	3.52		0.03	1.53
ET025B	67.32	0.45	14.43	1.14		0.03	1.26
ET025E	66.76	0.33	15.16	2.07		0.06	0.93
ET026C	65.41	0.51	16.25	3.19		0.05	1.29
ET026D	63.62	0.55	16.32	2.75		0.03	1.04
T016	63.48	0.61	18.75	3.38		0.04	1.05
T041D	56.73	0.83	17.17	5.83		0.08	3.31
T065C	57.47	0.66	15.41	4.67		0.05	2.39
T081	60.57	0.62	16.18	3.97		0.05	2.25
202-20	71.70	0.29	14.70	2.09	1.88	0.05	0.47
202-22	55.60	1.14	17.90	8.01	7.21	0.13	3.35
202-33	50.50	1.21	18.00	9.61	8.65	0.13	4.32
99-5-11-1a	68.90	0.60	15.60	2.92	2.63	0.06	1.04
99-5-11-2	72.70	0.16	14.50	1.67	1.50	0.03	0.22
99-5-4-2	70.80	0.36	14.70	2.78	2.50	0.04	0.55
99-5-5-4d	70.70	0.27	14.00	2.17	1.95	0.09	0.45
99-5-7-2a	77.50	0.05	12.30	1.25	1.12	0.02	0.03
99-5-7-3b	74.70	0.13	13.90	1.46	1.31	0.04	0.19
99-5-9-3	74.50	0.18	13.70	1.61	1.45	0.03	0.34
99-5-9-4a	79.90	0.15	11.30	1.46	1.31	0.02	0.17
99-7-26-1b	76.50	0.16	12.90	1.66	1.49	0.04	0.27
BD-3	74.30	0.16	13.50	1.76	1.58	0.06	0.22
BD-7	73.10	0.19	14.30	1.62	1.46	0.03	0.35
BD-8	78.80	0.07	12.00	0.53	0.48	0.00	0.03
GL-1	65.50	0.49	15.50	4.63	4.17	0.11	1.92

Sample data continued

Sample	CaO	Na2O	K2O	P2O5	LOI	Total	Source
DG02-1	0.18	3.71	4.43	0.03	1.06	100.35	Chen et al. (2013)
DG03-1	0.24	3.28	4.90	0.06	1.61	100.14	Chen et al. (2013)
DG05-1	2.20	3.32	3.71	0.16	2.44	99.56	Chen et al. (2013)
GRC02-1	3.27	2.35	3.65	0.10	2.18	99.54	Chen et al. (2013)
GRC03-1	7.69	4.77	1.00	0.45	3.60	100.42	Chen et al. (2013)
GRC03-2	3.08	3.59	3.19	0.11	3.18	99.78	Chen et al. (2013)
SZ01-1	5.31	2.04	3.41	0.12	3.82	99.86	Chen et al. (2013)
SZ01-2	3.89	1.96	3.39	0.13	2.72	99.80	Chen et al. (2013)
SZ02-1	6.24	2.04	2.68	0.14	3.28	99.90	Chen et al. (2013)
SZ03-1	5.68	1.81	2.54	0.14	2.50	99.84	Chen et al. (2013)
SZ04-1	5.91	1.70	2.72	0.14	2.18	99.98	Chen et al. (2013)
SZ04-2	5.97	1.67	2.72	0.14	2.13	100.15	Chen et al. (2013)
SZ05-1	4.01	2.93	3.19	0.12	2.41	100.33	Chen et al. (2013)
SZ05-2	3.72	2.75	3.22	0.12	2.10	100.00	Chen et al. (2013)
SZ05-2R	3.71	2.76	3.21	0.12	2.12	100.11	Chen et al. (2013)
SZ06-2	3.83	3.28	3.42	0.12	2.06	100.23	Chen et al. (2013)
SZ07-1	4.28	1.58	4.43	0.11	2.15	99.62	Chen et al. (2013)
SZ09-1	11.29	2.31	0.74	0.26	7.35	99.58	Chen et al. (2013)
SZ10-1	1.01	3.66	3.41	0.12	2.12	99.59	Chen et al. (2013)
SZ10-2	2.01	3.38	3.24	0.12	2.06	100.27	Chen et al. (2013)
SZ11-1	9.70	4.28	1.50	0.18	4.62	100.37	Chen et al. (2013)
SZ12-1	7.54	3.82	0.91	0.21	6.81	100.35	Chen et al. (2013)
SZ12-2	9.77	2.98	0.26	0.28	7.60	99.67	Chen et al. (2013)
SZ12-3	6.66	4.17	1.04	0.19	6.31	100.28	Chen et al. (2013)
ET023	3.53	4.19	2.95	0.19		98.55	Chung et al. (2003)
ET025B	1.85	3.15	5.69	0.05		95.37	Chung et al. (2003)
ET025E	2.70	3.63	3.43	0.14		95.21	Chung et al. (2003)
ET026C	3.47	4.25	2.78	0.17		97.37	Chung et al. (2003)
ET026D	3.40	4.61	2.71	0.21		95.24	Chung et al. (2003)
T016	3.98	4.57	1.89	0.20		97.95	Chung et al. (2003)
T041D	5.54	4.11	1.72	0.27		95.59	Chung et al. (2003)
T065C	5.29	3.60	2.71	0.26		92.51	Chung et al. (2003)
T081	3.68	5.35	2.01	0.18		94.86	Chung et al. (2003)
202-20	1.23	3.60	5.03	0.08	1.06	100.33	D'Andrea Kapp et al. (2005)
202-22	6.65	3.73	1.98	0.37	1.45	100.25	D'Andrea Kapp et al. (2005)
202-33	7.98	3.22	1.61	0.42	2.75	99.74	D'Andrea Kapp et al. (2005)
99-5-11-1a	2.30	4.22	3.25	0.20	0.40	99.51	D'Andrea Kapp et al. (2005)
99-5-11-2	1.16	3.37	6.03	0.05	0.25	100.19	D'Andrea Kapp et al. (2005)
99-5-4-2	1.72	3.55	5.36	0.11	0.32	100.36	D'Andrea Kapp et al. (2005)
99-5-5-4d	1.54	3.91	4.32	0.09	1.71	99.23	D'Andrea Kapp et al. (2005)
99-5-7-2a	0.32	3.82	4.63	0.01	0.29	100.22	D'Andrea Kapp et al. (2005)
99-5-7-3b	1.20	3.78	4.52	0.04	0.32	100.27	D'Andrea Kapp et al. (2005)
99-5-9-3	1.30	3.04	5.27	0.07	0.35	100.46	D'Andrea Kapp et al. (2005)
99-5-9-4a	1.24	3.43	2.54	0.03	0.22	100.48	D'Andrea Kapp et al. (2005)
99-7-26-1b	0.59	2.84	4.24	0.17	0.94	100.24	D'Andrea Kapp et al. (2005)
BD-3	0.72	3.59	5.33	0.06	0.63	100.28	D'Andrea Kapp et al. (2005)
BD-7	1.36	3.59	4.65	0.08	0.46	99.77	D'Andrea Kapp et al. (2005)
BD-8	0.49	2.62	5.31	0.02	0.45	100.40	D'Andrea Kapp et al. (2005)
GL-1	5.36	2.82	2.40	0.15	1.56	100.44	D'Andrea Kapp et al. (2005)

Table A.3: continued

Sample	SiO2	TiO2	Al2O3	Fe2O3	FeO	MnO	MgO
GL-11	77.40	0.14	11.80	1.63	1.47	0.03	0.16
GL-12	74.50	0.21	12.90	1.86	1.67	0.02	0.40
ND-13	53.60	1.06	16.80	9.16	8.24	0.17	3.53
ND-14	75.20	0.08	13.80	0.90	0.81	0.01	0.14
ND-15	68.30	0.33	15.50	2.83	2.55	0.07	0.70
ND-22	77.00	0.08	12.20	1.85	1.66	0.06	0.09
ND-3	69.10	0.49	15.00	3.38	3.04	0.07	0.98
ND-4	70.90	0.32	15.20	2.23	2.01	0.06	0.51
ND-9	67.20	0.42	16.60	3.43	3.09	0.07	1.00
QC14	68.90	0.30	14.90	2.39	2.15	0.06	0.46
QC17	74.30	0.11	14.20	1.00	0.90	0.03	0.11
QC18	74.40	0.14	14.20	1.29	1.16	0.04	0.22
QC19	75.00	0.08	13.30	0.85	0.76	0.04	0.07
QC2	72.80	0.27	13.60	1.85	1.66	0.05	0.30
QC4	76.80	0.07	12.80	0.68	0.61	0.02	0.01
QC5	73.00	0.02	15.00	0.31	0.28	0.05	0.02
YD-11	76.30	0.15	12.80	1.23	1.11	0.06	0.09
YD-13	74.60	0.17	13.40	1.61	1.45	0.08	0.28
YD-33	72.70	0.24	14.50	1.86	1.67	0.04	0.39
YD-37	76.80	0.16	12.70	1.25	1.12	0.04	0.21
YD-7	71.90	0.25	14.50	2.04	1.84	0.06	0.50
YD-8	73.60	0.23	13.80	1.78	1.60	0.06	0.47
98T57	51.02	0.92	16.31	7.57		0.22	0.65
99T132	49.71	1.08	11.85	7.49		0.24	7.18
99T134	68.54	0.66	14.07	3.15		0.14	1.11
99T145	65.02	0.66	14.67	3.39		0.16	1.50
99T152	60.45	0.98	13.71	4.82		0.17	3.82
99T154	56.81	0.97	12.71	5.58		0.19	4.59
99T53	60.15	1.24	14.47	3.76		0.12	2.06
99T56	59.45	1.22	13.91	4.19		0.13	3.07
99T57	56.79	1.43	13.29	5.07		0.16	3.24
99T60	59.22	1.26	14.02	4.16		0.13	3.36
99T62	58.90	1.26	13.93	4.16		0.16	3.51
CHZ-1	54.28	1.60	12.82	3.39	2.95	0.11	5.66
CHZ-10	53.90	1.63	12.73	3.51	2.68	0.11	6.03
CHZ-11	53.50	1.60	12.57	3.28	2.92	0.10	6.32
CHZ-12	54.58	1.61	12.78	3.31	2.95	0.11	5.88
CHZ-2	54.42	1.62	12.75	3.29	2.85	0.11	5.87
CHZ-3	55.20	1.66	12.98	2.69	3.48	0.10	5.71
CHZ-4	54.18	1.53	13.59	2.70	3.88	0.12	5.95
CHZ-5	54.37	1.51	13.70	2.89	3.67	0.11	5.74
CHZ-6	55.66	1.52	13.71	3.11	3.02	0.09	4.95
CHZ-7	54.00	1.59	12.79	3.30	2.93	0.12	6.05
CHZ-8	54.15	1.60	12.76	3.25	2.82	0.12	5.84
CHZ-9	54.07	1.62	12.64	3.43	2.68	0.12	5.90
Tl/03	54.72	1.43	11.53	5.05	1.58	0.08	6.60
Tl/06	60.92	1.22	14.16	3.11	1.05	0.06	2.74
Tl/08	56.64	1.61	13.49	4.56	1.40	0.07	4.65
Tl/10	53.33	1.68	10.87	2.64	3.22	0.10	8.13

Sample data continued

Sample	CaO	Na2O	K2O	P2O5	LOI	Total	Source
GL-11	0.12	2.74	5.43	0.04	0.98	100.47	D'Andrea Kapp et al. (2005)
GL-12	1.31	2.81	4.98	0.09	1.14	100.21	D'Andrea Kapp et al. (2005)
ND-13	7.29	2.98	4.39	0.58	0.72	100.31	D'Andrea Kapp et al. (2005)
ND-14	1.39	2.84	5.78	0.04	0.25	100.45	D'Andrea Kapp et al. (2005)
ND-15	2.03	3.42	5.50	0.12	0.47	99.24	D'Andrea Kapp et al. (2005)
ND-22	0.52	3.66	3.77	0.03	0.88	100.08	D'Andrea Kapp et al. (2005)
ND-3	2.08	3.28	4.49	0.17	0.95	100.05	D'Andrea Kapp et al. (2005)
ND-4	1.62	3.29	5.66	0.07	0.32	100.18	D'Andrea Kapp et al. (2005)
ND-9	2.80	3.94	3.91	0.18	0.87	100.44	D'Andrea Kapp et al. (2005)
QC14	1.77	3.24	5.41	0.10	0.45	98.30	D'Andrea Kapp et al. (2005)
QC17	1.23	3.39	5.08	0.02	0.40	100.00	D'Andrea Kapp et al. (2005)
QC18	1.36	3.79	4.50	0.03	0.35	100.28	D'Andrea Kapp et al. (2005)
QC19	0.98	3.29	4.95	0.02	0.60	99.20	D'Andrea Kapp et al. (2005)
QC2	1.69	3.09	4.92	0.06	0.35	99.10	D'Andrea Kapp et al. (2005)
QC4	0.74	3.15	4.92	0.01	0.45	99.80	D'Andrea Kapp et al. (2005)
QC5	0.38	2.58	8.19	0.04	0.25	99.90	D'Andrea Kapp et al. (2005)
YD-11	0.71	3.28	5.07	0.03	0.68	100.42	D'Andrea Kapp et al. (2005)
YD-13	1.08	3.59	4.98	0.05	0.26	100.17	D'Andrea Kapp et al. (2005)
YD-33	1.24	3.38	5.07	0.06	0.73	100.19	D'Andrea Kapp et al. (2005)
YD-37	1.05	2.07	5.18	0.04	0.59	100.02	D'Andrea Kapp et al. (2005)
YD-7	1.86	3.42	5.26	0.08	0.46	100.35	D'Andrea Kapp et al. (2005)
YD-8	1.79	3.26	4.75	0.07	0.54	100.31	D'Andrea Kapp et al. (2005)
98T57	4.81	3.68	6.58	0.11	6.04	97.91	Ding et al. (2003)
99T132	10.34	1.62	6.17	1.34	2.63	99.65	Ding et al. (2003)
99T134	1.24	2.68	6.54	0.37	1.21	99.71	Ding et al. (2003)
99T145	2.26	2.57	7.38	0.43	1.76	99.80	Ding et al. (2003)
99T152	4.86	2.41	7.53	0.59	0.67	100.00	Ding et al. (2003)
99T154	7.12	1.80	8.19	0.77	1.16	99.89	Ding et al. (2003)
99T53	2.79	1.92	10.55	0.57	1.78	99.41	Ding et al. (2003)
99T56	3.04	2.24	11.24	0.47	1.06	100.00	Ding et al. (2003)
99T57	3.70	2.34	8.62	0.56	4.18	99.38	Ding et al. (2003)
99T60	2.95	1.26	11.66	0.46	1.18	99.66	Ding et al. (2003)
99T62	3.92	1.96	10.09	0.67	1.01	99.57	Ding et al. (2003)
CHZ-1	6.48	1.59	8.10	1.22	0.84	98.20	Gao et al. (2007b)
CHZ-10	6.59	1.34	8.61	1.26	0.73	98.39	Gao et al. (2007b)
CHZ-11	7.12	1.61	7.70	1.32	0.91	98.04	Gao et al. (2007b)
CHZ-12	6.37	1.61	8.32	1.16	0.51	98.68	Gao et al. (2007b)
CHZ-2	6.48	1.79	7.92	1.22	0.80	98.32	Gao et al. (2007b)
CHZ-3	6.10	1.66	8.29	1.06	0.28	98.93	Gao et al. (2007b)
CHZ-4	6.54	1.61	7.50	0.93	0.66	98.53	Gao et al. (2007b)
CHZ-5	6.36	1.67	7.62	0.94	0.61	98.58	Gao et al. (2007b)
CHZ-6	5.78	1.81	8.20	0.90	0.43	98.75	Gao et al. (2007b)
CHZ-7	6.64	1.51	8.04	1.26	0.73	98.23	Gao et al. (2007b)
CHZ-8	6.67	1.46	8.27	1.20	0.84	98.14	Gao et al. (2007b)
CHZ-9	6.79	1.37	8.36	1.38	0.78	98.36	Gao et al. (2007b)
Tl/03	7.06	2.26	6.34	0.90	1.66	97.55	Gao et al. (2007b)
Tl/06	3.26	2.49	9.17	0.58	0.49	98.76	Gao et al. (2007b)
Tl/08	5.42	2.04	8.05	0.69	0.56	98.62	Gao et al. (2007b)
Tl/10	6.69	2.22	4.47	0.97	4.57	94.32	Gao et al. (2007b)

Table A.3: continued

Sample	SiO2	TiO2	Al2O3	Fe2O3	FeO	MnO	MgO
Tl/11	54.00	1.62	11.09	3.59	2.22	0.09	7.74
Tl/13	54.36	1.45	12.18	4.59	1.68	0.10	6.34
Tl/17	60.70	1.06	13.29	2.37	1.98	0.07	3.47
Tl/18	56.72	1.58	13.40	3.34	2.42	0.07	5.13
Tl/59	62.62	0.92	13.79	2.25	1.42	0.07	2.57
DZ-01	51.02	0.72	17.99	12.31		0.14	10.65
DZ-02	45.68	0.75	15.88	9.84		0.16	14.35
DZ-03	50.74	0.92	16.98	10.45		0.16	6.31
DZ-05	50.64	0.61	17.66	8.92		0.13	5.98
DZ-07	51.70	0.81	14.38	8.91		0.21	5.84
DZ-10	50.93	0.91	16.78	10.43		0.22	6.34
DZ-11	44.16	0.86	17.41	10.40		0.31	12.48
DZ-13	49.55	0.84	16.37	10.62		0.19	9.18
DZ-14	49.57	0.79	16.01	10.24		0.16	9.11
DZ-16	47.79	0.79	17.08	10.44		0.17	10.08
DZ-17	49.70	0.88	16.17	10.54		0.16	9.80
DZ-18	49.69	0.86	16.24	10.44		0.16	10.16
DZ-19	52.59	0.85	15.62	11.77		0.19	9.79
DZ-20	51.67	0.82	15.22	9.83		0.15	9.55
DZ-21	50.80	0.74	16.55	8.87		0.13	8.19
DZ-22	51.41	0.80	16.11	10.16		0.15	9.47
DZ-23	52.59	0.82	15.17	10.44		0.16	9.41
DZ-28	53.79	1.06	15.85	9.80		0.19	5.73
LKA-01	55.64	0.88	17.16	7.84		0.16	3.97
LKA-02	54.03	1.00	17.87	8.98		0.13	4.20
LKA-03	54.49	0.97	17.06	7.91		0.15	4.18
LKA-04	51.41	1.05	16.88	8.83		0.17	6.34
LKA-05	48.89	1.03	17.71	8.91		0.19	6.41
LKA-06	51.58	0.96	16.19	5.42		0.10	8.86
LKA-07	49.95	0.95	16.74	7.14		0.12	9.24
LKA-08	50.77	0.93	16.70	7.06		0.10	9.46
LKA-09	51.50	1.03	15.50	7.51		0.10	9.12
LKA-11	46.56	0.97	18.80	8.69		0.11	12.04
LKA-12	44.41	1.10	17.54	11.22		0.08	11.98
LKA-13	51.29	0.95	15.71	7.32		0.10	11.28
LKA-14	51.72	0.84	14.54	7.86		0.14	11.05
LKA-15	49.47	0.82	14.52	8.66		0.15	11.51
LKA-16	49.26	1.00	15.17	8.24		0.12	10.43
LKA-17	48.56	0.94	16.81	6.62		0.08	11.73
LKA-19	50.23	0.90	15.92	6.76		0.08	9.96
LKA-22	47.53	0.99	17.76	7.43		0.10	12.13
LKA-24	47.56	1.04	18.41	8.05		0.11	10.34
ML18-1	51.08	0.82	16.50	10.42		0.26	5.02
ML18-10	65.91	0.34	17.08	3.28		0.06	1.18
ML18-2	71.03	0.12	15.47	1.75		0.04	0.67
ML18-3	66.59	0.33	16.74	3.07		0.06	1.12
ML18-4	54.80	0.79	17.24	8.56		0.17	4.35
ML18-5	56.29	0.74	16.76	8.19		0.18	3.83
ML18-6	55.97	0.56	15.71	7.73		0.19	3.91

Sample data continued

Sample	CaO	Na2O	K2O	P2O5	LOI	Total	Source
Tl/11	6.83	1.33	7.33	0.76	2.37	96.60	Gao et al. (2007b)
Tl/13	6.74	2.29	6.99	0.87	1.37	97.59	Gao et al. (2007b)
Tl/17	4.04	2.78	8.21	0.70	0.46	98.67	Gao et al. (2007b)
Tl/18	5.27	2.08	8.02	0.67	0.61	98.70	Gao et al. (2007b)
Tl/59	2.58	2.65	8.74	0.51	0.63	98.12	Gao et al. (2007b)
DZ-01	5.89	2.33	0.71	0.19		101.95	Gao et al. (2008)
DZ-02	9.37	2.68	0.09	0.26		99.06	Gao et al. (2008)
DZ-03	9.24	3.60	0.37	0.32		99.09	Gao et al. (2008)
DZ-05	11.41	2.55	0.56	0.14		98.60	Gao et al. (2008)
DZ-07	12.74	3.86	0.13	0.23		98.81	Gao et al. (2008)
DZ-10	8.82	3.72	0.60	0.26		99.01	Gao et al. (2008)
DZ-11	9.40	2.90	0.18	0.19		98.29	Gao et al. (2008)
DZ-13	10.52	1.15	0.11	0.22		98.75	Gao et al. (2008)
DZ-14	12.31	0.31	0.09	0.18		98.77	Gao et al. (2008)
DZ-16	10.96	1.28	0.10	0.17		98.86	Gao et al. (2008)
DZ-17	10.69	0.63	0.10	0.17		98.84	Gao et al. (2008)
DZ-18	9.47	1.58	0.07	0.18		98.85	Gao et al. (2008)
DZ-19	6.02	1.65	0.11	0.14		98.73	Gao et al. (2008)
DZ-20	10.90	0.46	0.11	0.17		98.88	Gao et al. (2008)
DZ-21	13.02	0.48	0.13	0.15		99.06	Gao et al. (2008)
DZ-22	8.79	1.59	0.19	0.17		98.84	Gao et al. (2008)
DZ-23	9.61	0.33	0.12	0.18		98.83	Gao et al. (2008)
DZ-28	8.69	3.51	0.55	0.36		99.53	Gao et al. (2008)
LKA-01	7.28	3.06	1.63	0.26		97.88	Gao et al. (2008)
LKA-02	7.93	2.83	1.44	0.28		98.69	Gao et al. (2008)
LKA-03	6.52	3.26	2.00	0.30		96.84	Gao et al. (2008)
LKA-04	9.90	1.37	0.05	0.30		96.30	Gao et al. (2008)
LKA-05	11.85	1.64	0.02	0.24		96.89	Gao et al. (2008)
LKA-06	10.78	2.33	2.73	0.21		99.16	Gao et al. (2008)
LKA-07	10.36	1.66	2.64	0.20		99.00	Gao et al. (2008)
LKA-08	7.46	2.56	3.67	0.20		98.91	Gao et al. (2008)
LKA-09	8.59	2.42	2.72	0.45		98.94	Gao et al. (2008)
LKA-11	5.84	2.01	3.31	0.40		98.73	Gao et al. (2008)
LKA-12	5.57	2.85	3.23	0.48		98.46	Gao et al. (2008)
LKA-13	6.42	2.72	2.59	0.45		98.83	Gao et al. (2008)
LKA-14	8.99	3.05	0.41	0.28		98.88	Gao et al. (2008)
LKA-15	11.66	1.16	0.45	0.31		98.71	Gao et al. (2008)
LKA-16	11.20	2.13	0.82	0.49		98.86	Gao et al. (2008)
LKA-17	7.56	1.63	4.70	0.31		98.94	Gao et al. (2008)
LKA-19	9.34	1.96	3.47	0.29		98.91	Gao et al. (2008)
LKA-22	6.98	1.80	4.52	0.21		99.45	Gao et al. (2008)
LKA-24	8.24	1.38	4.65	0.22		100.00	Gao et al. (2008)
ML18-1	6.69	4.55	2.44	0.79	1.21	99.78	Guan et al. (2012)
ML18-10	3.33	5.43	3.01	0.19	0.48	100.29	Guan et al. (2012)
ML18-2	2.51	4.93	3.22	0.09	0.45	100.28	Guan et al. (2012)
ML18-3	3.46	5.50	2.41	0.17	0.63	100.08	Guan et al. (2012)
ML18-4	5.14	4.96	2.53	0.46	0.91	99.91	Guan et al. (2012)
ML18-5	5.49	4.80	2.36	0.70	1.00	100.34	Guan et al. (2012)
ML18-6	4.51	2.85	6.89	0.44	0.77	99.53	Guan et al. (2012)

Table A.3: continued

Sample	SiO2	TiO2	Al2O3	Fe2O3	FeO	MnO	MgO
ML18-7	66.35	0.32	16.92	3.24		0.06	1.18
ML18-8	65.26	0.26	17.68	2.75		0.05	1.03
ML18-9	68.07	0.27	16.45	2.53		0.05	0.89
1-Lt	73.60	0.06	14.84	0.77			0.09
2-Lmt	73.98	0.08	14.71	0.87			0.11
3-L2m	73.55	0.10	14.85	0.91			0.13
G68	57.44	1.16	18.37	7.92		0.13	0.91
G006	70.02	0.46	16.07	2.02		0.02	1.41
G016	68.82	0.23	16.01	1.42		0.03	1.30
G019	68.56	0.48	15.25	1.72		0.06	1.77
G025	66.52	0.44	17.57	2.80		0.05	1.73
G09	67.29	0.63	16.18	2.46		0.06	1.49
GUO37	59.22	0.74	18.13	5.93		0.07	2.95
GUO48	62.68	0.85	17.02	3.84		0.07	2.72
GUO51	68.15	0.48	16.31	2.95		0.07	2.24
GUO62	65.93	0.64	18.11	2.86		0.05	1.99
ZF09	66.47	0.91	16.07	2.35		0.07	2.20
ZFG17	69.36	0.65	17.08	2.36		0.10	2.59
G10	73.76	0.22	14.20	1.73		0.03	0.61
G100A	74.52	0.30	13.99	1.53		0.03	0.30
G100C	73.01	0.28	14.85	1.49		0.04	0.45
G100E	75.48	0.26	12.12	0.66	1.28	0.04	0.32
G101A	58.74	0.81	15.75	7.45		0.12	4.07
G101C	58.33	0.74	15.57	1.94	4.77	0.11	4.01
G101E	58.51	0.85	15.39	1.79	4.92	0.12	3.98
G101G	59.40	0.76	15.60	7.04		0.11	4.03
G117A	47.28	1.22	15.79	10.95		0.13	6.54
G117B	47.23	1.09	14.76	10.34		0.20	6.70
G118A	68.98	0.43	14.86	4.53		0.08	1.47
G118C	70.85	0.37	15.17	3.69		0.08	1.24
G118D	69.91	0.41	15.34	3.87		0.08	1.25
G118G	68.74	0.46	15.48	4.64		0.08	1.54
G12	65.96	0.75	15.41	4.98		0.07	1.56
G120A	70.25	0.23	15.22	0.00	2.01	0.07	1.00
G121B	62.45	0.59	17.19	0.03	4.58	0.10	2.60
G124A	62.28	0.79	16.74	5.49		0.09	2.76
G124C	62.86	0.82	16.99	5.87		0.10	2.66
G125A	63.15	0.70	16.33	0.00	5.01	0.09	2.51
G15A	60.00	0.83	16.86	7.24		0.14	2.80
G20	74.25	0.19	14.14	1.31		0.08	0.12
G26	69.30	0.43	15.77	2.99		0.09	0.98
G38E	73.22	0.37	12.43	1.97		0.03	0.60
G4	58.73	0.71	17.18	6.97		0.13	2.82
G40	72.12	0.29	14.68	2.20		0.03	0.45
G41B	71.76	0.35	14.60	2.57		0.06	0.80
G42A	72.23	0.31	15.46	2.06		0.03	0.39
G42B	71.35	0.32	14.74	1.97		0.04	0.32
G5	61.00	0.70	16.85	5.61		0.10	2.63
G57A	73.52	0.18	13.81	0.70	1.08	0.05	0.26

Sample data continued

Sample	CaO	Na2O	K2O	P2O5	LOI	Total	Source
ML18-7	3.39	5.46	2.63	0.18	0.63	100.36	Guan et al. (2012)
ML18-8	2.85	5.08	4.54	0.16	0.44	100.10	Guan et al. (2012)
ML18-9	3.06	5.53	2.84	0.17	0.38	100.24	Guan et al. (2012)
1-Lt	0.41	4.23	4.54	0.14	0.80	99.50	Guillot et al. (1995)
2-Lmt	0.45	4.06	4.46	0.13	0.90	99.75	Guillot et al. (1995)
3-L2m	0.56	4.04	4.50	0.12	0.90	99.65	Guillot et al. (1995)
G68	6.06	3.01	4.85	0.14	2.33	102.32	Guo et al. (2006)
G006	1.86	4.69	3.31	0.13	0.52	99.89	Guo et al. (2007)
G016	1.74	3.57	6.77	0.10	0.87	99.93	Guo et al. (2007)
G019	2.49	4.16	5.37	0.13	1.82	100.04	Guo et al. (2007)
G025	3.95	4.41	2.38	0.16	1.68	99.64	Guo et al. (2007)
G09	3.69	4.28	3.70	0.22	0.47	99.76	Guo et al. (2007)
GUO37	5.28	5.85	1.68	0.14	1.29	99.91	Guo et al. (2007)
GUO48	4.63	4.98	2.79	0.41	0.66	99.54	Guo et al. (2007)
GUO51	2.88	3.70	2.83	0.38	0.27	100.47	Guo et al. (2007)
GUO62	3.74	4.16	2.24	0.27	0.36	99.52	Guo et al. (2007)
ZF09	3.85	4.21	3.48	0.39	1.53	99.78	Guo et al. (2007)
ZFG17	1.71	3.72	2.15	0.26	1.06	99.63	Guo et al. (2007)
G10	1.71	3.00	5.53	0.05	0.21	101.05	Harris et al. (1988a)
G100A	0.94	3.07	5.44	0.05	0.42	100.59	Harris et al. (1988a)
G100C	1.20	3.75	5.35	0.06	0.51	100.99	Harris et al. (1988a)
G100E	0.54	2.82	5.80	0.04	0.28	99.76	Harris et al. (1988a)
G101A	6.49	3.02	2.94	0.20	0.64	100.23	Harris et al. (1988a)
G101C	6.40	2.88	2.94	0.15	0.37	99.54	Harris et al. (1988a)
G101E	6.31	2.91	3.01	0.15	0.33	99.53	Harris et al. (1988a)
G101G	6.22	2.64	2.98	0.19	0.65	99.62	Harris et al. (1988a)
G117A	11.12	3.20	0.92	0.12	0.52	97.89	Harris et al. (1988a)
G117B	14.79	1.87	0.80	0.14	0.84	98.76	Harris et al. (1988a)
G118A	3.30	3.74	1.54	0.10	0.76	99.79	Harris et al. (1988a)
G118C	2.97	5.03	1.33	0.05	0.36	101.14	Harris et al. (1988a)
G118D	3.05	4.39	1.39	0.08	0.39	100.16	Harris et al. (1988a)
G118G	3.44	4.20	1.61	0.14	0.44	100.77	Harris et al. (1988a)
G12	4.17	3.44	3.16	0.18	0.61	100.29	Harris et al. (1988a)
G120A	2.25	3.67	4.14	0.06	0.46	99.96	Harris et al. (1988a)
G121B	5.80	3.13	1.87	0.10	0.46	100.02	Harris et al. (1988a)
G124A	4.42	3.89	3.07	0.16	0.88	100.57	Harris et al. (1988a)
G124C	3.86	3.13	3.40	0.19	0.84	100.72	Harris et al. (1988a)
G125A	3.69	3.21	3.52	0.20	0.17	99.84	Harris et al. (1988a)
G15A	5.74	3.92	1.84	0.23	0.33	99.93	Harris et al. (1988a)
G20	1.02	3.43	5.18	0.00	0.21	99.93	Harris et al. (1988a)
G26	2.54	4.20	4.66	0.15	0.51	101.63	Harris et al. (1988a)
G38E	1.46	2.84	4.88	0.10	0.29	98.19	Harris et al. (1988a)
G4	6.15	3.99	2.55	0.20	0.35	99.78	Harris et al. (1988a)
G40	1.32	3.27	5.67	0.09	0.44	100.56	Harris et al. (1988a)
G41B	2.03	3.64	4.50	0.08	0.29	100.68	Harris et al. (1988a)
G42A	1.64	3.60	5.53	0.08	0.26	101.59	Harris et al. (1988a)
G42B	1.41	3.31	5.72	0.06	0.25	99.49	Harris et al. (1988a)
G5	5.34	4.25	3.27	0.28	0.32	100.35	Harris et al. (1988a)
G57A	0.89	2.86	5.58	0.15	0.29	99.93	Harris et al. (1988a)

Table A.3: continued

Sample	SiO2	TiO2	Al2O3	Fe2O3	FeO	MnO	MgO
G60A	68.98	0.58	14.01	3.14		0.06	2.05
G61A	70.00	0.46	14.18	2.62		0.06	1.54
G64A	71.56	0.39	14.76	2.16		0.04	0.50
G64C	70.75	0.51	15.54	2.72		0.04	0.69
G66A	70.09	0.46	14.21	0.00	3.42	0.06	0.78
G67A	66.84	0.43	15.89	4.16		0.09	1.46
G68A	64.27	0.53	16.62	5.19		0.10	2.43
G68B	71.80	0.20	14.88	0.00	1.58	0.00	0.71
G69A	77.41	0.05	12.44	0.54		0.02	0.14
G69C	76.79	0.05	12.17	0.00	0.91	0.02	0.19
G71	71.49	0.32	15.57	3.24		0.07	1.08
S70C	76.05	0.11	13.75	1.25		0.02	0.18
S70D	72.87	0.26	14.52	1.79		0.04	0.31
X45	65.60	0.46	15.80	4.41		0.10	1.83
NM-1	66.00	0.50	16.00	3.73		0.07	2.08
NM-2	69.50	0.36	15.20	1.43		0.04	1.07
NM-3	70.10	0.35	15.10	2.72		0.05	0.95
NM-4	60.80	0.60	17.40	5.17		0.09	2.80
NM-5	65.90	0.44	16.10	3.54		0.06	1.75
NM-6	66.20	0.46	15.80	3.63		0.06	1.76
NM-7	65.80	0.45	15.50	3.67		0.07	2.05
YANS-2	71.50	0.23	15.30	1.84		0.04	0.55
YANS-4	71.30	0.33	15.10	2.26		0.06	0.69
ZH-1-94	66.80	0.43	15.60	3.36		0.06	1.74
ZH-3-92	71.10	0.32	14.60	2.06		0.04	0.90
Cj-02	68.87	0.32	14.59	2.81		0.31	0.90
Cj-20	64.90	0.41	15.38	3.74		0.07	0.76
Cj-22	67.87	0.35	15.75	1.98		0.09	0.82
Dzl-01	72.42	0.30	15.23	1.56		0.03	0.55
Dzl-05	71.26	0.29	15.58	1.32		0.04	0.66
Dzl-06	70.09	0.29	15.78	2.27		0.02	0.66
Dzl-07	71.51	0.29	15.24	0.88		0.03	0.56
Jm-16	68.29	0.37	14.71	1.59		0.05	1.29
Jm-21	69.51	0.42	15.10	2.27		0.07	1.17
Jm-23	68.00	0.38	14.82	1.47		0.04	1.29
Jm-7	68.52	0.45	14.91	2.26		0.06	1.22
Jmy-01	68.59	0.39	14.62	1.89		0.03	1.36
Jmy-04	67.09	0.47	14.62	0.98		0.06	1.43
Jmy-07	68.14	0.42	14.44	1.85		0.05	1.41
Ng-16	68.46	0.47	15.86	2.27		0.03	0.92
Ng-18	68.79	0.46	15.76	2.26		0.02	0.75
Nmy-01	69.71	0.37	15.33	1.93		0.02	1.15
Nmy-02	69.24	0.38	15.78	2.33		0.01	0.81
Nmy-04	68.75	0.42	15.79	1.99		0.03	1.34
Nmy-05	69.58	0.38	15.51	3.28		0.02	1.27
Nmy-07	70.07	0.36	15.18	1.45		0.02	1.09
Nt-03	67.90	0.49	16.09	2.16		0.01	1.49
Nt-05	71.19	0.37	14.99	1.60		0.01	0.72
Nt-07	67.14	0.42	15.16	2.60		0.06	1.17

Sample data continued

Sample	CaO	Na2O	K2O	P2O5	LOI	Total	Source
G60A	2.59	2.84	5.20	0.20	0.80	100.45	Harris et al. (1988a)
G61A	2.23	2.39	5.61	0.17	1.33	100.59	Harris et al. (1988a)
G64A	2.02	3.28	4.89	0.10	0.57	100.27	Harris et al. (1988a)
G64C	2.13	2.95	5.27	0.18	0.57	101.35	Harris et al. (1988a)
G66A	2.01	2.96	5.00	0.17	0.34	100.13	Harris et al. (1988a)
G67A	4.09	2.66	3.30	0.11	0.61	99.64	Harris et al. (1988a)
G68A	5.21	2.55	2.34	0.13	0.75	100.12	Harris et al. (1988a)
G68B	1.50	3.04	5.51	0.09	0.23	100.26	Harris et al. (1988a)
G69A	0.69	2.35	5.95	0.07	0.50	99.71	Harris et al. (1988a)
G69C	0.75	1.95	6.29	0.09	0.14	99.63	Harris et al. (1988a)
G71	1.63	2.85	4.41	0.17	0.88	101.71	Harris et al. (1988a)
S70C	0.89	3.29	5.71	0.13	0.37	101.75	Harris et al. (1988a)
S70D	1.44	3.67	4.81	0.08	0.33	100.12	Harris et al. (1988a)
X45	4.22	2.84	3.30	0.08	0.56	99.20	Harris et al. (1988a)
NM-1	3.82	4.09	3.34	0.22	0.71	100.60	Harrison et al. (2000)
NM-2	3.68	3.81	4.45	0.18	0.72	100.50	Harrison et al. (2000)
NM-3	3.08	4.38	2.65	0.17	0.70	100.20	Harrison et al. (2000)
NM-4	5.43	4.52	2.55	0.34	0.95	100.70	Harrison et al. (2000)
NM-5	3.87	4.20	3.42	0.25	0.58	100.10	Harrison et al. (2000)
NM-6	3.84	4.27	3.10	0.27	0.55	100.00	Harrison et al. (2000)
NM-7	3.44	3.70	4.64	0.32	0.56	100.20	Harrison et al. (2000)
YANS-2	1.77	3.76	4.77	0.10	0.82	100.70	Harrison et al. (2000)
YANS-4	1.86	3.70	4.55	0.11	0.63	100.50	Harrison et al. (2000)
ZH-1-94	3.87	4.26	3.24	0.26	0.46	100.10	Harrison et al. (2000)
ZH-3-92	2.66	3.84	4.02	0.15	0.70	100.40	Harrison et al. (2000)
Cj-02	2.03	1.63	4.35	0.12		95.93	Hou et al. (2004)
Cj-20	1.24	3.22	4.08	0.15		93.95	Hou et al. (2004)
Cj-22	2.40	3.70	3.18	0.13		96.27	Hou et al. (2004)
Dzl-01	0.82	4.30	4.06	0.14		99.41	Hou et al. (2004)
Dzl-05	2.17	4.42	3.59	0.09		99.42	Hou et al. (2004)
Dzl-06	1.93	3.62	3.61	0.10		98.37	Hou et al. (2004)
Dzl-07	1.77	4.07	4.14	0.09		98.58	Hou et al. (2004)
Jm-16	1.30	3.25	7.43	0.17		98.45	Hou et al. (2004)
Jm-21	0.41	3.45	5.73	0.18		98.31	Hou et al. (2004)
Jm-23	2.01	2.31	8.56	0.11		98.99	Hou et al. (2004)
Jm-7	1.49	3.68	4.24	0.17		97.00	Hou et al. (2004)
Jmy-01	1.88	3.32	6.21	0.17		98.46	Hou et al. (2004)
Jmy-04	3.65	6.46	6.68	0.20		101.64	Hou et al. (2004)
Jmy-07	1.88	1.96	6.55	0.19		96.89	Hou et al. (2004)
Ng-16	2.88	4.80	2.97	0.17		98.83	Hou et al. (2004)
Ng-18	2.73	4.66	3.28	0.17		98.88	Hou et al. (2004)
Nmy-01	1.91	4.50	3.43	0.14		98.49	Hou et al. (2004)
Nmy-02	0.38	4.47	4.37	0.14		97.91	Hou et al. (2004)
Nmy-04	1.37	4.84	3.82	0.16		98.51	Hou et al. (2004)
Nmy-05	0.49	4.44	4.11	0.15		99.23	Hou et al. (2004)
Nmy-07	1.08	3.95	4.93	0.13		98.26	Hou et al. (2004)
Nt-03	1.53	4.61	3.51	0.19		97.98	Hou et al. (2004)
Nt-05	0.90	3.62	4.75	0.15		98.30	Hou et al. (2004)
Nt-07	2.91	4.13	3.49	0.17		97.25	Hou et al. (2004)

Table A.3: continued

Sample	SiO2	TiO2	Al2O3	Fe2O3	FeO	MnO	MgO
Nt-08	66.83	0.39	15.12	2.28		0.06	1.11
Nt-10	64.26	0.58	15.19	3.12		0.06	1.93
Nt-12	68.18	0.42	15.34	2.55		0.09	1.19
Nt-31	70.26	0.39	14.69	1.63		0.02	0.90
Nty-01	72.18	0.30	14.94	1.07		0.01	0.61
Nty-04	71.24	0.20	14.66	1.31		0.03	0.70
Nty-05	66.94	0.45	15.94	3.11		0.03	1.36
Nty-08	70.10	0.28	14.64	1.98		0.01	0.61
Nty-11	70.20	0.38	14.93	2.14		0.02	1.25
PI-18	68.43	0.40	16.30	2.40		0.04	0.96
PI-28	66.49	0.57	16.28	3.77		0.01	0.85
0321-08	48.35	3.58	14.27	12.02		0.30	4.43
0321-09	48.51	3.72	14.36	12.03		0.25	4.31
cb-154	70.18	0.21	16.05	1.29		0.02	0.76
cb-167	69.74	0.24	16.71	1.53		0.03	0.89
cb-168	70.80	0.26	16.07	1.62		0.03	0.86
cb-172	69.13	0.25	16.74	1.56		0.02	0.84
cb-178	70.75	0.26	16.12	1.59		0.03	0.92
cb-189	70.72	0.25	16.21	1.60		0.03	0.82
cb-193	70.63	0.25	15.84	1.58		0.03	0.82
cb-206	69.12	0.32	16.10	0.43		0.04	1.41
cb-207	67.45	0.46	16.82	0.68		0.04	2.08
cb-208	68.08	0.38	15.75	1.36		0.04	1.58
cb-209	68.29	0.35	16.26	1.09		0.02	1.40
cb-210	66.96	0.43	16.22	2.02		0.04	1.85
cb-211	65.14	0.45	17.44	1.85		0.06	1.80
cb-213-2	69.62	0.32	15.47	1.21		0.03	1.21
cb-31	70.44	0.28	14.40	1.86		0.02	0.79
cb-33	71.72	0.28	14.67	1.72		0.02	0.84
cb-34	76.44	0.11	12.57	0.12		0.01	0.11
cb-35	76.61	0.09	12.79	0.08		0.01	0.19
cb-36	76.31	0.11	12.69	0.08		0.01	0.04
cb-37	65.26	0.48	16.66	3.78		0.07	1.53
cb-38	79.08	0.10	10.96	0.09		0.01	0.22
cb-77	68.65	0.36	15.85	2.09		0.03	1.40
cb-77-1	69.25	0.34	16.18	2.17		0.03	1.41
cb-77-2	68.66	0.33	15.61	1.92		0.03	1.31
cb-77-3	69.25	0.33	15.70	2.03		0.03	1.55
cb-78	68.90	0.32	15.92	2.05		0.03	1.40
cb-79	68.31	0.32	15.94	2.06		0.03	1.39
CMD-1	65.98	0.49	15.28	3.63		0.05	1.77
CMD-10	66.52	0.46	15.52	3.52		0.06	1.69
CMD-16-1	69.30	0.42	15.64	2.27		0.02	1.25
CMD-17	63.97	0.44	17.70	2.84		0.03	1.52
CMD-18	67.62	0.43	16.44	2.48		0.03	1.39
CMD-19	70.10	0.40	15.21	2.73		0.03	1.43
CMD-20	66.27	0.46	17.14	2.97		0.03	1.53
CMD-21	69.47	0.39	14.99	3.03		0.03	1.06
CMD-30	65.22	0.47	16.00	3.66		0.06	1.93

Sample data continued

Sample	CaO	Na2O	K2O	P2O5	LOI	Total	Source
Nt-08	2.86	4.33	3.36	0.17		96.51	Hou et al. (2004)
Nt-10	3.38	3.94	3.63	0.23		96.32	Hou et al. (2004)
Nt-12	2.30	4.69	3.48	0.16		98.40	Hou et al. (2004)
Nt-31	0.72	3.12	6.01	0.18		97.92	Hou et al. (2004)
Nty-01	0.34	4.45	4.53	0.05		98.48	Hou et al. (2004)
Nty-04	1.68	4.24	3.07	0.07		97.20	Hou et al. (2004)
Nty-05	3.06	4.39	3.06	0.18		98.52	Hou et al. (2004)
Nty-08	0.40	3.41	6.57	0.12		98.12	Hou et al. (2004)
Nty-11	1.91	4.64	3.02	0.14		98.63	Hou et al. (2004)
PI-18	2.25	5.11	2.60	0.13		98.62	Hou et al. (2004)
PI-28	1.07	3.05	3.33	0.22		95.64	Hou et al. (2004)
0321-08	7.93	2.43	0.17	0.54		94.02	Hou et al. (2012)
0321-09	7.87	2.54	0.17	0.54		94.30	Hou et al. (2012)
cb-154	2.16	4.08	3.38	0.10		98.23	Hou et al. (2012)
cb-167	2.80	4.46	3.22	0.12		99.74	Hou et al. (2012)
cb-168	2.69	4.08	3.14	0.11		99.66	Hou et al. (2012)
cb-172	2.78	4.23	3.27	0.11		98.93	Hou et al. (2012)
cb-178	2.74	3.80	3.03	0.11		99.35	Hou et al. (2012)
cb-189	2.76	4.10	3.20	0.10		99.79	Hou et al. (2012)
cb-193	2.82	3.97	3.16	0.12		99.22	Hou et al. (2012)
cb-206	2.15	3.92	4.01	0.12		97.62	Hou et al. (2012)
cb-207	0.77	3.53	2.67	0.12		94.62	Hou et al. (2012)
cb-208	2.06	3.59	4.70	0.12		97.66	Hou et al. (2012)
cb-209	2.31	3.87	4.41	0.11		98.11	Hou et al. (2012)
cb-210	2.65	3.98	3.38	0.14		97.67	Hou et al. (2012)
cb-211	3.46	4.12	2.99	0.16		97.47	Hou et al. (2012)
cb-213-2	2.08	3.84	4.04	0.11		97.93	Hou et al. (2012)
cb-31	1.53	3.62	5.52	0.12		98.58	Hou et al. (2012)
cb-33	1.43	3.10	5.81	0.12		99.71	Hou et al. (2012)
cb-34	0.53	2.99	6.29	0.04		99.21	Hou et al. (2012)
cb-35	0.46	2.86	6.99	0.03		100.11	Hou et al. (2012)
cb-36	0.65	2.52	6.88	0.03		99.32	Hou et al. (2012)
cb-37	5.33	4.51	0.96	0.26		98.84	Hou et al. (2012)
cb-38	0.52	1.98	6.47	0.03		99.46	Hou et al. (2012)
cb-77	2.29	3.73	3.84	0.12		98.36	Hou et al. (2012)
cb-77-1	2.10	3.92	3.70	0.12		99.22	Hou et al. (2012)
cb-77-2	2.48	3.65	3.83	0.11		97.93	Hou et al. (2012)
cb-77-3	2.28	3.94	3.85	0.11		99.07	Hou et al. (2012)
cb-78	2.01	3.93	3.90	0.12		98.58	Hou et al. (2012)
cb-79	2.36	4.43	3.69	0.11		98.64	Hou et al. (2012)
CMD-1	3.37	4.22	3.79	0.26		98.84	Hou et al. (2012)
CMD-10	3.33	3.91	3.88	0.23		99.12	Hou et al. (2012)
CMD-16-1	2.71	3.83	3.40	0.12		98.96	Hou et al. (2012)
CMD-17	3.55	4.57	3.33	0.21		98.16	Hou et al. (2012)
CMD-18	3.43	4.48	2.65	0.17		99.12	Hou et al. (2012)
CMD-19	2.89	3.83	2.91	0.17		99.70	Hou et al. (2012)
CMD-20	3.50	4.20	3.13	0.20		99.43	Hou et al. (2012)
CMD-21	2.58	3.99	3.15	0.11		98.80	Hou et al. (2012)
CMD-30	3.79	4.83	3.58	0.27		99.81	Hou et al. (2012)

Table A.3: continued

Sample	SiO2	TiO2	Al2O3	Fe2O3	FeO	MnO	MgO
CMD-31	65.30	0.48	16.32	3.61		0.06	1.96
CMD-32	65.98	0.51	15.78	3.77		0.06	1.81
CMD-33	65.93	0.48	16.11	3.55		0.06	1.82
CMD-36	69.63	0.46	14.85	3.03		0.04	1.48
CMD-37	72.54	0.32	14.09	2.18		0.02	0.97
T0319-6	71.80	0.24	15.35	1.17		0.02	0.73
T0319-7	74.84	0.25	13.47	1.63		0.03	0.79
T0319-8	71.57	0.30	15.18	1.80		0.03	0.99
T0319-9	72.16	0.26	14.70	1.57		0.03	0.79
T0320-6	72.46	0.03	16.20	0.40		0.01	0.04
YX-10	68.30	0.33	16.58	2.16		0.04	1.14
YX-11	68.57	0.33	16.76	2.11		0.04	1.24
YX-12	68.31	0.31	16.27	2.07		0.04	1.02
YX-13	68.94	0.32	16.32	1.98		0.03	1.13
YX-14	68.48	0.33	15.90	2.05		0.03	1.47
06FW101	72.29	0.27	14.28	1.99		0.05	0.57
06FW104	71.71	0.37	14.26	2.52		0.08	0.83
06FW105	67.62	0.56	14.99	3.50		0.06	1.27
06FW108	62.25	0.75	15.62	6.23		0.10	2.71
06FW110	73.45	0.22	13.54	1.74		0.04	0.42
06FW111	66.49	0.50	15.10	4.32		0.08	1.69
06FW112	60.23	0.66	17.15	6.65		0.12	2.91
06FW118	73.27	0.24	13.53	1.75		0.03	0.54
06FW119	63.91	0.67	15.92	5.51		0.09	2.32
06FW120	51.94	1.43	17.25	10.47		0.18	3.87
06FW121	75.29	0.13	12.73	1.16		0.01	0.29
06FW126	56.62	1.15	18.46	6.91		0.12	2.65
06FW127	77.16	0.09	12.14	0.65		0.01	0.06
06FW128	54.99	0.76	17.12	8.80		0.20	4.43
06FW129	57.43	1.05	18.67	6.24		0.11	2.32
06FW131	69.90	0.28	15.28	2.14		0.04	0.71
06FW133	67.45	0.41	15.39	2.83		0.05	1.19
06FW134	70.57	0.28	14.41	1.97		0.04	0.68
06FW139	61.01	1.27	16.40	5.27		0.08	2.07
06FW140	70.99	0.25	14.97	1.89		0.05	0.54
06FW146	52.88	0.77	19.06	9.41		0.16	4.35
06FW147	61.42	0.71	16.83	6.18		0.11	2.66
06FW148	71.69	0.26	14.23	2.17		0.06	0.71
06FW151	56.09	1.08	17.43	8.40		0.14	3.48
06FW152-2	53.49	1.32	17.36	9.18		0.15	4.08
06FW154	75.43	0.23	12.37	1.71		0.05	0.32
06FW155	70.33	0.41	14.28	2.02		0.05	0.89
06FW156	67.99	0.46	15.40	3.28		0.06	1.11
06FW162	60.29	0.72	16.78	7.01		0.12	3.24
06FW163	71.58	0.48	14.33	2.88		0.04	0.80
06FW174	56.45	0.79	17.45	7.84		0.15	3.06
06FW175	57.57	0.78	17.59	7.24		0.14	3.06
06FW176	54.48	1.03	17.99	8.47		0.15	3.09
08FW51	66.35	0.56	15.31	4.69		0.06	1.97

Sample data continued

Sample	CaO	Na2O	K2O	P2O5	LOI	Total	Source
CMD-31	3.81	4.72	3.49	0.26		100.01	Hou et al. (2012)
CMD-32	3.64	4.20	3.81	0.26		99.82	Hou et al. (2012)
CMD-33	3.44	4.13	4.02	0.26		99.80	Hou et al. (2012)
CMD-36	2.42	3.60	3.53	0.20		99.24	Hou et al. (2012)
CMD-37	1.70	3.19	4.91	0.12		100.04	Hou et al. (2012)
T0319-6	1.91	4.41	3.52	0.11		99.26	Hou et al. (2012)
T0319-7	1.94	3.02	2.95	0.12		99.04	Hou et al. (2012)
T0319-8	2.08	3.36	3.38	0.11		98.80	Hou et al. (2012)
T0319-9	2.34	3.40	3.37	0.11		98.73	Hou et al. (2012)
T0320-6	4.17	4.80	0.82	0.03		98.96	Hou et al. (2012)
YX-10	2.73	3.94	3.29	0.13		98.64	Hou et al. (2012)
YX-11	2.85	3.92	3.20	0.12		99.14	Hou et al. (2012)
YX-12	2.59	3.87	3.22	0.14		97.84	Hou et al. (2012)
YX-13	2.50	4.25	3.27	0.13		98.87	Hou et al. (2012)
YX-14	2.36	4.69	3.37	0.14		98.82	Hou et al. (2012)
06FW101	2.24	4.13	3.62	0.07	0.33	99.51	Ji et al. (2012)
06FW104	2.32	4.00	3.28	0.10	0.45	99.47	Ji et al. (2012)
06FW105	3.14	3.48	4.25	0.16	0.37	99.03	Ji et al. (2012)
06FW108	5.17	3.21	2.90	0.16	0.37	99.10	Ji et al. (2012)
06FW110	1.78	3.18	4.81	0.05	0.55	99.23	Ji et al. (2012)
06FW111	3.71	3.84	3.30	0.16	0.68	99.19	Ji et al. (2012)
06FW112	6.39	3.90	1.85	0.19	0.43	100.05	Ji et al. (2012)
06FW118	1.76	2.90	5.22	0.05	0.35	99.29	Ji et al. (2012)
06FW119	4.65	3.64	3.21	0.19	0.48	100.11	Ji et al. (2012)
06FW120	8.10	4.21	1.52	0.48	0.55	99.45	Ji et al. (2012)
06FW121	1.43	2.60	5.26	0.03	0.40	98.93	Ji et al. (2012)
06FW126	5.67	4.71	2.36	0.42	0.60	99.07	Ji et al. (2012)
06FW127	0.68	2.30	5.86	0.01	0.40	98.96	Ji et al. (2012)
06FW128	7.03	3.83	1.66	0.20	1.18	99.02	Ji et al. (2012)
06FW129	5.27	4.73	2.71	0.37	0.60	98.90	Ji et al. (2012)
06FW131	2.22	4.23	4.16	0.12	0.73	99.08	Ji et al. (2012)
06FW133	2.72	4.25	4.60	0.21	0.67	99.10	Ji et al. (2012)
06FW134	1.90	4.00	4.74	0.13	0.62	98.72	Ji et al. (2012)
06FW139	4.10	4.09	4.50	0.82	1.00	99.61	Ji et al. (2012)
06FW140	1.99	4.10	4.16	0.10	0.38	99.04	Ji et al. (2012)
06FW146	8.37	3.88	0.55	0.34	-0.05	99.77	Ji et al. (2012)
06FW147	5.34	4.18	2.46	0.22	0.45	100.11	Ji et al. (2012)
06FW148	2.33	4.05	3.66	0.10	0.45	99.26	Ji et al. (2012)
06FW151	7.22	3.79	1.94	0.51	0.42	100.08	Ji et al. (2012)
06FW152-2	7.66	3.49	1.45	0.45	0.73	98.63	Ji et al. (2012)
06FW154	1.17	3.28	4.52	0.05	0.23	99.13	Ji et al. (2012)
06FW155	2.52	3.40	5.06	0.13	0.58	99.09	Ji et al. (2012)
06FW156	2.79	3.69	4.78	0.14	0.55	99.70	Ji et al. (2012)
06FW162	5.11	3.47	2.12	0.16	0.52	99.02	Ji et al. (2012)
06FW163	1.73	3.02	4.79	0.10	0.18	99.75	Ji et al. (2012)
06FW174	6.93	4.02	2.14	0.25	0.30	99.08	Ji et al. (2012)
06FW175	6.56	3.90	2.07	0.30	0.20	99.21	Ji et al. (2012)
06FW176	6.97	4.34	2.06	0.39	0.38	98.97	Ji et al. (2012)
08FW51	4.38	3.12	2.80	0.13	0.82	99.37	Ji et al. (2012)

Table A.3: continued

Sample	SiO2	TiO2	Al2O3	Fe2O3	FeO	MnO	MgO
09FW41	70.44	0.40	14.91	2.91		0.06	0.84
09FW42	69.74	0.31	14.99	2.93		0.05	0.99
09FW43	70.66	0.32	14.76	2.62		0.05	0.95
09FW50	67.85	0.40	15.31	3.93		0.07	1.63
ML06-1	65.72	0.39	17.09	3.27		0.07	1.24
SR01-1	62.52	0.57	15.54	4.91		0.07	2.11
SR02-1	72.05	0.21	14.88	1.91		0.05	0.59
SR03-1	71.48	0.24	14.79	2.71		0.08	0.74
SR04-1	61.81	0.59	17.04	5.86		0.11	2.24
07TB33a-1	58.96	0.97	16.62	6.44		0.10	3.36
07TB33a-2	52.17	1.05	17.07	8.46		0.13	5.57
07TB33b-1	58.48	1.01	15.80	6.95		0.09	3.12
07TB33b-2	59.26	0.97	16.60	6.68		0.10	3.18
07TB33c-1	52.77	0.55	18.80	7.44		0.14	5.55
07TB33d	52.86	0.58	18.69	7.04		0.13	5.54
07TB33e	57.69	0.97	16.75	6.47		0.10	3.55
Khan_1	60.62	1.01	16.55	7.94		0.14	2.68
Khan_103	50.82	0.42	11.95	9.63		0.28	10.22
Khan_104	46.60	0.63	7.18	15.53		0.21	11.56
Khan_106	46.63	0.46	5.53	14.99		0.21	13.43
Khan_108	46.59	0.64	7.35	16.32		0.24	11.66
Khan_111	74.70	0.10	14.00	1.69		0.05	0.44
Khan_16	49.38	0.51	12.14	11.41		0.20	9.52
Khan_17	53.06	0.53	12.69	9.31		0.28	6.97
Khan_18	46.77	0.52	13.98	11.81		0.17	9.79
Khan_2	70.31	0.23	14.95	2.62		0.09	0.74
Khan_20	74.62	0.18	14.11	1.52		0.07	0.40
Khan_33	51.85	1.21	17.81	11.69		0.24	4.90
Khan_34	53.00	1.20	17.78	10.37		0.28	4.55
Khan_38	71.00	0.41	14.92	2.68		0.08	0.78
Khan_41	51.33	1.38	17.73	10.10		0.20	6.51
Khan_47	48.67	0.61	19.71	9.77		0.20	5.61
Khan_52	41.67	1.05	18.82	15.75		0.16	7.23
Khan_59	52.03	0.68	17.43	8.42		0.22	4.21
Khan_61	48.25	1.11	19.06	11.41		0.18	5.48
Khan_63	56.23	0.73	21.38	4.93		0.08	1.60
Khan_67	70.31	0.26	15.29	3.07		0.07	0.86
Khan_69	59.23	0.57	18.41	6.43		0.21	5.11
Khan_70	72.26	0.26	15.03	2.20		0.05	0.72
Khan_72	55.17	0.64	16.24	9.29		0.18	5.48
Khan_76	52.29	0.57	15.90	9.14		0.26	7.95
Khan_8	63.40	0.78	17.09	4.96		0.06	1.94
Khan_9	57.34	0.94	16.88	8.35		0.13	3.56
Khan_96	71.15	0.38	14.64	3.06		0.07	0.97
Khan_99	63.22	0.69	17.67	4.61		0.10	1.60
ST055C	52.92	0.92	17.49	7.96		0.17	4.10
ST057A	59.69	0.80	17.64	5.82		0.07	2.11
ST060C	68.39	0.47	15.16	2.51		0.08	0.81
T036D	48.34	0.94	18.65	10.52		0.16	6.18

Sample data continued

Sample	CaO	Na2O	K2O	P2O5	LOI	Total	Source
09FW41	2.20	3.95	4.08	0.12	0.22	99.91	Ji et al. (2012)
09FW42	2.35	3.51	4.69	0.11	0.36	99.67	Ji et al. (2012)
09FW43	2.56	3.61	4.07	0.11	0.26	99.71	Ji et al. (2012)
09FW50	3.49	3.62	3.44	0.12	0.36	99.86	Ji et al. (2012)
ML06-1	3.65	5.19	2.61	0.21	0.70	99.44	Ji et al. (2012)
SR01-1	3.87	3.13	4.00	0.18	3.20	96.90	Ji et al. (2012)
SR02-1	1.75	4.01	3.82	0.09	0.58	99.36	Ji et al. (2012)
SR03-1	2.92	4.03	2.55	0.10	0.36	99.64	Ji et al. (2012)
SR04-1	4.64	4.05	2.49	0.24	1.08	99.07	Ji et al. (2012)
07TB33a-1	5.47	3.69	3.10	0.26	1.02	99.99	Jiang et al. (2012)
07TB33a-2	8.08	3.86	2.23	0.31	1.25	100.19	Jiang et al. (2012)
07TB33b-1	5.22	3.83	3.21	0.29	1.64	99.65	Jiang et al. (2012)
07TB33b-2	5.11	3.59	3.31	0.26	0.95	100.03	Jiang et al. (2012)
07TB33c-1	8.03	4.03	1.32	0.16	0.81	99.59	Jiang et al. (2012)
07TB33d	8.57	4.18	0.64	0.14	1.32	99.69	Jiang et al. (2012)
07TB33e	5.79	3.65	3.06	0.27	1.04	99.34	Jiang et al. (2012)
Khan_1	4.30	4.17	2.35	0.25		100.00	Khan et al. (2009)
Khan_103	14.22	1.79	0.39	0.27		100.00	Khan et al. (2009)
Khan_104	15.84	1.34	0.96	0.15		100.00	Khan et al. (2009)
Khan_106	17.61	0.66	0.36	0.11		100.00	Khan et al. (2009)
Khan_108	15.59	0.96	0.51	0.12		100.00	Khan et al. (2009)
Khan_111	2.99	3.82	2.17	0.04		100.00	Khan et al. (2009)
Khan_16	11.34	2.72	2.47	0.32		100.00	Khan et al. (2009)
Khan_17	12.95	3.66	0.19	0.37		100.00	Khan et al. (2009)
Khan_18	12.18	2.05	2.38	0.35		100.00	Khan et al. (2009)
Khan_2	3.65	5.48	1.85	0.07		100.00	Khan et al. (2009)
Khan_20	1.28	4.45	3.30	0.06		100.00	Khan et al. (2009)
Khan_33	6.15	3.71	2.18	0.27		100.00	Khan et al. (2009)
Khan_34	7.66	3.65	1.24	0.25		100.00	Khan et al. (2009)
Khan_38	2.47	4.46	3.09	0.12		100.00	Khan et al. (2009)
Khan_41	8.67	3.13	0.73	0.22		100.00	Khan et al. (2009)
Khan_47	11.11	3.07	1.12	0.12		100.00	Khan et al. (2009)
Khan_52	14.09	0.92	0.27	0.04		100.00	Khan et al. (2009)
Khan_59	13.07	3.11	0.66	0.15		100.00	Khan et al. (2009)
Khan_61	9.67	3.22	1.41	0.21		100.00	Khan et al. (2009)
Khan_63	8.57	4.22	1.97	0.29		100.00	Khan et al. (2009)
Khan_67	2.69	3.82	3.49	0.13		100.00	Khan et al. (2009)
Khan_69	5.99	3.36	0.50	0.19		100.00	Khan et al. (2009)
Khan_70	3.66	4.89	0.81	0.10		100.00	Khan et al. (2009)
Khan_72	8.62	3.73	0.52	0.13		100.00	Khan et al. (2009)
Khan_76	9.46	4.03	0.27	0.13		100.00	Khan et al. (2009)
Khan_8	3.81	4.40	3.17	0.40		100.00	Khan et al. (2009)
Khan_9	6.93	4.56	1.11	0.20		100.00	Khan et al. (2009)
Khan_96	2.69	3.37	3.56	0.11		100.00	Khan et al. (2009)
Khan_99	4.54	3.89	3.45	0.22		100.00	Khan et al. (2009)
ST055C	6.34	2.66	4.41	0.38	2.97	100.30	Lee et al. (2009)
ST057A	4.21	2.83	5.33	0.29	0.87	99.66	Lee et al. (2009)
ST060C	1.35	2.82	6.40	0.07	0.84	98.89	Lee et al. (2009)
T036D	9.28	3.31	0.72	0.23	0.51	98.83	Lee et al. (2009)

Table A.3: continued

Sample	SiO2	TiO2	Al2O3	Fe2O3	FeO	MnO	MgO
T040A	64.39	0.76	16.60	4.60		0.10	1.56
T041F	52.25	0.87	19.20	10.57		0.14	3.84
T047	50.87	1.24	22.41	7.53		0.11	2.75
T054A	56.49	1.21	17.64	8.92		0.19	2.74
T065A	73.90	0.51	10.87	3.95		0.07	2.26
T065B	75.87	0.29	13.82	2.16		0.03	0.22
73-164	73.61	0.33	14.34	1.93		0.05	0.27
73-540	70.44	0.26	14.54	1.58		0.03	0.58
73-720	69.86	0.41	14.51	2.83		0.04	1.09
73-721	64.09	0.70	16.13	4.66		0.09	1.89
73-73	73.33	0.22	14.68	1.80		0.05	0.30
73-750	51.24	1.24	20.76	8.89		0.17	3.34
ET103A	70.69	0.28	14.35	1.70		0.04	0.39
ET104B	73.04	0.21	13.77	2.02		0.06	0.43
ET105A	67.35	0.46	15.70	3.91		0.08	1.16
ET105B	73.49	0.18	14.47	1.71		0.04	0.54
ET105C	72.54	0.24	14.81	2.03		0.03	0.48
ET105D	73.06	0.24	14.27	2.20		0.05	0.74
ET105E	71.39	0.27	15.15	2.45		0.07	0.82
ET105F	72.05	0.26	14.73	2.36		0.06	0.79
ET105G	52.23	1.09	16.27	8.85		0.15	5.58
ET106A2	78.30	0.07	11.66	0.78		0.02	
ET107A	73.05	0.32	14.20	2.30		0.03	0.29
ET108B	72.90	0.17	14.56	1.41		0.04	0.12
ET111B	72.75	0.19	14.33	1.43		0.03	0.09
ET113A	72.35	0.24	14.25	1.46		0.04	0.35
ET115F1	74.05	0.25	13.79	1.49		0.03	0.16
ET115F2	74.05	0.25	13.79	1.49		0.03	0.16
ET116B	73.17	0.23	14.45	1.71		0.04	0.33
ET117A	62.72	0.63	15.95	4.88		0.08	3.23
ET117C	67.53	0.41	15.38	3.12		0.05	1.90
ET119A	64.14	0.47	15.43	4.05		0.07	2.17
ET120A	70.43	0.28	15.31	2.16		0.07	0.68
ET120C	55.23	1.09	17.93	7.91		0.13	3.33
ET120D	45.03	1.87	17.99	12.78		0.19	4.91
ET120E	51.13	0.98	16.59	8.94		0.19	6.94
ET122A	54.60	1.15	17.42	7.76		0.12	4.78
ET122B	69.06	0.37	15.73	2.38		0.04	0.83
ET122D	70.35	0.33	15.31	1.90		0.03	0.53
ET124C	71.68	0.11	15.22	0.91		0.01	0.19
ET124D	50.23	0.89	16.29	8.50		0.23	8.13
ET125A	68.32	0.47	15.00	2.61		0.06	0.80
ET203B	70.77	0.17	14.90	1.38		0.04	0.12
ET203D	71.14	0.18	14.51	1.40		0.04	0.11
ET219B2	75.61	0.08	12.39	0.72		0.02	
ET220B	74.17	0.08	12.89	0.78		0.02	
ET221B	75.27	0.08	12.32	0.79		0.02	
ET222B	76.14	0.08	12.25	0.77		0.02	
RAW11	57.63	1.11	15.20	6.47		0.13	1.57

Sample data continued

Sample	CaO	Na2O	K2O	P2O5	LOI	Total	Source
T040A	3.45	3.91	3.18	0.22	1.31	100.08	Lee et al. (2009)
T041F	7.23	3.06	1.00	0.23	1.63	100.03	Lee et al. (2009)
T047	6.33	4.25	2.55	0.35	0.96	99.35	Lee et al. (2009)
T054A	7.09	3.19	1.06	0.36	0.71	99.59	Lee et al. (2009)
T065A	1.80	1.00	3.09	0.10	1.91	99.45	Lee et al. (2009)
T065B	1.15	2.77	4.52	0.07	0.94	101.84	Lee et al. (2009)
73-164	1.52	2.57	5.17	0.08	0.55	100.42	Lin et al. (2012)
73-540	1.62	2.95	4.57	0.10	0.72	97.39	Lin et al. (2012)
73-720	2.93	3.23	3.71	0.08	1.00	99.69	Lin et al. (2012)
73-721	4.68	3.55	2.55	0.13	1.20	99.67	Lin et al. (2012)
73-73	1.20	2.99	4.68	0.16	1.10	100.51	Lin et al. (2012)
73-750	8.42	4.09	1.08	0.29	0.73	100.25	Lin et al. (2012)
ET103A	2.11	2.72	4.34	0.03	0.53	97.18	Lin et al. (2012)
ET104B	1.98	2.96	3.58	0.04	0.47	98.56	Lin et al. (2012)
ET105A	3.51	2.79	3.36	0.08	0.34	98.74	Lin et al. (2012)
ET105B	1.75	3.69	4.33	0.06	0.43	100.69	Lin et al. (2012)
ET105C	2.15	2.98	3.62	0.04	0.62	99.54	Lin et al. (2012)
ET105D	2.19	3.65	3.51	0.08	0.80	100.79	Lin et al. (2012)
ET105E	2.22	3.93	3.86	0.09	0.30	100.55	Lin et al. (2012)
ET105F	2.28	3.83	3.62	0.09	0.85	100.92	Lin et al. (2012)
ET105G	6.92	2.50	1.16	0.15	5.70	100.60	Lin et al. (2012)
ET106A2	0.56	2.64	4.45		0.81	99.29	Lin et al. (2012)
ET107A	1.34	2.63	5.36	0.05	0.77	100.34	Lin et al. (2012)
ET108B	1.30	3.22	4.68	0.03	0.53	98.96	Lin et al. (2012)
ET111B	1.26	2.45	5.47	0.03	0.80	98.83	Lin et al. (2012)
ET113A	1.93	2.14	5.23	0.04	0.90	98.93	Lin et al. (2012)
ET115F1	1.20	2.73	5.06	0.02	0.75	99.53	Lin et al. (2012)
ET115F2	1.20	2.73	5.06	0.02	0.75	99.53	Lin et al. (2012)
ET116B	1.25	2.64	4.72	0.12	0.72	99.38	Lin et al. (2012)
ET117A	4.84	2.68	2.85	0.09	1.50	99.45	Lin et al. (2012)
ET117C	3.27	2.79	3.20	0.08	1.20	98.93	Lin et al. (2012)
ET119A	3.24	3.25	3.31	0.11	2.80	99.04	Lin et al. (2012)
ET120A	2.47	3.27	3.76	0.05	0.32	98.80	Lin et al. (2012)
ET120C	7.00	2.80	1.78	0.24	1.30	98.74	Lin et al. (2012)
ET120D	10.76	2.53	0.86	1.03	0.57	98.52	Lin et al. (2012)
ET120E	8.79	2.42	1.12	0.16	1.10	98.36	Lin et al. (2012)
ET122A	6.74	2.67	2.48	0.28	0.67	98.67	Lin et al. (2012)
ET122B	2.47	3.09	4.40	0.09	0.50	98.96	Lin et al. (2012)
ET122D	2.04	2.74	5.11	0.07	0.42	98.83	Lin et al. (2012)
ET124C	1.45	2.25	6.31	0.01	0.40	98.54	Lin et al. (2012)
ET124D	8.75	1.78	1.99	0.17	1.60	98.56	Lin et al. (2012)
ET125A	2.18	3.01	4.48	0.09	0.57	97.59	Lin et al. (2012)
ET203B	1.40	3.30	4.94	0.03	0.38	97.43	Lin et al. (2012)
ET203D	1.35	3.20	4.90	0.03	0.30	97.16	Lin et al. (2012)
ET219B2	0.60	2.88	4.95		0.73	97.98	Lin et al. (2012)
ET220B	0.64	2.79	5.50		0.70	97.57	Lin et al. (2012)
ET221B	0.65	2.85	4.92		0.80	97.70	Lin et al. (2012)
ET222B	0.50	2.73	5.07		0.58	98.14	Lin et al. (2012)
RAW11	4.62	3.78	2.34	0.33	8.11	101.29	Lin et al. (2012)

Table A.3: continued

Sample	SiO2	TiO2	Al2O3	Fe2O3	FeO	MnO	MgO
RAW12	55.16	1.14	18.16	6.52		0.14	1.44
RAW13	60.67	0.99	17.78	6.10		0.09	0.63
RAW15	52.51	1.56	18.47	8.31		0.13	3.59
RAW17	68.63	0.48	16.99	2.58		0.06	3.59
RAW20	51.00	1.36	21.57	7.41		0.11	2.37
RAW22	53.64	1.43	17.00	7.93		0.13	2.36
RAW24	55.24	1.48	17.47	7.64		0.14	2.42
RAW25	50.38	1.52	17.33	8.60		0.12	4.22
RAW26	51.73	1.45	16.60	8.27		0.13	4.03
RAW29	54.48	1.45	17.21	8.86		0.13	4.09
RAW30	45.85	2.13	19.21	11.40		0.11	6.01
MB12-1	68.48	0.57	14.37	3.71		0.07	1.76
MB12-3	66.21	0.62	14.93	3.95		0.07	1.87
MB12-5	66.54	0.62	15.23	4.13		0.07	1.93
MB12-7	67.60	0.52	15.54	3.36		0.06	1.55
MB12-8	66.60	0.59	14.68	3.95		0.07	1.90
MB12-9	66.44	0.59	15.69	3.82		0.07	1.83
MB13-2	53.85	1.48	17.24	8.71		0.14	3.71
MB13-2R	53.96	1.50	17.32	8.72		0.14	3.72
MB13-3	51.53	1.34	17.27	9.50		0.18	5.25
MB14-2	57.58	1.02	15.00	7.72		0.17	4.67
MB14-4	67.22	0.61	14.99	4.07		0.08	1.89
MB14-5	57.23	1.05	16.10	6.43		0.15	4.44
MB16-1	66.63	0.56	15.65	3.70		0.07	1.71
MB17-1	67.46	0.53	15.06	3.61		0.07	1.68
TE007/93	64.07	0.72	13.90	4.67		0.09	2.96
TE008/93	60.62	0.86	12.88	5.51		0.10	5.06
TE011/93	56.96	1.01	13.87	5.73		0.10	5.06
TE025/93	64.91	0.59	14.51	3.81		0.10	1.99
TE047/93	77.86	0.31	10.39	2.23		0.05	0.42
TE117/93	57.98	1.01	12.14	5.87		0.12	6.83
TE118/93	57.41	1.03	12.35	6.21		0.15	6.72
TE125/93	56.45	1.32	12.99	6.55		0.13	4.75
TE126/93	53.48	1.34	13.91	7.47		0.11	6.87
TE127/93	55.13	1.37	13.18	7.25		0.11	6.68
TE131/93	53.76	1.29	14.32	6.70		0.10	6.82
TE136/93	67.16	0.63	15.26	3.54		0.02	1.41
TE137/93	53.64	0.91	12.05	6.65		0.12	10.16
TE138/93	57.73	0.87	12.18	6.31		0.12	7.14
TE148/93	64.11	0.62	15.75	3.59		0.03	0.92
TE150/93	65.38	0.59	16.47	3.49		0.03	0.79
TE153/93	69.42	0.61	14.06	3.44		0.06	0.82
TE154/93	65.48	0.59	15.95	3.52		0.08	1.45
TE189/93	64.75	0.69	18.46	2.55		0.02	0.84
TE192/93	72.89	0.59	12.45	1.67		0.03	0.48
CM045/93	65.67	0.50	15.58		3.70	0.09	1.53
CM070/93	46.94	1.48	16.63		12.00	0.18	7.30
CM108/93	54.93	0.91	18.46		7.22	0.14	3.64
HF092/93	59.94	0.52	18.71		4.55	0.15	0.97

Sample data continued

Sample	CaO	Na2O	K2O	P2O5	LOI	Total	Source
RAW12	4.41	4.02	2.34	0.33	7.56	101.29	Lin et al. (2012)
RAW13	2.99	2.46	3.09	0.30	4.40	99.50	Lin et al. (2012)
RAW15	6.59	3.14	0.93	0.40	3.32	98.95	Lin et al. (2012)
RAW17	1.59	2.37	2.84	0.08	2.22	98.44	Lin et al. (2012)
RAW20	5.17	2.74	3.19	0.38	3.32	98.62	Lin et al. (2012)
RAW22	4.65	3.18	2.44	0.40	5.97	99.13	Lin et al. (2012)
RAW24	5.76	3.20	3.07	0.42	2.63	99.47	Lin et al. (2012)
RAW25	5.85	2.85	2.08	0.36	6.64	99.95	Lin et al. (2012)
RAW26	6.24	3.87	1.29	0.34	3.91	97.86	Lin et al. (2012)
RAW29	5.35	3.60	1.79	0.33	3.24	100.53	Lin et al. (2012)
RAW30	4.62	3.49	1.29	0.48	3.85	98.44	Lin et al. (2012)
MB12-1	3.43	3.80	3.26	0.26	0.40	100.11	Meng et al. (2013)
MB12-3	3.24	3.63	4.14	0.28	0.93	99.87	Meng et al. (2013)
MB12-5	2.85	3.96	3.35	0.30	1.28	100.30	Meng et al. (2013)
MB12-7	3.65	4.14	3.10	0.23	0.36	100.10	Meng et al. (2013)
MB12-8	2.91	3.95	3.20	0.28	2.13	100.26	Meng et al. (2013)
MB12-9	3.85	4.12	3.10	0.26	0.46	100.23	Meng et al. (2013)
MB13-2	5.34	4.74	2.73	0.66	1.59	100.19	Meng et al. (2013)
MB13-2R	5.34	4.75	2.74	0.67	1.55	100.41	Meng et al. (2013)
MB13-3	5.72	4.39	2.81	0.50	1.06	99.55	Meng et al. (2013)
MB14-2	6.41	4.08	1.83	0.40	0.77	99.65	Meng et al. (2013)
MB14-4	3.87	4.14	2.57	0.27	0.37	100.08	Meng et al. (2013)
MB14-5	5.68	3.94	3.61	0.46	0.50	99.59	Meng et al. (2013)
MB16-1	3.51	4.18	3.63	0.28	0.32	100.24	Meng et al. (2013)
MB17-1	3.45	3.87	3.48	0.25	0.63	100.09	Meng et al. (2013)
TE007/93	3.91	3.44	4.40	0.30	0.11	98.57	Miller et al. (1999)
TE008/93	3.93	2.62	6.23	0.60	1.37	99.78	Miller et al. (1999)
TE011/93	3.99	2.17	6.86	0.61	2.77	99.13	Miller et al. (1999)
TE025/93	3.18	2.48	6.82	0.25	0.59	99.23	Miller et al. (1999)
TE047/93	1.76	2.43	2.90	0.09	1.10	99.54	Miller et al. (1999)
TE117/93	4.64	2.51	6.48	1.02	0.64	99.24	Miller et al. (1999)
TE118/93	4.62	2.47	6.29	0.97	0.72	98.94	Miller et al. (1999)
TE125/93	4.12	1.15	7.54	0.70	3.67	99.37	Miller et al. (1999)
TE126/93	4.65	2.17	6.34	0.83	1.84	99.01	Miller et al. (1999)
TE127/93	4.60	2.14	6.60	0.78	2.27	100.11	Miller et al. (1999)
TE131/93	5.53	2.52	5.98	0.83	1.13	98.98	Miller et al. (1999)
TE136/93	2.72	3.30	5.10	0.32	1.40	100.86	Miller et al. (1999)
TE137/93	4.65	1.62	6.71	1.10	0.86	98.47	Miller et al. (1999)
TE138/93	4.27	2.11	6.19	0.91	1.08	98.91	Miller et al. (1999)
TE148/93	2.40	3.15	6.30	0.35	1.30	98.52	Miller et al. (1999)
TE150/93	2.36	2.99	6.26	0.23	0.97	99.56	Miller et al. (1999)
TE153/93	2.40	3.04	6.06	0.28	0.36	100.55	Miller et al. (1999)
TE154/93	2.71	2.98	6.01	0.21	0.39	99.37	Miller et al. (1999)
TE189/93	3.39	3.76	3.75	0.16	0.77	99.14	Miller et al. (1999)
TE192/93	3.04	3.63	2.82	0.15	1.15	98.90	Miller et al. (1999)
CM045/93	2.52	3.37	4.89	0.31	0.76	98.92	Miller et al. (2000)
CM070/93	8.63	2.91	1.89	0.35	1.97	100.28	Miller et al. (2000)
CM108/93	6.22	4.08	2.86	0.38	0.66	99.50	Miller et al. (2000)
HF092/93	2.50	4.39	6.48	0.24	0.58	99.03	Miller et al. (2000)

Table A.3: continued

Sample	SiO2	TiO2	Al2O3	Fe2O3	FeO	MnO	MgO
HF095/93	62.32	0.63	17.92		4.29	0.15	1.02
HF197/93	61.89	0.68	16.11		5.18	0.12	1.89
TE059/93	68.70	0.29	16.06		2.15	0.06	0.59
TE073/93	48.24	1.50	15.49		10.59	0.17	4.97
TE082/93	50.35	1.13	18.09		8.93	0.17	5.05
TE086/93	61.09	0.87	15.33		5.85	0.10	2.43
TE110/93	54.58	1.10	18.29		8.98	0.23	2.77
HB06/97	71.65	0.11	15.55	0.81		0.05	0.02
HB18/97	69.73	0.65	13.89	4.46		0.06	1.14
HB25/97	69.27	0.58	13.89	4.13		0.08	1.11
HB26/97	74.92	0.13	13.92	0.88		0.09	0.06
HF05/92	71.83	0.35	13.92	2.93		0.06	0.74
HF143/90	69.83	0.50	13.86	3.71		0.04	0.89
HF144/90	70.95	0.45	14.58	3.14		0.03	0.67
HF59/91	48.77	1.45	16.34	9.56		0.15	8.30
HF61/91	51.11	0.69	15.94	6.39		0.07	9.65
HF63/91	71.45	0.55	12.52	3.21		0.02	0.97
HF64/91	66.38	0.86	15.70	4.09		0.03	1.29
HF66b/91	50.81	1.53	17.37	8.57		0.10	6.93
HF67/91	75.45	0.13	13.85	1.38		0.01	0.08
HF73/91	72.40	0.45	13.39	2.87		0.07	0.85
HF94/90	59.25	1.03	15.94	6.09		0.10	3.67
HF95/90	48.69	1.09	16.93	8.46		0.13	9.29
HF98/90	73.70	0.17	13.50	1.88		0.06	0.52
KAW883	74.28	0.13	13.81	1.27		0.02	0.14
WAP25	68.01	0.39	14.68	3.55		0.06	1.62
BD-103	67.93	0.36	13.56	2.99	0.55	0.10	0.84
BD-145	61.57	0.62	15.88	5.46	2.02	0.11	1.77
BD-151	57.46	0.64	18.04	5.28	2.80	0.11	1.91
BD-160	58.77	0.71	17.11	7.42	0.25	0.10	1.77
BD-55	74.01	0.12	11.78	1.47	0.35	0.09	0.43
BD-58	43.33	0.99	15.62	9.96	5.25	0.18	3.85
BD-65	49.69	0.92	17.08	9.46	1.88	0.17	3.27
BD-77	68.98	0.25	18.09	0.72	0.15	0.01	0.27
D-15	58.05	0.68	15.92	6.75	2.70	0.15	2.53
D-2	59.16	0.70	16.02	6.21	2.10	0.15	3.66
L060	77.64	0.12	11.42	1.50	0.48	0.04	0.21
LZ9912	44.68	0.99	16.37	9.70	4.15	0.14	3.44
LZ9916	79.64	0.31	9.75	2.39	0.32	0.02	0.23
LZ9917	75.58	0.30	11.21	2.60	0.38	0.03	0.48
LZ9921	74.69	0.13	12.03	1.58	0.50	0.03	0.45
LZ994	71.56	0.46	12.40	3.53	0.28	0.12	0.53
P-1	74.06	0.17	13.33	1.33	0.38	0.08	0.28
Y-2	63.07	0.80	15.70	5.34	0.28	0.02	0.94
Y-4	75.03	0.45	12.40	1.56	0.15	0.01	0.48
ZB1	56.44	1.24	13.48	6.53	1.32	0.09	4.21
ZB10	56.48	1.23	13.51	6.58	1.42	0.10	4.46
ZB12	57.13	1.25	13.71	6.22	1.05	0.09	4.10
ZB4	55.90	1.25	13.52	6.46	2.42	0.09	4.32

Sample data continued

Sample	CaO	Na2O	K2O	P2O5	LOI	Total	Source
HF095/93	2.20	3.96	7.27	0.17	0.70	100.63	Miller et al. (2000)
HF197/93	4.72	3.72	3.78	0.23	0.76	99.08	Miller et al. (2000)
TE059/93	2.06	2.95	3.88	0.13	3.04	99.91	Miller et al. (2000)
TE073/93	11.92	3.16	1.47	0.49	1.74	99.74	Miller et al. (2000)
TE082/93	10.04	3.63	0.56	0.36	2.14	100.45	Miller et al. (2000)
TE086/93	4.97	3.47	4.15	0.54	1.39	100.19	Miller et al. (2000)
TE110/93	8.04	3.28	0.64	0.27	1.26	99.44	Miller et al. (2000)
HB06/97	0.65	3.63	4.98	0.34	1.43	99.22	Miller et al. (2001)
HB18/97	2.13	2.42	4.06	0.19	0.79	99.52	Miller et al. (2001)
HB25/97	2.02	2.72	4.44	0.14	0.75	99.13	Miller et al. (2001)
HB26/97	0.80	3.04	4.85	0.07	0.65	99.41	Miller et al. (2001)
HF05/92	1.23	2.74	4.54	0.23	0.64	99.21	Miller et al. (2001)
HF143/90	1.91	3.58	4.28	0.17	0.45	99.22	Miller et al. (2001)
HF144/90	0.91	2.10	5.10	0.18	0.93	99.04	Miller et al. (2001)
HF59/91	10.63	2.93	1.10	0.14	0.70	100.07	Miller et al. (2001)
HF61/91	11.51	2.45	0.34	0.10	0.31	98.56	Miller et al. (2001)
HF63/91	1.74	2.35	4.71	0.30	0.67	98.49	Miller et al. (2001)
HF64/91	2.31	2.83	5.56	0.30	0.61	99.96	Miller et al. (2001)
HF66b/91	9.41	2.96	1.46	0.15	0.80	100.09	Miller et al. (2001)
HF67/91	0.58	3.14	4.71	0.22	0.84	100.39	Miller et al. (2001)
HF73/91	1.06	2.92	4.61	0.16	1.18	99.96	Miller et al. (2001)
HF94/90	6.20	3.20	2.20	0.22	0.82	98.72	Miller et al. (2001)
HF95/90	10.11	2.37	0.43	0.14	0.77	98.41	Miller et al. (2001)
HF98/90	1.36	2.82	4.39	0.09	0.43	98.92	Miller et al. (2001)
KAW883	0.58	3.06	4.72	0.23	0.69	98.93	Miller et al. (2001)
WAP25	2.68	2.28	4.54	0.10	0.81	98.72	Miller et al. (2001)
BD-103	2.78	2.83	4.60	0.14	3.39	99.52	Mo et al. (2008)
BD-145	5.62	3.03	2.35	0.17	3.48	100.06	Mo et al. (2008)
BD-151	7.92	2.61	1.20	0.18	4.56	99.91	Mo et al. (2008)
BD-160	3.13	5.63	2.49	0.22	3.07	100.42	Mo et al. (2008)
BD-55	2.35	2.41	3.90	0.03	3.09	99.68	Mo et al. (2008)
BD-58	11.39	1.61	2.30	0.35	10.78	100.36	Mo et al. (2008)
BD-65	8.67	2.86	2.60	0.44	5.03	100.19	Mo et al. (2008)
BD-77	0.28	4.15	5.26	0.06	1.68	99.75	Mo et al. (2008)
D-15	6.49	2.73	1.88	0.17	4.22	99.57	Mo et al. (2008)
D-2	3.67	4.11	2.39	0.19	3.62	99.88	Mo et al. (2008)
L060	1.60	3.46	1.72	0.03	2.12	99.86	Mo et al. (2008)
LZ9912	12.06	2.40	1.39	0.47	8.42	100.06	Mo et al. (2008)
LZ9916	0.39	2.30	3.68	0.16	1.12	99.99	Mo et al. (2008)
LZ9917	0.59	1.71	5.55	0.14	1.77	99.96	Mo et al. (2008)
LZ9921	2.28	2.31	2.52	0.03	3.68	99.73	Mo et al. (2008)
LZ994	2.34	3.81	2.41	0.09	3.30	100.55	Mo et al. (2008)
P-1	1.06	3.33	5.43	0.04	0.80	99.91	Mo et al. (2008)
Y-2	1.75	3.30	6.06	0.65	2.23	99.86	Nomade et al. (2004)
Y-4	0.57	1.32	6.12	0.27	2.41	100.62	Nomade et al. (2004)
ZB1	5.93	3.14	6.53	1.16	0.76	99.51	Nomade et al. (2004)
ZB10	6.22	3.08	6.32	1.13	0.64	99.75	Nomade et al. (2004)
ZB12	5.62	3.25	6.54	0.98	0.77	99.66	Nomade et al. (2004)
ZB4	5.92	3.12	6.41	1.12	0.73	98.84	Nomade et al. (2004)

Table A.3: continued

Sample	SiO2	TiO2	Al2O3	Fe2O3	FeO	MnO	MgO
B29a	93.15	0.22	3.25	0.44		0.00	0.45
B29b	68.20	0.59	16.18	4.67		0.02	1.73
B36a	76.93	0.94	11.49	2.64		0.01	1.91
B39	63.99	0.92	19.83	7.94		0.17	1.77
B41	70.50	0.52	14.19	3.31		0.04	1.72
B45	75.75	0.30	13.10	2.26		0.03	1.20
B50	74.69	0.79	12.63	4.97		0.10	1.65
B51	84.05	0.59	7.91	3.53		0.07	0.99
B68	74.23	0.29	13.42	2.43		0.04	0.96
B71b	95.79	0.12	3.47	1.30		0.03	0.34
B75	97.89	0.08	2.62	0.63		0.01	0.53
B81	69.11	0.77	17.75	5.61		0.12	1.22
B83	58.04	1.05	19.88	11.40		0.21	1.97
B85b	71.93	0.73	13.97	6.37		0.05	1.95
B87	69.25	0.78	15.99	6.53		0.08	1.72
B88b	65.55	0.77	17.30	6.35		0.08	1.58
YH01-1	50.90	1.12	14.90	9.40		0.16	5.41
YH01-2	73.98	0.14	12.45	1.03		0.04	0.30
YH02-1	55.11	0.89	12.29	7.41		0.16	7.11
YH02-2	75.35	0.12	12.37	1.49		0.05	0.18
YH03-1	80.64	0.10	12.66	0.57		0.01	0.27
YH10-2	63.06	0.67	16.09	5.27		0.11	2.14
YH10-3	55.45	0.96	16.57	8.15		0.17	3.59
YH10-4	62.33	0.68	15.93	5.20		0.12	2.06
YH10-6	57.40	1.50	16.40	7.80		0.20	3.40
YH22-1	48.82	1.03	14.95	10.55		0.24	8.35
YH22-2	45.90	1.09	14.28	12.09		0.22	11.25
YH22-3	75.56	0.12	13.04	1.17		0.03	0.30
YH22-4	75.54	0.11	12.83	1.11		0.03	0.26
RG-13	63.66	0.76	15.68	6.19		0.11	2.54
RG-14	57.75	1.07	17.17	7.98		0.15	3.13
RG-16	68.68	0.45	14.88	3.76		0.09	1.28
RG-20	66.75	0.55	15.18	3.84		0.07	1.59
RG-6	75.20	0.20	13.08	1.89		0.07	0.42
T024	69.53	0.26	17.65		2.22	0.07	0.58
T026	70.11	0.16	15.95		1.41	0.04	0.32
T027	66.45	0.36	16.57		2.87	0.09	0.83
T212	65.93	0.36	16.56		3.16	0.07	0.95
T213	65.07	0.36	18.04		3.43	0.11	1.00
T215	68.28	0.24	17.20		2.14	0.06	0.49
T216A	67.89	0.30	17.04		2.52	0.05	0.61
T217	68.78	0.23	17.59		1.83	0.06	0.44
T218B	67.79	0.29	16.96		2.50	0.06	0.63
JPT14.2	61.54	0.77	17.33	4.05		0.06	2.16
T11B	62.60	0.73	16.50	3.96		0.06	2.23
T2A	51.27	0.96	10.98	6.42		0.11	11.38
T3B	56.05	1.05	14.37	6.74		0.10	5.23
T4A	51.66	1.00	13.70	6.03		0.08	6.86
T5A	56.97	0.68	11.19	4.19		0.09	4.34

Sample data continued

Sample	CaO	Na2O	K2O	P2O5	LOI	Total	Source
B29a	0.04	0.01	1.23	0.02	0.71	99.52	Richards et al. (2006)
B29b	0.09	0.16	5.28	0.08	2.63	99.63	Richards et al. (2006)
B36a	0.12	0.11	4.08	0.10	1.93	100.27	Richards et al. (2006)
B39	0.33	0.45	3.93	0.05	1.47	100.84	Richards et al. (2006)
B41	1.92	2.67	3.81	0.14	0.96	99.78	Richards et al. (2006)
B45	1.73	3.42	2.12	0.16	0.59	100.65	Richards et al. (2006)
B50	0.36	0.34	3.12	0.22	1.62	100.50	Richards et al. (2006)
B51	0.24	0.27	1.97	0.17	1.16	100.95	Richards et al. (2006)
B68	1.10	2.97	3.78	0.13	0.82	100.17	Richards et al. (2006)
B71b	0.02	0.02	2.01	0.03	0.41	103.54	Richards et al. (2006)
B75	0.04	0.01	0.79	0.03	0.52	103.16	Richards et al. (2006)
B81	0.24	0.71	4.34	0.06	2.10	102.03	Richards et al. (2006)
B83	1.15	1.56	4.18	0.29	2.64	102.37	Richards et al. (2006)
B85b	0.96	1.04	3.51	0.11	1.64	102.27	Richards et al. (2006)
B87	0.79	1.75	3.92	0.09	0.67	101.57	Richards et al. (2006)
B88b	0.96	2.57	3.00	0.07	1.61	99.82	Richards et al. (2006)
YH01-1	7.20	3.03	1.29	0.17	6.55	100.13	Sui et al. (2013)
YH01-2	3.14	1.43	2.59	0.05	4.69	99.84	Sui et al. (2013)
YH02-1	6.15	2.84	1.70	0.22	6.40	100.28	Sui et al. (2013)
YH02-2	2.31	2.84	2.07	0.04	3.47	100.29	Sui et al. (2013)
YH03-1	0.10	0.12	3.59	0.02	1.98	100.05	Sui et al. (2013)
YH10-2	4.36	4.50	2.52	0.18	1.41	100.31	Sui et al. (2013)
YH10-3	6.73	4.07	1.38	0.24	2.74	100.05	Sui et al. (2013)
YH10-4	5.38	3.78	1.96	0.18	2.33	99.95	Sui et al. (2013)
YH10-6	5.70	4.30	1.70	0.20	2.00	100.40	Sui et al. (2013)
YH22-1	10.62	1.99	1.19	0.21	1.62	99.57	Sui et al. (2013)
YH22-2	8.71	2.12	0.31	0.16	3.42	99.55	Sui et al. (2013)
YH22-3	0.56	3.31	5.55	0.06	0.71	100.41	Sui et al. (2013)
YH22-4	1.02	3.37	4.71	0.04	1.16	100.18	Sui et al. (2013)
RG-13	5.38	3.98	1.38	0.18		100.20	Upadhyay et al. (2008)
RG-14	6.86	3.86	1.85	0.32		100.60	Upadhyay et al. (2008)
RG-16	3.56	4.27	2.18	0.13		99.63	Upadhyay et al. (2008)
RG-20	3.88	4.41	3.23	0.27		100.40	Upadhyay et al. (2008)
RG-6	1.29	3.82	3.98	0.06		100.20	Upadhyay et al. (2008)
T024	3.54	4.41	1.73	0.10		100.09	Wen et al. (2008)
T026	2.61	4.38	2.20	0.04		97.22	Wen et al. (2008)
T027	3.83	4.13	1.84	0.14		97.11	Wen et al. (2008)
T212	3.35	3.68	2.97	0.13		97.16	Wen et al. (2008)
T213	4.40	4.18	2.12	0.14		98.85	Wen et al. (2008)
T215	3.21	4.48	2.09	0.06		98.25	Wen et al. (2008)
T216A	3.44	4.46	1.82	0.08		98.21	Wen et al. (2008)
T217	3.32	4.46	2.10	0.06		98.87	Wen et al. (2008)
T218B	3.45	4.26	2.15	0.09		98.18	Wen et al. (2008)
JPT14.2	4.96	4.41	2.70	0.26	0.99	99.23	Williams et al. (2001)
T11B	4.65	4.35	2.82	0.25	2.27	100.41	Williams et al. (2001)
T2A	5.35	1.14	7.69	1.29	2.50	99.09	Williams et al. (2001)
T3B	3.73	2.14	5.96	0.80	3.25	99.41	Williams et al. (2001)
T4A	5.75	2.14	6.52	0.97	4.10	98.97	Williams et al. (2001)
T5A	7.08	2.02	5.03	0.64	7.38	99.61	Williams et al. (2001)

Table A.3: continued

Sample	SiO2	TiO2	Al2O3	Fe2O3	FeO	MnO	MgO
ZC-05	48.97	0.96	16.33		9.00	0.20	6.61
ZC-186	53.28	0.87	13.79		9.53	0.31	6.99
ZC-192	51.59	0.72	16.36		10.26	0.16	6.73
ZC-206	46.84	0.18	14.12		12.28	0.21	12.91
ZC-232	49.67	0.94	14.80		13.45	0.11	4.74
GL-22	49.60	2.10	17.00	11.70		0.18	5.20
GL-24	46.20	2.47	16.30	13.40		0.18	6.22
GL-8	49.80	1.22	15.43	9.53		0.14	8.22
GLS-16	48.53	2.42	16.19	12.89		0.19	6.37
GLS-21	42.35	1.00	9.40	14.51		0.20	19.51
GLS-27	50.70	1.57	14.05	13.31		0.21	6.27
TL-2	49.14	1.38	16.08	10.87		0.15	7.09
TL-3	49.51	1.41	16.16	10.86		0.16	6.90
TL-4	51.31	1.30	16.78	10.18		0.51	3.90
TL-7	57.31	0.82	17.59	7.84		0.11	3.46
T339	69.25	0.45	15.21	2.64		0.02	1.40
T358	66.09	0.41	15.37	2.55		0.08	1.00
T379	67.63	0.38	15.53	3.12		0.05	1.37
T380	68.44	0.33	15.90	2.59		0.05	1.11
T381	68.61	0.36	15.64	2.72		0.05	1.15
T399	67.95	0.42	15.44	2.39		0.03	1.00
T400	67.93	0.46	15.34	2.55		0.04	1.15
T401	69.75	0.33	15.01	2.01		0.03	0.78
T402	71.50	0.33	14.03	2.06		0.04	0.91
T403	69.68	0.31	14.93	1.80		0.04	0.85
T404	72.09	0.33	13.80	1.82		0.03	0.75
0319-06	71.80	0.24	15.35		1.17	0.02	0.73
0321-031	74.98	0.05	14.84		0.53		0.23
0321-041	74.54	0.05	15.02		0.45	0.01	0.22
0321-07	76.11	0.05	13.80		0.51		0.30
0321-12	72.98	0.02	15.03		0.05		0.08
0322-01	72.54	0.07	15.46		0.67	0.01	0.16
0322-04	71.94	0.05	15.67		0.48	0.01	0.13
0323-01	72.76	0.03	15.69		0.27	0.02	0.06
0323-03	72.91	0.03	15.37		0.30		0.17
0323-04	73.40	0.03	15.30		0.21	0.01	0.05
T0317-01	69.08	0.25	16.04		1.49	0.03	0.83
T0317-02	69.30	0.24	16.52		1.40	0.03	0.75
T0317-03	68.85	0.25	16.79		1.48	0.02	0.81
T0317-04	69.04	0.23	16.78		1.35	0.02	0.71
T0317-05	69.12	0.23	16.87		1.41	0.02	0.73
T0317-06	68.65	0.24	17.01		1.47	0.02	0.76
T0319-06	71.80	0.24	15.35		1.17	0.02	0.73
T0319-07	74.84	0.25	15.04		1.13	0.03	0.79
T0319-08	71.57	0.30	15.18		1.80	0.03	0.99
T0319-09	72.16	0.26	15.70		1.57	0.03	0.79
T0319-10	73.51	0.26	15.27		1.53	0.02	0.67
T0319-11	72.92	0.25	15.84		1.43	0.02	0.81
T0319-12	72.54	0.27	14.43		1.72	0.03	0.91

Sample data continued

Sample	CaO	Na2O	K2O	P2O5	LOI	Total	Source
ZC-05	10.98	3.54	0.24	0.18	2.67	99.68	Xu et al. (2004)
ZC-186	6.82	4.87	0.14	0.10	2.67	99.37	Xu et al. (2004)
ZC-192	9.09	2.78	0.28	0.15	1.76	99.88	Xu et al. (2004)
ZC-206	9.59	0.87	0.18	0.04	1.98	99.21	Xu et al. (2004)
ZC-232	7.59	4.19	0.20	0.10	4.36	100.15	Xu et al. (2004)
GL-22	7.69	3.98	0.51	0.39	1.80	100.00	Xu et al. (2008)
GL-24	7.88	2.76	1.13	0.26	3.08	99.80	Xu et al. (2008)
GL-8	8.33	1.95	2.15	0.20	2.63	99.60	Xu et al. (2008)
GLS-16	7.72	3.46	1.50	0.42	0.59	100.26	Xu et al. (2008)
GLS-21	7.12	0.32	0.16	0.09	5.80	100.46	Xu et al. (2008)
GLS-27	8.24	3.64	0.26	0.17	2.25	100.68	Xu et al. (2008)
TL-2	7.12	3.10	1.34	0.28	3.70	100.25	Xu et al. (2008)
TL-3	7.27	3.18	1.37	0.29	3.12	100.22	Xu et al. (2008)
TL-4	7.87	3.38	1.68	0.31	2.58	99.79	Xu et al. (2008)
TL-7	5.89	2.99	1.55	0.12	2.51	100.17	Xu et al. (2008)
T339	2.13	3.80	4.00	0.18	0.61	99.69	Xu et al. (2010)
T358	2.79	4.11	3.59	0.17	3.38	99.54	Xu et al. (2010)
T379	3.04	4.03	3.67	0.19	0.52	99.53	Xu et al. (2010)
T380	2.72	4.18	3.86	0.15	0.27	99.60	Xu et al. (2010)
T381	2.69	4.03	3.72	0.15	0.49	99.61	Xu et al. (2010)
T399	2.45	4.61	4.21	0.14	0.96	99.60	Xu et al. (2010)
T400	2.22	4.60	4.11	0.16	1.03	99.59	Xu et al. (2010)
T401	2.24	4.23	4.82	0.11	0.29	99.60	Xu et al. (2010)
T402	2.15	4.32	4.00	0.16	0.20	99.70	Xu et al. (2010)
T403	1.89	4.15	5.56	0.13	0.29	99.63	Xu et al. (2010)
T404	1.90	4.34	4.21	0.13	0.27	99.67	Xu et al. (2010)
0319-06	1.91	4.41	3.52	0.11	0.61	99.87	Zeng et al. (2009)
0321-031	1.55	4.68	1.73	0.04	1.03	99.65	Zeng et al. (2009)
0321-041	1.45	4.94	2.02	0.05	0.53	99.27	Zeng et al. (2009)
0321-07	1.55	4.59	1.57	0.03	1.38	99.88	Zeng et al. (2009)
0321-12	1.24	3.98	5.62	0.02	0.10	99.12	Zeng et al. (2009)
0322-01	0.99	3.77	5.08	0.17	0.87	99.79	Zeng et al. (2009)
0322-04	0.81	4.43	5.17	0.07	0.79	99.55	Zeng et al. (2009)
0323-01	0.90	5.39	3.76	0.04	0.49	99.41	Zeng et al. (2009)
0323-03	0.96	5.19	3.80	0.05	0.75	99.53	Zeng et al. (2009)
0323-04	0.82	5.12	3.80	0.05	0.70	99.49	Zeng et al. (2009)
T0317-01	2.67	4.01	3.23	0.12	1.47	99.22	Zeng et al. (2011)
T0317-02	2.92	4.30	3.06	0.12	0.86	99.50	Zeng et al. (2011)
T0317-03	2.79	4.20	3.41	0.14	0.68	99.42	Zeng et al. (2011)
T0317-04	2.91	4.43	3.12	0.13	0.54	99.26	Zeng et al. (2011)
T0317-05	2.90	4.20	3.18	0.12	0.64	99.42	Zeng et al. (2011)
T0317-06	2.83	4.20	3.52	0.14	0.54	99.38	Zeng et al. (2011)
T0319-06	1.91	4.41	3.52	0.11	0.63	99.89	Zeng et al. (2011)
T0319-07	1.94	3.22	2.95	0.12	0.68	100.99	Zeng et al. (2011)
T0319-08	2.08	3.66	3.38	0.11	1.13	100.23	Zeng et al. (2011)
T0319-09	2.34	3.40	3.37	0.11	0.95	100.68	Zeng et al. (2011)
T0319-10	1.84	3.27	3.00	0.12	1.11	100.60	Zeng et al. (2011)
T0319-11	2.02	3.73	2.93	0.10	0.91	100.96	Zeng et al. (2011)
T0319-12	2.21	3.31	3.16	0.11	0.89	99.58	Zeng et al. (2011)

Table A.3: continued

Sample	SiO2	TiO2	Al2O3	Fe2O3	FeO	MnO	MgO
T0320-06	72.46	0.03	16.20		0.40	0.01	0.04
T0389-0	68.30	0.33	15.93		2.04	0.03	1.44
T0389-10	68.86	0.33	15.85		2.18	0.04	1.45
T0389-11	68.74	0.35	15.61		2.08	0.03	1.37
T0389-12	69.22	0.32	15.73		2.02	0.03	1.45
T0389-4	68.64	0.33	16.15		1.83	0.03	1.33
T0389-5	68.79	0.31	15.71		1.85	0.03	1.32
T0389-6	69.13	0.33	15.86		2.13	0.04	1.44
T0389-7	69.26	0.33	15.65		1.96	0.03	1.33
T0389-8	68.96	0.31	15.14		1.86	0.03	1.21
T0389-9	68.76	0.33	15.77		2.07	0.04	1.45
T100	74.04	0.11	14.78	0.04	0.80	0.03	0.47
T101	73.65	0.10	14.92	0.13	0.73	0.03	0.40
T104	73.90	0.12	14.70	0.19	0.88	0.03	0.41
T105	73.94	0.07	15.11	0.10	0.60	0.03	0.33
T110	72.58	0.29	15.16	0.01	1.83	0.03	0.94
T111	72.35	0.29	15.31	0.13	1.58	0.03	0.83
T113	70.97	0.39	15.53	0.21	2.17	0.03	1.10
T114	71.78	0.35	14.84	0.01	2.20	0.03	0.99
T117	73.85	0.10	14.81	0.22	0.87	0.03	0.35
T118	74.24	0.08	14.75	0.01	0.85	0.03	0.31
T120	74.06	0.12	14.23	0.15	0.77	0.02	0.26
T121	73.38	0.10	14.99	0.15	0.98	0.03	0.37
T136	74.69	0.22	13.50	0.38	0.18	0.03	0.55
T71	74.66	0.20	13.22	1.69	1.22	0.03	0.45
T72	74.48	0.19	13.25	1.68	1.20	0.03	0.43
T73	74.48	0.12	14.42	1.18	1.05	0.04	0.31
T74	74.54	0.12	14.60	1.14	1.00	0.04	0.33
T75	72.79	0.21	15.32	1.60	1.38	0.03	0.54
T76	74.63	0.02	14.25	0.59	0.62	0.01	0.10
T77	74.10	0.03	14.92	0.70	0.40	0.02	0.14
T97-26	72.94	0.11	14.71	1.22	0.95	0.02	0.28
T97-57	73.86	0.09	15.31	0.78	0.62	0.02	0.19
T97-61	73.36	0.21	13.89	2.10	1.48	0.05	0.47
T519	74.15	0.09	14.45	1.04		0.05	0.24
T520	73.72	0.13	14.60	1.35		0.06	0.31
T521	74.70	0.10	14.61	1.10		0.04	0.25
T522	72.87	0.10	14.99	1.15		0.06	0.25
T523	73.26	0.09	14.67	1.12		0.04	0.24
T524	72.88	0.14	14.82	1.64		0.04	0.36
T529	73.93	0.15	13.58	1.69		0.02	0.44
T632	71.18	0.38	15.20	2.42		0.02	0.70
T633	73.35	0.24	14.22	1.70		0.03	0.41
T634	69.48	0.43	15.77	2.72		0.04	0.84
T636	65.81	0.60	17.46	3.69		0.03	1.14
T637	72.07	0.33	15.07	2.24		0.02	0.58
T638	67.33	0.55	16.69	3.47		0.04	1.10
GZ-11	72.88	0.31	13.67	1.52	0.25	0.08	0.47
GZ-12	66.64	0.45	15.25	4.01	0.23	0.09	0.36

Sample data continued

Sample	CaO	Na2O	K2O	P2O5	LOI	Total	Source
T0320-06	4.17	4.80	0.82	0.03	0.78	99.74	Zeng et al. (2011)
T0389-0	2.35	3.81	3.63	0.13	1.47	99.46	Zeng et al. (2011)
T0389-10	2.08	3.81	3.52	0.13	0.97	99.22	Zeng et al. (2011)
T0389-11	2.15	3.68	3.66	0.11	1.50	99.28	Zeng et al. (2011)
T0389-12	2.01	3.98	3.42	0.11	1.08	99.37	Zeng et al. (2011)
T0389-4	1.53	3.89	3.50	0.14	2.08	99.45	Zeng et al. (2011)
T0389-5	1.89	3.82	3.42	0.12	1.97	99.23	Zeng et al. (2011)
T0389-6	2.02	3.82	3.46	0.12	0.83	99.18	Zeng et al. (2011)
T0389-7	1.66	3.59	3.47	0.12	1.97	99.37	Zeng et al. (2011)
T0389-8	2.54	3.71	3.16	0.14	2.33	99.39	Zeng et al. (2011)
T0389-9	2.24	3.77	3.39	0.13	1.37	99.32	Zeng et al. (2011)
T100	1.71	3.17	3.99	0.05	0.69	99.88	Zhang et al. (2004)
T101	1.86	3.30	4.10	0.05	0.75	100.02	Zhang et al. (2004)
T104	1.66	3.29	3.80	0.05	0.80	99.83	Zhang et al. (2004)
T105	2.00	3.38	3.58	0.04	0.67	99.85	Zhang et al. (2004)
T110	1.55	3.16	3.11	0.09	1.09	99.84	Zhang et al. (2004)
T111	1.37	3.34	3.42	0.07	1.11	99.83	Zhang et al. (2004)
T113	1.62	2.97	3.57	0.11	1.05	99.72	Zhang et al. (2004)
T114	1.84	3.46	3.14	0.10	1.08	99.82	Zhang et al. (2004)
T117	0.94	3.34	4.36	0.19	0.80	99.86	Zhang et al. (2004)
T118	1.02	3.54	4.27	0.13	0.65	99.88	Zhang et al. (2004)
T120	1.05	3.65	4.59	0.13	0.81	99.84	Zhang et al. (2004)
T121	0.95	3.43	4.66	0.16	0.65	99.85	Zhang et al. (2004)
T136	1.58	2.72	4.36	0.05	0.58	98.84	Zhang et al. (2004)
T71	1.54	2.98	4.68	0.06	0.25	99.76	Zhang et al. (2004)
T72	1.53	3.01	4.72	0.05	0.22	99.59	Zhang et al. (2004)
T73	0.82	3.53	4.10	0.17	0.50	99.67	Zhang et al. (2004)
T74	0.86	3.58	3.99	0.17	0.53	99.90	Zhang et al. (2004)
T75	1.18	3.54	3.97	0.15	0.69	100.02	Zhang et al. (2004)
T76	0.78	3.93	4.27	0.15	0.94	99.67	Zhang et al. (2004)
T77	0.93	4.27	4.38	0.13	0.42	100.04	Zhang et al. (2004)
T97-26	0.97	3.80	4.93	0.11	0.82	99.91	Zhang et al. (2004)
T97-57	0.67	4.03	4.55	0.16	0.19	99.85	Zhang et al. (2004)
T97-61	1.89	3.28	4.11	0.06	0.09	99.51	Zhang et al. (2004)
T519	1.61	3.72	3.62	0.05	0.50	99.52	Zhang et al. (2010)
T520	1.66	3.72	3.62	0.06	0.51	99.74	Zhang et al. (2010)
T521	1.51	3.60	3.75	0.06	0.53	100.25	Zhang et al. (2010)
T522	1.42	3.78	4.11	0.06	0.81	99.60	Zhang et al. (2010)
T523	1.45	3.81	3.97	0.06	0.84	99.55	Zhang et al. (2010)
T524	2.12	3.78	3.19	0.06	0.49	99.52	Zhang et al. (2010)
T529	1.71	2.73	4.86	0.05	0.37	99.53	Zhang et al. (2010)
T632	2.75	3.92	2.62	0.12	0.67	99.98	Zhang et al. (2010)
T633	1.59	3.12	4.74	0.08	0.48	99.96	Zhang et al. (2010)
T634	3.04	4.23	2.63	0.15	0.66	99.99	Zhang et al. (2010)
T636	3.92	4.18	2.12	0.26	0.88	100.09	Zhang et al. (2010)
T637	2.59	3.64	2.65	0.08	0.68	99.95	Zhang et al. (2010)
T638	3.67	4.35	1.91	0.23	0.72	100.06	Zhang et al. (2010)
GZ-11	0.80	3.25	4.90	0.15		99.75	Zhao et al. (2001)
GZ-12	1.75	3.51	4.72	0.18		99.75	Zhao et al. (2001)

Table A.3: continued

Sample	SiO2	TiO2	Al2O3	Fe2O3	FeO	MnO	MgO
GZ-14	64.05	0.45	14.88	4.01	0.08	0.14	0.43
GZ-3	72.97	0.29	14.70	1.39	0.22	0.03	0.34
GZ-5	66.94	0.48	15.15	4.10	0.15	0.08	0.57
GZ-6	69.56	0.31	13.84	1.31	0.75	0.04	0.81
GZ-7	54.08	0.99	16.09	3.80	1.92	0.08	1.96
GZ-8	70.85	0.32	14.11	1.92	0.25	0.03	0.51
GZ-9	64.63	0.45	14.38	3.71	0.15	0.07	0.41
CQ01	51.79	1.42	11.41	6.82	4.08	0.10	10.92
CQ02	55.80	1.32	14.86	6.55	3.08	0.11	4.29
CQ03	51.48	1.56	11.53	7.11	4.52	0.11	9.96
D9103	56.07	1.35	14.25	6.15	0.20	0.09	4.99
DR01-1	61.62	0.88	14.13	3.90	1.20	0.06	2.50
DR01-2	59.08	0.93	13.55	4.19	1.58	0.07	2.91
DR03	60.98	0.90	13.92	3.98	1.45	0.06	2.53
DR04	59.28	0.88	13.92	3.95	1.40	0.06	2.62
GGP-7	45.39	0.83	10.34	7.88	2.75	0.13	12.30
SL0618	58.90	1.30	13.90	5.70	5.10	0.10	5.50
SL0619	58.84	1.35	14.00	5.63	5.10	0.11	5.33
SL0620	59.00	1.30	13.70	5.50	5.00	0.10	5.40
SL0621	54.60	1.40	13.00	6.80	6.10	0.10	9.00
SL0622	57.90	1.40	14.40	5.80	5.20	0.10	5.30
SL0623	56.40	1.30	12.10	6.40	5.80	0.10	8.90
SL0624	56.80	1.40	12.10	6.50	5.90	0.10	9.30
SL0625	56.70	1.40	13.50	6.60	6.00	0.10	6.20
SL0628	60.61	1.22	14.53	5.76	5.20	0.06	4.18
SL0630	54.07	1.59	12.50	6.72	6.00	0.10	9.51
SL0631	55.70	1.40	13.60	6.80	6.10	0.10	7.50
XR01-1	59.40	0.99	13.76	5.23	0.80	0.08	3.81
XR01-3	52.22	1.41	11.51	6.99	3.95	0.11	10.99
XR02-1	52.47	1.51	12.76	6.07	2.88	0.10	6.42
Z8030-18	55.23	1.57	13.64	5.92	2.32	0.07	4.75
Z8030-5	55.96	1.37	13.60	4.47	1.30	0.06	4.12
ZB11	55.98	1.24	13.55	6.57	1.62	0.10	4.94
ZB14	57.69	1.18	13.77	6.05	1.20	0.08	3.93
ZB16	57.67	1.18	13.83	6.08	2.22	0.09	4.17
ZB18	55.52	1.27	13.44	6.44	2.58	0.10	4.52
ZB20	55.29	1.25	13.31	6.44	2.00	0.09	4.43
ZB21	55.02	1.35	14.40	7.14	2.78	0.13	2.59
ZB22	58.31	1.27	14.94	6.24	0.10	0.11	2.93
ZB3	56.12	1.24	13.45	6.59	2.42	0.10	4.98
ZB6	55.73	1.23	13.46	6.46	2.55	0.10	4.88
ZB8	56.86	1.23	13.75	6.48	1.75	0.10	4.90
ZB9	55.04	1.21	13.17	6.38	1.70	0.09	4.90
GZ-10	64.07	0.52	15.80	3.28	1.42	0.04	1.64
GZ-15	66.31	0.53	15.72	3.14	0.98	0.04	0.66
GZ-16	64.75	0.64	16.54	3.42	3.07	0.05	1.17
GZ-18	61.34	0.59	15.18	3.70	3.32	0.10	2.03
Y-1-1	68.60	0.69	14.07	3.89	0.25	0.02	0.75
Y-3	68.22	0.47	15.24	2.46	0.15	0.02	0.45

Sample data continued

Sample	CaO	Na2O	K2O	P2O5	LOI	Total	Source
GZ-14	4.16	3.54	4.40	0.17		99.75	Zhao et al. (2001)
GZ-3	0.30	3.25	4.48	0.11		99.77	Zhao et al. (2001)
GZ-5	1.55	2.99	4.70	0.18		99.72	Zhao et al. (2001)
GZ-6	1.69	3.27	5.23	0.14		99.69	Zhao et al. (2001)
GZ-7	5.42	4.43	3.62	0.54		99.62	Zhao et al. (2001)
GZ-8	2.07	2.13	3.73	0.14		99.79	Zhao et al. (2001)
GZ-9	4.21	3.38	4.34	0.17		99.73	Zhao et al. (2001)
CQ01	5.92	1.91	6.57	1.09	0.54	98.49	Zhao et al. (2009)
CQ02	5.95	2.75	6.35	0.78	0.62	99.38	Zhao et al. (2009)
CQ03	6.03	1.48	6.45	1.26	1.14	98.11	Zhao et al. (2009)
D9103	4.84	2.72	7.19	1.06	0.90	99.61	Zhao et al. (2009)
DR01-1	2.79	2.69	8.67	0.53	1.24	99.01	Zhao et al. (2009)
DR01-2	3.72	2.71	8.31	0.57	2.81	98.85	Zhao et al. (2009)
DR03	3.29	2.59	8.46	0.54	2.27	99.52	Zhao et al. (2009)
DR04	2.92	2.37	8.83	0.56	2.74	98.13	Zhao et al. (2009)
GGP-7	10.09	1.42	5.96	0.66	1.81	96.81	Zhao et al. (2009)
SL0618	4.90	2.50	5.60	0.70	0.70	99.80	Zhao et al. (2009)
SL0619	4.80	2.45	5.67	0.71	0.94	99.83	Zhao et al. (2009)
SL0620	4.80	2.20	5.90	0.70	1.30	99.90	Zhao et al. (2009)
SL0621	5.50	1.70	5.90	0.90	0.70	99.70	Zhao et al. (2009)
SL0622	4.90	2.50	5.70	0.80	0.80	99.50	Zhao et al. (2009)
SL0623	5.20	1.60	5.90	0.80	0.90	99.50	Zhao et al. (2009)
SL0624	5.10	1.70	5.90	0.80	0.10	99.80	Zhao et al. (2009)
SL0625	5.00	2.20	5.70	0.80	1.50	99.80	Zhao et al. (2009)
SL0628	4.71	2.75	4.66	0.57	1.26	100.31	Zhao et al. (2009)
SL0630	5.45	1.69	6.60	0.94	0.47	99.64	Zhao et al. (2009)
SL0631	5.70	2.50	5.30	0.80	0.40	99.80	Zhao et al. (2009)
XR01-1	4.68	3.11	7.41	0.56	0.53	99.56	Zhao et al. (2009)
XR01-3	6.06	2.04	6.14	1.12	0.73	99.32	Zhao et al. (2009)
XR02-1	6.17	1.87	8.03	1.18	0.90	97.48	Zhao et al. (2009)
Z8030-18	4.90	2.08	7.77	0.67	0.80	97.40	Zhao et al. (2009)
Z8030-5	4.39	2.53	7.47	0.68	2.95	97.60	Zhao et al. (2009)
ZB11	6.24	3.06	6.24	1.12	0.68	99.70	Zhao et al. (2009)
ZB14	5.30	3.41	6.60	0.93	1.02	99.96	Zhao et al. (2009)
ZB16	5.38	3.31	6.54	0.95	0.46	99.66	Zhao et al. (2009)
ZB18	6.48	3.11	6.42	1.09	1.12	99.51	Zhao et al. (2009)
ZB20	6.88	3.04	6.31	1.08	1.68	99.80	Zhao et al. (2009)
ZB21	3.65	2.98	8.77	0.65	1.86	98.54	Zhao et al. (2009)
ZB22	2.76	3.92	7.83	0.71	0.70	99.72	Zhao et al. (2009)
ZB3	6.19	3.15	6.24	1.12	0.39	99.57	Zhao et al. (2009)
ZB6	6.59	3.18	6.18	1.10	1.07	99.98	Zhao et al. (2009)
ZB8	6.08	3.14	6.32	1.12	0.39	100.37	Zhao et al. (2009)
ZB9	7.03	2.97	6.11	1.11	1.51	99.52	Zhao et al. (2009)
GZ-10	3.49	3.98	3.16	0.19	4.39	100.56	Zhou et al. (2010)
GZ-15	2.89	3.17	3.73	0.20	4.01	100.40	Zhou et al. (2010)
GZ-16	4.03	4.37	3.06	0.25		97.95	Zhou et al. (2010)
GZ-18	5.68	4.12	2.90	0.23		95.49	Zhou et al. (2010)
Y-1-1	1.80	3.35	5.20	0.58	1.45	100.40	Zhou et al. (2010)
Y-3	0.66	2.60	9.13	0.28	0.83	100.36	Zhou et al. (2010)

Table A.3: continued

Sample	SiO2	TiO2	Al2O3	Fe2O3	FeO	MnO	MgO
DX13-1	68.05	0.58	14.74	4.07		0.12	0.98
DX19-1	71.10	0.35	14.53	2.95		0.06	0.94
DX2-1	66.48	0.75	15.15	5.15		0.12	1.33
DX21-1	75.30	0.10	13.48	1.43		0.05	0.55
DXL1-3	73.95	0.14	10.94	1.31		0.04	0.77
GB-8	68.43	0.29	13.66	2.88		0.21	0.65
NX5-2	67.52	0.51	15.36	4.18		0.06	1.36
NX5-3	57.41	0.78	16.38	8.04		0.22	3.64
SZ39	76.58	0.06	12.39	1.54		0.02	0.06
SZ43	72.66	0.22	14.29	2.20		0.03	0.29
SZ48	60.47	0.77	15.02	8.75		0.15	3.19
SZ52	64.97	0.57	14.66	6.80		0.08	1.59
CY1-01	70.57	0.54	13.95	3.43		0.05	0.93
CY1-02	70.74	0.48	13.86	3.14		0.04	0.77
CY1-02R	70.78	0.47	13.85	3.14		0.04	0.76
CY1-1	69.92	0.45	14.63	3.04		0.04	0.67
CY2-1	76.77	0.26	11.63	2.03		0.02	0.37
CY3-1	75.40	0.22	12.44	1.92		0.03	0.23
CY4-1	74.47	0.31	13.08	2.32		0.03	0.44
CY6-1	75.40	0.24	12.56	1.65		0.02	0.31
GBJD-1	70.47	0.34	14.76	2.46		0.04	0.59
GBJD-2	72.47	0.35	13.73	2.72		0.05	0.64
GBJD-3	71.80	0.35	14.03	2.70		0.05	0.62
PK01-1	73.37	0.31	13.67	2.55		0.04	0.66
PK01-2	72.84	0.33	13.56	2.60		0.04	0.69
PK01-3	73.02	0.33	13.63	2.58		0.04	0.67
PK01-4	71.61	0.31	14.31	2.58		0.04	0.68
PK01-5	73.00	0.29	13.78	2.35		0.04	0.56
PK01-6	73.64	0.29	13.39	2.34		0.04	0.61
MM02-2	56.82	0.80	15.47	4.94		0.08	5.81
MM02-3	55.87	0.96	18.12	6.53		0.05	5.48
MM02-4	59.86	0.88	17.57	5.01		0.06	3.51
MM02-5	57.77	0.98	17.78	4.34		0.06	5.83
MM02-6	62.98	0.95	16.61	6.07		0.07	4.41
T203A	58.05	1.10	18.97	5.88		0.06	4.03

Sample data continued

Sample	CaO	Na2O	K2O	P2O5	LOI	Total	Source
DX13-1	2.96	3.37	2.93	0.14	1.99	99.93	Zhu et al. (2009)
DX19-1	3.21	3.37	2.81	0.09	0.85	100.26	Zhu et al. (2009)
DX2-1	3.13	3.65	2.76	0.17	1.53	100.22	Zhu et al. (2009)
DX21-1	0.28	3.94	4.23	0.02	0.84	100.22	Zhu et al. (2009)
DXL1-3	2.35	3.83	1.41	0.03	4.76	99.53	Zhu et al. (2009)
GB-8	2.22	1.63	7.07	0.08	2.46	99.58	Zhu et al. (2009)
NX5-2	3.74	3.25	2.92	0.13	0.66	99.69	Zhu et al. (2009)
NX5-3	6.53	3.64	2.04	0.16	0.78	99.62	Zhu et al. (2009)
SZ39	0.23	2.99	5.22	0.01	0.75	99.52	Zhu et al. (2009)
SZ43	0.58	2.96	5.21	0.04	1.60	99.53	Zhu et al. (2009)
SZ48	3.66	3.77	2.16	0.12	3.73	99.57	Zhu et al. (2009)
SZ52	3.10	2.83	2.54	0.13	4.79	99.86	Zhu et al. (2009)
CY1-01	2.12	2.57	5.05	0.12	0.20	99.53	Zhu et al. (2009)
CY1-02	1.75	2.55	5.73	0.10	0.41	99.57	Zhu et al. (2009)
CY1-02R	1.75	2.55	5.72	0.10	0.37	99.53	Zhu et al. (2009)
CY1-1	1.89	3.24	5.39	0.11	0.17	99.55	Zhu et al. (2009)
CY2-1	1.25	2.69	4.37	0.06	0.14	99.59	Zhu et al. (2009)
CY3-1	0.91	2.78	5.62	0.05	0.25	99.85	Zhu et al. (2009)
CY4-1	1.50	2.92	4.57	0.07	0.22	99.93	Zhu et al. (2009)
CY6-1	1.35	2.72	4.84	0.06	0.94	100.09	Zhu et al. (2009)
GBJD-1	1.34	3.30	4.99	0.16	0.75	99.19	Zhu et al. (2009)
GBJD-2	1.36	2.91	4.48	0.15	0.67	99.52	Zhu et al. (2009)
GBJD-3	1.35	2.98	4.82	0.16	0.67	99.52	Zhu et al. (2009)
PK01-1	1.33	2.74	5.10	0.15	0.41	100.33	Zhu et al. (2009)
PK01-2	1.29	2.73	5.25	0.13	0.50	99.96	Zhu et al. (2009)
PK01-3	1.27	2.71	5.25	0.13	0.50	100.13	Zhu et al. (2009)
PK01-4	1.30	2.83	5.51	0.14	0.33	99.64	Zhu et al. (2009)
PK01-5	1.40	2.91	4.69	0.12	0.42	99.56	Zhu et al. (2009)
PK01-6	1.20	2.57	5.24	0.13	0.50	99.95	Zhu et al. (2009)
MM02-2	10.05	3.85	1.69	0.48	2.67	99.99	Zhu et al. (2009a)
MM02-3	5.45	4.61	2.40	0.53	1.57	100.00	Zhu et al. (2009a)
MM02-4	7.62	3.30	1.87	0.30	1.47	99.98	Zhu et al. (2009a)
MM02-5	5.33	5.17	2.23	0.51	1.55	100.00	Zhu et al. (2009a)
MM02-6	4.18	2.56	1.92	0.26	2.22	100.01	Zhu et al. (2009a)
T203A	6.52	2.75	2.37	0.27		100.00	Zhu et al. (2009a)

Table A.4: Whole rock geochemistry (ICPMS - Trace elements) for Lhasa terrane and Himalayan literature samples. All measurements reported in ppm.

Sample	Rb	Sr	Y	Zr	Nb	Ba	Pb	Sc	V	Cr	Ni	Cu	Zn
NDG-01	8.00	171.00	14.00	23.00	1.00	25.00	3.00	48.00		538.00	92.00	24.00	27.00
NDG-02	9.00	168.00	11.00	14.00	1.00	28.00	3.00		210.00	720.00	88.00	22.00	31.00
NDG-03	13.00	167.00	28.00	56.00	2.00	47.00	4.00			213.00	50.00	29.00	33.00
NDG-04	4.00	186.00	19.00	48.00	2.00	30.00	3.00	44.00		107.00	18.00	19.00	
NDG-05	1.00	102.00	4.00	6.00	1.00	9.00	1.00		181.00	352.00	70.00	10.00	10.00
NDG-06	2.00	88.00	6.00	11.00	1.00	9.00	2.00			298.00	89.00	18.00	51.00
NDG-07	3.00	143.00	5.00	11.00	1.00	5.00	4.00	41.00		319.00	82.00	2.00	7.00
NDG-08	1.00	91.00	4.00	10.00	2.00	19.00	1.00		194.00	322.00	75.00	10.00	50.00
NDG-09	4.00	65.00	8.00	39.00	3.00	5.00	4.00	43.00		324.00	68.00	2.00	8.00
NDV-01	3.00	58.00	34.00	89.00	4.00	90.00	6.00	24.00		209.00	17.00	50.00	100.00
NDV-04	3.00	83.00	24.00	64.00	3.00	53.00	6.00	43.00		256.00	73.00	74.00	79.00
NDV-05	1.00	50.00	19.00	44.00	3.00	27.00	1.00	44.00	349.00	79.00	28.00	172.00	109.00
NDV-1S	1.00	67.00	32.00	119.00	3.00	22.00	0.00	36.00	413.00	30.00	14.00	7.00	29.00
NDV-2S	6.00	155.00	32.00	72.00	2.00	49.00	3.00	38.00		96.00	33.00	19.00	68.00
NDV-3S	4.00	154.00	21.00	51.00	3.00	23.00	5.00	41.00		287.00	60.00	144.00	76.00
NDV-4S	4.00	108.00	35.00	99.00	3.00	48.00	5.00	33.00		94.00	27.00	117.00	109.00
NN-13	2.00	124.00	6.00	12.00	1.00	4.00	3.00	36.00		179.00	130.00	32.00	37.00
NN-14	2.00	169.00	10.00	18.00	2.00	20.00	7.00	36.00		176.00	105.00	19.00	43.00
NN-15	3.00	157.00	7.00	10.00	2.00	29.00	4.00	43.00		140.00	101.00	23.00	41.00
NN-19	3.00	180.00	7.00	16.00	2.00	29.00	1.00			106.00	74.00	15.00	47.00
NV-01	4.40	55.00	29.00	64.00	3.00	144.00		24.00		181.00	19.00	81.00	76.00
NV-02	3.70	46.00	25.00	58.00	3.00	157.00		19.00		311.00	21.00	35.00	77.00
NV-03	6.70	50.00	30.00	66.00	4.00	164.00		21.00		210.00	27.00	40.00	73.00
NV-04	3.60	40.00	32.00	64.00	5.00	159.00		22.00		219.00	30.00	46.00	66.00
NV-05	3.20	50.00	30.00	71.00	4.00	163.00		19.00		150.00	18.00	94.00	97.00
NV-06	4.10	46.00	29.00	66.00	4.00	143.00		23.00		142.00	18.00	32.00	74.00
NV-07	3.20	45.00	27.00	64.00	4.00	152.00		23.00		140.00	26.00	61.00	93.00
NV-08	40.50	86.00	29.00	105.00	6.00	217.00		20.00		355.00	160.00	88.00	77.00
NV-09	4.70	52.00	33.00	70.00	4.00	148.00		21.00		223.00	18.00	74.00	94.00
NV-10	3.60	44.00	29.00	65.00	4.00	142.00		22.00		203.00	28.00	127.00	84.00
NV-11	3.20	54.00	28.00	71.00	4.00	135.00		22.00		207.00	18.00	77.00	89.00
93BG1	283.00	54.70	4.40	40.00	5.70	59.00	89.00						
93G18	290.00	67.70	8.90	40.00	6.20	134.00	86.00						
93G2	253.00	110.00	13.50	52.00	12.50	248.00	102.00						

Sample data continued

Sample	Ga	La	Ce	Pr	Nd	Sm	Eu	Gd	Tb	Dy	Ho	Er	Tm
NDG-01	16.00	1.49	3.70	0.71	3.58	1.29	0.69	1.28	0.29	2.11	0.47	1.18	0.20
NDG-02	12.00	1.15	2.53	0.59	2.75	1.11	0.59	1.07	0.25	1.84	0.41	0.99	0.16
NDG-03	15.00												
NDG-04	18.00	2.10	5.74	0.98	4.92	1.66	0.64	1.70	0.37	2.65	0.60	1.54	0.26
NDG-05	11.00	0.71	0.73	0.23	0.68	0.31	0.23	0.34	0.09	0.73	0.18	0.44	0.08
NDG-06	15.00	0.79	1.14	0.27	0.87	0.34	0.22	0.35	0.08	0.64	0.16	0.42	0.08
NDG-07	13.00	0.81	1.22	0.33	0.95	0.35	0.20	0.36	0.08	0.67	0.16	0.43	0.08
NDG-08	11.00	0.51	0.64	0.17	0.51	0.20	0.16	0.21	0.06	0.43	0.11	0.29	0.05
NDG-09	12.00	0.94	1.83	0.39	1.48	0.49	0.30	0.48	0.11	0.85	0.20	0.53	0.09
NDV-01	17.00	1.99	5.91	0.99	5.10	1.90	0.52	2.04	0.48	3.53	0.89	2.34	0.43
NDV-04	17.00	2.53	7.29	1.28	6.10	2.06	0.80	2.13	0.46	3.24	0.76	1.87	0.31
NDV-05	14.00	1.84	5.26	0.90	4.46	1.58	0.58	1.67	0.37	2.72	0.65	1.61	0.28
NDV-1S	19.00	3.73	11.73	1.89	9.01	2.73	0.71	2.88	0.60	4.29	1.00	2.54	0.42
NDV-2S	19.00	2.18	6.64	1.15	6.01	2.25	0.77	2.31	0.55	4.10	0.98	2.44	0.43
NDV-3S	18.00	2.31	5.72	0.95	5.70	2.40	0.75	2.67	0.56	2.57	0.60	1.52	0.27
NDV-4S	22.00	3.47	9.93	1.67	8.15	2.79	0.99	2.85	0.60	4.28	1.01	2.50	0.42
NN-13	11.00	0.68	0.99	0.34	0.94	0.43	0.27	0.42	0.10	0.73	0.17	0.41	0.07
NN-14	15.00	1.04	2.34	0.48	2.11	0.82	0.50	0.80	0.19	1.36	0.32	0.78	0.13
NN-15	14.00	0.71	1.31	0.30	1.20	0.48	0.34	0.47	0.11	0.79	0.18	0.44	0.07
NN-19	14.00	0.85	1.62	0.37	1.50	0.59	0.37	0.58	0.14	1.04	0.24	0.62	0.11
NV-01	11.00	3.09	9.02	1.44	7.47	2.77	0.93	2.91	0.63	4.77	1.12	2.91	0.50
NV-02	12.00	2.40	8.64	1.13	5.80	2.06	0.67	2.19	0.49	3.54	0.87	2.22	0.39
NV-03	11.00	2.82	8.33	1.36	7.10	2.49	0.83	2.84	0.60	4.51	1.10	2.89	0.52
NV-04	13.00	2.82	8.62	1.39	7.22	2.55	0.83	2.95	0.62	4.63	1.09	2.88	0.51
NV-05	12.00	2.92	8.43	1.31	6.50	2.34	0.76	2.53	0.53	3.89	0.89	2.33	0.40
NV-06	13.00	2.87	8.66	1.39	7.05	2.50	0.81	2.80	0.60	4.37	1.04	2.69	0.47
NV-07	12.00	2.68	8.39	1.36	7.05	2.40	0.80	2.75	0.57	4.20	0.98	2.57	0.44
NV-08	11.00	10.27	24.32	2.93	12.17	3.27	0.86	3.92	0.63	4.24	0.98	2.55	0.43
NV-09	13.00	3.38	9.97	1.58	8.05	2.93	0.93	3.14	0.69	5.10	1.21	3.10	0.54
NV-10	14.00	3.71	12.01	1.78	8.00	2.36	0.86	2.76	0.52	3.84	0.90	2.41	0.43
NV-11	13.00	2.85	8.06	1.38	6.98	2.44	0.83	2.71	0.57	4.26	0.98	2.57	0.45
93BG1		7.20	11.70			2.20	0.19		0.12				
93G18		6.30	12.30		6.50	1.40	0.29		0.32				
93G2		9.90	22.40		10.80	2.20	0.50		0.44				

Sample data continued

Sample	Yb	Lu	Th	U	Hf	Ta	Co	Source
NDG-01	1.20	0.18						Ahmad et al. (2008)
NDG-02	0.96	0.15						Ahmad et al. (2008)
NDG-03								Ahmad et al. (2008)
NDG-04	1.65	0.25						Ahmad et al. (2008)
NDG-05	0.51	0.08						Ahmad et al. (2008)
NDG-06	0.51	0.08						Ahmad et al. (2008)
NDG-07	0.51	0.08						Ahmad et al. (2008)
NDG-08	0.34	0.06						Ahmad et al. (2008)
NDG-09	0.59	0.09						Ahmad et al. (2008)
NDV-01	2.81	0.44						Ahmad et al. (2008)
NDV-04	2.06	0.31						Ahmad et al. (2008)
NDV-05	1.87	0.29						Ahmad et al. (2008)
NDV-1S	2.64	0.38						Ahmad et al. (2008)
NDV-2S	2.67	0.40						Ahmad et al. (2008)
NDV-3S	1.70	0.32						Ahmad et al. (2008)
NDV-4S	2.70	0.41						Ahmad et al. (2008)
NN-13	0.40	0.07						Ahmad et al. (2008)
NN-14	0.79	0.12						Ahmad et al. (2008)
NN-15	0.44	0.07						Ahmad et al. (2008)
NN-19	0.66	0.10						Ahmad et al. (2008)
NV-01	3.29	0.52						Ahmad et al. (2008)
NV-02	2.57	0.40						Ahmad et al. (2008)
NV-03	3.41	0.55						Ahmad et al. (2008)
NV-04	3.30	0.51						Ahmad et al. (2008)
NV-05	2.59	0.42						Ahmad et al. (2008)
NV-06	3.11	0.49						Ahmad et al. (2008)
NV-07	2.89	0.45						Ahmad et al. (2008)
NV-08	2.79	0.45						Ahmad et al. (2008)
NV-09	3.50	0.54						Ahmad et al. (2008)
NV-10	2.77	0.43						Ahmad et al. (2008)
NV-11	2.99	0.47						Ahmad et al. (2008)
93BG1	0.83	0.14	2.70					Ayres et al. (1997)
93G18	0.90	0.13	2.80	6.80				Ayres et al. (1997)
93G2	1.32	0.16	4.20	12.80				Ayres et al. (1997)

Table A.4: continued

Sample	Rb	Sr	Y	Zr	Nb	Ba	Pb	Sc	V	Cr	Ni	Cu	Zn
93G8	257.00	140.00	11.00	39.00	15.70	271.00	80.00						
93ZP3	314.00	41.50	8.50	27.00	9.20	54.00	69.00						
MA88.1	189.00	153.00	17.70	51.50	10.30	302.00	90.00						
MA97.3	248.00	75.50	13.20	40.00	9.70	166.00	90.00						
MN14	255.00	86.10	16.60	56.00	8.10	314.00	49.00						
PAN2	188.00	88.90	34.20	199.00	12.10	583.00	22.00						
DG01-1	237.00	38.30	58.10	332.00	15.90	315.00	30.90	5.54	11.70	6.14	6.29	10.70	80.30
DG01-2	229.00	26.30	61.50	320.00	16.20	327.00	28.90	5.63	10.10	5.29	3.25	6.53	58.80
DG02-1	205.00	26.50	65.20	342.00	17.00	485.00	44.70	4.53	2.64	2.18	0.82	7.26	72.30
DG03-1	253.00	45.00	51.50	469.00	16.00	481.00	26.70	10.90	7.63	2.56	1.35	3.80	9.79
DG05-1	179.00	92.80	59.50	443.00	15.80	403.00	36.20	13.40	33.60	10.50	5.35	17.70	88.50
GRC02-1	160.00	204.00	22.20	136.00	9.01	507.00	24.20	14.60	93.70	16.00	6.47	30.79	62.20
GRC03-1	28.04	491.00	33.00	170.00	10.10	252.00	7.63	29.30	277.00	27.20	14.90	43.60	115.00
GRC03-2	137.00	288.00	19.00	126.00	8.31	481.00	27.40	11.90	81.90	8.66	3.90	7.34	56.50
SZ01-1	120.00	146.00	27.00	153.00	9.63	770.00	23.30	14.20	87.00	15.30	4.71	10.10	74.70
SZ01-2	153.00	164.00	30.10	167.00	9.77	620.00	28.10	15.90	104.00	16.20	5.55	7.01	74.10
SZ02-1	106.00	194.00	32.90	188.00	12.30	559.00	25.20	22.80	130.00	55.00	11.20	14.70	83.40
SZ03-1	101.00	199.00	33.20	190.00	12.60	563.00	24.20	24.50	138.00	53.00	8.59	20.60	83.10
SZ04-1	112.00	178.00	31.80	185.00	12.10	542.00	27.60	23.00	135.00	50.20	8.54	16.80	82.00
SZ04-2	113.00	184.00	32.60	187.00	12.30	546.00	23.10	23.20	134.00	54.70	8.25	17.80	80.90
SZ05-1	129.00	235.00	22.70	142.00	9.46	424.00	28.00	15.00	108.00	15.90	5.14	10.80	63.40
SZ05-2	142.00	221.00	19.70	153.00	9.53	398.00	22.70	14.10	102.00	25.00	10.40	10.30	63.50
SZ05-2R	143.00	223.00	19.70	142.00	9.47	400.00	22.70	14.00	103.00	16.70	6.36	10.20	64.50
SZ06-2	144.00	249.00	25.00	147.00	9.34	431.00	30.10	14.70	106.00	15.20	5.40	9.75	62.60
SZ07-1	138.00	143.00	28.50	150.00	9.56	556.00	24.80	15.70	98.50	17.90	5.10	7.44	71.90
SZ09-1	28.61	390.00	27.70	139.00	6.57	131.00	8.12	26.20	186.00	102.00	57.00	31.30	76.00
SZ10-1	155.00	212.00	22.60	144.00	9.86	469.00	28.10	16.90	125.00	19.40	6.75	3.51	93.30
SZ10-2	147.00	208.00	18.00	144.00	9.51	447.00	50.70	14.70	104.00	15.60	5.04	8.31	90.60
SZ11-1	64.82	429.00	26.10	132.00	4.58	158.00	3.37	26.60	168.00	206.00	95.90	35.30	67.10
SZ12-1	31.44	297.00	28.10	132.00	5.01	148.00	14.70	27.40	188.00	201.00	94.70	32.80	73.30
SZ12-2	5.93	262.00	29.00	128.00	6.90	151.00	7.51	25.60	184.00	174.00	117.00	64.90	83.10
SZ12-3	41.37	431.00	26.50	124.00	4.62	178.00	4.39	26.50	177.00	214.00	94.00	49.90	73.30
ET023	85.90	1048.00	8.20	89.00	3.67	755.00	12.60						
ET025B	337.00	360.00	8.30	129.00	6.94	748.00	20.50						
ET025E	159.00	689.00	6.90	102.00	4.28	823.00	31.60						

Sample data continued

Sample	Ga	La	Ce	Pr	Nd	Sm	Eu	Gd	Tb	Dy	Ho	Er	Tm
93G8		9.40	18.70			2.60	0.51		0.39				
93ZP3		3.50	7.30		3.60	0.78	0.19		0.25				
MA88.1		11.10	22.40			2.90	0.71		0.54				
MA97.3		6.50	15.90		7.90	1.50	0.39		0.40				
MN14		12.70	29.10			4.40	0.78		0.88				
PAN2		41.00	84.10		37.10	7.00	1.23		1.09				
DG01-1	21.10	36.80	90.70	9.07	35.50	8.03	0.90	8.15	1.52	9.84	2.22	6.16	0.96
DG01-2	20.60	51.80	105.00	12.10	48.50	10.50	1.08	10.20	1.74	10.80	2.33	6.54	0.99
DG02-1	21.70	57.90	128.00	14.00	55.00	12.00	1.15	11.10	1.88	11.60	2.49	6.95	1.03
DG03-1	17.90	35.90	80.30	8.97	36.30	8.04	0.90	7.42	1.30	8.50	1.90	5.52	0.88
DG05-1	21.00	43.90	92.40	11.00	44.40	9.74	1.69	9.79	1.65	9.98	2.18	5.95	0.92
GRC02-1	17.10	30.90	59.00	6.20	22.00	4.34	1.04	3.98	0.62	3.69	0.79	2.14	0.34
GRC03-1	20.10	27.30	58.00	6.98	30.30	6.49	1.86	6.32	0.97	5.80	1.19	3.21	0.47
GRC03-2	15.70	30.50	56.30	5.75	20.10	3.83	0.90	3.50	0.54	3.20	0.68	1.89	0.30
SZ01-1	14.30	31.40	59.40	6.17	23.90	4.39	1.04	4.19	0.66	4.12	0.88	2.47	0.37
SZ01-2	16.00	29.90	60.10	6.60	25.70	5.19	1.20	5.00	0.80	4.76	1.01	2.78	0.41
SZ02-1	20.60	39.70	79.10	8.69	34.10	6.73	1.36	6.21	0.97	5.83	1.24	3.43	0.51
SZ03-1	20.10	40.70	80.80	8.89	35.50	6.86	1.41	6.39	0.99	5.94	1.26	3.53	0.51
SZ04-1	19.60	38.90	77.90	8.60	33.90	6.63	1.33	6.09	0.96	5.71	1.22	3.38	0.50
SZ04-2	19.20	39.30	78.20	8.76	34.20	6.63	1.36	6.18	0.97	5.81	1.23	3.43	0.51
SZ05-1	17.00	31.40	60.00	6.35	24.00	4.64	1.06	4.28	0.68	4.06	0.87	2.44	0.37
SZ05-2	17.20	33.90	63.40	6.56	24.60	4.62	1.02	4.15	0.64	3.72	0.77	2.16	0.33
SZ05-2R	17.30	34.40	64.50	6.65	24.60	4.67	1.02	4.16	0.63	3.75	0.77	2.16	0.33
SZ06-2	17.20	33.70	63.50	6.76	25.30	4.86	1.09	4.63	0.73	4.35	0.93	2.58	0.39
SZ07-1	19.10	31.60	57.50	6.05	24.00	4.69	1.01	4.58	0.74	4.61	0.99	2.81	0.42
SZ09-1	16.50	14.50	34.00	4.39	20.10	4.75	1.44	4.87	0.82	5.04	1.07	2.93	0.42
SZ10-1	17.90	30.10	63.60	6.09	23.20	4.26	0.92	3.94	0.64	3.92	0.85	2.35	0.34
SZ10-2	17.70	28.50	52.70	5.80	21.40	4.06	0.94	3.64	0.55	3.27	0.70	2.04	0.33
SZ11-1	15.20	9.90	23.40	3.15	14.30	3.84	1.29	4.17	0.73	4.59	1.00	2.75	0.40
SZ12-1	15.70	10.80	26.10	3.57	16.20	4.31	1.38	4.73	0.81	5.10	1.10	3.01	0.44
SZ12-2	16.50	13.40	31.70	4.30	19.70	4.83	1.43	5.01	0.85	5.26	1.12	3.06	0.45
SZ12-3	15.70	10.20	24.20	3.33	14.80	3.97	1.34	4.28	0.75	4.68	1.02	2.80	0.40
ET023		21.90	45.90	5.51	22.50	3.96	0.99	2.81	0.31	1.56	0.27	0.72	0.10
ET025B		26.80	50.80	5.43	19.60	3.09	0.79	2.43	0.27	1.24	0.21	0.60	0.08
ET025E		24.40	47.70	5.30	19.80	3.22	0.87	2.43	0.27	1.25	0.21	0.60	0.08

Sample data continued

Sample	Yb	Lu	Th	U	Hf	Ta	Co	Source
93G8	1.20	0.19	3.60					Ayres et al. (1997)
93ZP3	1.05	0.15	1.30	7.00				Ayres et al. (1997)
MA88.1	1.47	0.21	4.10					Ayres et al. (1997)
MA97.3	1.17	0.14	2.50	14.10				Ayres et al. (1997)
MN14	1.16	0.16	8.10					Ayres et al. (1997)
PAN2	3.90	0.58	15.90	2.90				Ayres et al. (1997)
DG01-1	6.16	0.91	27.90	5.37	9.09	1.50	1.97	Chen et al. (2013)
DG01-2	6.37	0.92	26.70	4.56	8.77	1.53	1.02	Chen et al. (2013)
DG02-1	6.63	0.95	29.50	7.21	9.40	1.61	0.43	Chen et al. (2013)
DG03-1	5.68	0.84	29.50	7.01	12.00	1.37	0.28	Chen et al. (2013)
DG05-1	5.77	0.87	22.20	4.99	10.30	1.32	7.07	Chen et al. (2013)
GRC02-1	2.18	0.34	21.80	4.68	3.89	1.01	12.20	Chen et al. (2013)
GRC03-1	3.02	0.45	4.28	0.87	4.00	0.60	28.00	Chen et al. (2013)
GRC03-2	1.94	0.30	22.70	3.54	3.64	0.96	9.57	Chen et al. (2013)
SZ01-1	2.56	0.38	25.30	4.37	4.16	1.10	12.00	Chen et al. (2013)
SZ01-2	2.71	0.40	21.40	4.20	4.54	1.08	12.40	Chen et al. (2013)
SZ02-1	3.31	0.49	17.80	2.69	5.11	0.98	16.80	Chen et al. (2013)
SZ03-1	3.39	0.50	18.60	2.78	5.20	1.01	17.10	Chen et al. (2013)
SZ04-1	3.27	0.48	17.70	2.68	5.00	0.96	17.30	Chen et al. (2013)
SZ04-2	3.34	0.49	18.00	2.73	5.10	0.98	17.00	Chen et al. (2013)
SZ05-1	2.50	0.38	21.50	4.60	3.96	1.05	12.20	Chen et al. (2013)
SZ05-2	2.26	0.34	23.40	5.00	4.26	1.10	11.50	Chen et al. (2013)
SZ05-2R	2.24	0.34	23.80	4.94	4.00	1.11	11.60	Chen et al. (2013)
SZ06-2	2.60	0.39	22.90	4.84	4.16	1.09	11.80	Chen et al. (2013)
SZ07-1	2.94	0.44	21.50	4.78	4.05	1.03	12.70	Chen et al. (2013)
SZ09-1	2.69	0.40	2.12	0.34	3.26	0.44	34.10	Chen et al. (2013)
SZ10-1	2.41	0.36	20.50	4.05	3.88	1.00	14.40	Chen et al. (2013)
SZ10-2	2.30	0.34	22.30	4.59	4.05	1.10	12.10	Chen et al. (2013)
SZ11-1	2.61	0.39	1.90	0.35	2.94	0.34	37.10	Chen et al. (2013)
SZ12-1	2.80	0.41	1.53	0.29	3.12	0.36	35.90	Chen et al. (2013)
SZ12-2	2.87	0.42	1.57	0.18	3.43	0.47	36.30	Chen et al. (2013)
SZ12-3	2.64	0.38	1.59	0.30	2.90	0.34	38.90	Chen et al. (2013)
ET023	0.65	0.09	8.83	2.52	2.54	0.30		Chung et al. (2003)
ET025B	0.56	0.09	19.20	5.13	3.74	0.46		Chung et al. (2003)
ET025E	0.53	0.08	14.20	5.09	3.42	0.33		Chung et al. (2003)

Table A.4: continued

Sample	Rb	Sr	Y	Zr	Nb	Ba	Pb	Sc	V	Cr	Ni	Cu	Zn
ET026C	66.80	902.00	6.40	108.00	2.93	713.00	18.40						
ET026D	61.40	1051.00	5.60	85.00	3.10	1032.00	22.80						
T016	78.70	921.00	5.40	210.00	3.01	537.00	29.30						
T041D	30.50	911.00	9.50	99.00	3.80	490.00	16.40						
T065C	81.30	1121.00	9.00	123.00	4.66	1008.00	47.90						
T081	48.20	1004.00	7.10	101.00	3.64	689.00	17.10						
202-20	174.00	249.00	29.30	215.00	6.20	1300.00	12.34		12.00				
202-22	66.00	863.00	25.80	377.00	4.40	659.00			134.00		41.00	15.00	60.00
202-33	56.00	926.00	27.10	325.00	3.50	446.00	5.88		189.00		40.00	24.00	102.00
99-5-11-1a	352.00	517.00	11.00	174.00	9.40	807.00	28.00		41.00		22.00	23.00	61.00
99-5-11-2	326.67	121.48	14.64	155.65	5.08	391.68	39.44		9.46				44.00
99-5-4-2	272.01	402.42	48.30	326.23	19.85	1140.00	22.91		37.16			35.49	77.00
99-5-5-4d	203.00	168.00	24.70	196.00	11.40	324.00	21.00		18.00				
99-5-7-2a	266.00	20.00	53.30	78.00	10.30	22.00	22.00						
99-5-7-3b	210.00	134.00	19.60	105.00	7.00	702.00	16.00		9.00				
99-5-9-3	318.62	235.71	18.93	157.77	15.41	790.13	18.65		19.72			16.02	
99-5-9-4a	164.00	73.00	9.90	112.00	15.70	174.00	34.00		8.00				34.00
99-7-26-1b	415.00	62.00	23.00	78.00	13.50	134.00	87.00		11.00				41.00
BD-3	444.00	144.00	18.20	131.00	22.00	376.00	39.72		8.00		55.00		50.00
BD-7	236.00	336.00	10.20	124.00	5.10	830.00	30.02		14.00		23.00		41.00
BD-8	190.00	97.00	13.80	73.00	5.80	392.00						10.00	
GL-1	111.00	346.00	21.60	151.00	6.00	479.00	18.54		92.00		128.00	14.00	61.00
GL-11	238.00	54.00	47.40	139.00	7.50	459.00	13.58						
GL-12	195.00	131.00	30.70	122.00	6.40	538.00	12.73		16.00				
ND-13	203.00	750.00	36.00	151.00	6.40	632.00			204.00		34.00	23.00	65.00
ND-14	218.00	281.00	20.50	66.00	12.70	475.00	33.00		9.00		20.00		
ND-15	278.00	334.00	24.00	193.00	13.90	623.00	32.00		28.00				46.00
ND-22	221.00	57.00	65.10	122.00	17.60	288.00	58.00						48.00
ND-3	244.00	334.00	35.20	289.00	22.00	586.00	29.00		39.00				63.00
ND-4	427.52	381.68	18.76	256.74	22.39	1200.00	5.24		28.88			11.73	
ND-9	186.00	423.00	56.50	257.00	26.30	878.00	23.09		35.00				55.00
QC14	435.00	290.00	31.00	279.00	48.00	956.00			28.00		6.00	5.70	63.50
QC17	392.00	106.00	44.00	121.00	26.00	311.00			8.00		17.00	3.50	30.90
QC18	335.00	113.00	44.50	104.00	17.30	330.00	41.00		7.00			11.00	37.00
QC19	409.00	56.60	60.00	89.00	23.00	148.00			4.00		2.00	4.70	37.20

Sample data continued

Sample	Ga	La	Ce	Pr	Nd	Sm	Eu	Gd	Tb	Dy	Ho	Er	Tm
ET026C		21.30	43.80	5.08	19.90	3.35	0.95	2.53	0.28	1.24	0.20	0.54	0.07
ET026D		21.60	46.70	5.64	22.40	3.67	1.06	2.59	0.27	1.13	0.19	0.52	0.06
T016		52.90	104.00	11.20	41.30	5.68	1.26	3.44	0.27	1.02	0.13	0.52	0.08
T041D		17.80	40.10	5.12	21.80	4.19	1.21	3.46	0.43	2.03	0.35	0.93	0.12
T065C		37.60	75.80	8.93	35.00	5.79	1.58	4.36	0.45	1.95	0.31	0.82	0.10
T081		13.10	28.40	3.47	14.40	2.79	0.84	2.23	0.29	1.33	0.22	0.59	0.07
202-20	15.00	57.80	91.00	10.40	35.30	5.53	1.26	5.01	0.77	4.50	0.93	2.72	0.44
202-22	2.00	32.40	57.60	7.81	32.50	6.19	2.07	6.01	0.86	4.66	0.94	2.58	0.37
202-33	21.00	26.70		7.38	32.00	6.43	2.16	6.29	0.92	4.96	0.97	2.66	0.38
99-5-11-1a	25.00	42.40	82.60	8.23	29.50	4.46	1.06	3.57	0.41	1.97	0.38	1.08	0.18
99-5-11-2	20.95	42.71	73.04	8.57	28.96	5.61	0.61	4.96	0.69	3.05	0.49	1.25	0.18
99-5-4-2	21.63	81.64	139.00	16.90	59.81	9.58	1.34	7.80	1.11	6.62	1.47	4.72	0.85
99-5-5-4d	16.00	43.80	80.30	8.03	27.80	4.90	0.70	4.28	0.62	3.81	0.84	2.58	0.41
99-5-7-2a	16.00	12.60	38.70	4.51	20.50	7.45	0.07	7.63	1.68	10.50	2.09	6.37	1.00
99-5-7-3b	14.00	34.80	68.50	6.93	24.20	4.08	0.61	3.11	0.54	3.37	0.68	2.18	0.34
99-5-9-3	20.32	32.46	51.92	5.77	19.17	3.58	0.59	3.68	0.64	3.58	0.64	1.57	0.22
99-5-9-4a	14.00	27.60	53.90	5.58	20.50	4.25	0.48	3.66	0.50	2.39	0.35	0.77	0.09
99-7-26-1b	20.00	16.10	39.00	3.90	14.40	3.41	0.26	3.13	0.68	4.07	0.78	2.24	0.37
BD-3	21.00	60.10	105.00	12.40	41.20	7.15	0.57	6.01	0.82	3.71	0.60	1.57	0.25
BD-7	22.00	40.90	67.60	7.57	25.80	3.87	0.78	3.16	0.38	1.85	0.33	0.94	0.13
BD-8	10.00	29.20	48.30	5.28	18.00	3.06	0.44	2.35	0.39	2.28	0.46	1.51	0.25
GL-1	17.00	41.30	67.40	7.84	27.40	4.68	1.18	4.63	0.69	3.84	0.79	2.20	0.33
GL-11	16.00	54.80	98.90	12.60	46.90	9.14	0.83	8.88	1.45	8.10	1.66	4.55	0.74
GL-12	16.00	29.30	50.30	6.08	22.00	4.30	0.85	4.59	0.80	4.72	1.02	2.84	0.47
ND-13	20.00	76.70	136.00	17.40	68.90	12.70	3.25	11.60	1.48	7.18	1.32	3.36	0.43
ND-14	15.00	16.10	30.40	3.23	11.70	2.81	0.50	2.78	0.48	2.97	0.62	1.97	0.31
ND-15	18.00	47.30	87.70	8.82	31.90	5.71	1.22	4.76	0.65	3.88	0.80	2.48	0.38
ND-22	17.00	31.80	63.60	6.93	27.10	6.99	0.49	7.44	1.44	9.21	2.04	6.77	1.05
ND-3	19.00	65.80	122.00	12.50	44.90	8.10	1.39	7.02	0.95	5.75	1.18	3.52	0.55
ND-4	18.62	66.54	100.75	10.77	33.62	3.60	0.94	2.69	0.39	2.52	0.54	1.83	0.32
ND-9	22.00	91.70	137.00	15.30	51.70	10.00	1.05	10.10	1.77	10.00	1.98	5.41	0.90
QC14	17.00	89.60	159.00	15.00	49.30	6.30	1.09	4.80	0.60	4.60	0.93	3.70	0.60
QC17	15.00	35.80	69.40	6.90	25.90	5.50	0.43	5.40	1.00	6.70	1.43	4.40	0.70
QC18	18.00	30.60	59.80	6.18	21.80	4.63	0.46	4.21	1.00	6.70	1.42	4.69	0.75
QC19	13.00	26.60	53.40	5.70	20.60	5.30	0.37	1.20	1.20	9.60	1.91	6.20	1.00

Sample data continued

Sample	Yb	Lu	Th	U	Hf	Ta	Co	Source
ET026C	0.44	0.06	7.49	2.65	3.11	0.18		Chung et al. (2003)
ET026D	0.38	0.05	8.86	2.34	2.64	0.18		Chung et al. (2003)
T016	0.46	0.05	7.84	0.99	5.07	0.36		Chung et al. (2003)
T041D	0.74	0.11	3.27	0.64	2.77	0.23		Chung et al. (2003)
T065C	0.61	0.09	17.90	4.02	3.22	0.31		Chung et al. (2003)
T081	0.46	0.06	3.68	0.76	2.97	0.23		Chung et al. (2003)
202-20	2.94	0.43	22.02	12.93			115.00	D'Andrea Kapp et al. (2005)
202-22	2.53	0.39	10.28	2.55			50.00	D'Andrea Kapp et al. (2005)
202-33	2.51	0.38	6.09	1.39			44.00	D'Andrea Kapp et al. (2005)
99-5-11-1a	1.15	0.18	19.50	3.37			58.00	D'Andrea Kapp et al. (2005)
99-5-11-2	1.10	0.16	34.10	7.84			1.00	D'Andrea Kapp et al. (2005)
99-5-4-2	5.34	0.67	95.50	14.21			2.00	D'Andrea Kapp et al. (2005)
99-5-5-4d	2.69	0.40	33.70	6.13			71.00	D'Andrea Kapp et al. (2005)
99-5-7-2a	6.26	0.86	28.30	5.28			2.00	D'Andrea Kapp et al. (2005)
99-5-7-3b	2.34	0.34	12.70	1.29				D'Andrea Kapp et al. (2005)
99-5-9-3	1.26	0.17	25.50	16.23			2.00	D'Andrea Kapp et al. (2005)
99-5-9-4a	0.46	0.05	13.40	2.12				D'Andrea Kapp et al. (2005)
99-7-26-1b	2.33	0.31	18.70	3.95			101.00	D'Andrea Kapp et al. (2005)
BD-3	1.60	0.24	62.39	10.27			6.00	D'Andrea Kapp et al. (2005)
BD-7	0.85	0.13	28.59	4.44			1.00	D'Andrea Kapp et al. (2005)
BD-8	1.77	0.28	17.80	3.68			2.00	D'Andrea Kapp et al. (2005)
GL-1	2.15	0.33	25.72	3.91			7.00	D'Andrea Kapp et al. (2005)
GL-11	4.57	0.66	33.67	3.39			1.00	D'Andrea Kapp et al. (2005)
GL-12	3.04	0.45	23.95	3.85			2.00	D'Andrea Kapp et al. (2005)
ND-13	2.83	0.39	4.93	1.77			18.00	D'Andrea Kapp et al. (2005)
ND-14	2.24	0.37	20.60	8.37			2.00	D'Andrea Kapp et al. (2005)
ND-15	2.51	0.39	24.40	5.61			3.00	D'Andrea Kapp et al. (2005)
ND-22	6.94	1.06	32.80	7.21				D'Andrea Kapp et al. (2005)
ND-3	3.60	0.52	31.30	6.31			75.00	D'Andrea Kapp et al. (2005)
ND-4	2.08	0.30	41.58	4.41			3.00	D'Andrea Kapp et al. (2005)
ND-9	5.57	0.76	18.09	4.84			4.00	D'Andrea Kapp et al. (2005)
QC14	4.40	0.60					3.00	D'Andrea Kapp et al. (2005)
QC17	4.60	0.63					2.00	D'Andrea Kapp et al. (2005)
QC18	4.91	0.70	39.70	21.30			2.00	D'Andrea Kapp et al. (2005)
QC19	6.30	0.85					2.00	D'Andrea Kapp et al. (2005)

Table A.4: continued

Sample	Rb	Sr	Y	Zr	Nb	Ba	Pb	Sc	V	Cr	Ni	Cu	Zn
QC2	331.00	122.00	25.00	221.00	31.00	331.00			13.00		6.00	1.50	45.10
QC4	335.00	37.40	21.00	37.00	19.00	91.00			2.00		5.00	2.30	22.50
QC5	599.00	115.00	18.00	27.00	23.00	361.00					4.00	1.70	11.00
YD-11	185.00	118.00	22.40	123.00	5.80	508.00	16.34		6.00				
YD-13	203.00	146.00	23.70	130.00	7.60	531.00	15.69		6.00				47.00
YD-33	153.00	250.00	24.80	170.00	6.90	1350.00	10.94		11.00				66.00
YD-37	178.00	122.00	21.10	124.00	6.00	863.00	15.87		7.00				
YD-7	199.29	238.66	17.36	166.51	5.81	776.82	16.56		22.43		29.00		35.00
YD-8	188.22	207.38	18.01	130.63	7.27	622.43	14.52		17.54				
98T57	101.00	15352.00	66.00	882.00	69.00	3421.00	167.00	4.50		17.00	1.90	1.40	251.00
99T132	676.00	1490.00	40.00	511.00	25.00	3209.00	93.00			123.00	117.00	65.00	7.00
99T134	479.00	552.00	14.00	197.00	23.00	1256.00	62.00			114.00	45.00	22.00	5.40
99T145	506.00	745.00	22.00	271.00	28.00	1594.00	54.00			68.00	44.00	29.00	7.10
99T152	586.00	843.00	23.00	352.00	29.00	1757.00	55.00			154.00	100.00	40.00	4.80
99T154	619.00	1556.00	27.00	428.00	24.00	2108.00	113.00			131.00	101.00	54.00	7.70
99T53	372.00	1377.00	20.00	1154.00	73.00	3648.00	167.00			124.00	68.00	26.00	6.50
99T56	455.00	1077.00	23.00	929.00	50.00	3574.00	116.00			129.00	74.00	23.00	7.30
99T57	353.00	1760.00	30.00	1534.00	106.00	5160.00	201.00			139.00	67.00	62.00	10.10
99T60	432.00	1028.00	18.00	786.00	43.00	3167.00	87.00			181.00	102.00	32.00	6.00
99T62	416.00	1907.00	22.00	679.00	53.00	3035.00	92.00			134.00	103.00	32.00	7.40
CHZ-1	880.00	810.00	36.10	1101.00	73.20	2989.00	166.00	18.80	136.00	313.00	186.00		
CHZ-10	529.00	861.00	35.50	965.00	75.00	3263.00	144.00	19.10	145.00	322.00	188.00		
CHZ-11	811.00	855.00	34.50	749.00	50.40	3287.00	125.00	19.50	142.00	357.00	194.00		
CHZ-12	795.00	790.00	37.40	853.00	80.60	2968.00	147.00	20.10	152.00	351.00	193.00		
CHZ-2	702.00	798.00	34.90	893.00	68.50	2939.00	116.00	18.30	137.00	299.00	176.00		
CHZ-3	784.00	704.00	32.20	806.00	66.30	2498.00	81.20	18.50	141.00	286.00	158.00		
CHZ-4	712.00	660.00	29.60	834.00	54.90	2134.00	82.40	18.60	147.00	297.00	172.00		
CHZ-5	781.00	739.00	32.90	884.00	57.90	2346.00	105.00	20.10	164.00	329.00	202.00		
CHZ-6	785.00	688.00	32.70	917.00	70.70	2151.00	158.00	17.40	134.00	269.00	151.00		
CHZ-7	871.00	844.00	35.50	983.00	65.80	3167.00	150.00	19.30	151.00	326.00	179.00		
CHZ-8	564.00	1072.00	35.40	1000.00	73.80	3819.00	166.00	18.20	137.00	316.00	174.00		
CHZ-9	538.00	911.00	35.60	935.00	70.90	3336.00	110.00	19.50	135.00	324.00	188.00		
Tl/03	611.00	1260.00	23.90	783.00	46.40	3051.00	101.50	20.30	140.00	342.80	187.90		
Tl/06	441.00	1371.00	19.90	990.00	63.00	2369.00	132.80	8.70	70.60	89.40	55.60		
Tl/08	598.00	1207.00	24.10	787.00	34.50	2537.00	89.40	14.80	114.30	239.20	124.50		

Sample data continued

Sample	Ga	La	Ce	Pr	Nd	Sm	Eu	Gd	Tb	Dy	Ho	Er	Tm
QC2	16.00	134.00	275.00	27.10	98.50	16.20	1.05	11.60	1.20	5.80	0.86	2.30	0.30
QC4	14.00	9.60	20.20	2.20	7.50	2.30	0.25	2.70	0.50	3.50	0.68	2.10	0.30
QC5	16.00	10.70	22.20	2.40	9.00	2.40	0.56	2.20	0.40	2.90	0.50	1.70	0.30
YD-11	14.00	32.60	61.30	5.90	20.00	3.35	0.68	3.19	0.55	3.22	0.70	2.16	0.37
YD-13	15.00	30.10	50.60	5.89	21.30	4.06	0.79	3.82	0.64	3.77	0.77	2.29	0.38
YD-33	15.00	64.40	98.50	10.80	36.50	5.41	1.24	4.96	0.74	3.95	0.81	2.41	0.38
YD-37	14.00	62.20	99.10	11.20	37.00	5.39	0.90	4.83	0.66	3.54	0.69	2.07	0.32
YD-7	15.82	32.88	53.45	6.19	21.04	3.49	0.83	3.23	0.48	2.70	0.56	1.65	0.27
YD-8	14.15	37.66	60.94	6.65	22.41	3.57	0.76	3.12	0.49	2.83	0.59	1.75	0.30
98T57		538.00	955.00	75.00	257.00	34.00	7.70	19.00	2.90	13.00	2.00	5.60	0.80
99T132		142.00	314.00	39.00	156.00	31.00	7.10	22.00	2.50	9.80	1.50	3.80	0.40
99T134		97.00	198.00	20.00	77.00	11.00	2.70	5.60	0.90	3.50	0.50	1.40	0.20
99T145		111.00	229.00	25.00	95.00	17.00	3.50	9.80	1.40	5.00	0.80	2.00	0.20
99T152		110.00	250.00	30.00	118.00	22.00	4.20	11.00	1.50	5.90	0.90	2.30	0.30
99T154		116.00	252.00	32.00	131.00	25.00	4.90	14.00	1.90	6.40	1.00	2.80	0.30
99T53		232.00	486.00	56.00	203.00	29.00	5.80	17.00	1.70	5.50	0.80	2.70	0.20
99T56		288.00	560.00	69.00	253.00	31.00	6.70	21.00	2.00	5.30	0.80	2.80	0.30
99T57		292.00	591.00	68.00	246.00	38.00	7.90	24.00	2.20	6.90	1.20	3.50	0.40
99T60		254.00	514.00	57.00	207.00	26.00	5.00	17.00	1.80	4.90	0.70	2.00	0.20
99T62		247.00	507.00	58.00	213.00	29.00	5.60	19.00	1.80	5.20	0.80	2.40	0.30
CHZ-1	27.90	139.00	351.00	54.70	244.00	46.40	6.83	26.20	2.43	9.56	1.44	3.33	0.41
CHZ-10	28.10	139.00	354.00	54.20	243.00	45.70	6.86	26.60	2.45	9.61	1.43	3.34	0.40
CHZ-11	26.60	138.00	336.00	53.10	237.00	45.10	6.75	25.90	2.37	9.14	1.38	3.16	0.38
CHZ-12	29.40	140.00	361.00	56.30	254.00	48.00	6.90	27.70	2.52	9.84	1.51	3.47	0.42
CHZ-2	27.20	138.00	352.00	54.80	247.00	45.70	6.72	26.00	2.43	9.50	1.42	3.24	0.39
CHZ-3	27.40	139.00	334.00	52.00	231.00	42.90	6.20	24.60	2.20	8.65	1.34	3.01	0.37
CHZ-4	24.90	123.00	290.00	45.10	199.00	36.80	5.36	21.10	1.97	7.81	1.23	2.86	0.35
CHZ-5	27.00	133.00	310.00	48.20	215.00	40.60	5.91	22.90	2.17	8.63	1.36	3.12	0.40
CHZ-6	27.40	143.00	329.00	50.30	221.00	40.40	5.80	23.20	2.17	8.67	1.37	3.12	0.40
CHZ-7	27.00	140.00	347.00	53.50	236.00	45.00	6.73	25.80	2.38	9.46	1.45	3.24	0.39
CHZ-8	27.10	141.00	344.00	52.10	234.00	43.70	6.68	24.90	2.31	9.13	1.39	3.21	0.39
CHZ-9	28.00	135.00	361.00	56.30	247.00	47.50	7.06	26.90	2.47	9.69	1.49	3.29	0.40
Tl/03	20.20	154.00	359.00	46.60	182.80	28.20	4.60	13.71	1.41	5.78	0.91	2.10	0.28
Tl/06	27.10	241.00	469.00	54.50	185.60	22.90	3.90	11.01	1.15	4.67	0.73	1.68	0.23
Tl/08	23.80	133.00	329.00	45.80	189.60	30.80	4.80	14.67	1.44	5.87	0.92	2.11	0.28

Sample data continued

Sample	Yb	Lu	Th	U	Hf	Ta	Co	Source
QC2	1.60	0.20					130.00	D'Andrea Kapp et al. (2005)
QC4	1.90	0.23						D'Andrea Kapp et al. (2005)
QC5	2.00	0.29						D'Andrea Kapp et al. (2005)
YD-11	2.60	0.39	20.44	3.00				D'Andrea Kapp et al. (2005)
YD-13	2.57	0.39	13.57	3.14				D'Andrea Kapp et al. (2005)
YD-33	2.63	0.41	15.85	2.79			2.00	D'Andrea Kapp et al. (2005)
YD-37	2.13	0.32	27.10	2.94			1.00	D'Andrea Kapp et al. (2005)
YD-7	1.87	0.30	28.50	9.01			2.00	D'Andrea Kapp et al. (2005)
YD-8	2.02	0.32	21.56	4.98			2.00	D'Andrea Kapp et al. (2005)
98T57	5.00	0.70	96.00	15.00	19.00	4.00	3.10	Ding et al. (2003)
99T132	2.30	0.30	129.00	18.00	13.00	1.60	30.00	Ding et al. (2003)
99T134	1.00	0.10	108.00	17.00	6.30	1.60	9.20	Ding et al. (2003)
99T145	1.40	0.20	145.00	21.00	8.50	2.40	9.50	Ding et al. (2003)
99T152	1.60	0.20	117.00	25.00	9.70	2.10	19.00	Ding et al. (2003)
99T154	1.70	0.20	116.00	8.40	11.40	1.90	22.00	Ding et al. (2003)
99T53	1.70	0.20	214.00	23.00	30.00	4.30	13.00	Ding et al. (2003)
99T56	1.80	0.20	223.00	12.00	26.00	5.20	13.00	Ding et al. (2003)
99T57	2.10	0.30	283.00	43.00	40.00	5.20	15.00	Ding et al. (2003)
99T60	1.20	0.20	160.00	5.20	24.00	3.70	15.00	Ding et al. (2003)
99T62	1.70	0.20	176.00	4.80	19.00	3.30	17.00	Ding et al. (2003)
CHZ-1	2.43	0.33	204.40	22.40	30.10	4.06	25.90	Gao et al. (2007b)
CHZ-10	2.31	0.32	139.30	24.50	26.50	4.17	25.70	Gao et al. (2007b)
CHZ-11	2.15	0.30	231.70	18.20	20.60	2.70	25.80	Gao et al. (2007b)
CHZ-12	2.50	0.35	198.60	24.00	24.40	4.54	25.70	Gao et al. (2007b)
CHZ-2	2.36	0.32	187.60	28.20	25.00	3.90	24.10	Gao et al. (2007b)
CHZ-3	2.27	0.31	154.00	23.70	23.30	3.77	23.80	Gao et al. (2007b)
CHZ-4	2.13	0.30	166.60	20.20	22.80	3.21	24.80	Gao et al. (2007b)
CHZ-5	2.40	0.34	202.30	23.30	24.20	3.37	27.00	Gao et al. (2007b)
CHZ-6	2.33	0.33	184.10	27.70	25.80	3.62	21.70	Gao et al. (2007b)
CHZ-7	2.34	0.33	219.10	23.90	26.60	3.59	25.00	Gao et al. (2007b)
CHZ-8	2.30	0.32	202.30	29.40	27.20	3.72	23.60	Gao et al. (2007b)
CHZ-9	2.36	0.32	213.50	21.90	26.20	3.88	25.30	Gao et al. (2007b)
Tl/03	1.69	0.24	183.10	17.00	21.01	2.49	32.70	Gao et al. (2007b)
Tl/06	1.37	0.19	145.10	16.00	25.80	3.24	11.60	Gao et al. (2007b)
Tl/08	1.70	0.24	152.00	13.60	21.63	1.89	22.10	Gao et al. (2007b)

Table A.4: continued

Sample	Rb	Sr	Y	Zr	Nb	Ba	Pb	Sc	V	Cr	Ni	Cu	Zn
Tl/10	790.00	1421.00	25.00	974.00	47.30	3340.00	127.50	17.30	131.30	370.00	236.90		
Tl/11	550.00	1564.00	25.20	994.00	48.80	3931.00	128.50	16.90	128.00	368.60	226.90		
Tl/13	391.00	1633.00	25.80	862.00	34.90	3452.00	107.70	17.60	119.70	320.90	174.80		
Tl/17	939.00	1004.00	28.60	966.00	54.20	2835.00	101.20	19.50	122.30	564.60	338.60		
Tl/18	576.00	1196.00	25.40	784.00	34.00	2531.00	85.20	15.00	124.30	239.10	132.30		
Tl/59	442.00	930.00	16.90	340.00	56.50	2869.00	109.50	7.70	65.00	75.90	51.00		
DZ-01	25.20	342.00	16.90	102.00	4.33	199.00	2.88	39.60	276.00	134.00	68.30		
DZ-02	3.11	308.00	15.60	63.80	2.78	68.40	2.75	40.60	240.00	631.00	209.00		
DZ-03	12.60	748.00	22.10	96.90	4.89	141.00	7.11	37.80	259.00	133.00	51.20		
DZ-05	20.60	482.00	17.50	85.40	3.22	273.00	4.86	29.90	190.00	166.00	66.80		
DZ-07	3.57	488.00	19.70	84.60	4.32	104.00	6.48	33.10	205.00	131.00	49.50		
DZ-10	18.50	488.00	20.20	79.80	4.82	366.00	6.87	36.80	231.00	142.00	55.10		
DZ-11	5.96	322.00	18.50	95.60	3.44	67.00	2.93	35.90	237.00	422.00	163.00		
DZ-13	4.29	258.00	17.50	81.20	3.33	34.80	1.93	39.60	266.00	181.00	68.30		
DZ-14	2.16	77.10	14.60	46.50	1.81	30.20	5.10	32.70	258.00	124.00	60.10		
DZ-16	2.55	163.00	15.20	45.80	1.97	29.10	3.15	39.20	277.00	194.00	69.80		
DZ-17	3.28	251.00	16.50	56.50	2.25	43.80	2.63	37.30	229.00	164.00	64.00		
DZ-18	1.79	225.00	16.80	52.70	1.95	31.60	1.91	40.10	250.00	181.00	70.30		
DZ-19	3.22	269.00	16.40	48.60	2.21	28.70	4.74	39.10	258.00	174.00	68.80		
DZ-20	2.99	381.00	17.00	56.40	2.19	72.60	4.56	37.20	226.00	163.00	64.20		
DZ-21	4.87	196.00	15.10	50.50	2.24	49.40	4.14	34.50	238.00	158.00	63.70		
DZ-22	9.41	274.00	17.70	50.10	2.67	78.70	4.32	37.90	250.00	167.00	67.50		
DZ-23	4.40	225.00	16.70	46.50	2.23	42.80	3.51	37.10	234.00	165.00	66.20		
DZ-28	19.80	577.00	24.30	124.00	7.64	336.00	9.42	35.90	264.00	109.00	45.40		
LKA-01	23.50	554.00	13.30	82.50	4.44	328.00	4.21	20.90	174.00	79.20	19.60		
LKA-02	21.10	677.00	12.40	93.40	4.08	300.00	5.75	19.00	197.00	96.60	21.10		
LKA-03	47.20	514.00	12.40	96.50	4.31	481.00	4.08	17.70	180.00	108.00	17.60		
LKA-04	0.74	171.00	20.90	57.70	4.14	11.60	3.18	32.20	258.00	134.00	57.20		
LKA-05	0.27	177.00	19.00	54.40	3.54	10.90	2.89	34.80	262.00	165.00	63.30		
LKA-06	264.00	364.00	16.60	35.30	2.39	23.40	3.59	35.60	260.00	424.00	133.00		
LKA-07	200.00	291.00	16.60	41.90	2.35	23.50	3.47	35.70	264.00	411.00	139.00		
LKA-08	313.00	201.00	17.00	44.70	2.23	49.30	2.63	35.40	254.00	408.00	123.00		
LKA-09	320.00	200.00	16.50	51.70	3.92	40.20	3.24	38.30	303.00	596.00	168.00		
LKA-11	218.00	290.00	18.80	79.00	3.62	19.40	1.38	39.10	289.00	545.00	211.00		
LKA-12	257.00	132.00	18.20	59.40	3.41	21.20	0.80	37.70	307.00	442.00	163.00		

Sample data continued

Sample	Ga	La	Ce	Pr	Nd	Sm	Eu	Gd	Tb	Dy	Ho	Er	Tm
Tl/10	22.10	200.00	452.00	57.20	218.70	31.20	5.47	15.46	1.57	6.33	0.98	2.16	0.29
Tl/11	22.30	200.00	456.00	57.00	217.10	31.00	5.47	15.21	1.56	6.33	0.97	2.16	0.28
Tl/13	20.60	165.00	364.00	44.80	168.60	24.60	4.73	12.96	1.40	6.02	0.98	2.35	0.31
Tl/17	20.50	156.00	397.00	56.50	241.30	42.70	5.93	20.00	1.89	7.28	0.54	2.42	0.32
Tl/18	23.80	138.00	337.00	46.80	196.10	32.00	4.93	15.27	1.51	6.12	0.96	2.20	0.30
Tl/59	24.10	204.00	418.00	47.20	165.40	21.80	3.91	10.51	1.08	4.29	0.64	1.42	0.18
DZ-01	16.50	12.10	24.10	3.43	14.60	3.38	1.18	3.64	0.56	3.39	0.70	1.97	0.28
DZ-02	13.70	7.50	14.80	2.24	10.10	2.66	0.86	3.21	0.50	3.29	0.68	1.84	0.26
DZ-03	16.90	10.80	22.90	3.50	15.90	4.02	1.56	4.47	0.71	4.48	0.93	2.65	0.37
DZ-05	15.90	9.59	20.00	3.04	13.20	3.28	1.01	3.61	0.57	3.44	0.73	2.09	0.29
DZ-07	14.50	9.88	19.80	2.94	13.20	3.33	1.53	3.86	0.61	3.81	0.81	2.34	0.33
DZ-10	14.80	10.60	21.80	3.29	14.60	3.69	1.34	4.18	0.68	4.15	0.86	2.38	0.33
DZ-11	14.60	9.58	18.20	2.71	11.90	2.99	1.05	3.55	0.58	3.58	0.76	2.07	0.30
DZ-13	16.30	12.00	22.90	3.25	14.20	3.52	1.25	3.88	0.60	3.64	0.75	2.14	0.30
DZ-14	17.50	6.98	13.90	2.14	10.00	2.61	0.93	3.03	0.48	3.11	0.62	1.77	0.25
DZ-16	14.40	7.50	15.00	2.28	10.50	2.56	0.81	3.05	0.50	3.19	0.66	1.89	0.26
DZ-17	15.30	8.35	16.10	2.46	10.70	2.96	1.29	3.23	0.54	3.25	0.70	1.91	0.27
DZ-18	15.20	8.27	16.10	2.48	11.10	2.84	1.19	3.36	0.52	3.38	0.69	1.95	0.28
DZ-19	14.40	7.76	14.90	2.34	10.60	2.77	1.13	3.22	0.52	3.34	0.69	1.96	0.27
DZ-20	15.10	8.58	16.60	2.47	10.90	2.88	1.33	3.49	0.53	3.44	0.69	1.94	0.28
DZ-21	14.40	7.92	16.00	2.30	10.40	2.58	0.88	3.08	0.46	3.09	0.61	1.73	0.24
DZ-22	14.60	9.86	19.60	2.82	12.40	3.27	1.16	3.60	0.56	3.62	0.72	2.04	0.29
DZ-23	14.70	8.13	16.20	2.43	10.90	2.89	1.14	3.38	0.53	3.41	0.70	1.97	0.27
DZ-28	18.60	17.10	33.70	4.71	20.20	4.98	1.69	5.27	0.81	4.99	1.02	2.85	0.41
LKA-01	17.40	13.50	29.30	3.93	16.80	3.79	1.06	3.39	0.48	2.68	0.52	1.38	0.20
LKA-02	20.00	12.00	27.40	3.72	16.30	3.75	1.19	3.35	0.47	2.53	0.49	1.27	0.18
LKA-03	18.70	12.70	28.40	3.83	16.60	3.71	1.17	3.38	0.46	2.51	0.48	1.26	0.18
LKA-04	16.50	8.76	20.80	2.94	13.40	3.46	1.20	3.82	0.63	3.91	0.84	2.35	0.34
LKA-05	16.50	8.27	18.70	2.61	11.80	3.05	1.25	3.44	0.56	3.51	0.75	2.13	0.31
LKA-06	12.60	6.14	14.40	2.09	9.64	2.61	0.87	3.09	0.50	3.13	0.66	1.81	0.26
LKA-07	14.80	6.23	14.50	2.08	9.62	2.60	1.03	3.08	0.50	3.09	0.66	1.82	0.26
LKA-08	14.20	6.09	14.00	2.02	9.34	2.52	0.94	3.04	0.50	3.14	0.67	1.86	0.27
LKA-09	14.20	8.43	18.80	2.60	11.60	2.99	0.94	3.37	0.53	3.20	0.66	1.78	0.25
LKA-11	17.90	11.30	24.20	3.19	13.80	3.33	0.76	3.70	0.59	3.61	0.75	2.07	0.30
LKA-12	21.10	4.46	11.70	1.78	8.48	2.80	0.68	3.58	0.61	3.77	0.76	2.03	0.28

Sample data continued

Sample	Yb	Lu	Th	U	Hf	Ta	Co	Source
Tl/10	1.65	0.23	130.70	14.00	26.32	2.50	27.60	Gao et al. (2007b)
Tl/11	1.65	0.23	131.90	9.60	26.45	2.50	26.60	Gao et al. (2007b)
Tl/13	1.87	0.27	112.00	10.90	23.27	1.83	24.50	Gao et al. (2007b)
Tl/17	1.88	0.26	224.30	22.00	27.02	2.90	36.20	Gao et al. (2007b)
Tl/18	1.74	0.24	150.80	13.70	21.72	1.89	19.30	Gao et al. (2007b)
Tl/59	1.07	0.15	153.00	14.50	12.29	2.86	10.70	Gao et al. (2007b)
DZ-01	1.84	0.27	1.05	0.60	2.55	0.25	41.00	Gao et al. (2008)
DZ-02	1.72	0.25	0.64	0.48	2.09	0.15	44.80	Gao et al. (2008)
DZ-03	2.36	0.34	0.87	0.64	2.66	0.28	29.60	Gao et al. (2008)
DZ-05	1.96	0.30	0.88	1.02	2.85	0.21	35.90	Gao et al. (2008)
DZ-07	2.17	0.31	0.71	0.47	2.29	0.26	27.80	Gao et al. (2008)
DZ-10	2.17	0.31	0.72	0.74	2.33	0.28	32.10	Gao et al. (2008)
DZ-11	1.93	0.29	0.54	0.34	2.52	0.19	35.20	Gao et al. (2008)
DZ-13	1.99	0.28	0.84	0.54	2.23	0.18	35.80	Gao et al. (2008)
DZ-14	1.58	0.23	0.59	0.51	1.52	0.11	35.30	Gao et al. (2008)
DZ-16	1.69	0.24	0.60	0.43	1.58	0.15	35.10	Gao et al. (2008)
DZ-17	1.70	0.25	0.77	0.29	1.59	0.14	32.00	Gao et al. (2008)
DZ-18	1.75	0.26	0.57	0.27	1.50	0.12	35.50	Gao et al. (2008)
DZ-19	1.81	0.26	0.55	0.39	1.44	0.14	34.40	Gao et al. (2008)
DZ-20	1.69	0.25	0.65	0.49	1.63	0.12	31.70	Gao et al. (2008)
DZ-21	1.56	0.24	0.70	1.17	1.45	0.14	31.50	Gao et al. (2008)
DZ-22	1.81	0.26	1.03	0.64	1.58	0.18	34.20	Gao et al. (2008)
DZ-23	1.75	0.26	0.68	0.39	1.46	0.13	33.40	Gao et al. (2008)
DZ-28	2.66	0.39	1.49	0.65	3.16	0.42	29.00	Gao et al. (2008)
LKA-01	1.20	0.17	1.07	0.38	2.28	0.24	31.80	Gao et al. (2008)
LKA-02	1.10	0.16	0.94	0.32	2.42	0.22	29.90	Gao et al. (2008)
LKA-03	1.10	0.16	1.00	0.34	2.48	0.23	27.00	Gao et al. (2008)
LKA-04	2.19	0.32	0.94	0.31	1.58	0.23	46.00	Gao et al. (2008)
LKA-05	2.00	0.30	0.87	0.30	1.50	0.20	34.20	Gao et al. (2008)
LKA-06	1.64	0.23	0.62	0.24	1.19	0.14	36.50	Gao et al. (2008)
LKA-07	1.67	0.24	0.68	0.30	1.30	0.14	38.00	Gao et al. (2008)
LKA-08	1.71	0.25	0.61	0.25	1.33	0.13	35.00	Gao et al. (2008)
LKA-09	1.57	0.23	0.75	0.38	1.55	0.20	29.30	Gao et al. (2008)
LKA-11	1.93	0.29	0.90	0.41	2.04	0.18	43.90	Gao et al. (2008)
LKA-12	1.69	0.24	0.79	0.38	1.61	0.18	36.00	Gao et al. (2008)

Table A.4: continued

Sample	Rb	Sr	Y	Zr	Nb	Ba	Pb	Sc	V	Cr	Ni	Cu	Zn
LKA-13	175.00	290.00	15.50	48.40	3.62	41.10	1.65	36.70	265.00	542.00	170.00		
LKA-14	18.50	315.00	12.70	35.80	2.51	37.30	1.03	35.90	240.00	844.00	261.00		
LKA-15	33.10	129.00	13.60	44.00	2.53	29.60	1.22	33.20	234.00	765.00	268.00		
LKA-16	42.60	290.00	16.10	52.40	3.41	43.40	1.14	36.40	284.00	605.00	190.00		
LKA-17	270.00	413.00	16.20	57.00	2.64	30.50	2.76	34.70	260.00	436.00	139.00		
LKA-19	419.00	298.00	15.90	42.20	2.70	17.90	1.66	39.30	286.00	559.00	189.00		
LKA-22	462.00	265.00	17.60	22.10	2.49	33.00	3.13	38.00	280.00	403.00	135.00		
LKA-24	457.00	270.00	18.00	22.00	2.50	31.00	3.33	37.90	282.00	407.00	136.00		
ML18-1	143.00	675.00	16.70	291.00	12.20	370.00	37.10	21.60	184.00	85.20	27.50	169.00	206.00
ML18-10	85.40	1223.00	9.59	157.00	9.56	1441.00	46.30	4.43	63.90	7.06	5.62	19.50	59.40
ML18-2	82.10	961.00	4.43	89.40	4.71	1094.00	43.10	2.65	33.50	3.87	3.04	10.30	34.30
ML18-3	72.20	1106.00	8.42	127.00	8.87	811.00	41.10	4.36	59.60	6.21	5.09	19.50	55.00
ML18-4	154.00	859.00	6.97	113.00	6.45	503.00	33.20	10.60	152.00	97.30	95.80	23.60	165.00
ML18-5	139.00	944.00	13.00	243.00	9.66	545.00	32.80	13.20	144.00	66.00	26.10	54.00	154.00
ML18-6	212.00	868.00	14.10	166.00	9.62	2801.00	66.00	15.50	145.00	61.70	20.70	22.20	146.00
ML18-7	75.20	1203.00	8.16	132.00	7.54	1027.00	41.10	4.53	59.10	7.14	5.71	13.80	56.60
ML18-8	110.00	1309.00	7.87	133.00	7.62	3120.00	53.40	3.88	53.20	5.94	4.97	17.10	50.80
ML18-9	79.00	1212.00	8.09	137.00	7.99	1344.00	44.20	3.50	47.60	8.36	4.86	21.70	44.80
1-Lt	391.00	41.00	9.69			133.00							
2-Lmt	348.00	66.00	9.78			193.00							
3-L2m	312.00	96.00	13.33			263.00							
G68	357.00	6369.00	56.80	787.00	75.90	6929.00	188.90	6.49	79.10	23.80	5.57	6.84	118.30
G006	158.00	317.00	4.17	92.60	5.33	729.00	29.20	8.44	55.50	46.80	29.80	19.00	21.50
G016	401.00	422.00	6.23	124.00	7.34	981.00	103.00	3.04	34.80	55.00	20.10	88.60	53.60
G019	369.00	448.00	5.51	109.00	8.05	783.00	68.60	3.95	42.20	42.70	23.90	124.00	47.50
G025	84.20	1003.00	6.18	185.00	4.98	461.00	31.50	6.46	48.00	56.80	28.10	53.50	63.20
G09	252.00	785.00	12.90	173.00	15.20	819.00	28.90	5.05	38.60	46.90	32.60	12.60	33.40
GUO37	92.80	1133.00	10.10	114.00	4.85	478.00	19.20	6.75	72.10	89.00	39.20	21.40	23.80
GUO48	88.30	1024.00	8.53	126.00	6.51	766.00	27.70	5.27	70.60	81.90	31.50	14.40	23.80
GUO51	188.00	689.00	8.90	122.00	7.83	762.00	29.10	4.88	45.10	52.20	16.50	10.30	25.20
GUO62	167.00	490.00	11.20	135.00	6.67	660.00	33.40	5.10	58.50	78.70	30.60	10.10	22.30
ZF09	135.00	819.00	11.00	130.00	7.76	840.00	35.20	5.95	41.90	59.00	18.90	10.30	26.40
ZFG17	188.00	889.00	10.10	167.00	5.34	845.00	40.90	4.82	57.50	57.90	20.00	13.90	24.40
G10	137.00	242.00	5.00	99.00	3.00	370.00							
G100A	348.00	104.00	24.00	165.00	13.00	250.00							

Sample data continued

Sample	Ga	La	Ce	Pr	Nd	Sm	Eu	Gd	Tb	Dy	Ho	Er	Tm
LKA-13	13.80	8.16	18.10	2.50	11.20	2.89	0.90	3.20	0.50	2.99	0.61	1.67	0.24
LKA-14	10.60	5.69	12.70	1.80	8.13	2.20	0.61	2.51	0.41	2.45	0.50	1.38	0.20
LKA-15	13.60	5.73	12.90	1.80	8.18	2.23	0.76	2.61	0.42	2.56	0.53	1.49	0.21
LKA-16	13.70	7.97	18.00	2.53	11.40	2.96	1.03	3.35	0.52	3.07	0.64	1.71	0.24
LKA-17	13.90	6.54	14.80	2.08	9.53	2.56	1.15	3.09	0.50	3.05	0.64	1.76	0.26
LKA-19	14.10	7.16	15.80	2.22	10.20	2.74	0.68	3.18	0.51	3.10	0.64	1.76	0.25
LKA-22	15.00	6.38	15.30	2.22	10.20	2.78	0.94	3.29	0.54	3.34	0.70	1.94	0.27
LKA-24	15.10	6.49	15.60	2.25	10.40	2.81	0.94	3.34	0.55	3.43	0.72	1.98	0.28
ML18-1	30.45	139.00	239.00	25.70	83.20	10.70	1.76	6.94	0.74	3.20	0.58	1.58	0.24
ML18-10	20.13	54.60	95.70	10.80	37.50	5.68	1.38	3.79	0.45	2.04	0.34	0.91	0.14
ML18-2	16.86	24.70	43.70	4.89	16.60	2.46	0.72	1.64	0.20	0.91	0.15	0.42	0.07
ML18-3	19.69	43.70	78.70	8.83	30.50	4.79	1.14	3.21	0.38	1.76	0.32	0.78	0.12
ML18-4	25.81	49.70	88.70	9.62	32.20	4.31	0.78	2.90	0.32	1.39	0.25	0.65	0.10
ML18-5	25.64	128.00	217.00	23.40	75.50	9.42	1.57	5.97	0.63	2.63	0.47	1.21	0.20
ML18-6	20.30	72.90	130.00	14.90	52.50	7.93	1.81	5.60	0.67	2.99	0.53	1.34	0.22
ML18-7	19.18	46.80	82.60	9.31	32.10	4.82	1.17	3.20	0.39	1.68	0.31	0.77	0.12
ML18-8	19.02	51.80	91.60	10.10	34.40	4.95	1.50	3.25	0.38	1.61	0.30	0.75	0.12
ML18-9	18.58	43.20	77.60	8.77	30.70	4.70	1.20	3.13	0.38	1.72	0.30	0.75	0.12
1-Lt		8.76	11.00		4.30	1.46	0.27	1.56		1.80		0.79	
2-Lmt		8.14	17.35		7.27	2.35	0.44	2.46		2.11		0.85	
3-L2m		13.37	21.30		9.16	2.88	0.48	2.77		2.46		0.92	
G68	26.40	348.00	589.00	57.20	166.00	27.30	5.38	15.70	2.01	9.58	1.65	4.37	0.61
G006	18.20	8.61	14.80	1.68	6.22	1.24	0.45	0.81	0.11	0.58	0.12	0.33	0.05
G016	17.10	30.90	56.70	6.70	23.40	3.15	0.81	1.88	0.23	1.13	0.21	0.56	0.08
G019	15.20	28.10	49.50	5.74	20.80	3.00	0.79	1.63	0.22	1.14	0.20	0.49	0.07
G025	16.10	36.00	69.30	7.62	26.50	4.14	1.19	2.66	0.30	1.30	0.22	0.59	0.09
G09	16.00	18.30	40.80	5.82	20.70	3.21	1.24	2.90	0.35	1.64	0.28	0.72	0.10
GUO37	17.20	18.10	36.90	5.01	19.20	3.77	1.23	2.89	0.36	1.78	0.32	0.82	0.12
GUO48	14.90	23.90	53.60	6.67	25.40	5.02	1.48	3.05	0.42	1.89	0.31	0.80	0.11
GUO51	16.70	27.10	45.60	5.83	18.40	3.55	1.68	2.31	0.30	1.54	0.28	0.70	0.11
GUO62	14.90	22.80	47.60	6.04	17.20	4.09	1.51	2.64	0.38	1.99	0.33	0.76	0.11
ZF09	18.60	32.60	55.10	6.84	26.90	5.47	1.89	3.10	0.43	2.32	0.39	0.91	0.13
ZFG17	16.80	18.20	35.60	4.71	19.30	3.64	1.38	3.93	0.36	1.72	0.31	0.78	0.11
G10					14.00	1.70							
G100A													

Sample data continued

Sample	Yb	Lu	Th	U	Hf	Ta	Co	Source
LKA-13	1.45	0.21	0.73	0.30	1.48	0.18	36.90	Gao et al. (2008)
LKA-14	1.19	0.18	0.55	0.23	1.15	0.13	44.50	Gao et al. (2008)
LKA-15	1.33	0.20	0.56	0.24	1.31	0.13	48.60	Gao et al. (2008)
LKA-16	1.50	0.22	0.62	0.28	1.54	0.16	37.70	Gao et al. (2008)
LKA-17	1.61	0.24	0.66	0.30	1.56	0.13	37.50	Gao et al. (2008)
LKA-19	1.51	0.21	0.63	0.24	1.20	0.13	45.30	Gao et al. (2008)
LKA-22	1.65	0.23	0.65	0.22	0.79	0.14	40.80	Gao et al. (2008)
LKA-24	1.68	0.24	0.65	0.24	0.79	0.14	41.90	Gao et al. (2008)
ML18-1	1.53	0.27	73.40	7.50	8.12	0.52	24.50	Guan et al. (2012)
ML18-10	0.84	0.12	30.80	3.41	4.07	0.59	6.38	Guan et al. (2012)
ML18-2	0.39	0.06	14.30	2.33	2.51	0.29	3.56	Guan et al. (2012)
ML18-3	0.74	0.11	24.80	4.01	3.42	0.52	6.07	Guan et al. (2012)
ML18-4	0.62	0.11	23.10	2.05	2.92	0.14	20.90	Guan et al. (2012)
ML18-5	1.10	0.20	68.60	5.99	6.29	0.37	19.10	Guan et al. (2012)
ML18-6	1.22	0.18	36.20	4.21	4.37	0.51	17.70	Guan et al. (2012)
ML18-7	0.67	0.11	25.90	2.68	3.34	0.46	6.23	Guan et al. (2012)
ML18-8	0.66	0.10	30.10	3.16	3.32	0.46	5.56	Guan et al. (2012)
ML18-9	0.70	0.11	26.30	3.99	3.52	0.50	4.83	Guan et al. (2012)
1-Lt	1.01	0.11	4.00	10.00				Guillot et al. (1995)
2-Lmt	0.70	0.12	4.00	11.00				Guillot et al. (1995)
3-L2m	0.82	0.13	5.00	6.00				Guillot et al. (1995)
G68	4.12	0.64	56.90	12.84	14.00	3.41	11.40	Guo et al. (2006)
G006	0.33	0.05	12.60	1.82	3.68	0.53	9.12	Guo et al. (2007)
G016	0.48	0.06	29.80	8.46	3.39	0.81	14.90	Guo et al. (2007)
G019	0.44	0.06	16.40	5.37	3.47	0.69	28.30	Guo et al. (2007)
G025	0.56	0.08	10.40	2.14	6.37	0.53	18.90	Guo et al. (2007)
G09	0.65	0.09	42.30	3.67	4.48	0.80	11.50	Guo et al. (2007)
GUO37	0.71	0.09	3.14	0.91	3.11	0.36	18.30	Guo et al. (2007)
GUO48	0.67	0.10	10.10	2.12	3.56	0.41	8.34	Guo et al. (2007)
GUO51	0.73	0.11	21.40	15.30	4.78	0.88	6.03	Guo et al. (2007)
GUO62	0.76	0.12	16.70	20.30	3.89	0.91	6.22	Guo et al. (2007)
ZF09	0.88	0.13	16.50	13.30	6.71	0.79	5.77	Guo et al. (2007)
ZFG17	0.68	0.11	21.60	4.11	4.15	0.37	8.66	Guo et al. (2007)
G10			21.00	4.00				Harris et al. (1988a)
G100A			55.00	4.00				Harris et al. (1988a)

Table A.4: continued

Sample	Rb	Sr	Y	Zr	Nb	Ba	Pb	Sc	V	Cr	Ni	Cu	Zn
G100C	169.00	128.00	39.00	182.00	18.00	260.00							
G100E	72.00	149.00	27.00	230.00		493.00							
G101A		310.00	29.00	200.00	10.00	350.00							
G101C		278.00	22.00	200.00		399.00							
G101E		278.00	24.00	210.00		414.00							
G101G		295.00	28.00	245.00	10.00	710.00							
G117A		19.00		370.00	16.00	140.00							
G117B		38.00		370.00	12.00	151.00							
G118A		140.00		410.00		168.00							
G118C	125.00	128.00	17.00	154.00	14.00	270.00							
G118D	129.00	137.00	23.00	137.00	14.00	280.00							
G118G	147.00	175.00	17.00	153.00	11.00	490.00							
G12	108.00	304.00	36.00	208.00	7.00	620.00							
G120A		167.00	21.00	167.00		717.00							
G121B		254.00	20.00	130.00		387.00							
G124A	198.00	262.00	35.00	212.00	16.00	450.00							
G124C	204.00	269.00	36.00	238.00	15.00	770.00							
G125A		207.00	21.00	290.00		766.00							
G15A	57.00	470.00	20.00	101.00	7.00	381.00							
G20	229.00	152.00	30.00	119.00	13.00	358.00							
G26	174.00	368.00	24.00	190.00	10.00	886.00							
G38E	220.00	345.00	13.00	147.00	25.00	250.00							
G4	58.00	645.00	19.00	127.00	6.00	623.00							
G40	331.00	224.00	22.00	225.00	10.00	480.00							
G41B	240.00	180.00	24.00	133.00	11.00	630.00							
G42A	236.00	303.00	14.00	225.00	8.00	330.00							
G42B	319.00	302.00	8.00	241.00	14.00	660.00							
G5	110.00	867.00	18.00	174.00	13.00	660.00							
G57A	319.00	64.00	26.00	140.00		484.00							
G60A	325.00	272.00	26.00	300.00	19.00	80.00							
G61A	353.00	221.00	19.00	236.00	15.00	532.00							
G64A	387.00	227.00	14.00	246.00	19.00	280.00							
G64C		276.00	27.00	292.00	24.00	540.00							
G66A		110.00	26.00	88.00	12.00	230.00							
G67A	168.00	296.00	24.00	119.00	12.00	290.00							

Sample data continued

Sample	Ga	La	Ce	Pr	Nd	Sm	Eu	Gd	Tb	Dy	Ho	Er	Tm
G100C													
G100E		68.00											
G101A													
G101C		43.00											
G101E		46.00											
G101G													
G117A													
G117B													
G118A													
G118C													
G118D													
G118G													
G12													
G120A		36.00											
G121B		19.00											
G124A		25.00	52.00		29.00	6.60	1.40		1.00				
G124C													
G125A		71.00											
G15A		21.00	41.00		21.00	4.30	1.20		0.68				0.34
G20		34.00	69.00		26.00	5.60	0.77		0.89				0.52
G26		53.00	101.00		36.00	6.00	1.30		0.75				0.36
G38E													
G4													
G40													
G41B													
G42A		90.00	167.00		54.00	7.20	1.00		1.10				
G42B													
G5													
G57A		45.00											
G60A													
G61A													
G64A		90.00	147.00		48.00	9.20	0.97		1.10				
G64C													
G66A		27.00											
G67A													

Sample data continued

Sample	Yb	Lu	Th	U	Hf	Ta	Co	Source
G100C			62.00	4.00				Harris et al. (1988a)
G100E								Harris et al. (1988a)
G101A			25.00	4.00				Harris et al. (1988a)
G101C								Harris et al. (1988a)
G101E								Harris et al. (1988a)
G101G			25.00	4.00				Harris et al. (1988a)
G117A			29.00	3.00	84.00	10.00		Harris et al. (1988a)
G117B			30.00	3.00	79.00	11.00		Harris et al. (1988a)
G118A			22.00	17.00	156.00	11.00		Harris et al. (1988a)
G118C			9.00	3.00				Harris et al. (1988a)
G118D			14.00	3.00				Harris et al. (1988a)
G118G			19.00	3.00				Harris et al. (1988a)
G12			6.00	3.00				Harris et al. (1988a)
G120A								Harris et al. (1988a)
G121B								Harris et al. (1988a)
G124A	2.90	0.49	14.00	7.00	6.70	1.70		Harris et al. (1988a)
G124C			26.00	4.00				Harris et al. (1988a)
G125A								Harris et al. (1988a)
G15A	2.10	0.34	4.00	0.97	3.90	0.44		Harris et al. (1988a)
G20	3.30	0.46	21.00	3.00	3.80	1.60		Harris et al. (1988a)
G26	2.80	0.42	17.00	3.40	5.50	1.20		Harris et al. (1988a)
G38E			78.00	5.00				Harris et al. (1988a)
G4			6.00	3.00				Harris et al. (1988a)
G40			73.00	4.00				Harris et al. (1988a)
G41B			28.00	4.00				Harris et al. (1988a)
G42A	1.50	0.25	73.00	8.90	6.90	3.00		Harris et al. (1988a)
G42B			52.00	4.00	5.30	0.92		Harris et al. (1988a)
G5			27.00	6.00				Harris et al. (1988a)
G57A								Harris et al. (1988a)
G60A			50.00	4.00				Harris et al. (1988a)
G61A			46.00	4.00				Harris et al. (1988a)
G64A	1.30	0.19			6.80	1.30		Harris et al. (1988a)
G64C			86.00	6.00				Harris et al. (1988a)
G66A								Harris et al. (1988a)
G67A			17.00	4.00				Harris et al. (1988a)

Table A.4: continued

Sample	Rb	Sr	Y	Zr	Nb	Ba	Pb	Sc	V	Cr	Ni	Cu	Zn
G68A	130.00	301.00	42.00	126.00	6.00	310.00							
G68B		115.00	40.00	310.00		459.00							
G69A	296.00	62.00	18.00	51.00		190.00							
G69C	391.00	64.00	14.00	61.00		152.00							
G71	303.00	112.00	21.00	119.00	16.00	270.00							
S70C	339.00	127.00	25.00	118.00	17.00	210.00							
S70D	264.00	236.00	18.00	175.00	10.00	750.00							
X45	174.00	300.00	26.00	127.00	10.00	370.00							
NM-1	128.00	997.00	11.00	134.00	9.00	1280.00	27.00		85.00	27.00	27.00	16.00	60.00
NM-2	174.00	635.00	9.00	166.00	12.00	672.00	15.00		46.00	38.00	51.00	26.00	40.00
NM-3	118.00	645.00	9.00	137.00	16.00	293.00	19.00		53.00		33.00	10.00	41.00
NM-4	105.00	1160.00	13.00	148.00	10.00	1110.00	31.00		117.00	41.00	40.00	48.00	90.00
NM-5	113.00	926.00	11.00	143.00	10.00	1180.00	21.00		75.00	35.00	30.00		49.00
NM-6	121.00	882.00	11.00	177.00	10.00	835.00	28.00		75.00	34.00	30.00		53.00
NM-7	192.00	743.00	11.00	183.00	9.00	1230.00	27.00		74.00	59.00	47.00	31.00	55.00
YANS-2	205.00	399.00	9.00	161.00	7.00	741.00	37.00		27.00				47.00
YANS-4	219.00	379.00	16.00	179.00	12.00	617.00	31.00		35.00				47.00
ZH-1-94	134.00	869.00	11.00	152.00	12.00	879.00	24.00		75.00	47.00	31.00	49.00	69.00
ZH-3-92	170.00	605.00	10.00	158.00	14.00	664.00	33.00		45.00	27.00	29.00	32.00	51.00
Cj-02	280.00	118.00	5.10	69.00	6.90	555.00		3.50					
Cj-20	195.00	309.00	5.10	91.60	6.90	711.00		3.50					
Cj-22	134.00	290.00	5.00	72.20	7.60	710.00		3.20					
Dzl-01	117.00	348.00	5.80	51.00	6.10	829.00		2.80					
Dzl-05	125.00	656.00	6.00	61.00	5.30	829.00		6.00					
Dzl-06	91.00	490.00	5.20	33.00	4.90	691.00		1.90					
Dzl-07	132.00	570.00	6.80	40.00	6.50	673.00		3.20					
Jm-16	434.00	239.00	8.00	111.00	7.10	742.00		3.50					
Jm-21	494.00	448.00	4.10	103.00	5.80	701.00		2.90					
Jm-23	494.00	282.00	5.50	108.00	7.50	701.00		4.00					
Jm-7	218.00	320.00	4.60	112.00	6.10	957.00		3.10					
Jmy-01	392.00	444.00	5.60	106.00	7.90	823.00		3.70					
Jmy-04	424.00	267.00	6.10	95.00	8.00	796.00		3.90					
Jmy-07	380.00	409.00	5.50	107.00	8.30	930.00		3.90					
Ng-16	51.00	729.00	4.30	95.00	4.90	770.00		2.60					
Ng-18	53.00	685.00	3.90	94.00	4.60	787.00		1.80					

Sample data continued

Sample	Ga	La	Ce	Pr	Nd	Sm	Eu	Gd	Tb	Dy	Ho	Er	Tm
G68A		19.00	40.00		23.00	6.20	1.10		1.20				
G68B		57.00											
G69A													
G69C		10.00											
G71		29.00	61.00		27.00	5.40	0.74		0.75				
S70C					38.00	8.10							
S70D		54.00	108.00		38.00	6.30	0.83		0.95				
X45													
NM-1	20.00	42.40	82.40	8.65	30.30	4.70	1.29	3.30	0.40	2.00	0.40	1.00	0.13
NM-2	19.00	38.60	77.80	7.77	26.50	3.90	0.97	2.60	0.30	1.60	0.30	0.80	0.12
NM-3	20.00	50.30	89.10	8.36	27.80	3.90	1.03	2.70	0.30	1.60	0.30	0.80	0.12
NM-4	22.00	42.60	88.30	9.33	34.50	5.50	1.59	4.00	0.50	2.50	0.40	1.20	0.17
NM-5	19.00	51.20	100.00	10.20	35.50	5.10	1.40	3.60	0.40	2.00	0.40	1.00	0.12
NM-6	20.00	57.60	106.00	10.50	36.70	5.40	1.37	3.60	0.40	2.00	0.40	1.00	0.13
NM-7	19.00	58.20	101.00	9.97	35.10	5.10	1.17	3.60	0.40	2.10	0.40	1.00	0.13
YANS-2	19.00	40.00	69.50	6.41	20.70	3.00	0.72	2.10	0.30	1.40	0.30	0.80	0.13
YANS-4	19.00	38.10	80.90	9.00	31.90	5.40	1.09	3.80	0.50	2.80	0.50	1.50	0.21
ZH-1-94	21.00	59.10	108.00	10.60	36.70	5.30	1.39	3.70	0.40	2.10	0.40	1.00	0.14
ZH-3-92	19.00	37.20	73.70	7.55	26.00	3.80	0.97	2.80	0.30	1.60	0.30	0.90	0.12
Cj-02		20.90	42.00	4.68	18.10	2.97	0.77	2.08	0.21	1.12	0.14	0.50	0.05
Cj-20		20.80	40.20	4.74	18.80	3.00	0.86	2.28	0.23	1.25	0.15	0.51	0.04
Cj-22		18.30	45.90	4.11	16.00	2.73	0.71	1.99	0.20	1.09	0.14	0.47	0.04
Dzl-01		18.60	37.70	3.97	16.60	2.51	0.69	1.89	0.21	1.08	0.17	0.51	0.08
Dzl-05		19.40	40.90	4.50	16.60	2.63	0.81	2.01	0.20	1.14	0.16	0.53	0.09
Dzl-06		17.80	37.80	3.88	14.30	2.29	0.65	1.75	0.17	0.99	0.13	0.47	0.06
Dzl-07		26.40	55.60	5.78	21.80	2.90	0.94	2.59	0.20	1.45	0.20	0.63	0.08
Jm-16		27.48	44.11	5.50	19.16	2.92	0.71	2.11	0.29	1.51	0.27	0.75	0.11
Jm-21		19.68	45.48	4.69	16.69	2.48	0.57	1.48	0.20	0.95	0.16	0.42	0.07
Jm-23		29.50	52.52	5.79	19.44	2.85	0.68	1.83	0.24	1.09	0.21	0.53	0.09
Jm-7		28.77	50.25	6.03	21.93	3.24	0.79	1.88	0.23	1.10	0.19	0.48	0.07
Jmy-01		28.24	48.24	5.66	19.86	3.05	0.73	1.90	0.25	1.12	0.21	0.57	0.09
Jmy-04		31.06	58.63	6.45	22.41	3.35	0.76	2.10	0.27	1.28	0.23	0.61	0.09
Jmy-07		25.17	51.64	5.77	19.94	2.98	0.76	1.91	0.25	1.17	0.20	0.56	0.09
Ng-16		19.60	45.70	4.84	18.90	3.08	0.84	2.08	0.20	1.02	0.12	0.42	0.03
Ng-18		17.10	41.70	4.41	17.50	3.02	0.82	2.03	0.18	0.93	0.10	0.36	0.02

Sample data continued

Sample	Yb	Lu	Th	U	Hf	Ta	Co	Source
G68A	3.90	0.68	7.30	3.10				Harris et al. (1988a)
G68B								Harris et al. (1988a)
G69A			8.00	4.00				Harris et al. (1988a)
G69C								Harris et al. (1988a)
G71	1.36	0.23	17.00	2.90	3.70	2.70		Harris et al. (1988a)
S70C			55.00	31.00	4.20	0.98		Harris et al. (1988a)
S70D	1.60	0.25	43.00	6.30				Harris et al. (1988a)
X45			22.00	4.00				Harris et al. (1988a)
NM-1	0.90	0.13	19.20	3.00	4.20	1.20	36.00	Harrison et al. (2000)
NM-2	0.80	0.13	25.90	7.10	5.10	1.40	20.00	Harrison et al. (2000)
NM-3	0.80	0.14	32.60	7.80	4.40	1.70	27.00	Harrison et al. (2000)
NM-4	1.00	0.16	13.70	5.50	4.50	1.20	39.00	Harrison et al. (2000)
NM-5	0.90	0.14	32.40	3.70	4.30	1.10	24.00	Harrison et al. (2000)
NM-6	0.90	0.13	26.10	3.70	5.60	1.20	27.00	Harrison et al. (2000)
NM-7	0.90	0.14	28.10	5.90	5.70	1.40	54.00	Harrison et al. (2000)
YANS-2	0.90	0.14	30.60	5.50	5.30	1.10	27.00	Harrison et al. (2000)
YANS-4	1.40	0.21	36.10	4.80	6.00	1.60	16.00	Harrison et al. (2000)
ZH-1-94	0.90	0.13	32.00	8.10	4.70	1.50	32.00	Harrison et al. (2000)
ZH-3-92	0.90	0.13	31.70	9.20	5.00	2.00	38.00	Harrison et al. (2000)
Cj-02	0.44	0.05	14.30	5.90	2.30	0.40		Hou et al. (2004)
Cj-20	0.44	0.04	11.40	2.90	3.00	0.30		Hou et al. (2004)
Cj-22	0.43	0.04	10.70	4.40	2.50	0.40		Hou et al. (2004)
Dzl-01	0.47	0.08	8.50	2.20	2.00	0.40		Hou et al. (2004)
Dzl-05	0.50	0.08	8.60	0.30	2.10	0.30		Hou et al. (2004)
Dzl-06	0.45	0.06	6.80	1.90	1.40	0.30		Hou et al. (2004)
Dzl-07	0.55	0.09	7.50	2.10	1.70	0.30		Hou et al. (2004)
Jm-16	0.69	0.12	24.60	8.30	3.30	0.50		Hou et al. (2004)
Jm-21	0.38	0.06	18.90	3.30	3.40	0.50		Hou et al. (2004)
Jm-23	0.55	0.09	12.00	5.80	3.50	0.50		Hou et al. (2004)
Jm-7	0.42	0.07	18.30	3.30	3.40	0.50		Hou et al. (2004)
Jmy-01	0.54	0.09	27.70	8.00	3.50	0.70		Hou et al. (2004)
Jmy-04	0.57	0.09	26.00	7.10	3.00	0.70		Hou et al. (2004)
Jmy-07	0.54	0.09	25.10	8.50	3.50	0.80		Hou et al. (2004)
Ng-16	0.39	0.03	7.20	2.20	2.90	0.20		Hou et al. (2004)
Ng-18	0.33	0.02	7.10	2.40	2.90	0.20		Hou et al. (2004)

Table A.4: continued

Sample	Rb	Sr	Y	Zr	Nb	Ba	Pb	Sc	V	Cr	Ni	Cu	Zn
Nmy-01	97.00	564.00	5.00	150.00	5.00	989.00		4.80					
Nmy-02	144.00	310.00	3.20	125.00	5.10	1000.00		3.80					
Nmy-04	134.00	599.00	4.20	98.00	5.90	884.00		3.80					
Nmy-05	137.00	421.00	3.40	106.00	4.70	789.00		3.90					
Nmy-07	149.00	501.00	5.00	88.00	4.50	892.00		3.60					
Nt-03	140.00	686.00	8.00	146.00	7.40	992.00		4.60					
Nt-05	148.00	538.00	6.60	134.00	7.20	868.00		3.30					
Nt-07	144.00	640.00	6.10	148.00	7.70	771.00		3.80					
Nt-08	138.00	586.00	6.20	150.00	7.70	813.00		3.80					
Nt-10	137.00	637.00	6.80	164.00	9.70	918.00		5.80					
Nt-12	112.00	592.00	5.90	158.00	7.40	878.00		4.40					
Nt-31	258.00	388.00	4.80	142.00	7.50	1206.00		4.30					
Nty-01	112.00	428.00	2.90	84.00	5.20	887.00		3.10					
Nty-04	89.90	523.00	2.90	64.00	3.40	723.00		2.00					
Nty-05	974.00	903.00	5.90	115.00	4.50	892.00		5.20					
Nty-08	194.00	358.00	3.20	102.00	5.30	1096.00		3.20					
Nty-11	918.00	632.00	3.40	85.00	4.00	632.00		3.50					
PI-18	41.00	469.00	6.20	102.00	6.30	785.00		3.10					
PI-28	120.00	500.00	6.90	102.00	8.00	621.00		4.70					
0321-08	2.55	252.00	63.90	308.00	13.30	40.40		50.50	420.00	40.30	18.70		
0321-09	3.02	268.00	57.80	305.00	15.00	37.20		48.30	436.00	36.50	15.20		
cb-154	162.00	340.00	6.21	102.00	5.13	457.00		3.43	17.80	6.56	3.32		
cb-167	146.00	380.00	5.77	117.00	4.65	527.00		4.18	22.70	8.16	3.64		
cb-168	150.00	365.45	6.44	116.00	4.77	461.00		4.05	24.20	9.30	3.84		
cb-172	142.00	390.91	6.03	115.00	4.34	564.00		3.71	21.80	8.03	3.50		
cb-178	147.50	363.18	6.22	112.50	4.80	407.50		3.76	22.85	9.15	3.77		
cb-189	146.00	399.09	6.64	114.00	5.02	600.00		4.17	21.00	7.26	3.05		
cb-193	156.00	363.64	6.11	110.00	3.73	464.00		3.91	21.30	6.19	3.09		
cb-206	220.00	353.00	8.03	121.00	10.10	451.00		5.43	33.00	34.20	19.10		
cb-207	220.00	233.00	13.00	133.00	7.85	340.00		9.95	63.50	55.30	24.50		
cb-208	258.00	296.00	10.20	135.00	9.33	444.00		6.51	40.20	43.50	24.80		
cb-209	195.00	338.00	9.13	133.00	8.58	468.00		6.14	35.70	37.40	22.00		
cb-210	225.00	363.00	11.70	139.00	9.18	492.00		8.20	52.20	49.80	28.00		
cb-211	151.00	403.00	10.40	142.00	11.00	507.00		8.23	42.50	24.90	7.50		
cb-213-2	196.00	296.00	8.55	116.00	8.11	412.00		5.32	30.20	30.90	17.90		

Sample data continued

Sample	Ga	La	Ce	Pr	Nd	Sm	Eu	Gd	Tb	Dy	Ho	Er	Tm
Nmy-01		17.39	34.40	3.93	14.27	2.45	0.69	1.64	0.21	1.04	0.18	0.48	0.08
Nmy-02		6.03	13.98	1.46	5.51	1.06	0.29	0.76	0.11	0.57	0.11	0.32	0.05
Nmy-04		18.40	34.20	4.06	15.23	2.43	0.64	1.49	0.17	0.84	0.16	0.40	0.06
Nmy-05		9.03	16.91	1.98	7.28	1.31	0.35	0.87	0.12	0.65	0.12	0.35	0.06
Nmy-07		15.89	28.49	3.48	12.60	2.08	0.60	1.45	0.18	0.91	0.17	0.46	0.07
Nt-03		19.93	53.64	6.77	25.59	4.49	1.05	2.91	0.39	1.68	0.32	0.81	0.12
Nt-05		18.98	43.28	5.56	21.02	3.45	0.75	2.19	0.31	1.43	0.25	0.65	0.10
Nt-07		27.70	58.27	6.26	22.51	3.57	0.87	2.25	0.31	1.40	0.23	0.59	0.09
Nt-08		25.64	51.00	5.58	19.75	3.17	0.80	2.02	0.27	1.19	0.21	0.54	0.08
Nt-10		29.77	67.47	7.10	25.90	4.09	1.04	2.55	0.34	1.56	0.27	0.66	0.10
Nt-12		27.81	54.03	5.65	20.35	3.23	0.81	2.06	0.28	1.36	0.23	0.60	0.09
Nt-31		26.27	46.83	5.48	19.10	2.92	0.66	1.80	0.22	0.99	0.17	0.46	0.07
Nty-01		5.52	11.20	1.35	5.71	1.04	0.29	0.70	0.11	0.53	0.11	0.30	0.05
Nty-04		8.64	17.00	2.09	7.70	1.27	0.35	0.85	0.11	0.53	0.10	0.27	0.05
Nty-05		19.18	40.42	4.89	18.58	3.06	0.84	1.03	0.24	1.19	0.23	0.57	0.09
Nty-08		8.26	20.80	2.33	8.78	1.50	0.34	0.92	0.12	0.63	0.12	0.33	0.06
Nty-11		14.19	26.81	2.96	10.65	1.68	0.48	1.06	0.15	0.72	0.13	0.35	0.05
PI-18		16.90	47.40	4.32	15.60	2.90	0.77	2.15	0.24	1.26	0.18	0.61	0.06
PI-28		33.10	64.50	7.74	29.40	4.82	1.13	3.39	0.32	1.64	0.22	0.68	0.07
0321-08		29.50	64.40	8.63	34.90	9.66	3.11	11.30	1.93	12.00	2.31	6.72	0.98
0321-09		27.50	59.80	7.68	33.00	9.27	2.96	10.90	1.83	11.30	2.28	6.52	0.96
cb-154		20.60	43.40	4.70	17.50	3.63	0.91	2.47	0.29	1.19	0.20	0.56	0.07
cb-167		28.90	59.30	6.43	23.40	4.63	1.15	2.97	0.32	1.24	0.20	0.53	0.07
cb-168		26.10	54.60	5.86	21.80	4.22	1.07	2.93	0.33	1.30	0.23	0.64	0.08
cb-172		28.60	58.90	6.39	23.40	4.67	1.18	3.14	0.35	1.33	0.21	0.57	0.06
cb-178		25.95	54.10	5.90	21.65	4.36	1.09	2.85	0.32	1.32	0.21	0.58	0.07
cb-189		27.00	56.30	6.07	22.30	4.55	1.10	3.08	0.33	1.35	0.22	0.59	0.08
cb-193		24.50	51.40	5.53	20.70	4.03	1.06	2.83	0.32	1.29	0.21	0.56	0.07
cb-206		28.00	55.70	6.00	21.50	4.26	1.16	3.26	0.37	1.67	0.29	0.79	0.11
cb-207		33.20	65.30	7.20	26.30	5.08	1.20	4.19	0.52	2.64	0.47	1.34	0.18
cb-208		32.60	66.90	7.18	26.20	5.32	1.06	4.06	0.46	2.15	0.38	1.03	0.14
cb-209		29.70	60.10	6.40	23.80	4.79	1.17	3.55	0.41	1.91	0.33	0.87	0.11
cb-210		32.30	65.20	6.93	25.10	5.02	1.25	3.80	0.46	2.28	0.43	1.18	0.16
cb-211		31.10	61.50	6.70	24.30	4.69	1.23	3.59	0.41	2.03	0.39	1.08	0.14
cb-213-2		31.20	63.30	6.71	24.40	4.78	1.05	3.58	0.40	1.88	0.31	0.87	0.12

Sample data continued

Sample	Yb	Lu	Th	U	Hf	Ta	Co	Source
Nmy-01	0.47	0.07	9.40	0.80	4.40	0.50		Hou et al. (2004)
Nmy-02	0.35	0.06	13.80	1.20	3.90	0.50		Hou et al. (2004)
Nmy-04	0.41	0.07	14.40	1.60	3.40	0.50		Hou et al. (2004)
Nmy-05	0.36	0.06	11.10	1.40	3.50	0.50		Hou et al. (2004)
Nmy-07	0.45	0.07	8.20	1.80	3.30	0.50		Hou et al. (2004)
Nt-03	0.72	0.11	14.50	2.80	4.40	0.50		Hou et al. (2004)
Nt-05	0.55	0.09	12.40	2.70	4.00	0.50		Hou et al. (2004)
Nt-07	0.50	0.08	22.80	5.30	4.40	0.50		Hou et al. (2004)
Nt-08	0.46	0.07	21.90	4.60	4.40	0.70		Hou et al. (2004)
Nt-10	0.54	0.09	19.90	4.70	4.90	1.00		Hou et al. (2004)
Nt-12	0.50	0.08	16.10	4.10	4.60	0.60		Hou et al. (2004)
Nt-31	0.42	0.06	34.90	6.40	4.10	0.50		Hou et al. (2004)
Nty-01	0.34	0.06	7.90	2.00	3.00	0.50		Hou et al. (2004)
Nty-04	0.30	0.05	5.50	2.40	2.60	0.50		Hou et al. (2004)
Nty-05	0.53	0.08	9.50	0.80	19.00	0.50		Hou et al. (2004)
Nty-08	0.38	0.07	11.90	0.90	4.00	0.50		Hou et al. (2004)
Nty-11	0.34	0.05	11.60	2.20	3.00	0.50		Hou et al. (2004)
PI-18	0.60	0.06	8.50	2.40	3.00	0.30		Hou et al. (2004)
PI-28	0.56	0.06	13.70	3.10	3.30	0.40		Hou et al. (2004)
0321-08	6.04	0.97	6.26	0.89	8.30	0.95	42.10	Hou et al. (2012)
0321-09	6.06	0.95	6.08	0.95	7.97	1.13	40.00	Hou et al. (2012)
cb-154	0.47	0.06	8.63	3.39	2.89	0.60	2.02	Hou et al. (2012)
cb-167	0.42	0.06	12.60	2.32	3.05	0.45	2.52	Hou et al. (2012)
cb-168	0.47	0.07	11.10	2.74	3.18	0.37	2.75	Hou et al. (2012)
cb-172	0.44	0.06	12.10	1.97	3.06	0.31	2.43	Hou et al. (2012)
cb-178	0.46	0.07	10.95	2.11	3.12	0.42	2.58	Hou et al. (2012)
cb-189	0.48	0.07	11.10	2.10	2.99	0.37	2.43	Hou et al. (2012)
cb-193	0.43	0.06	10.10	2.23	2.98	0.18	2.33	Hou et al. (2012)
cb-206	0.66	0.10	12.80	3.17	3.26	0.98	4.99	Hou et al. (2012)
cb-207	1.15	0.16	12.90	3.49	3.48	0.61	4.21	Hou et al. (2012)
cb-208	0.82	0.13	15.40	4.11	3.57	0.89	6.23	Hou et al. (2012)
cb-209	0.75	0.11	13.50	3.70	3.47	0.66	5.87	Hou et al. (2012)
cb-210	1.05	0.14	13.70	4.11	3.60	0.69	7.99	Hou et al. (2012)
cb-211	0.90	0.14	12.20	3.45	3.56	0.75	6.80	Hou et al. (2012)
cb-213-2	0.75	0.10	14.40	3.62	3.18	0.72	3.55	Hou et al. (2012)

Table A.4: continued

Sample	Rb	Sr	Y	Zr	Nb	Ba	Pb	Sc	V	Cr	Ni	Cu	Zn
cb-31	214.00	473.00	11.30	173.33	26.40	761.00		4.18	28.00	13.30	8.07		
cb-33	224.00	473.00	9.18	146.67	26.50	782.00		4.02	31.80	10.20	7.95		
cb-34	245.00	155.00	3.49	74.33	32.60	102.00		1.47	3.07	1.29	1.09		
cb-35	247.00	174.00	3.76	78.29	29.55	113.00		1.59	3.69	1.69	1.28		
cb-36	246.00	163.00	3.56	77.25	33.80	129.00		1.64	3.79	1.13	1.28		
cb-37	50.80	1242.00	9.23	105.00	5.33	408.00		6.17	64.80	4.81	7.19		
cb-38	221.00	153.00	3.41	62.50	31.70	124.00		1.37	3.42	0.66	1.10		
cb-77	190.00	331.82	7.43	125.00	7.05	468.00		5.03	34.50	34.20	19.80		
cb-77-1	185.00	314.55	7.90	130.00	7.00	449.00		5.24	34.60	52.40	24.10		
cb-77-2	182.00	346.36	7.33	123.00	7.20	427.00		4.97	32.70	35.20	20.30		
cb-77-3	192.00	313.18	8.19	121.50	8.32	454.50		5.29	35.10	37.30	20.60		
cb-78	201.00	324.55	7.53	115.00	7.06	463.00		4.85	31.20	36.10	20.00		
cb-79	192.00	317.27	8.33	125.00	6.30	448.00		4.86	32.90	37.10	19.60		
CMD-1	134.00	776.36	10.70	115.00	12.20	1009.00		5.96	66.70	26.30	17.10		
CMD-10	144.00	755.45	10.40	118.00	12.10	837.00		5.85	68.00	25.20	17.00		
CMD-16-1	127.00	678.18	12.80	138.00	9.14	874.00		6.63	46.60	15.00	20.60		
CMD-17	129.00	860.00	6.81	58.10	8.76	769.00		5.04	54.70	22.40	16.10		
CMD-18	109.00	831.82	7.64	82.50	10.20	648.00		4.12	49.40	18.40	14.90		
CMD-19	111.00	660.91	10.90	98.10	9.24	626.00		5.95	53.80	19.90	20.40		
CMD-20	121.00	851.82	6.66	62.50	8.98	753.00		5.62	56.40	22.90	16.70		
CMD-21	111.00	587.27	8.27	114.00	8.73	660.00		5.79	58.90	52.60	22.50		
CMD-30	133.00	840.91	10.60	130.00	11.50	915.00		6.51	72.70	27.90	18.80		
CMD-31	126.00	886.36	10.70	133.00	11.70	949.00		6.43	73.20	27.70	19.50		
CMD-32	130.00	802.73	11.20	147.00	12.70	1005.00		6.18	71.20	25.20	17.50		
CMD-33	134.00	810.91	9.71	146.00	10.80	999.00		5.86	66.40	23.60	17.20		
CMD-36	130.00	587.73	6.21	109.00	8.84	713.50		4.26	54.90	26.20	19.30		
CMD-37	156.00	462.73	3.86	96.80	5.81	670.00		2.95	39.60	20.50	13.50		
T0319-6	195.00	349.00	3.74	120.00	4.12	397.00		2.34	14.20				
T0319-7	244.00	310.00	6.86	119.00	4.57	357.00		3.37	25.50				
T0319-8	155.00	313.00	6.77	126.00	5.58	483.00		4.53	37.30				
T0319-9	152.00	338.00	6.16	124.00	4.61	503.00		3.49	26.30				
T0320-6	30.00	1564.00	6.24	41.50	1.16	112.00		1.40	6.40				
YX-10	159.00	295.91	8.19	131.50	5.68	451.50		4.53	33.00	20.05	7.34		
YX-11	152.00	330.91	8.24	136.00	5.10	494.00		4.56	33.40	18.70	7.29		
YX-12	167.00	301.82	7.44	120.00	5.27	450.00		4.51	29.80	16.90	6.56		

Sample data continued

Sample	Ga	La	Ce	Pr	Nd	Sm	Eu	Gd	Tb	Dy	Ho	Er	Tm
cb-31		68.90	126.00	11.40	35.70	4.94	0.90	3.43	0.41	2.03	0.37	1.12	0.15
cb-33		69.30	124.00	11.10	33.70	4.43	0.83	3.07	0.35	1.71	0.31	0.94	0.13
cb-34		19.90	35.90	3.29	9.53	1.12	0.27	0.74	0.09	0.48	0.10	0.34	0.06
cb-35		31.55	52.60	4.37	11.80	1.36	0.26	0.97	0.11	0.53	0.11	0.38	0.06
cb-36		20.20	35.80	3.25	9.29	1.15	0.26	0.83	0.09	0.53	0.10	0.36	0.06
cb-37		30.00	62.20	6.98	26.20	4.12	1.03	3.07	0.36	1.71	0.32	0.90	0.11
cb-38		21.60	36.10	3.13	8.80	0.98	0.24	0.76	0.09	0.46	0.10	0.34	0.06
cb-77		29.20	60.80	6.43	23.30	4.62	1.20	3.21	0.37	1.54	0.26	0.75	0.09
cb-77-1		24.20	49.60	5.35	19.20	3.89	1.20	2.89	0.36	1.57	0.27	0.80	0.09
cb-77-2		25.70	52.90	5.61	20.30	4.01	1.16	2.68	0.35	1.50	0.26	0.72	0.09
cb-77-3		26.20	54.15	5.78	20.90	4.21	1.10	2.98	0.37	1.57	0.28	0.78	0.10
cb-78		24.10	50.30	5.38	19.40	3.93	1.10	2.83	0.35	1.48	0.27	0.71	0.10
cb-79		27.40	57.30	5.96	21.70	4.44	1.22	3.22	0.39	1.75	0.30	0.83	0.11
CMD-1		50.30	98.30	10.20	34.80	5.17	1.25	3.51	0.45	1.99	0.37	1.03	0.14
CMD-10		50.20	94.40	9.65	32.50	4.98	1.20	3.23	0.42	1.82	0.34	0.96	0.13
CMD-16-1		33.00	55.70	5.34	17.30	3.07	1.01	2.71	0.42	2.30	0.45	1.22	0.17
CMD-17		24.70	42.50	4.29	14.70	2.31	1.07	1.81	0.24	1.21	0.24	0.73	0.10
CMD-18		34.60	59.90	5.88	19.10	2.71	1.00	1.76	0.26	1.21	0.23	0.75	0.11
CMD-19		57.80	100.00	9.67	30.90	4.36	0.99	2.92	0.39	1.80	0.36	1.10	0.15
CMD-20		24.10	40.80	4.15	14.30	2.27	1.02	1.71	0.23	1.15	0.23	0.67	0.10
CMD-21		55.50	94.50	8.61	26.70	3.71	0.94	2.46	0.34	1.53	0.29	0.83	0.11
CMD-30		51.40	98.70	10.10	34.30	5.31	1.26	3.46	0.45	1.94	0.36	0.98	0.14
CMD-31		52.50	101.00	10.40	35.50	5.47	1.33	3.60	0.45	2.01	0.35	1.03	0.14
CMD-32		53.30	106.00	11.10	37.30	5.69	1.38	3.83	0.48	2.04	0.38	1.08	0.14
CMD-33		48.90	93.00	9.58	32.50	4.87	1.22	3.32	0.41	1.85	0.34	0.94	0.12
CMD-36		51.90	78.00	6.86	21.15	2.89	0.85	2.01	0.25	1.14	0.20	0.59	0.08
CMD-37		49.40	71.90	6.01	18.00	2.19	0.67	1.47	0.18	0.68	0.13	0.36	0.05
T0319-6		22.30	43.30	4.62	17.00	3.55	1.07	2.54	0.26	0.96	0.13	0.38	0.05
T0319-7		29.60	60.10	6.83	25.10	5.16	0.86	3.16	0.29	1.61	0.27	0.73	0.10
T0319-8		39.70	80.50	9.37	35.10	6.98	1.10	4.37	0.40	2.27	0.37	0.98	0.13
T0319-9		33.30	67.20	7.62	28.30	5.48	0.99	3.26	0.28	1.54	0.24	0.67	0.08
T0320-6		7.17	12.70	1.39	4.64	1.26	0.74	1.38	0.21	1.04	0.18	0.50	0.07
YX-10		31.35	64.45	7.13	26.00	5.05	1.33	3.49	0.42	1.73	0.29	0.75	0.10
YX-11		34.10	69.50	7.59	28.00	5.37	1.42	3.68	0.43	1.77	0.28	0.77	0.10
YX-12		28.40	59.40	6.29	23.40	4.62	1.27	3.35	0.38	1.62	0.27	0.74	0.09

Sample data continued

Sample	Yb	Lu	Th	U	Hf	Ta	Co	Source
cb-31	1.12	0.17	91.50	17.50	5.53	2.48	3.50	Hou et al. (2012)
cb-33	0.87	0.14	77.70	15.70	4.97	2.56	3.97	Hou et al. (2012)
cb-34	0.51	0.09	33.10	11.80	3.77	3.40	0.38	Hou et al. (2012)
cb-35	0.52	0.10	33.10	16.65	3.88	3.23	0.24	Hou et al. (2012)
cb-36	0.51	0.09	35.00	21.30	3.93	3.47	0.27	Hou et al. (2012)
cb-37	0.75	0.11	9.14	2.76	2.99	0.35	9.61	Hou et al. (2012)
cb-38	0.49	0.08	25.00	24.10	3.15	3.20	0.30	Hou et al. (2012)
cb-77	0.60	0.09	13.20	2.97	3.23	0.49	4.85	Hou et al. (2012)
cb-77-1	0.61	0.10	11.40	3.15	3.40	0.57	5.67	Hou et al. (2012)
cb-77-2	0.58	0.09	11.90	2.66	3.17	0.59	5.09	Hou et al. (2012)
cb-77-3	0.64	0.10	12.40	3.35	3.11	0.68	5.30	Hou et al. (2012)
cb-78	0.65	0.09	11.60	3.02	3.08	0.70	4.77	Hou et al. (2012)
cb-79	0.72	0.10	13.60	3.25	3.27	0.51	4.95	Hou et al. (2012)
CMD-1	0.87	0.13	42.90	6.39	2.95	1.11	9.49	Hou et al. (2012)
CMD-10	0.83	0.12	30.80	6.07	2.96	1.10	9.35	Hou et al. (2012)
CMD-16-1	1.02	0.16	33.90	4.06	3.35	0.71	8.75	Hou et al. (2012)
CMD-17	0.66	0.11	9.77	5.79	1.65	0.76	9.14	Hou et al. (2012)
CMD-18	0.75	0.12	25.80	9.57	2.10	0.86	8.82	Hou et al. (2012)
CMD-19	0.98	0.15	43.80	3.99	2.62	0.85	9.46	Hou et al. (2012)
CMD-20	0.64	0.09	11.30	5.12	1.59	0.73	9.66	Hou et al. (2012)
CMD-21	0.79	0.12	43.80	7.81	3.07	0.81	8.82	Hou et al. (2012)
CMD-30	0.86	0.13	36.30	8.02	3.18	0.98	10.20	Hou et al. (2012)
CMD-31	0.85	0.13	31.30	7.66	3.19	1.00	10.40	Hou et al. (2012)
CMD-32	0.95	0.14	33.60	7.03	3.61	1.13	9.66	Hou et al. (2012)
CMD-33	0.84	0.12	36.40	7.63	3.47	0.93	9.26	Hou et al. (2012)
CMD-36	0.52	0.09	29.30	5.23	2.85	0.64	9.19	Hou et al. (2012)
CMD-37	0.38	0.06	35.80	5.41	2.59	0.39	6.34	Hou et al. (2012)
T0319-6	0.32	0.05	11.30	1.01	3.53	0.35		Hou et al. (2012)
T0319-7	0.60	0.08	10.60	2.31	3.30	0.38		Hou et al. (2012)
T0319-8	0.78	0.11	12.10	2.62	3.55	0.45		Hou et al. (2012)
T0319-9	0.54	0.08	11.60	2.39	3.53	0.42		Hou et al. (2012)
T0320-6	0.41	0.06	7.10	9.31	1.50	0.42		Hou et al. (2012)
YX-10	0.59	0.09	12.75	2.94	3.38	0.45	3.99	Hou et al. (2012)
YX-11	0.61	0.09	14.20	3.07	3.42	0.35	3.91	Hou et al. (2012)
YX-12	0.56	0.08	12.60	3.25	3.08	0.41	3.56	Hou et al. (2012)

Table A.4: continued

Sample	Rb	Sr	Y	Zr	Nb	Ba	Pb	Sc	V	Cr	Ni	Cu	Zn
YX-13	161.00	290.00	8.25	125.00	5.30	421.00		4.73	34.00	22.30	7.18		
YX-14	164.00	282.73	8.47	120.00	5.54	434.00		4.62	32.80	18.20	7.08		
07TB33a-1	91.40	716.00	16.00	143.00	7.60	366.00		13.20	138.00	50.00	27.00	74.70	72.10
07TB33a-2	41.30	937.00	13.40	57.00	4.00	297.00		16.80	220.00	86.00	48.00	78.30	111.00
07TB33b-1	102.00	693.00	17.50	97.00	8.30	357.00		14.60	143.00	45.00	41.00	336.00	70.20
07TB33b-2	87.10	735.00	16.60	127.00	8.20	437.00		13.80	136.00	43.00	27.00	79.00	73.40
07TB33c-1	42.40	656.00	10.50	43.00	0.80	144.00		20.80	165.00	18.00	11.00	46.60	66.60
07TB33d	20.20	745.00	10.80	41.00	1.20	128.00		24.20	203.00	23.00	12.00	30.20	80.50
07TB33e	82.40	762.00	15.80	155.00	7.10	393.00		14.10	144.00	55.00	31.00	49.30	73.30
Khan_1	62.72	717.61	38.82	200.72	6.82	298.07	8.03						
Khan_103													
Khan_104	22.00	368.02	11.88	16.49	0.62	53.06	2.05						
Khan_106													
Khan_108	9.17	399.92	12.23	15.31	0.51	45.26	2.99						
Khan_111	22.28	253.99	30.56	71.47	9.43	954.14	9.43						
Khan_16													
Khan_17													
Khan_18	73.40	282.31	14.60	32.57	1.37	75.80	2.78						
Khan_2	30.03	184.25	22.83	146.61	5.39	239.99	9.37						
Khan_20	261.28	676.36	90.72	551.32	37.63	2461.67	56.78						
Khan_33	78.44	306.88	24.97	54.59	3.89	166.69	8.32						
Khan_34													
Khan_38	66.38	216.62	22.35	78.10	6.64	377.96	7.11						
Khan_41	92.75	2542.70	123.57	259.06	50.25	722.90	20.14						
Khan_47													
Khan_52	2.16	477.39	9.22	16.15	0.60	85.93	1.66						
Khan_59													
Khan_61													
Khan_63													
Khan_67	382.95	1439.74	94.43	506.22	39.73	1670.89	32.62						
Khan_69													
Khan_70													
Khan_72													
Khan_76	12.50	1716.62	67.95	141.14	4.44	477.11	13.72						
Khan_8	259.55	3596.30	53.57	939.22	90.28	2950.86	64.24						

Sample data continued

Sample	Ga	La	Ce	Pr	Nd	Sm	Eu	Gd	Tb	Dy	Ho	Er	Tm
YX-13		32.50	67.30	7.24	26.40	5.10	1.30	3.67	0.43	1.76	0.29	0.76	0.09
YX-14		32.30	67.20	7.24	26.50	5.07	1.21	3.63	0.43	1.78	0.28	0.80	0.10
07TB33a-1	17.00	28.30	59.50	7.41	29.20	5.05	1.29	3.99	0.57	3.02	0.57	1.56	0.23
07TB33a-2	16.80	20.20	42.40	5.54	21.90	4.03	1.28	3.28	0.48	2.58	0.50	1.35	0.19
07TB33b-1	16.60	30.00	62.20	7.83	30.80	5.48	1.30	4.29	0.63	3.32	0.63	1.72	0.25
07TB33b-2	18.30	29.90	62.30	7.74	30.40	5.24	1.32	4.07	0.59	3.12	0.59	1.65	0.24
07TB33c-1	13.70	8.30	18.10	2.55	11.20	2.37	0.85	2.05	0.32	1.91	0.39	1.11	0.17
07TB33d	17.00	11.30	22.40	2.92	12.40	2.50	1.04	2.25	0.35	2.01	0.41	1.17	0.18
07TB33e	17.20	27.30	56.70	7.19	28.20	4.84	1.28	3.84	0.54	3.04	0.58	1.54	0.23
Khan_1		14.68	38.36	4.66	19.46	5.19	1.41	5.71	0.93	6.16	1.25	3.55	
Khan_103													
Khan_104		8.15	17.41	2.51	11.17	3.18	0.92	2.91	0.39	2.23	0.43	1.21	
Khan_106													
Khan_108		6.86	15.56	2.41	11.42	3.26	0.91	3.04	0.41	2.32	0.44	1.23	
Khan_111		11.75	26.75	3.11	10.85	2.98	0.33	3.18	0.59	4.07	0.90	2.84	
Khan_16													
Khan_17													
Khan_18		16.52	30.48	4.02	16.78	3.83	1.10	3.35	0.45	2.56	0.50	1.40	
Khan_2		16.04	33.72	3.85	14.09	3.17	0.90	3.21	0.52	3.32	0.70	2.11	
Khan_20		113.35	212.98	22.76	75.29	14.37	3.22	13.10	2.05	12.74	2.64	8.27	
Khan_33		10.66	24.42	3.47	15.12	3.92	1.14	4.36	0.70	4.34	0.89	2.44	
Khan_34													
Khan_38		15.37	30.30	3.34	11.68	2.64	0.79	2.85	0.47	3.09	0.68	2.13	
Khan_41		74.18	165.53	21.92	89.39	21.64	7.31	22.96	3.70	22.33	4.39	11.44	
Khan_47													
Khan_52		2.36	5.78	0.90	4.36	1.44	0.54	1.69	0.26	1.73	0.34	0.93	
Khan_59													
Khan_61													
Khan_63													
Khan_67		115.24	223.02	23.94	83.27	17.50	3.80	15.62	2.34	13.92	2.89	8.60	
Khan_69													
Khan_70													
Khan_72													
Khan_76		16.18	36.30	5.37	24.89	7.74	3.38	9.76	1.68	11.26	2.36	6.81	
Khan_8		189.47	393.74	43.23	149.77	26.44	6.66	19.38	2.33	11.31	1.79	4.45	

Sample data continued

Sample	Yb	Lu	Th	U	Hf	Ta	Co	Source
YX-13	0.62	0.09	13.80	3.08	3.14	0.46	3.95	Hou et al. (2012)
YX-14	0.65	0.08	13.90	2.80	3.01	0.48	3.82	Hou et al. (2012)
07TB33a-1	1.44	0.22	12.10	2.72	3.52	0.52	16.90	Jiang et al. (2012)
07TB33a-2	1.20	0.19	3.25	0.89	1.61	0.26	23.80	Jiang et al. (2012)
07TB33b-1	1.53	0.24	14.00	2.42	2.50	0.60	20.50	Jiang et al. (2012)
07TB33b-2	1.49	0.23	10.90	2.69	3.22	0.54	17.50	Jiang et al. (2012)
07TB33c-1	1.06	0.18	0.75	0.23	1.21	0.05	14.40	Jiang et al. (2012)
07TB33d	1.16	0.18	1.77	0.53	1.17	0.08	14.10	Jiang et al. (2012)
07TB33e	1.41	0.22	7.19	1.87	3.85	0.44	15.80	Jiang et al. (2012)
Khan_1	3.65	0.58	6.32	1.32	4.47	0.46		Khan et al. (2009)
Khan_103								Khan et al. (2009)
Khan_104	1.10	0.16	2.85		0.69	0.05		Khan et al. (2009)
Khan_106								Khan et al. (2009)
Khan_108	1.09	0.16	2.31		0.69	0.04		Khan et al. (2009)
Khan_111	3.41	0.55	21.26	5.16	2.72	0.93		Khan et al. (2009)
Khan_16								Khan et al. (2009)
Khan_17								Khan et al. (2009)
Khan_18	1.33	0.21	6.25		0.95	0.09		Khan et al. (2009)
Khan_2	2.41	0.40	10.08	1.47	3.39	0.39		Khan et al. (2009)
Khan_20	10.14	1.65	66.83	7.02	13.44	2.89		Khan et al. (2009)
Khan_33	2.20	0.32	2.88		1.53	0.25		Khan et al. (2009)
Khan_34								Khan et al. (2009)
Khan_38	2.52	0.40	9.10	1.64	2.10	0.59		Khan et al. (2009)
Khan_41	9.94	1.52	17.48		6.84	3.43		Khan et al. (2009)
Khan_47								Khan et al. (2009)
Khan_52	0.83	0.13	0.44	0.08	0.52	0.04		Khan et al. (2009)
Khan_59								Khan et al. (2009)
Khan_61								Khan et al. (2009)
Khan_63								Khan et al. (2009)
Khan_67	9.74	1.61	78.61	13.88	12.71	4.29		Khan et al. (2009)
Khan_69								Khan et al. (2009)
Khan_70								Khan et al. (2009)
Khan_72								Khan et al. (2009)
Khan_76	6.61	1.03	4.14		3.69	0.30		Khan et al. (2009)
Khan_8	3.70	0.54	55.55	7.07	19.88	4.96		Khan et al. (2009)

Table A.4: continued

Sample	Rb	Sr	Y	Zr	Nb	Ba	Pb	Sc	V	Cr	Ni	Cu	Zn
Khan_9	89.33	1671.79	155.58	300.28	23.35	1116.59	19.96						
Khan_96													
Khan_99													
ST055C	160.00	1066.00	29.00	139.00	7.80	657.00	32.60	20.70	230.00	54.40	28.90	12.00	164.00
ST057A	252.00	805.00	28.50	250.00	13.70	849.00	32.90	15.30	118.00	34.20	15.10	13.00	63.90
ST060C	426.00	378.00	39.70	254.00	24.60	219.00	23.60	11.60	30.30	6.90	5.10	2.50	63.80
T036D	19.70	746.00	14.70	12.10	2.20	229.00	3.91	21.80	214.00	38.60	24.00	50.00	68.50
T040A	110.00	453.00	24.80	127.00	10.00	545.00	19.80	14.70	73.10	2.30	2.40	8.60	59.10
T041F	21.30	703.00	15.40	31.90	1.90	275.00	7.51	19.40	203.00	1.80	7.30	21.30	63.50
T047	120.00	445.00	26.10	89.50	10.10	459.00	17.90	23.30	175.00	47.60	18.80	5.80	83.20
T054A	33.60	557.00	27.70	108.00	5.20	290.00	8.20	16.80	105.00	0.53	1.90	6.30	110.00
T065A	131.00	108.00	26.20	72.80	12.90	483.00	39.30	11.70	63.30	54.80	22.50	18.30	86.20
T065B	183.00	131.00	29.60	78.60	13.60	470.00	37.90	6.30	14.60	0.48	1.50	6.80	45.40
06FW101	100.00	197.00	27.16	108.00	9.11	415.00	13.82	4.35	23.53	2.66	1.85	1.62	24.47
06FW104	93.00	201.00	23.78	171.00	9.08	523.00	10.91	4.90	31.73	1.84	1.09	1.69	32.84
06FW105	154.00	315.00	21.38	171.00	10.33	661.00	25.90	6.82	54.85	9.17	5.14	4.20	42.89
06FW108	91.00	332.00	20.03	164.00	6.82	497.00	21.04	12.88	119.18	20.89	11.86	24.43	69.43
06FW110	202.00	143.00	29.89	132.00	9.18	380.00	15.51	4.30	19.93	1.59	1.25	3.56	20.24
06FW111	66.00	324.00	11.32	187.00	5.81	454.00	11.52	6.81	81.57	9.95	5.85	6.71	44.90
06FW112	20.00	386.00	24.55	98.00	7.08	370.00	13.27	11.93	151.34	13.31	7.23	27.82	64.66
06FW118	131.00	229.00	6.70	115.00	2.75	555.00	14.75	3.99	26.56	3.36	2.39	4.36	21.50
06FW119	119.00	476.00	13.10	179.00	5.19	690.00	13.70	10.93	124.42	19.20	10.53	13.31	62.11
06FW120	34.00	627.00	15.16	72.00	9.21	359.00	10.13	25.54	267.94	0.35	5.04	220.41	113.99
06FW121	120.00	371.00	1.54	98.00	0.68	1438.00	14.17	0.32	26.93	1.09	1.06	5.81	13.96
06FW126	78.00	919.00	31.13	378.00	15.70	850.00	10.04	11.79	128.44	12.24	7.69	26.05	96.08
06FW127	103.00	603.00	1.32	145.00	1.08	3084.00	18.11	0.18	11.10	1.06	1.07	3.86	7.69
06FW128	106.00	591.00	19.11	90.00	6.89	223.00	11.51	22.34	220.48	12.09	9.43	40.28	102.23
06FW129	65.00	942.00	25.33	339.00	13.52	1273.00	10.12	10.50	112.71	10.10	6.46	21.87	91.11
06FW131	225.00	454.00	7.28	135.00	7.18	632.00	52.53	3.36	33.85	3.46	3.46	26.09	35.33
06FW133	289.00	568.00	11.59	207.00	14.62	752.00	47.56	5.00	56.87	15.07	9.25	4.31	32.54
06FW134	302.00	434.00	7.52	135.00	11.13	617.00	65.44	3.02	35.97	7.50	5.09	5.79	44.14
06FW139	216.00	874.00	14.82	411.00	20.24	943.00	31.15	7.44	91.60	17.13	9.60	36.83	116.16
06FW140	181.00	417.00	9.53	115.00	8.21	750.00	36.03	3.28	29.17	1.87	2.10	21.99	45.57
06FW146	4.00	865.00	13.54	30.00	1.39	200.00	4.84	12.73	189.90	16.67	12.01	23.17	89.93
06FW147	58.00	559.00	18.78	173.00	5.22	452.00	17.61	12.26	132.75	12.79	9.15	45.77	73.56

Sample data continued

Sample	Ga	La	Ce	Pr	Nd	Sm	Eu	Gd	Tb	Dy	Ho	Er	Tm
Khan_9		62.48	154.23	19.53	81.38	22.36	6.41	24.08	3.84	25.27	5.09	14.66	
Khan_96													
Khan_99													
ST055C	21.10	46.80	93.50	10.30	41.30	8.22	2.19	7.22	1.04	5.35	1.01	2.72	0.38
ST057A	21.00	58.60	117.00	12.40	46.60	8.60	2.23	7.26	1.00	5.05	0.96	2.68	0.38
ST060C	19.30	89.20	198.00	17.80	62.10	10.70	1.15	8.92	1.25	6.46	1.26	3.61	0.54
T036D	18.90	7.96	19.00	2.66	12.60	3.05	1.01	2.98	0.48	2.67	0.56	1.54	0.21
T040A	18.70	30.30	61.90	7.09	27.50	5.37	1.31	5.01	0.74	4.00	0.82	2.30	0.33
T041F	19.80	8.46	19.10	2.62	12.10	2.86	1.13	2.80	0.45	2.58	0.54	1.50	0.21
T047	24.50	26.30	55.30	6.64	27.60	5.79	1.54	5.65	0.86	4.69	0.96	2.61	0.35
T054A	19.50	18.10	40.70	5.35	23.80	5.49	1.66	5.47	0.88	4.95	1.03	2.85	0.40
T065A	15.80	35.30	70.60	7.85	29.10	5.46	1.06	5.13	0.77	4.22	0.87	2.48	0.36
T065B	15.80	36.00	65.30	8.39	30.70	5.55	0.81	5.28	0.79	4.40	0.95	2.82	0.43
06FW101	14.45	29.70	58.95	6.90	25.45	4.86	0.78	4.26	0.69	4.46	0.92	2.70	0.44
06FW104	14.57	28.80	52.66	6.54	24.04	4.48	0.78	3.96	0.61	4.04	0.81	2.39	0.38
06FW105	15.97	40.23	74.76	8.17	29.49	5.00	1.09	4.21	0.61	3.84	0.74	2.13	0.33
06FW108	17.00	23.91	48.46	5.70	21.63	4.31	1.01	3.95	0.59	3.65	0.71	1.97	0.29
06FW110	13.39	24.80	50.82	5.90	22.90	4.63	0.61	4.23	0.70	4.87	0.98	2.94	0.48
06FW111	15.91	20.80	37.50	4.08	13.96	2.41	0.71	2.06	0.30	1.90	0.39	1.15	0.19
06FW112	17.15	15.45	31.82	4.69	19.25	4.24	1.02	3.97	0.63	4.16	0.87	2.49	0.38
06FW118	11.04	13.63	25.88	2.79	10.16	1.79	0.61	1.41	0.21	1.20	0.23	0.61	0.10
06FW119	15.86	17.44	33.38	3.80	13.98	2.93	0.83	2.41	0.37	2.13	0.45	1.21	0.19
06FW120	19.32	28.96	55.28	6.64	25.64	5.14	1.34	3.98	0.56	2.81	0.55	1.37	0.21
06FW121	9.48	4.42	5.51	0.48	1.48	0.22	0.30	0.21	0.03	0.18	0.04	0.16	0.03
06FW126	20.62	45.68	97.73	12.27	46.95	8.95	2.08	6.70	0.96	5.34	1.07	2.87	0.45
06FW127	7.65	4.77	7.18	0.60	1.91	0.28	0.43	0.24	0.03	0.17	0.04	0.14	0.03
06FW128	17.81	13.80	28.64	3.63	14.67	3.54	1.01	3.10	0.50	3.00	0.66	1.84	0.29
06FW129	20.24	42.50	90.86	11.70	44.89	8.53	2.08	6.19	0.88	4.69	0.93	2.44	0.37
06FW131	17.33	27.26	49.16	5.05	17.18	2.80	0.65	1.90	0.24	1.22	0.23	0.60	0.09
06FW133	19.29	52.92	100.03	10.57	34.95	5.74	1.05	3.72	0.44	2.12	0.38	0.99	0.15
06FW134	18.33	45.51	75.36	7.16	22.51	3.38	0.69	2.25	0.26	1.31	0.23	0.64	0.09
06FW139	24.30	136.48	283.36	31.47	102.59	13.90	2.41	8.21	0.84	3.55	0.53	1.26	0.15
06FW140	17.09	23.07	43.32	4.74	16.21	2.78	0.60	1.91	0.27	1.46	0.29	0.80	0.13
06FW146	18.16	9.61	22.75	3.17	13.42	3.37	1.29	2.85	0.43	2.35	0.51	1.30	0.19
06FW147	16.60	17.44	36.84	4.75	17.98	4.13	1.01	3.40	0.54	2.95	0.66	1.81	0.28

Sample data continued

Sample	Yb	Lu	Th	U	Hf	Ta	Co	Source
Khan_9	14.99	2.29	24.22	2.51	8.70	1.55		Khan et al. (2009)
Khan_96								Khan et al. (2009)
Khan_99								Khan et al. (2009)
ST055C	2.37	0.36	10.10	2.12	3.80	0.56	25.20	Lee et al. (2009)
ST057A	2.43	0.36	27.30	4.83	6.07	1.03	9.20	Lee et al. (2009)
ST060C	3.56	0.54	54.50	8.24	7.12	1.93	3.20	Lee et al. (2009)
T036D	1.37	0.20	1.48	0.23	0.62	0.12	29.80	Lee et al. (2009)
T040A	2.15	0.32	0.88	2.51	3.36	0.71	7.80	Lee et al. (2009)
T041F	1.38	0.21	8.33	0.13	0.97	0.10	23.00	Lee et al. (2009)
T047	2.24	0.31	0.57	1.03	1.92	0.59	16.70	Lee et al. (2009)
T054A	2.61	0.39	1.21	0.70	2.86	0.31	13.60	Lee et al. (2009)
T065A	2.26	0.33	15.40	2.01	1.93	0.95	9.70	Lee et al. (2009)
T065B	2.89	0.45	21.10	2.17	2.44	1.05	1.90	Lee et al. (2009)
06FW101	3.19	0.46	15.70	4.03	3.37	0.87	2.50	Li et al. (2012)
06FW104	2.76	0.42	12.33	2.63	4.66	0.77	3.56	Li et al. (2012)
06FW105	2.44	0.36	36.36	7.82	4.54	0.92	7.24	Li et al. (2012)
06FW108	1.96	0.29	13.36	3.03	4.24	0.54	16.42	Li et al. (2012)
06FW110	3.64	0.52	34.40	7.97	4.69	1.21	2.62	Li et al. (2012)
06FW111	1.45	0.23	18.11	4.00	4.73	0.51	10.20	Li et al. (2012)
06FW112	2.66	0.38	4.98	1.45	2.43	0.49	15.46	Li et al. (2012)
06FW118	0.68	0.11	29.49	5.41	3.42	0.16	3.38	Li et al. (2012)
06FW119	1.26	0.21	11.35	2.74	4.68	0.40	14.97	Li et al. (2012)
06FW120	1.45	0.24	7.03	1.86	1.80	1.07	26.09	Li et al. (2012)
06FW121	0.28	0.06	10.75	2.40	3.01	0.06	2.69	Li et al. (2012)
06FW126	3.10	0.48	10.16	2.69	8.82	1.11	14.03	Li et al. (2012)
06FW127	0.28	0.05	4.08	1.81	5.15	0.07	0.48	Li et al. (2012)
06FW128	1.90	0.31	4.44	1.74	2.54	0.54	25.89	Li et al. (2012)
06FW129	2.25	0.34	6.82	1.97	8.02	0.88	12.43	Li et al. (2012)
06FW131	0.66	0.10	29.28	7.15	3.83	0.72	4.12	Li et al. (2012)
06FW133	0.97	0.15	65.79	7.47	5.82	1.53	7.00	Li et al. (2012)
06FW134	0.68	0.11	41.98	8.10	4.01	1.20	4.25	Li et al. (2012)
06FW139	0.85	0.12	41.72	6.69	10.29	1.01	11.66	Li et al. (2012)
06FW140	0.92	0.14	20.42	4.20	3.65	0.98	3.38	Li et al. (2012)
06FW146	1.20	0.19	0.42	0.16	0.88	0.08	24.56	Li et al. (2012)
06FW147	1.79	0.29	4.71	1.63	4.79	0.37	16.48	Li et al. (2012)

Table A.4: continued

Sample	Rb	Sr	Y	Zr	Nb	Ba	Pb	Sc	V	Cr	Ni	Cu	Zn
06FW148	81.00	456.00	7.01	96.00	4.95	681.00	26.21	2.76	37.42	5.47	2.77	21.85	38.05
06FW151	56.00	580.00	20.82	121.00	5.33	503.00	13.33	15.45	160.39	32.53	14.91	57.01	78.68
06FW152-2	43.00	690.00	24.34	150.00	8.33	501.00	16.44	20.52	240.36	26.59	12.23	6.21	94.98
06FW154	206.00	122.00	32.50	119.00	16.60	189.00	12.15	3.41	15.96	1.03	0.97	4.54	19.62
06FW155	168.00	306.00	17.16	127.00	11.30	563.00	12.50	5.12	30.34	6.44	2.28	9.56	24.39
06FW156	173.00	366.00	17.69	150.00	10.61	665.00	11.71	6.15	58.17	8.12	3.38	3.24	30.62
06FW162	79.00	452.00	26.01	138.00	8.90	517.00	14.40	17.45	172.50	4.71	4.03	43.84	79.90
06FW163	146.00	245.00	15.12	345.00	9.20	937.00	16.29	6.91	151.87	10.55	6.66	18.95	77.94
06FW174	42.00	677.00	34.08	160.00	7.87	370.00	11.30	8.65	182.95	4.66	5.72	59.81	81.43
06FW175	14.00	542.00	18.02	82.00	5.10	264.00	10.74	18.67	159.80	10.94	11.38	56.12	72.59
06FW176	10.00	515.00	29.67	205.00	7.34	230.00	7.57	4.84	50.81	1.94	1.99	6.41	34.10
08FW51	89.90	338.00	23.10	129.00	5.80	617.00	15.60	12.80	106.00	20.60	10.10	63.90	48.90
09FW41	159.00	251.00	27.13	123.00	12.70	530.00	12.80	6.17	41.40	2.32	2.06	3.09	34.30
09FW42	178.00	378.00	16.39	106.00	10.40	839.00	18.70	5.96	49.40	6.86	3.02	3.80	28.60
09FW43	157.00	378.00	16.43	99.00	11.10	638.00	17.00	5.47	44.50	5.11	2.78	9.99	27.80
09FW50	100.00	486.00	12.90	65.00	5.04	631.00	25.70	7.43	72.20	9.30	6.98	20.90	51.60
ML06-1	80.40	1136.00	9.88	124.00	8.81	1073.00	41.20	4.90	71.60	5.45	5.41	23.60	65.60
SR01-1	128.00	449.00	20.74	165.00	8.19	603.00	17.20	10.60	97.30	21.90	10.40	9.22	52.00
SR02-1	215.00	393.00	7.29	104.00	7.40	736.00	41.00	2.84	23.90	0.92	1.04	9.59	32.40
SR03-1	70.30	357.00	15.81	82.00	6.88	311.00	20.90	3.40	30.50	1.32	1.51	12.90	51.60
SR04-1	119.00	532.00	22.53	168.00	9.55	330.00	23.60	9.63	89.40	2.99	3.75	22.10	74.70
73-164	306.00	157.00	33.90	197.00	26.00	747.00	47.40	36.50	13.30	37.80	4.56		
73-540	360.00	168.00	15.60	123.00	18.20	610.00	64.80	29.40	20.70	47.30	8.87		
73-720	156.00	206.00	28.80	153.00	12.60	706.00	11.40	36.80	49.90	44.10	6.06		
73-721	126.00	288.00	25.20	253.00	11.70	636.00	15.20	12.70	82.90	59.50	8.40		
73-73	385.00	129.00	38.50	127.00	25.90	548.00	49.00	48.70	18.90	88.80	7.49		
73-750	67.30	503.00	27.40	167.00	8.99	355.00	7.36	32.80	123.00	52.80	15.70		
ET103A	170.00	145.00	14.30	127.00	13.10	418.00	33.10	4.11	14.30	7.60	2.15		44.10
ET104B	176.00	105.00	15.40	108.00	8.65	183.00	20.90	9.82		1.60	0.83	0.97	13.60
ET105A	161.00	163.00	19.10	153.00	8.85	310.00	19.50	9.96	19.10	6.90	1.98	1.95	32.90
ET105B	240.00	94.20	26.30	71.90	10.40	283.00	30.50	6.82	14.20	3.08	1.01	2.00	23.70
ET105C	242.00	135.00	19.60	62.70	10.10	379.00	30.50	8.35	21.40	3.09	1.40	7.64	21.10
ET105D	219.00	133.00	17.60	57.70	8.01	339.00	25.10	6.99	21.90	2.97	1.54	1.66	33.20
ET105E	253.00	132.00	21.60	66.20	10.60	296.00	27.40	9.03	24.40	3.43	1.63	4.87	47.10
ET105F	248.00	132.00	20.90	60.60	9.55	344.00	27.50	10.60	22.70	95.20	2.75	4.38	37.70

Sample data continued

Sample	Ga	La	Ce	Pr	Nd	Sm	Eu	Gd	Tb	Dy	Ho	Er	Tm
06FW148	14.65	27.30	47.17	4.79	15.32	2.50	0.62	1.75	0.22	1.14	0.22	0.60	0.09
06FW151	16.89	17.74	40.89	5.26	20.16	4.72	1.22	3.90	0.60	3.35	0.75	2.00	0.32
06FW152-2	17.76	17.62	40.56	5.35	21.83	5.25	1.46	4.51	0.72	4.02	0.89	2.38	0.36
06FW154	12.11	20.76	48.90	6.43	23.85	5.58	0.49	4.36	0.76	4.47	1.01	2.97	0.53
06FW155	13.32	32.71	61.54	6.46	20.83	3.66	0.80	2.87	0.43	2.52	0.54	1.57	0.27
06FW156	15.16	33.81	60.68	6.41	20.82	3.90	0.86	3.04	0.46	2.64	0.58	1.63	0.28
06FW162	20.42	22.08	47.84	5.83	23.06	4.81	1.05	4.38	0.68	4.45	0.93	2.65	0.42
06FW163	17.27	17.48	35.97	4.31	17.65	3.42	0.88	3.00	0.44	2.86	0.55	1.56	0.23
06FW174	20.15	24.73	63.59	8.69	37.20	8.04	1.66	6.86	1.01	6.34	1.25	3.46	0.51
06FW175	17.62	14.18	31.12	4.59	19.60	4.29	1.17	3.73	0.57	3.57	0.72	2.00	0.31
06FW176	14.23	21.28	49.25	7.92	34.77	7.53	1.67	6.27	0.93	5.75	1.15	3.17	0.46
08FW51	16.40	19.10	39.70	4.76	18.90	4.17	0.95	4.05	0.67	3.93	0.78	2.30	0.35
09FW41	16.80	36.10	71.50	8.20	29.90	5.84	0.99	4.71	0.75	4.42	0.89	2.65	0.39
09FW42	15.20	42.30	76.70	8.00	27.10	4.60	0.92	3.36	0.50	2.75	0.54	1.52	0.24
09FW43	15.60	45.60	82.70	8.50	28.40	4.75	0.92	3.40	0.50	2.66	0.54	1.62	0.25
09FW50	16.30	37.40	66.90	6.82	23.00	3.50	0.73	2.82	0.39	2.18	0.44	1.20	0.17
ML06-1	21.10	44.80	82.40	9.01	32.40	5.03	1.29	3.48	0.41	1.94	0.32	0.88	0.12
SR01-1	16.70	29.40	62.60	7.36	28.20	5.39	1.13	4.63	0.65	3.67	0.69	2.03	0.31
SR02-1	16.30	20.80	37.00	3.88	13.20	2.11	0.56	1.63	0.22	1.25	0.24	0.70	0.10
SR03-1	16.90	13.60	27.20	3.23	12.40	2.68	0.62	2.51	0.39	2.46	0.49	1.53	0.24
SR04-1	19.80	31.00	61.70	7.29	27.90	5.36	1.07	4.58	0.66	3.88	0.76	2.15	0.34
73-164	20.00	87.40	165.00	18.90	64.70	11.60	0.86	8.59	1.30	6.79	1.23	3.36	0.45
73-540	22.00	30.40	62.40	7.40	25.90	5.13	0.68	4.26	0.63	3.12	0.53	1.44	0.21
73-720	15.60	37.20	73.00	8.38	28.10	5.40	0.84	4.81	0.81	4.87	0.98	3.00	0.45
73-721	18.30	33.70	63.70	7.41	26.30	4.92	1.05	4.62	0.73	4.36	0.90	2.63	0.42
73-73	23.00	26.70	56.20	6.76	23.80	5.61	0.56	5.85	1.07	6.51	1.29	3.62	0.54
73-750	22.50	15.60	36.30	4.85	19.60	4.34	1.37	4.89	0.80	4.89	1.03	2.91	0.44
ET103A	16.20	49.80	94.10	9.69	33.40	5.54	0.87	4.51	0.61	2.88	0.55	1.41	0.19
ET104B	13.70	22.10	39.80	4.01	13.90	2.53	0.50	2.36	0.38	2.15	0.46	1.38	0.22
ET105A	15.90	22.50	41.70	4.28	15.40	2.89	0.71	2.84	0.46	2.70	0.57	1.71	0.27
ET105B	15.70	34.50	63.30	6.34	21.90	4.41	0.58	4.11	0.69	3.91	0.81	2.43	0.39
ET105C	16.50	34.60	63.50	6.17	20.40	3.59	0.69	3.31	0.48	2.64	0.55	1.62	0.26
ET105D	15.90	30.10	55.40	5.31	17.90	3.32	0.72	3.04	0.47	2.63	0.54	1.60	0.25
ET105E	17.20	33.90	63.50	6.09	20.80	3.91	0.74	3.67	0.58	3.31	0.68	1.99	0.32
ET105F	16.70	35.20	62.60	5.96	19.90	3.67	0.74	3.43	0.55	3.14	0.65	1.91	0.30

Sample data continued

Sample	Yb	Lu	Th	U	Hf	Ta	Co	Source
06FW148	0.64	0.10	12.61	2.11	2.72	0.41	4.29	Li et al. (2012)
06FW151	1.99	0.33	4.19	1.30	3.45	0.39	20.23	Li et al. (2012)
06FW152-2	2.23	0.37	6.17	1.67	4.37	0.56	24.71	Li et al. (2012)
06FW154	3.75	0.61	18.03	5.09	3.86	2.02	1.69	Li et al. (2012)
06FW155	1.88	0.32	25.38	5.63	3.61	1.07	5.88	Li et al. (2012)
06FW156	1.87	0.32	18.64	5.07	4.22	0.99	5.81	Li et al. (2012)
06FW162	2.96	0.44	11.11	3.57	3.77	0.79	18.19	Li et al. (2012)
06FW163	1.66	0.25	3.63	1.21	8.88	0.50	16.02	Li et al. (2012)
06FW174	3.36	0.47	9.77	2.18	4.44	0.43	19.08	Li et al. (2012)
06FW175	2.04	0.30	2.65	0.69	2.12	0.28	19.29	Li et al. (2012)
06FW176	3.04	0.44	3.23	1.09	4.79	0.29	4.46	Li et al. (2012)
08FW51	2.31	0.37	9.47	1.21	3.98	0.50	11.80	Li et al. (2012)
09FW41	2.77	0.40	26.20	4.61	3.78	1.38	4.48	Li et al. (2012)
09FW42	1.72	0.26	27.20	5.84	3.06	0.94	5.62	Li et al. (2012)
09FW43	1.73	0.29	28.40	5.11	2.89	1.01	4.67	Li et al. (2012)
09FW50	1.23	0.19	13.10	2.01	1.94	0.43	9.94	Li et al. (2012)
ML06-1	0.79	0.12	25.20	3.29	3.28	0.51	7.12	Li et al. (2012)
SR01-1	2.07	0.32	22.60	5.82	4.86	0.69	12.60	Li et al. (2012)
SR02-1	0.73	0.12	11.70	3.28	3.26	0.74	2.74	Li et al. (2012)
SR03-1	1.81	0.30	4.45	1.52	2.72	0.89	4.63	Li et al. (2012)
SR04-1	2.31	0.38	21.10	4.47	4.68	0.79	12.40	Li et al. (2012)
73-164	2.75	0.40	52.80	7.14	6.50	2.36	2.13	Lin et al. (2012)
73-540	1.32	0.19	24.80	6.63	4.21	1.93	3.49	Lin et al. (2012)
73-720	3.09	0.44	24.10	4.31	5.17	1.32	4.84	Lin et al. (2012)
73-721	2.64	0.43	22.50	3.69	7.59	1.07	8.66	Lin et al. (2012)
73-73	3.38	0.49	24.40	5.49	4.30	4.01	2.69	Lin et al. (2012)
73-750	2.62	0.39	2.86	1.13	4.39	0.79	19.80	Lin et al. (2012)
ET103A	1.16	0.18	20.10	10.70	3.65	0.95	2.46	Lin et al. (2012)
ET104B	1.58	0.26	22.20	3.65	3.08	1.07	2.66	Lin et al. (2012)
ET105A	1.87	0.30	21.50	2.97	3.86	0.92	6.26	Lin et al. (2012)
ET105B	2.67	0.42	33.20	3.80	2.86	1.65	2.56	Lin et al. (2012)
ET105C	1.78	0.28	33.20	3.80	2.02	1.65	3.65	Lin et al. (2012)
ET105D	1.76	0.27	23.50	2.87	2.08	1.11	3.77	Lin et al. (2012)
ET105E	2.18	0.33	27.10	3.03	2.35	1.36	4.19	Lin et al. (2012)
ET105F	2.07	0.32	26.50	3.08	2.14	1.22	4.13	Lin et al. (2012)

Table A.4: continued

Sample	Rb	Sr	Y	Zr	Nb	Ba	Pb	Sc	V	Cr	Ni	Cu	Zn
ET105G	58.80	220.00	24.10	103.00	7.19	152.00	10.30	15.90	139.00	155.00	64.80	38.30	90.50
ET106A2	491.00	6.46	115.00	90.80	16.20		30.70	16.30		3.40		16.80	
ET107A	330.00	63.90	44.10	254.00	16.90	170.00	38.90	17.90		3.36	1.74	4.25	26.80
ET108B	192.00	179.00	31.70	173.00	13.60	509.00	36.90	12.50		5.25	0.63	2.78	39.20
ET111B	335.00	78.30	38.40	192.00	27.50	245.00	64.00	11.50		6.13	0.75	6.46	42.90
ET113A	226.00	214.00	23.30	240.00	8.82	355.00	43.10	10.20		1.32	2.23	6.61	95.20
ET115F1	396.00	69.70	36.60	208.00	11.80	297.00	40.90	7.28		3.90	0.61	1.57	4.69
ET115F2	402.00	72.10	37.00	210.00	11.80	319.00	41.60	7.94		4.55	1.03	2.03	3.84
ET116B	345.00	81.50	37.10	110.00	19.50	301.00	48.80	21.80		5.57	2.44	4.26	23.80
ET117A	177.00	229.00	23.90	184.00	11.20	314.00	17.40	20.90	52.60	229.00	35.10	10.10	54.10
ET117C	186.00	218.00	14.10	114.00	10.20	252.00	22.50	14.10	5.06	60.90	24.50	6.50	16.50
ET119A	139.00	694.00	23.70	138.00	11.70	429.00	35.40	12.20	86.80	76.70	10.40	18.30	44.10
ET120A	204.00	230.00	12.30	139.00	7.02	353.00	16.50	6.86		1.81	0.79	1.83	4.10
ET120C	55.70	546.00	24.10	173.00	9.36	415.00	14.90	13.70	162.00	9.98	13.10	29.60	82.60
ET120D	31.10	425.00	39.90	62.10	8.45	103.00	5.96	23.80	206.00	1.74	1.68	21.40	98.30
ET120E	50.20	273.00	23.70	113.00	5.68	127.00	2.83	19.50	171.00	208.00	90.50	25.70	65.70
ET122A	91.70	723.00	27.30	178.00	11.50	618.00	10.20	18.70	113.00	46.70	31.70	5.77	73.10
ET122B	179.00	400.00	16.20	194.00	13.10	655.00	25.60	16.10		9.55	4.78	3.16	21.60
ET122D	167.00	321.00	8.45	208.00	10.60	684.00	30.40	18.70		5.87	2.23	2.10	8.84
ET124C	209.00	501.00	8.62	153.00	5.59	1228.00	66.20	5.27	13.20	2.82	1.08	5.09	21.10
ET124D	140.00	264.00	23.70	119.00	5.81	118.00	3.07	22.60	174.00	348.00	133.00	6.69	100.00
ET125A	181.00	195.00	30.70	211.00	14.20	643.00	37.40	7.04	31.10	6.03	3.63		55.20
ET203B	207.00	163.00	33.10	193.00	13.50	696.00	38.10	3.84	4.88	1.03	0.82		52.10
ET203D	221.00	156.00	31.60	176.00	13.70	662.00	36.70	3.95	8.07	3.20	0.67		60.20
ET219B2	644.00	8.91	108.00	105.00	18.40	10.70	55.20	4.51	1.05	1.37	4.21		23.90
ET220B	713.00	11.50	135.00	89.10	19.10	46.20	58.50	3.82	3.75	4.72	0.63		14.70
ET221B	675.00	9.57	135.00	102.00	19.80	14.70	51.50	10.70	0.71	1.18	0.21		13.90
ET222B	658.00	9.15	130.00	98.10	17.60	10.20	49.50	6.92		1.82	0.39		11.10
RAW11	89.40	185.00	35.40	287.00	14.70	214.00	20.00	7.51	49.50	4.92	3.66	14.20	69.20
RAW12	96.80	146.00	36.80	284.00	13.90	114.00	16.80	7.64	50.30	4.32	3.98	9.57	68.50
RAW13	124.00	108.00	45.50	316.00	20.00	238.00	23.60	11.90	18.00	1.60	1.33	7.17	57.50
RAW15	30.70	319.00	31.60	244.00	16.20	148.00	12.40	13.00	110.00	41.40	26.80	26.60	78.40
RAW17	157.00	64.30	26.90	92.60	8.44	339.00	11.20	5.14	31.20	3.45	2.22	2.99	37.40
RAW20	40.40	233.00	24.70	345.00	18.30	223.00	11.50	6.16	96.00	16.30	13.50	34.40	66.20
RAW22	134.00	265.00	56.20	429.00	24.90	203.00	24.80	17.40	123.00	25.10	15.80	48.20	117.00

Sample data continued

Sample	Ga	La	Ce	Pr	Nd	Sm	Eu	Gd	Tb	Dy	Ho	Er	Tm
ET105G	14.00	21.10	39.80	5.11	20.90	4.83	1.29	4.64	0.77	4.61	0.94	2.61	0.36
ET106A2	18.70	20.10	49.50	6.21	25.10	8.22	0.05	9.56	2.18	14.60	3.20	9.52	1.53
ET107A	20.60	61.00	123.00	14.20	52.50	10.10	0.62	8.73	1.33	7.00	1.35	3.77	0.56
ET108B	20.10	26.50	56.10	6.55	26.00	5.51	0.79	5.15	0.85	4.71	0.92	2.58	0.37
ET111B	22.80	77.30	156.00	17.20	60.80	11.80	0.61	9.63	1.43	7.17	1.30	3.45	0.46
ET113A	17.80	52.40	108.00	12.10	46.10	9.38	0.82	7.69	1.04	4.65	0.74	1.78	0.23
ET115F1	17.70	52.90	109.00	11.70	41.30	7.05	0.50	5.87	0.83	4.20	0.82	2.34	0.36
ET115F2	17.70	49.60	102.00	11.10	39.40	6.79	0.48	5.74	0.81	4.11	0.80	2.26	0.34
ET116B	22.00	26.00	53.60	5.97	22.20	5.04	0.58	4.93	0.92	5.41	1.05	2.86	0.42
ET117A	18.70	23.60	47.50	5.39	21.20	4.20	0.84	3.95	0.64	3.56	0.71	2.01	0.30
ET117C	17.40	28.90	51.90	5.16	17.70	3.00	0.67	2.76	0.39	2.08	0.41	1.19	0.18
ET119A	18.10	38.70	78.90	9.05	33.60	6.59	1.08	5.47	0.82	4.46	0.87	2.42	0.33
ET120A	14.90	31.80	54.30	5.25	17.50	2.57	0.62	2.30	0.31	1.61	0.34	1.01	0.16
ET120C	16.90	25.20	53.40	6.54	27.10	5.71	1.58	5.13	0.78	4.43	0.89	2.47	0.34
ET120D	20.60	24.60	56.20	7.49	33.80	8.27	2.19	8.05	1.32	7.63	1.53	4.10	0.54
ET120E	15.30	14.50	31.30	4.04	17.10	4.11	1.15	4.03	0.69	4.13	0.87	2.40	0.34
ET122A	20.20	24.90	57.10	7.38	31.80	6.61	1.43	5.56	0.85	4.39	0.84	2.24	0.31
ET122B	18.10	40.10	72.20	7.25	25.20	3.96	0.80	3.42	0.45	2.26	0.44	1.29	0.20
ET122D	17.40	43.90	79.30	7.94	27.40	3.99	0.77	3.16	0.35	1.49	0.25	0.68	0.09
ET124C	17.50	37.30	67.70	7.05	24.10	3.44	1.05	2.63	0.30	1.45	0.28	0.81	0.12
ET124D	15.90	15.50	33.90	4.33	18.30	4.31	1.16	4.18	0.69	4.21	0.85	2.39	0.33
ET125A	16.90	46.50	91.90	10.00	37.30	6.92	1.47	6.18	0.95	5.30	1.08	3.03	0.44
ET203B	19.10	29.10	60.60	7.07	26.90	5.80	0.96	5.43	0.93	5.36	1.08	2.97	0.44
ET203D	18.80	38.80	81.10	9.38	35.80	7.47	0.96	6.40	1.03	5.42	1.02	2.76	0.39
ET219B2	20.10	33.70	80.10	9.62	36.60	10.60	0.11	11.10	2.42	15.60	3.38	10.00	1.57
ET220B	20.70	35.20	83.50	10.10	38.90	11.80	0.15	12.80	2.84	18.70	4.01	11.80	1.86
ET221B	20.50	36.20	86.40	10.50	40.30	12.20	0.13	13.10	2.90	19.10	4.09	12.10	1.89
ET222B	19.70	32.40	77.40	9.43	36.80	11.30	0.11	12.20	2.69	17.60	3.78	11.20	1.77
RAW11	17.00	32.60	67.70	7.77	30.70	6.41	1.62	6.37	1.03	5.85	1.22	3.43	0.50
RAW12	17.60	32.50	66.50	7.77	30.90	6.59	1.63	6.63	1.07	6.05	1.26	3.53	0.51
RAW13	20.20	42.40	93.30	10.40	41.30	8.61	2.06	8.50	1.36	7.67	1.57	4.40	0.40
RAW15	20.10	28.40	60.80	7.19	29.10	6.19	1.76	6.04	0.97	5.42	1.00	3.04	0.43
RAW17	14.30	28.10	56.80	6.09	22.40	4.46	0.83	4.40	0.72	4.20	0.88	2.53	0.37
RAW20	20.70	15.80	72.10	5.09	21.30	4.99	1.24	5.11	0.89	5.27	1.11	3.15	0.47
RAW22	27.00	48.90	109.00	12.20	48.70	10.30	2.52	10.20	1.63	9.25	1.92	5.42	0.78

Sample data continued

Sample	Yb	Lu	Th	U	Hf	Ta	Co	Source
ET105G	2.43	0.35	6.79	1.23	3.13	0.61	24.80	Lin et al. (2012)
ET106A2	9.90	1.43	48.60	13.10	4.23	2.47	0.29	Lin et al. (2012)
ET107A	3.67	0.54	54.40	6.93	6.82	2.70	2.59	Lin et al. (2012)
ET108B	2.34	0.34	13.10	2.82	4.68	1.61	0.97	Lin et al. (2012)
ET111B	3.01	0.42	47.00	7.75	6.22	2.69	1.03	Lin et al. (2012)
ET113A	1.42	0.21	44.20	2.53	6.30	0.93	1.71	Lin et al. (2012)
ET115F1	2.38	0.37	38.90	4.65	4.20	0.85	1.38	Lin et al. (2012)
ET115F2	2.33	0.36	40.10	4.84	4.10	0.83	1.31	Lin et al. (2012)
ET116B	2.69	0.38	24.10	7.98	3.18	2.77	2.20	Lin et al. (2012)
ET117A	1.89	0.28	18.90	2.19	4.58	0.92	14.60	Lin et al. (2012)
ET117C	1.21	0.18	27.50	3.47	3.07	1.23	8.86	Lin et al. (2012)
ET119A	2.20	0.32	18.20	2.92	4.33	1.18	10.60	Lin et al. (2012)
ET120A	1.13	0.19	16.00	1.84	3.30	0.57	3.00	Lin et al. (2012)
ET120C	2.26	0.33	5.11	0.77	4.46	0.63	18.70	Lin et al. (2012)
ET120D	3.36	0.46	2.78	0.56	2.12	0.61	20.60	Lin et al. (2012)
ET120E	2.27	0.34	3.15	0.65	2.83	0.40	29.80	Lin et al. (2012)
ET122A	1.91	0.28	6.24	0.87	3.98	0.69	21.60	Lin et al. (2012)
ET122B	1.30	0.19	36.50	3.83	4.56	1.46	4.04	Lin et al. (2012)
ET122D	0.57	0.09	45.30	4.50	4.94	0.42	2.70	Lin et al. (2012)
ET124C	0.97	0.16	23.70	13.90	4.90	0.95	1.26	Lin et al. (2012)
ET124D	2.23	0.33	3.48	0.63	2.94	0.40	28.30	Lin et al. (2012)
ET125A	2.93	0.45	27.40	3.32	5.88	1.12	4.09	Lin et al. (2012)
ET203B	2.89	0.41	11.00	2.37	5.41	1.26	1.08	Lin et al. (2012)
ET203D	2.47	0.35	15.30	2.36	4.95	1.28	1.12	Lin et al. (2012)
ET219B2	10.30	1.48	44.40	5.71	4.73	4.02	0.55	Lin et al. (2012)
ET220B	12.10	1.74	43.70	6.84	3.92	4.11	0.53	Lin et al. (2012)
ET221B	12.40	1.78	47.10	8.80	4.67	4.05	0.51	Lin et al. (2012)
ET222B	11.60	1.67	45.50	6.31	4.58	3.88	0.50	Lin et al. (2012)
RAW11	3.25	0.49	13.20	2.57	6.78	1.24	8.56	Lin et al. (2012)
RAW12	3.30	0.50	12.80	2.59	6.76	1.20	9.16	Lin et al. (2012)
RAW13	4.12	0.62	12.10	1.90	7.64	1.51	3.88	Lin et al. (2012)
RAW15	2.78	0.42	7.22	1.38	5.67	1.22	17.80	Lin et al. (2012)
RAW17	2.45	0.36	18.00	3.22	2.96	0.83	3.95	Lin et al. (2012)
RAW20	3.07	0.46	5.48	2.38	7.77	1.38	13.20	Lin et al. (2012)
RAW22	5.06	0.77	17.40	3.17	9.82	1.85	17.80	Lin et al. (2012)

Table A.4: continued

Sample	Rb	Sr	Y	Zr	Nb	Ba	Pb	Sc	V	Cr	Ni	Cu	Zn
RAW24	95.60	273.00	45.10	393.00	21.10	324.00	17.60	13.60	112.00	19.30	14.70	8.11	112.00
RAW25	91.00	223.00	30.30	230.00	13.20	194.00	5.39	16.10	142.00	51.30	39.60	4.22	82.10
RAW26	57.60	290.00	30.50	222.00	12.70	112.00	6.56	16.30	145.00	52.90	38.60	4.50	74.00
RAW29	77.50	293.00	29.80	218.00	12.40	231.00	7.72	16.50	137.00	50.90	37.20	28.70	61.30
RAW30	69.30	243.00	42.60	299.00	17.50	105.00	11.50	18.10	189.00	46.80	45.60	111.00	82.70
MB12-1	133.00	725.00	12.30	187.00	13.10	420.00	18.00	6.85	71.10	27.40	12.30	3.31	53.80
MB12-1R	135.00	736.00	12.50	185.00	13.40	420.00	18.30	6.95	73.40	27.70	13.40	3.51	54.30
MB12-3	154.00	758.00	14.50	176.00	15.10	887.00	20.40	7.70	78.50	30.30	13.50	3.03	59.00
MB12-5	121.00	742.00	12.00	184.00	13.00	487.00	16.30	6.97	68.90	28.80	12.50	2.66	54.80
MB12-7	115.00	746.00	11.80	167.00	12.60	360.00	17.70	5.80	59.70	22.70	10.20	3.03	45.90
MB12-8	136.00	738.00	11.30	177.00	12.80	400.00	17.30	7.31	75.40	30.50	14.10	2.90	59.20
MB12-9	101.00	766.00	12.40	191.00	13.90	381.00	18.00	6.65	75.00	28.30	13.10	2.62	57.40
MB13-3	199.00	576.00	29.00	263.00	30.40	296.00	18.00	12.30	184.00	13.00	13.80	28.10	119.00
MB14-2	123.00	627.00	20.00	198.00	22.40	189.00	14.20	19.80	177.00	156.00	36.50	10.50	106.00
MB14-2R	117.00	588.00	18.80	177.00	21.10	178.00	13.50	18.40	166.00	144.00	34.00	9.63	98.50
MB14-4	144.00	738.00	10.80	175.00	12.10	489.00	19.50	6.70	70.20	26.50	12.50	2.74	59.20
MB14-5	194.00	555.00	18.30	207.00	20.10	482.00	21.40	15.40	147.00	100.00	51.60	6.55	97.80
MB16-1	133.00	680.00	11.10	156.00	12.60	481.00	19.10	6.76	65.70	28.60	12.00	3.54	49.10
MB17-1	117.00	755.00	13.00	202.00	14.50	244.00	16.40	7.81	79.40	31.10	14.10	2.96	59.00
TE007/93	386.00	684.00	18.00	285.00	21.00	1562.00	125.00	10.00	83.00	129.00	54.00	28.00	59.00
TE008/93	528.00	849.00	25.00	446.00	28.00	2351.00	118.00	16.00	107.00	314.00	144.00	38.00	68.00
TE011/93	574.00	772.00	25.00	418.00	38.00	2715.00	128.00	15.00	111.00	332.00	145.00	31.00	76.00
TE025/93	438.00	500.00	14.00	412.00	22.00	1165.00	109.00	10.00	76.00	82.00	17.00	14.00	67.00
TE047/93	155.00	452.00	8.00	117.00	8.00	778.00	31.00	5.00	36.00	25.00	8.00	12.00	28.00
TE117/93	753.00	842.00	27.00	461.00	29.00	2160.00	52.00	12.00	120.00	377.00	193.00	53.00	62.00
TE118/93	712.00	802.00	28.00	454.00	26.00	2292.00	53.00	14.00	128.00	419.00	169.00	39.00	80.00
TE125/93	632.00	621.00	27.00	511.00	38.00	1863.00	47.00	18.00	133.00	295.00	87.00	33.00	87.00
TE126/93	465.00	792.00	24.00	635.00	37.00	2718.00	93.00	17.00	128.00	496.00	203.00	55.00	74.00
TE127/93	437.00	787.00	24.00	609.00	38.00	2715.00	88.00	18.00	130.00	494.00	212.00	53.00	77.00
TE131/93	466.00	802.00	26.00	589.00	40.00	2397.00	88.00	18.00	109.00	384.00	202.00	73.00	56.00
TE136/93	340.00	772.00	17.00	316.00	17.00	1988.00	67.00	9.00	67.00	130.00	74.00	39.00	65.00
TE137/93	702.00	990.00	30.00	392.00	23.00	3488.00	79.00	13.00	115.00	528.00	358.00	63.00	72.00
TE138/93	523.00	1042.00	28.00	387.00	24.00	3416.00	87.00	12.00	109.00	368.00	230.00	58.00	75.00
TE148/93	381.00	415.00	14.00	358.00	14.00	989.00	83.00	9.00	52.00	65.00	22.00	15.00	78.00
TE150/93	411.00	425.00	17.00	364.00	14.00	941.00	85.00	7.00	49.00	63.00	19.00	21.00	78.00

Sample data continued

Sample	Ga	La	Ce	Pr	Nd	Sm	Eu	Gd	Tb	Dy	Ho	Er	Tm
RAW24	21.30	43.50	91.40	10.50	41.00	8.51	1.91	8.41	1.33	7.50	1.54	4.39	0.63
RAW25	19.20	27.20	57.70	6.65	26.60	5.67	1.29	5.73	0.91	5.11	1.05	2.94	0.42
RAW26	18.50	28.50	58.80	6.79	27.30	5.80	1.56	5.90	0.92	5.16	1.05	2.92	0.42
RAW29	17.30	30.60	61.90	7.08	28.10	5.84	1.64	5.88	0.91	5.01	1.02	2.82	0.40
RAW30	21.90	28.60	63.90	7.77	32.20	7.18	1.47	7.29	1.20	6.87	1.42	3.98	0.56
MB12-1	19.60	45.00	85.70	9.37	33.10	5.27	1.36	3.82	0.47	2.35	0.44	1.16	0.17
MB12-1R	20.10	44.40	85.70	9.56	33.70	5.43	1.34	3.87	0.47	2.48	0.45	1.19	0.17
MB12-3	20.00	67.50	113.00	11.70	40.90	6.24	1.54	4.53	0.55	2.78	0.52	1.40	0.19
MB12-5	19.10	64.10	103.00	10.20	34.60	5.24	1.26	3.71	0.47	2.28	0.43	1.15	0.16
MB12-7	18.80	66.80	102.00	10.20	34.40	5.24	1.30	3.63	0.45	2.33	0.42	1.12	0.15
MB12-8	19.90	44.00	79.60	8.82	30.90	4.87	1.21	3.52	0.44	2.20	0.41	1.07	0.15
MB12-9	21.50	40.50	76.00	9.18	32.70	5.23	1.38	3.79	0.47	2.48	0.45	1.18	0.16
MB13-3	28.90	77.20	167.00	19.50	69.70	11.10	2.68	8.38	1.07	5.50	1.03	2.79	0.39
MB14-2	23.40	51.10	111.00	12.80	46.50	7.87	1.92	5.92	0.76	3.81	0.70	1.88	0.26
MB14-2R	21.90	49.10	105.00	12.20	44.30	7.47	1.84	5.62	0.72	3.64	0.69	1.80	0.25
MB14-4	19.90	62.70	97.20	9.56	32.00	4.77	1.21	3.33	0.42	2.12	0.38	1.03	0.15
MB14-5	22.10	55.70	117.00	13.20	47.40	7.76	2.16	5.65	0.71	3.57	0.67	1.74	0.24
MB16-1	18.90	46.80	84.50	8.84	30.90	4.71	1.18	3.41	0.43	2.15	0.40	1.02	0.15
MB17-1	20.70	41.40	84.00	9.49	34.00	5.48	1.38	3.84	0.49	2.50	0.45	1.24	0.18
TE007/93	17.00	95.00	178.00										
TE008/93	17.00	112.00	275.00	34.00	157.00	28.00	4.50	15.00	1.70	6.70	0.99	2.20	0.23
TE011/93	22.00	115.00	251.00	34.00	158.00	28.00	2.80	16.00	1.70	6.60	0.91	2.30	0.26
TE025/93	25.00	87.00	173.00	19.00	68.00	11.00	1.80	6.00	0.70	2.90	0.45	1.10	0.13
TE047/93	15.00	29.00	59.00	6.00	22.00	4.00	0.90	2.00	0.30	1.70	0.29	0.80	0.11
TE117/93	20.00	81.00	197.00	29.00	145.00	31.00	4.80	15.00	1.60	6.60	0.91	2.30	0.26
TE118/93	23.00	85.00	203.00	30.00	135.00	30.00	4.90	14.00	1.50	5.80	0.91	2.30	0.28
TE125/93	22.00	72.00	185.00	24.00	109.00	25.00	4.00	14.00	1.50	6.50	1.06	2.50	0.33
TE126/93	21.00	119.00	284.00	39.00	200.00	31.00	4.40	16.00	1.50	6.20	0.81	2.20	0.23
TE127/93	22.00	118.00	290.00	39.00	171.00	32.00	4.60	17.00	1.70	6.60	0.90	2.20	0.26
TE131/93	20.00	112.00	269.00	36.00	155.00	29.00	4.30	15.00	1.50	5.60	0.79	2.00	0.23
TE136/93	22.00	93.00	191.00	22.00	83.00	15.00	2.40	8.00	0.90	4.30	0.64	1.60	0.19
TE137/93	16.00	84.00	207.00	30.00	144.00	30.00	5.30	16.00	1.80	7.80	1.14	2.50	0.31
TE138/93	19.00	89.00	206.00	29.00	145.00	29.00	4.70	16.00	1.70	6.90	1.01	2.50	0.29
TE148/93	29.00	87.00	176.00	19.00	73.00	11.00	1.70	6.00	0.70	3.10	0.50	1.40	0.15
TE150/93	28.00	92.00	162.00	20.00	78.00	12.00	1.80	8.00	0.80	3.30	0.54	1.40	0.18

Sample data continued

Sample	Yb	Lu	Th	U	Hf	Ta	Co	Source
RAW24	4.16	0.62	17.80	3.26	8.93	1.58	23.32	Lin et al. (2012)
RAW25	2.73	0.41	9.20	1.74	5.23	1.02	23.30	Lin et al. (2012)
RAW26	2.67	0.40	9.04	1.84	5.06	0.99	22.70	Lin et al. (2012)
RAW29	2.59	0.39	8.93	1.62	4.93	0.96	21.80	Lin et al. (2012)
RAW30	3.64	0.55	9.13	1.74	6.44	1.22	41.10	Lin et al. (2012)
MB12-1	1.07	0.16	26.90	3.11	4.63	0.93	8.88	Meng et al. (2013)
MB12-1R	1.13	0.17	26.20	3.29	4.61	0.96	8.97	Meng et al. (2013)
MB12-3	1.27	0.18	25.20	3.83	4.41	1.10	9.65	Meng et al. (2013)
MB12-5	1.05	0.17	32.40	3.67	4.58	0.90	9.22	Meng et al. (2013)
MB12-7	1.03	0.15	21.00	3.02	4.22	0.94	7.30	Meng et al. (2013)
MB12-8	0.99	0.16	22.90	4.16	4.41	0.86	9.84	Meng et al. (2013)
MB12-9	1.15	0.18	22.60	3.04	4.68	0.96	9.29	Meng et al. (2013)
MB13-3	2.64	0.41	19.10	6.89	6.64	2.21	21.00	Meng et al. (2013)
MB14-2	1.80	0.28	12.90	4.52	5.06	1.61	21.30	Meng et al. (2013)
MB14-2R	1.67	0.26	12.70	4.04	4.60	1.54	19.90	Meng et al. (2013)
MB14-4	0.95	0.15	21.60	2.97	4.28	0.82	8.98	Meng et al. (2013)
MB14-5	1.58	0.24	13.10	2.92	5.03	1.25	20.30	Meng et al. (2013)
MB16-1	1.00	0.16	19.80	2.53	3.97	0.89	8.13	Meng et al. (2013)
MB17-1	1.23	0.18	14.90	2.87	5.14	1.02	9.61	Meng et al. (2013)
TE007/93			106.00				13.00	Miller et al. (1999)
TE008/93	1.60	0.23	114.00	23.00	12.20	1.80	20.00	Miller et al. (1999)
TE011/93	1.40	0.22	136.00	27.00	13.00	1.80	20.00	Miller et al. (1999)
TE025/93	1.00	0.15	47.00				17.00	Miller et al. (1999)
TE047/93	0.80	0.13	18.00	21.00	3.30	0.80	4.00	Miller et al. (1999)
TE117/93	1.70	0.25	165.00	23.00	12.50	1.60	21.00	Miller et al. (1999)
TE118/93	1.60	0.24	186.00	26.00	13.00	1.60	25.00	Miller et al. (1999)
TE125/93	2.00	0.31	114.00	25.00	15.60	2.80	21.00	Miller et al. (1999)
TE126/93	1.30	0.24	192.00	20.00	17.70	2.50	25.00	Miller et al. (1999)
TE127/93	1.40	0.22	188.00	21.00	18.20	2.70	26.00	Miller et al. (1999)
TE131/93	1.30	0.22	160.00	22.00	19.10	2.80	30.00	Miller et al. (1999)
TE136/93	1.40	0.21	104.00	17.00	8.80	1.40	8.00	Miller et al. (1999)
TE137/93	2.10	0.30	169.00	22.00	11.20	1.30	28.00	Miller et al. (1999)
TE138/93	1.90	0.27	157.00	20.00	10.00	1.30	24.00	Miller et al. (1999)
TE148/93	1.00	0.19	35.00	9.00	10.30	1.40	4.00	Miller et al. (1999)
TE150/93	1.20	0.19	39.00	11.00	10.30	1.40	3.00	Miller et al. (1999)

Table A.4: continued

Sample	Rb	Sr	Y	Zr	Nb	Ba	Pb	Sc	V	Cr	Ni	Cu	Zn
TE153/93	396.00	418.00	11.00	370.00	14.00	964.00	80.00	8.00	63.00	63.00	21.00	16.00	76.00
TE154/93	413.00	420.00	13.00	373.00	18.00	810.00	85.00	7.00	74.00	67.00	21.00	15.00	72.00
TE189/93	156.00	969.00	12.00	175.00	8.00	998.00	28.00	6.00	94.00	50.00	17.00	9.00	39.00
TE192/93	118.00	756.00	12.00	123.00	6.00	781.00	45.00	6.00	57.00	33.00	14.00	14.00	48.00
CM045/93	221.00	601.00	11.00	219.00	19.00	1035.00	87.00	6.00	67.00	36.00	17.00	21.00	50.00
CM070/93	89.00	573.00	20.00	148.00	5.00	539.00	10.00	28.00	391.00	12.00	25.00	97.00	115.00
CM108/93	98.00	698.00	18.00	176.00	11.00	727.00	33.00	14.00	151.00	36.00	23.00	44.00	87.00
HF092/93	385.00	399.00	46.00	621.00	56.00	382.00	22.00	5.00	32.00	12.00	6.00	18.00	67.00
HF095/93	309.00	268.00	42.00	529.00	44.00	445.00	35.00	6.00	23.00	5.00	2.00	17.00	98.00
HF197/93	156.00	524.00	19.00	183.00	10.00	674.00	17.00	10.00	116.00	22.00	17.00	28.00	50.00
TE059/93	209.00	403.00	14.00	135.00	10.00	908.00	39.00	11.00	29.00	11.00	7.00	6.00	41.00
TE073/93	30.00	770.00	17.00	116.00	5.00	517.00	9.00	19.00	213.00	67.00	38.00	43.00	90.00
TE082/93	11.00	742.00	19.00	127.00	11.00	220.00	141.00	19.00	235.00	67.00	22.00	49.00	87.00
TE086/93	190.00	1147.00	23.00	220.00	9.00	1711.00	46.00	15.00	152.00	94.00	33.00	33.00	67.00
TE110/93	17.00	344.00	27.00	97.00	4.00	205.00	9.00	24.00	120.00	17.00	8.00	14.00	107.00
HB06/97	413.00	42.00	12.00	46.00	17.00	128.00	33.00	3.00	3.00	6.00	0.30	1.00	64.00
HB18/97	206.00	106.00	31.00	250.00	15.00	611.00	26.00	9.00	61.00	30.00	10.00	12.00	67.00
HB25/97	260.00	94.00	40.00	205.00	13.00	518.00	29.00	10.00	40.00	24.00	10.00	5.00	50.00
HB26/97	300.00	35.00	50.00	78.00	8.00	138.00	34.00	5.00	50.00	14.00	5.00	2.00	62.00
HF05/92	353.00	64.00	27.00	150.00	17.00	359.00		7.00	51.00	40.00	13.00	40.00	91.00
HF143/90	257.00	104.00	34.00	191.00	16.00	514.00	16.00	9.00	56.00	105.00	5.00	0.00	62.00
HF144/90	356.00	74.00	10.00	225.00	9.00	469.00	17.00	6.00	43.00	75.00	3.00	14.00	76.00
HF59/91	55.00	249.00	29.00	128.00	3.00	119.00	9.00		210.00	326.00	95.00	63.00	102.00
HF61/91	19.00	275.00	15.00	71.00	2.00	80.00	3.90		134.00	525.00	159.00	67.00	45.00
HF63/91	257.00	114.00	17.00	222.00	20.00	445.00	42.00		46.00	51.00	7.00	10.00	70.00
HF64/91	315.00	151.00	26.00	408.00	19.00	927.00	44.00		56.00	43.00	9.00	17.00	70.00
HF66b/91	76.00	244.00	25.00	117.00	5.00	187.00	12.00	10.00	168.00	273.00	82.00	57.00	70.00
HF67/91	467.00	21.00	10.00	58.00	19.00	56.00	29.00		7.00	29.00	6.00	6.00	65.00
HF73/91	359.00	46.00	20.00	135.00	11.00	420.00	28.00		31.00	49.00	11.00	10.00	50.00
HF94/90	155.00	196.00	27.00	149.00	3.00	259.00		23.00	143.00	127.00	25.00	11.00	64.00
HF95/90	25.00	270.00	21.00	83.00	2.00	53.00		5.00	165.00	242.00	198.00	43.00	57.00
HF98/90	260.00	70.00	27.00	70.00	10.00	309.00	26.00	6.00	23.00	57.00	7.00	0.00	26.00
KAW883	487.00	14.00	6.00	39.00	16.00	55.00	5.00	2.00	4.00	36.00	2.00	2.00	61.00
WAP25	180.00	114.00	17.00	116.00	3.00	986.00	24.00	9.00	63.00	73.00	30.00	12.00	42.00
BD-103	123.00	307.00	21.40	150.00	12.00	745.00		5.66					

Sample data continued

Sample	Ga	La	Ce	Pr	Nd	Sm	Eu	Gd	Tb	Dy	Ho	Er	Tm
TE153/93	28.00	84.00	176.00	19.00	68.00	11.00	1.80	6.00	0.70	2.80	0.40	1.10	0.14
TE154/93	27.00	89.00	160.00	20.00	75.00	12.00	1.80	7.00	0.70	3.40	0.55	1.50	0.19
TE189/93	17.00	40.00	79.00	9.00	35.00	6.00	1.70	4.00	0.50	2.60	0.43	1.10	0.15
TE192/93	17.00	30.00	60.00	7.00	28.00	5.00	1.30	3.00	0.40	2.10	0.36	0.90	0.13
CM045/93	19.00	52.00	107.00	12.00	39.00	6.00	1.20	4.00	0.50	2.10	0.38	1.00	0.12
CM070/93	20.00	15.00	36.00	5.00	21.00	5.00	1.50	4.00	0.70	3.70	0.75	1.90	0.29
CM108/93	21.00	37.00	72.00	8.00	29.00	5.00	1.60	4.00	0.60	3.50	0.69	1.60	0.27
HF092/93	21.00	100.00	19.30	18.00	6.30	11.00	1.30	9.00	1.30	7.20	1.70	4.30	0.74
HF095/93	20.00	77.00	160.00	16.00	56.00	10.00	1.60	9.00	1.30	7.80	1.67	4.30	0.71
HF197/93	19.00	37.00	74.00	8.00	30.00	6.00	1.40	4.00	0.60	3.50	0.77	1.90	0.28
TE059/93	18.00	37.00	76.00	8.00	30.00	5.00	1.00	4.00	0.50	2.70	0.51	1.40	0.20
TE073/93	19.00	29.00	60.00	7.00	30.00	6.00	1.90	5.00	0.70	3.30	0.71	1.60	0.24
TE082/93	19.00	22.00	45.00	6.00	24.00	5.00	1.50	4.00	0.60	3.60	0.78	2.00	0.26
TE086/93	18.00	53.00	109.00	13.00	50.00	9.00	2.30	6.00	0.80	3.80	0.68	1.80	0.24
TE110/93	20.00	10.00	23.00	3.00	14.00	4.00	1.40	4.00	0.70	3.90	0.92	2.40	0.38
HB06/97	23.00	9.00	18.00	2.00	8.00	2.00	0.60	2.00	0.40	2.10	0.30	0.60	0.10
HB18/97	20.00	45.00	89.00	11.00	40.00	9.00	1.30	7.00	1.10	5.80	1.00	2.70	0.40
HB25/97	19.00	39.00	80.00	10.00	37.00	7.00	1.10	7.00	1.00	6.30	1.23	3.50	0.55
HB26/97	16.00	17.00	37.00	5.00	17.00	5.00	0.40	5.00	1.00	7.10	1.55	4.60	0.90
HF05/92		34.00	73.00	8.80	32.00	7.30	0.80	5.30	0.82	4.80	0.88	2.40	0.35
HF143/90		53.00	106.00	13.00	56.00	10.00	1.30	10.00	1.10	6.20	1.10	2.90	0.37
HF144/90		87.00	132.00	18.00	75.00	12.00	1.50	13.00	1.50	8.70	1.70	3.70	0.50
HF59/91	19.00	10.00	27.00	3.70	18.00	4.70	1.50	4.40	0.77	5.00	1.10	2.70	0.39
HF61/91		6.00	16.00	2.20	10.00	2.60	0.90	2.40	0.41	2.50	0.57	1.50	0.21
HF63/91	22.00	58.00	132.00	15.00	56.00	11.00	1.10	7.60	0.91	3.90	0.66	1.60	0.19
HF64/91	23.00	97.00	218.00	26.00	101.00	16.00	1.50	11.00	1.20	5.90	1.00	2.50	0.31
HF66b/91	18.00	15.00	37.00	4.80	22.00	5.20	1.50	4.50	0.72	4.30	1.00	2.30	0.38
HF67/91		15.00	34.00	4.10	15.00	3.70	0.20	2.60	0.41	2.00	0.31	0.70	0.13
HF73/91		28.00	59.00	7.00	25.00	6.00	0.70	5.00	0.87	5.30	1.10	2.40	0.37
HF94/90	20.00	23.00	56.00	7.20	29.00	7.10	1.70	7.60	0.84	5.10	0.98	2.60	0.38
HF95/90	16.00	7.00	18.00	2.70	13.00	3.70	1.20	4.00	0.60	3.80	0.78	2.20	0.31
HF98/90	17.00	14.00	30.00	3.50	13.00	3.20	0.60	3.90	0.58	3.60	0.72	2.10	0.32
KAW883	2.00	9.00	21.00	2.70	11.00	2.90	0.30	3.00	0.27	1.50	0.20	0.60	0.09
WAP25	16.00	20.00	41.00	5.00	19.00	4.40	1.20	5.10	0.46	2.90	0.60	1.50	0.23
BD-103		40.30	72.80	8.04	28.50	5.51	1.21	5.61	0.73	4.00	0.76	2.08	0.31

Sample data continued

Sample	Yb	Lu	Th	U	Hf	Ta	Co	Source
TE153/93	0.80	0.14	34.00	10.00	10.30	1.40	13.00	Miller et al. (1999)
TE154/93	1.30	0.22	45.00	7.00	9.70	1.30	5.00	Miller et al. (1999)
TE189/93	0.90	0.14	10.00	3.00	4.50	0.80	7.00	Miller et al. (1999)
TE192/93	0.80	0.12	9.00	10.00			7.00	Miller et al. (1999)
CM045/93	0.80	0.12	61.00	9.00	6.00	1.50	7.00	Miller et al. (2000)
CM070/93	2.00	0.31	6.00	1.00	4.30	114.00	6.00	Miller et al. (2000)
CM108/93	1.80	0.28	12.00	1.00	5.00	0.70	9.00	Miller et al. (2000)
HF092/93	5.30	0.88	75.00	12.00	14.00	3.80	5.00	Miller et al. (2000)
HF095/93	4.90	0.77	55.60	7.00	12.30	2.80	4.00	Miller et al. (2000)
HF197/93	2.00	0.32	24.00	4.00	4.70	0.97	13.00	Miller et al. (2000)
TE059/93	1.40	0.25	19.00	5.00	4.00	1.40	3.00	Miller et al. (2000)
TE073/93	1.50	0.24	5.64	1.00	3.30	0.30	40.00	Miller et al. (2000)
TE082/93	1.90	0.28	4.00	1.00	3.50	0.40	44.00	Miller et al. (2000)
TE086/93	1.60	0.26	24.00	2.00			10.00	Miller et al. (2000)
TE110/93	2.50	0.42	5.00	4.00			5.00	Miller et al. (2000)
HB06/97	0.50	0.07	5.50	13.00	1.50	4.90	1.00	Miller et al. (2001)
HB18/97	2.30	0.40	27.30	3.00	6.90	2.30	8.00	Miller et al. (2001)
HB25/97	3.50	0.52	25.70	4.00	6.30	1.60	8.00	Miller et al. (2001)
HB26/97	5.70	0.92	16.70	12.00	3.40	2.40	1.70	Miller et al. (2001)
HF05/92	2.40	0.36					2.00	Miller et al. (2001)
HF143/90	2.10	0.28	34.00	4.50	0.22	9.60	9.00	Miller et al. (2001)
HF144/90	3.10	0.40					7.00	Miller et al. (2001)
HF59/91	2.70	0.37	4.50	1.50	4.20	0.28	41.00	Miller et al. (2001)
HF61/91	1.30	0.21	2.20	0.40	2.10	0.10	34.00	Miller et al. (2001)
HF63/91	1.40	0.20	38.00	4.00	7.00	1.50	7.00	Miller et al. (2001)
HF64/91	2.10	0.29	79.00	5.00	13.00	1.40	74.00	Miller et al. (2001)
HF66b/91	2.40	0.39	7.50	1.90	3.80	0.60	43.00	Miller et al. (2001)
HF67/91	0.70	0.10	13.00	3.00	2.50	3.50	1.00	Miller et al. (2001)
HF73/91	2.50	0.32	16.00	2.20	5.00	1.80	2.00	Miller et al. (2001)
HF94/90	2.38	0.33	16.00	4.00	0.50	5.90	39.00	Miller et al. (2001)
HF95/90	1.90	0.27	3.00	0.20	1.50			Miller et al. (2001)
HF98/90	2.10	0.28	12.00	4.70	0.30	1.90	3.00	Miller et al. (2001)
KAW883	0.42	0.07	11.00	2.40	0.30	2.00	6.00	Miller et al. (2001)
WAP25	1.27	0.21	13.00	3.60	0.40	5.60	12.00	Miller et al. (2001)
BD-103	2.25	0.35	27.70	6.23	3.93	0.89		Mo et al. (2008)

Table A.4: continued

Sample	Rb	Sr	Y	Zr	Nb	Ba	Pb	Sc	V	Cr	Ni	Cu	Zn
BD-145	63.10	351.00	22.10	129.00	7.29	428.00		13.30					
BD-151	21.80	436.00	23.30	156.00	6.14	390.00		12.60					
BD-160	71.30	566.00	22.70	134.00	5.88	392.00		11.80					
BD-55	105.00	132.00	29.50	114.00	8.56	581.00		6.35					
BD-58	62.10	763.00	27.00	118.00	7.94	636.00		20.40					
BD-65	53.20	1021.00	39.30	149.00	10.80	1023.00		16.30					
BD-77	123.00	335.00	28.90	234.00	19.40	919.00		3.28					
D-15	51.50	386.00	23.30	118.00	5.39	354.00		15.20					
D-2	41.40	450.00	23.30	136.00	7.04	965.00		15.30					
L060	81.00	178.00	35.50	112.00	11.00	279.00							
LZ9912	29.90	967.00	28.50	145.00	10.10	586.00		19.20					
LZ9916	88.70	206.00	13.70	101.00	7.88	1304.00		2.48					
LZ9917	163.00	164.00	17.70	113.00	8.67	813.00		4.20					
LZ9921	81.40	76.50	24.30	95.60	7.56	363.00		6.74					
LZ994	59.90	183.00	17.80	117.00	7.48	240.00		5.37					
P-1	198.00	235.00	17.80	142.00	11.90	691.00		2.50					
Y-2	254.00	1007.00	24.00	419.00	21.00	2599.00	45.00		88.00	53.00	24.00		
Y-4	274.00	583.00	15.00	255.00	14.00	2258.00	55.00		48.00	28.00	9.00		
ZB1	350.00	1441.00	26.00	298.00	34.00	2507.00	77.00		113.00	126.00	83.00		
ZB10	357.00	1626.00	28.00	334.00	36.00	2775.00	78.00		125.00	145.00	96.00		
ZB12	425.00	1495.00	29.00	424.00	50.00	2919.00	119.00		112.00	116.00	72.00		
ZB4	379.00	1638.00	28.00	335.00	38.00	2823.00	79.00		124.00	138.00	92.00		
YH01-1	44.10	457.00	24.00	118.00	11.40	322.00	7.70	29.50	253.00	84.20	26.70	36.30	91.40
YH01-2	118.00	77.00	10.80	119.00	18.80	480.00	16.70	2.35	16.10	5.05	2.62	2.89	19.00
YH02-1	43.80	402.00	17.40	118.00	10.70	318.00	3.99	19.50	144.00	529.00	152.00	60.10	64.80
YH02-2	83.00	82.90	9.89	107.00	17.30	709.00	5.39	2.22	13.20	3.85	2.45	2.40	17.00
YH03-1	144.00	7.39	9.01	91.80	17.50	102.00	3.17	1.54	8.85	2.35	0.58	6.27	7.10
YH10-2	58.60	556.00	13.80	101.00	8.58	706.00	7.65	11.10	116.00	13.00	5.84	14.30	59.00
YH10-3	30.20	466.00	18.20	92.20	7.01	431.00	8.68	20.70	193.00	14.50	7.95	202.00	96.20
YH10-4	45.50	536.00	13.80	102.00	8.82	642.00	9.21	10.90	118.00	12.40	5.92	36.00	59.10
YH10-6	40.20	523.50	17.10	82.50	13.10	496.00	8.78	17.20	196.40	14.60	7.17	36.90	74.70
YH22-1	47.10	448.00	18.90	82.20	5.84	112.00	18.30	33.00	257.00	310.00	75.80	177.00	136.00
YH22-2	12.90	379.00	14.90	57.50	3.26	78.50	7.06	38.50	279.00	496.00	152.00	55.60	128.00
YH22-3	187.00	193.00	10.30	109.00	17.50	635.00	17.00	1.60	10.50	3.81	2.34	4.93	30.50
YH22-4	163.00	172.00	10.10	113.00	17.10	546.00	12.20	1.55	10.10	3.04	2.16	3.97	24.80

Sample data continued

Sample	Ga	La	Ce	Pr	Nd	Sm	Eu	Gd	Tb	Dy	Ho	Er	Tm
BD-145		22.30	45.30	5.30	21.00	4.44	1.12	4.58	0.68	3.94	0.80	2.15	0.32
BD-151		20.00	41.40	5.17	21.80	4.78	1.24	4.82	0.71	4.17	0.85	2.24	0.33
BD-160		19.90	38.70	4.93	21.00	4.61	1.22	4.65	0.70	4.02	0.82	2.11	0.31
BD-55		31.90	63.00	7.24	27.70	5.71	0.72	5.96	0.90	5.23	1.08	2.89	0.43
BD-58		34.50	69.70	8.44	36.20	7.88	1.99	7.77	1.03	5.39	1.00	2.50	0.34
BD-65		48.20	87.90	11.10	45.90	9.29	2.33	9.02	1.11	5.69	1.01	2.54	0.36
BD-77		62.90	105.00	12.40	42.50	6.74	1.48	6.92	0.88	4.82	0.95	2.63	0.40
D-15		19.80	39.70	4.73	19.10	4.25	1.10	4.30	0.66	3.94	0.82	2.17	0.33
D-2		21.70	44.90	5.47	22.00	4.58	1.23	4.57	0.66	3.91	0.80	2.15	0.32
L060		40.90	88.80	10.90	34.70	7.58	1.09	6.95	1.12	5.88	1.27	3.24	0.52
LZ9912		48.80	106.00	12.00	51.30	9.73	2.58	8.38	1.28	6.26	1.04	2.77	0.33
LZ9916		28.20	44.00	6.21	23.00	4.27	0.96	3.24	0.46	2.51	0.49	1.29	0.20
LZ9917		38.30	60.70	8.24	29.10	5.32	1.10	4.02	0.57	3.47	0.60	1.71	0.23
LZ9921		33.70	64.70	8.12	29.60	5.67	0.58	4.58	0.68	4.31	0.89	2.43	0.34
LZ994		28.60	60.50	7.31	27.40	5.11	0.97	4.15	0.62	3.97	0.79	2.17	0.31
P-1		36.60	65.30	6.72	22.90	4.10	0.75	4.22	0.55	3.11	0.63	1.78	0.28
Y-2	21.00	96.70	196.40	28.00	107.00	16.30	3.40	12.10	1.20	5.30		2.00	
Y-4	18.00	65.70	114.60	16.30	60.40	9.10	2.10	6.90	0.70	3.20		1.20	
ZB1	17.00	62.20	121.80	19.80	86.60	16.80	3.30	10.90	1.20	5.30		2.00	
ZB10	20.00	67.60	136.10	21.70	93.20	18.00	3.60	11.90	1.30	5.80		2.20	
ZB12	21.00	69.40	138.10	21.70	91.20	17.90	3.50	12.00	1.30	6.10		2.30	
ZB4	21.00	72.00	138.90	22.80	97.90	19.10	3.70	12.40	1.30	5.90		2.30	
YH01-1	16.90	20.20	41.50	5.34	21.40	4.96	1.28	4.67	0.74	4.45	0.92	2.48	0.38
YH01-2	12.10	30.90	49.10	4.75	14.40	2.24	0.47	1.91	0.29	1.73	0.36	1.07	0.18
YH02-1	13.20	19.90	38.20	4.56	17.50	3.68	1.04	3.53	0.55	3.29	0.65	1.90	0.28
YH02-2	11.00	29.40	47.30	4.48	13.50	2.08	0.45	1.77	0.26	1.66	0.34	1.01	0.18
YH03-1	13.70	32.20	51.30	4.85	14.40	2.18	0.36	1.79	0.25	1.49	0.30	0.93	0.16
YH10-2	16.60	15.60	31.10	3.88	15.40	3.20	1.00	2.92	0.43	2.57	0.51	1.38	0.21
YH10-3	20.20	13.90	28.70	3.74	15.50	3.48	1.09	3.41	0.55	3.38	0.68	1.94	0.29
YH10-4	18.60	16.00	31.10	3.95	15.70	3.11	1.00	2.90	0.43	2.58	0.52	1.43	0.21
YH10-6	19.80	15.70	33.90	4.62	19.10	4.20	1.28	3.87	0.58	3.37	0.65	1.83	0.25
YH22-1	15.20	17.40	37.20	4.98	21.00	5.00	1.34	4.73	0.70	3.87	0.75	2.02	0.29
YH22-2	15.70	15.50	31.10	3.99	16.60	3.73	1.06	3.50	0.53	3.10	0.63	1.74	0.24
YH22-3	12.40	33.40	53.80	5.08	15.30	2.46	0.48	1.94	0.29	1.73	0.34	1.07	0.19
YH22-4	12.20	31.80	51.70	4.85	14.40	2.35	0.45	1.89	0.28	1.61	0.36	1.06	0.18

Sample data continued

Sample	Yb	Lu	Th	U	Hf	Ta	Co	Source
BD-145	2.34	0.35	11.10	2.32	3.54	0.56		Mo et al. (2008)
BD-151	2.41	0.36	9.10	1.99	4.17	0.44		Mo et al. (2008)
BD-160	2.31	0.34	7.65	1.42	3.57	0.42		Mo et al. (2008)
BD-55	3.23	0.48	19.10	3.24	3.99	0.71		Mo et al. (2008)
BD-58	2.41	0.35	9.10	1.48	2.94	0.32		Mo et al. (2008)
BD-65	2.49	0.36	13.90	2.08	3.69	0.46		Mo et al. (2008)
BD-77	2.92	0.46	24.00	6.13	5.77	1.05		Mo et al. (2008)
D-15	2.39	0.35	9.32	1.85	3.14	0.40		Mo et al. (2008)
D-2	2.39	0.36	9.17	1.88	3.50	0.47		Mo et al. (2008)
L060	3.08	0.49	13.00	2.85	3.22	0.71		Mo et al. (2008)
LZ9912	2.31	0.31	9.86	2.44	3.48	0.57		Mo et al. (2008)
LZ9916	1.28	0.19	13.20	5.48	2.55	0.54		Mo et al. (2008)
LZ9917	1.62	0.24	21.00	4.23	3.08	0.74		Mo et al. (2008)
LZ9921	2.33	0.34	16.50	3.66	3.66	0.90		Mo et al. (2008)
LZ994	2.23	0.33	14.00	2.70	4.19	0.75		Mo et al. (2008)
P-1	2.17	0.34	35.30	6.76	4.01	1.08		Mo et al. (2008)
Y-2	1.60	0.20	63.00	11.00	12.00	1.10		Nomade et al. (2004)
Y-4	1.00	0.10	49.00	7.00	7.00	0.80		Nomade et al. (2004)
ZB1	1.70	0.20	56.00	15.00	8.00	1.80		Nomade et al. (2004)
ZB10	1.90	0.30	59.00	16.00	9.00	1.90		Nomade et al. (2004)
ZB12	1.90	0.30	94.00	21.00	12.00	2.80		Nomade et al. (2004)
ZB4	1.90	0.30	64.00	15.00	10.00	2.00		Nomade et al. (2004)
YH01-1	2.30	0.36	5.25	1.23	3.19	0.79	31.10	Sui et al. (2013)
YH01-2	1.19	0.19	23.10	5.84	3.67	2.13	1.63	Sui et al. (2013)
YH02-1	1.76	0.27	7.86	2.19	2.97	0.99	33.50	Sui et al. (2013)
YH02-2	1.22	0.20	24.10	4.56	3.39	2.04	1.68	Sui et al. (2013)
YH03-1	1.15	0.19	23.50	3.64	2.94	2.17	0.22	Sui et al. (2013)
YH10-2	1.36	0.21	3.04	1.17	2.82	0.69	11.30	Sui et al. (2013)
YH10-3	1.91	0.29	2.35	0.84	2.62	0.52	20.10	Sui et al. (2013)
YH10-4	1.41	0.21	3.20	1.22	2.80	0.72	11.50	Sui et al. (2013)
YH10-6	1.62	0.25	2.26	0.86	2.40	0.86	18.60	Sui et al. (2013)
YH22-1	1.83	0.27	3.46	0.77	2.26	0.39	40.70	Sui et al. (2013)
YH22-2	1.45	0.21	4.88	0.93	1.80	0.23	46.90	Sui et al. (2013)
YH22-3	1.28	0.19	23.80	4.78	3.50	2.13	2.59	Sui et al. (2013)
YH22-4	1.23	0.20	23.50	4.41	3.48	2.11	1.28	Sui et al. (2013)

Table A.4: continued

Sample	Rb	Sr	Y	Zr	Nb	Ba	Pb	Sc	V	Cr	Ni	Cu	Zn
RG-13	39.50	366.90	25.70	174.30	0.00	323.30	7.60	18.10	133.00	13.70		29.10	62.60
RG-14	75.90	437.80	33.10	181.60	0.00	302.00	15.20	23.10	162.60	22.20		62.30	101.60
RG-16	67.10	321.50	18.50	141.90	0.00	425.30	3.40	9.70	59.10	111.70		29.50	36.90
RG-20	131.60	840.80	13.80	227.60	0.00	1378.00	62.80	6.00	71.90	14.80		29.70	45.90
RG-6	133.00	113.10	18.00	119.20	0.00	389.30	13.70	0.00	12.70	126.10		23.30	8.80
T024	40.90	738.00	5.00	139.00	4.05	461.00	16.90	6.10	11.80	11.40	5.80	28.10	51.20
T026	53.30	626.00	9.10	135.00	3.07	619.00	17.80	3.00	87.70	4.45	1.20	11.50	42.20
T027	41.30	622.00	9.30	106.00	4.95	407.00	12.40	7.30	32.40	9.07	5.20	558.50	60.90
T212	90.30	622.00	9.90	120.00	5.22	492.00	13.70	10.20	4.40	0.19	1.60	37.00	53.40
T213	45.10	688.00	11.60	102.00	3.73	479.00	16.20	9.40			1.10	15.10	62.40
T215	54.50	757.00	6.80	137.00	3.31	534.00	16.50	10.10			0.40	8.40	49.00
T216A	35.90	768.00	4.10	139.00	2.97	462.00	14.90	6.90			0.40	5.50	46.70
T217	49.90	780.00	7.10	122.00	3.46	534.00	18.70	9.90			0.70	8.60	44.30
T218B	42.60	719.00	5.00	117.00	2.79	600.00	14.50	7.20			0.50	12.50	49.30
JPT14.2	67.34	856.27	9.17	130.45	5.93	733.93	24.89						
T11B	99.76	996.22	8.82	139.34	6.22	740.06	25.82						
T2A	642.61	920.95	36.34	323.33	18.56	4220.68	10.26						
T3B	325.63	1114.95	35.82	367.91	20.36	2695.74	52.69						
T4A	401.00	698.87	26.98	484.50	23.78	2736.72	59.81						
T5A	283.93	767.48	22.31	253.46	14.40	1593.45	47.01						
Zc-05	2.70	184.00	24.00	51.00	1.20	17.00	0.89	30.00	235.00	222.00	47.00	39.00	
ZC-186	1.00	60.00	21.00	45.00	0.70	9.00	1.26	31.00	186.00	309.00	44.00	33.00	
ZC-192	3.30	116.00	20.00	48.00	0.60	9.00	2.14	34.00	219.00	592.00	41.00	38.00	
ZC-206	0.90	45.00	3.00	3.00	0.00	7.00	0.88	40.00	155.00	95.00	158.00	65.00	
ZC-232	2.40	95.00	24.00	63.00	0.60	15.00		31.00	224.00	2612.00	42.00	32.00	
GL-22	28.00	389.00	37.10	220.00	19.70	153.00	6.56	21.10	182.00	58.40	50.50	72.20	115.00
GL-24	49.40	405.00	33.30	193.00	18.10	214.00	1.93	19.20	201.00	118.00	67.10	74.80	105.00
GL-8	206.10	260.70	21.75	134.30	9.74	145.70	8.25	19.66	162.00	314.50	138.60	50.78	71.45
GLS-16	29.64	370.50	40.22	215.40	19.87	233.90	7.22	21.53	194.90	98.73	67.35	65.78	118.80
GLS-21	5.82	4.90	20.61	63.90	4.20	9.80	2.20	27.23	186.20	1145.20	696.80	204.20	84.88
GLS-27	6.79	232.90	36.97	129.70	11.63	98.80	5.21	40.31	324.70	77.54	49.44	169.90	101.90
TL-2	27.62	387.40	23.81	123.00	12.06	385.80	5.33	20.68	137.20	132.00	84.35	34.86	85.98
TL-3	29.76	391.80	31.52	127.50	12.75	411.40	6.23	21.30	139.80	151.20	142.40	34.79	123.40
TL-4	37.75	461.20	43.75	171.10	14.30	529.60	9.12	20.58	161.60	157.00	71.29	28.30	106.60
TL-7	157.20	235.30	24.36	118.20	8.57	215.50	17.93	17.80	190.20	13.25	9.49	34.60	82.06

Sample data continued

Sample	Ga	La	Ce	Pr	Nd	Sm	Eu	Gd	Tb	Dy	Ho	Er	Tm
RG-13	16.40	57.10	48.20	5.20	19.90	0.00	0.90	0.00	0.60				
RG-14	18.70	62.60	60.00	0.00	34.80	5.50	1.40	0.00	0.70				
RG-16	0.00	50.40	27.10	0.00	19.90	4.40	1.10	0.00	0.60				
RG-20	17.50	105.10	136.60	10.10	51.70	7.90	2.30	4.90	0.70				
RG-6	0.00	59.70	37.80	0.00	21.40	2.20	0.30	4.00	0.50				
T024	19.60	14.90	27.30	2.90	10.23	1.62	0.52	1.27	0.15	0.82	0.16	0.45	0.06
T026	16.00	26.50	49.20	5.04	17.61	2.61	0.68	1.91	0.27	1.31	0.27	0.84	0.14
T027	17.30	18.30	35.40	3.95	14.41	2.51	0.81	2.02	0.28	1.54	0.30	0.87	0.13
T212	18.70	21.50	36.30	4.53	16.80	3.03	0.81	2.30	0.33	1.69	0.31	0.86	0.13
T213	18.50	16.20	27.50	3.60	13.92	2.68	0.79	2.15	0.33	1.88	0.36	1.05	0.17
T215	17.90	22.20	35.40	4.17	14.53	2.09	0.68	1.50	0.17	0.85	0.18	0.63	0.11
T216A	17.80	21.20	33.70	4.06	14.41	2.23	0.71	1.56	0.19	0.81	0.14	0.38	0.05
T217	18.20	19.60	31.30	3.77	13.25	2.17	0.67	1.66	0.23	1.20	0.22	0.62	0.09
T218B	17.70	13.50	21.70	2.61	9.44	1.63	0.66	1.31	0.18	0.89	0.16	0.43	0.06
JPT14.2		26.82	53.20	6.49	25.01	4.18	1.08	3.08	0.36	1.73	0.30	0.76	0.11
T11B		28.53	56.16	6.78	26.31	4.28	1.11	3.11	0.36	1.70	0.29	0.73	0.10
T2A		145.85	314.84	40.72	167.12	30.13	5.33	19.92	2.05	8.20	1.17	2.70	0.35
T3B		95.95	198.94	25.13	101.55	18.19	3.49	12.67	1.52	7.07	1.19	2.96	0.42
T4A		133.70	284.13	40.47	164.95	27.24	4.58	15.53	1.50	5.93	0.87	2.06	0.27
T5A		56.43	123.50	16.12	66.96	11.90	2.17	7.89	0.91	4.24	0.72	1.84	0.27
Zc-05		2.45	8.66	1.40	7.76	2.57	0.95	3.14	0.57	3.89	1.00	2.57	0.41
ZC-186		1.48	5.99	1.02	5.94	2.13	0.81	2.63	0.48	3.28	0.86	2.16	0.35
ZC-192		1.94	6.96	1.16	6.50	2.24	0.84	2.68	0.48	3.19	0.84	2.06	0.34
ZC-206		0.15	0.41	0.04	0.27	0.10	0.11	0.12	0.02	0.30	0.10	0.31	0.06
ZC-232		2.45	8.88	1.50	8.28	2.71	1.01	3.20	0.57	3.92	1.01	2.55	0.41
GL-22	21.10	24.10	54.80	7.55	33.10	6.93	2.19	7.39	1.19	6.72	1.35	3.34	0.48
GL-24	19.30	16.60	43.10	6.43	27.90	6.32	2.11	6.63	1.05	6.15	1.30	3.58	0.54
GL-8	16.89	18.91	37.68	4.73	18.51	4.10	1.25	4.20	0.71	3.93	0.82	2.40	0.35
GLS-16	20.43	25.95	59.50	8.35	36.53	7.80	2.51	8.39	1.32	7.72	1.52	3.82	0.56
GLS-21	11.46	5.78	12.79	1.82	8.85	2.49	0.78	3.45	0.59	3.79	0.78	2.00	0.30
GLS-27	16.97	16.55	34.08	4.44	19.85	4.79	1.50	6.35	1.06	6.59	1.38	3.54	0.54
TL-2	18.00	25.05	46.79	5.74	22.49	4.52	1.45	4.80	0.74	4.48	0.83	2.16	0.32
TL-3	17.65	27.42	50.10	6.01	24.50	4.70	1.59	5.30	0.85	5.02	1.04	2.61	0.36
TL-4	18.75	41.29	71.04	8.38	33.01	6.07	1.76	6.30	1.02	6.11	1.24	3.35	0.45
TL-7	19.42	19.19	38.80	4.72	18.61	4.12	1.05	4.25	0.73	4.52	0.89	2.44	0.36

Sample data continued

Sample	Yb	Lu	Th	U	Hf	Ta	Co	Source
RG-13	2.20		1.90	0.00	0.00		15.70	Upadhyay et al. (2008)
RG-14	3.00		11.60	0.00	0.00		18.50	Upadhyay et al. (2008)
RG-16	1.50		6.60	0.00	7.50		6.90	Upadhyay et al. (2008)
RG-20	0.90		56.40	3.50	5.00		8.50	Upadhyay et al. (2008)
RG-6	1.60		15.90	0.00	0.10		2.00	Upadhyay et al. (2008)
T024	0.45	0.07	2.38	0.41	3.63	0.18	3.10	Wen et al. (2008)
T026	0.95	0.16	6.69	0.83	3.44	0.24	1.60	Wen et al. (2008)
T027	0.94	0.15	3.45	0.87	2.98	0.36	4.40	Wen et al. (2008)
T212	0.79	0.13	6.95	1.79	3.23	0.42	4.10	Wen et al. (2008)
T213	1.11	0.18	5.29	1.60	2.87	0.33	4.40	Wen et al. (2008)
T215	0.72	0.11	4.06	0.54	3.48	0.27	2.00	Wen et al. (2008)
T216A	0.36	0.06	4.03	0.38	3.43	0.14	2.50	Wen et al. (2008)
T217	0.59	0.10	4.21	0.57	3.12	0.20	1.90	Wen et al. (2008)
T218B	0.38	0.06	1.84	0.38	2.89	0.10	2.70	Wen et al. (2008)
JPT14.2	0.65	0.10	9.20	2.03	3.49	0.39		Williams et al. (2001)
T11B	0.61	0.09	9.37	1.96	3.64	0.39		Williams et al. (2001)
T2A	2.15	0.31	117.98	13.64	8.38	0.99		Williams et al. (2001)
T3B	2.55	0.38	68.32	10.35	9.62	1.25		Williams et al. (2001)
T4A	1.64	0.24	146.91	21.27	12.62	1.28		Williams et al. (2001)
T5A	1.62	0.24	79.29	13.85	6.88	0.76		Williams et al. (2001)
Zc-05	2.59	0.42	0.17	0.09	1.89			Xu et al. (2004)
ZC-186	2.16	0.35	0.17	0.11	1.67			Xu et al. (2004)
ZC-192	2.10	0.34	0.13	0.08	1.78			Xu et al. (2004)
ZC-206	0.46	0.09	0.11	0.08	0.06			Xu et al. (2004)
ZC-232	2.51	0.42	0.11	0.10	2.21			Xu et al. (2004)
GL-22	2.89	0.43	2.74	0.53	6.24	1.33	34.70	Xu et al. (2008)
GL-24	3.33	0.52	1.82	0.35	5.46	1.34	38.20	Xu et al. (2008)
GL-8	2.13	0.33	5.58	0.88	3.73	0.83	37.06	Xu et al. (2008)
GLS-16	3.38	0.50	3.29	0.55	6.46	1.46	39.97	Xu et al. (2008)
GLS-21	1.80	0.26	0.88	0.18	2.20	0.32	82.71	Xu et al. (2008)
GLS-27	3.14	0.47	4.57	0.84	4.30	0.89	44.12	Xu et al. (2008)
TL-2	1.87	0.26	5.49	0.70	3.55	0.75	40.63	Xu et al. (2008)
TL-3	2.18	0.33	5.89	0.79	3.63	0.79	62.39	Xu et al. (2008)
TL-4	2.69	0.41	7.31	0.79	4.86	0.89	62.38	Xu et al. (2008)
TL-7	2.24	0.34	8.22	1.37	4.08	0.57	21.16	Xu et al. (2008)

Table A.4: continued

Sample	Rb	Sr	Y	Zr	Nb	Ba	Pb	Sc	V	Cr	Ni	Cu	Zn
T339	201.00	726.00	8.29	84.10	7.52	889.00	24.30	5.34	52.70	18.60	10.70	365.00	23.00
T358	145.00	673.00	6.69	103.00	6.25	855.00	43.20	4.27	47.50	11.20	7.31	13.40	91.10
T379	153.00	766.00	8.42	90.80	7.83	845.00	33.50	5.44	58.80	23.50	10.40	7.00	41.10
T380	158.00	814.00	6.20	73.90	5.78	1042.00	37.00	4.46	45.00	15.20	8.02	14.20	42.20
T381	162.00	724.00	7.17	110.00	6.91	800.00	39.90	4.52	48.30	14.10	7.70	4.94	47.10
T399	204.00	713.00	7.99	94.90	7.92	825.00	31.90	3.91	47.70	8.90	7.94	4.50	49.00
T400	187.00	683.00	10.40	122.00	7.83	773.00	36.30	4.21	52.00	10.50	9.23	30.00	47.60
T401	187.00	583.00	7.75	107.00	8.94	794.00	31.00	3.44	36.40	6.79	5.31	2.56	29.60
T402	302.00	469.00	7.41	99.90	10.80	347.00	55.40	3.66	36.10	17.10	8.73	16.10	44.00
T403	372.00	628.00	7.12	88.30	10.20	1146.00	58.30	3.17	33.00	13.80	7.90	11.90	38.10
T404	270.00	582.00	7.08	116.00	8.54	672.00	52.90	3.49	33.70	10.10	6.08	31.20	44.50
T0317-01	168.00	355.00	5.97	107.00	5.06	473.00		3.42	23.00				
T0317-02	170.00	404.00	6.30	117.00	4.95	435.00		3.28	21.10				
T0317-03	171.00	416.00	5.82	123.00	4.91	508.00		3.51	22.60				
T0317-04	167.00	388.00	6.57	126.00	4.65	384.00		3.24	20.60				
T0317-05	148.00	378.00	6.39	125.00	4.41	466.00		3.22	22.00				
T0317-06	164.00	405.00	6.47	119.00	4.68	612.00		3.40	22.20				
T0319-06	195.00	349.00	3.74	120.00	4.12	397.00		2.34	14.20				
T0319-07	244.00	310.00	6.86	119.00	4.57	357.00		3.37	25.50				
T0319-08	155.00	313.00	6.77	126.00	5.58	483.00		4.53	37.30				
T0319-09	152.00	338.00	6.16	124.00	4.61	503.00		3.49	26.30				
T0319-10	161.00	323.00	6.66	121.00	4.61	412.00		3.49	24.80				
T0319-11	163.00	318.00	6.85	112.00	4.25	417.00		3.57	25.90				
T0319-12	167.00	315.00	6.43	124.00	4.79	411.00		3.88	28.70				
T0320-06	30.00	1564.00	6.24	42.00	1.16	112.00		1.40	6.40				
T0389-0	190.00	347.00	7.64	134.00	9.10	465.00		3.20	37.70				
T0389-10	190.00	334.00	8.07	126.00	9.20	449.00		2.68	40.30				
T0389-11	171.00	297.00	7.91	118.00	8.08	452.00		3.31	41.70				
T0389-12	152.00	319.00	7.39	124.00	7.95	483.00		2.61	41.30				
T0389-4	213.00	252.00	7.68	121.00	8.22	386.00		2.87	38.70				
T0389-5	196.00	341.00	7.34	121.00	7.87	417.00		3.32	36.70				
T0389-6	176.00	310.00	8.04	122.00	8.06	398.00		3.27	40.00				
T0389-7	187.00	299.00	8.20	128.00	7.63	421.00		3.57	40.20				
T0389-8	179.00	305.00	7.47	128.00	8.08	360.00		3.56	37.40				
T0389-9	184.00	339.00	7.88	119.00	8.31	436.00		3.25	40.90				

Sample data continued

Sample	Ga	La	Ce	Pr	Nd	Sm	Eu	Gd	Tb	Dy	Ho	Er	Tm
T339	18.40	28.60	62.40	7.00	26.20	4.44	1.00	2.62	0.31	1.45	0.27	0.68	0.11
T358	19.40	28.40	60.60	6.58	24.60	3.88	0.96	2.32	0.27	1.28	0.21	0.59	0.10
T379	19.80	32.90	68.90	7.58	27.00	4.37	1.08	2.82	0.34	1.55	0.28	0.77	0.10
T380	19.10	24.60	52.30	5.94	21.00	3.58	0.93	2.09	0.26	1.22	0.20	0.59	0.07
T381	19.80	29.60	60.20	6.70	23.80	4.00	0.93	2.42	0.29	1.40	0.24	0.62	0.09
T399	22.20	35.90	70.50	7.56	26.30	4.48	0.97	2.65	0.34	1.63	0.24	0.78	0.09
T400	21.90	39.90	78.70	8.59	30.00	5.11	1.03	3.13	0.42	2.02	0.32	0.92	0.13
T401	21.10	35.50	71.00	7.31	24.50	3.96	0.88	2.44	0.31	1.56	0.22	0.75	0.09
T402	20.30	32.00	66.10	7.29	25.90	4.55	0.80	2.50	0.31	1.48	0.23	0.74	0.09
T403	20.00	34.20	67.70	7.38	25.70	4.55	1.01	2.63	0.31	1.41	0.23	0.69	0.09
T404	20.50	45.40	90.20	8.81	29.00	4.80	0.88	2.67	0.32	1.37	0.23	0.68	0.08
T0317-01		27.70	54.40	5.97	22.00	4.23	1.04	3.22	0.33	1.35	0.21	0.58	0.06
T0317-02		28.70	55.50	6.20	22.40	4.36	1.10	3.27	0.33	1.26	0.23	0.62	0.08
T0317-03		29.20	57.90	6.16	22.70	4.45	1.17	3.24	0.36	1.21	0.21	0.53	0.07
T0317-04		28.00	53.30	6.14	22.70	4.22	1.08	3.28	0.34	1.32	0.21	0.63	0.09
T0317-05		28.60	54.70	6.27	21.40	4.42	1.15	3.33	0.34	1.39	0.20	0.59	0.07
T0317-06		30.40	57.10	6.53	23.10	4.73	1.20	3.58	0.35	1.47	0.22	0.65	0.07
T0319-06		22.30	43.30	4.62	17.00	3.55	1.07	2.54	0.26	0.96	0.13	0.38	0.05
T0319-07		29.60	60.10	6.83	25.10	5.16	0.86	3.16	0.29	1.61	0.27	0.73	0.10
T0319-08		39.70	80.50	9.37	35.10	6.98	1.10	4.37	0.40	2.27	0.37	0.98	0.13
T0319-09		33.30	67.20	7.62	28.30	5.48	0.99	3.26	0.28	1.54	0.24	0.67	0.08
T0319-10		33.00	66.00	7.54	28.00	5.46	0.94	3.27	0.30	1.67	0.27	0.77	0.09
T0319-11		28.50	57.60	6.51	24.10	4.83	0.91	2.97	0.30	1.70	0.29	0.80	0.11
T0319-12		30.90	62.80	7.09	26.50	5.33	0.92	3.41	0.29	1.61	0.26	0.69	0.09
T0320-06		7.17	12.70	1.39	4.64	1.26	0.74	1.38	0.21	1.04	0.18	0.50	0.07
T0389-0		23.90	41.30	5.55	20.50	4.34	1.08	3.13	0.36	1.52	0.25	0.71	0.09
T0389-10		19.10	41.30	4.74	17.60	3.94	1.05	3.00	0.34	1.63	0.27	0.71	0.10
T0389-11		25.00	51.50	5.53	19.70	3.96	1.05	2.96	0.34	1.53	0.25	0.65	0.09
T0389-12		18.60	39.30	4.38	16.00	3.65	0.98	2.66	0.31	1.42	0.25	0.69	0.09
T0389-4		20.60	31.50	4.84	17.90	3.79	0.85	2.90	0.34	1.51	0.24	0.65	0.09
T0389-5		20.90	35.30	4.84	18.00	3.86	1.05	2.83	0.33	1.43	0.24	0.67	0.09
T0389-6		23.20	47.90	5.37	19.60	4.00	1.04	2.98	0.36	1.64	0.27	0.73	0.10
T0389-7		27.60	49.90	6.20	22.30	4.43	1.07	3.16	0.38	1.62	0.27	0.68	0.09
T0389-8		19.60	34.90	4.39	16.40	3.44	0.96	2.53	0.31	1.40	0.23	0.65	0.09
T0389-9		26.50	53.50	5.75	20.80	4.28	1.13	3.12	0.34	1.55	0.25	0.70	0.11

Sample data continued

Sample	Yb	Lu	Th	U	Hf	Ta	Co	Source
T339	0.65	0.11	27.20	5.34	2.85	0.71	134.00	Xu et al. (2010)
T358	0.50	0.08	21.60	4.62	3.10	0.53	65.20	Xu et al. (2010)
T379	0.59	0.10	31.90	6.19	2.77	0.67	118.00	Xu et al. (2010)
T380	0.48	0.08	22.60	2.66	2.14	0.55	158.00	Xu et al. (2010)
T381	0.54	0.09	29.10	5.13	3.28	0.60	146.00	Xu et al. (2010)
T399	0.76	0.10	21.90	4.31	2.84	0.67	5.92	Xu et al. (2010)
T400	0.86	0.12	21.90	5.39	3.38	0.62	6.63	Xu et al. (2010)
T401	0.70	0.10	26.80	4.04	3.19	0.84	3.68	Xu et al. (2010)
T402	0.69	0.10	51.70	12.70	3.25	0.88	4.90	Xu et al. (2010)
T403	0.66	0.09	44.90	12.70	2.79	0.82	4.45	Xu et al. (2010)
T404	0.57	0.09	29.50	5.13	3.33	0.66	4.05	Xu et al. (2010)
T0317-01	0.46	0.07	12.10	1.74	3.30	0.49		Zeng et al. (2011)
T0317-02	0.47	0.07	12.30	1.18	3.59	0.48		Zeng et al. (2011)
T0317-03	0.46	0.08	12.00	1.30	3.51	0.41		Zeng et al. (2011)
T0317-04	0.49	0.08	11.60	2.44	3.52	0.41		Zeng et al. (2011)
T0317-05	0.51	0.08	11.80	1.88	3.85	0.39		Zeng et al. (2011)
T0317-06	0.47	0.08	12.00	1.07	3.64	0.35		Zeng et al. (2011)
T0319-06	0.32	0.05	11.30	1.01	3.53	0.35		Zeng et al. (2011)
T0319-07	0.60	0.08	10.60	2.31	3.30	0.38		Zeng et al. (2011)
T0319-08	0.78	0.11	12.10	2.62	3.55	0.45		Zeng et al. (2011)
T0319-09	0.54	0.08	11.60	2.39	3.53	0.42		Zeng et al. (2011)
T0319-10	0.60	0.09	12.20	2.20	3.40	0.38		Zeng et al. (2011)
T0319-11	0.67	0.10	9.80	1.05	3.27	0.38		Zeng et al. (2011)
T0319-12	0.54	0.08	11.00	1.09	3.55	0.33		Zeng et al. (2011)
T0320-06	0.41	0.06	7.10	9.31	1.50	0.42		Zeng et al. (2011)
T0389-0	0.56	0.07	10.70	1.80	3.67	0.81		Zeng et al. (2011)
T0389-10	0.65	0.09	10.20	2.03	3.61	0.92		Zeng et al. (2011)
T0389-11	0.64	0.09	12.20	2.53	3.45	0.75		Zeng et al. (2011)
T0389-12	0.59	0.08	9.60	2.10	3.50	0.74		Zeng et al. (2011)
T0389-4	0.56	0.08	11.20	1.84	3.44	0.79		Zeng et al. (2011)
T0389-5	0.60	0.09	10.40	2.08	3.61	0.82		Zeng et al. (2011)
T0389-6	0.62	0.09	11.30	2.32	3.48	0.69		Zeng et al. (2011)
T0389-7	0.60	0.10	12.40	2.22	3.61	0.72		Zeng et al. (2011)
T0389-8	0.55	0.09	10.20	2.25	3.62	0.74		Zeng et al. (2011)
T0389-9	0.63	0.09	12.80	2.35	3.47	0.88		Zeng et al. (2011)

Table A.4: continued

Sample	Rb	Sr	Y	Zr	Nb	Ba	Pb	Sc	V	Cr	Ni	Cu	Zn
T100	156.00	61.00	21.00	48.00	9.00	218.00							
T101	180.00	60.00	30.00	58.00	10.00	191.00							
T104	119.00	41.00	29.00	53.00	16.00	271.00							
T105	145.00	70.00	29.00	30.00	8.00	205.00							
T107	126.00	152.00	42.00	209.00	24.00	452.00							
T110	41.00	64.00	10.00	78.00	9.00	334.00							
T111	87.00	123.00	13.00	89.00	8.00	442.00							
T113	66.00	131.00	16.00	92.00	9.00	594.00							
T114	70.00	139.00	17.00	114.00	9.00	494.00							
T117	276.00	33.00	8.00	52.00	14.00	171.00							
T118	257.00	36.00	8.00	58.00	14.00	201.00							
T120	297.00	26.00	6.00	35.00	14.00	135.00							
T121	321.00	30.00	9.00	56.00	15.00	158.00							
T125	207.00	85.00	34.00	191.00	19.00	1335.00							
T129	131.00	32.00	31.00	178.00	15.00	1151.00							
T135	127.00	57.00	34.00	160.00	17.00	483.00							
T136	173.00	44.00	21.00	139.00	13.00	420.00							
T137	114.00	49.00	18.00	161.00	16.00	553.00							
T71	159.00	43.00	29.00	153.00	12.00	436.00							
T72	141.00	34.00	24.00	138.00	11.00	434.00							
T73	227.00	68.00	8.00	43.00	8.00	252.00							
T74	216.00	58.00	9.00	47.00	8.00	141.00							
T75	137.00	104.00	10.00	83.00	8.00	394.00							
T76	238.00	21.00	13.00	51.00	9.00	37.00							
T77	302.00	12.00	4.00	23.00	9.00	15.00							
T97-26	256.00	72.00	7.00	50.00	16.00	294.00							
T97-57	309.00	36.00	3.00	37.00	13.00	108.00							
T97-61	144.00	86.00	25.00	78.00	13.00	448.00							
T519	94.60	326.00	9.40	59.00	5.70	573.00							
T520	105.30	356.00	10.10	72.00	7.40	624.00							
T521	117.80	306.00	11.70	60.00	7.00	630.00							
T522	115.30	286.00	11.40	64.00	8.40	604.00							
T523	115.10	287.00	12.10	63.00	7.90	562.00							
T524	67.40	477.00	7.40	87.00	5.50	910.00							
T529	106.60	304.00	8.30	43.00	2.70	1012.00							

Sample data continued

Sample	Ga	La	Ce	Pr	Nd	Sm	Eu	Gd	Tb	Dy	Ho	Er	Tm
T100		5.30	11.30	1.21	4.90	1.34	0.28	1.64	0.37	2.71	0.67	2.10	
T101		7.50	15.90	1.72	6.90	1.85	0.34	2.28	0.52	3.78	0.94	2.93	
T104		3.90	8.50	0.93	3.80	1.08	0.24	1.59	0.41	3.36	0.89	2.76	
T105		6.30	13.20	1.41	5.70	1.72	0.47	2.31	0.54	3.88	0.92	2.79	
T107		55.90	115.80	11.99	45.50	8.81	1.47	7.69	1.19	6.85	1.45	3.98	
T110		13.20	28.20	3.09	12.20	2.73	0.56	2.38	0.35	1.76	0.33	0.85	
T111		16.30	34.70	3.78	14.90	3.35	0.74	2.96	0.45	2.29	0.44	1.13	
T113		25.90	55.00	5.94	23.30	5.05	1.00	4.33	0.62	3.11	0.59	1.46	
T114		22.50	47.70	5.14	20.10	4.40	0.93	3.84	0.57	2.93	0.57	1.46	
T117		9.20	19.20	2.04	7.80	1.96	0.24	1.76	0.29	1.47	0.25	0.59	
T118		8.90	18.60	1.96	7.40	1.76	0.17	1.64	0.27	1.46	0.27	0.68	
T120		6.30	13.00	1.35	5.10	1.25	0.19	1.15	0.20	1.01	0.18	0.44	
T121		11.10	23.30	2.46	9.20	2.33	0.23	2.11	0.35	1.77	0.31	0.74	
T125		50.00	103.20	10.58	40.10	7.97	1.33	6.89	1.09	6.09	1.25	3.38	
T129		28.80	61.20	6.60	25.70	5.57	0.99	5.04	0.87	5.16	1.10	3.09	
T135		45.20	94.30	9.86	37.30	7.25	1.18	6.45	1.04	6.01	1.29	3.58	
T136		19.80	40.80	4.16	15.30	3.30	0.38	3.03	0.53	3.13	0.67	1.87	
T137		30.50	64.30	6.86	26.50	5.30	0.84	4.30	0.62	3.30	0.68	1.94	
T71		21.30	43.70	4.41	16.30	3.65	0.40	3.62	0.67	4.15	0.93	2.63	
T72		14.80	31.10	3.29	12.50	2.94	0.34	2.91	0.54	3.35	0.74	2.13	
T73		9.60	20.10	2.11	8.10	1.84	0.35	1.63	0.27	1.45	0.27	0.74	
T74		10.30	21.40	2.23	8.60	1.95	0.32	1.72	0.29	1.53	0.29	0.75	
T75		19.20	41.00	4.45	17.40	3.83	0.68	3.05	0.42	1.95	0.35	0.84	
T76		4.30	9.20	1.01	3.80	1.25	0.09	1.43	0.33	2.07	0.43	1.21	
T77		2.00	4.30	0.45	1.70	0.59	0.04	0.62	0.13	0.68	0.11	0.26	
T97-26		11.50	24.00	2.51	9.60	2.28	0.47	2.06	0.31	1.47	0.26	0.60	
T97-57		4.90	10.10	1.04	3.80	1.02	0.14	1.00	0.17	0.79	0.12	0.25	
T97-61		28.30	58.80	6.11	23.10	4.59	0.69	3.53	0.63	3.40	0.74	2.22	
T519		17.30	33.70	3.70	12.80	2.32	0.71	1.72	0.29	1.74	0.30	0.79	0.12
T520		17.40	33.50	3.64	12.90	2.46	0.69	1.71	0.28	1.66	0.32	0.87	0.14
T521		15.90	31.40	3.58	12.80	2.39	0.71	1.92	0.33	2.09	0.36	1.07	0.15
T522		16.10	31.40	3.53	12.60	2.44	0.65	1.93	0.34	2.08	0.32	1.10	0.16
T523		16.40	32.20	3.61	12.60	2.52	0.67	1.93	0.34	2.17	0.36	1.00	0.15
T524		24.20	46.40	5.08	17.60	2.75	1.01	1.89	0.26	1.27	0.22	0.65	0.10
T529		31.40	63.60	7.29	26.40	4.75	1.19	3.26	0.45	1.94	0.31	0.79	0.09

Sample data continued

Sample	Yb	Lu	Th	U	Hf	Ta	Co	Source
T100	2.24	0.33	3.70	1.89	1.22	1.19		Zhang et al. (2004)
T101	3.13	0.45	5.40	1.26	1.90	1.64		Zhang et al. (2004)
T104	2.73	0.38	3.10	1.80	1.72	2.60		Zhang et al. (2004)
T105	2.92	0.42	4.20	1.09	1.08	1.56		Zhang et al. (2004)
T107	3.76	0.56	28.20	3.86	5.73	1.95		Zhang et al. (2004)
T110	0.80	0.11	6.60	1.15	2.43	1.19		Zhang et al. (2004)
T111	1.07	0.16	7.90	1.81	2.67	1.23		Zhang et al. (2004)
T113	1.24	0.18	12.10	2.07	2.66	0.59		Zhang et al. (2004)
T114	1.24	0.18	10.60	1.18	3.24	0.88		Zhang et al. (2004)
T117	0.53	0.07	4.70	1.14	1.94	4.35		Zhang et al. (2004)
T118	0.61	0.08	5.00	2.07	2.07	4.04		Zhang et al. (2004)
T120	0.39	0.05	3.30	1.97	1.29	5.00		Zhang et al. (2004)
T121	0.62	0.08	6.10	1.80	2.07	4.80		Zhang et al. (2004)
T125	3.35	0.52	27.20	3.17	5.42	1.65		Zhang et al. (2004)
T129	3.07	0.46	14.20	1.89	5.09	1.38		Zhang et al. (2004)
T135	3.49	0.53	20.50	2.51	4.59	1.52		Zhang et al. (2004)
T136	1.93	0.29	16.30	2.18	4.15	1.53		Zhang et al. (2004)
T137	2.01	0.31	14.40	2.01	4.61	1.30		Zhang et al. (2004)
T71	2.62	0.39	18.40	2.92	4.47	1.01		Zhang et al. (2004)
T72	2.14	0.33	13.40	2.42	4.10	0.89		Zhang et al. (2004)
T73	0.72	0.10	4.10	1.49	1.36	1.24		Zhang et al. (2004)
T74	0.72	0.10	4.40	1.74	1.56	1.27		Zhang et al. (2004)
T75	0.75	0.11	9.00	1.58	2.52	1.09		Zhang et al. (2004)
T76	1.29	0.18	2.60	2.16	2.13	1.34		Zhang et al. (2004)
T77	0.24	0.03	1.30	1.41	1.14	1.59		Zhang et al. (2004)
T97-26	0.50	0.07	6.20	3.17	1.70	3.51		Zhang et al. (2004)
T97-57	0.16	0.02	2.70	1.65	1.47	2.77		Zhang et al. (2004)
T97-61	2.34	0.35	18.20	4.75	2.53	1.60		Zhang et al. (2004)
T519	0.71							Zhang et al. (2010)
T520	0.93							Zhang et al. (2010)
T521	0.93							Zhang et al. (2010)
T522	0.98							Zhang et al. (2010)
T523	0.98							Zhang et al. (2010)
T524	0.62							Zhang et al. (2010)
T529	0.58							Zhang et al. (2010)

Table A.4: continued

Sample	Rb	Sr	Y	Zr	Nb	Ba	Pb	Sc	V	Cr	Ni	Cu	Zn
T529/2	114.80	301.00	8.10	56.00	2.20	948.00							
T632	90.70	595.00	8.60	118.00	5.90	879.00							
T633	146.00	286.00	11.10	136.00	10.10	651.00							
T634	75.30	716.00	9.50	99.00	4.50	778.00							
T636	92.80	748.00	11.60	104.00	7.60	388.00							
T637	64.20	509.00	9.20	139.00	7.30	852.00							
T638	83.90	816.00	5.20	84.00	3.80	530.00							
CQ01	451.00	1144.00	32.20	643.00	32.70	3387.00	89.00	17.50	125.00	561.00	372.00	52.00	79.00
CQ02	487.00	1260.00	28.80	525.00	29.30	1853.00	41.00	14.40	116.00	103.00	70.00	31.00	84.00
CQ03	331.00	1343.00	39.50	831.00	43.20	5513.00	121.00	19.60	127.00	610.00	341.00	59.00	85.00
D9103	486.00	1020.00	34.10	611.00	33.60	2984.00	89.00	15.00	76.00	364.00	209.00	33.00	70.00
DR01-1	435.00	967.00	20.80	898.00	60.10	3038.00	154.00	8.40	64.00	70.00	52.00	30.00	63.00
DR01-2	419.00	1075.00	21.60	849.00	53.80	3354.00	167.00	9.40	72.00	92.00	64.00	27.00	64.00
DR03	416.00	1283.00	20.50	903.00	58.50	3299.00	182.00	8.60	65.00	74.00	53.00	29.00	62.00
DR04	459.00	1286.00	20.90	868.00	52.80	3966.00	220.00	9.40	76.00	82.00	61.00	29.00	66.00
GGP-7	298.00	2169.00	39.00	283.00	12.80	10170.00	284.00	22.30	125.00	401.00	319.00	65.00	85.00
SL0618	494.00	888.00	25.20	527.00	26.70	2542.00	57.00	14.60	114.00	235.00	133.00	23.00	79.00
SL0619	497.00	893.00	24.80	528.00	26.96	2583.01	62.00	14.48	112.76	227.00	142.03	25.00	83.00
SL0620	533.00	870.00	25.00	519.00	25.90	2504.00	58.00	14.40	112.00	232.00	119.00	24.00	81.00
SL0621	389.00	942.00	29.50	568.00	33.90	2474.00	56.00	18.70	138.00	470.00	283.00	29.00	86.00
SL0622	469.00	896.00	27.20	534.00	26.60	2549.00	68.00	14.80	110.00	236.00	138.00	33.00	83.00
SL0623	499.00	814.00	26.20	540.00	31.40	2084.00	49.00	17.70	128.00	459.00	309.00	42.00	78.00
SL0624	583.00	873.00	27.20	562.00	30.70	2310.00	50.00	17.30	130.00	426.00	252.00	34.00	77.00
SL0625	507.00	761.00	28.20	517.00	30.70	2137.00	44.00	17.80	130.00	364.00	124.00	34.00	95.00
SL0628	391.00	787.00	20.40	381.00	22.13	1692.19	36.00	14.08	107.55	196.00	105.89	33.00	86.00
SL0630	601.00	939.00	30.40	621.00	34.48	2480.37	44.00	18.25	144.69	496.00	144.46	20.00	85.00
SL0631	434.00	1003.00	25.10	491.00	29.60	2269.00	49.00	17.30	144.00	368.00	209.00	28.00	86.00
XR01-1	650.00	893.00	27.80	484.00	30.20	1737.00	71.00	12.70	75.00	147.00	83.00	31.00	77.00
XR01-3	2518.00	1264.00	33.60	679.00	34.60	4044.00	99.00	18.60	125.00	670.00	395.00	42.00	79.00
XR02-1	873.00	1057.00	38.10	809.00	54.30	2893.00	133.00	17.10	114.00	266.00	165.00	41.00	86.00
Z8030-18	595.00	1225.00	27.40	794.00	35.30	2751.00	95.00	16.20	130.00	229.00	141.00	34.00	89.00
Z8030-5	1574.00	1226.00	20.00	870.00	55.80	2760.00	121.00	12.90	95.00	213.00	124.00	31.00	81.00
ZB11	354.00	1700.00	28.20	341.00	37.00	2859.00	87.00	13.70	127.30	138.00	92.20	58.00	102.00
ZB14	450.00	1489.00	28.20	442.00	52.20	2871.00	111.00	11.95	106.50	106.00	73.60	78.00	95.00
ZB16	420.00	1504.00	28.40	440.00	50.60	2899.00	90.00	11.87	114.60	106.00	71.10	55.00	96.00

Sample data continued

Sample	Ga	La	Ce	Pr	Nd	Sm	Eu	Gd	Tb	Dy	Ho	Er	Tm
T529/2		28.90	58.50	6.66	24.00	4.40	0.93	3.13	0.38	1.77	0.31	0.69	0.09
T632		26.60	51.20	6.06	20.40	3.18	1.10	2.25	0.28	1.57	0.30	0.80	0.12
T633		41.20	77.30	8.70	28.20	4.86	0.82	3.63	0.45	2.22	0.39	0.97	0.15
T634		37.30	72.40	8.82	30.10	4.57	1.07	3.05	0.36	1.93	0.35	0.86	0.13
T636		40.80	79.70	9.69	33.50	5.73	1.05	4.51	0.59	2.78	0.43	0.87	0.10
T637		85.30	148.00	16.10	51.30	6.77	1.20	4.50	0.45	2.00	0.34	0.84	0.10
T638		18.80	36.90	4.66	17.00	3.00	1.06	2.12	0.23	1.05	0.18	0.47	0.08
CQ01	20.60	126.80	344.00	54.20	261.00	48.60	7.56	27.60	2.69	9.70	1.22	3.17	0.31
CQ02	20.40	99.50	220.00	30.60	124.00	20.90	3.64	14.30	1.53	6.50	1.00	2.57	0.31
CQ03	22.10	175.30	455.00	67.20	310.00	59.50	8.65	33.20	3.19	11.90	1.44	3.79	0.37
D9103	21.60	100.40	232.00	36.30	159.00	29.00	4.62	18.20	1.96	8.30	1.26	3.29	0.39
DR01-1	25.40	217.10	433.00	51.60	191.00	25.50	4.21	17.80	1.55	6.00	0.77	2.21	0.23
DR01-2	24.10	204.00	411.00	50.30	187.00	25.60	4.34	17.70	1.56	6.20	0.80	2.28	0.24
DR03	24.90	208.40	416.00	50.70	188.00	25.20	4.22	17.60	1.54	5.90	0.77	2.21	0.24
DR04	25.50	220.70	446.00	49.00	177.00	23.70	4.25	16.60	1.44	5.70	0.74	2.03	0.23
GGP-7	14.60	144.00	257.00	33.70	133.00	25.00	7.46	20.20	2.23	9.60	1.46	3.55	0.42
SL0618	21.70	124.60	311.00	42.70	178.00	33.00	5.31	16.60	1.57	5.90	0.90	2.26	0.27
SL0619	22.14	126.20	307.00	43.00	177.00	32.60	5.29	16.40	1.57	5.80	0.88	2.22	0.27
SL0620	21.50	119.90	288.00	39.70	171.00	31.00	5.07	15.90	1.51	5.70	0.87	2.21	0.27
SL0621	21.00	104.10	271.00	37.80	169.00	31.90	5.00	16.00	1.58	6.40	1.07	2.70	0.34
SL0622	22.20	125.80	307.00	42.70	180.00	33.00	5.39	16.90	1.59	6.10	0.96	2.31	0.29
SL0623	19.60	97.40	258.00	36.10	162.00	29.90	4.52	14.60	1.45	5.90	0.96	2.48	0.32
SL0624	20.10	102.80	266.00	37.80	168.00	32.10	4.96	15.60	1.53	6.20	0.99	2.59	0.33
SL0625	21.30	98.60	232.00	32.80	142.00	26.50	4.15	13.90	1.39	5.90	0.97	2.52	0.32
SL0628	20.99	83.70	185.00	25.20	107.00	19.10	3.24	10.00	1.04	4.50	0.78	1.98	0.26
SL0630	22.09	118.50	310.00	46.30	206.00	40.00	6.11	19.50	1.83	7.30	1.12	2.74	0.35
SL0631	21.40	102.40	257.00	36.00	156.00	29.70	4.80	15.10	1.44	5.90	0.93	2.33	0.29
XR01-1	21.40	112.00	243.00	33.50	136.00	24.70	3.78	15.70	1.66	7.00	0.99	2.62	0.30
XR01-3	20.60	146.60	386.00	59.10	269.00	51.60	7.52	28.90	2.79	10.30	1.28	3.39	0.33
XR02-1	22.60	128.40	335.00	52.70	239.00	48.50	6.80	28.00	2.88	11.00	1.44	3.67	0.38
Z8030-18	26.60	148.50	354.00	49.50	209.00	34.10	5.01	19.80	1.86	7.30	1.00	2.58	0.30
Z8030-5	28.40	209.80	419.00	53.70	199.00	25.50	3.83	18.10	1.57	6.10	0.77	2.23	0.23
ZB11	20.40	68.10	139.00	21.90	95.00	18.30	3.60	12.00	1.33	5.90	0.88	2.27	0.29
ZB14	21.70	69.50	138.00	21.20	89.00	17.00	3.37	11.40	1.28	5.70	0.87	2.23	0.29
ZB16	21.00	69.10	139.00	21.20	89.00	17.20	3.41	11.50	1.29	5.90	0.86	2.23	0.29

Sample data continued

Sample	Yb	Lu	Th	U	Hf	Ta	Co	Source
T529/2	0.52							Zhang et al. (2010)
T632	0.67							Zhang et al. (2010)
T633	0.92							Zhang et al. (2010)
T634	0.78							Zhang et al. (2010)
T636	0.53							Zhang et al. (2010)
T637	0.64							Zhang et al. (2010)
T638	0.44							Zhang et al. (2010)
CQ01	2.10	0.30	215.60	32.25	18.60	1.90	58.00	Zhao et al. (2009)
CQ02	1.97	0.29	81.20	15.97	13.80	1.85	41.00	Zhao et al. (2009)
CQ03	2.37	0.33	298.00	19.52	22.80	2.44	51.00	Zhao et al. (2009)
D9103	2.54	0.38	123.30	20.71	19.10	2.46	43.00	Zhao et al. (2009)
DR01-1	1.52	0.23	158.60	18.63	26.20	3.42	44.00	Zhao et al. (2009)
DR01-2	1.57	0.24	139.20	16.89	24.50	3.05	43.00	Zhao et al. (2009)
DR03	1.54	0.23	152.40	18.21	26.70	3.36	54.00	Zhao et al. (2009)
DR04	1.52	0.22	172.20	19.40	24.00	3.13	54.00	Zhao et al. (2009)
GGP-7	2.65	0.39	69.60	11.38	6.70	0.71	54.00	Zhao et al. (2009)
SL0618	1.69	0.23	179.00	20.76	14.00	1.47	23.00	Zhao et al. (2009)
SL0619	1.73	0.24	178.91	19.94	14.10	1.47	23.00	Zhao et al. (2009)
SL0620	1.63	0.23	171.00	20.74	13.50	1.40	21.00	Zhao et al. (2009)
SL0621	2.19	0.29	189.00	21.82	15.70	1.89	33.00	Zhao et al. (2009)
SL0622	1.78	0.25	178.00	20.00	13.90	1.46	23.00	Zhao et al. (2009)
SL0623	1.88	0.27	174.00	21.68	14.70	1.75	33.00	Zhao et al. (2009)
SL0624	2.03	0.28	188.00	23.65	15.30	1.73	31.00	Zhao et al. (2009)
SL0625	1.94	0.28	147.00	19.22	13.90	1.64	28.00	Zhao et al. (2009)
SL0628	1.57	0.23	105.23	13.25	9.80	1.20	19.00	Zhao et al. (2009)
SL0630	2.13	0.29	217.61	25.01	16.90	1.88	33.00	Zhao et al. (2009)
SL0631	1.71	0.23	170.00	19.92	13.00	1.60	30.00	Zhao et al. (2009)
XR01-1	1.96	0.29	112.10	27.00	13.80	2.13	43.00	Zhao et al. (2009)
XR01-3	2.15	0.30	239.40	33.89	19.60	2.02	55.00	Zhao et al. (2009)
XR02-1	2.40	0.35	242.00	41.13	25.10	3.30	40.00	Zhao et al. (2009)
Z8030-18	1.94	0.28	173.80	16.66	23.10	2.24	37.00	Zhao et al. (2009)
Z8030-5	1.47	0.22	100.80	7.45	26.00	3.19	29.00	Zhao et al. (2009)
ZB11	1.87	0.27	61.00	14.39	9.40	1.94	21.00	Zhao et al. (2009)
ZB14	1.89	0.26	96.00	23.57	12.00	2.81	16.00	Zhao et al. (2009)
ZB16	1.86	0.27	97.50	23.88	12.10	2.80	17.00	Zhao et al. (2009)

Table A.4: continued

Sample	Rb	Sr	Y	Zr	Nb	Ba	Pb	Sc	V	Cr	Ni	Cu	Zn
ZB18	442.00	1544.00	29.60	388.00	48.20	2743.00	83.00	13.14	128.10	116.00	66.80	36.00	98.00
ZB20	443.00	1497.00	28.80	378.00	47.90	2661.00	82.00	13.72	128.60	117.00	67.40	46.00	99.00
ZB21	788.00	1315.00	34.80	1433.00	122.00	3087.00	169.00	10.50	121.00	52.00	40.00	39.00	121.00
ZB22	669.00	872.00	29.70	1001.00	77.40	2231.00	126.00	10.20	106.00	53.00	44.00	26.00	91.00
ZB3	359.00	1673.00	29.10	333.00	36.60	2698.00	82.00	14.34	139.60	126.00	89.10	47.00	94.00
ZB6	349.00	1620.00	27.90	324.00	37.80	2656.00	87.00	14.41	130.40	130.00	87.30	57.00	93.00
ZB8	356.00	1695.00	28.70	334.00	38.50	2858.00	88.00	13.92	129.30	135.00	92.40	65.00	105.00
ZB9	337.00	1682.00	27.50	334.00	35.60	2719.00	81.00	13.62	127.30	132.00	89.60	64.00	101.00
GZ-11	326.00	282.00	8.02	171.00	17.20	792.00	48.00	2.40	29.00	19.10	7.30	7.40	52.30
GZ-12	203.00	370.00	14.30	180.00	12.80	581.00	42.30	4.20	62.00	4.00	1.30	7.90	89.20
GZ-14	167.00	442.00	13.70	176.00	11.50	639.00	19.90	2.40	63.00	4.70	1.90	12.30	47.90
GZ-3	248.00	139.00	4.36	156.00	14.20	657.00	48.80	2.30	28.00	16.60	5.30	9.80	50.50
GZ-5	176.00	376.00	14.70	168.00	11.70	884.00	33.10	5.20	71.00	8.60	5.00	18.20	39.00
GZ-6	312.00	487.00	8.41	173.00	17.80	1031.00	67.60	2.80	30.00	21.10	10.20	10.70	39.10
GZ-7	132.00	808.00	9.86	209.00	18.50	1524.00	50.70	8.90	130.00	68.40	35.80	22.00	84.50
GZ-8	196.00	203.00	6.05	162.00	10.90	469.00	29.30	3.10	25.00	21.30	9.20	11.20	55.60
GZ-9	167.00	461.00	13.80	177.00	11.40	700.00	19.40	4.80	66.00	8.20	2.80	12.40	9.20
GZ-10	116.00	779.00	7.70	144.00	6.40	904.00	37.90	4.84	61.50	21.10	12.50	23.30	52.90
GZ-15	153.00	696.00	7.60	143.00	6.50	988.00	35.60	4.32	63.70	19.10	11.30	15.20	50.80
GZ-16	116.39	1030.40	7.08	157.68	5.04	914.93	39.00				18.48		
GZ-18	97.85	965.51	6.95	138.50	4.65	809.79	37.70				14.64		
Y-1-1	212.00	1065.00	18.10	364.00	19.30	2359.00	56.90	6.43	64.90	56.10	22.70	17.90	34.50
Y-3	423.00	424.00	17.50	317.00	20.40	1841.00	72.50	4.65	26.10	16.60	8.00	18.60	47.50
DX13-1	109.00	175.00	46.30	257.00	12.20	719.00	17.40	12.70	42.70	3.22	2.73	6.84	
DX19-1	96.00	231.00	24.00	134.00	6.42	599.00	12.90	9.44	43.80	3.41	1.98	5.62	
DX2-1	103.00	194.00	48.80	289.00	12.40	633.00	16.00	16.60	68.60	4.47	3.66	11.00	
DX21-1	126.00	49.90	23.50	92.50	8.18	750.00	4.75	3.32	4.16	2.18	1.67	2.52	
DXL1-3	57.20	79.20	17.30	85.80	8.87	200.00	26.90	4.27	28.80	3.23	2.97	10.60	
GB-8	264.00	114.00	20.80	151.00	8.07	1280.00	184.00	7.04	31.60	4.34	1.88	12.10	
NX5-2	106.00	260.00	22.10	139.00	7.05	452.00	12.20	9.06	71.70	6.91	4.03	4.51	
NX5-3	80.10	261.00	42.90	104.00	7.90	328.00	12.60	21.30	186.00	36.80	8.42	14.10	
SZ39	194.00	53.40	28.10	96.00	12.40	355.00	27.40	2.31	1.03	91.30	1.37	1.22	
SZ43	167.00	160.00	30.20	185.00	12.10	1230.00	28.70	4.27	12.50	65.50	1.10	2.95	
SZ48	83.50	273.00	25.30	130.00	8.24	661.00	19.70	20.90	147.00	26.70	7.91	19.80	
SZ52	131.50	124.00	27.10	181.00	10.20	190.00	14.40	11.20	65.80	20.70	3.88	9.10	

Sample data continued

Sample	Ga	La	Ce	Pr	Nd	Sm	Eu	Gd	Tb	Dy	Ho	Er	Tm
ZB18	20.50	68.40	138.00	21.70	93.00	17.90	3.54	12.00	1.35	6.00	0.90	2.33	0.29
ZB20	19.90	67.40	140.00	21.60	92.00	17.60	3.52	11.80	1.30	5.90	0.88	2.27	0.29
ZB21	25.10	123.90	265.00	35.80	141.00	26.30	5.07	18.20	2.06	8.90	1.34	3.41	0.44
ZB22	24.70	106.80	225.00	30.50	120.00	21.90	4.16	15.20	1.68	7.20	1.11	2.89	0.37
ZB3	20.20	68.90	135.00	21.70	94.00	18.10	3.55	12.00	1.32	5.80	0.89	2.25	0.29
ZB6	19.80	67.90	135.00	21.70	93.00	18.10	3.51	11.90	1.29	5.70	0.85	2.22	0.28
ZB8	20.40	70.10	138.00	22.10	96.00	18.70	3.67	12.30	1.34	5.90	0.86	2.25	0.28
ZB9	19.80	67.50	136.00	21.60	93.00	17.90	3.56	11.90	1.28	5.80	0.85	2.20	0.27
GZ-11	19.80	36.90	67.40	8.41	28.30	4.38	0.82	2.70	0.36	1.60	0.31	0.80	0.13
GZ-12	15.10	24.20	44.40	6.09	22.20	3.99	0.98	3.15	0.45	2.49	0.52	1.51	0.24
GZ-14	19.80	27.40	53.90	6.97	23.20	4.10	1.07	3.33	0.51	2.65	0.59	1.74	0.24
GZ-3	18.60	14.50	37.70	4.14	13.60	2.20	0.45	1.33	0.16	0.85	0.17	0.48	0.09
GZ-5	15.20	26.60	53.90	6.49	22.20	3.92	0.97	3.10	0.48	2.69	0.54	1.67	0.27
GZ-6	18.10	43.80	88.30	9.87	33.40	5.03	0.93	3.04	0.40	1.75	0.34	0.85	0.14
GZ-7	20.00	58.30	107.00	12.90	46.80	6.89	1.59	4.36	0.55	2.34	0.43	0.96	0.14
GZ-8	20.10	27.50	48.60	6.90	23.40	3.67	0.72	2.23	0.28	1.26	0.24	0.60	0.10
GZ-9	12.30	25.10	46.20	6.10	21.50	3.78	0.98	3.09	0.47	2.58	0.53	1.55	0.25
GZ-10	19.40	26.70	55.00	6.80	26.00	4.30	1.02	3.22	0.35	1.64	0.26	0.68	0.09
GZ-15	19.90	27.20	56.00	6.80	26.40	4.30	1.01	3.26	0.35	1.62	0.25	0.65	0.08
GZ-16													
GZ-18													
Y-1-1	18.80	82.10	169.00	24.00	90.40	13.40	2.70	9.84	0.96	4.09	0.55	1.55	0.18
Y-3	18.10	76.30	149.00	20.10	71.30	10.20	1.85	8.20	0.83	3.71	0.57	1.61	0.21
DX13-1	18.10	40.20	81.50	9.62	37.30	7.77	1.70	8.13	1.22	7.86	1.70	4.79	0.67
DX19-1	15.00	29.50	55.70	5.97	22.70	4.30	0.92	3.97	0.63	3.77	0.77	2.35	0.36
DX2-1	16.70	40.00	82.60	9.96	40.00	8.45	1.91	9.17	1.38	8.91	1.94	5.46	0.76
DX21-1	12.70	31.20	57.90	5.86	20.30	3.94	0.59	3.94	0.56	3.63	0.82	2.52	0.39
DXL1-3	11.10	21.70	44.70	4.85	17.60	3.85	0.53	3.63	0.53	3.33	0.69	1.97	0.29
GB-8	11.40	31.60	56.50	5.66	20.50	3.95	0.79	3.48	0.56	3.30	0.69	2.10	0.34
NX5-2	15.60	31.00	57.40	5.92	21.30	4.08	1.07	4.11	0.58	3.64	0.81	2.35	0.34
NX5-3	17.60	30.80	69.20	8.37	33.40	7.23	1.74	7.24	1.08	7.09	1.55	4.60	0.68
SZ39	13.30	22.00	54.70	5.92	22.60	5.32	0.55	5.17	0.91	5.36	1.06	3.01	0.46
SZ43	16.40	62.00	123.00	14.30	50.90	8.28	1.64	8.10	1.06	5.76	1.04	3.00	0.42
SZ48	15.10	27.00	53.10	6.00	23.70	4.60	1.13	4.81	0.73	4.31	0.86	2.55	0.39
SZ52	16.40	35.10	67.80	7.48	29.10	5.31	1.11	5.57	0.82	4.74	0.95	2.77	0.41

Sample data continued

Sample	Yb	Lu	Th	U	Hf	Ta	Co	Source
ZB18	1.90	0.28	82.90	24.11	10.80	2.58	18.00	Zhao et al. (2009)
ZB20	1.92	0.28	82.90	22.26	10.60	2.56	18.00	Zhao et al. (2009)
ZB21	2.94	0.45	322.50	76.18	38.80	7.79	33.00	Zhao et al. (2009)
ZB22	2.47	0.38	264.60	55.21	27.60	3.85	56.00	Zhao et al. (2009)
ZB3	1.89	0.27	59.70	14.37	9.30	1.89	22.00	Zhao et al. (2009)
ZB6	1.81	0.28	61.20	14.05	9.20	1.99	20.00	Zhao et al. (2009)
ZB8	1.86	0.26	61.90	14.01	9.30	1.98	21.00	Zhao et al. (2009)
ZB9	1.82	0.26	59.50	14.88	9.10	1.88	21.00	Zhao et al. (2009)
GZ-11	0.74	0.12	46.20	12.50	5.20	1.00	4.00	Zhao et al. (2011)
GZ-12	1.48	0.24	21.50	2.90	3.90	0.70	4.90	Zhao et al. (2011)
GZ-14	1.44	0.23	21.40	4.70	4.30	0.90	6.10	Zhao et al. (2011)
GZ-3	0.49	0.09	42.90	6.10	4.30	0.80	4.30	Zhao et al. (2011)
GZ-5	1.76	0.26	24.00	3.80	4.60	0.90	8.00	Zhao et al. (2011)
GZ-6	0.83	0.13	46.50	13.60	5.40	1.10	5.00	Zhao et al. (2011)
GZ-7	0.77	0.10	27.30	3.40	4.80	1.40	17.10	Zhao et al. (2011)
GZ-8	0.59	0.09	37.10	9.00	4.40	0.70	5.10	Zhao et al. (2011)
GZ-9	1.60	0.25	21.80	3.90	4.50	0.90	5.40	Zhao et al. (2011)
GZ-10	0.59	0.09	18.70	3.70	3.93	0.43	3.00	Zhou et al. (2010)
GZ-15	0.56	0.08	19.50	3.30	3.98	0.45	0.90	Zhou et al. (2010)
GZ-16			19.96					Zhou et al. (2010)
GZ-18			16.77					Zhou et al. (2010)
Y-1-1	1.23	0.18	55.10	7.30	10.08	0.96	1.70	Zhou et al. (2010)
Y-3	1.44	0.22	64.40	11.50	9.08	1.23	0.03	Zhou et al. (2010)
DX13-1	4.43	0.66	16.00	2.51	6.73	1.05	6.34	Zhu et al. (2009)
DX19-1	2.40	0.37	14.40	1.34	3.57	0.58	4.28	Zhu et al. (2009)
DX2-1	4.95	0.72	15.00	2.36	7.90	1.09	8.72	Zhu et al. (2009)
DX21-1	2.81	0.44	23.20	3.48	3.06	1.09	1.13	Zhu et al. (2009)
DXL1-3	2.06	0.30	20.30	1.93	2.81	1.22	2.26	Zhu et al. (2009)
GB-8	2.25	0.35	16.00	2.16	3.84	0.89	2.14	Zhu et al. (2009)
NX5-2	2.39	0.36	13.30	1.55	3.62	0.81	7.91	Zhu et al. (2009)
NX5-3	4.71	0.71	10.60	0.94	2.95	0.81	18.40	Zhu et al. (2009)
SZ39	3.24	0.49	28.50	2.93	4.13	1.40	0.96	Zhu et al. (2009)
SZ43	3.03	0.44	28.50	2.18	5.56	1.07	1.10	Zhu et al. (2009)
SZ48	2.76	0.43	15.40	2.30	3.80	0.78	17.80	Zhu et al. (2009)
SZ52	2.90	0.43	19.20	3.10	5.01	1.07	7.64	Zhu et al. (2009)

Table A.4: continued

Sample	Rb	Sr	Y	Zr	Nb	Ba	Pb	Sc	V	Cr	Ni	Cu	Zn
CY1-01	203.00	144.00	30.30	230.00	13.40	694.00	30.60	7.42	40.70	10.50	4.33	4.70	46.60
CY1-02	275.00	108.00	48.70	191.00	14.30	498.00	35.40	8.56	32.70	8.25	3.59	4.32	47.80
CY1-02R	269.00	109.00	46.40	240.00	13.90	489.00	34.50	8.48	33.30	8.19	3.52	6.34	49.90
CY1-1	248.00	101.00	51.20	216.00	15.00	605.00	33.00	8.35	29.00	7.49	3.69	6.31	41.10
CY2-1	203.00	58.50	34.10	157.00	9.23	249.00	27.40	3.82	17.20	3.70	1.95	2.39	31.80
CY3-1	312.00	51.70	53.60	221.00	12.10	254.00	42.90	3.90	7.80	2.28	1.22	2.92	32.20
CY4-1	191.00	77.70	27.10	212.00	9.38	338.00	26.50	4.53	20.90	4.19	2.42	3.23	34.00
CY6-1	189.00	73.30	24.60	226.00	8.95	382.00	29.10	3.05	14.30	3.44	1.86	2.44	25.30
GBJD-1	195.00	170.00	26.30	188.00	27.20	302.00	22.00	4.01	25.30	11.40			
GBJD-2	200.00	157.00	28.30	209.00	29.60	340.00	27.00	4.12	25.40	12.90			
GBJD-3	204.00	172.00	27.60	224.00	28.80	352.00	24.50	4.15	24.90	13.30			
PK01-1	143.00	168.00	30.20	178.00	29.30	408.00	22.50	3.95	22.90	15.00	7.32		
PK01-2	197.00	173.00	27.60	192.00	29.50	403.00	27.30	4.19	23.40	13.80	7.49		
PK01-3	197.00	171.00	27.50	185.00	30.40	395.00	27.40	4.24	23.50	16.60	8.51		
PK01-4	227.00	186.00	26.70	184.00	30.20	540.00	29.80	4.29	23.50	15.70	7.37		
PK01-5	207.00	155.00	31.50	177.00	26.40	266.00	31.50	3.96	20.20	13.20	6.26		
PK01-6	209.00	174.00	26.40	150.00	27.10	491.00	28.20	3.82	21.60	12.30	6.85		
MM02-2	40.10	836.00	11.50	125.00	9.58	1158.00	16.10	13.40	125.00	190.00	21.00	130.00	5.19
MM02-3	129.00	530.00	11.90	149.00	10.60	577.00	11.20	15.50	137.00	176.00	27.00	133.00	30.30
MM02-4	62.10	631.00	11.20	125.00	10.70	477.00	15.20	11.40	100.00	225.00	24.00	105.00	63.10
MM02-5	65.40	692.00	11.30	158.00	10.80	973.00	11.50	14.80	123.00	190.00	20.00	143.00	23.60
MM02-6	57.70	476.00	8.70	133.00	11.00	475.00	10.50	8.50	85.20	225.00	22.00	139.00	298.00
T203A	86.90	633.00	13.50	156.00	10.70	724.00	12.00	19.30	25.00	220.00	20.00	108.00	220.00

Sample data continued

Sample	Ga	La	Ce	Pr	Nd	Sm	Eu	Gd	Tb	Dy	Ho	Er	Tm
CY1-01	18.60	67.10	126.00	12.90	47.80	8.21	1.33	6.92	1.01	5.55	1.06	2.98	0.44
CY1-02	19.00	77.40	149.00	15.70	59.00	11.20	1.11	10.00	1.57	9.18	1.75	4.78	0.70
CY1-02R	19.10	67.60	130.00	13.80	52.10	10.20	1.10	9.16	1.48	8.62	1.64	4.57	0.66
CY1-1	19.30	49.20	98.90	11.00	43.80	9.86	1.02	9.35	1.62	9.61	1.86	5.03	0.73
CY2-1	15.70	46.30	89.00	9.12	33.70	6.42	0.74	5.73	0.91	5.45	1.12	3.39	0.53
CY3-1	18.90	76.10	148.00	15.40	55.80	10.60	0.89	9.35	1.53	9.05	1.84	5.36	0.82
CY4-1	17.90	66.40	124.00	12.50	44.90	7.43	0.93	6.17	0.90	4.87	0.94	2.64	0.39
CY6-1	16.10	55.20	105.00	10.50	37.60	6.43	0.87	5.48	0.80	4.41	0.86	2.45	0.37
GBJD-1		49.50	92.10	10.10	35.20	6.08	1.15	5.84	0.88	4.86	0.91	2.60	0.36
GBJD-2		50.90	95.10	10.60	36.40	6.51	1.00	6.10	0.91	5.03	0.99	2.80	0.39
GBJD-3		51.70	96.20	10.50	36.90	6.32	1.10	6.05	0.89	4.98	0.98	2.74	0.38
PK01-1	19.10	45.80	87.40	9.28	33.80	6.36	0.95	5.53	0.90	5.29	1.08	2.83	0.41
PK01-2	19.50	44.00	84.20	8.91	32.20	5.99	1.00	5.27	0.85	4.96	0.99	2.63	0.38
PK01-3	19.80	44.20	83.80	8.77	31.60	5.97	1.00	5.17	0.84	4.94	0.99	2.60	0.38
PK01-4	20.50	46.50	87.60	9.19	32.70	6.11	1.11	5.28	0.83	4.91	0.98	2.55	0.37
PK01-5	19.70	43.80	84.70	8.87	31.30	5.91	0.88	5.24	0.88	5.33	1.11	3.04	0.46
PK01-6	18.60	42.10	78.60	8.34	29.50	5.54	1.03	4.83	0.79	4.65	0.95	2.51	0.37
MM02-2	63.20	30.80	59.60	6.87	26.50	4.79	1.69	3.33	0.44	2.41	0.43	1.19	0.16
MM02-3	48.90	26.00	50.30	5.77	22.70	4.03	1.66	3.49	0.46	2.39	0.44	1.25	0.16
MM02-4	157.00	24.10	53.10	6.43	25.00	4.52	1.26	3.21	0.45	2.45	0.44	1.21	0.16
MM02-5	57.40	22.30	44.20	5.14	20.10	3.69	1.27	3.17	0.43	2.25	0.41	1.23	0.16
MM02-6	62.30	20.00	44.10	5.04	20.00	3.79	1.09	2.62	0.37	1.99	0.35	0.94	0.12
T203A	58.00	28.50	53.40	7.21	28.30	5.03	1.38	3.89	0.54	2.76	0.49	1.28	0.18

Sample data continued

Sample	Yb	Lu	Th	U	Hf	Ta	Co	Source
CY1-01	2.67	0.38	24.40	2.87	5.82	1.15	5.86	Zhu et al. (2009)
CY1-02	4.10	0.56	85.90	8.66	5.15	1.25	4.52	Zhu et al. (2009)
CY1-02R	3.96	0.55	48.90	5.45	6.45	1.18	4.53	Zhu et al. (2009)
CY1-1	4.23	0.58	27.20	2.57	5.80	1.20	4.57	Zhu et al. (2009)
CY2-1	3.34	0.48	73.60	7.36	4.52	1.46	2.62	Zhu et al. (2009)
CY3-1	5.09	0.71	55.80	8.25	6.18	1.46	1.71	Zhu et al. (2009)
CY4-1	2.45	0.35	33.30	2.51	5.55	0.84	3.20	Zhu et al. (2009)
CY6-1	2.26	0.34	34.30	3.94	6.22	0.77	2.21	Zhu et al. (2009)
GBJD-1	2.28	0.33	17.70	1.67	4.59	2.83		Zhu et al. (2009)
GBJD-2	2.48	0.35	19.70	1.94	5.21	2.91		Zhu et al. (2009)
GBJD-3	2.44	0.35	20.40	1.99	5.53	2.71		Zhu et al. (2009)
PK01-1	2.60	0.37	20.30	3.39	4.75	2.36	3.31	Zhu et al. (2009)
PK01-2	2.47	0.35	22.20	2.26	5.11	2.76	4.36	Zhu et al. (2009)
PK01-3	2.47	0.35	22.70	2.32	5.02	2.83	4.89	Zhu et al. (2009)
PK01-4	2.40	0.33	22.50	2.80	5.03	3.27	3.93	Zhu et al. (2009)
PK01-5	2.98	0.42	25.50	3.03	5.02	2.65	3.44	Zhu et al. (2009)
PK01-6	2.36	0.33	20.20	2.14	4.07	2.40	3.59	Zhu et al. (2009)
MM02-2	0.97	0.14	2.45	1.32	3.25	0.49		Zhu et al. (2009a)
MM02-3	1.00	0.15	2.85	1.43	3.40	0.60		Zhu et al. (2009a)
MM02-4	0.99	0.14	2.48	0.62	3.43	0.56		Zhu et al. (2009a)
MM02-5	0.96	0.14	3.24	1.29	3.68	0.61		Zhu et al. (2009a)
MM02-6	0.71	0.10	2.22	0.38	3.78	0.58		Zhu et al. (2009a)
T203A	1.08	0.16	4.03	1.06	3.60	0.68		Zhu et al. (2009a)

APPENDIX B

Table B.1: Apatite (U-Th)/He results

Sample	Age (Ma)	± (Ma)	U (ppm)	Th (ppm)	Sm (ppm)	Th/U	He (ncc/mg)	mass (mg)	Ft	StDev
02PX05-1	7.2	0.4	10.5	38.7	3.7	12.1	3.9		0.70	
02PX05-2	5.4	0.3	12.2	50.3	4.1	10.2	2.9		0.64	
02PX05-3	7.7	0.4	5.7	23.3	4.1	6.3	2.0		0.60	
02PX05	**6.8**	**0.3**	**9.5**	**37.4**	**4.0**	**9.5**	**2.9**		**0.65**	**1.2**
04GB02-4	10.0	0.6	16.9	50.4	181.6	3.0	1.2	25.8	0.72	
04GB02-5	8.9	0.5	11.0	35.1	139.6	3.2	0.7	26.9	0.72	
04GB02-6	9.0	0.5	8.2	27.3	183.7	3.3	0.6	25.1	0.72	
04GB02	**9.3**	**0.6**	**12.1**	**37.6**	**168.3**	**3.2**	**0.8**	**25.9**	**0.72**	**0.6**
04GB04-4	24.3	1.5	61.4	164.3	147.2	2.7	8.7	12.2	0.65	
04GB04-5	22.3	1.3	62.8	45.3	191.1	0.7	5.9	11.1	0.65	
04GB04-6	15.1	0.9	139.1	16.9	97.1	0.1	7.9	9.2	0.67	
04GB04	**20.6**	**1.2**	**87.8**	**75.5**	**145.1**	**1.2**	**7.5**	**10.8**	**0.66**	**4.8**
04XI03-1	45.5	2.3	24.7	80.2	3.2	171.6		4.3	0.71	
04XI03-2	36.1	1.8	31.9	110.5	3.5	171.3		2.7	0.67	
04XI03-3	40.4	2.0	37.8	124.3	3.3	232.0		3.4	0.70	
04XI03	**40.6**	**2.0**	**31.5**	**105.0**	**3.3**	**191.7**		**3.5**	**0.70**	**4.7**
04XI04-1*	117.9	7.1	7.1	25.0	206.4	3.5	6.0	9.5	0.64	
04XI04-2	8.9	0.5	12.0	58.8	292.2	4.9	0.9	9.2	0.64	
04XI04-3	9.3	0.6	15.1	144.0	286.8	9.6	1.6	9.4	0.63	
04XI04	**9.1**	**0.5**	**13.5**	**101.4**	**289.5**	**7.2**	**1.3**	**9.3**	**0.63**	**0.3**
04XI05-1	12.6	0.8	30.9	339.4	260.4	11.0	5.1	9.5	0.66	
04XI05-2	14.2	0.9	22.4	206.0	231.5	9.2	3.7	9.7	0.66	
04XI05-3	16.6	1.0	18.8	227.2	208.1	12.1	4.4	9.0	0.65	
04XI05	**14.5**	**0.9**	**24.0**	**257.5**	**233.3**	**10.8**		**9.4**	**0.66**	**2.0**
04XI08-1	8.7	0.4	5.4	22.3	4.2	8.0		5.8	0.72	
04XI08-2	11.8	0.6	4.4	21.6	4.9	9.5		5.3	0.70	
04XI08-3	12.0	0.6	6.5	30.6	4.7	14.8		4.6	0.74	
04XI08	**10.8**	**0.5**	**5.4**	**24.8**	**4.6**	**10.8**		**5.2**	**0.72**	**1.8**
04XI18-1	75.9	3.8	4.4	21.1	4.8	63.1		7.5	0.73	
04XI18-2	58.0	2.9	8.4	47.6	5.7	95.1		4.6	0.69	
04XI18-3	58.7	2.9	7.6	35.0	4.6	83.0		5.3	0.73	
04XI18-4	75.4	3.8	5.9	18.3	3.1	76.6		7.4	0.82	
04XI18	**64.0**	**3.2**	**7.3**	**33.6**	**4.4**	**84.9**		**5.8**	**0.74**	**9.8**
04XI20-1	12.3	0.6	5.0	3.2	0.6	6.5		5.0	0.75	
04XI20-2	18.2	0.9	4.6	1.3	0.3	7.9		6.8	0.73	
04XI20-3	14.7	0.7	4.8	1.7	0.3	6.4		4.4	0.69	
04XI20	**15.1**	**0.8**	**4.8**	**2.0**	**0.4**	**6.9**		**5.4**	**0.72**	**2.9**
04XI29-1	45.8	2.3	392.3	501.3	325.1	1.3	114.5	5.1	0.68	
04XI29-2	46.6	2.3	636.0	321.2	379.0	0.5	280.6	3.5	0.66	
04XI29-3	42.4	2.1	278.1	442.3	330.4	1.6	118.7	2.8	0.56	
04XI29	**44.9**	**2.2**	**435.5**	**421.6**	**344.9**	**1.1**	**171.3**	**3.8**	**0.64**	**2.2**
04XI32-1	69.7	3.5	7.6	53.0	7.0	111.4		3.2	0.65	
04XI32-2*	121.6	6.1	9.6	53.6	5.6	222.9		2.9	0.68	
04XI32-3	71.0	3.5	8.8	38.1	4.3	109.4		4.0	0.71	
04XI32	**70.3**	**3.5**	**8.2**	**45.6**	**5.7**	**110.4**		**3.6**	**0.68**	**0.9**
04XI36-1	4.4	0.3	6.7	37.9	552.5	5.6	6.4	2.8	0.59	
04XI36-2	2.5	0.2	5.2	24.0	452.5	4.6	2.7	2.8	0.61	
04XI36-3	2.3	0.1	7.2	39.7	511.1	5.5	3.4	4.2	0.60	

Table B.1: continued

Sample	Age (Ma)	± (Ma)	U (ppm)	Th (ppm)	Sm (ppm)	Th/U	He (ncc/mg)	mass (mg)	Ft	StDev
04XI36	**3.1**	**0.2**	**6.4**	**33.9**	**505.4**	**5.2**	**4.2**	**3.3**	**0.60**	**1.2**
04XIA01-1*	10.6	0.5	10.4	70.2	6.8	24.2	1.7		0.70	
04XIA01-2	6.4	0.3	1.6	13.5	8.2	2.6	1.9		0.71	
04XIA01-3	6.3	0.3	8.1	51.9	6.4	9.6	0.9		0.62	
04XIA01-4*	16.2	0.8	6.7	41.4	6.1	22.2	1.3		0.68	
04XIA01-5	8.0	0.4	6.1	67.8	11.1	14.7	1.3		0.68	
04XIA01	**6.9**	**0.3**	**5.3**	**44.4**	**8.6**	**9.0**	**1.4**		**0.67**	**1.0**
04XIA02-1	7.5	0.4	5.6	40.8	7.3	8.8	2.1		0.63	
04XIA02-2	11.4	0.6	4.9	42.2	8.6	13.8	2.6		0.67	
04XIA02-3	9.6	0.5	9.7	79.9	8.2	21.4	2.0		0.64	
04XIA02-6*	3.8	0.2	33.8	54.9	202.8	1.6	0.6	7.2	0.62	
04XIA02-7*	17.7	1.1	8.9	50.5	194.2	5.7	1.3	7.1	0.61	
04XIA02-8	10.8	0.6	7.1	58.1	235.8	8.1	0.8	8.0	0.62	
04XIA02	**9.8**	**0.5**	**6.9**	**55.3**	**65.0**	**13.0**	**1.9**	**8.0**	**0.64**	**9.8**
04XIA03-1	7.4	0.4	21.7	91.1	4.2	27.0	2.0		0.70	
04XIA03-2	6.3	0.3	4.9	33.9	6.9	7.1	2.5		0.72	
04XIA03-3	6.5	0.3	8.7	62.8	7.3	13.2	2.3		0.71	
04XIA03-4	5.5	0.3	5.9	41.5	7.0	7.6	2.5		0.72	
04XIA03-5	8.3	0.4	3.6	27.5	7.6	7.4	2.6		0.73	
04XIA03-6	7.2	0.4	8.2	58.4	184.6	7.2	0.6	20.7	0.69	
04XIA03-7	8.0	0.5	11.4	75.7	212.8	6.7	0.9	22.3	0.70	
04XIA03-8	7.1	0.4	9.9	76.5	252.8	7.7	0.8	23.6	0.70	
04XIA03	**7.0**	**0.4**	**9.3**	**58.4**	**85.4**	**10.5**	**1.8**	**22.2**	**0.71**	**0.9**
04XIA04-1	9.9	0.6	34.4	36.6	116.5	1.1	1.6	10.6	0.66	
04XIA04-2	9.8	0.6	31.7	28.7	110.1	0.9	1.4	10.9	0.66	
04XIA04-3	11.1	0.7	63.9	22.7	119.7	0.4	2.8	9.1	0.66	
04XIA04	**10.2**	**0.6**	**43.4**	**29.3**	**115.4**	**0.8**	**1.9**	**10.2**	**0.66**	**0.7**
04XIA05-1	13.2	0.8	24.4	27.9	100.2	1.1	1.5	14.8	0.67	
04XIA05-2	9.7	0.6	39.3	63.7	169.8	1.6	1.9	13.8	0.66	
04XIA05-3	15.1	0.9	87.2	51.4	155.8	0.6	5.5	13.6	0.67	
04XIA05	**12.7**	**0.8**	**50.3**	**47.7**	**141.9**	**1.1**	**3.0**	**14.1**	**0.67**	**2.7**
04XIA06-1	9.6	0.6	51.4	44.4	141.2	0.9	2.3	17.8	0.70	
04XIA06-2	10.4	0.6	38.0	40.8	150.6	1.1	1.9	17.1	0.69	
04XIA06-3	12.5	0.7	38.8	35.3	166.4	0.9	2.3	16.7	0.69	
04XIA06	**10.8**	**0.7**	**42.7**	**40.2**	**152.7**	**0.9**	**2.1**	**17.2**	**0.69**	**1.5**
04XIA07-1	10.4	0.6	50.5	56.9	159.7	1.1	2.1	8.1	0.58	
04XIA07-2	8.8	0.5	51.4	28.9	126.9	0.6	1.8	11.0	0.65	
04XIA07-3	15.6	0.9	8.1	53.3	183.3	6.6	1.2	15.0	0.67	
04XIA07	**11.6**	**0.7**	**36.7**	**46.4**	**156.6**	**2.8**	**1.7**	**11.4**	**0.63**	**3.6**
04XIE85-1	6.4	0.4	15.9	66.7	105.3	4.2	17.4	6.5	0.69	
04XIE85-2	6.6	0.4	20.3	61.3	108.9	3.0	22.7	11.3	0.79	
04XIE85-3	6.4	0.4	13.5	59.7	100.1	4.4	16.6	13.1	0.75	
04XIE85-4	6.3	0.4	13.3	51.3	96.3	3.8	14.7	10.8	0.73	
04XIE85-5	7.6	0.5	13.3	50.3	93.8	3.8	16.6	10.4	0.69	
04XIE85	**6.7**	**0.4**	**15.3**	**57.9**	**100.9**	**3.9**	**17.6**	**10.4**	**0.73**	**0.5**
05XI67-1	44.0	2.6	13.4	79.6	329.4	6.0	5.4	12.9	0.65	
05XI67-2	31.3	1.9	20.8	118.8	368.7	5.7	5.8	13.9	0.66	
05XI67-3*	188.1	11.3	25.4	159.8	450.4	6.3	44.4	13.3	0.65	

Table B.1: continued

Sample	Age (Ma)	± (Ma)	U (ppm)	Th (ppm)	Sm (ppm)	Th/U	He (ncc/mg)	mass (mg)	Ft	StDev
05XI67	**37.7**	**2.3**	**17.1**	**99.2**	**349.0**	**5.8**	**5.6**	**13.4**	**0.7**	**9.0**
05XI80-1	5.5	0.3								
05XI80-2	4.9	0.3								
05XI80-3	8.5	0.5								
05XI80	**6.3**	**0.4**								**1.9**
05XI90-1	9.3	0.6								
05XI90-2	8.8	0.5								
05XI90-3	10.9	0.7								
05XI90	**9.7**	**0.6**								**1.1**
05XI91-1	6.2	0.4								
05XI91-2	6.8	0.4								
05XI91-3	7.2	0.4								
05XI91	**6.7**	**0.4**								**0.5**
05XI92-1	2.5	0.1								
05XI92-1	2.5	0.2								
05XI92-3	2.1	0.1								
05XI92	**2.4**	**0.1**								**0.3**
05XI94-1	8.1	0.5								
05XI94-2	9.5	0.6								
05XI94-3	8.9	0.5								
05XI94-4	8.4	0.5								
05XI94-5	8.1	0.5								
05XI94	**8.6**	**0.5**								**0.6**
05XIB50-1	36.7	2.2	5.5	42.9	308.4	7.8	45.3	1.9	0.56	
05XIB50-2	17.2	1.0	8.9	85.2	430.3	9.6	42.2	1.8	0.62	
05XIB50-3	26.8	1.6	7.5	74.6	441.6	9.9	62.7	2.6	0.67	
05XIB50-4	19.4	1.2	8.4	77.1	375.9	9.2	46.4	2.8	0.66	
05XIB50	***25.0***	***1.5***	***7.6***	***70.0***	***389.1***	***9.1***	***49.1***	***2.3***	***0.63***	**8.8**
05XID68-1	8.7	0.5	45.1	235.4	1112.4	5.2	69.4	4.1	0.60	
05XID68-2	9.3	0.6	19.5	96.0	716.5	4.9	32.7	4.1	0.60	
05XID68-3	10.4	0.6	28.0	160.8	989.0	5.7	60.3	4.3	0.65	
05XID68	**9.5**	**0.6**	**30.9**	**164.0**	**939.3**	**5.3**	**54.2**	**4.2**	**0.62**	**0.9**
05XID69-1	8.0	0.5	24.9	132.7	892.8	5.3	43.9	5.6	0.71	
05XID69-2*	21.2	1.3	30.0	190.1	870.5	6.3	137.9	3.3	0.65	
05XID69-3	13.5	0.8	20.3	106.2	709.1	5.2	47.6	3.1	0.57	
05XID69-4	9.2	0.6	25.1	118.4	763.9	4.7	41.6	3.1	0.63	
05XID69-5	9.7	0.6	25.1	141.8	360.2	5.7	2.2	14.9	0.67	
05XID69-6	11.9	0.7	25.9	156.6	404.0	6.1	2.8	14.2	0.66	
05XID69-7	11.2	0.7	27.4	168.7	413.6	6.2	2.8	14.7	0.66	
05XID69	**10.6**	**0.6**	**24.8**	**137.4**	**590.6**	**5.5**	**23.5**	**9.3**	**0.65**	**2.0**
05XID70-1	9.8	0.6	19.4	109.8	1042.6	5.7	43.1	5.0	0.67	
05XID70-2	11.8	0.7	29.2	148.0	1237.1	5.1	69.4	4.4	0.65	
05XID70-3	8.1	0.5	25.5	131.9	922.2	5.2	43.1	3.4	0.68	
05XID70-4	10.4	0.6	19.6	95.3	714.5	4.9	37.9	3.3	0.63	
05XID70	**10.0**	**0.6**	**23.4**	**121.3**	**979.1**	**5.2**	**48.4**	**4.0**	**0.66**	**1.6**
05XID71-1	12.9	0.8	12.2	58.9	567.8	4.8	32.5	2.9	0.68	
05XID71-2	10.8	0.6	12.1	51.7	385.8	4.3	23.6	2.3	0.66	
05XID71-3	13.4	0.8	38.1	205.5	573.8	5.4	4.6	18.9	0.69	

Table B.1: continued

Sample	Age (Ma)	± (Ma)	U (ppm)	Th (ppm)	Sm (ppm)	Th/U	He (ncc/mg)	mass (mg)	Ft	StDev
05XID71-4	10.8	0.6	34.7	197.5	484.8	5.7	3.5	19.9	0.69	
05XID71-5	12.1	0.7	27.9	152.3	459.3	5.5	3.0	17.5	0.68	
05XID71	**12.0**	**0.7**	**25.0**	**133.2**	**494.3**	**5.1**	**13.4**	**12.3**	**0.68**	**1.2**
05XID72-1	8.9	0.5	29.3	144.9	1067.4	4.9	49.3	5.3	0.63	
05XID72-2	8.5	0.5	25.2	118.9	1051.8	4.7	42.1	6.4	0.66	
05XID72-3	8.4	0.5	18.3	89.7	765.5	4.9	31.7	6.1	0.68	
05XID72-4	9.3	0.6	21.2	100.4	1021.6	4.7	44.0	6.1	0.74	
05XID72	**8.8**	**0.5**	**23.5**	**113.5**	**976.6**	**4.8**	**41.8**	**6.0**	**0.68**	**0.4**
05XID73-1*	22.5	1.4	15.0	68.0	461.2	4.5	50.8	0.8	0.53	
05XID73-2	12.5	0.7	18.4	86.8	622.6	4.7	39.3	1.3	0.59	
05XID73-3*	23.5	1.4	11.3	49.2	410.9	4.4	45.7	1.5	0.61	
05XID73-4	13.7	0.8	23.0	113.8	381.5	5.0	2.7	18.3	0.68	
05XID73-5	13.1	0.8	17.9	88.6	329.2	4.9	2.0	18.2	0.68	
05XID73-6	12.0	0.7	18.9	103.7	329.2	5.5	2.0	17.2	0.68	
05XID73	**12.8**	**0.8**	**19.6**	**98.2**	**415.6**	**5.0**	**11.5**	**13.8**	**0.66**	**0.7**
05XID74-1*	16.2	1.0	17.0	74.9	752.4	4.4	55.1	6.5	0.69	
05XID74-2	9.4	0.6	17.2	80.6	661.0	4.7	30.8	3.9	0.65	
05XID74-3	9.1	0.5	17.9	104.2	695.2	5.8	34.4	4.2	0.65	
05XID74	**9.2**	**0.6**	**17.5**	**92.4**	**678.1**	**5.3**	**32.6**	**4.1**	**0.65**	**0.3**
05XIE81-1	5.5	0.3	17.4	75.9	92.3	4.4	15.5	5.9	0.64	
05XIE81-2	8.2	0.5	16.9	78.0	80.9	4.6	22.5	4.9	0.63	
05XIE81-3	5.7	0.3	16.6	68.7	88.7	4.1	15.5	7.2	0.67	
05XIE81	**6.5**	**0.4**	**17.0**	**74.2**	**87.3**	**4.4**	**17.8**	**6.0**	**0.64**	**1.5**
05XIE82-1	7.1	0.4	17.7	71.0	122.2	4.0	20.1	6.7	0.66	
05XIE82-2*	123.5	7.4	22.2	63.5	88.4	2.9	364.7	5.2	0.64	
05XIE82-3	8.6	0.5	20.0	61.1	87.3	3.1	24.2	6.6	0.66	
05XIE82	**7.9**	**0.5**	**18.8**	**66.0**	**104.8**	**3.5**	**22.1**	**6.7**	**0.66**	**1.1**
05XIE83-1	7.2	0.4	15.6	68.6	101.6	4.4	17.8	5.0	0.63	
05XIE83-2	7.6	0.5	14.0	57.2	89.1	4.1	17.9	8.0	0.68	
05XIE83-3	6.9	0.4	14.3	81.1	112.3	5.7	18.0	5.4	0.63	
05XIE83	**7.2**	**0.4**	**14.6**	**69.0**	**101.0**	**4.7**	**17.9**	**6.1**	**0.65**	**0.4**
05XIE84-1	7.1	0.4	16.0	62.9	107.9	3.9	19.9	13.9	0.73	
05XIE84-2	6.9	0.4	13.9	58.5	93.4	4.2	18.1	13.5	0.76	
05XIE84-3*	79.5	4.8	15.8	64.0	102.2	4.1	215.2	10.6	0.70	
05XIE84	**7.0**	**0.4**	**15.0**	**60.7**	**100.6**	**4.1**	**19.0**	**13.7**	**0.74**	**0.1**
05XIE86-1	7.1	0.4	196.4	657.8	82.5	3.3	20.1	6.0	0.65	
05XIE86-2	10.9	0.5	236.6	787.0	112.0	3.3	39.4	9.3	0.69	
05XIE86-3_2	6.8	0.3	186.9	660.8	123.3	3.5	20.4	7.0	0.69	
05XIE86-4*	1.4	0.1	546.2	511.8	8643.9	0.9	17.8	8.9	0.78	
05XIE86-5	6.7	0.3	155.3	588.4	96.4	3.8	19.1	9.3	0.78	
05XIE86	**7.9**	**0.4**	**193.8**	**673.5**	**103.5**	**3.5**	**24.8**	**7.9**	**0.70**	**2.0**
05XIE87-1	7.0	0.4	137.7	592.2	89.7	4.3	16.1	4.5	0.66	
05XIE87-2	8.0	0.4	134.8	554.9	95.6	4.1	18.6	10.9	0.70	
05XIE87-3	8.5	0.4	115.0	509.8	81.1	4.4	17.9	8.1	0.72	
05XIE87-4	7.4	0.4	136.4	578.5	107.1	4.2	20.4	14.6	0.81	
05XIE87-5	7.6	0.4	158.4	641.6	127.0	4.1	23.4	11.3	0.79	
05XIE87-6	8.0	0.4	161.7	601.4	108.0	3.7	24.2	12.0	0.80	
05XIE87	**7.7**	**0.4**	**140.7**	**579.7**	**101.4**	**4.1**	**20.1**	**10.2**	**0.75**	**0.5**

Table B.1: continued

Sample	Age (Ma)	± (Ma)	U (ppm)	Th (ppm)	Sm (ppm)	Th/U	He (ncc/mg)	mass (mg)	Ft	StDev
05XIE88-1	7.7	0.4	158.0	704.2	138.9	4.5	22.4	8.0	0.72	
05XIE88-2	7.5	0.4	142.7	575.3	97.9	4.0	19.0	9.5	0.73	
05XIE88-3	8.1	0.4	153.3	704.3	103.9	4.6	24.7	14.2	0.76	
05XIE88	**7.8**	**0.4**	**151.3**	**661.3**	**113.6**	**4.4**	**22.0**	**10.6**	**0.74**	**0.3**
05XIE89-4	6.7	0.4	14.6	33.0	126.2	2.3	13.3	7.4	0.69	
05XIE89-5	6.5	0.4	15.3	48.7	91.2	3.2	13.9	5.9	0.64	
05XIE89-6*	21.1	1.3	16.8	58.7	122.3	3.5	49.0	4.4	0.60	
05XIE89	**6.6**	**0.4**	**14.9**	**40.9**	**108.7**	**2.7**	**13.6**	**6.7**	**0.67**	**0.2**

Bold entries represent average values from individual aliquot analysis.
Aliquots denoted with (*) were excluded from the calculation of the mean age

Table B.2: Zircon (U-Th)/He results

Sample	Age (Ma)	± (Ma)	U (ppm)	Th (ppm)	Sm (ppm)	Th/U	He (ncc/mg)	mass (mg)	Ft	StDev
Z04XIA01-1	14.7	1.2	85.8	115.3		1.34	139.8	3.1	0.69	
Z04XIA01-2	14.5	1.2	502.7	375.6		0.75	689.2	2.0	0.66	
Z04XIA01-3	17.7	1.4	172.4	221.1		1.28	327.8	3.4	0.68	
Z04XIA01-4	16.1	1.3	326.4	277.5	2.1	0.9	25.54	5.4	0.75	
Z04XIA01-5	23.5	1.9	367.3	259.9	2.4	0.7	40.06	4.3	0.74	
Z04XIA01-6	18.4	1.5	828.1	620.1	4.2	0.7	71.82	5.2	0.74	
Z04XIA01	**17.5**	**1.4**	**380.5**	**311.6**	**2.9**	**0.9**	**215.7**	**3.9**	**0.7**	**3.3**
Z04XIA02-1	17.7	1.4	94.4	109.7		1.16	194.3	5.8	0.75	
Z04XIA02-2	20.7	1.7	95.5	132.8		1.39	233.4	5.0	0.73	
Z04XIA02-4	18.4	1.5	584.7	461.9		0.79	1062.3	2.7	0.68	
Z04XIA02-5	14.4	1.2	936.8	567.5		0.61	1288.3	2.6	0.68	
Z04XIA02-6	21.4	1.7	533.2	446.3	3.3	0.8	53.41	3.9	0.72	
Z04XIA02-7	15.7	1.3	356.5	268.5	3.8	0.8	26.34	4.4	0.74	
Z04XIA02-8	24.5	2.0	933.7	858.3	3.2	0.9	112.76	4.8	0.75	
Z04XIA02	**19.0**	**1.5**	**505.0**	**406.4**	**3.4**	**0.9**	**424.4**	**4.2**	**0.7**	**3.5**
Z04XIA03-1	17.4	1.4	1689.9	465.8		0.28	2609.6	2.7	0.68	
Z04XIA03-2	14.9	1.2	1449.7	402.6		0.28	2008.8	3.6	0.71	
Z04XIA03-3*	26.0	2.1	700.9	529.5		0.76	1872.1	4.0	0.71	
Z04XIA03-4	13.1	1.1	1177.6	230.4		0.20	1440.8	4	0.73	
Z04XIA03-5	12.8	1.0	1261.3	417.1		0.33	1561.4	4.4	0.74	
Z04XIA03-6	26.6	2.1	676.4	307.4	3.4	0.5	85.96	9.7	0.80	
Z04XIA03-7	40.1	3.2	653.8	494.2	1.3	0.8	132.04	10.0	0.79	
Z04XIA03-8	23.0	1.8	854.4	387.9	2.5	0.5	95.49	12.6	0.81	
Z04XIA03	**21.8**	**1.7**	**1058.0**	**404.4**	**2.4**	**0.4**	**1225.8**	**6.4**	**0.7**	**9.2**
Z04XIA04-1	16.1	1.3	513.1	340.1		0.66	808.7	3.0	0.70	
Z04XIA04-2	13.8	1.1	816.0	269.8		0.33	1027.9	2.8	0.69	
Z04XIA04-3	21.6	1.7	1122.4	485.7		0.43	2304.7	3.7	0.71	
Z04XIA04-4	13.9	1.1	1054.0	515.1		0.49	1470.1	4.7	0.74	
Z04XIA04-5	11.3	0.9	1652.2	529.8		0.32	1729.9	3.6	0.71	
Z04XIA04-6	19.5	1.6	892.4	440.6	2.0	0.5	80.88	5.9	0.77	
Z04XIA04-7	16.4	1.3	611.7	285.3	1.7	0.5	47.61	8.1	0.79	
Z04XIA04-8	16.6	1.3	525.1	218.9	1.2	0.4	42.79	13.9	0.83	
Z04XIA04	**16.2**	**1.3**	**898.4**	**385.7**	**1.6**	**0.5**	**939.1**	**5.7**	**0.7**	**3.3**
Z04XIA05-1	11.8	0.9	359.5	207.8		0.58	414.8	3.3	0.71	
Z04XIA05-3	16.1	1.3	826.2	384.4		0.47	1246.8	3.0	0.69	
Z04XIA05-4	9.5	0.8	405.3	170.9		0.42	377.2	3.9	0.73	
Z04XIA05-5	21.7	1.7	345.9	163.8	1.1	0.5	36.64	12.0	0.81	
Z04XIA05-6	12.6	1.0	115.6	74.0	1.8	0.6	7.44	13.7	0.82	
Z04XIA05-7*	60.6	4.9	66.8	49.5	1568.7	0.7	24.39	11.6	0.81	
Z04XIA05	**14.3**	**1.1**	**410.5**	**200.2**	**1.4**	**0.5**	**416.6**	**7.2**	**0.8**	**4.7**
Z04XIA06-1	13.2	1.1	1206.0	825.2		0.68	1629.8	4.2	0.72	
Z04XIA06-2	18.1	1.5	781.4	403.9		0.52	1390.0	4.0	0.72	
Z04XIA06-3	12.4	1.0	647.8	450.0		0.69	791.4	3.0	0.70	
Z04XIA06-4	18.1	1.5	1298.7	699.2	2.1	0.5	104.13	3.6	0.73	
Z04XIA06-5	14.3	1.1	914.0	457.9	1.9	0.5	58.75	4.6	0.74	
Z04XIA06-6	18.5	1.5	797.1	453.8	2.4	0.6	67.52	4.8	0.75	
Z04XIA06	**15.8**	**1.3**	**940.8**	**548.3**	**2.2**	**0.6**	**673.6**	**4.0**	**0.7**	**2.8**
Z04XIA07-1*	793.4	63.5	23.6	25.3		1.072	2000.9	2.5	0.66	

Table B.2: continued

Sample	Age (Ma)	± (Ma)	U (ppm)	Th (ppm)	Sm (ppm)	Th/U	He (ncc/mg)	mass (mg)	Ft	StDev
Z04XIA07-3	12.6	1.0	1286.9	413.7		0.321	1401.6	2.0	0.66	
Z04XIA07-4	11.3	0.9	1280.1	296.0		0.23	1373.7	4.6	0.74	
Z04XIA07-5	14.0	1.1	1620.5	345.2		0.21	1935.3	2	0.67	
Z04XIA07	**12.6**	**1.0**	**1286.9**	**413.7**		**0.321**	**1401.6**	**2.0**	**0.66**	**1.4**
Z05XIB41-1	69.0	5.5	132.7	184.2	4.7	1.4	1200.8	13.3	0.81	
Z05XIB41-2	61.2	4.9	200.9	476.4	5.4	2.4	1715.3	4.2	0.73	
Z05XIB41-3	65.2	5.2	210.0	259.3	9.3	1.2	1630.7	6.7	0.75	
Z05XIB41	**65.1**	**5.2**	**181.2**	**306.7**	**6.4**	**1.66**	**1515.6**	**8.1**	**0.77**	**3.9**
Z05XIB42-1	55.6	4.4	90.4	108.0	5.9	1.2	608.5	8.1	0.77	
Z05XIB42-2	61.7	4.9	93.4	125.2	15.2	1.3	984.6	12.7	0.80	
Z05XIB42-3	54.9	4.4	161.5	213.2	7.0	1.3	1078.7	6.2	0.76	
Z05XIB42	**57.4**	**4.6**	**115.1**	**148.8**	**9.4**	**1.29**	**890.6**	**9.0**	**0.78**	**3.7**
Z05XIB43-1	52.1	4.2								
Z05XIB43-2	51.7	4.1								
Z05XIB43-3	44.0	3.5								
Z05XIB43	**49.3**	**3.9**								**4.6**
Z05XIB45-1	53.5	4.3								
Z05XIB45-2	51.1	4.1								
Z05XIB45-3	56.8	4.5								
Z05XIB45	**53.8**	**4.3**								**2.9**
Z05XIB46-1	58.9	4.7	174.7	192.0	5.4	1.1	1219.1	7.2	0.77	
Z05XIB46-2	43.8	3.5	80.9	168.8	5.6	2.1	496.9	6.9	0.77	
Z05XIB46-3	53.4	4.3	90.1	174.8	6.0	1.9	380.1	3.0	0.71	
Z05XIB46	**52.0**	**4.2**	**115.2**	**178.5**	**5.7**	**1.71**	**698.7**	**5.7**	**0.75**	**7.6**
Z05XIB47-1	53.4	4.3	184.8	342.4	7.0	1.9	1262.2	3.9	0.73	
Z05XIB47-2	54.0	4.3	116.2	210.4	4.9	1.8	841.9	7.0	0.77	
Z05XIB47-3	56.4	4.5	46.8	98.1	3.9	2.1	394.6	14.8	0.82	
Z05XIB47	**54.6**	**4.4**	**115.9**	**217.0**	**5.2**	**1.92**	**832.9**	**8.6**	**0.77**	**1.6**
Z05XIB49-1	70.4	5.6	121.4	195.2	3.6	1.6	1064.3	5.0	0.74	
Z05XIB49-2	97.7	7.8	119.7	160.6	5.5	1.3	1426.2	5.8	0.76	
Z05XIB49-3	111.6	8.9	218.7	192.8	2.6	0.9	2738.0	6.0	0.76	
Z05XIB49	**93.2**	**7.5**	**153.3**	**182.9**	**3.9**	**1.28**	**1742.8**	**5.6**	**0.75**	**21.0**
Z05XIB50-1	33.3	2.7	169.7	177.4	3.6	1.0	641.3	5.6	0.75	
Z05XIB50-2	84.6	6.8	102.9	118.4	1.6	1.2	1015.5	5.5	0.75	
Z05XIB50-3	64.2	5.1	242.2	54.6	1.0	0.2	1573.3	6.7	0.79	
Z05XIB50	**60.7**	**4.9**	**171.6**	**116.8**	**2.1**	**0.81**	**1076.7**	**5.9**	**0.76**	**25.8**
Z05XIC56-1	76.7	6.1	193.6	160.1	3.0	0.8	1673.1	7.5	0.77	
Z05XIC56-2	120.8	9.7	165.9	136.6	4.2	0.8	2329.8	9.7	0.79	
Z05XIC56-3	99.0	7.9	183.2	115.9	4.6	0.6	2115.5	17.8	0.83	
Z05XIC56	**98.8**	**7.9**	**180.9**	**137.5**	**3.9**	**0.76**	**2039.5**	**11.7**	**0.80**	**22.0**
Z05XIC57-1	49.2	3.9	153.9	165.4	5.3	1.1	871.6	4.7	0.75	
Z05XIC57-2	79.0	6.3	175.6	222.6	6.3	1.3	1588.7	4.3	0.72	
Z05XIC57-3	74.9	6.0	319.1	343.9	11.7	1.1	2698.8	4.5	0.74	
Z05XIC57	**67.7**	**5.4**	**216.2**	**244.0**	**7.8**	**1.14**	**1719.7**	**4.5**	**0.74**	**16.2**
Z05XID68-1	30.6	2.5	655.4	371.8		0.57	2074.7	4.8	0.75	
Z05XID68-2	25.9	2.1	360.3	308.9		0.86	1014.2	4.8	0.74	
Z05XID68-3	38.6	3.1	928.2	530.5		0.57	3677.9	5.1	0.74	
Z05XID68-4	30.5	2.4	502.3	279.0	1.7	0.6	70.74	6.0	0.76	

Table B.2: continued

Sample	Age (Ma)	± (Ma)	U (ppm)	Th (ppm)	Sm (ppm)	Th/U	He (ncc/mg)	mass (mg)	Ft	StDev
Z05XID68-5	33.6	2.7	487.0	303.3	6.6	0.6	77.26	6.6	0.76	
Z05XID68-6	30.2	2.4	687.6	238.9	3.1	0.3	89.84	4.9	0.74	
Z05XID68	**31.6**	**2.5**	**603.5**	**338.7**	**3.8**	**0.6**	**1167.4**	**5.4**	**0.748**	**4.2**
Z05XID69-1	34.3	2.7	1337.5	586.2		0.44	4653.1	4.8	0.75	
Z05XID69-2	24.9	2.0	137.2	126.5		0.92	388.9	5.8	0.77	
Z05XID69-3	24.8	2.0	695.1	315.6		0.45	1753.2	4.9	0.75	
Z05XID69-4	30.8	2.5	917.7	386.7	1.8	0.4	125.08	5.0	0.75	
Z05XID69-5	32.3	2.6	657.8	483.9	3.0	0.7	97.55	3.8	0.72	
Z05XID69-6	35.2	2.8	1316.1	598.8	3.4	0.5	204.14	4.9	0.74	
Z05XID69	**30.4**	**2.4**	**843.5**	**416.3**	**2.7**	**0.6**	**1203.7**	**4.9**	**0.747**	**4.6**
Z05XID70-1	28.5	2.3	507.1	355.8		0.70	1489.3	4.1	0.73	
Z05XID70-2	28.5	2.3	274.3	203.9		0.74	850.0	6.5	0.76	
Z05XID70-3	37.1	3.0	614.8	315.4		0.51	2359.1	6.5	0.76	
Z05XID70-4	30.1	2.4	505.4	246.6	2.2	0.5	68.58	5.3	0.75	
Z05XID70-5	34.7	2.8	559.9	281.4	2.0	0.5	89.55	6.9	0.76	
Z05XID70-6	24.2	1.9	947.7	500.4	4.7	0.5	106.80	7.1	0.77	
Z05XID70	**30.5**	**2.4**	**568.2**	**317.2**	**3.0**	**0.6**	**827.2**	**6.1**	**0.754**	**4.7**
Z05XID71-1	29.8	2.4	1065.8	420.3	3.6	0.4	3216.2	5.6	0.76	
Z05XID71-2	34.5	2.8	859.4	369.7	4.3	0.4	2968.9	4.7	0.75	
Z05XID71-3	32.6	2.6	1050.7	336.3	4.0	0.3	3579.7	9.1	0.80	
Z05XID71-4	31.6	2.5	744.7	241.2	1.3	0.3	104.01	5.7	0.76	
Z05XID71-5	34.5	2.8	360.0	171.7	1.5	0.5	57.13	6.7	0.77	
Z05XID71-6	36.8	2.9	609.9	337.9	3.4	0.6	102.24	5.2	0.75	
Z05XID71	**33.3**	**2.7**	**781.7**	**312.8**	**3.0**	**0.4**	**1671.4**	**6.2**	**0.763**	**2.5**
Z05XID72-1	25.7	2.1	377.4	206.1		0.55	992.2	4.9	0.74	
Z05XID72-2	26.0	2.1	374.4	200.3		0.54	998.6	4.7	0.75	
Z05XID72-3	24.0	1.9	295.9	179.3		0.61	732.9	4.4	0.74	
Z05XID72-4	29.7	2.4	735.2	273.2	1.5	0.4	98.13	6.1	0.77	
Z05XID72-5	31.8	2.5	517.5	272.5	4.5	0.5	77.09	7.2	0.77	
Z05XID72-6	29.1	2.3	588.7	259.3	1.6	0.4	77.23	6.4	0.76	
Z05XID72	**27.7**	**2.2**	**481.5**	**231.8**	**2.5**	**0.5**	**496.0**	**5.6**	**0.755**	**3.0**
Z05XID73-1	20.0	1.6	442.8	213.6		0.48	864.2	2.9	0.72	
Z05XID73-2	27.8	2.2	978.1	388.1		0.40	2504.9	2.3	0.69	
Z05XID73-3	23.4	1.9	623.9	274.6		0.44	1422.7	3.4	0.72	
Z05XID73-4	30.8	2.5	964.1	292.1	1.5	0.3	129.39	4.4	0.75	
Z05XID73-5	23.1	1.8	325.9	183.1	4.6	0.6	35.25	6.1	0.77	
Z05XID73-6	34.4	2.8	497.2	310.0	3.0	0.6	78.67	4.2	0.74	
Z05XID73	**26.6**	**2.1**	**638.7**	**276.9**	**3.0**	**0.5**	**839.2**	**3.9**	**0.733**	**5.4**
Z05XID74-1	20.0	1.6	435.5	373.4		0.86	901.0	2.9	0.71	
Z05XID74-2	17.9	1.4	368.1	281.1		0.76	693.9	4.2	0.73	
Z05XID74-3	27.8	2.2	590.6	242.9		0.41	1607.2	3.9	0.73	
Z05XID74	**21.9**	**1.8**	**464.8**	**299.1**		**0.68**	**1067.3**	**3.7**	**0.724**	**5.2**
Z05XIE81-1	7.3	0.6	728.0	922.2		1.27	582.6	2.7	0.69	
Z05XIE81-2	7.4	0.6	821.6	971.0		1.18	676.1	3.2	0.71	
Z05XIE81-3	7.2	0.6	864.1	1035.9		1.20	678.8	2.8	0.70	
Z05XIE81	**7.3**	**0.6**	**804.6**	**976.4**		**1.22**	**645.8**	**2.9**	**0.70**	**0.1**
Z05XIE82-1	7.3	0.6	1389.2	549.3		0.40	1021.5	5.2	0.76	
Z05XIE82-2	8.2	0.7	935.4	1389.3		1.49	939.1	5.3	0.75	

Table B.2: continued

Sample	Age (Ma)	± (Ma)	U (ppm)	Th (ppm)	Sm (ppm)	Th/U	He (ncc/mg)	mass (mg)	Ft	StDev
Z05XIE82-3	6.7	0.5	2270.7	941.0		0.41	1482.4	3.8	0.73	
Z05XIE82	**7.4**	**0.6**	**1531.8**	**959.9**		**0.77**	**1147.7**	**4.8**	**0.74**	**0.7**
Z05XIE83-1	6.9	0.5	1742.5	477.2		0.27	1148.6	4.5	0.74	
Z05XIE83-2	7.9	0.6	1107.7	702.7		0.63	912.8	4.5	0.74	
Z05XIE83-3	9.0	0.7	764.3	443.0		0.58	707.8	4.5	0.75	
Z05XIE83	**7.9**	**0.6**	**1204.8**	**541.0**		**0.50**	**923.1**	**4.5**	**0.74**	**1.1**
Z05XIE84-1	6.4	0.5	1842.1	747.2		0.41	1203.8	5.2	0.76	
Z05XIE84-2	7.0	0.6	847.0	353.4		0.42	627.1	9.0	0.79	
Z05XIE84-3	7.2	0.6	1064.0	274.1		0.26	780.3	7.3	0.79	
Z05XIE84	**6.9**	**0.5**	**1251.0**	**458.3**		**0.36**	**870.4**	**7.2**	**0.78**	**0.4**
Z05XIE85-1	8.4	0.7	1012.5	416.0		0.41	874.8	6.4	0.77	
Z05XIE85-2	8.2	0.7	864.0	462.0		0.53	763.8	7.5	0.78	
Z05XIE85-3	7.1	0.6	1441.6	698.5		0.48	1092.8	8.8	0.78	
Z05XIE85	**7.9**	**0.6**	**1106.0**	**525.5**		**0.48**	**910.5**	**7.6**	**0.78**	**0.7**
Z05XIE86-1	6.0	0.5	2035.0	1101.5		0.54	1273.6	5.4	0.76	
Z05XIE86-2*	4.3	0.3	350.3	934.4		2.67	231.6	7.4	0.78	
Z05XIE86-3	6.6	0.5	975.1	576.3		0.59	684.1	5.9	0.77	
Z05XIE86	**6.3**	**0.5**	**1505.1**	**838.9**		**0.57**	**978.8**	**5.7**	**0.76**	**0.4**
Z05XIE87-1	7.4	0.6	750.8	347.3		0.46	565.7	4.6	0.75	
Z05XIE87-2	6.0	0.5	1872.1	663.4		0.35	1124.2	5.0	0.75	
Z05XIE87-3	7.2	0.6	843.2	485.3		0.58	629.0	4.9	0.75	
Z05XIE87	**6.9**	**0.6**	**1155.4**	**498.7**		**0.46**	**773.0**	**4.8**	**0.75**	**0.7**
Z05XIE88-1	7.7	0.6	777.9	454.4		0.58	654.3	8.2	0.79	
Z05XIE88-2*	11.7	0.9	1993.4	807.8		0.41	2380.7	5.3	0.76	
Z05XIE88-3	6.6	0.5	1408.0	561.7		0.40	970.3	6.5	0.78	
Z05XIE88	**7.2**	**0.6**	**1093.0**	**508.1**		**0.49**	**812.3**	**7.4**	**0.8**	**0.7**
Z05XIE89-1	9.3	0.7	3077.7	1543.2		0.50	2727.5	2.5	0.70	
Z05XIE89-2	6.8	0.5	1617.4	441.4		0.27	1128.4	8.5	0.80	
Z05XIE89-3	8.4	0.7	486.6	355.8		0.73	447.2	5.5	0.76	
Z05XIE89	**8.2**	**0.7**	**1727.2**	**780.1**		**0.50**	**1434.4**	**5.5**	**0.75**	**1.3**
Z04XI03-1	53.0	4.2	564.7	363.8		0.644	3089.8	4.9	0.73	
Z04XI03-2	60.7	4.9	414.7	243.8		0.588	2719.2	8.5	0.78	
Z04XI03-3	60.4	4.8	496.1	330.4		0.666	3251.0	8.0	0.77	
Z04XI03	**58.0**	**4.6**	**491.8**	**312.7**		**0.633**	**3020.0**	**7.1**	**0.76**	**4.4**
Z04XI04-1	21.4	1.7	168.4	369.7		2.20	469.1	4.1	0.71	
Z04XI04-2	19.8	1.6	254.7	280.8		1.10	539.7	4.7	0.70	
Z04XI04-3	18.7	1.5	145.9	94.8		0.65	270.2	3.4	0.71	
Z04XI04	**19.9**	**1.6**	**189.7**	**248.4**		**1.32**	**426.3**	**4.1**	**0.70**	**1.3**
Z04XI05-1	16.3	1.3	278.3	190.1		0.68	439.9	3	0.68	
Z04XI05-2	12.5	1.0	212.7	269.0		1.26	283.0	2.6	0.67	
Z04XI05-3	19.8	1.6	160.9	109.3		0.68	320.5	3.9	0.71	
Z04XI05	**16.2**	**1.3**	**217.3**	**189.4**		**0.9**	**347.8**	**3.2**	**0.7**	**3.7**
Z04XI07-1	47.4	3.8	188.3	121.6		0.65	847.2	2.8	0.67	
Z04XI07-2	48.3	3.9	158.6	142.6		0.90	780.6	3.4	0.69	
Z04XI07-3	50.9	4.1	283.9	132.1		0.47	1483.0	6.5	0.76	
Z04XI07-4	44.5	3.6	238.1	179.0	1.9	0.8	55.12	12.2	0.82	
Z04XI07-5*	93.0	7.4	117.8	84.6	0.8	0.7	55.52	10.6	0.80	
Z04XI07-6	46.1	3.7	114.0	95.1	7.6	0.8	27.50	11.5	0.81	

Table B.2: continued

Sample	Age (Ma)	± (Ma)	U (ppm)	Th (ppm)	Sm (ppm)	Th/U	He (ncc/mg)	mass (mg)	Ft	StDev
Z04XI07	**47.5**	**3.8**	**196.6**	**134.1**	**4.7**	**0.7**	**638.7**	**7.3**	**0.7**	**2.4**
Z04XI08-1	25.8	2.1	411.7	238.8		0.580	962.9	2.0	0.65	
Z04XI08-2	26.3	2.1	348.6	214.7		0.616	868.1	2.6	0.68	
Z04XI08-3	30.6	2.4	237.5	193.4		0.815	697.9	2.4	0.66	
Z04XI08	**27.6**	**2.2**	**332.6**	**215.6**		**0.670**	**843.0**	**2.3**	**0.66**	**2.6**
Z04XI12-1	40.2	3.2	376.0	190.7		0.507	1489.3	4.2	0.72	
Z04XI12-2	34.6	2.8	407.2	208.7		0.513	1380.5	3.5	0.72	
Z04XI12-3	34.0	2.7	314.7	280.4		0.891	1103.6	3.8	0.70	
Z04XI12	**36.3**	**2.9**	**366.0**	**226.6**		**0.637**	**1324.5**	**3.8**	**0.71**	**3.4**
Z04XI16-1	23.8	1.9	223.7	194.8		0.87	499.7	1.9	0.64	
Z04XI16-2	15.7	1.3	448.1	359.9		0.80	716.6	3.6	0.70	
Z04XI16-3	17.3	1.4	299.8	271.3		0.91	506.0	2.3	0.66	
Z04XI16	**18.9**	**1.5**	**323.9**	**275.4**		**0.9**	**574.1**	**2.6**	**0.7**	**4.3**
Z04XI17-1	16.0	1.3	190.3	166.2		0.874	314.7	3.5	0.70	
Z04XI17-2	20.1	1.6	138.4	96.8		0.700	271.2	3.1	0.69	
Z04XI17-3	10.8	0.9	43.1	42.5		0.986	44.8	1.8	0.64	
Z04XI17	**15.6**	**1.3**	**123.9**	**101.9**		**0.853**	**210.2**	**2.8**	**0.68**	**4.7**
Z04XI18-1	71.6	5.7	226.2	119.8		0.53	1709.1	8.1	0.77	
Z04XI18-2	70.8	5.7	135.2	129.6		0.96	1019.8	3.8	0.71	
Z04XI18-3	67.2	5.4	46.1	43.9		0.95	343.4	5.7	0.74	
Z04XI18	**69.9**	**5.6**	**135.8**	**97.8**		**0.8**	**1024.1**	**5.9**	**0.7**	**2.3**
Z04XI19-1	40.7	3.3								
Z04XI19-2	33.8	2.7								
Z04XI19-3	48.6	3.9								
Z04XI19	**41.0**	**3.3**								**7.4**
Z04XI20-1	54.3	4.3	406.6	252.4		0.62	2135.6	3.3	0.69	
Z04XI20-2	57.0	4.6	66.9	67.6		1.01	423.1	5	0.73	
Z04XI20-3	65.7	5.3	169.6	68.9		0.41	1093.6	4.6	0.73	
Z04XI20	**59.0**	**4.7**	**214.4**	**129.6**		**0.7**	**1217.4**	**4.3**	**0.7**	**6.0**
Z04XI22-1	110.6	8.8								
Z04XI22-2	115.0	9.2								
Z04XI22-3	105.3	8.4								
Z04XI22	**110.3**	**8.8**								**4.9**
Z04XI25-1	77.3	6.2	312.6	304.4		0.97	2560.3	3.8	0.70	
Z04XI25-2	68.4	5.5	172.1	195.5		1.14	1337.0	5.6	0.73	
Z04XI25-3	81.1	6.5	116.9	153.6		1.31	1055.6	3.6	0.70	
Z04XI25	**75.6**	**6.0**	**200.5**	**217.9**		**1.1**	**1651.0**	**4.3**	**0.7**	**6.5**
Z04XI30-1	63.0	5.0	86.1	60.0		0.696	636.8	18.3	0.82	
Z04XI30-2	83.3	6.7	62.7	62.3		0.993	633.9	14.0	0.80	
Z04XI30-3	82.2	6.6	51.1	50.9		0.996	534.0	29.8	0.84	
Z04XI30	**76.2**	**6.1**	**66.6**	**57.7**		**0.895**	**601.5**	**20.7**	**0.82**	**11.4**
Z04XI31-1	93.0	7.4	310.2	260.2		0.84	3179.2	6.6	0.75	
Z04XI31-2	86.3	6.9	172.5	97.3		0.56	1537.9	5.3	0.74	
Z04XI31-3	81.7	6.5	210.6	192.6		0.91	1803.7	4.0	0.71	
Z04XI31	**87.0**	**7.0**	**231.1**	**183.4**		**0.77**	**2173.6**	**5.3**	**0.73**	**5.7**
Z04XI32-1	86.5	6.9	370.1	230.3		0.622	3172.5	3.4	0.71	
Z04XI32-2	77.0	6.2	88.0	78.8		0.895	726.1	4.6	0.72	
Z04XI32-3	102.9	8.2	406.4	243.3		0.599	3980.4	2.8	0.68	

Table B.2: continued

Sample	Age (Ma)	± (Ma)	U (ppm)	Th (ppm)	Sm (ppm)	Th/U	He (ncc/mg)	mass (mg)	Ft	StDev
Z04XI32	**88.8**	**7.1**	**288.2**	**184.1**		**0.705**	**2626.3**	**3.6**	**0.70**	**13.1**
Z04XI36-1	73.4	5.9	185.7	104.7		0.56	1527.0	11.3	0.81	
Z04XI36-2	72.3	5.8	115.4	99.4		0.86	959.9	8.2	0.78	
Z04XI36-3	62.9	5.0	115.9	89.3		0.77	826.8	9.3	0.78	
Z04XI36-4*	48.1	3.9	96.8	105.5		1.09	515.9	3.2	0.72	
Z04XI36	**69.5**	**5.6**	**139.0**	**97.8**		**0.7**	**1104.5**	**9.6**	**0.8**	**5.8**
Z04XI38-1	47.0	3.8	410.5	384.6		0.937	2107.5	5.1	0.73	
Z04XI38-2	47.3	3.8	430.9	365.0		0.847	2159.1	3.8	0.72	
Z04XI38	**47.2**	**3.8**	**420.7**	**374.8**		**0.892**	**2133.3**	**4.5**	**0.73**	**0.3**
Z05XI52-1	63.2	5.1								
Z05XI52-2	59.5	4.8								
Z05XI52-3	54.4	4.4								
Z05XI52	**59.0**	**4.7**								**4.4**
Z05XI59-2	53.1	4.2								
Z05XI59-3	50.8	4.1								
Z05XI59	**51.9**	**4.2**								**1.6**
Z05XI60-1	44.3	3.5								
Z05XI60-2	48.8	3.9								
Z05XI60-3	60.8	4.9								
Z05XI60	**51.3**	**4.1**								**8.6**
Z05XI63-1	21.9	1.7								
Z05XI63-2	21.5	1.7								
Z05XI63-3*	13.1	1.0								
Z05XI63	**21.7**	**1.7**								**0.3**
Z05XI67-1	28.2	2.3								
Z05XI67-2	25.5	2.0								
Z05XI67-3	37.1	3.0								
Z05XI67	**30.2**	**2.4**								**6.1**
Z05XI79-1*	6.5	0.5								
Z05XI79-2	22.9	1.8								
Z05XI79-3	21.6	1.7								
Z05XI79	**22.2**	**1.8**								**0.9**
Z05XI80-1	7.4	0.6								
Z05XI80-2	8.1	0.6								
Z05XI80-3	9.4	0.8								
Z05XI80	**8.3**	**0.7**								**1.0**
Z05XI90-1	20.0	1.6								
Z05XI90-2	23.0	1.8								
Z05XI90-3	17.5	1.4								
Z05XI90	**20.2**	**1.6**								**2.8**
Z05XI91-1	10.0	0.8								
Z05XI91-2	11.3	0.9								
Z05XI91-3	10.4	0.8								
Z05XI91	**10.6**	**0.8**								**0.7**
Z05XI92-1	7.3	0.6								
Z05XI92-2	8.0	0.6								
Z05XI92-3	8.2	0.7								
Z05XI92	**7.8**	**0.6**								**0.5**

Table B.2: continued

Sample	Age (Ma)	± (Ma)	U (ppm)	Th (ppm)	Sm (ppm)	Th/U	He (ncc/mg)	mass (mg)	Ft	StDev
Z05XI93-1	13.2	1.1								
Z05XI93-2	13.6	1.1								
Z05XI93-3	13.1	1.0								
Z05XI93	**13.3**	**1.1**								**0.3**
Z05XI94-1	18.1	1.5								
Z05XI94-2	20.4	1.6								
Z05XI94-3	19.0	1.5								
Z05XI94	**19.2**	**1.5**								**1.2**
ZPX01-1*	154.0	7.7	66.1	750.9		11.37	3242.7	4.4	0.71	
ZPX01-2	16.2	0.8	309.6	188.0		0.61	496.2	3.8	0.71	
ZPX01-3	14.2	0.7	424.3	255.8		0.60	581.9	3.0	0.69	
ZPX01	**15.2**	**0.8**	**367.0**	**221.9**		**0.61**	**539.1**	**3.4**	**0.70**	**1.4**
ZPX03-1	15.7	0.8	297.7	197.4		0.66	503.0	6.7	0.76	
ZPX03-2*	32.2	1.6	642.4	702.4		1.09	2251.1	3.8	0.71	
ZPX03-3	15.3	0.8	889.7	497.2		0.56	1293.9	3.2	0.69	
ZPX03	**15.5**	**0.8**	**593.7**	**347.3**		**0.61**	**898.5**	**5.0**	**0.73**	**0.3**
ZPX04-1	12.2	0.6	449.2	251.8		0.56	582.0	8.9	0.77	
ZPX04-2	17.2	0.9	395.3	222.2		0.56	744.0	10.8	0.79	
ZPX04-3*	33.6	1.7	284.6	149.9		0.53	994.6	6.3	0.76	
ZPX04-4	28.4	1.4	485.5	247.7		0.51	1396.2	4.8	0.74	
ZPX04-5	19.5	1.0	400.8	243.1		0.61	755.0	2.9	0.69	
ZPX04	**22.2**	**0.7**	**422.3**	**237.0**		**0.56**	**663.0**	**9.9**	**0.78**	**3.5**
ZPX05-1	13.8	0.7	1797.4	2256.9		1.26	2680.1	3.0	0.69	
ZPX05-2*	19.1	1.0	512.6	228.2		0.45	925.2	2.9	0.70	
ZPX05-3	9.4	0.5	469.9	357.9		0.76	476.6	6.5	0.75	
ZPX05-4	14.7	0.7	1101.4	879.7		0.80	1754.1	5.4	0.75	
ZPX05-5	12.9	0.6	228.2	181.1		0.79	342.8	12.6	0.81	
ZPX05	**12.7**	**0.6**	**899.2**	**918.9**		**0.9**	**1313.4**	**6.9**	**0.75**	**2.3**
ZPX06-1	50.2	2.5	498.8	363.5		0.73	2420.1	2.3	0.68	
ZPX06-2	49.4	2.5	1018.7	669.3		0.66	5084.6	3.6	0.72	
ZPX06-3	48.1	2.4	758.7	533.3		0.70	3528.6	2.6	0.68	
ZPX06	**49.2**	**2.5**	**758.7**	**522.0**		**0.70**	**3677.8**	**2.8**	**0.69**	**1.1**
Z04GB04-1	42.7	3.4								
Z04GB04-2	47.4	3.8								
Z04GB04-3	40.2	3.2								
Z04GB04	**43.5**	**3.5**								**3.7**

APPENDIX C

Table C.1: Results from HeFTy - HeMP comparison based on four different thermal histories.

Mineral*	Model	radius (µm)	U (ppm)	Th (ppm)	Sm (ppm)	Age HF (Ma)	Age HP (Ma)	dAge (%)	Age HF (Ma)	Age HP (Ma)	dAge (%)	Age HF (Ma)	Age HP (Ma)	dAge (%)
t-T History 1							**100 Myrs**			**50 Myrs**			**10 Myrs**	
Apatite	Durango	50	10	0	0	55.4	55.7	0.5	29.9	30.0	0.2	7.1	7.1	0.0
Apatite	RDAAM	60	10	0	0	48.1	48.3	0.3	25.4	25.4	0.1	6.2	6.2	0.1
Apatite	RDAAM	60	20	0	0	52.5	52.6	0.1	26.3	26.3	-0.1	6.2	6.2	0.1
Apatite	RDAAM	60	30	0	0	56.1	56.1	0.0	27.3	27.3	0.1	6.2	6.2	0.1
Apatite	RDAAM	60	40	0	0	58.9	58.9	0.1	28.3	28.3	0.1	6.2	6.2	0.1
Apatite	RDAAM	60	50	0	0	61.2	61.2	0.0	29.3	29.2	-0.3	6.2	6.2	0.0
Apatite	RDAAM	60	60	0	0	63.1	63.1	0.0	30.1	30.0	-0.2	6.2	6.2	0.1
Apatite	RDAAM	60	70	0	0	64.7	64.7	0.0	30.8	30.8	-0.1	6.2	6.2	0.0
Apatite	RDAAM	60	80	0	0	66.1	66.1	0.0	31.5	31.4	-0.3	6.3	6.3	0.0
Apatite	RDAAM	60	90	0	0	67.4	67.4	0.0	32.1	32.0	-0.3	6.3	6.3	-0.1
Apatite	RDAAM	60	100	0	0	68.5	68.5	0.0	32.6	32.5	-0.2	6.3	6.3	-0.1
Apatite	RDAAM	60	110	0	0	69.5	69.5	0.0	33.0	33.0	0.1	6.3	6.3	-0.1
Apatite	RDAAM	60	120	0	0	70.4	70.4	0.0	33.4	33.5	0.2	6.4	6.4	-0.1
Apatite	RDAAM	60	130	0	0	71.2	71.2	0.0	33.9	33.9	0.0	6.4	6.4	-0.1
Apatite	RDAAM	60	140	0	0	71.9	72.0	0.1	34.3	34.3	-0.1	6.4	6.4	-0.1
Apatite	RDAAM	60	150	0	0	72.7	72.7	0.0	34.6	34.6	0.1	6.5	6.5	-0.1
Zircon	Reiners	30	100	50	10	65.1	64.9	-0.3	33.8	33.6	-0.6	7.3	7.4	0.8
Zircon	Reiners	40	100	50	10	67.2	67.1	-0.2	34.9	34.7	-0.5	7.6	7.6	0.8
Zircon	Reiners	50	100	50	10	68.8	68.7	-0.1	35.7	35.6	-0.3	7.7	7.8	0.5
Zircon	Reiners	60	100	50	10	70.1	70.1	0.0	36.4	36.3	-0.4	7.9	7.9	0.5
Zircon	Reiners	70	100	50	10	71.2	71.2	0.0	36.9	36.9	-0.1	8.0	8.0	0.4
Zircon	Reiners	80	100	50	10	72.1	72.2	0.2	37.4	37.4	-0.1	8.1	8.2	0.4
Zircon	Reiners	90	100	50	10	73.0	73.1	0.2	37.9	37.8	-0.2	8.2	8.2	0.2
Zircon	Reiners	100	100	50	10	73.7	73.9	0.3	38.3	38.2	-0.2	8.3	8.3	0.4
Zircon-zon.	Reiners	60/30	100/200	40/80	0/0	69.7	69.6	-0.1	36.2	36.0	-0.5	7.8	7.9	0.6
Zircon-zon.	Reiners	60/24	100/200	40/80	0/0	69.4	69.3	-0.1	36.0	35.9	-0.3	7.8	7.9	0.6
Zircon-zon.	Reiners	60/18	100/200	40/80	0/0	69.2	69.1	-0.1	35.9	35.8	-0.3	7.8	7.8	0.6
Zircon-zon.	Reiners	60/12	100/200	40/80	0/0	69.3	69.2	-0.1	35.9	35.8	-0.2	7.8	7.8	0.5
Zircon-zon.	Reiners	60/6	100/200	40/80	0/0	69.5	69.5	0.0	36.1	36.0	-0.3	7.8	7.9	0.5
t-T History 2							**100 Myrs**			**50 Myrs**			**10 Myrs**	
Apatite	Durango	50	10	0	0	52.0	52.1	0.2	26.3	26.3	-0.2	5.4	5.4	-0.2

Table C.1: continued

Mineral*	Model	radius (µm)	U (ppm)	Th (ppm)	Sm (ppm)	Age HF (Ma)	Age HP (Ma)	dAge (%)	Age HF (Ma)	Age HP (Ma)	dAge (%)	Age HF (Ma)	Age HP (Ma)	dAge (%)
Apatite	RDAAM	60	10	0	0	51.0	51.2	0.3	25.7	25.7	0.2	5.3	5.3	-0.1
Apatite	RDAAM	60	20	0	0	51.1	51.3	0.4	25.8	25.8	0.1	5.3	5.3	-0.3
Apatite	RDAAM	60	30	0	0	51.2	51.3	0.2	25.8	25.8	0.2	5.3	5.3	-0.2
Apatite	RDAAM	60	40	0	0	51.2	51.3	0.3	25.8	25.9	0.2	5.3	5.3	-0.2
Apatite	RDAAM	60	50	0	0	51.2	51.4	0.3	25.8	25.9	0.2	5.3	5.3	-0.2
Apatite	RDAAM	60	60	0	0	51.3	51.4	0.2	25.9	25.9	-0.2	5.3	5.3	-0.1
Apatite	RDAAM	60	70	0	0	51.3	51.4	0.2	25.9	25.9	-0.1	5.3	5.3	-0.1
Apatite	RDAAM	60	80	0	0	51.4	51.4	0.1	25.9	25.9	-0.1	5.3	5.3	-0.1
Apatite	RDAAM	60	90	0	0	51.4	51.5	0.2	25.9	25.9	-0.1	5.3	5.3	-0.1
Apatite	RDAAM	60	100	0	0	51.5	51.5	0.0	25.9	25.9	-0.1	5.3	5.3	-0.1
Apatite	RDAAM	60	110	0	0	51.6	51.5	-0.1	25.9	25.9	0.0	5.3	5.3	-0.3
Apatite	RDAAM	60	120	0	0	51.6	51.6	0.0	26.0	25.9	-0.4	5.3	5.3	-0.3
Apatite	RDAAM	60	130	0	0	51.7	51.6	-0.1	26.0	25.9	-0.4	5.3	5.3	-0.3
Apatite	RDAAM	60	140	0	0	51.7	51.7	-0.1	26.0	25.9	-0.3	5.3	5.3	-0.2
Apatite	RDAAM	60	150	0	0	51.8	51.7	-0.2	26.0	25.9	-0.3	5.3	5.3	-0.2
Zircon	Reiners	30	100	50	10	52.4	52.5	0.1	26.3	26.3	0.0	5.3	5.3	-0.2
Zircon	Reiners	40	100	50	10	52.6	52.7	0.2	26.5	26.4	-0.3	5.4	5.4	-0.2
Zircon	Reiners	50	100	50	10	52.8	52.9	0.2	26.5	26.5	0.1	5.4	5.4	-0.2
Zircon	Reiners	60	100	50	10	52.9	53.0	0.3	26.6	26.6	0.0	5.4	5.4	-0.4
Zircon	Reiners	70	100	50	10	53.1	53.2	0.1	26.7	26.7	-0.1	5.4	5.4	-0.2
Zircon	Reiners	80	100	50	10	53.2	53.3	0.2	26.7	26.7	0.1	5.4	5.4	-0.2
Zircon	Reiners	90	100	50	10	53.3	53.4	0.2	26.8	26.8	-0.1	5.4	5.4	-0.2
Zircon	Reiners	100	100	50	10	53.3	53.5	0.3	26.8	26.8	0.1	5.5	5.4	-0.2
Zircon-zon.	Reiners	60/30	100/200	40/80	0/0	52.9	53.0	0.2	26.6	26.6	-0.1	5.4	5.4	-0.2
Zircon-zon.	Reiners	60/24	100/200	40/80	0/0	52.8	53.0	0.3	26.6	26.6	-0.2	5.4	5.4	-0.4
Zircon-zon.	Reiners	60/18	100/200	40/80	0/0	52.8	52.9	0.2	26.6	26.5	-0.2	5.4	5.4	-0.2
Zircon-zon.	Reiners	60/12	100/200	40/80	0/0	52.8	52.9	0.2	26.6	26.6	-0.2	5.4	5.4	-0.2
Zircon-zon.	Reiners	60/6	100/200	40/80	0/0	52.8	53.0	0.3	26.6	26.6	-0.1	5.4	5.4	-0.2
t-T History 3							**100 Myrs**			**50 Myrs**			**10 Myrs**	
Apatite	Durango	50	10	0	0	44.8	45.5	1.5	29.0	29.3	1.0	8.1	8.1	0.0
Apatite	RDAAM	60	10	0	0	30.3	30.6	0.9	16.3	16.5	1.4	6.1	6.1	0.6
Apatite	RDAAM	60	20	0	0	48.3	48.5	0.5	20.6	20.8	1.0	6.1	6.1	0.6
Apatite	RDAAM	60	30	0	0	60.7	61.0	0.5	25.5	25.7	0.6	6.1	6.2	0.7

Table C.1: continued

Mineral*	Model	radius (μm)	U (ppm)	Th (ppm)	Sm (ppm)	Age HF (Ma)	Age HP (Ma)	dAge (%)	Age HF (Ma)	Age HP (Ma)	dAge (%)	Age HF (Ma)	Age HP (Ma)	dAge (%)
Apatite	RDAAM	60	40	0	0	68.8	69.1	0.5	29.5	29.6	0.4	6.2	6.2	0.6
Apatite	RDAAM	60	50	0	0	74.3	74.6	0.4	32.5	32.6	0.5	6.3	6.3	0.6
Apatite	RDAAM	60	60	0	0	78.1	78.5	0.5	34.9	35.0	0.2	6.4	6.4	0.5
Apatite	RDAAM	60	70	0	0	80.9	81.3	0.5	36.7	36.8	0.2	6.5	6.5	0.4
Apatite	RDAAM	60	80	0	0	83.0	83.4	0.5	38.1	38.2	0.2	6.6	6.7	0.4
Apatite	RDAAM	60	90	0	0	84.6	85.0	0.5	39.3	39.3	0.1	6.8	6.8	0.3
Apatite	RDAAM	60	100	0	0	85.9	86.3	0.5	40.2	40.3	0.1	6.9	6.9	0.3
Apatite	RDAAM	60	110	0	0	86.9	87.4	0.5	41.0	41.0	0.1	7.1	7.1	0.2
Apatite	RDAAM	60	120	0	0	87.7	88.2	0.6	41.6	41.7	0.2	7.2	7.2	0.1
Apatite	RDAAM	60	130	0	0	88.4	88.9	0.6	42.1	42.2	0.3	7.3	7.3	0.1
Apatite	RDAAM	60	140	0	0	89.0	89.5	0.6	42.6	42.7	0.2	7.4	7.4	0.2
Apatite	RDAAM	60	150	0	0	89.5	90.1	0.6	43.0	43.1	0.2	7.5	7.5	0.1
Zircon	Reiners	30	100	50	10	37.4	36.3	-3.0	23.2	22.5	-3.0	6.9	6.7	-2.6
Zircon	Reiners	40	100	50	10	44.6	43.6	-2.2	27.2	26.6	-2.3	7.5	7.4	-2.0
Zircon	Reiners	50	100	50	10	50.5	49.7	-1.6	30.2	29.7	-1.6	8.0	7.8	-1.5
Zircon	Reiners	60	100	50	10	55.3	54.8	-1.0	32.5	32.1	-1.1	8.2	8.1	-1.2
Zircon	Reiners	70	100	50	10	59.4	59.0	-0.7	34.4	34.0	-1.0	8.5	8.4	-0.9
Zircon	Reiners	80	100	50	10	62.8	62.5	-0.4	35.8	35.6	-0.6	8.6	8.6	-0.8
Zircon	Reiners	90	100	50	10	65.7	65.5	-0.3	37.0	36.8	-0.5	8.8	8.7	-0.7
Zircon	Reiners	100	100	50	10	68.2	68.1	-0.2	38.0	37.9	-0.4	8.9	8.8	-0.6
Zircon-zon.	Reiners	60/30	100/200	40/80	0/0	53.9	53.0	-1.8	31.8	31.2	-1.9	8.1	8.0	-1.6
Zircon-zon.	Reiners	60/24	100/200	40/80	0/0	53.1	52.2	-1.8	31.4	30.8	-2.0	8.1	7.9	-1.6
Zircon-zon.	Reiners	60/18	100/200	40/80	0/0	52.5	51.6	-1.7	31.0	30.5	-1.8	8.0	7.9	-1.6
Zircon-zon.	Reiners	60/12	100/200	40/80	0/0	52.6	52.0	-1.2	31.1	30.6	-1.5	8.0	7.9	-1.4
Zircon-zon.	Reiners	60/6	100/200	40/80	0/0	53.5	52.9	-1.1	31.6	31.2	-1.4	8.1	8.0	-1.4
t-T History 4							**100 Myrs**			**50 Myrs**			**10 Myrs**	
Apatite	Durango	50	10	0	0	36.5	36.6	0.2	19.6	19.7	0.4	5.4	5.4	0.6
Apatite	RDAAM	60	10	0	0	32.8	32.8	-0.1	16.9	17.0	0.3	4.1	4.1	0.3
Apatite	RDAAM	60	20	0	0	36.7	36.7	-0.1	17.8	17.8	-0.2	4.1	4.1	0.1
Apatite	RDAAM	60	30	0	0	39.9	39.8	-0.2	18.8	18.7	-0.4	4.1	4.1	0.3
Apatite	RDAAM	60	40	0	0	42.4	42.3	-0.1	19.7	19.7	-0.2	4.1	4.1	0.0
Apatite	RDAAM	60	50	0	0	45.5	45.3	-0.5	20.5	20.5	0.0	4.2	4.2	0.2
Apatite	RDAAM	60	60	0	0	50.2	50.0	-0.5	21.3	21.3	-0.1	4.2	4.2	0.0

Table C.1: continued

Mineral*	Model	radius (μm)	U (ppm)	Th (ppm)	Sm (ppm)	Age HF (Ma)	Age HP (Ma)	dAge (%)	Age HF (Ma)	Age HP (Ma)	dAge (%)	Age HF (Ma)	Age HP (Ma)	dAge (%)
Apatite	RDAAM	60	70	0	0	56.2	55.9	-0.4	22.3	22.2	-0.4	4.2	4.2	0.2
Apatite	RDAAM	60	80	0	0	62.2	62.0	-0.3	23.5	23.4	-0.3	4.2	4.2	0.0
Apatite	RDAAM	60	90	0	0	67.6	67.4	-0.3	25.1	25.0	-0.3	4.3	4.3	0.1
Apatite	RDAAM	60	100	0	0	72.1	72.0	-0.1	27.0	26.9	-0.4	4.3	4.3	0.1
Apatite	RDAAM	60	110	0	0	75.9	75.9	0.0	29.0	28.9	-0.5	4.4	4.4	0.0
Apatite	RDAAM	60	120	0	0	79.0	79.1	0.1	30.9	30.8	-0.4	4.4	4.4	0.0
Apatite	RDAAM	60	130	0	0	81.6	81.7	0.2	32.6	32.6	-0.1	4.5	4.5	0.0
Apatite	RDAAM	60	140	0	0	83.8	83.9	0.2	34.3	34.2	-0.3	4.5	4.5	0.0
Apatite	RDAAM	60	150	0	0	85.6	85.8	0.2	35.7	35.7	-0.1	4.6	4.6	-0.2
Zircon	Reiners	30	100	50	10	33.8	33.6	-0.6	17.6	17.4	-1.0	3.8	3.8	-0.8
Zircon	Reiners	40	100	50	10	34.9	34.7	-0.5	18.1	18.0	-0.6	4.0	3.9	-0.8
Zircon	Reiners	50	100	50	10	35.7	35.6	-0.4	18.5	18.4	-0.4	4.0	4.0	-0.7
Zircon	Reiners	60	100	50	10	36.4	36.3	-0.4	18.9	18.8	-0.6	4.1	4.1	-0.5
Zircon	Reiners	70	100	50	10	36.9	36.9	-0.1	19.2	19.1	-0.6	4.2	4.2	-0.5
Zircon	Reiners	80	100	50	10	37.4	37.4	-0.1	19.4	19.4	-0.2	4.2	4.2	-0.5
Zircon	Reiners	90	100	50	10	37.9	37.8	-0.2	19.6	19.6	-0.1	4.3	4.3	-0.2
Zircon	Reiners	100	100	50	10	38.3	38.2	-0.2	19.8	19.8	0.0	4.3	4.3	-0.5
Zircon-zon.	Reiners	60/30	100/200	40/80	0/0	36.2	36.0	-0.5	18.8	18.7	-0.7	4.1	4.1	-0.7
Zircon-zon.	Reiners	60/24	100/200	40/80	0/0	36.0	35.9	-0.3	18.7	18.6	-0.6	4.1	4.1	-0.5
Zircon-zon.	Reiners	60/18	100/200	40/80	0/0	35.9	35.8	-0.3	18.6	18.5	-0.3	4.1	4.0	-0.7
Zircon-zon.	Reiners	60/12	100/200	40/80	0/0	35.9	35.8	-0.2	18.7	18.6	-0.7	4.1	4.0	-0.5
Zircon-zon.	Reiners	60/6	100/200	40/80	0/0	36.1	36.0	-0.3	18.7	18.6	-0.3	4.1	4.1	-0.5

* radius values for zoned zircons (Zircon-zon.) refer to grain size and width of the outer rim, parent concentrations are given for the core and rim of the grain. HF - HeFTy, HP - HeMP